WHEEL FAILURE MECHANISMS
OF RAILROAD CARS

FINAL REPORT

Volume 2
(Technical Task Summaries)

FRA Contract Number DTFR53-82-C-00282, Task Order #6

Association of American Railroads

Britto R. Rajkumar
Transportation Test Center
Pueblo, Colorado
&
Daniel H. Stone
AAR Technical Center
Chicago, Illinois

ASSOCIATION OF AMERICAN RAILROADS
RESEARCH AND TEST DEPARTMENT

WHEEL FAILURE MECHANISMS
OF RAILROAD CARS
FINAL REPORT
VOLUME II
(TECHNICAL TASK SUMMARIES)

REPORT NO. R-680

FRA CONTRACT NO. DTFR 53-82-C-00282, TASK ORDER #6

Association of American Railroads
Transportation Test Center

B. R. RAJKUMAR
D. H. STONE

NOVEMBER, 1987

DISCLAIMER

This report is disseminated by the AAR for informational purposes only and is given to, and accepted by, the recipient at its sole risk. The AAR makes no representations or warranties, either express or implied, with respect to the report or its contents. The AAR assumes no liability to anyone for special, collateral, exemplary, indirect, incidental, consequential or any other kind of damage resulting from the use or application of this report or its content. Any attempt to apply the information contained in this paper is done at the recipient's own risk.

1. REPORT NO. R-680 - Volume II	2. REPORT DATE November, 1987	3. PERIOD COVERED September, 1983 - January, 1987

4. TITLE AND SUBTITLE

Wheel Failure Mechanisms of Railroad Cars
Volume II - Technical Task Summaries

5. AUTHOR(S)

Britto R. Rajkumar, Section Manager
Daniel H. Stone, Director - Metallurgy

6. PERFORMING ORGANIZATION NAME AND ADDRESS Association of American Railroads Transportation Test Center P. O. Box 11130 Pueblo, Colorado 81001	7. TYPE OF REPORT 8. CONTRACT OR GRANT NO. DTFR53-82-C-00282
9. SPONSORING AGENCY NAME AND ADDRESS United States Department of Transportation Federal Railroad Administration 400 7th Street, S. W. Washington, D. C. 20590	10. NO. OF PAGES 11. NO. OF REFERENCES

12. SUPPLEMENTARY NOTES

FRA Task Order 6 - Final Report

13. ABSTRACT

This report summaries an extensive research program into the causes of wheel thermal failure. Results of material property tests, review of failure data, dynamometer tests, roll dynamics unit, track tests, and theoretical and experimental stress analysis show that heat-treated wheels of designs which meet the requirements of AAR Standard S.660 (low-stress wheels) are significantly more resistant to failure.

Volume II is a detailed reporting of the data and results, while Volume I gives a shorter summary of the program. Volume III is an appendix of highly detailed research data.

14. SUBJECT TERMS Residual Stress, Thermal Cracking, Wheel Failure, Wheel Steel Fatigue, Wheel Stress Analysis, Wheels	15. AVAILABILITY STATEMENT Assistant Vice President Association of American Railroads Technical Center 3140 South Federal Street Chicago, Illinois 60616

EXECUTIVE SUMMARY

This report presents the results of an extensive study into the causes of thermally induced wheel failure. Major issues addressed include the effects of wheel plate design, heat-treatment, ability to resist thermal damage, the relationship between discoloration and residual stress reversal, and the amount of brake energy required to cause changes in the residual stress in a wheel.

Results of this study show that heat-treated, curved plate (low stress) wheels are the most resistant to thermal and mechanical damage and, therefore, resistant to failure.

A survey of wheel performance was made using data based on wheel removals and derailments. Results of this study indicate that derailments due to thermally induced wheel failure are highly seasonal, with the majority of failures occurring during the winter months. The number of derailments due to thermally induced wheel failure has declined significantly over the last seven years as have all other categories of derailments. It was found that mechanical damage (i.e. tread metal flow, excessive wear, metallurgical transformation) is necessary for the initiation of thermal cracks and thus failure. Further, derailment data show that wheels with curved plate designs are several times less likely to fail than wheels of straight plate design; lack of population and mileage data for heat-treated wheels preclude use of derailment data to assess the role of heat-treatment in failure rate.

Additional information was gathered from an extensive program of saw cutting wheels that had been in service. Experimental programs were conducted using a dynamometer, the roll-dynamics unit, and on-track testing. Heat-treated curved plate wheels are more resistant to both stress-reversal and mechanical damage than any other combination of design and heat-treatment, and therefore more resistant to thermally induced failure. Over-hanging brake shoes and non-uniform tread heating were found to be conditions which will increase the probability of wheel failure.

Specific combinations of speed, time and brake shoe force are required to produce thermal damage in the rim for each wheel design and heat-treatment. These data should be used to promote brake system performance specifications.

It was found that discoloration*, while it indicates thermal input, is not necessarily evidence of destructive thermal damage. Discoloration indicates a greater probability of an adverse change in residual stress. However, it should be noted that research indicates some nondiscolored wheels may have developed high residual tensile stresses. The following diagram presents the schematic distribution of wheel population and illustrates that the derailment rate is higher for discolored wheels than nondiscolored wheels, while the absolute number of derailments is higher for nondiscolored wheels.
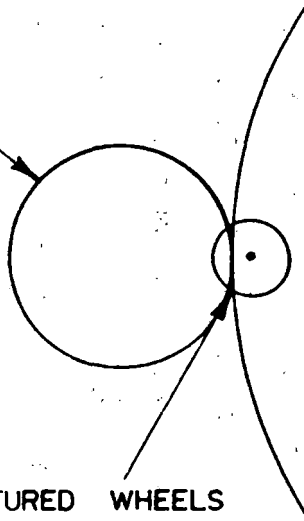
---

*Discoloration is defined as "a pattern of 'reddish brown' or 'blue' discoloration from heat on front and back face of rim, 4-inches into the plate with decreasing intensity."

~500,000
DISCOLORED
WHEELS

iv

FRACTURED WHEELS
INVOLVED IN
DERAILMENT

SCHEMATIC   DISTRIBUTION

~11,200,000

NON-DISCOLORED
WHEELS

OF   WHEEL   POPULATION

WHEEL FAILURE MECHANISMS
CONTROLLING FACTORS AND FINAL REPORT (VOLUME TWO) SECTION REFERENCES

FRACTURE STAGE	PRIMARY REQUIREMENTS	OPERATING CAUSE	BEST CLASS	BEST DESIGN	BEST DETECTION
CRACK INITIATION	SURFACE DAMAGE	WHEEL MECHANICAL ABUSE	C	ANY S AND CURVED	VISUAL INSP. & MEASUREMENT SWEEP FREQ. ULTR
	SECTION 2 SECTION 11	SECTION 2	SECTION 4		SECTION 14
INCREMENTAL CRACK GROWTH	RESIDUAL STRESS DEVELOPMENT & MECH. LOAD	THERMAL BRAKING ABUSE	SAME FOR ALL	S AND CURVED	MAGNETIC/ ULTRASONIC
	SECTION 11	SECTION 2 SECTION 3 SECTION 6	SECTION 4 SECTION 7	SECTION 7	SECTION 14
WHEEL FRACTURE	CRITICAL STRESS	IMPACT	B	S AND CURVED	-------
	SECTION 2	SECTION 2	SECTION 4	SECTION 2	

GLOSSARY OF TERMS

Cast Iron Brake Shoe: A brake shoe made of a high phosphorus (0.4 to 3.0 percent) cast iron.

Cast Wheel: A wheel that is manufactured by casting steel into a wholly or partially graphite mold.

Composition Brake Shoe: A brake shoe formed of a rubber, steel powder, and knolin composite adhesively bonded to a steel backing plate.

Crack Initiation: The formation of a crack large enough to grow under alternating stress.

Curved Plate Wheel: A wheel whose plate profile has a fully parabolic shape (see Low Stress Wheel).

Class B Wheel: A wheel which is rim quenched to yield a hardness of 277 to 341 Brinell. Grade B wheels contain 0.57 to 0.67 percent carbon.

Class C Wheel: A wheel which is rim quenched to yield a hardness of 321 to 363 Brinell. Grade C wheels contain 0.67 to 0.77 percent carbon.

Class U Wheel: An unheat-treated wheel which contains 0.65 to 0.80 percent carbon.

Discolored Wheel: A wheel which has a pattern of redish-brown or blue discoloration from heat on the front and back face of the rim, four inches or more into the rim with decreasing intensity.

Fracture: Rapid, unstable growth of a crack at rate approaching the speed of sound.

H-36 or CH-36 Wheel: A 36-inch diameter one-wear wheel for service on 100-ton cars. The C prefix indicates that the wheel is cast whereas the lack of a C prefix indicates a wrought wheel.

High Stress Wheel: A wheel of a design which does not meet the requirements of AAR Standard S-660.

Incremental Crack Growth: The slow, stable growth of a crack by fatigue.

J-33 or CJ-33 Wheel: A 33-inch diameter one-wear wheel for service on 70-ton cars. The C prefix indicates that the wheel is cast whereas the lack of a C prefix indicates a wrought wheel.

<u>J-36 or CJ-36 Wheel</u>:   A 36-inch diameter two-wear wheel for service on 100-ton cars. The C prefix indicates that the wheel is cast whereas the lack of a C prefix indicates a wrought wheel.

<u>K_{Ic}</u>:   The critical stress intensity factor, or fracture toughness, of a material. K_{Ic} defines the level of stress and crack size.

<u>Low Stress Wheel</u>:   A wheel of a design which meets the requirements of AAR Standard S-660 (Finite Element Analysis).

<u>S-Plate Wheel</u>:   A wheel whose plate profile has an S shape (see Low Stress Wheel).

<u>Straight Plate Wheel</u>:   A wheel whose plate profile has a straight section between the rim and hub filets (see High Stress Wheel).
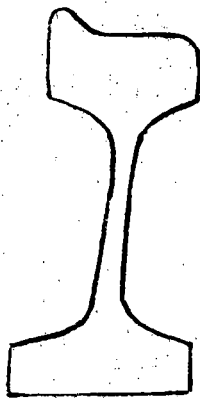
<u>Thermally Damaged Wheel</u>:   Any wheel, which through excessive brake shoe heating, has developed tensile residual hoop stresses in its rim.

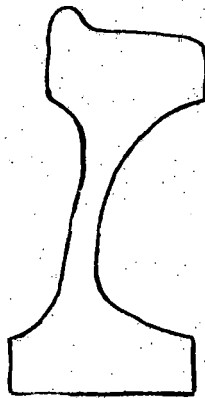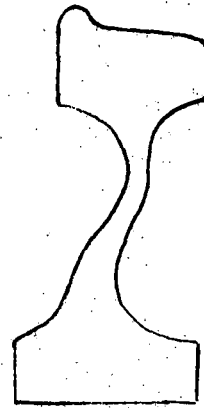<u>Wrought Wheel</u>:   A wheel which is manufactured by a process of forging and rolling.

FLANGE

RIM

PLATE

HUB

TREAD
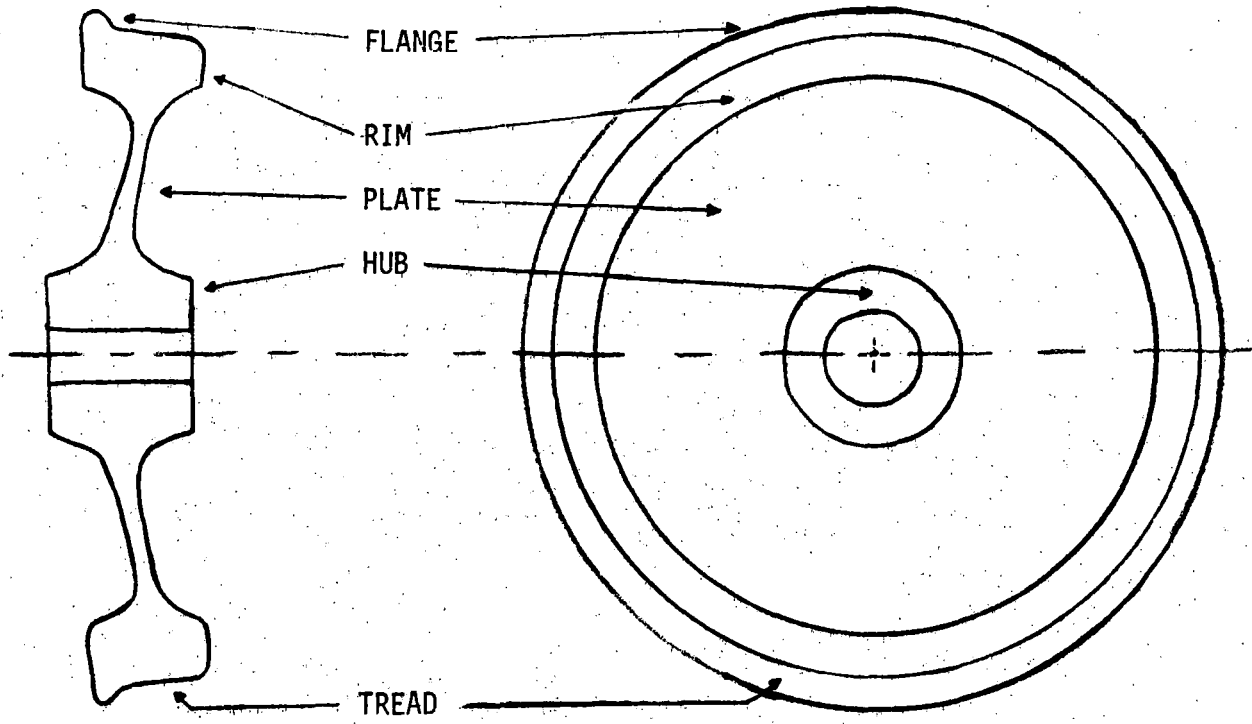
SIDE VIEW

FRONT VIEW

STRAIGHT
PLATE

PARABOLIC
PLATE

"S"
PLATE

BASIC WHEEL TYPES AND TERMINOLOGY

ACKNOWLEDGMENTS

Name	Contribution to the Project
Mr. George Carpenter AAR Technical Center Chicago	Brake Dynamometer testing in support of Technical Tasks T4, T6, and T8; data reduction and analysis; interim report preparation; reporting of results on individual tasks.
Mr. Tom Guins AAR, Washington Systems Center Washington, D.C.	National Study of Wheel Removal Guidelines
Mr. Robert Larson, Jr. TTC, Pueblo	Track testing in support of Technical Tasks T5, T6, and T7; data reduction and analysis; reporting of results on individual tasks performed.
Dr. Shirish Patil TTC, Pueblo	2D-mathematical model for computation of net rim forces in wheels from saw-cut displacement data.

Name	Contribution to the Project
Mr. Larry O. Daniels TTC, Pueblo	Track testing in support of Technical Task T8, and reporting of results.
Mr. Walt Halstead TTC, Pueblo	Stress Analysis - Technical Task T4
Mr. Michael Fec, AAR Technical Center Chicago	Wheel Material Properties, testing and reports - Technical Task T3.
Dr. Arthur Opinsky & Mr. Michael Joerms AAR Technical Center Chicago	Finite Element Analysis in support of Technical Tasks T10 and T11.
Mr. Aaron Tanzer AAR Technical Center Chicago	Wheel cracking behavior and data analysis of Technical Task T3
Mr. Dave Utrata AAR Technical Center Chicago	NDE Techniques - Technical Task T14.

Name	Contribution to the Project
Mr. M. Dembosky and his staff, TTC Pueblo	Development of data collection software for RDU and track testing.
Mrs. V. Rajkumar TTC, Pueblo	Software development for data analysis of Technical Tasks T4 and T5, and pilot technology survey.
Ms. Anita Medina TTC, Pueblo	Data reduction in support of Technical Tasks T4, T5, and T6, and overall data base management of the program.

TABLE OF CONTENTS

TABLE OF CONTENTS (Continued)

xvii

TABLE OF CONTENTS (Continued)

TABLE OF CONTENTS (Continued)

TABLE OF CONTENTS (Continued)

1.0 OVERVIEW

The life of a railroad wheel is determined by various factors such as wear, plastic deformation, fatigue cracking of the wheel plate, shelling and thermal cracking of the wheel tread, and wheel fracture. The incidence of heat related wheel failure, which is initiated by a thermal crack in the wheel rim, has become of great importance in the railroad industry. A relatively large number of wheels are removed from service on the basis of discoloration* of the wheel plate caused by severe thermal loads. The problem of identifying a thermally damaged wheel in service is very complex. Research has shown that a similar percentage of both nondiscolored and discolored wheels develop high levels of residual tensile stress in the rim. These stress levels promote the propagation of radial rim cracks and eventually lead to catastrophic wheel failures. Research has indicated that the initial residual stresses in the rim are altered by the effect of thermal stresses due to severe braking operation. Additionally, the effect of alternating stresses due to the mechanical loads at the wheel/rail interface are not well understood.

---

*Discoloration is defined as "a pattern of 'reddish brown' or 'blue' discolorations from heat on front and back face of rim, 4-inches into the plate with decreasing intensity".

To improve the safety performance of railcar wheels, the FRA supported the Wheel Failure Mechanisms Program to better understand important wheel failure mechanisms, and to develop technically sound wheel removal criteria and guidelines for safe operation. This project encompassed 14 Technical Tasks ranging from a technology survey through a national study of wheel removal guidelines to individual technical problem-oriented tasks which included laboratory and track testing and analyses. FRA also funded an independent study of M-2 fleet car axle/bearing failure modes, under Technical Task T15, included in the same contract covered by Task Order No. 6.

The individual technical tasks of this project were grouped into major subprojects for the purpose of clarity for the specific areas of wheel safety investigation. This grouping is illustrated in Figure 1.1.

1.1 Objectives

1.1.1 Overview and Program Control (Subproject 1)

The purpose of this subproject was to provide overall safety guidelines for wheel removal based on a continuing review and evaluation of national wheel safety statistics. The data base and pertinent analysis techniques were developed and managed under this subproject. In addition, the research results developed within the other Technical Subprojects were monitored within this subproject.

TECHNICAL TASKS

T1 - NATIONAL STUDY OF WHEEL REMOVAL GUIDELINES
T2 - CONDUCT PILOT TECHNOLOGY SURVEY - LITERATURE SEARCH
T3 - DETERMINATION OF MATERIAL PROPERTIES
T4 - HEAT TRANSFER AND RAIL LOADING - ANALYTICAL STUDY AND LABORATORY TESTING
T5 - PRELIMINARY TRACK TESTING AT T.T.C.
T6 - COMPREHENSIVE TESTING ON TRACK AND DYNAMOMETER
T7 - BRAKE SHOE EFFECT TESTING ON TRACK AND DYNAMOMETER
T8 - CRACK INITIATION TESTING
T9 - TREAD SHELLING
T10 - COMPREHENSIVE FAILURE MODEL
T11 - DETAILED RESIDUAL STRESS ANALYSIS
T12 - FURNISH BRAKE DYNAMOMETER AT A.A.R. TECH CENTER
T13 - MODIFY ROLL DYNAMICS UNIT (FOR T4 AND T15)
T14 - EVALUATION OF NDE TECHNIQUES
T15 - STUDY OF M-2 AXLE/BEARING FAILURE MODE

PLANNING TASKS

P2 - NATIONAL WHEEL STUDY PLAN
P1 - PILOT TECHNOLOGY SURVEY PLAN
P7 - LABORATORY MATERIALS TEST PLAN
P4 - ROLL DYNAMICS UNIT TEST PLAN
P3 - BRAKE DYNAMOMETER UTILIZATION PLAN
P8 - INDUCTION HEATING PLAN
P10 - MECHANICAL ANALYSES PLAN
P6 - TTC TRACK TEST PLAN
P11 - DATA BASE DESIGN PLAN (COVERS TECHNICAL TASKS T3 THRU T11)
P9 - DESTRUCTIVE TEST PLAN
P13 - M-2 CAR AXLE/BEARING STUDY PLAN
P5 - NONDESTRUCTIVE TEST EVALUATION PLAN

SUB PROJECTS

SP1 OVERVIEW AND PROGRAM CONTROL (WASHINGTON, CHICAGO & PUEBLO)
SP2 FAILURE MECHANISMS, VERIFICATIONS AND COUNTERMEASURES (CHICAGO)
SP3 THE STATE OF SAFETY RISKS DUE TO OVER HEATED WHEELS (PUEBLO)
SP4 NON-DESTRUCTIVE METHODS TO DETECT OVER HEATED WHEELS (PUEBLO)
SP5 SAFETY OF COMMUTER CARS WITH HOLLOW AXLES (PUEBLO)

FIGURE 1.1   WHEEL FAILURE MECHANISMS OF RAILROAD CARS

1.1.2 Failure Mechanisms, Verifications and Countermeasures (Subproject 2)

The purpose of this subproject was to determine the mechanisms of wheel failure, demonstrate these mechanisms by causing a wheel failure under controlled conditions and to suggest methods for preventing wheel failure.

It was very difficult to cause a wheel failure, but it was finally accomplished with the aid of an artificially induced defect in a straight plate, Class U wheel after prolonged severe drag and stop braking on the AAR wheel dynamometer.

1.1.3 The State of Safety Risks Due to Overheated Wheels (Subproject 3)

The purpose of this subproject was to determine the effects of wheel design/material/size and brake application history on the development of residual stress. The state of residual stress in the over-heated wheels due to severe modes of braking applications was evaluated. Duration and force levels of braking application, and the sequence of reapplication required to accumulate critical levels of residual stress in the test wheels were monitored.

Careful experimental study under controlled conditions in the laboratory and extensive track testing was performed to meet the objective of this subproject. The data accumulated in these and other tasks were analyzed and compiled into this report.

1.1.4 Nondestructive Methods to Detect Damaged Wheels (Subproject 4)

This portion of the program addressed the goal of developing technically sound wheel removal criteria. It included the critical evaluation of nondestructive testing techniques, since they represented candidate methods for possible future wheel removal criteria. Two specific residual stress measurements were identified under this program.

1.1.5 Safety of Commuter Cars with Hollow Axles (Subproject 5)

This project was regarded as a stand-alone task performed independently over and above the Scope of the Wheel Failure Mechanisms Program. The objective of this test program was to examine the thermal properties of bearings that have service worn grooves between the axle and roller bearing assembly, and to take static measurements of bearing cup and seal wear ring movement, and any wear which might have occurred between the bearing cones and the axle. The dynamic performance of a "bent" solid axle with a straight hollow axle was also compared.

The Roll Dynamics Unit (RDU) was utilized to determine rates of fretting wear and thermal runaway on hollow axle/bearing/wheel assemblies of commuter railcars (M-2 Fleet). Test runs of up to 11,000 miles each, with a M-2 truck were performed on the RDU and dynamic measurements of bearing

temperature and bending strain were monitored. Investigations on two axle/bearing/wheel assemblies were made during each test run. All the information was sent to the Transportation Systems Center, Cambridge, Massachusetts, and this task was reported separately.

2.0 NATIONAL STUDY OF WHEEL REMOVAL GUIDELINES (TECHNICAL
     TASK T1)

2.1 Introduction

The removal and failure trends of railroad freight car
wheels were monitored to determine and define the thermal
patterns developing in service. The methods used and the data
sources of information chosen were:

1.   The AAR Car Repair Billing System Data Base,

2.   The AAR Wheel Failure Report Data Base,

3.   The FRA Accident-Incident Reports Data Base, and

4.   The AAR Car Maintenance Cost Data Base.

The method used to monitor the wheel removal and failure
patterns is the control chart. The control charts have been
established with control limits for one quarter, two consecutive
quarters and three consecutive quarters. One control chart has
been established for each combination of data source and
normalizing factor (car miles, active cars, or ton miles). The
control limits have been established to provide 95% confidence
such that when the data source mean has shifted significantly,
the limits have been exceeded.

This section contains the data sources chosen and the
trends for each data source quarterly from 1980 to the latest
quarter for which information is available.

2.2 Data Sources

Four sources of data have been identified which may be used to monitor the impact of a change in the definition of an overheated wheel. These are as follows:

1. The AAR Car Repair Billing Exchange System Data (CRB) – These data contain foreign car repair billing on the majority of the North American freight car fleet. The job codes and why made codes in this system support the determination of the number of wheels removed due to thermal damage and/or discoloration.

2. The AAR Mechanical Division Wheel Failure Report (or MD-115) – These forms are voluntarily completed and submitted to the AAR Mechanical Division for all cracked or broken plates, rims or flanges. The why made codes permit the number of wheel failures due to thermal damage to be determined.

3. The FRA Accident/Incident Reports – Railroad accidents (derailments/collisions) resulting in damage exceeding a minimal threshold ($3,700 in 1984) must be reported to FRA. These reports permit the number of accidents caused by thermally damaged wheels to be estimated. Since the actual cause of a cracked or broken wheel can not be determined from these data, we assume all cracked or broken wheels are the result of thermal damage.

4. The AAR Car Maintenance Cost Data Base – These data are

maintained by the AAR Research and Test Department, and the data base contains both system and foreign repairs to freight cars owned by eight participating roads. These railroads voluntarily submit this information for approximately 500,000 freight cars. The repair information in this data base is in a form consistent with the CRB system. Thus, the number of wheels removed due to thermal damage and discoloration can be determined.

2.3 Trends

The purpose of monitoring data on wheel removals, failures and accidents/incidents is primarily to detect significant increases in the number of thermally damaged wheels in service or the number of wheel thermal damage related accidents. This has been accomplished by the use of control charts for each variable of interest. The control chart is a plot of the data over the relevant period of time. Control limits are established to detect the occurrence of a significant change in process average. Control limits may be set for a variety of occurrences. For example, there may be limits for a single point, for two consecutive points, for three consecutive points, etc. The limits in this report are the 95% confidence intervals for one, two and three consecutive quarters.

Figure 2.1 shows the trend for the rate of wheel removals due to discoloration (why made code 89 from Field Manual of the

2-3

CONTROL CHART
RATE OF WHEEL REMOVALS DUE TO DISCOLORATION
FROM THE CAR MAINTENANCE COST DATA BASE — APRIL, 1986
NUMBER OF WHEELS REMOVED 10,000 ACTIVE CARS
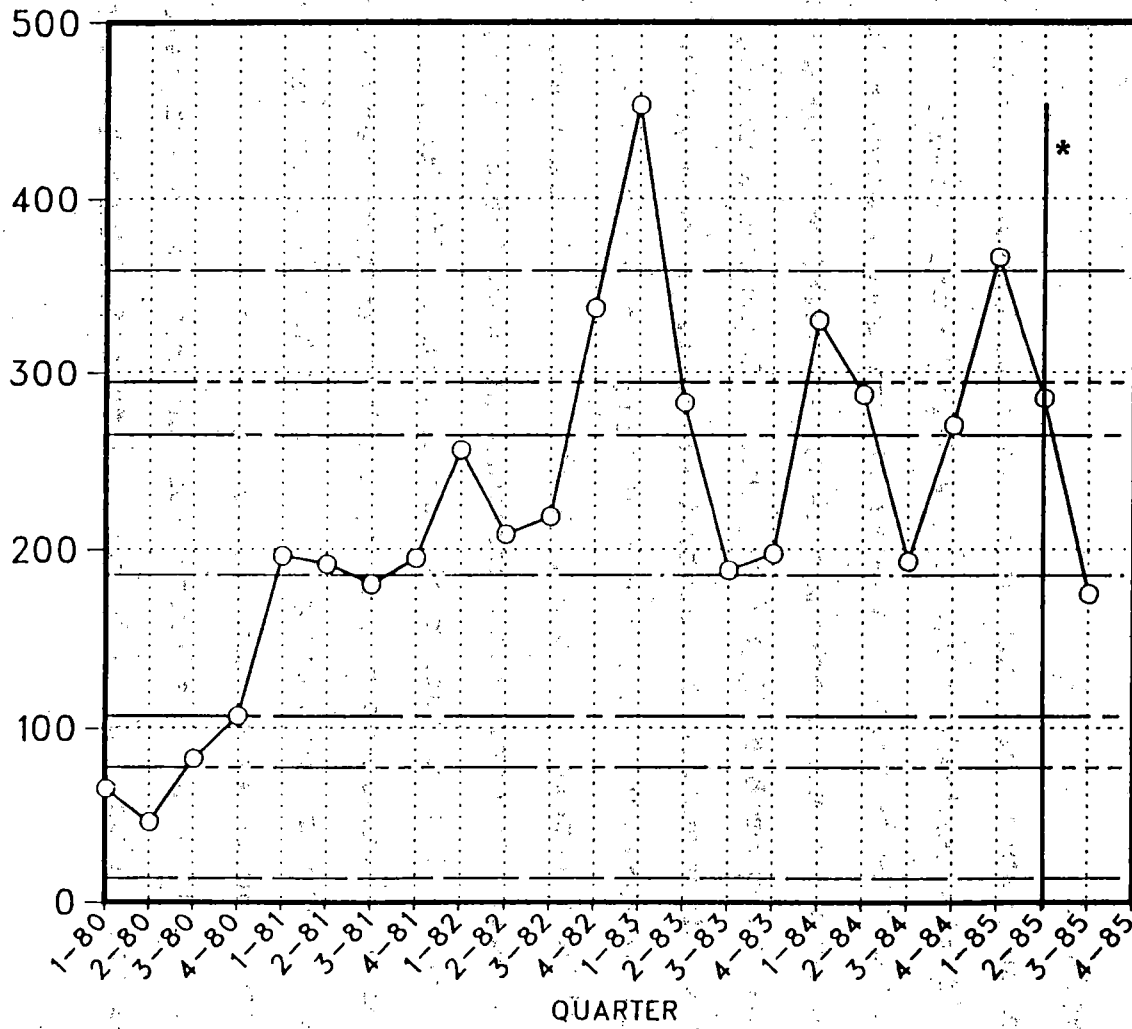
* CHANGE IN DISCOLORATION
  RULE

O WHEEL REMOVALS
  MEAN
  UCL—ONE POINT
  UCL—TWO POINTS
  UCL—THREE POINTS
  LCL—THREE POINTS
  LCL—TWO POINTS
  LCL—ONE POINT

QUARTER

FIGURE 2.1   RATE OF WHEEL REMOVALS PER 10,000 CARS DUE TO DISCOLORATION

<u>AAR Interchange Rules</u>) per 10,000 active cars (an active car is defined as a car which moved a minimum of 250 miles in the quarter) from the Car Maintenance Cost Data Base. This average rate of removals is approximately 175 per 10,000 active cars per quarter. The rate exceeded the upper control limit during the first quarter of 1983 but has settled back into statistical control.

The trend for the rate of wheel removals per million car miles due to discoloration is shown in Figure 2.2. The trend is very similar to the previous figure.

The rate of wheel removals per 10,000 active cars due to thermal damage is shown in Figure 2.3.

The why made codes from the <u>Field Manual of the AAR Interchange Rules</u> are:

- o 66-flange cracked or broken,
- o 68-rim cracked or broken,
- o 69-thermal cracks with overheating,
- o 74-thermal cracks, and
- o 83-cracked or broken plate.

This chart indicates an average of approximately 22 wheels removed per 10,000 active cars per quarter due to thermal damage. The rate of wheel removals due to thermal damage has been quite low in the last four quarters. The rate of wheel removal due to thermal damage does not show any obvious trends.

The rate of wheel removals per million car miles due to thermal damage is shown in Figure 2.4. This chart is very similar in all aspects to the previous figure.
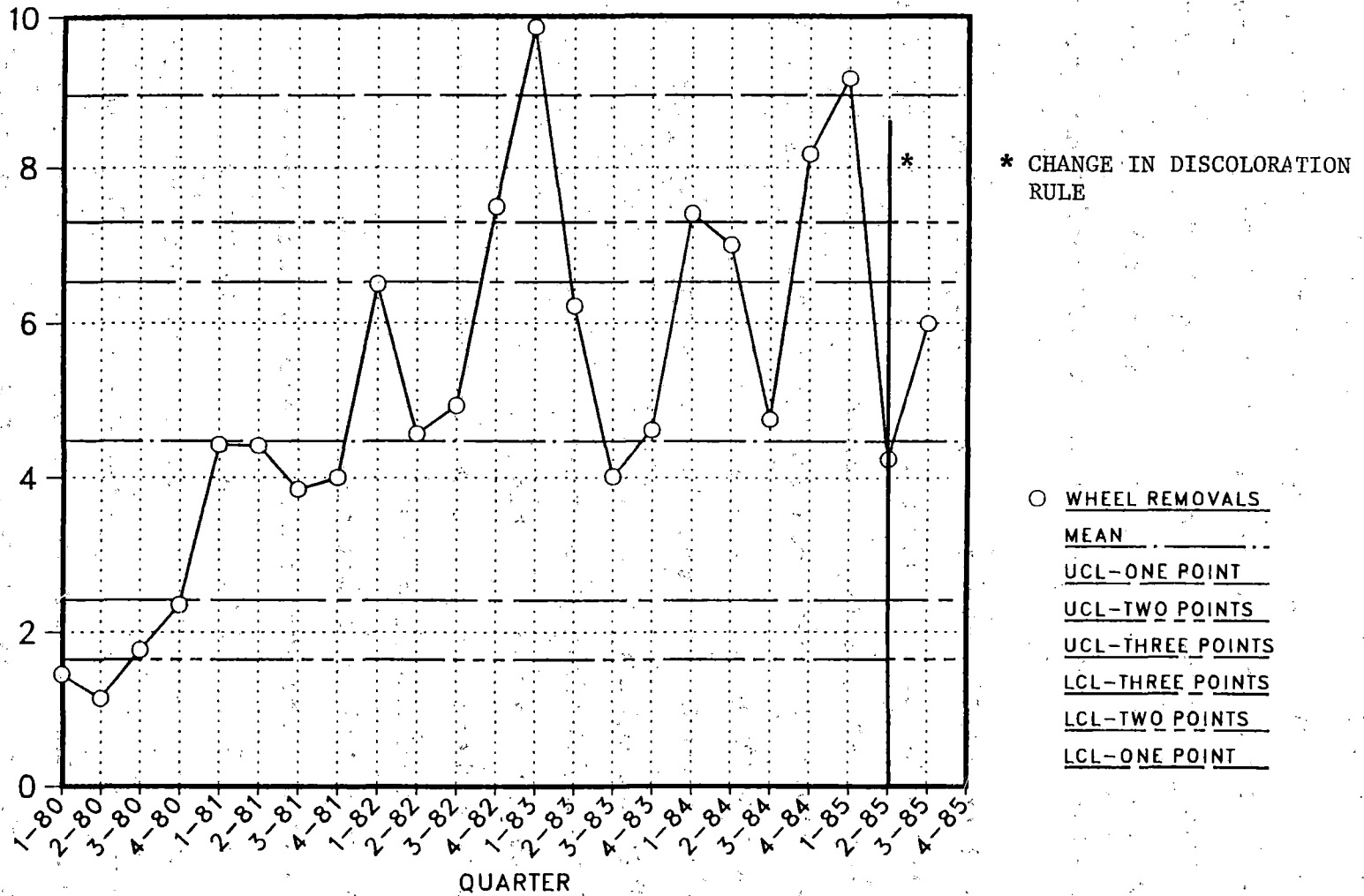
CONTROL CHART
RATE OF WHEEL REMOVALS DUE TO DISCOLORATION
FROM THE CAR MAINTENANCE COST DATA BASE — APRIL, 1986

FIGURE 2.2   RATE OF WHEEL REMOVALS PER MILLION CAR MILES DUE TO DISCOLORATION

CONTROL CHART
RATE OF WHEEL REMOVALS DUE TO THERMAL DAMAGE
FROM THE CAR MAINTENANCE COST DATA BASE — APRIL, 1986

RATE OF WHEEL REMOVALS PER 10,000 ACTIVE CARS
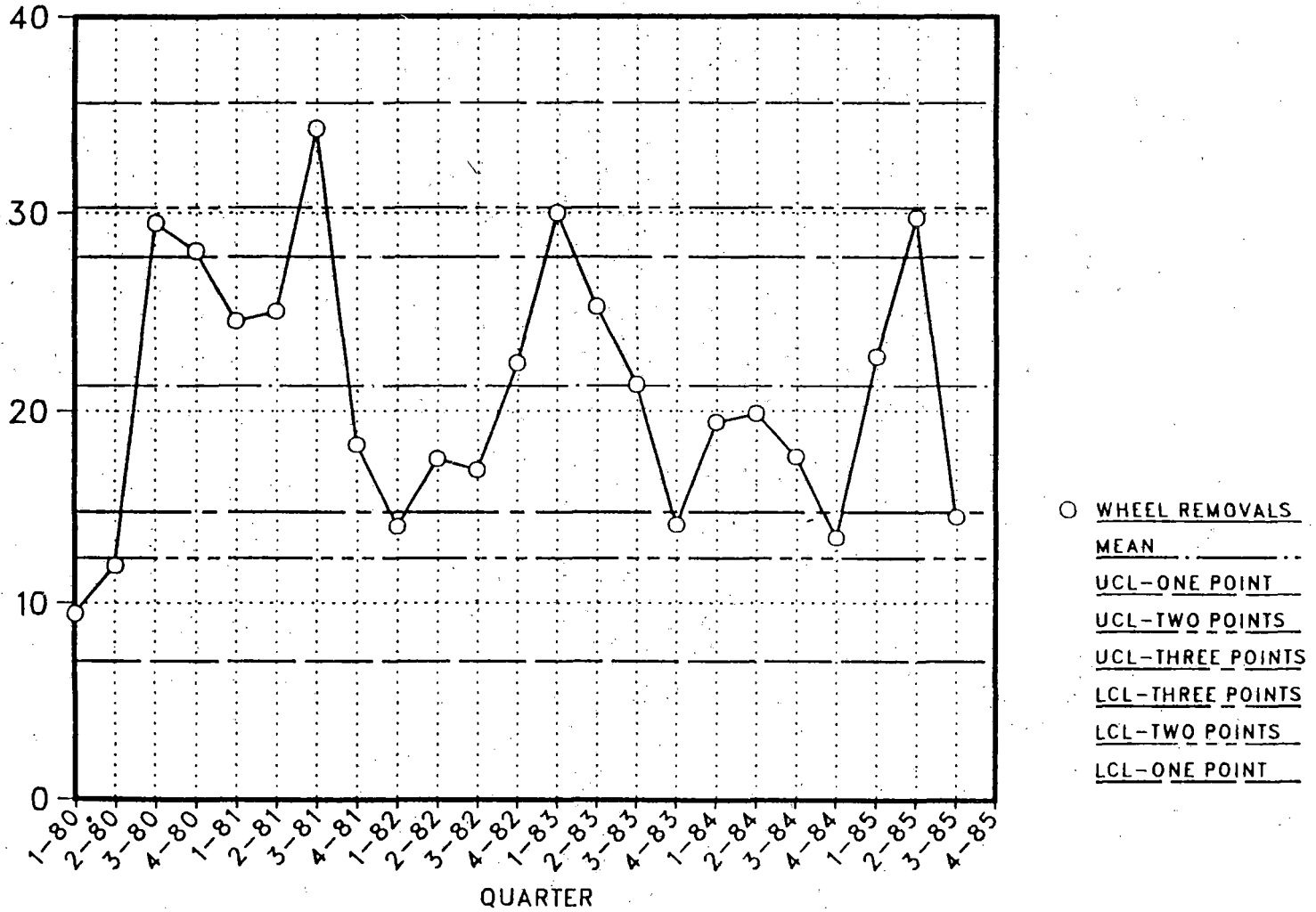
FIGURE 2.3   RATE OF WHEEL REMOVALS PER 10,000 CARS DUE TO THERMAL DAMAGE

CONTROL CHART
RATE OF WHEEL REMOVALS DUE TO THERMAL DAMAGE
FROM THE CAR MAINTENANCE COST DATA BASE — APRIL, 1986

RATE OF WHEEL REMOVALS PER MILLION CAR MILES

O   WHEEL REMOVALS

 ·   MEAN

UCL–ONE POINT

UCL–TWO POINTS

UCL–THREE POINTS

LCL–THREE POINTS

LCL–TWO POINTS

LCL–ONE POINT

QUARTER
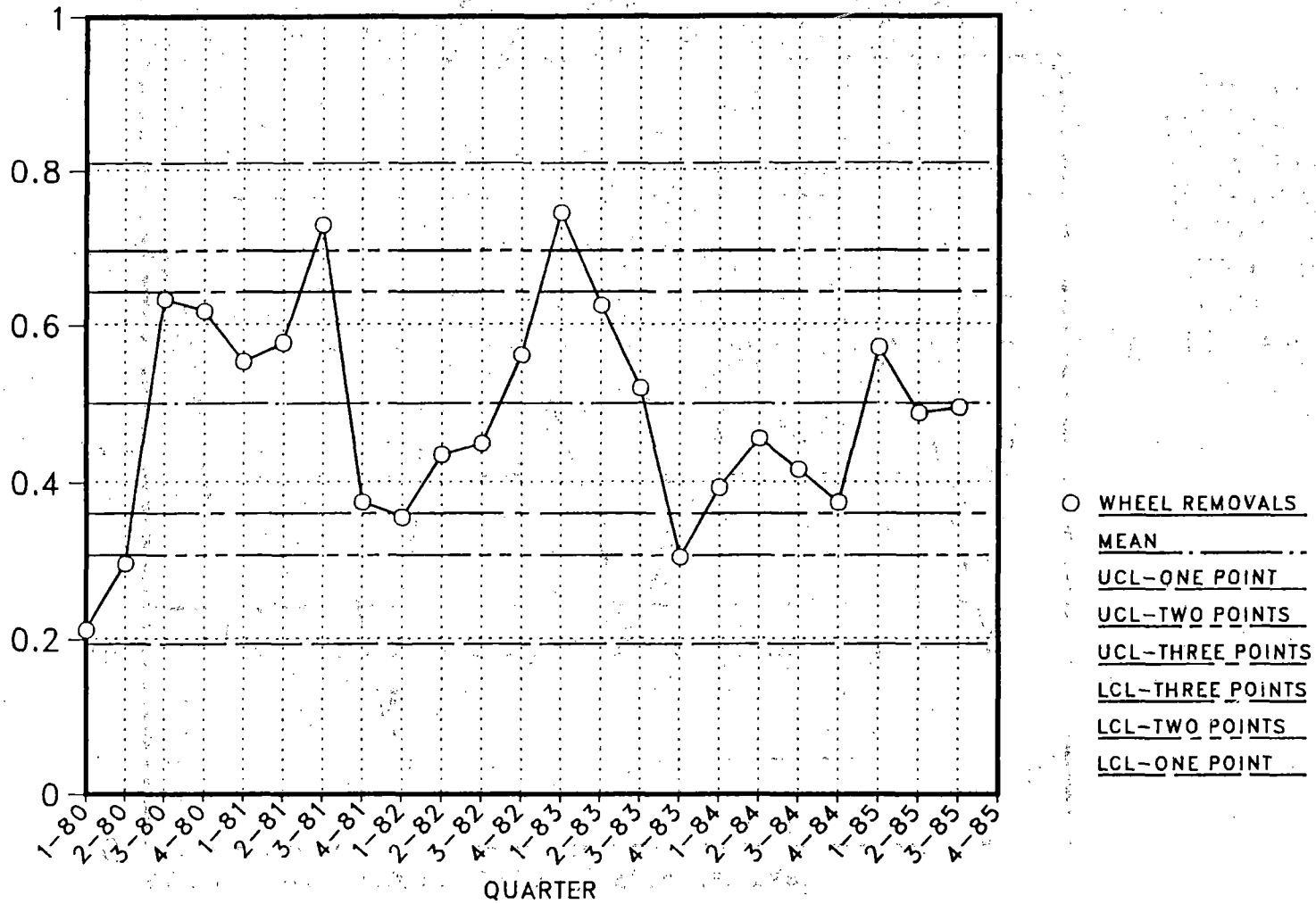
FIGURE 2.4   RATE OF WHEEL REMOVALS PER MILLION CAR MILES DUE TO THERMAL DAMAGE

The rate of wheel removals per billion ton miles due to thermal damage from the Car Repair Billing Data Base is presented in Figure 2.5. This shows a very high rate of removals during the period from the first quarter of 1982 through the first quarter of 1983. The rate of removals for the last eleven quarters suggests the rate of removals due to thermal damage has shifted dramatically. The reduction appears to be on the order of 2.5 wheels per billion ton-miles.

The rate of wheel removals per billion ton-miles due to discoloration is presented in Figure 2.6. This shows a very high rate of removals during the period from the first quarter of 1982 through the first quarter of 1983. The rate of removals then falls back into statistical control temporarily. However, the rate has been quite variable between the first quarter of 1983 and the second quarter of 1985. The rate then dropped dramatically in response to the rule change to discoloration front _and_ back in the second quarter of 1985. The average removal rate since the first quarter of 1981 is above 120 wheels per billion ton-miles, but in 1985 dropped to approximately 75 wheels per billion ton miles.

Except for the fact that wheel removals on account of discolored wheels and removals on account of cracked wheels peaked during the first quarter of 1983, the two causes do not seem to move exactly with each other. It should also be noted that the rate of removals for discoloration is approximately ten times that of wheels removed for cracking.

The trend in the rate of wheel failure reports submitted to

CONTROL CHART
FOR THE RATE OF WHEEL REMOVALS DUE TO THERMAL DAMAGE
FROM THE CAR REPAIR BILLING DATA BASE — February, 1987

RATE OF WHEELS REMOVALS PER BILLION TON MILES
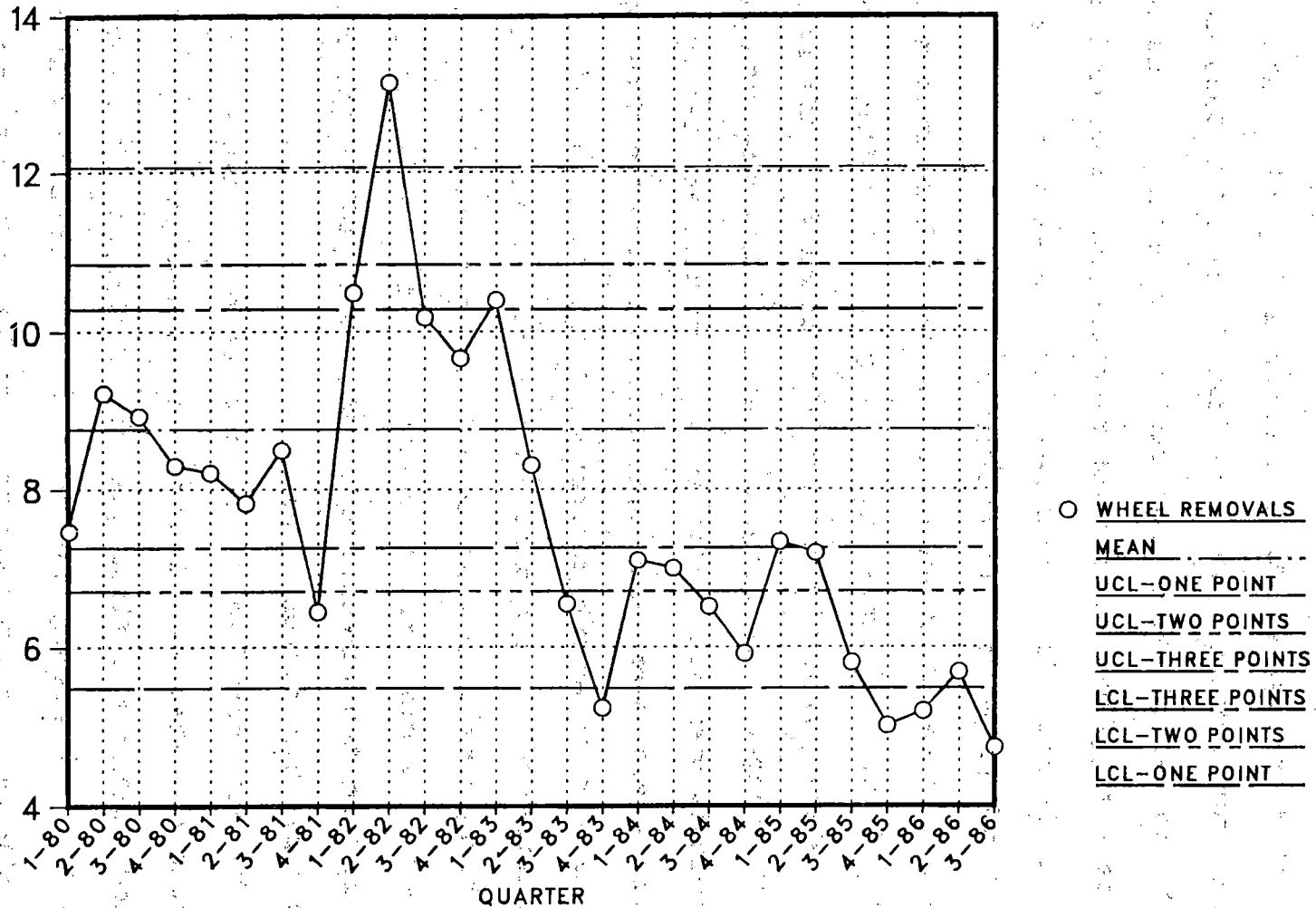
FIGURE 2.5   RATE OF WHEEL REMOVALS PER BILLION TON MILES DUE TO THERMAL DAMAGE

CONTROL CHART
FOR THE RATE OF WHEEL REMOVALS DUE TO DISCOLORATION
FROM THE CAR REPAIR BILLING DATA BASE —FEBRUARY, 1987
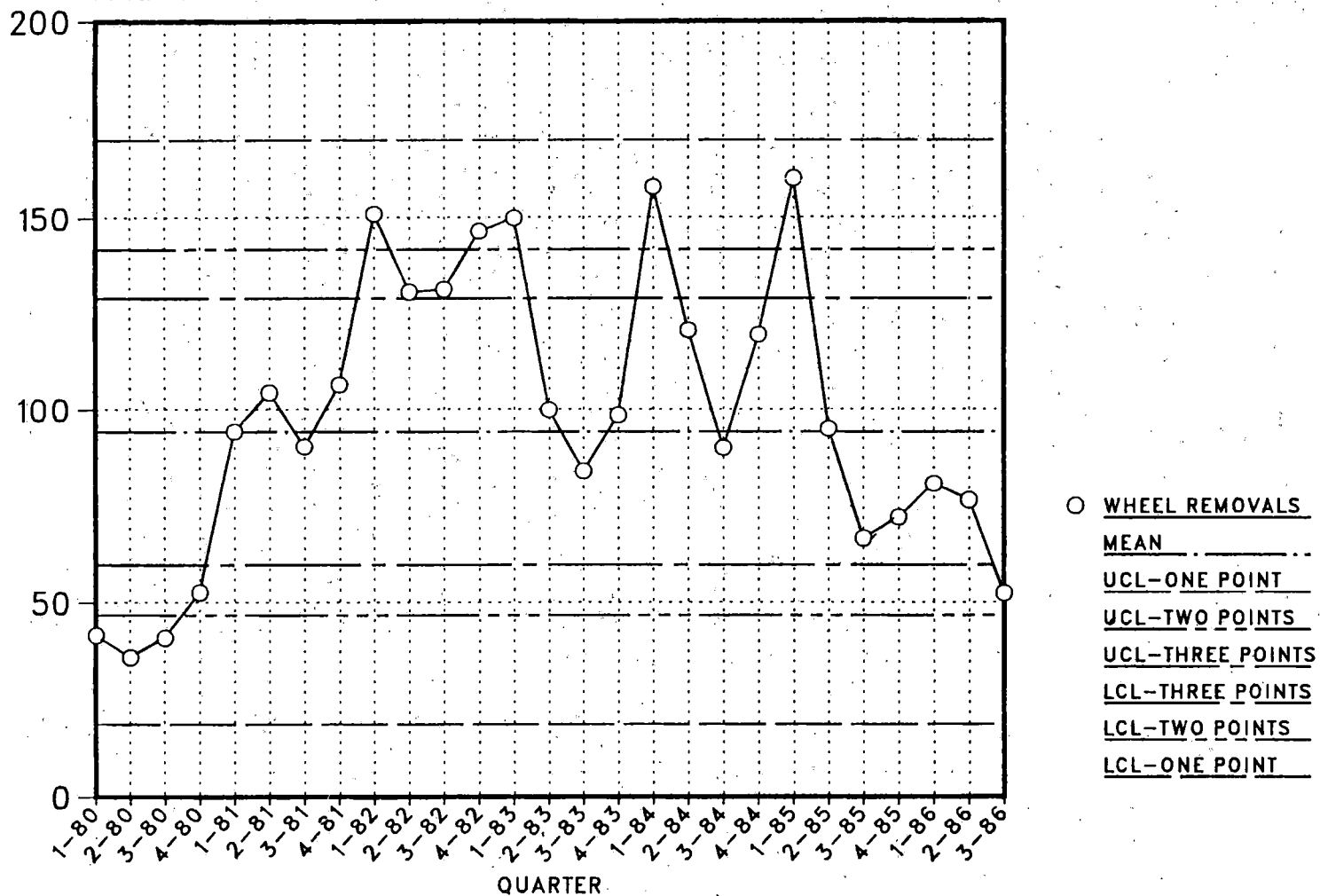
FIGURE 2.6   RATE OF WHEEL REMOVALS PER BILLION TON MILES DUE TO DISCOLORATION

the AAR per billion ton-miles is shown in Figure 2.7. Only those failure reports which indicate an associated derailment are included. This figure shows a great deal of variation in these data. However, the rate has for the most part remained in statistical control.

There is also a clear seasonal pattern to the derailment data with the number of derailments peaking during the winter quarter to produce approximately as many derailments as occur in the remaining nine months. It is suggested that there are probably two major reasons for this behavior: 1) the increase in brake valve malfunctions due to freezing, and 2) the increased track modulus due to road bed freezing, and hence greater dynamic loading.

The data in the wheel failure reports contain information on the type of wheel that failed and whether or not it was discolored. It is possible to use this information to make qualitative comparisons of wheel failure rates for different categories of wheels. Table 2.1 summarizes this information. The table is based on the analysis of 157 wheel failures in 1984 and 1985. As indicated in the table, it is estimated that there were 411 billion wheel miles in this period so that the overall wheel failure rate can be estimated at 38 failures per 100 billion wheel miles. Since only 28 of the 157 wheel failures were curved-plate wheels, it is obvious that the wheel failure rate for curved-plate wheels is significantly less than for straight-plate wheels because curved-plate wheel miles substantially exceed straight-plate wheel miles, inasmuch as

CONTROL CHART
FOR THE RATE OF WHEEL FAILURE REPORTS
DUE TO THERMAL DAMAGE CAUSING A DERAILMENT
FROM THE AAR WHEEL FAILURE DATA BASE – september, 1986

RATE OF WHEEL FAILURES PER BILLION TON MILES

O WHEEL FAILURE RATE
MEAN
UCL–ONE POINT
UCL–TWO POINTS
UCL–THREE POINTS
LCL–THREE POINTS
LCL–TWO POINTS
LCL–ONE POINT

QUARTER
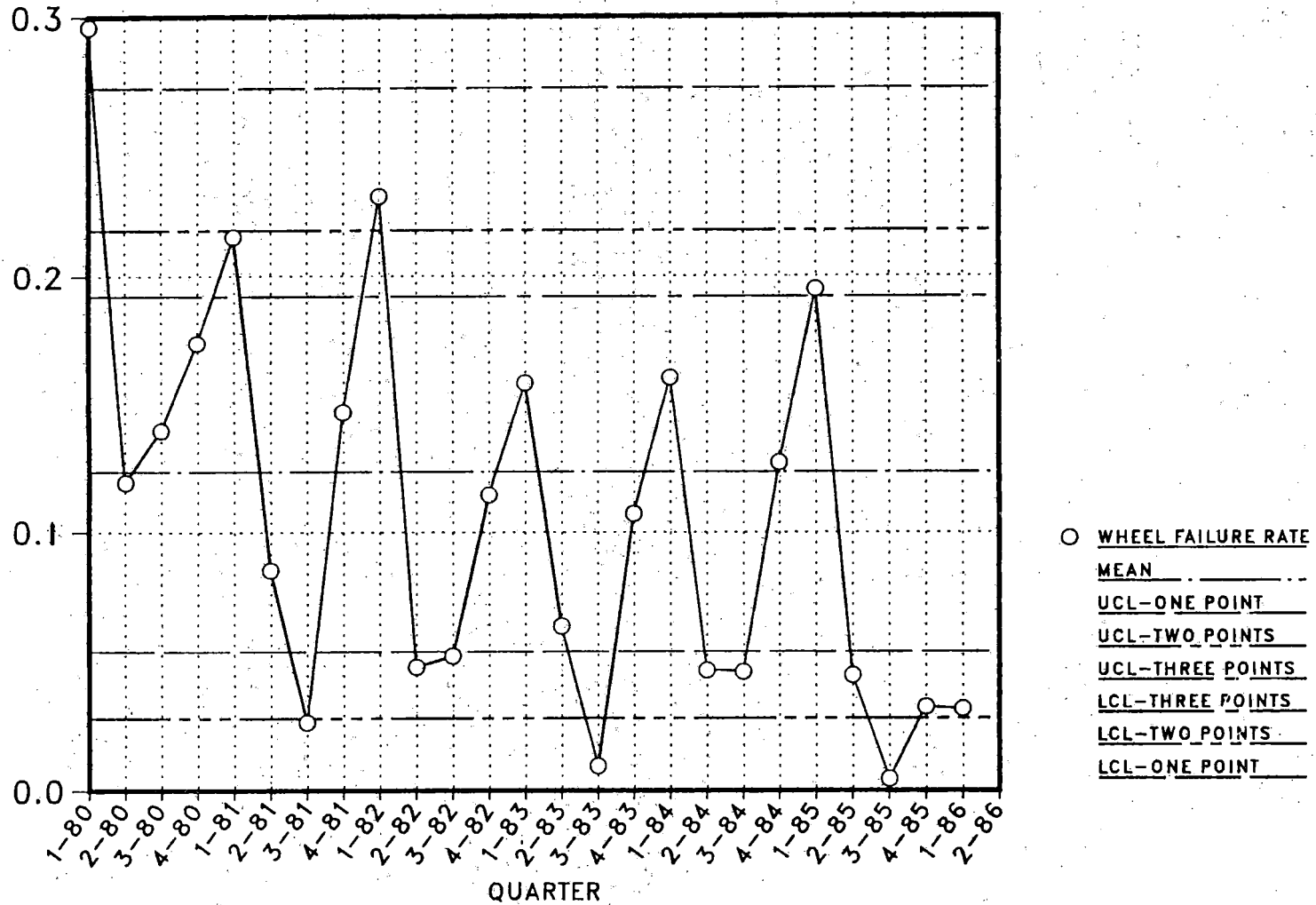
FIGURE 2.7   RATE OF WHEEL FAILURES PER BILLION TON MILES DUE TO THERMAL DAMAGE

TABLE 2.1
WHEEL FAILURE DATA FOR CURVED-PLATE AND STRAIGHT-PLATE,
DISCOLORED AND NONDISCOLORED, RAILROAD CAR WHEELS
FROM AAR DATA BASE (1) (1984 AND 1985 DATA)

Condition	Wheel Failures

Overall Failure Rate (2)   157/411 = 38 failures per 100 billion wheel miles

	Curved-Plate			Straight-Plate		
Curved-Plate, Straight-Plate Breakdown	28			129		
	NonDiscolored	Discolored		NonDiscolored	Discolored	
NonDiscolored, Discolored Breakdown	22	6		81	48	
	B & C	U	B & C	U	B & C	U	B & C	U
Heat Treatment Breakdown	6	16	2	4	22	59	18	30

(1) Wheel failures in period include:

    22 curved-plate nondiscolored wheels
     6 curved-plate discolored wheels
    81 straight-plate nondiscolored wheels
    48 straight-plate discolored wheels
   157 total wheel failures

(2) 411 billion wheel miles based on 922 billion ton miles in 1984 and 884 billion ton miles in 1985; 34.9 and 35.4 (estimated) ton miles per car mile in 1984 and 1985 respectively; and 8 wheel miles per car mile.

they are generally on newer, more active cars.

The table also shows a breakdown for discolored and nondiscolored wheels in both the straight- and curved-plate categories. Note that for each of these wheel types the discolored wheels represent about 1/3 of the failures. Since discolored wheels represent less than 5 percent of the population, the discolored wheel miles must be much less than nondiscolored wheel miles, it is obvious that the wheel failure rate for discolored wheels must be larger than for nondiscolored wheels.

The table also shows the breakdown in wheel failures by heat treatment. Because the number of failures is small, it is difficult to develop any discernible trends from the data. However, lacking data on the heat-treated versus non-heat treated wheel population and mileage, no conclusions on the effectiveness of heat treated wheels in resisting fracture can be drawn. The benefits of heat-treated wheels will be supported by other evidence to follow.

The trend in the rate of FRA reportable accidents caused by thermally damaged wheels is shown in Figure 2.8. The rate of accidents due to thermally damaged wheels has declined steadily since 1980. This trend has continued throughout 1986.

The FRA cause codes which are considered to be related to thermal damage are the following:

o   460 - broken flange,

o   461 - broken rim,

o   462 - broken plate,

CONTROL CHART
FOR THE NUMBER OF ACCIDENTS CAUSED BY THERMALLY DAMAGED WHEELS
FROM THE FRA ACCIDENT DATA BASE — FEBRUARY, 1987

RATE OF ACCIDENTS PER BILLION TON MILES

Legend:
O ACCIDENT RATE
MEAN
UCL—ONE POINT
UCL—TWO POINTS
UCL—THREE POINTS
LCL—THREE POINTS
LCL—TWO POINTS
LCL—ONE POINT

QUARTER
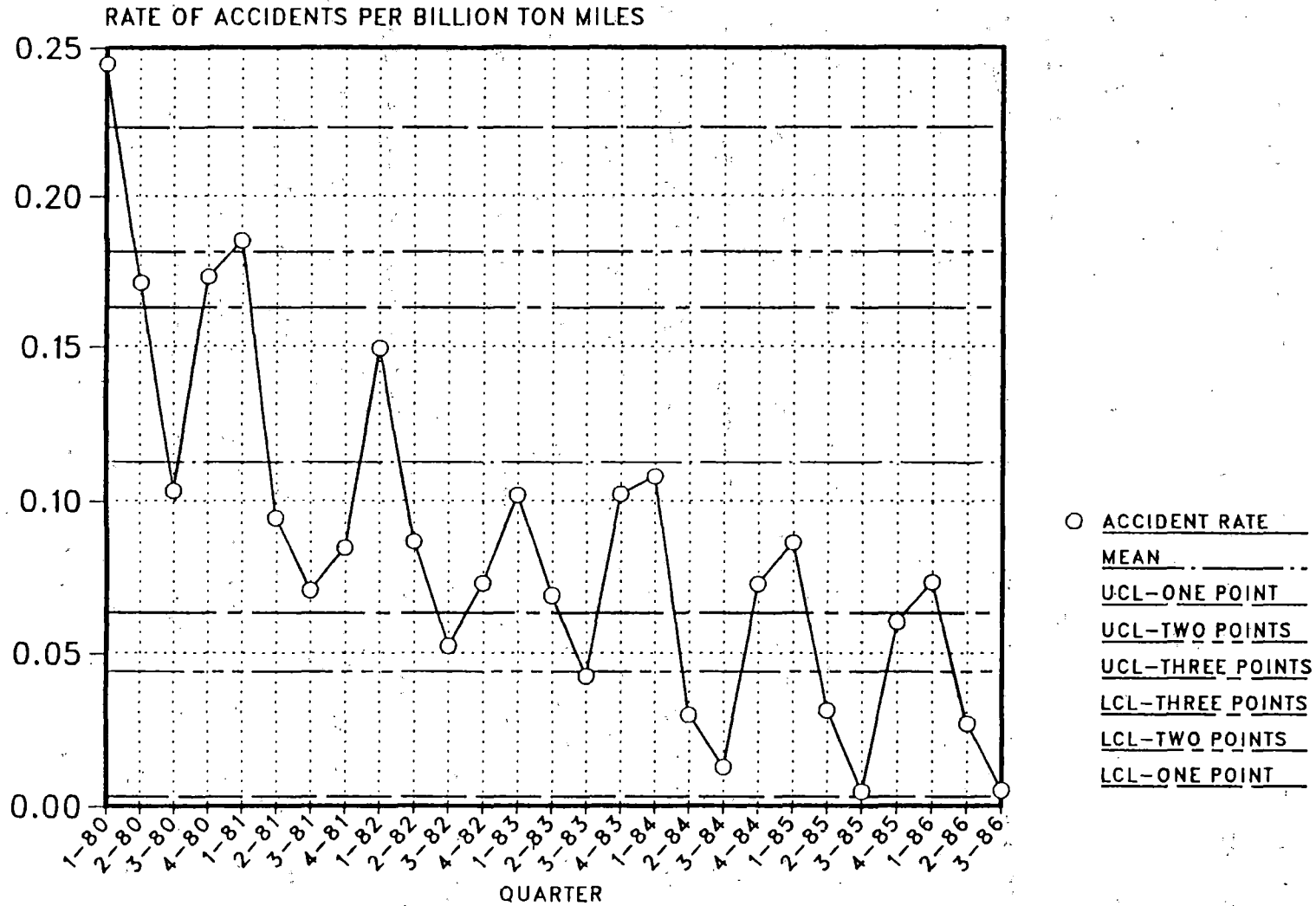
FIGURE 2.8   TREND IN THE RATE OF REPORTABLE ACCIDENTS CAUSED BY THERMALLY DAMAGED WHEELS

o   463 - broken hub, and

o   468 - thermal damage.

Any accidents involving locomotives are not included in these data.

Complete wheel failure data from AAR MD-115 forms is tabulated in Appendix 2.0 for 1983-1986.

2.4   Status of Investigation of Wheel Failures

A wide variety of investigations have been made during the past 25 years on the subject of wheel fracture. The reports which were issued were focused on selective aspects of the fracture problem and not brought together in a cohesive analysis.

In retrospect, the sequence of investigations was remarkably effective. It identified specific technical problems that were subsequently resolved and resulted in reduced wheel failures. In addition, it provided a technological base that can now be used in the development of a rational explanation of the total problem of wheel fracture.

The sequence is outlined below:

1.   First Step Investigations. Fracture mechanics tests were used to determine the effects of composition and heat treatment on fracture and fatigue properties of wheels. (References 1, 2, and 3.)

2.   Second Step Investigations. Samples of fractured wheels were examined to determine the fracture-critical combination of observed crack size and calculated stress. Fracture properties (K_{IC}) and fatigue

2-17

properties (da/dN) were determined for the sample wheels. The sampling was drawn from a wide variety of railroad sources. The primary investigation, Reference (4), is of major importance because it represents the first data base which is large enough for adequate analysis of wheel fractures.

3. Third Step Investigations. The wheel fracture experience (1969-1983) for a single railroad (UP) was examined for the case of fractures which caused derailments. This investigation, Reference (5), determined the distribution and range of fracture-critical crack sizes. Fracture mechanics calculations were made for determining fracture-critical stresses for specific crack sizes. The average K_{IC} fracture value was used for the calculations.

4. Other Investigations. The subject of thermally-induced stresses and residual stress systems was investigated over a long period (1970 to 1985). In recent years, investigations of this type represented the major thrust of research. The results were correlated in this study with the information developed by References (4) and (5). The primary reports include References (6), (7), and (8).

Despite these extensive studies, full advantage has not been taken of the large amount of critically-important information in the fracture analysis reports of the railroads

for cases of wheel fractures resulting in derailment. This information includes the nature of damage to the wheel rim and the flange metal, damage that results in the development of cracks. The damage involves abusive wear, hard-brittle spots (martensite) due to localized frictional heating, severe metal flow, localized work hardening, and dimensional changes such as wear of the flange and the development of sharp points at flange tips. This damage can be related to misalignment of brake shoes, improper brake shoe selection, or other problems relating to brakes. Except for cracks at the flange tip, the other cracks in wheels are all due to stress concentration points arising from wear or plastic flow or metal embrittlement effects, not related to fatigue initiation.

On an individual basis, railroads applied this information to minimize the metal damage responsible for development of cracks. A large reduction in the rate of wheel fractures causing derailment was achieved during the 1970 to 1985 period as a result of improvement in brake rigging, better control over brake alignment, and a change from cast iron to composition brake shoes.

This report is the first general attempt to relate abusive damage of the rim and the flange to the incidence of crack development. The data were originally developed on an ad-hoc basis for specific groups of cars and specific service conditions of particular railroads.

Information that some of the wheels that fractured and caused derailments also showed plate discoloration due to

overheating was developed as a result of railroad experience. This observation resulted in the AAR rule and the FRA regulation that wheels which showed more than four inches discoloration should be removed from service. The benefits of this rule are presently the subject of intensive debate. In particular, the value of this rule as applied to wheels of <u>high stress</u> and <u>low stress</u> design is still being evaluated.

This part of the overall Wheel Research Program is intended to add information, <u>derived from a review of railroad failure analysis reports for cases of fractures causing derailments</u>. This information and the prior information described by the previously cited steps of technology evolution, and particularly the primary reports of References (4), (5), (6), (7), and (8), places the current wheel failure problem in a much more comprehensive context.

In reviewing the railroad failure analysis reports, curved and straight plate design wheels and wheels discolored in excess of the four inch rule are identified and discussed appropriately.

Approximately 600 railroad failure analysis reports from the Union Pacific, Santa Fe, and Norfolk Southern railroads were reviewed. Special attention was given to approximately 400 reports that provided a sufficiently complete description of facts to permit a comprehensive failure analysis. These are cited in this report as "good file data."

The data from the Union Pacific covers the period for 1969 to 1983; for the Santa Fe from 1977 to 1985; and from the Norfolk Southern from 1981 to 1985.

2.4.1 Description of Fracture Critical Cracks

2.4.1.1 Type and Percentage Distribution

Fracture critical cracks (FCC) are defined as the cracks described in the failure analysis reports prepared by the individual railroad, which caused fracture resulting in a derailment.

Figure 2.9 describes the crack locations, relative percentage, and the typical causes for cracks studied by the UP and the Santa Fe railroads. Metallurgical examination (cross sectioning and etching adjacent to the fracture surface) established those cases in which there were hard-brittle spots due to localized surface overheating (in excess of 1350 degrees F) which produced martensite and a larger surrounding zone of spheroidized pearlite.

Figure 2.9 also presents a summary of crack types and metal damage. The Figure 2.9 codes of "typical" severe metal damage means that over 80 to 90% of the cases (for each crack location) involved severe metal damage as cited in the failure analysis reports.

The percentage of inner flange and back rim cracks for the Union Pacific and Santa Fe reports is remarkably similar and in the order of 32 to 35% for each type.

The percentages of center rim and rim edge cracks are different for the two railroads. Santa Fe explains its low percentage of rim edge cracks are due to action to eliminate
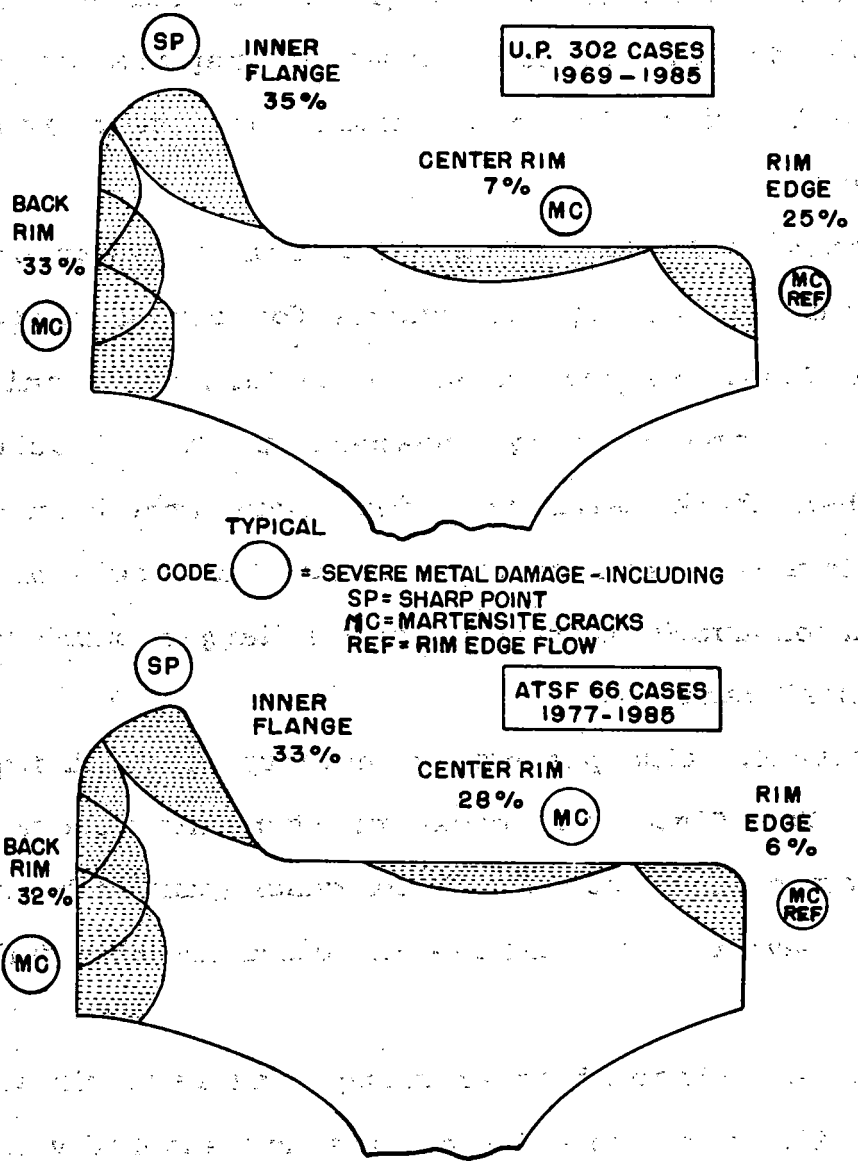
FIGURE 2.9   LOCATION AND FREQUENCY OF THERMAL CRACKS REMOVED
FROM UNION PACIFIC AND SANTA FE RAILROADS

over-riding brake shoes after 1977.   Before this time, the percentage of rim edge cracks was high and led to the action to correct this brake problem.

The higher percentage of center rim cracks for the Santa Fe was described as due to more extensive use of cast iron brake shoes.   Cast iron shoes cause higher local temperatures than composition brake shoes.   This leads to localized (shallow) surface heating (resulting in martensite).   The composition brake shoes produce deeper but lower surface temperatures.   The UP Railroad had a major campaign in the early 1970's to retrofit all cars with composition shoes.

Back rim cracks were attributed, in most cases, to retarder shoe and/or guard rail action.   The prohibition by AAR on rim stamping at critical locations has virtually eliminated this cause of failures.

The high percentage of inner flange cracks observed in reports from both railroads is due to sharp points at the top of the inner face of the flange.   These points are a result of the planing off of the flange and the development of a straight metal surface that intersects the top of the flange at a sharp point.   In over 90% of the inner-flange crack cases, the crack had originated at this sharp point as shown in the photographs in Section 9.

Similar types of cracks were also observed by the Norfolk Southern railroad.   Percentages are not cited for this railroad because of the smaller number of reports that were available for review.   Primary attention in the reports of the Southern

railroad was given to a unique type of crack described as "shattered rim defect." Shattered rim defects were developed as a result of large slag inclusions in wrought steel wheels. There was a history of such failures in wheels made for the Southern before 1977 by one supplier who furnished most of the Southern's wheels. The pre-1977 wheels were cast by top pouring from the ladle, which trapped slag inclusions at edges. After 1977, the Southern required bottom pouring, which eliminated slag inclusions. Shattered rim failures were no longer a problem after the change was made in the manufacturing method. This is an excellent example of reduction of derailment-causing fractures by manufacturing process changes which resulted in metallurgical improvement.

2.4.1.2   Differences Between Low and High Stress Wheel Failures

It is interesting to note that there is a significant difference in fracture behavior between low and high stress wheels. Virtually none of the failures of low stress wheels originated at rim cracks. The point of crack initiation for these wheels was at the intersection of the planed metal surface and the flange. This sharp point was the site of high stress concentrations and led to development of a fatigue crack and ultimate failure even in these wheels with their much better overall failure record.

REFERENCES

1. K. Hirakawa and H. Sakamoto, "Effect of Design Variation on Railroad Wheel Fracture," ASME Paper 81-WA/RT-4, November, 1981.

2. G. J. Fowler, "Fatigue Crack Initiation and Propagation in Pearlitic Rail Steels," PhD Thesis, UCLA, 1976.

3. A. Martin Meizoso, and J. Gil Sevillano, "Thermal: A Computer Code for Life Prediction of Wheels," Proceedings of the Eighth International Wheelset Congress, Paper II.2, Madrid, April, 1985.

4. C. S. Carter, R. G. Caton, and J. L. Guthrie, "Fracture Resistance and Fatigue Crack Growth Characteristics of Railroad Wheels and Axles," Report DOT-TSC-617, April, 1976.

5. A. J. Opinsky, "An Analysis of Some Railroad Wheel Tread Fractures," AAR Report No. R-609, July, 1985.

6. M. R. Johnson, R. E. Welch, and K. S. Yeung, "Analysis of Thermal Stresses and Residual Stress Changes in Railroad Wheels Caused by Severe Drag Braking," ASME Paper 75-WA/RT-3, November, 1975.

7. M. R. Johnson, R. R. Robinson, A. J. Opinsky, and D. H. Stone, "Residual Stress Calculations on 33-Inch Diameter One-Wear Freight Car Wheels Under Simulated Unreleased Hand Brake Conditions," ASME Paper 82-WA/RT-11, November, 1982.

8. M. R. Johnson, R. R. Robinson, A. J. Opinsky, M. W. Joerms, and D. H. Stone, "Calculation of Residual Stresses in Wheels from Saw Cut Displacement Data," ASME Paper 84-WA/RT-17, November, 1985.

TABLE 2.2
DERAILMENT DATA FROM AAR MD-115
WHEEL FAILURE FORMS

| Year | Straight Plate3 | | Curved Plate | |
	Non-Discolored*	Discolored	Non-Discolored	Discolored
1983*	12 (60%)	7 (35%)	1 (5%)	0 (0%)
1984	38 (49%)	28 (36%)	8 (10%)	4 (5%)
1985	45 (54%)	22 (27%)	14 (17%)	2 (2%)
1986*	11 (69%)	1 (6%)	4 (25%)	0 (0%)
Total	106 (54%)	58 (29%)	27 (14%)	6 (3%)

* DATA INCOMPLETE FOR ENTIRE YEAR

3.0 PILOT TECHNOLOGY SURVEY (TECHNICAL TASK T2)

As part of this research project, a comprehensive technology search was conducted. It should serve as an example of the cost and benefits to be derived for use on future projects. For the literature search, the Railroad Research Information System data base was included. Reports and other documentation were considered and experts in the technology field were also contacted. After the literature search, a small library of applicable documents for this particular project was established.

3.1 Major Findings and Current Status

A survey of technological literature was conducted by (i) searching the available literature on this and related subjects, and (ii) contacting experts who have made or are currently making contributions in the field of wheel failure mechanisms. A small library of applicable documents for this particular project was established at the Transportation Test Center. The small library includes a computerized information retrieval system with each listing accompanied by a special annotation prepared by the technical staff associated with the project. This was performed after a comprehensive evaluation of the various documents compiled in the small library.

Initial Survey

A file search on <u>Railroad Wheels</u> was acquired from the Railroad Research Information System. The following key phrases were used by the RRIS for this search:

wheel residual stresses	wheel thermal stress
crack propagation in wheel	finite element analysis of wheels
wheel fracture	plasticity in wheels
wheel designs	wheel metallurgy
mechanical properties of wheels	

The RRIS Field Search was then compared with the TTC Technical Library holdings to determine items that are currently on hand. Other items from the Field Search that seemed relevant and promising were identified for acquisition. These items were located and purchased, and gathered together into a separate library of research literature for this project.

The project personnel then conducted a limited, yet comprehensive evaluation of this "separate library" to decide which documents will be used. They also contacted appropriate experts in this technology field to become acquainted with on-going activity elsewhere. The rationale for their selection and organization of information is described below.

Computerized Information Retrieval System

The references, details, subject classification and special notations made by the project technical staff were then entered into the TTC Computerized Information Retrieval System so that research personnel could rapidly sort through this special "library" and locate references especially pertinent to their particular technical tasks. A detailed description of the TTC Computerized Information Retrieval System is given in Appendix 3.1.

The computer program used at TTC to establish this Information Retrieval System is the DATATRIEVE Program.

The preliminary criterion for selecting a particular reference to include in this select bibliography was direct applicability to at least one of the technical tasks of the FRA Wheel Program. In addition, certain references of indirect applicability were selected if they contained good fundamental information or technology of general applicability to the research program.

Format Evaluation

The bibliographic reference details and special notations that appear in the listing are explained in the following.

TTC Document Number

The initial number or alphanumeric string is given in the upper left corner of each reference entry in the TTC Library assigned document number. This number serves as the "license plate" to identify a particular reference. Typical document numbers of various character types are: 100 000, 200 000, 300 000, FRA, etc.

Standard Reference Detail

Following the document number, a standard identification of the reference by article, title, author(s), volume or periodical name and number, publishing organization, date and page number is listed.

Special Classification Notes

Following the reference identification are selected subject categories and key words or phrases.

The first phrase listed is the primary subject group selected by the reviewing research personnel for classifying this particular reference. The ten primary groups established are:

1. Service Evaluations
2. Experimental Stress Studies
   a. Nondestructive

b.   Semidestructive

c.   Destructive

3. Tread Contact Stress, Cracks or Hot Spots

4. Brake Shoe Studies

5. Material Properties

6. Crack Propagation

7. Finite Element Simulation

8. Laboratory Simulation

9. Track Tests

10. General Applicability

After the primary subject, the primary program technical
task number to which the reference applies is listed. Then the
specific wheel type(s) and class of steel (if available) are
listed. If there are any secondary subjects to which the
reference may apply, these are also listed in decreasing order
of applicability. Closing out this group of key phrases are any
pertinent ones listed on the standard library reference card.

Special Annotation

On some of the reference listings, a special abstract or
annotation is provided by research personnel. This brief
annotation focuses primarily on the purposes and conclusions of
the particular references that are especially applicable to the
Wheel Failure Program. They sometimes contain an evaluation of
the pertinence and quality of some aspect of work cited but
generally do not attempt to abstract the entire document.

Other Selected References

The annotated bibliography is supplemented by the selected references that either have not been specially annotated or are judged to be secondary, but of general interest to the program.

Annotated Listings

Annotated listing of references according to the order of assigned numbering system is presented in Appendix 3.2.

Listings of annotated references can be retrieved using TTC's computerized information retrieval system under typical key words, "THERMAL", "STRESS", "CRACK", "FATIGUE", "BRAKING", etc.

3.2 Application of Pilot Technology to Wheel Failure Mechanism Program

Because of the annotation processes the program's principal investigators were required to review each of the approximately 200 references, a review of the status of current technology more extensive than is normally undertaken. The benefits of the study are demonstrated, however, in the fact that fracture crack growth and fracture toughness investigations were, for example, deemed unnecessary since sufficient data existed in the literature.

4.0   PERTINENT MATERIAL PROPERTIES (TECHNICAL TASK T3)

The requirements of this task calls for the determination of the cyclic behavior of Class B, C, and U wheels at ambient and elevated temperatures. The effect of martensite on thermal cracking of the classes of wheels selected for this study was to be determined with an appropriate test rig. Four wheels of each class were to be tested. Tests were to be completed to characterize wheel materials in terms of their ability to arrest a running crack. A minimum of 12 specimens of each class were to be tested. In order to make statistical distribution of dangerous wheels among nondiscolored wheels in service, a minimum of 100 wheels were to be saw cut. Standardized test data from cooperating laboratories were to be analyzed.

The final lab materials test plan was designed to enhance the applicability (to variable strain and temperature cycles) of elevated temperature, mechanical property data, which was more representative of actual wheel braking cycles, particularly at slow strain rates.

Introduction

In order to develop some understanding of critical wheel material properties, the following experiments were performed:

1.   Low-cycle fatigue tests of Class B, C, and U wheels at ambient and elevated temperatures.

4-1

2. Fracture crack arrest tests of Class U and C wheels.

3. Laboratory induced thermal cracking of Class B, C, and U wheels.

4. Investigation of the effect of slow strain rate on wheel steel flow properties.

5. Radial saw-cutting of wheels (in order to provide a basis for estimating the statistical distribution of dangerous wheels).

Detailed test conditions, results, and conclusions corresponding to each of the above experiments follow.

4.1   Elevated Temperature Cyclic Behavior Task

Low-cycle fatigue tests were conducted on Class B, C, and U wheel materials at ambient and elevated temperatures. The specimens were taken from the rim sections of B, C, and U wheels and were subjected to constant strain amplitude fatigue cycles on a 22-kip test frame. Detailed test conditions, as well as results and conclusions, were reported in the form of an ASME paper (presented at the 1985 ASME Annual Railroad Transportation meeting). A copy of this report is attached as Appendix 4.1.

The data gathered in the Cyclic Behavior Task are being used primarily in Technical Tasks T4 and T10 to provide actual stress-strain curves for the temperatures of interest in the elastic/plastic finite element analyses.

It was generally observed that cyclic performance deteriorated with increasing temperature as shown in Table 4.1 and Figures 4.1a, b, and c . The heat-treated Classes B and C

TABLE 4.1
FATIGUE PROPERTIES FOR CLASSES B, C, AND U WHEEL STEEL

Wheel Steel	Temp. °C	σ_f' (ksi)	b	e_f'	c	K' (ksi)	n'
B	25	224	-0.106	0.631	-0.606	243	0.175
B	200	303	-0.156	0.257	-0.595	433	0.263
B	400	196	-0.114	2.590	-0.879	174	0.130
B	600	76	-0.093	0.918	-0.739	77	0.125
C	25	260	-0.111	1.850	-0.721	237	0.154
C	200	222	-0.092	0.147	-0.468	324	0.196
C	400	187	-0.096	8.700	-0.982	152	0.098
C	600	68	-0.075	1.921	-0.828	64	0.091
U	25	180	-0.101	0.528	-0.587	201	0.172
U	200	159	-0.102	0.147	-0.448	246	0.228
U	400	166	-0.118	1.685	-0.771	153	0.153
U	600	81	-0.104	0.762	-0.698	84	0.148

σ_f' -- Fatigue strength coefficient   (1 ksi = 6.8948 MPa)
b -- Fatigue strength exponent
e_f' -- Fatigue ductility coefficient
c -- Fatigue ductility exponent
K' -- Cyclic strength coefficient
n' -- Cyclic strain hardening exponent

1.   Steady state stress amplitude =

   $$K' \text{ (steady state plastic strain)}^{n'}$$

2. $$\frac{\text{Strain range}}{2} = \frac{f'}{E} (2N_f)^b + e_f' (2N_f)^c$$

   N_f = No. of cycles failures

3. $$n' = \frac{b}{c}$$

4. $$k' = \frac{F^1}{(e_f^1)n}$$
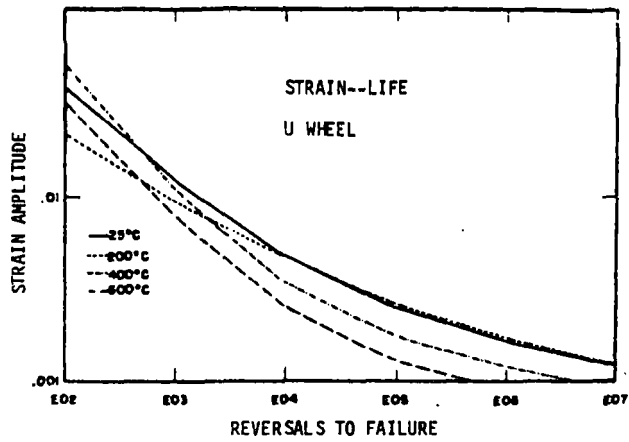
FIGURE 4.1A   STRAIN AMPLITUDE-LIFE CURVES FOR U WHEEL MATERIAL
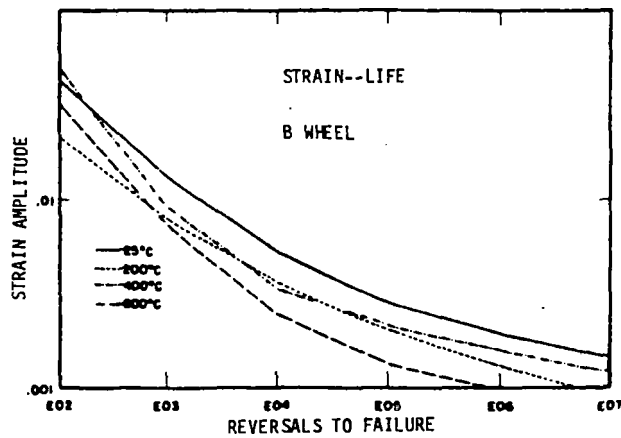
FIGURE 4.1B   STRAIN AMPLITUDE-LIFE CURVES FOR B WHEEL MATERIAL
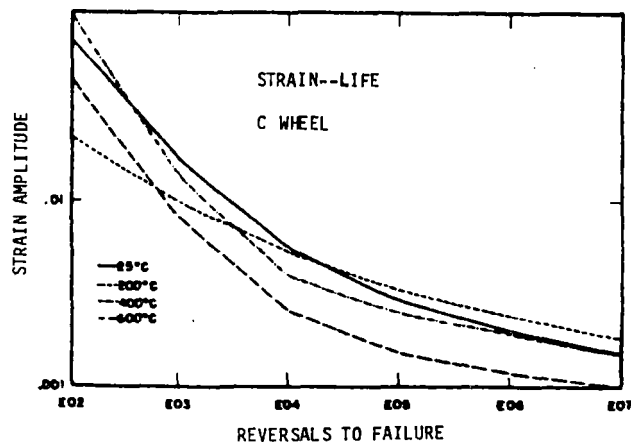
FIGURE 4.1C   STRAIN AMPLITUDE-LIFE CURVES FOR C WHEEL MATERIAL

4-4

materials performed better than the nonheat-treated Class U material. The differences in carbon level had a noticeable effect on fatigue performance.

4.1.1 Fatigue Test Conclusions

1. The cyclic fatigue lives at all temperatures tested converged at strains exceeding one percent.

2. At strains less than one percent, fatigue lives are considerably reduced as the test temperature is increased.

3. Differences in material performance are more pronounced at longer lives (low strain amplitudes) than at shorter lives (high strain amplitudes).

4. The heat-treated wheel materials (C and B) exhibit a higher resistance to fatigue than the nonheat-treated (U) material.

5. The Class C material with higher carbon content shows better resistance to fatigue than the Class B material with lower carbon content.

4.2 Fracture Crack Arrest Tests

The crack arrest fracture toughness (K_{Ia}) properties of Class U and C wheel steels were examined. Notched test specimens, taken from the rim portion of appropriate wheels, were wedge-loaded until rapid crack extension occurred. A

complete description of test conditions, results, and conclusions appears in Appendix 4.2. The results of this study indicate that the crack arrest fracture toughness of heat-treated Class C wheel steel is somewhat higher than untreated Class U steel at room temperature, and that this difference increases with temperature (Figure 4.1D).

A dependency of K_{Ia} values on test temperature was noted for Class C steel, while Class U steel appeared fairly insensitive to temperature. This difference appears to be related to the effect of interlamellar pearlite spacing on crack propagation in the steel.

Based solely on the K_{Ia} data, it may also be concluded that rim heat-treated wheels could arrest larger thermal cracks, prior to unstable propagation, than untreated wheels. The critical flaw size tolerated would increase with temperature for the Class C wheels. This behavior would not appear in Class U wheels which are tested below 100°C.

A comparison of actual wheel failure data revealing critical flaw size prior to full failure showed fairly good agreement for Class U data, but suggested that predictions for critical flaw size tolerance for the Class C wheels based on K_{Ia} values were too large.

4.3 <u>Thermal Cracking Test</u>

The purpose of these tests was to develop a laboratory technique to produce thermal cracking in wheels and to evaluate

4-6

CRITICAL FLAW SIZE VERSUS STRESS

Based on crack arrest data
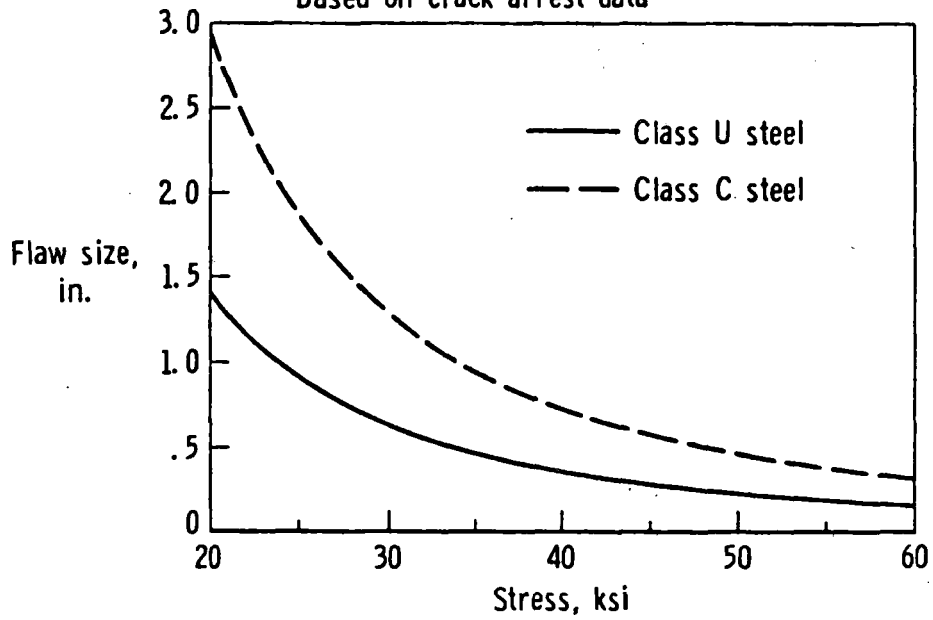
FIGURE 4.1D   CRITICAL FLAW SIZE -VS- STRESS FOR WHEEL STEELS, BASED ON CRACK ARREST DATA

the relative resistance to such cracking of Class B, C, and U wheels. The mechanism for the cracking being studied is the restrained contraction of untempered martensite, which is similar to the mechanism of quench cracking.

To produce this condition, a localized portion of the wheel tread is heated to a temperature exceeding 1333°F to obtain some transformation to austenite. Then this localized region is cooled fast enough for the austenite to transform to martensite. The restraint provided by the unheated remainder of the wheel during subsequent cooling should produce sufficiently high stresses to crack the brittle martensitic region. An apparatus was constructed and runs were conducted with instrumented wheels.

4.3.1 Apparatus

To enforce the above conditions, a machine was constructed to support the wheel in a vertical position by the bore and to turn it at speeds of 1 rpm and slower. Further, an oxygen-acetylene burner was supported and clamped so that the distance from the torch tip could be adjusted. A steel pan, measuring 10 inches wide by 48 inches long by 11 inches deep, was fitted with a standpipe and drain, placed beneath the wheel, so that the lower 9 inches of the wheel was submerged in water. The make up water was provided by two low pressure nozzles directed at the wheel plate about 12 inches above the water level in the pan. The general arrangement of the test rig is shown in Figure 4.2.

FIGURE 4.2   GENERAL ARRANGEMENT OF THE TEST RIG FOR THERMAL CRACKING

The trial wheel was fitted with eight 1/16 inch diameter sheathed thermocouples in holes drilled to the mid-tread positions from the back face of the rim. The 1/8 inch diameter holes were centered 1/4", 1/2", and 1" from the tread. After the thermocouples were placed in the holes, steel wool was packed around the thermocouples. The thermocouple data were acquired by a modified personal computer for data acquisition, storage and printout.

4.3.2 Test Specimens

All of the wheels for these tests were CJ33 with a parabolic plate. Four Class B, four Class C, and five Class U wheels were designated for these tests. One of the Class U wheels was drilled for the placement of thermocouples in the rim. This wheel was used for development of the test procedure.

4.3.3 Thermal Cracking Test Conditions, Results

Several preliminary trials were conducted with about 1/4 of the wheel to determine the gas pressure, torch-tip/wheel proximity, and wheel speed that would result in the desired apparent surface temperature. After this was accomplished, additional preliminary trials were conducted to enhance the quenching of the heated spot. Subsequently, trials were conducted with full rotation of the wheel to determine if cracking would occur. The conditions for these trials were based on the results of the preliminary trials. There were

as follows:

1. Rego tip TWP2579-56 - gas pressures of 20 psi oxygen and 10 psi acetylene to provide heat output of about 50,000 Btu/hr.

2. Torch tip to wheel tread distance - 1 inch.

3. Wheel speed about 1/20 rpm or 5 in/min.

4. Water sprays directed at wheel plate and water immersion of lower 9 inches of wheel.

Three classes of wheels (Class U, B, and C) were tested. It was theorized that for each of the transients, Class U wheels would take the least amount of time to crack. This is because they are not heat treated and have a relatively high carbon content. The next class of wheel to crack would be the Class C wheels since they have the same relative carbon content but are heat treated. Finally, Class B wheels should have taken the longest amount of time to crack since they have lower carbon content than the others and are heat treated. For each transient, two wheels were tested from each class. The results which are give below show there is no difference in the crackability between the different classes of wheels. However, they do fit well with the empirical model developed by Fec and Sehitoglu[1].

Two methods were used to determine wheel crackability. The first method was to note the revolution when the first crack was observed. The other method was to note when 25" of cracks were observed in the tread. This latter method has the advantage of not being dependent on localized conditions.

Temperatures in the interior of the rim region were measured by three thermocouples placed at depths of 1/2", 3/4" and 1". These thermocouples entered the rim from holes drilled in the side face to the above depths underneath the center of the rim. Data were automatically collected every second using a Compaq Plus computer attached to a Data Translation 2805 low-level A-to-D converter with cold junction circuitry. The problem with collecting data from the thermocouples was that their presence affected test results. The holes drilled for their placement created local stress risers. During the tests, most of the cracks would originate at these holes and grow to the tread. For this reason, thermocouples were only placed in wheels used to test the setup. The thermocouples were used to determine temperatures under test conditions. During the actual testing, no thermocouples were used.

Surface temperature was determined by using a Hughes Probeye infrared thermal vision with frame filter. Temple sticks were used to confirm that when the thermal vision was giving a temperature reading of 900°C, the actual hot spot temperature was between 899°C and 927°C.

The first series of tests were done at 900°C. The subsequent cracking which developed on the surface of the tread was dramatic. The transient was so severe that all cracking could be observed with the naked eye.

Figure 4.3 shows a typical wheel after a test. Cracking was uniform around the wheel. Most cracks started at the interface between the hot spot and the rest of the wheel. They then grew
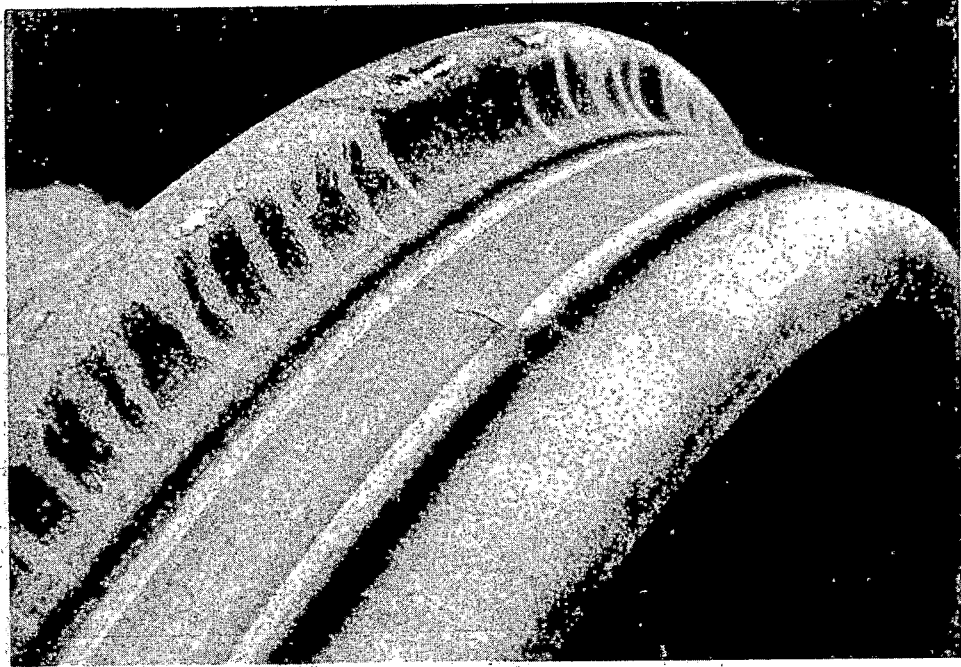
FIGURE 4.3   TYPICAL EXAMPLE OF UNIFORM CRACKING

towards the center of the wheel, meeting with cracks from the other side of the hot spot. These cracks started at 45° to the direction the wheel was rotating in. These cracks grew then towards the center of the hot spot. As they grew towards the center, their orientation changed to perpendicular to the direction of wheel rotation.

On some of the wheels tested at this temperature, a more localized form of cracking networks occurred (Figure 4.4). The cracking was not as uniform as with the other wheels. This type of cracking is due to more localized conditions. These crack networks opened quickly. As a result, more stress was relieved quickly and it took longer for wheels experiencing this type of cracking to meet the 25" criteria.

Contrary to prediction, at $900^{\circ}C$, there was no difference between the three classes of wheels in terms of the number of revolutions for cracking to occur. This is regardless of whether initial or 25" criteria is used. The results at $900^{\circ}C$ are presented in Figure 4.5.

As expected, martensite was produced in the hot spot. Most of the cracking occurred in the martensitic region.

At $700^{\circ}C$, the thermal strain is less severe. This means both that, it will take longer for cracking to develop and that when it does, the cracks will be less visible. This is because not enough thermal stress has developed yet to open the cracks as fully as was the case at $900^{\circ}C$. Cracks were found by spraying dye penetrant on tread. This method found cracking quicker than the magnetic particle tester which was in use when
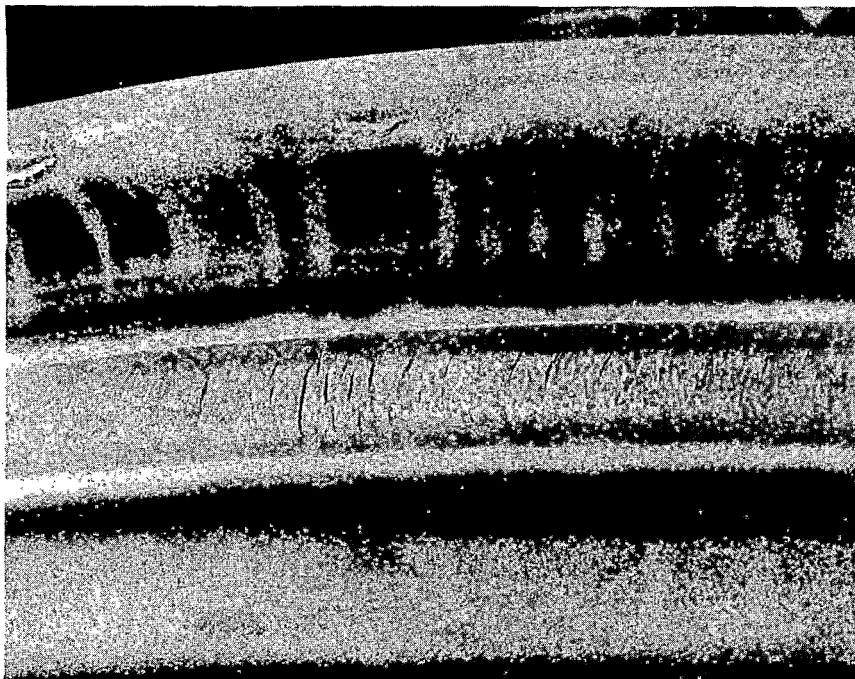
FIGURE 4.4   LOCALIZED FORM OF CRACKING NETWORKS
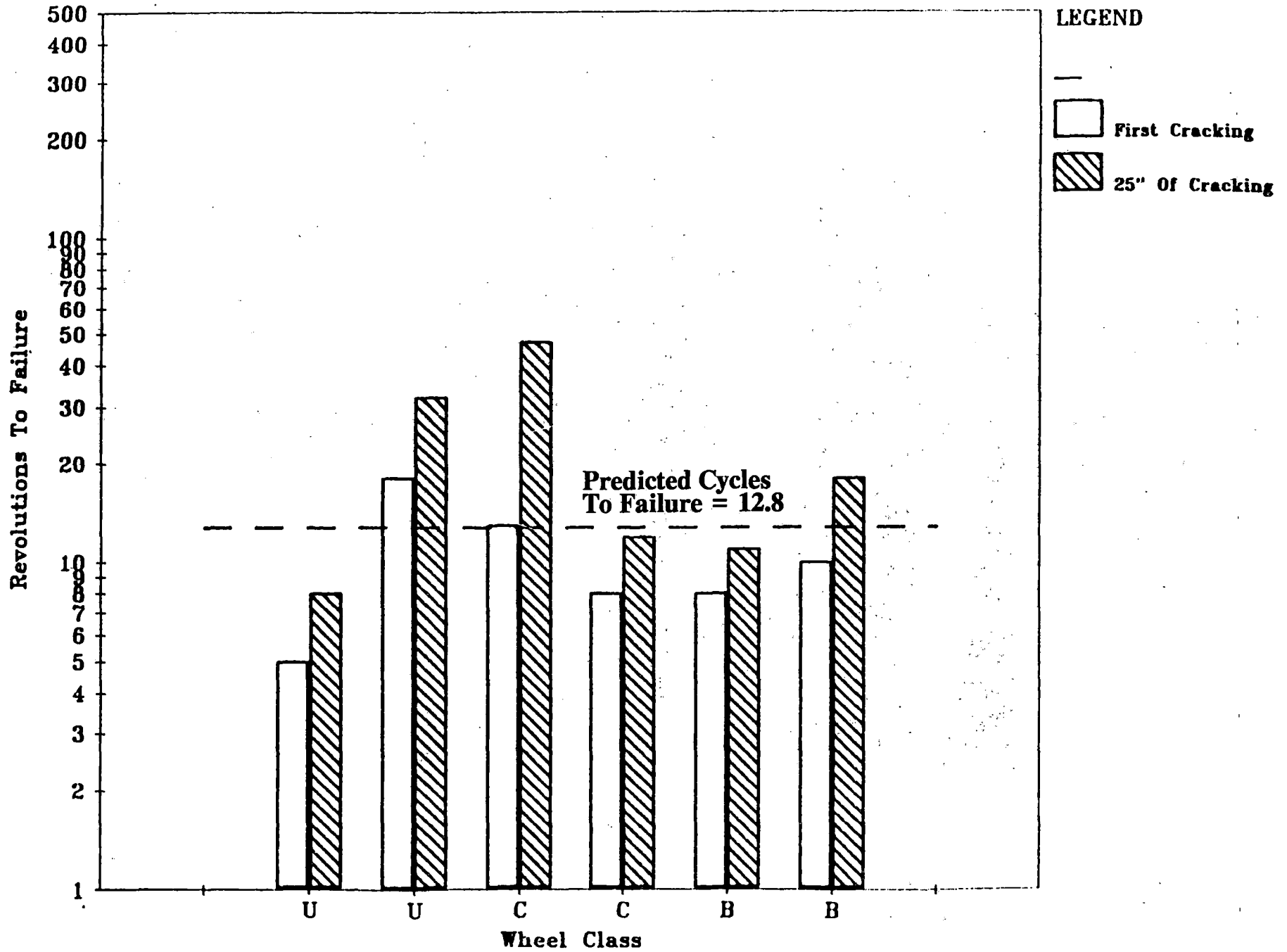
FIGURE 4.5   REVOLUTIONS TO FAILURE AT 900°C DURING THERMAL CRACKING TEST

the testing was initiated. Because of the longer amount of time for cracking to occur, only the initial cracking criterion was used in this test.

The observed cracks were of the hairline type. They tended to develop in the center of the flame-impingement region. Figure 4.6 shows that again, there is no difference between the different classes of wheels with regard to when cracking will occur.

While the material is affected less severely, the flame still influences it. Figure 4.7 shows a cross section of a Class U rim after it was macroetched in a 10% ammonium persulfate solution.

The etchant shows regions which have been affected by heat. In this case, a small region by the tread can be seen which has been heated enough to show up when macroetched.

4.3.4 Discussion of Thermal Cracking Test Results

As Figures 4.5 and 4.6 clearly show, there is no significant difference between the different classes of wheels with regard to when they will crack. At both temperatures, the wheels cracked at about the same number of revolutions.

An explanation for the lack of difference between the different classes of wheels can be found in work by Fec and Sehitoglu [1]. They used hourglass-shaped specimens made out of Class U wheel material. These specimens were rigidly held at each end in water-cooled grips while the center was cyclically
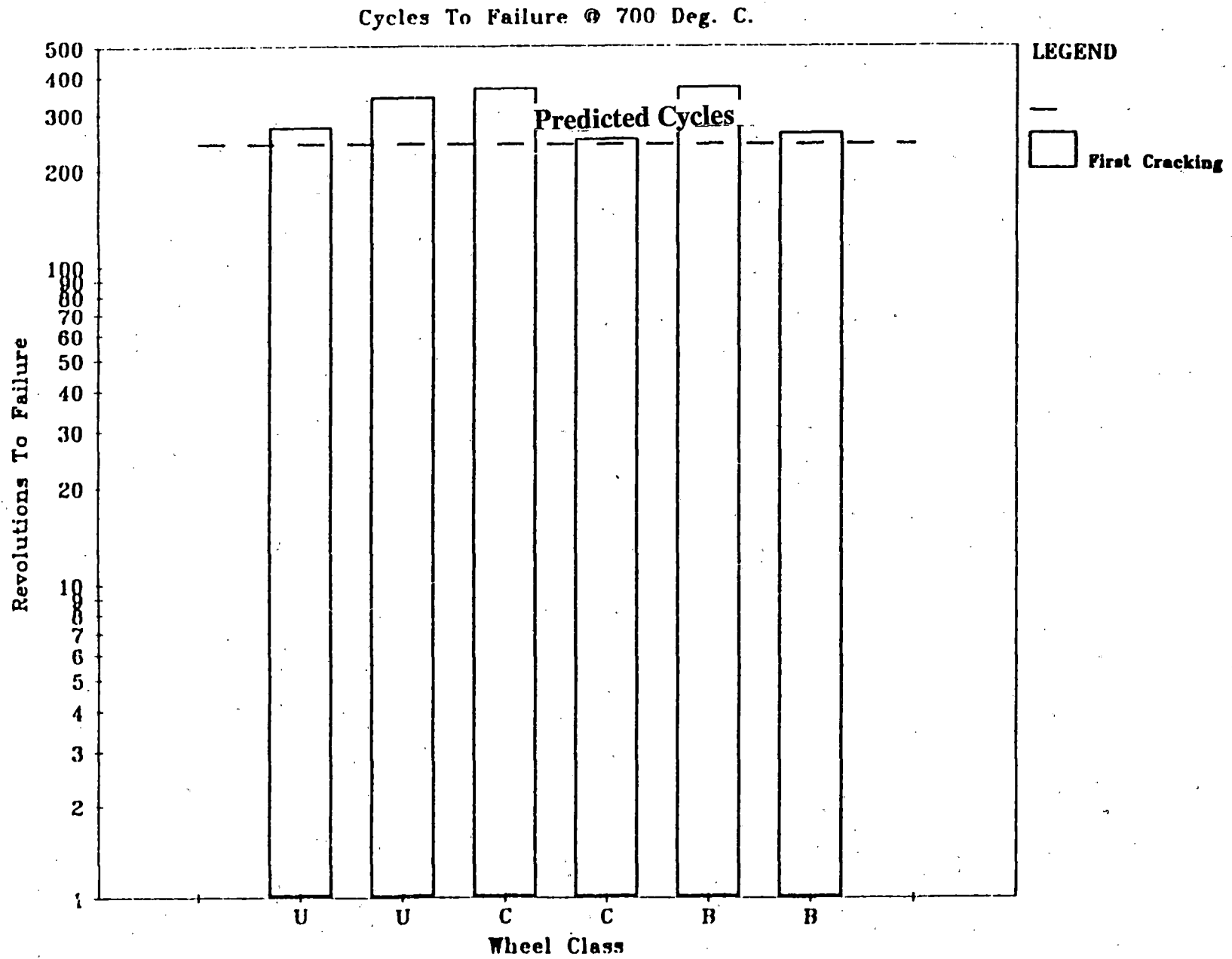
FIGURE 4.6   REVOLUTIONS TO FAILURE AT 700°C DURING THERMAL CRACKING TEST

Class U Wheel
Tested @ 700 Deg. C.
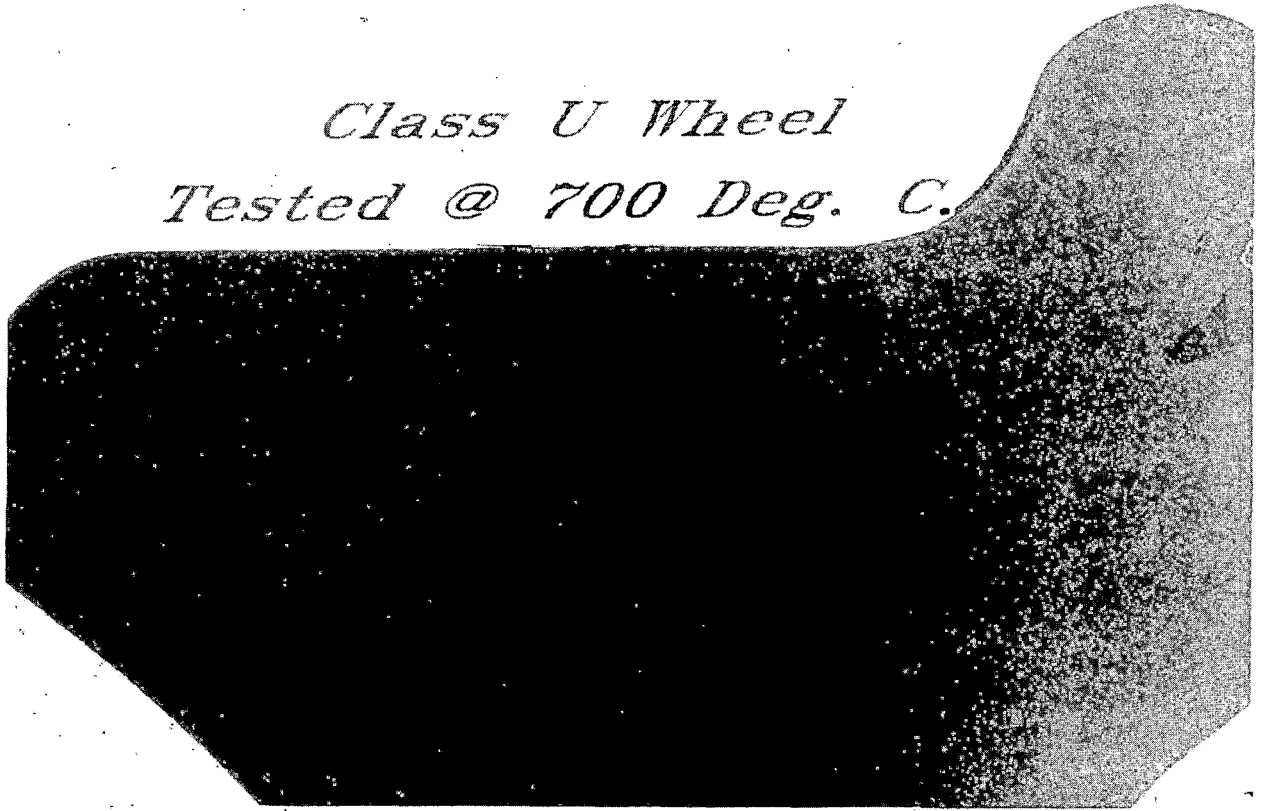
FIGURE 4.7   CROSS-SECTION OF A CLASS U RIM AFTER TESTING

heated by an induction heater until the specimen cracked. The
net strain from such cycling is 0, as shown in the equation.

$$e_{th} + e_m = 0 \qquad [1]$$

where e_{th} is the thermal strain and e_m is the mechanical
strain. Then,

$$\Delta e_{th} + \Delta e_m = 0 \qquad [2]$$

The thermal strain is defined as:

$$\Delta e_{th} = \alpha \Delta T \qquad [3]$$

where α is the thermal expansion coefficient and ΔT is the
difference between maximum and minimum temperatures of the
thermal cycle.

The mechanical strain can be defined by the Coffin-Manson
Law:

$$\Delta e_m = a N_f^{-b} \qquad [4]$$

a and b are constants, while N_f is the number of cycles
for cracking to occur.

Fec and Sehitoglu determined that the value of a is 0.01595
and b is 0.1148. α was measured to be 0.000017/°C. For plain
carbon wheel steels, this value of the thermal expansion

coefficient changes insignificantly between the different wheel classes.

By substituting Equations 3 and 4 into Equation 2 and rearranging, Fec and Sehitoglu defined the cycles to failure as:

$$N_f = (0.000017(\ T)/0.01595)^{(-1/.1148)} \qquad [5]$$

Figure 4.8 shows a plot of the results of this equation, cycles to failure versus ΔT.

To apply Equation 5 to the lazy susan results, ΔT has first to be determined. The minimum temperature in the cycle is $38^{\circ}C$. If the maximum temperature in the cycle is assumed to be the temperature of the hot spot, then for the $900^{\circ}C$ test T would be $862^{\circ}C$. However, the maximum temperature is really a gradient which involves the cooler material surrounding the hot spot. Thus, an effective ΔT has to be established. Based on the thermocouple data taken from the rim region, it was established that for a hot spot temperature of $900^{\circ}C$, the effective ΔT is $700^{\circ}C$.

At a hot spot temperature of $700^{\circ}C$ the effective ΔT is $500^{\circ}C$. Then, at a surface temperature of $900^{\circ}C$ the expected number of revolutions to failure is 12.8 while for a surface temperature of $700^{\circ}C$ the predicted number of revolutions to failure is 240. These predicted values have been plotted on the graphs in Figure 4.5 and 4.6.

The predicted number of cycles to failure agrees well with the number of cycles before first cracking is observed in the
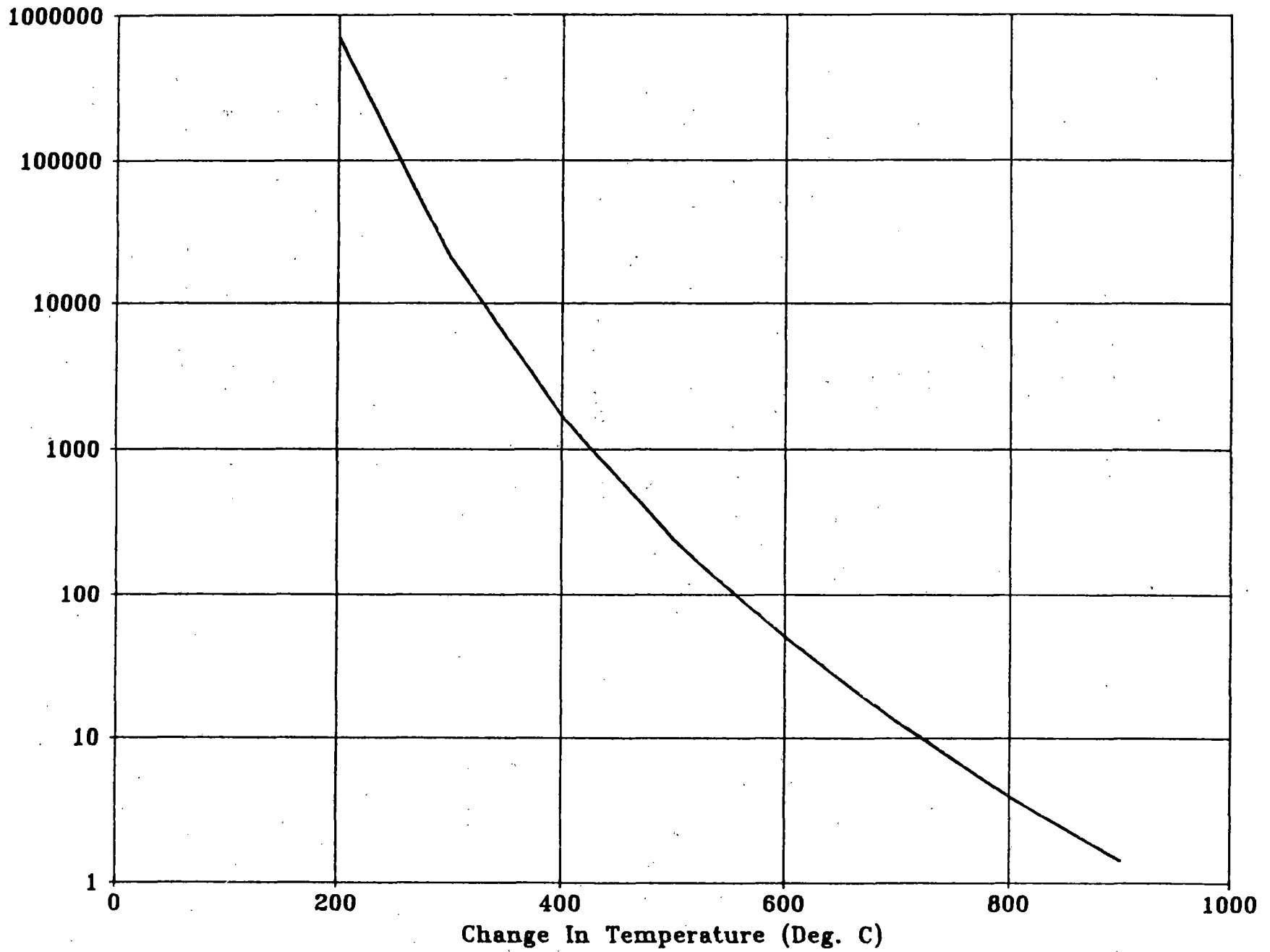
FIGURE 4.8   CYCLES TO FAILURE -VS- CHANGE IN TEMPERATURE FOR B, C, AND U WHEELS

wheel, particularly at 900°C. At 700°C, note that the number of cycles for first cracking to occur was higher than predicted in all cases. The reason for this is that the liquid penetrant was not sensitive enough to pick up initial cracking. Near the end of testing, a new magnetic particle tester was subsequently obtained to detect cracking. This unit found cracks 50 to 60 revolutions before the dye penetrant did on the two wheels it was used on. It is felt that at 700°C the results would be closer to the predicted values if this magnetic particle detector had been used. (For the sake of comparison, none of the results reported at 700°C were based on the magnetic particle detector. Rather, results were reported based on the dye penetrant test.)

4.3.5 Conclusions

Based on the thermal cycling testing performed, there is not any significant difference in performance between the Class B, Class C, and Class U wheels in regard to when they will first crack. It should be noted that in the case of wheel crack initiation, this process is "short circuited" by the production of stress risers because of the occurrence of wear. Rather, cracking can be predicted by the empirical model developed by Fec and Sehitoglu [1]:

$$N_f = (\alpha \Delta T / 0.01595)^{(-1/0.1148)}$$

The only part of this equation based on material properties is the thermal expansion coefficient, α , which varies little between the three classes of wheels. Here it was assumed to be a value of 0.000017/$^\circ$C.

Based on both the logic behind the model and the agreement of the lazy susan experimental results with it, it is felt that the Fec and Sehitoglu model can adequately predict the number of cycles to failure, in this situation.

4.4   Effect of Slow Strain Rate

Almost all the monotonic and cyclic mechanical property tests conducted to date have been performed at a conventional strain rate of 0.002/Sec. However, it has been observed that actual strain rates enforced on the hot rim steel of wheels subjected to prolonged drag braking are usually below 0.000002/Sec. or some three orders of magnitude slower than conventional test rates. Therefore, preliminary tests were conducted to gain some insight into the possible rate sensitivity of wheel steel flow properties (cyclic and monotonic) at elevated temperature.

Preliminary results indicate that a three order of magnitude reduction in strain rate could cause a significant reduction in flow stress, that is, greater than 20% at 400°C (752°F). This indication is based on some cyclic property data obtained recently from Prof. Huseyin Sehitoglu at the University of Illinois and from a monotonic tensile test with

step changes in strain rate conducted at AAR Chicago.

The effect of a one order reduction in strain rate on cyclic 0.2% offset yield was tested by Prof. Sehitoglu at the University of Illinois. An 11% reduction in flow stress at 400°C was observed for a reduction in strain rate of one order of magnitude. No effect of strain rate was seen at 200°C.

The effect of step reduction and subsequent increases in strain rate over four orders of magnitude in a special tension test of Class U steel at 400°C is shown in Figure 4.9. After uniform strain hardening was established at a strain of about 2.6%, the strain rate was abruptly reduced in steps from 0.002/ Sec. to 0.000002/Sec. and subsequently increased back to 0.002/ Sec. This procedure was repeated but to a slower rate, 0.000002/Sec., at higher strain in the same test. As seen in the figure, the drop in flow stress and subsequent rise are essentially identical for the same strain rate increment. A reduction of strain rate of two orders of magnitude to 0.00002/ Sec. causes a flow stress reduction of between 9.6 and 12.1%. At the slower rate of 0.000002/Sec., the flow stress continues to relax during the period of straining but seems to reestablish at a flow stress level at least 21.6% below that for conventional rate. Even greater relaxation rate was indicated at the slowest rate of 0.000002/Sec., but the test was too short to establish a steady flow stress.

From this preliminary test at 400°C a strain rate sensitivity, m, of at least 0.03 may be expected where the relation between flow stress and strain rate is given by:
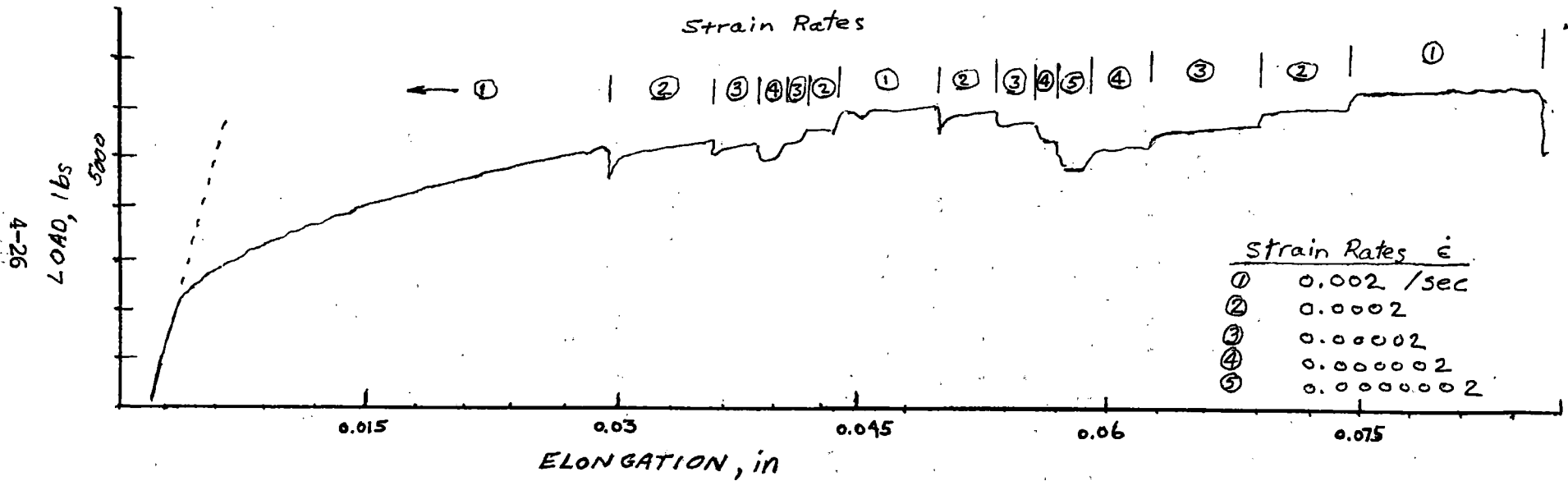
FIGURE 4.9   EFFECT OF STRAIN RATE ON FLOW CHARACTERISTICS OF

CLASS U WHEEL STEEL AT 400°C (752°F)

$$\sigma = C \; (\dot{\varepsilon})^m$$

(at a given value of strain and temperature)

This relationship was proposed originally by Zener and Hollaman in 1944. As Dieter (<u>Mechanical Metallurgy</u>, 1961) has observed, this parameter can be obtained from a test where strain rate is rapidly changed from one value to another.

$$m = \frac{\log \; (\sigma_2 / \sigma_1)}{\log \; (\varepsilon_2 / \varepsilon_1)}$$

It is expected that the strain rate sensitivity will increase with temperature.

4.5   Wheel Saw-Cutting

The purpose of this subtask was to estimate the number of unsafe wheels of various designs, at different levels of discoloration and usage.

To differentiate between wheels with potentially dangerous levels of tensile rim stresses and wheels with compressive rim stresses sufficient to inhibit crack growth, a destructive saw-cutting procedure was applied to a population of 387 wheels. In this procedure a given wheel was cut radially from the flange in towards the hub, and resulting flange tip displacements were measured as a function of saw-cut depth.

In addition to the 387 wheels which were saw-cut at the TTC,

188 wheels were cut in separate research programs by the Norfolk Southern, Union Pacific, and Santa Fe railroads.

Flange displacement data for the 188 wheels were provided by the railroads and were used to augment data collected at the TTC.

The freight car wheels selected for this study included:

1. Wheels taken out of service by visual inspection of wheel discoloration that extends 4 inches (102 mm) from the rim into the plate region on one side (AAR Why Made Code 89) and those subsequently taken out of service due to discoloration on both sides (there are 123 wheels in this data set),

2. Wheels taken out of service due to thermal cracks (AAR Why Made Code 74),

3. Wheels taken out of service due to reasons other than AAR Why Made Codes 89 and 74, and

4. 26 new wheels.

In addition, 23 wheels from dynamometer testing were saw-cut.

4.5.1 Radial Saw-Cutting Procedure

A Rockwell Model 28-345 band saw unit was modified at TTC, to facilitate radial saw-cutting of railroad wheels. This type of band saw has a movable table which is retrofitted with linear bearings, while the saw blade is mounted on a fixed column (Figure 4.10). A constant force feed is provided by a pulley

Wheel Failure Guard

Table Plate,
Roller Mtd. W/
Guides

Rockwell Model 28-345
Band Saw

Feed Table

Weights,
Constant Cutting Force

Front View

Wheel Failure Guard

Throat Width 19 ⅞"
Max. Work Height 11¾"
Blade Width Cap. ¹⁄₁₆" – 1"
Blade Speed 50 - 4500 fpm

Table Travel - One
Direction

Side View
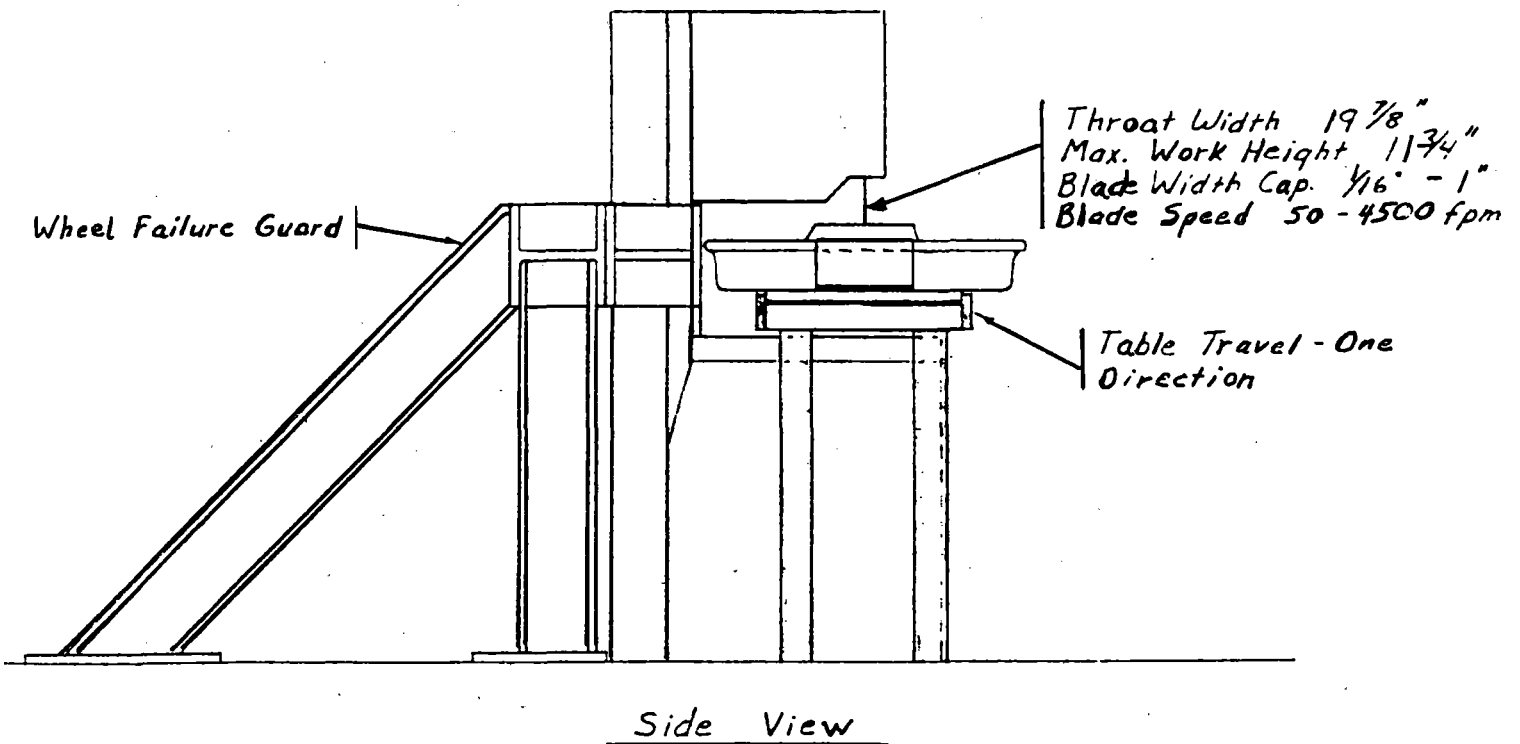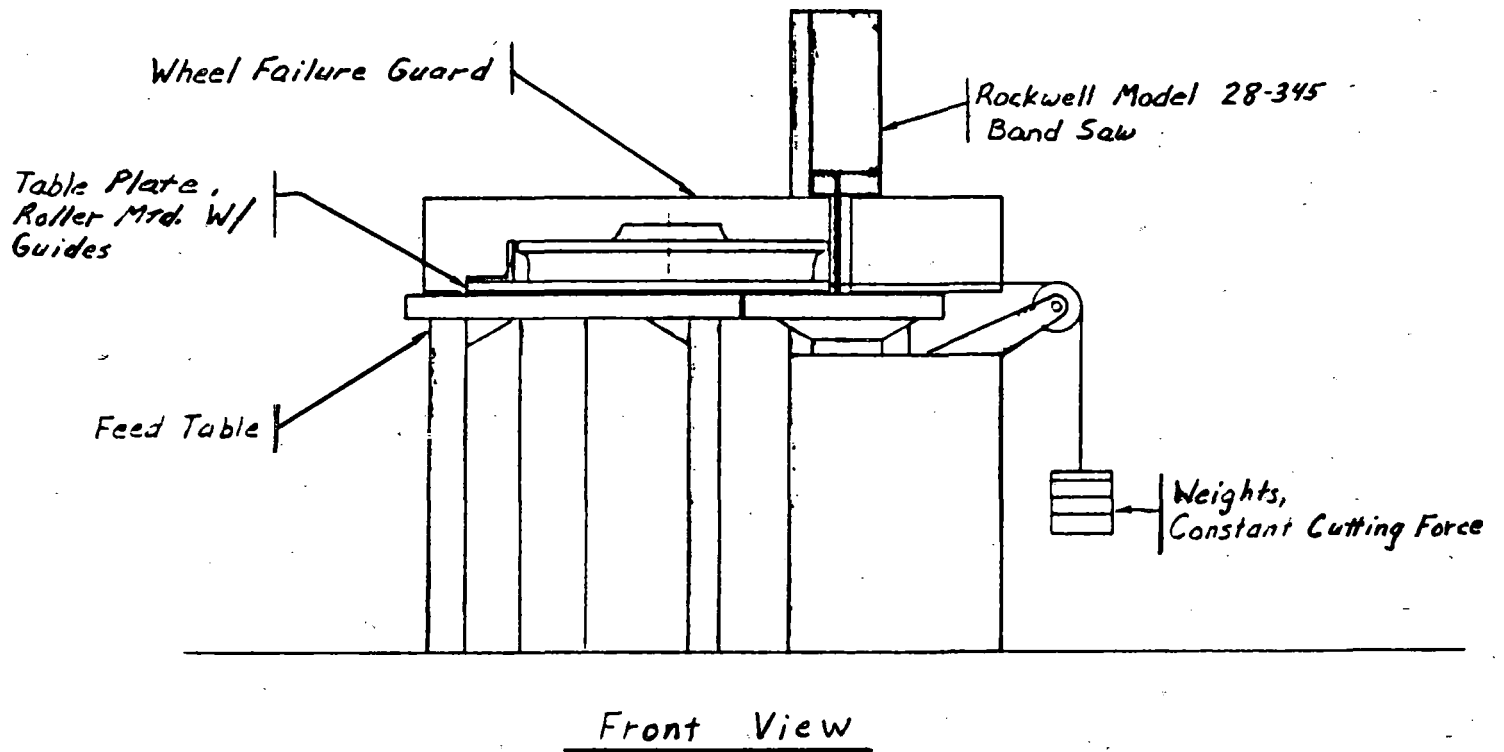
FIGURE 4.10   SCHEMATIC OF SAW-CUTTING UNIT AT PUEBLO

and weight system. A wheel failure guard is fabricated around the saw unit to protect personnel and the saw in case a catastrophic wheel failure should occur.

Instrumentation for the radial saw-cutting unit consists of appropriate transducers, electronic signal conditioners, and data acquisition system. To monitor the movement of the table supporting the railroad wheel, a calibrated string pot system is provided. An MTS clip gage with a range of 0.1" to 0.3" is used to measure the circumferential displacement that occurs at the flange tip during the radial cut. The clip gage is attached to knife edges that affix to the back of the wheel flange with the wheel mounted on the band saw table (Figure 4.11). An x-y plotter automatically records the MTS clip gage displacement versus the depth of cut during the cutting operation.

To prepare a wheel for cutting, the clip gage mount is attached to the back rim face. The wheel is placed flat on the band saw table and the blade is centered between the two knife edges. The band saw unit is started and the saw blade is allowed to cut through the knife edge support bracket until it just reaches the flange tip. At this point, the band saw unit is stopped and the clip gage is mounted on the knife edges around the cutting blade. The x-y plotter is initialized to zero displacement and zero depth of cut before the band saw unit is once again started to initiate the radial cut. A typical response of the clip gage is shown in Figure 4.12, with the superimposed wheel cross section, to the same scale as the depth of cut.
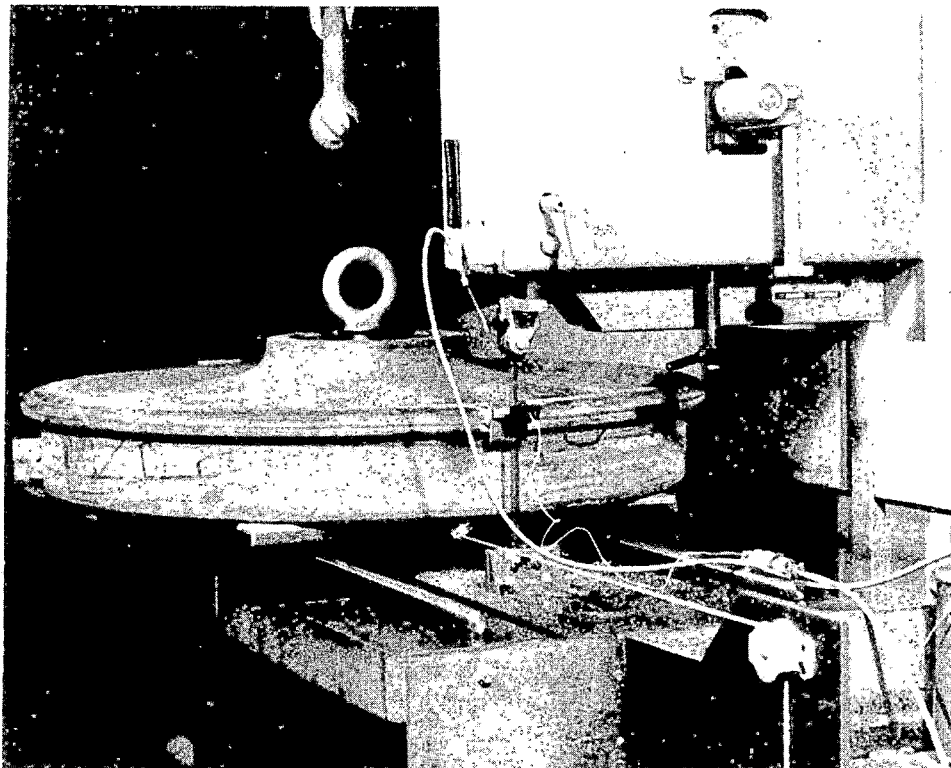
FIGURE 4.11   SAW-CUTTING UNIT WITH CLIP GAGE MOUNTED ON THE
              FLANGE TIP OF TEST WHEEL
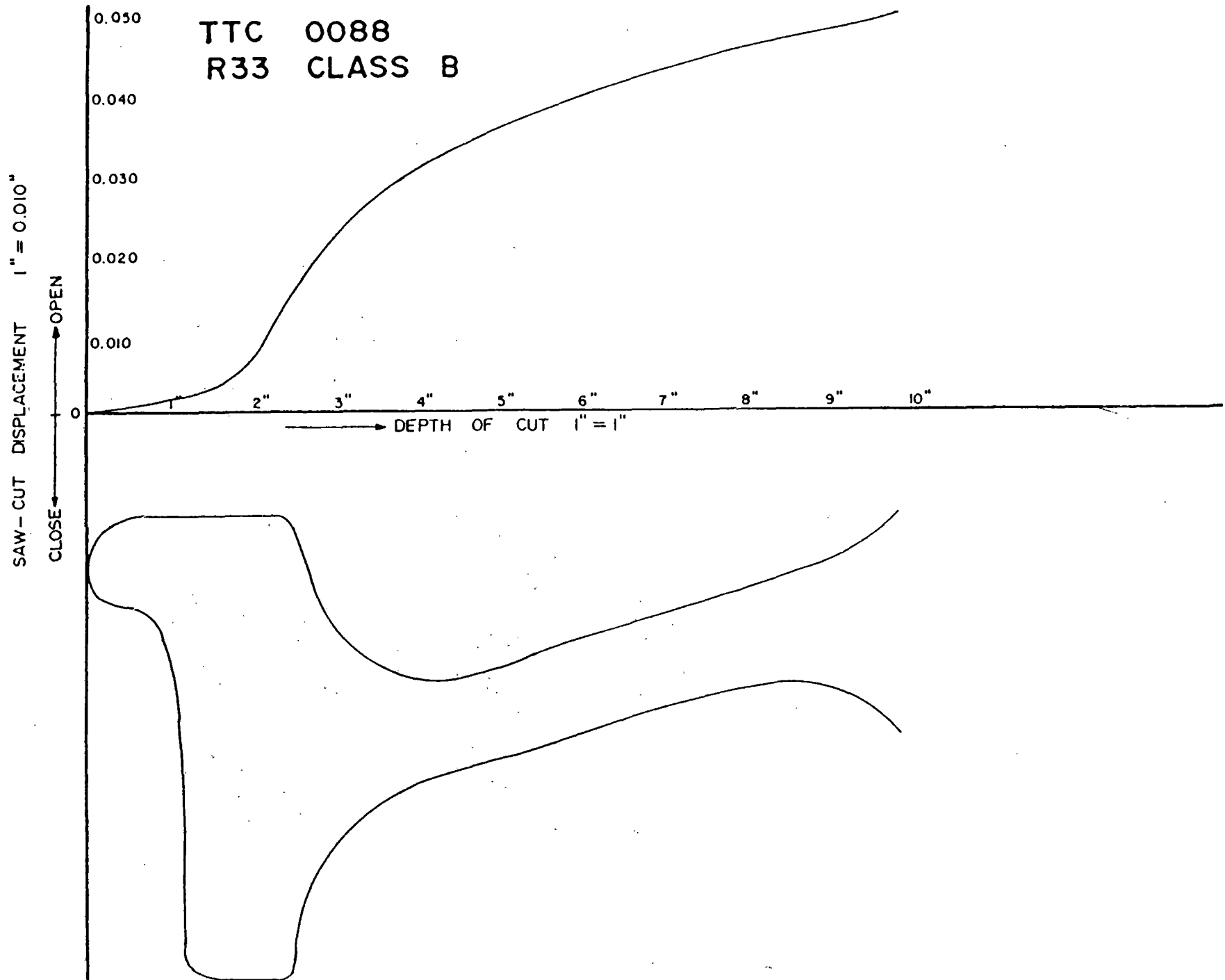
FIGURE 4.12   TYPICAL RESPONSE OF THE CLIP GAGE TO RADIAL SAW-CUTTING

An informal standardization of the saw-cutting method was agreed upon by the AAR, Norfolk Southern, Union Pacific, Santa Fe, and FRA to ensure ease of data interpretation between laboratories.

After the saw-cutting program at Pueblo was well underway, an additional saw-cut opening measurement capability was installed. Due to obvious differences in the opening/closing behavior of flange tip and tread surface (toward front face) for a number of test wheels, an extended arm clip-on displacement gage with a range of 0.5 inches to 1.0 inches (13 mm to 25 mm) was provided (Figure 4.13) with a special mounting bracket and knife edges. This additional clip-on displacement gage measured the displacement of the front tread surface. As saw-cutting progressed through the flange and the tread, the saw blade was allowed to cut through the mounting bracket of the extended arm clip gage, which was tack-welded to the tread position toward the front face, after which the saw unit was stopped and the second clip gage displacement on the x-y plot was initiated to zero. A typical response of both the clip gages is shown in Figure 4.14. The cross section of the saw-cut wheels is superimposed to the same scale as the depth of cut.

4.5.2 Typical Saw-Cutting Responses

If a rail car wheel is cut radially, one of three general types of behavior will usually be observed. A new or undamaged Class U wheel will show a relatively low compressive stress as
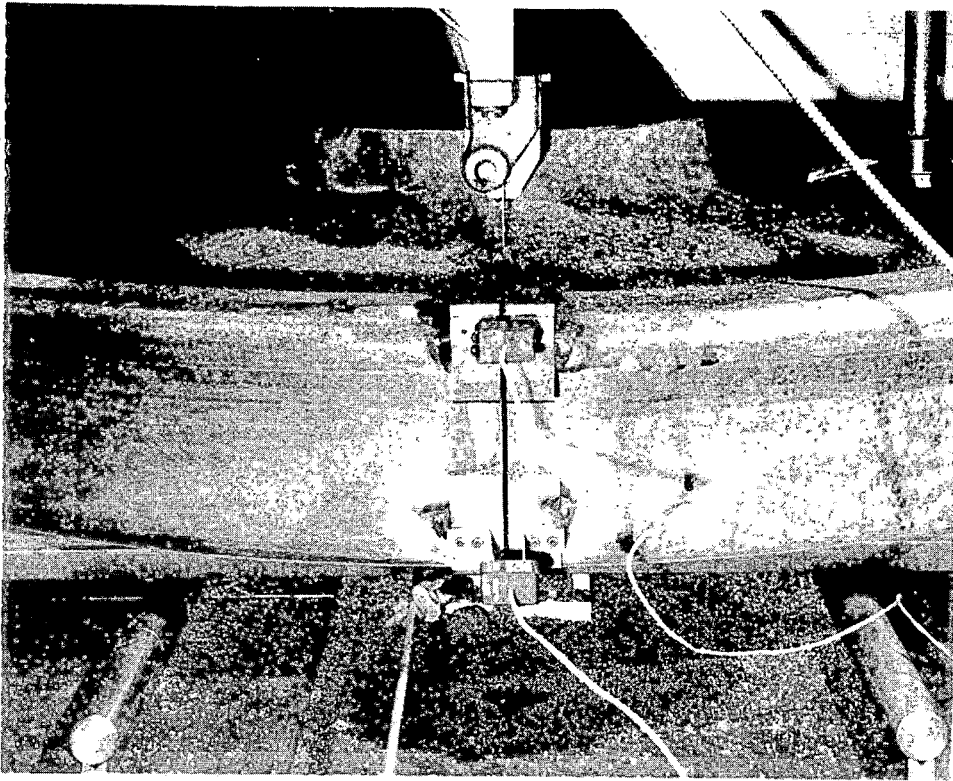
FIGURE 4.13   TWO CLIP GAGES MOUNTED ON THE TEST WHEEL TO
MEASURE THE RESPONSES OF FLANGE TIP (BACK FACE)
AND TREAD (FRONT FACE)
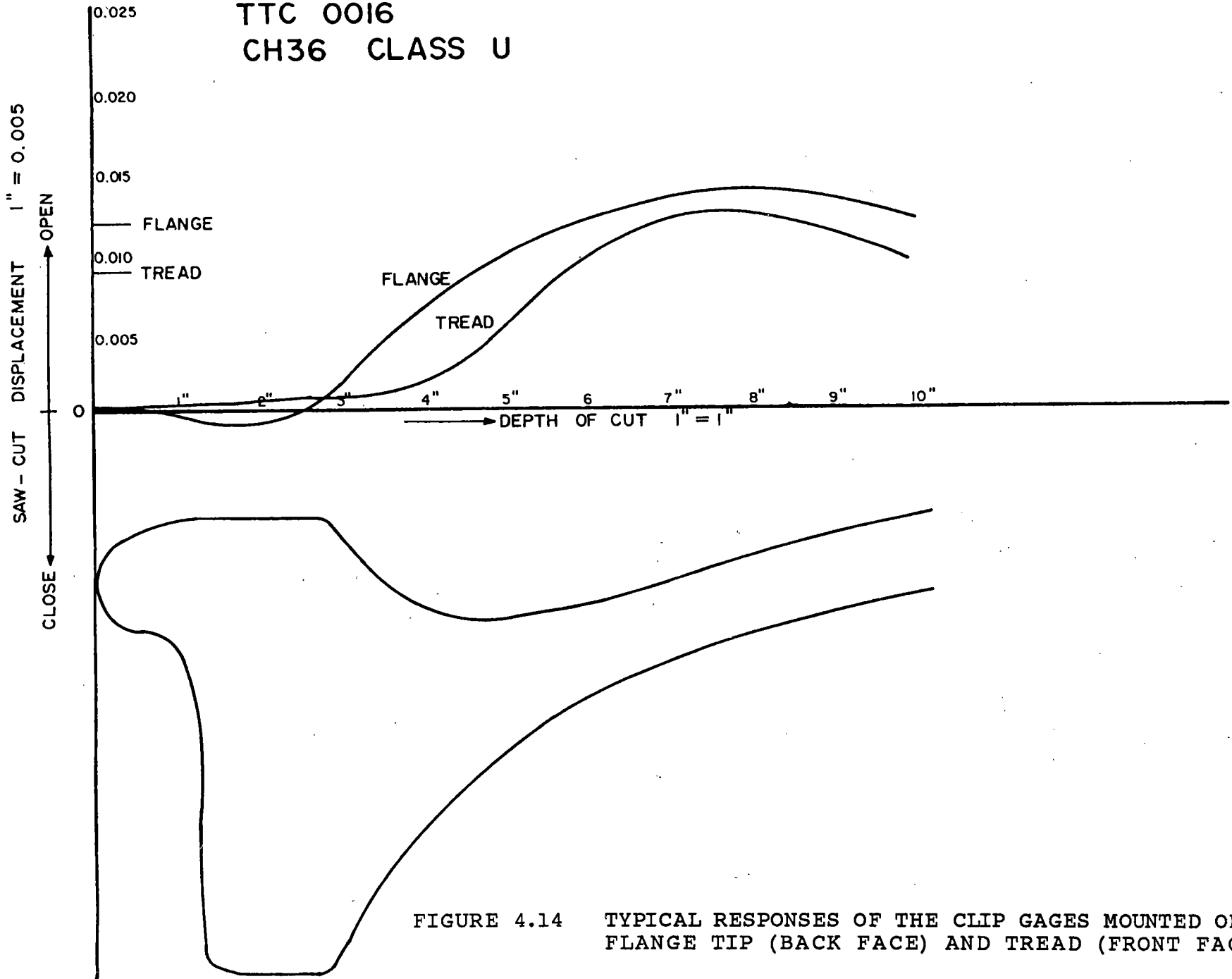
FIGURE 4.14   TYPICAL RESPONSES OF THE CLIP GAGES MOUNTED ON THE
FLANGE TIP (BACK FACE) AND TREAD (FRONT FACE)

the cut proceeds into the rim. As the cut approaches the bottom of the rim, the circumferential displacement measured at the flange tip begins to increase in the positive direction as shown in Figure 4.15. A heat-treated wheel (Class B or C) which is new or undamaged exhibits a continually increasing compressive residual stress to a point approximately two inches into the plate where a constant high level of compressive stress is maintained, as shown in Figure 4.16. A thermally damaged wheel, on the other hand develops an increased level of opening at the flange tip as the cut proceeds inward, as shown in Figure 4.17. A crack located in this area of tensile stress would probably be able to propagate with no possibility of arrest.

4.5.3   Determination of Residual Stress in the Test Wheels Prior to Saw-Cutting by Hole Drilling-Strain Gaging Method

During the course of the saw-cutting program, it was decided to determine the residual stress in the test wheel at certain strategic locations such as back side rim face, back rim fillet region and front fillet region, before the wheel was actually saw-cut. This was done to see if a suitable correlation exists between the saw-cut displacement and the original residual stress at certain locations in the wheel before the actual saw-cut. For this purpose, the hole drilling-strain gaging method of determining surface residual stresses was used for selected wheels, prior to saw-cutting.
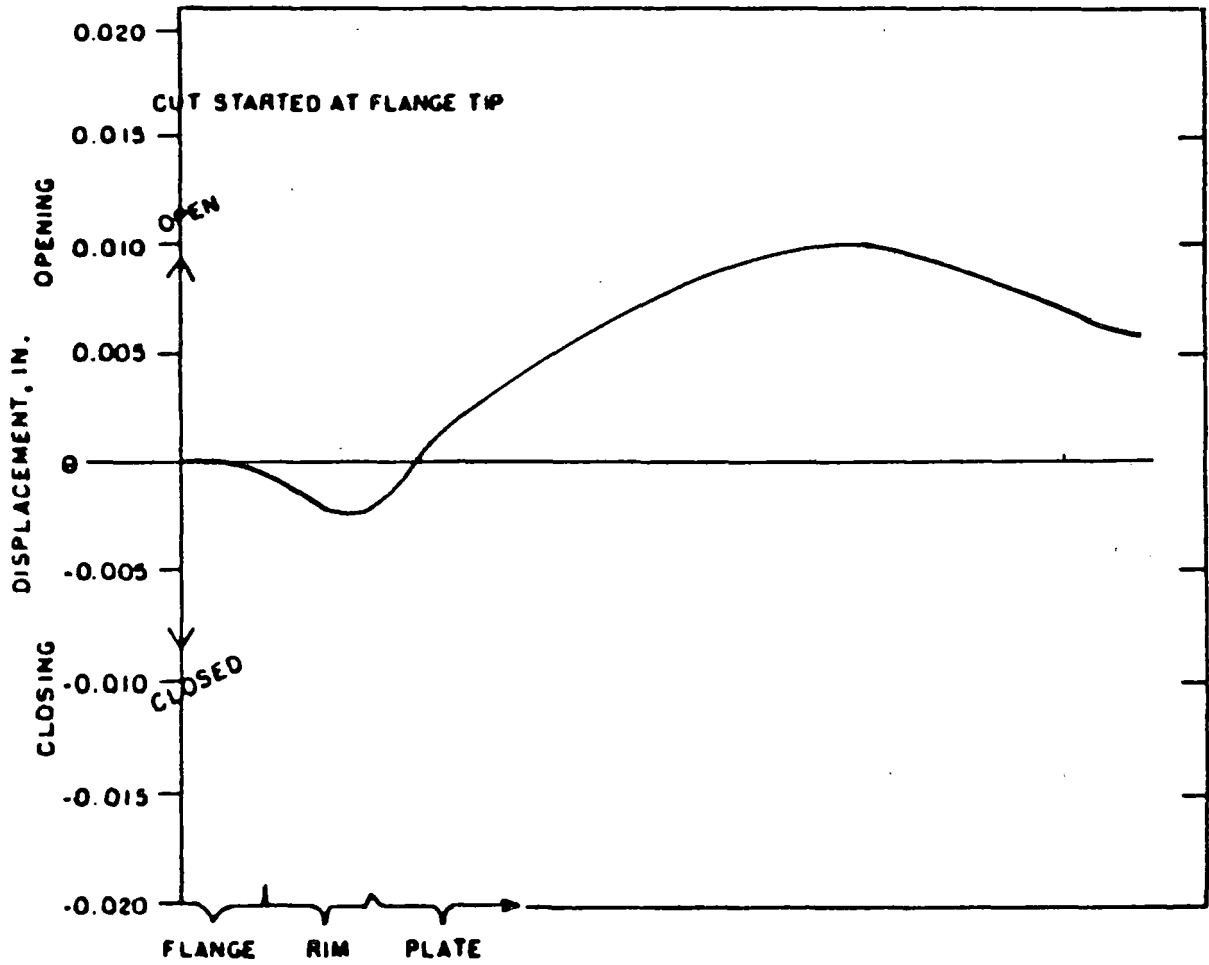
FIGURE 4.15   TYPICAL SAW-CUT DISPLACEMENT BEHAVIOR OF A NEW OR
UNDAMAGED CLASS U WHEEL
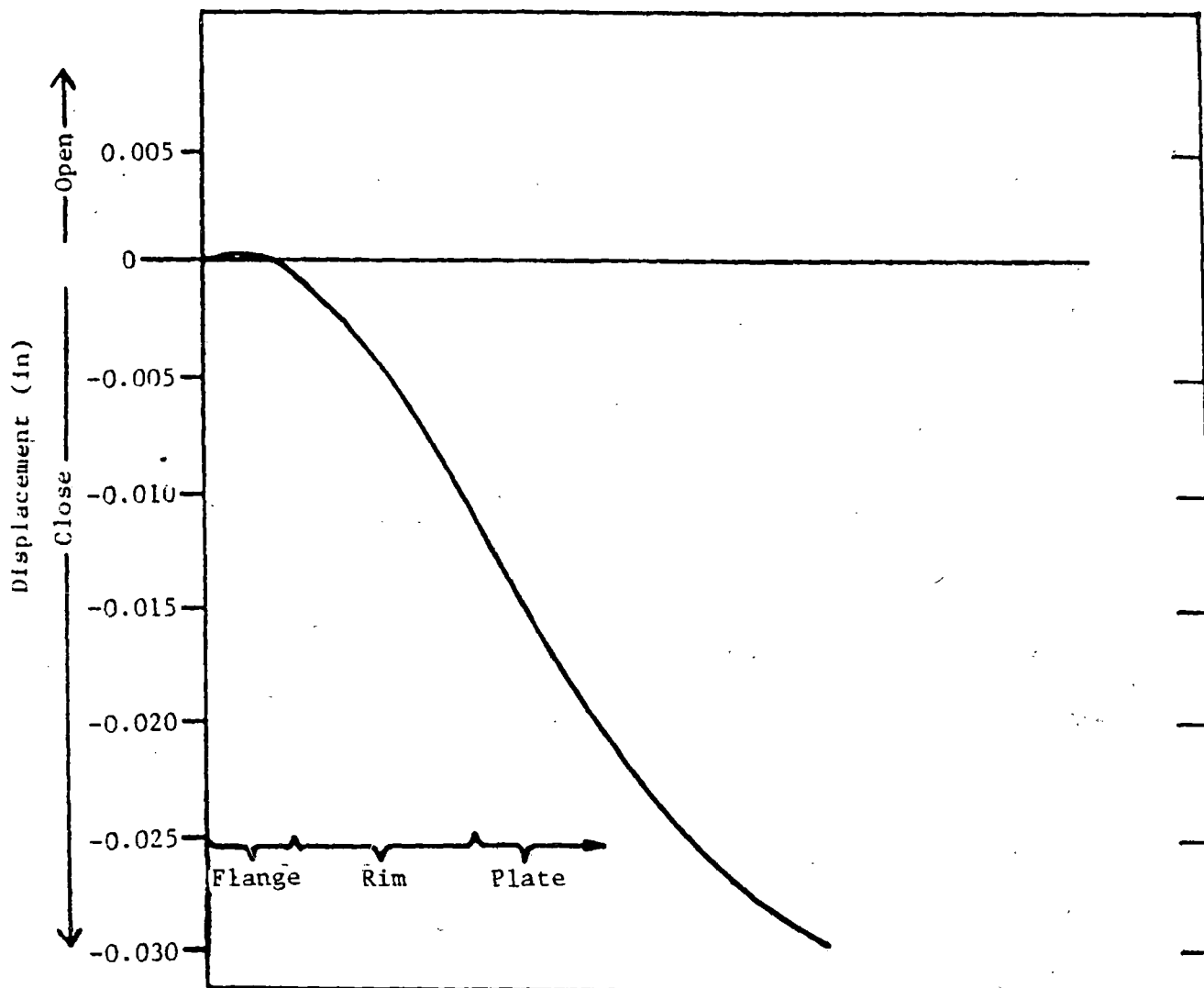
FIGURE 4.16   TYPICAL SAW-CUT DISPLACEMENT BEHAVIOR OF NEW OR
                UNDAMAGED CLASS B OR C WHEELS
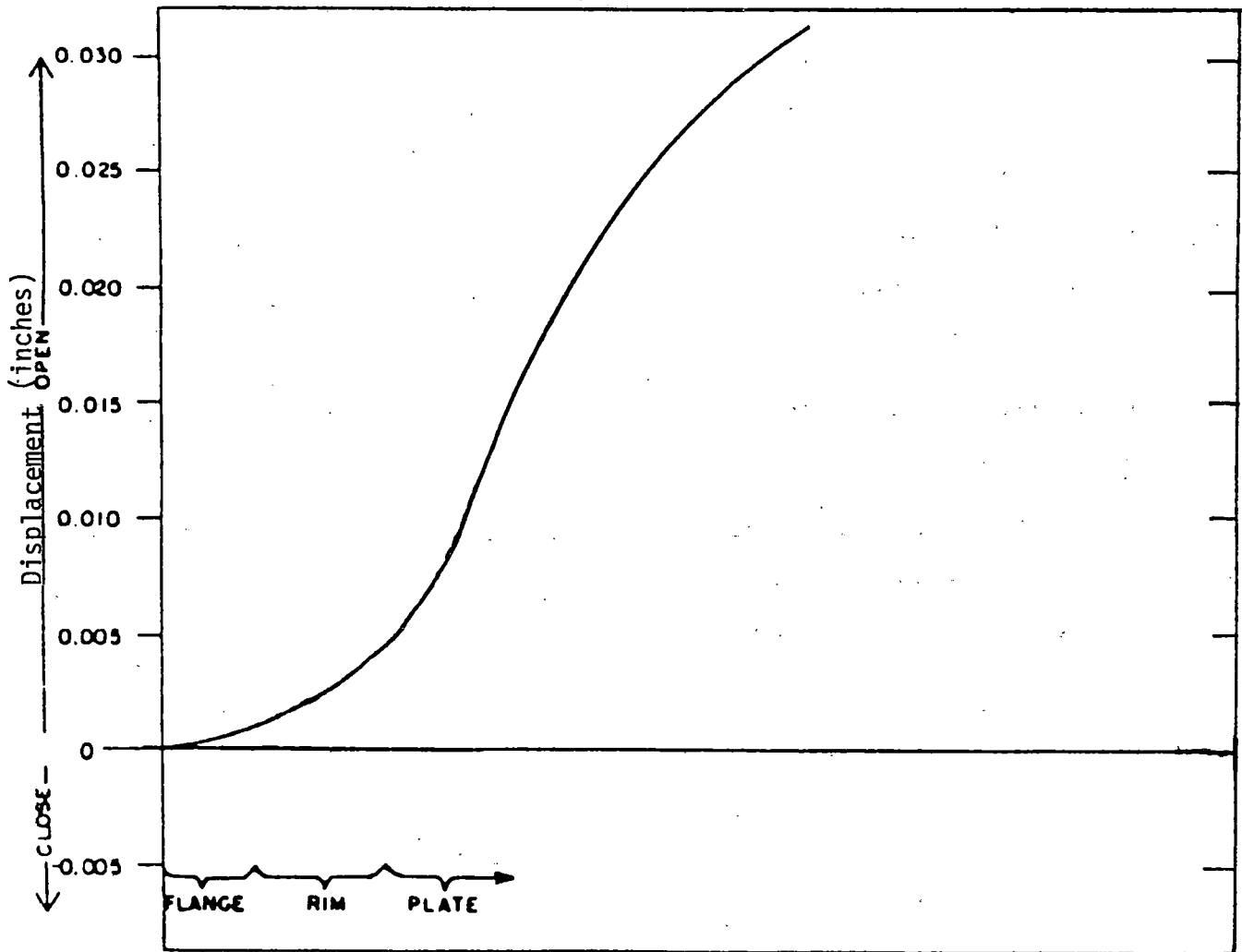
FIGURE 4.17   TYPICAL SAW-CUT DISPLACEMENT BEHAVIOR OF A
THERMALLY DAMAGED WHEEL

The hole drilling-strain gaging method is a semi-destructive method for measuring residual stresses near the surface of isotropic elastic material. The method involves placing a strain gage rosette on the surface, drilling a hole in the vicinity of the gages to a depth greater than its diameter, and measuring the relaxation strains. The residual stresses in the area surrounding the drilled hole relax, and the relaxation is nearly complete when the depth of the drilled hole approaches 1.2 times the diameter.

The measured strains are then related to relieved principal stresses through a series of equations.

The surface strains relieved are related to the relieved principal stresses by the following relationship:

$$\varepsilon_r = (A + B \cos 2\alpha)\, \sigma_x + (A - B \cos 2\alpha)\sigma_y \qquad [1]$$

where

ε_r = radial strain relieved at point P,

A $= -\dfrac{1+\nu}{2E} \times \dfrac{1}{r^2}$

B $= -\dfrac{1+\nu}{2E} \left(\dfrac{4}{\nu+1} \times \dfrac{1}{r^2} - \dfrac{3}{r^4}\right),$

σ_x, σ_y = principal stresses present in the structure before drilling

α = angle between the directions of r and x,

E = Young's modulus,

ν = Poisson's ratio,

r $= \dfrac{D}{D_0}$ (see Figure 4.18)
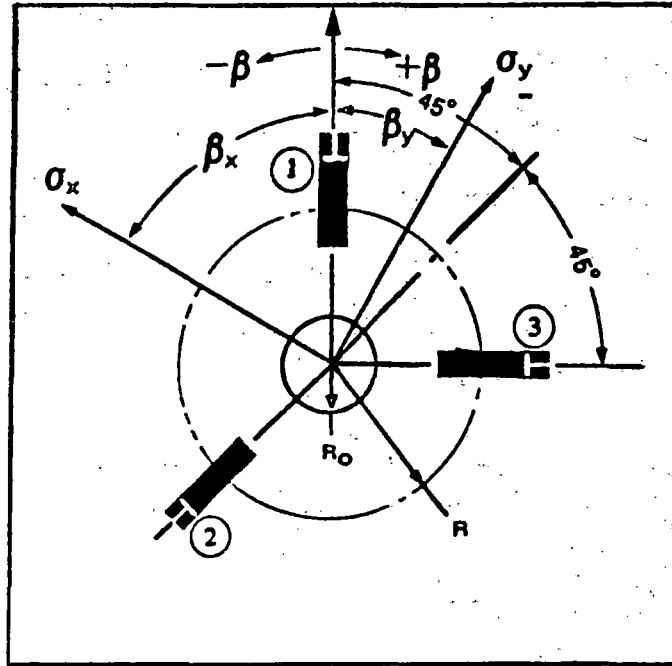
FIGURE 4.18   STRAIN GAGE ROSETTE ARRANGEMENT FOR DETERMINING
RESIDUAL STRESSES

D   = diameter of gage circle, and

D_0 = diameter of drilled hole

Measuring the relieved radial strain ϵ_1, ϵ_2, and ϵ_3 provides sufficient information to calculate the principal stresses σ_x and σ_y and their orientation, β, with respect to an arbitrary selected reference.

Solving for principal stresses and direction yields:

$$\sigma_x = \frac{\epsilon_1 + \epsilon_3}{4\,\bar{A}} + \frac{\sqrt{2}}{4\bar{B}}\sqrt{(\epsilon_1 - \epsilon_2)^2 + (\epsilon_2 - \epsilon_3)^2} \qquad (2)$$

$$\sigma_y = \frac{\epsilon_1 + \epsilon_3}{4\,\bar{A}} - \frac{\sqrt{2}}{4\bar{B}}\sqrt{(\epsilon_1 - \epsilon_2)^2 + (\epsilon_2 - \epsilon_3)^2} \qquad (3)$$

$$\tan 2\beta = \frac{\epsilon_1 - 2\epsilon_2 + \epsilon_3}{\epsilon_3 - \epsilon_1}$$

where $\bar{A}$ and $\bar{B}$ (both of which are negative) are determined from Figure 4.19. Equations (2) and (3) define the maximum (σ_x) and minimum (σ_y) principal stresses. Direction angle β is referenced to gage 1 where clockwise is positive (+) direction and:

$$\beta = \beta_x \quad \text{IF} \quad (\epsilon_1 + \epsilon_3)/2 < \epsilon_1$$

$$\beta = \beta_y \quad \text{IF} \quad (\epsilon_1 + \epsilon_3)/2 > \epsilon_1$$

$$\beta = 45° \quad \text{IF} \quad \epsilon_1 = \epsilon_3$$

$$\bar{A} = -\frac{1 + \mathcal{V}}{2E} \cdot \bar{a}$$

$$\bar{B} = -\frac{1}{2E} \cdot \bar{b}$$

The following graphs of Figure 4.19 are extracted from Technical Note TN-503-1 of Measurements Group Inc., Raleigh, North Carolina 27611.
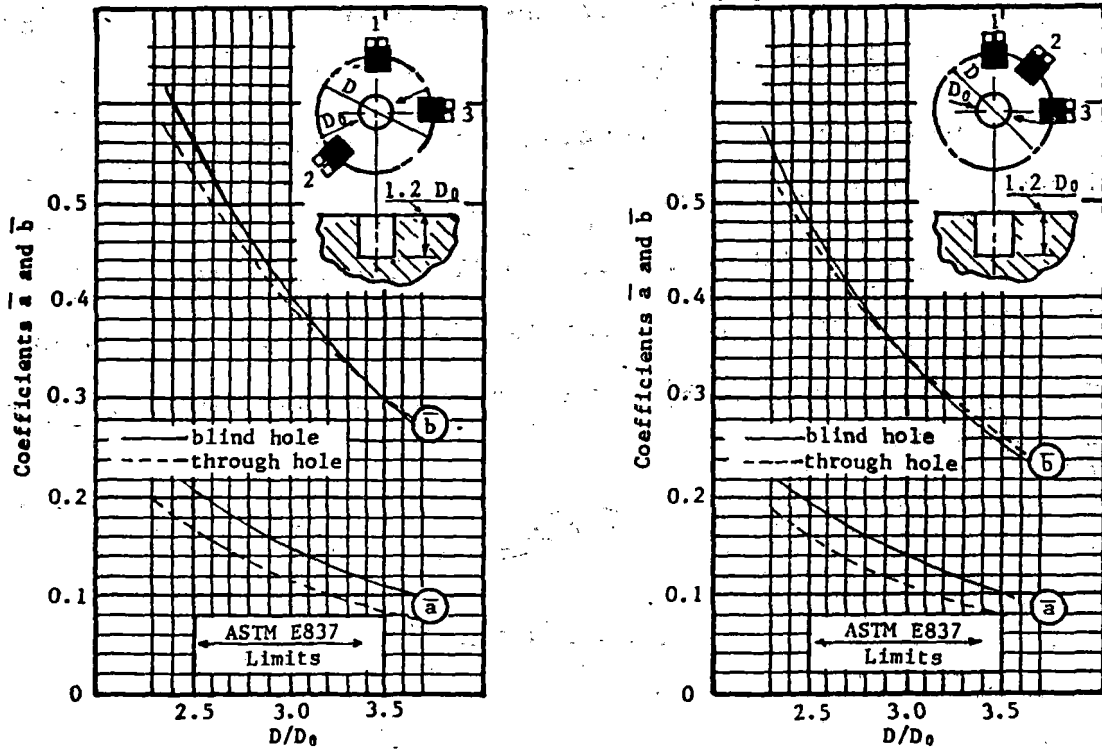
FIGURE 4.19   DATA REDUCTION COEFFICIENTS A AND B -VS- D/D$_O$.
LEFT GRAPH FOR UM GAGE, RIGHT GRAPH FOR RE & RK
GAGES

It is determined experimentally that when the depth of the hole equals the diameter, 100% of the strain is relieved and, thereafter, the change in the relieved strain is minimal. For our analysis, the calculated principal stresses at the point where depth equals diameter are regarded as the residual stresses at location B1.

Once σ_x and σ_y are determined, σ_1 and σ_2 (which can be hoop or radial stresses, depending on the orientation of gage #1 on the wheel) can be calculated from the Mohr Circle relationships:

$$\sigma_{1,2} = \frac{\sigma_x + \sigma_y}{2} \pm \frac{\sigma_x - \sigma_y}{2} \cos 2\beta \qquad \text{IF } \beta = \beta_x$$

$$\text{AND} \qquad \sigma_{1,2} = \frac{\sigma_x + \sigma_y}{2} \pm \frac{\sigma_y - \sigma_x}{2} \cos 2\beta \qquad \text{IF } \beta = \beta_y$$

Figures 4.20 and 4.21 show typical arrangements of the hole drilling-strain gaging method for railroad wheels.

A plate bending experiment was conducted in order to verify the accuracy of stresses obtained from the hole drilling method. In this test, a 5 1/2" x 15 x 9/16" steel plate was subjected to 4 point elastic bending with .08" displacement at the plate ends. Hole drillings were performed before and after the bending, and longitudinal and transverse strains resulting from the bending were measured on the surface of the plate midway between the ends. Surface stresses induced by the bending were then calculated using the following three independent methods:
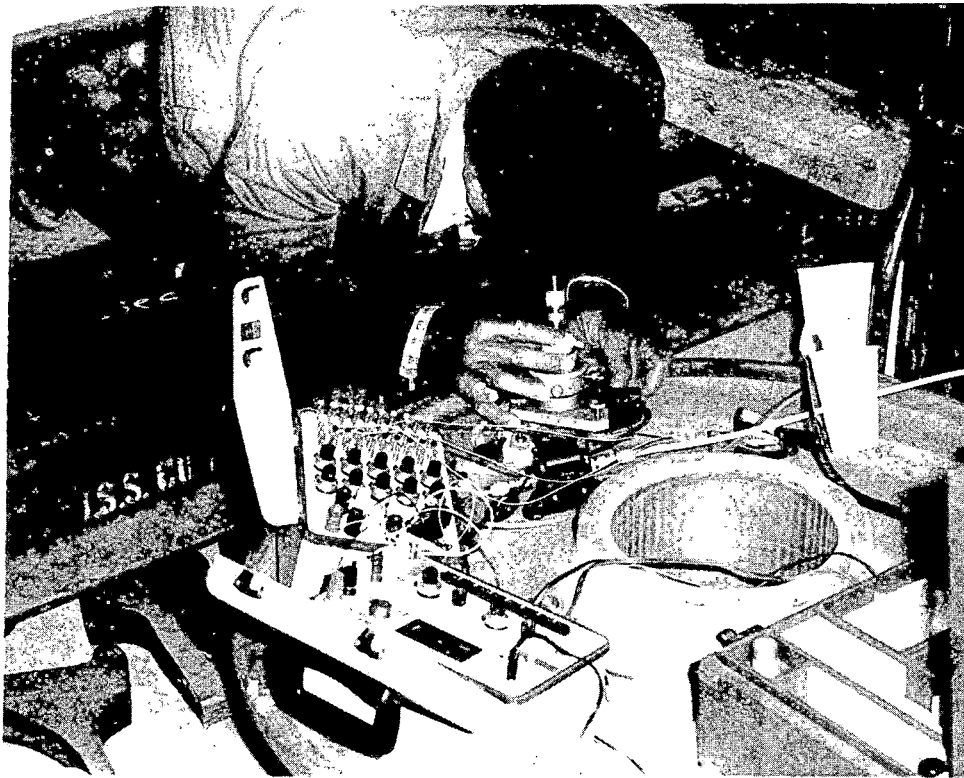
FIGURE 4.20   SETUP FOR HOLE DRILLING STRAIN GAGE METHOD TO
                EVALUATE RESIDUAL STRESSES IN RAILROAD WHEELS
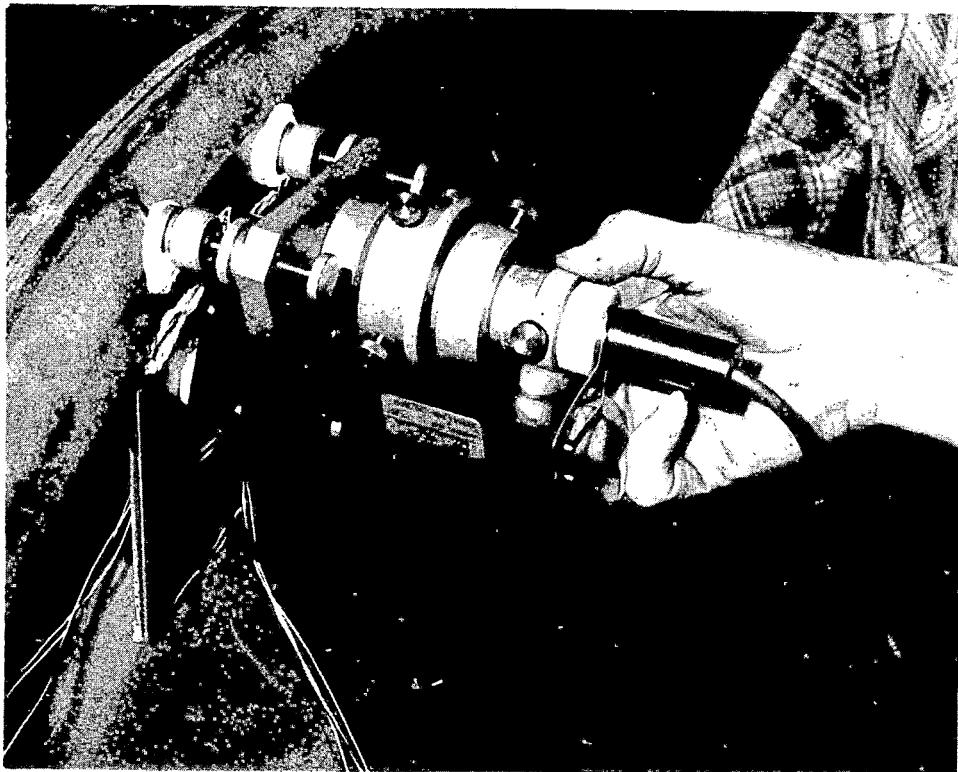
FIGURE 4.21   HOLE DRILLING UNIT SETUP ON BACK FACE RIM OF A
                WHEEL RESTING ON THE ROLL DYNAMICS UNIT AT PUEBLO

1. The hole drilling method.

2. Direct calculation of stresses from measured strains by assuming pure tension.

3. Theoretical estimation of the stresses based on the enforced displacements.

The stresses calculated from the hole drilling method showed good agreement with those calculated from measured strains and displacements. A detailed report of this experiment is given in Appendix 4.

4.5.4 Correlation Attempt Between Saw-Cut Displacement Behavior and Residual Stress Before the Saw-Cut at Selected Locations of the Wheel

Surface residual stress determination was used at selected locations for numerous wheels before the saw-cutting. The study presented here, refers to the correlation attempts made for a representative group of wheels (see Table 4.3) between the surface residual stresses at selected locations of the wheel and the saw-cut displacement behavior. See Figure 4.22 for the description of selected locations B1, B2, B3, and B4.

The results of the hole drilling-strain gaging method applied to measure the residual stresses at B1, B2, and B4 locations were obtained for the above group of wheels and these selected test wheels were saw-cut and individual wheel responses (in the hoop direction) to radial saw-cut were recorded with MTS clip gages as described under "Radial Saw-Cutting Procedure."

TABLE 4.3
GENERAL INFORMATION ABOUT SELECTED TEST WHEELS
FOR EXPERIMENTAL STRESS ANALYSIS

TTC ID	Mfg. Date	Serial No.	Class	Design	AAR Why Made Code	Discoloration
0009	78/02	42183	U	CH36	89	Yes
0010	78/02	45459	U	CH36	89	Yes
0011	80/03	61258	U	CH36	89	Yes
0031	82/02	24190	U	CH36	89	Yes
0046	76/10	4102	U	CH36	89	Yes
0047	82/03	61430	U	CH36	89	Yes
0051	75/10	51585	U	CH36	89	Yes
0054	75/10	51933	U	CH36	89	Yes
0070	64/09	18187	U	CJ36	--	No
0095	71/01	587204	C	CJ36	--	No

(0,0) ——

B1 ◯ + 0.32"
—— (0,0)

B2 ◯ — 3.02"

— 6.73" ◯ B3
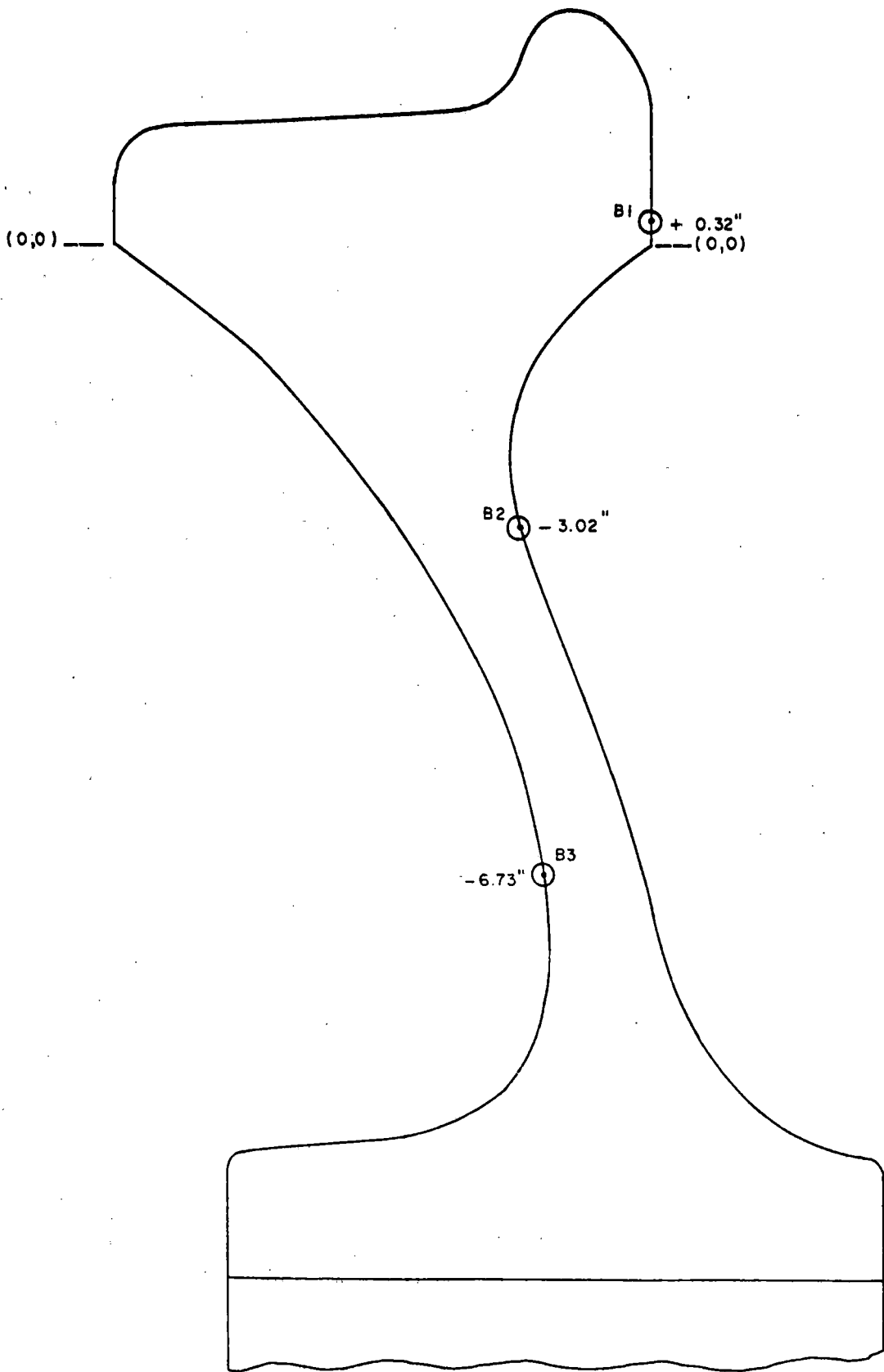
FIGURE 4.22   A TYPICAL 33 INCH (CURVED PLATE) TEST WHEEL,
SHOWING LOCATIONS (B1, B2, & B3) OF HIGH
TEMPERATURE STRAIN GAGES AND THERMOCOUPLES

Analysis of flange tip displacement (in the hoop direction) to saw-cutting at various depths of cut was carried out, and it was seen that at a given depth of cut, the flange tip displacement exhibited a certain relationship with the biaxial state of stress at B1, B2, and B4 locations, as measured by hole drilling-strain gaging method.

σ_H = Hoop Component of Residual Stress

σ_R = Radial Component of Residual Stress

Equivalent undirectional stress in the hoop direction, $\sigma = \sigma_H - \nu\sigma_R$.

It may be noted that hoop strain in a biaxial state of stress is given by $(1/\nu)(\sigma_H - \nu\sigma_R)$.

Figures 4.23 and 4.24 show the linear relationship between $\sigma = (\sigma_h - \nu\sigma_r)$ measured at the B1 location and flange tip displacement at 2 inches (51 mm) and 2.5 inches (64 mm) depth of cut, respectively.

In Figure 4.25 the average of values at B1 and B4 locations is plotted against the flange tip displacements at 2.5 inches (64 mm), 5.5 inches (140 mm), and 10 inches (254 mm) depth of cut for three test wheels. They also seem to hold a linear relationship.

Figure 4.26 presents the linear relationship between values measured at the B2 location, 5.5 inches (140 mm) radially down from flange tip for six test wheels and the corresponding
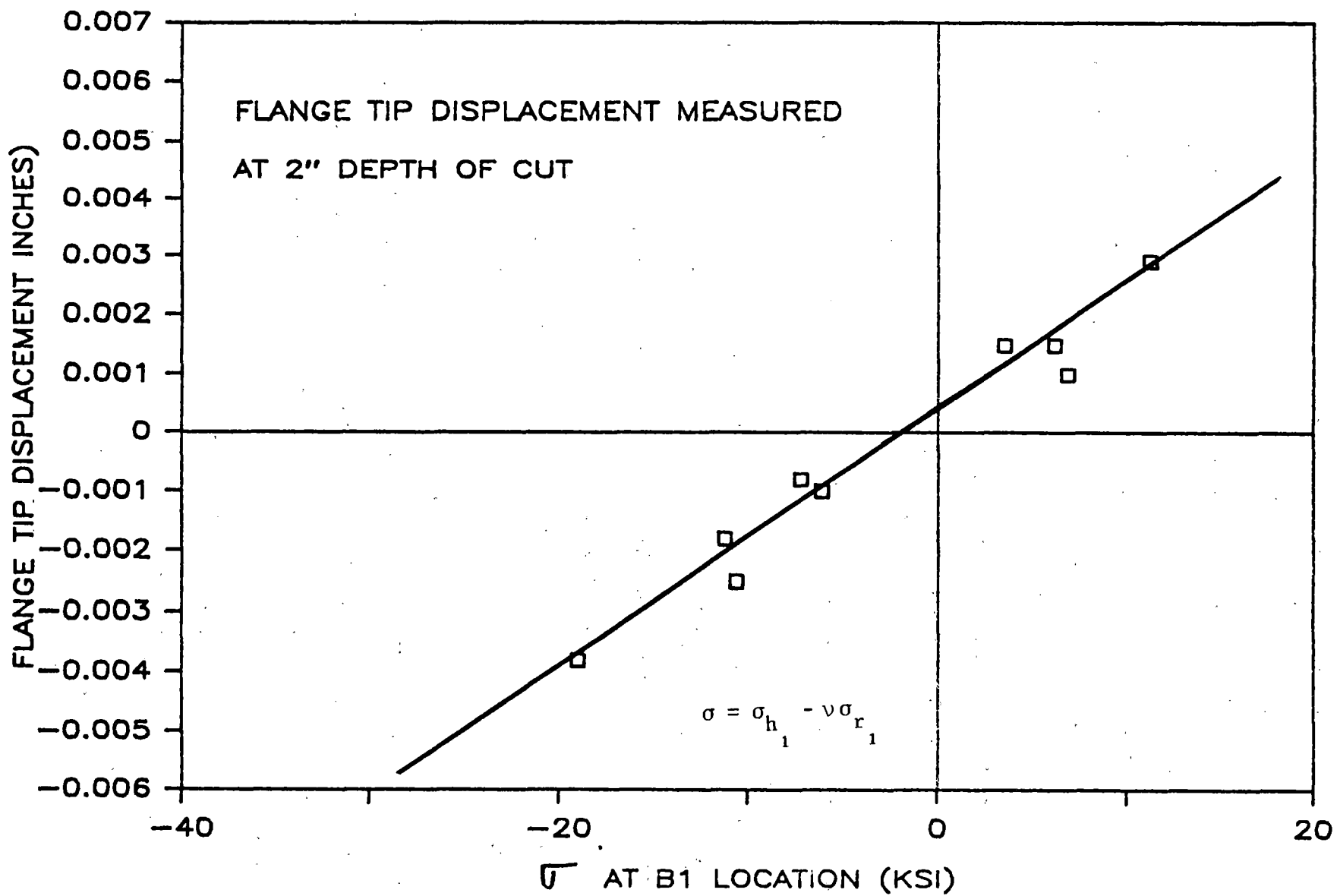
FIGURE 4.23   FLANGE TIP DISPLACEMENT AT 2 INCHES DEPTH OF CUT -VS- σ AT B1 LOCATION ($\sigma = \sigma_{h_1} - \nu\sigma_{r_1}$)
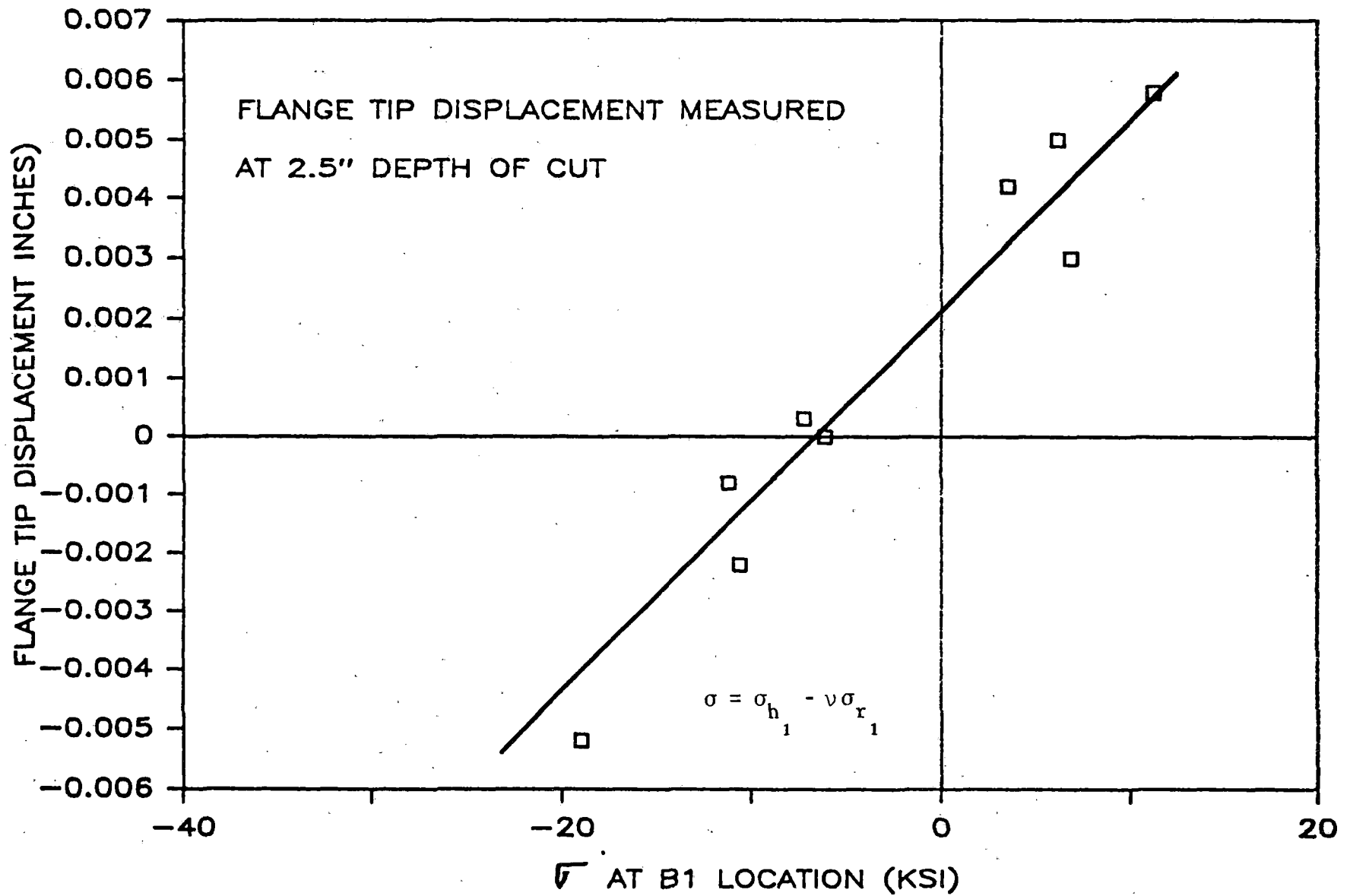
FIGURE 4.24   FLANGE TIP DISPLACEMENT AT 2.5 INCHES DEPTH OF CUT
-VS- σ AT B1 LOCATION ($\sigma = \sigma_{h_1} - \nu\sigma_{r_1}$)

FLANGE TIP DISPLACEMENT MEASURED
AT 2.5", 5.5", & 10" DEPTH OF CUT

□   = 2.5"
+   = 5.5"
◇   =10.0"

$$\sigma = \tfrac{1}{2} [(\sigma_{h_1} - \nu\sigma_{r_1}) + (\sigma_{h_4} - \nu\sigma_{r_4})]$$

AVERAGE σ AT B1 & B4 (KSI)
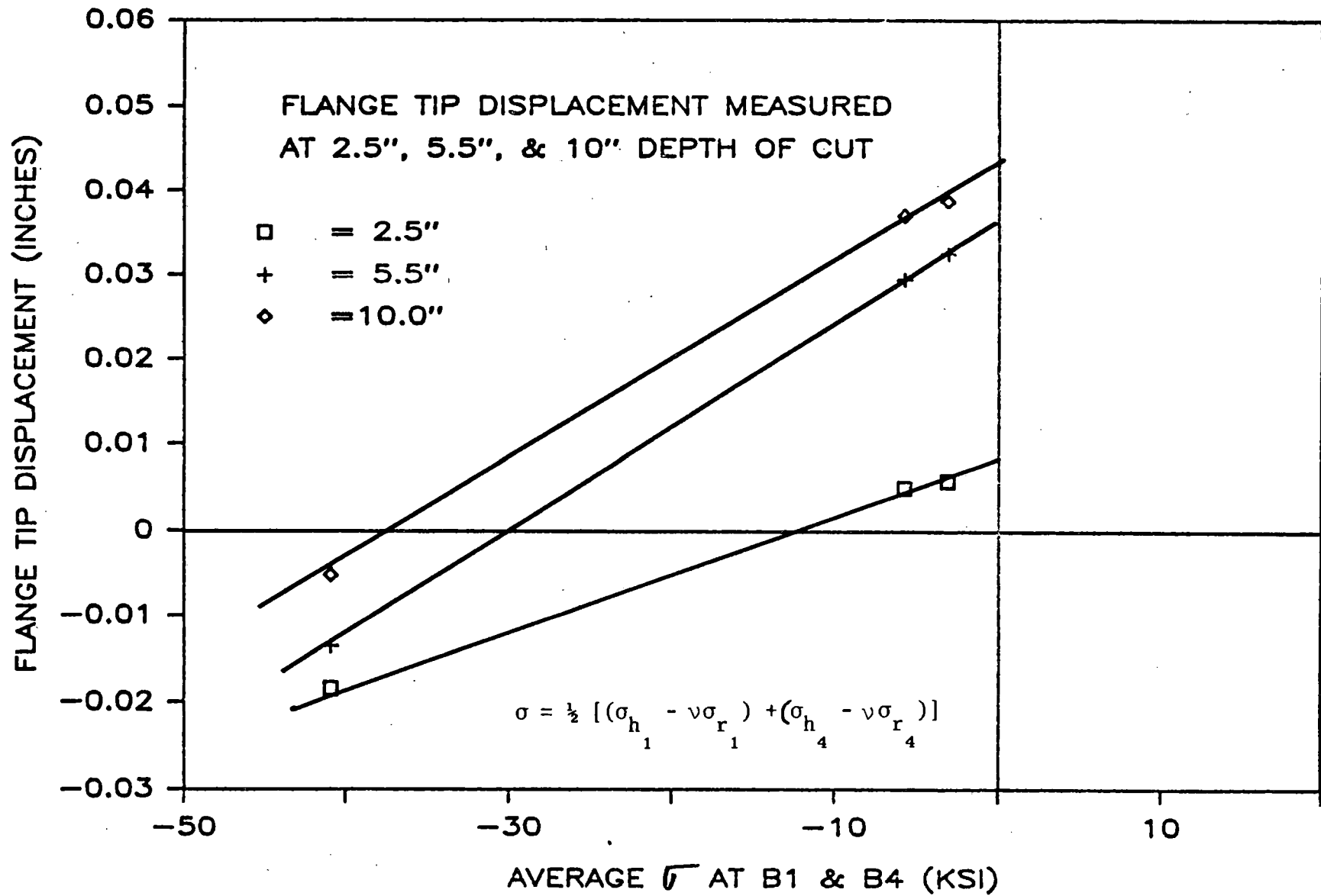
FIGURE 4.25   FLANGE TIP DISPLACEMENT AT 2.5 INCHES, 5.5 INCHES,
AND 10 INCHES DEPTH OF CUT -VS- AVERAGE OF σ VALUES
AT B1 AND B4 LOCATIONS

FLANGE TIP DISPLACEMENT
AT 5.5" DEPTH OF CUT

$\sigma = \sigma_{h_2} - \nu\sigma_{r_2}$

FIGURE 4.26   FLANGE TIP DISPLACEMENT AT 5.5 INCHES DEPTH OF CUT
-VS- σ AT B2 LOCATION ($\sigma = \sigma_{h_2} - \nu\sigma_{r_2}$)

flange tip displacement at 5.5 inches (140 mm) depth of cut. The same values are plotted against maximum flange tip opening during the saw-cutting operation in Figure 4.27 which is also a linear relationship.

This selective study showed that the response of the wheel to radial saw-cut (flange tip displacement in the hoop direction) at a given depth of cut has a linear relationship with equivalent uniaxial stress in the hoop direction at selected locations on the rim and rim fillet regions.

4.5.5 Data Base for Saw-Cutting Results

A data base was created as a means of storing characteristic flange tip displacement data for each of the wheels. A given flange tip displacement versus saw-cut depth plot was characterized by four variables as shown in Figure 4.28.

In addition to the measured values C.O.1, C.O.2, min, and max., the following information was entered into the table:

1. Plate shape (straight or curved), wheel design, and manufacturer

2. Amount of discoloration

3. Whether the wheel opened continuously, closed continuously, or exhibited a combination of both displacements

4. Residual stresses calculated from hole drilling (for selected wheels only)
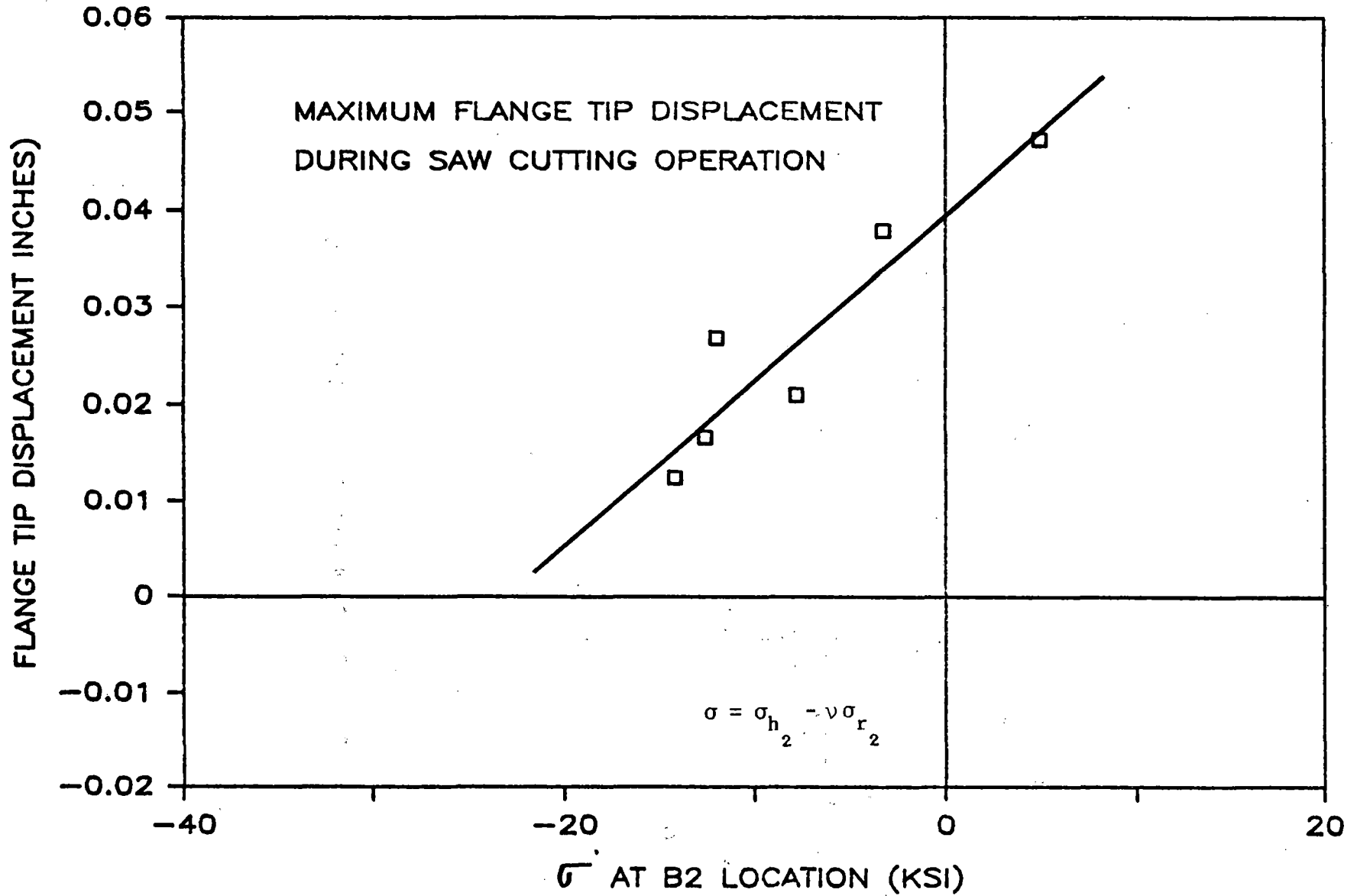
FIGURE 4.27   MAXIMUM FLANGE TIP DISPLACEMENT DURING SAW-CUT
OPERATION -VS- σ AT B2 LOCATION ($\sigma = \sigma_{h_2} - \nu \sigma_{r_2}$)
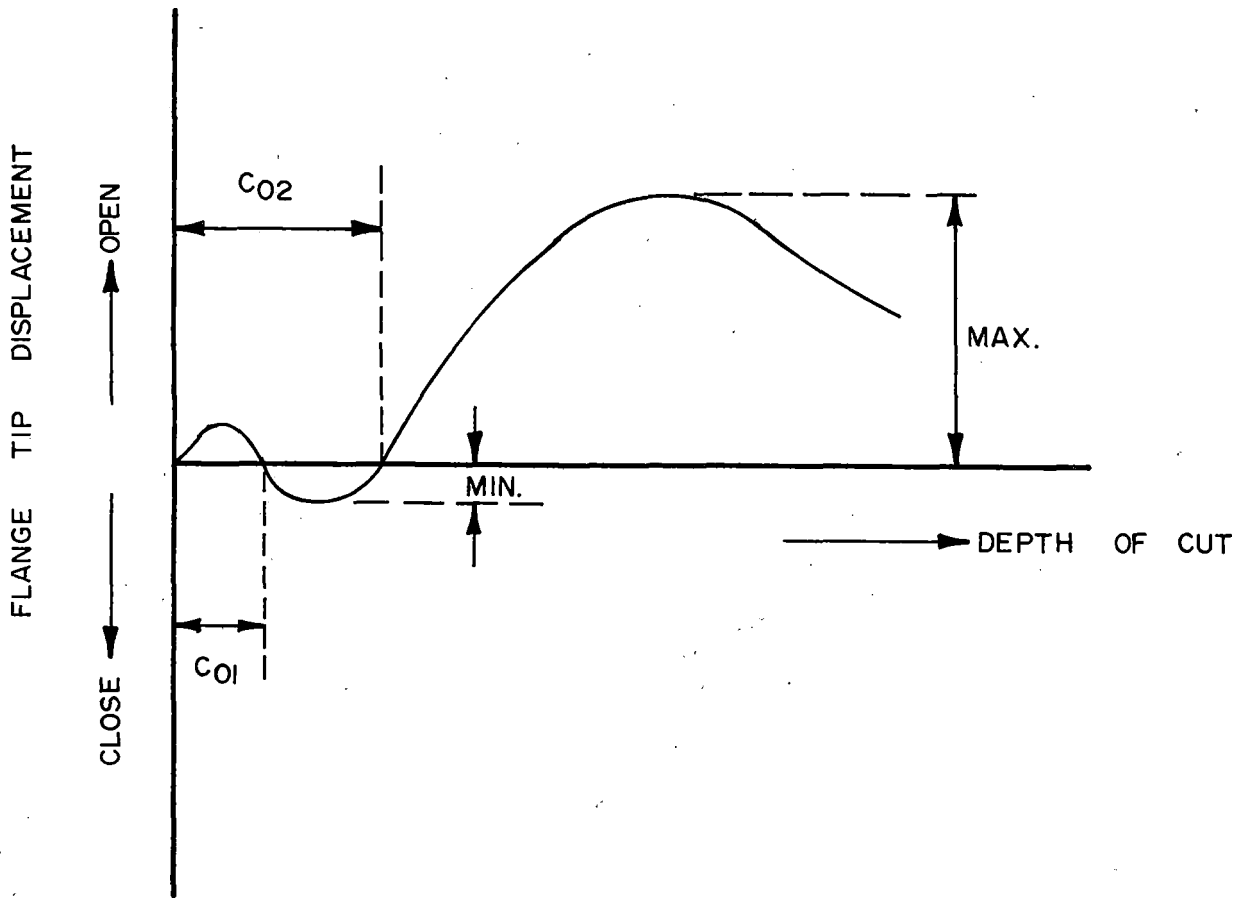
FIGURE 4.28   TYPICAL SAW-CUT DISPLACEMENT NOMENCLATURE

4-56

5. Calculated net "rim force" corresponding to the outer 3" of the rim. (For details, see the 'closed form solution for the interpretation of residual stress from saw-cut displacement data'.)

The complete data base is maintained at Pueblo. A representative sample of data base containing saw-cut information is presented in Appendix 4.3.

The classification of railroad wheels saw-cut at TTC, so far, is presented in Figure 4.29. The classification of railroad wheels whose saw-cut details are available in the data base at TTC, is presented in Figure 4.30. This includes wheels which are saw-cut at TTC as well as those saw-cut at participating railroad laboratories. This figure shows the logical classification of wheels in terms of class, design, and size. The next figure (Figure 4.31) shows the classification of saw-cut wheels into discolored and non-discolored types in each category of class, design, and size.

4.5.6 Saw-Cut Opening Analysis

The saw-cut displacement data obtained by radial saw-cutting of rail car wheels can be analyzed to obtain an indication of the magnitude and distribution of the residual stresses within a wheel. The saw-cut opening displacement curve by itself is not a good representation of the residual stresses in a wheel.

During the implementation of the Wheel Failure Mechanism Program, two different approaches were taken to evaluate the

```
┌─────────────────────────────────┐           ┌─────────────────────────────────┐
│ TOTAL NUMBER OF SAW-CUT          │           │ DETAILED SAW-CUT OPENING        │
│ WHEELS FOR WHICH INFORMATION     │           │ MEASUREMENTS WERE MADE ON       │
│ IS AVAILABLE AT TTC              │           │ 31 WHEELS FOR FINITE            │
│                                  │           │ ELEMENT ANALYSIS                │
│                                  │           │ ACCOMPLISHED BY 11TR1           │
│              614                 │           │                                 │
│                                  │           │                                 │
└─────────────────────────────────┘           └─────────────────────────────────┘


     SERVICE WHEELS                          TEST WHEELS
         552                                     62
```
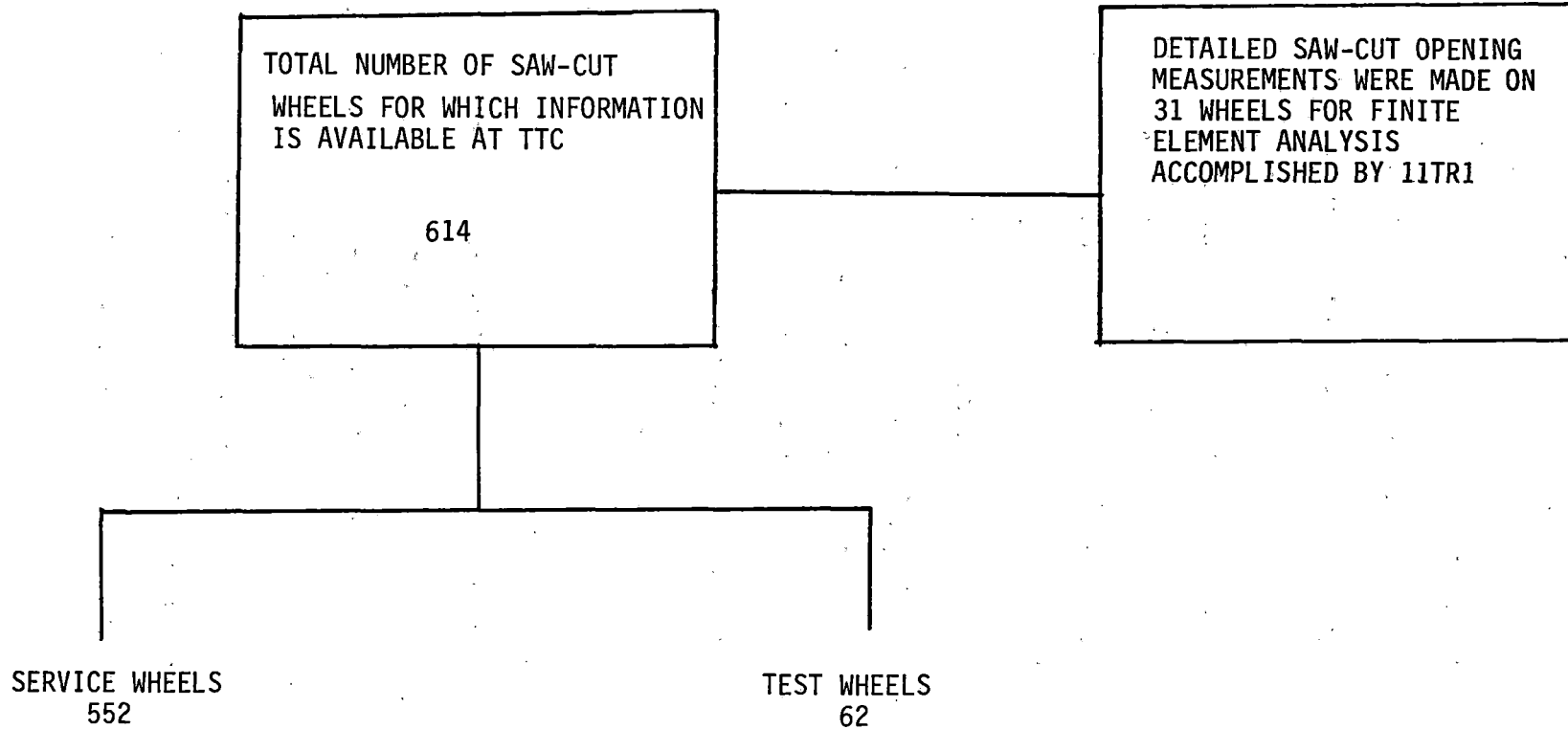
FIGURE 4.29   NUMBER OF SERVICE AND TEST WHEELS SAW-CUT AT TTC
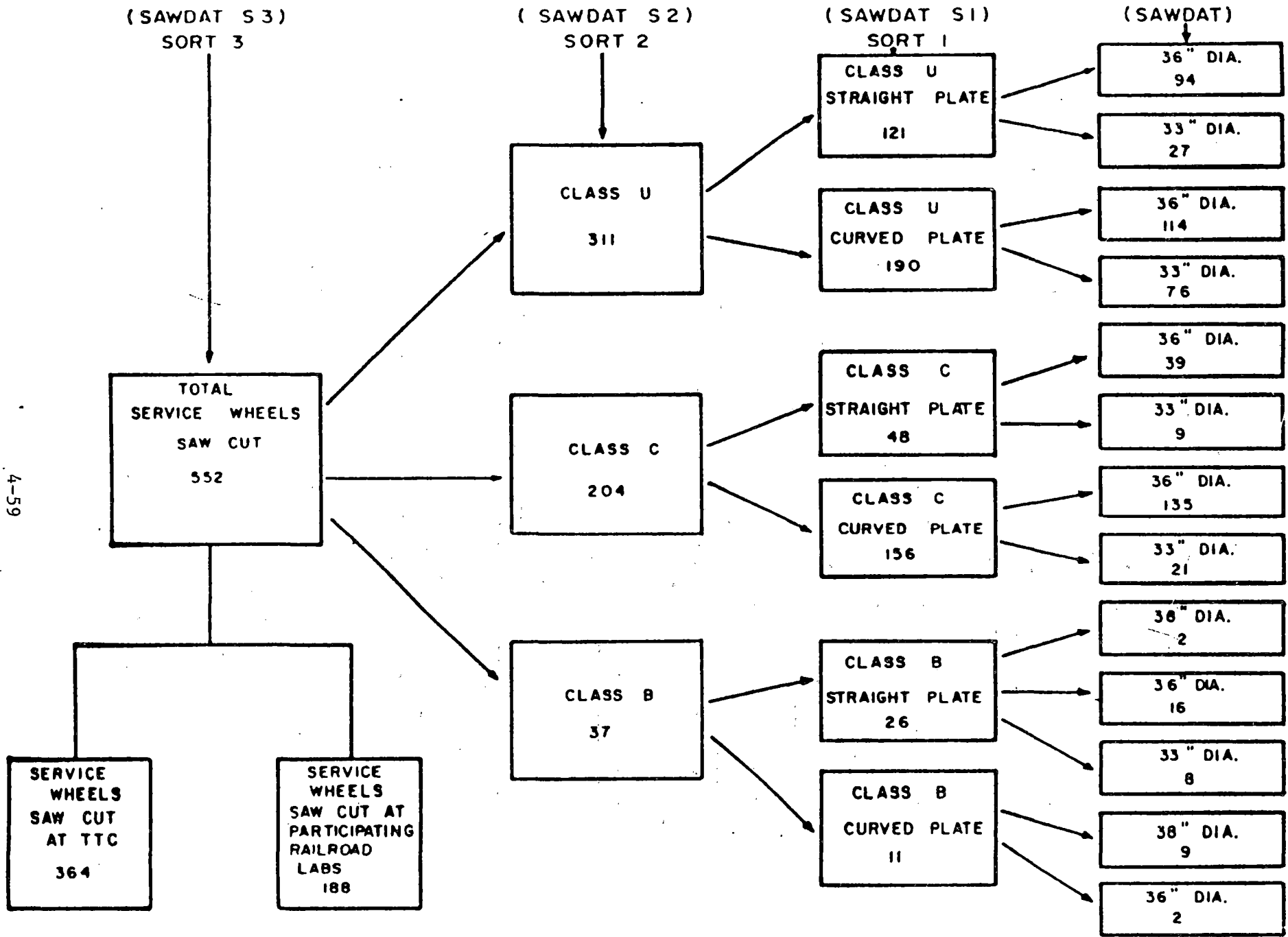
FIGURE 4.30   CLASSIFICATION OF SERVICE WHEELS USED IN SAW-CUTTING PROGRAM

4-59

SORT 4
(SAWDAT S4)

		OPEN	CLOSE	MIXED OPEN

CLASS U STRAIGHT PLATE, 36" — 94
- DISCOLORED (40) → 6 + 8 + 1 | 14 | 2 + 9
- NON-DISCOLORED (54) → 0 + 4 + 3 | 27 | 3 + 17

CLASS U STRAIGHT PLATE, 33" — 27
- DISCOLORED (8) → 0 + 1 + 0 | 5 | 1 + 1
- NON-DISCOLORED (19) → 1 + 3 + 0 | 12 | 0 + 3

CLASS U CURVED PLATE, 36" — 114
- DISCOLORED (66) → 4 + 20 + 2 | 8 | 8 + 23
- NON-DISCOLORED (48) → 0 + 8 + 1 | 6 | 5 + 19

CLASS U CURVED PLATE, 33" — 76
- DISCOLORED (17) → 0 + 3 + 0 | 1 | 3 + 10
- NON-DISCOLORED (59) → 0 + 2 + 0 | 27 | 1 + 29

CLASS C STRAIGHT PLATE, 36" — 39
- DISCOLORED (13) → 0 + 2 + 0 | 11 | ——
- NON-DISCOLORED (26) → 3 + 1 + 0 | 21 | 1 + 0

CLASS C STRAIGHT PLATE, 33" — 9
- DISCOLORED (0) → —— | —— | ——
- NON-DISCOLORED (9) → 0 + 1 + 0 | 4 | 0 + 4

CLASS C CURVED PLATE, 36" — 135
- DISCOLORED (131) → 0 + 2 + 0 | 115 | 5 + 9
- NON-DISCOLORED (4) → —— | 1 | 0 + 3

CLASS C CURVED PLATE, 33" — 21
- DISCOLORED (4) → —— | 4 | ——
- NON-DISCOLORED (17) → —— | 16 | 0 + 1

CLASS B STRAIGHT PLATE, 38", 36", 33" — 26
- DISCOLORED (5) → —— | 5 | ——
- NON-DISCOLORED (21) → 1 + 2 + 0 | 14 | 2 + 2

CLASS B CURVED PLATE, 38", 36", 33", 28" — 11
- DISCOLORED (6) → 0 + 0 + 1 | 4 | 1 + 0
- NON-DISCOLORED (5) → 0 | 5 | M

BROKEN   >0.02"   <0.02"   >0.02"   <0.02"

FIGURE 4.31   CLASSIFICATION OF SERVICE WHEELS USED IN SAW-CUTTING PROGRAM

4-60

residual stresses from the saw-cut displacement data. The first approach consisted of measuring the saw-cut opening displacement on both sides of the wheel along the entire length of a cut. A three-dimensional finite element analysis was performed to determine the stresses that result when the cut is closed. A circumferential displacement loading was assumed on the free surface. The stresses that are calculated for the plane of the cut are then an indication of the stresses that existed before the wheel was cut.

The second approach consisted of the development of a simple mathematical model for determining the average hoop stress distribution from the saw-cut displacement data.

The model assumes that the cut portion of the wheel consists of several interconnected rings. Using the reverse saw-cut displacement response, the rings are brought to their original position. During this process, stresses are developed on the interface of adjacent rings. The stresses required to bring the rings back to the original position are the original residual stresses and they depend on the displacement response as well as the stresses on the interface. Equations based on theory of elasticity are formulated for individual rings. The individual rings are then reconnected, generating in the process, the entire shear and hoop stress distribution along the radial cut. In the second approach, the results from the analysis were used to calculate the total circumferential force in the rim of the wheel and this force is suggested as a measure of the safety of the wheel.

Total rim forces were computed for all service wheels which exhibited an opening or mixed opening/closing flange tip displacement during the radial saw cutting procedure. Wheels which exhibited a monotonic closing displacement were assumed to have a negative rim force. The distribution of computed rim forces for all saw-cut service wheels is given in Table 4.4.

Figure 4.32 and 4.33 show the saw-cutting data segregated on the basis of net rim force for Class U and Class C wheels. These data show that heat-treatment is as effective as design in resisting thermal damage. Heat treatment appears to be more effective in curved plate wheels than in straight plate wheels.

An effective graphical method of presenting distribution information is cumulative probability plotting. Figure 4.34 presents the cumulative percentage of curved plate wheel population versus the net rim forces computed from the saw-cut displacement data.

Figure 4.35 presents the similar information for straight plate wheel population that were saw-cut.

As an example of the interpretation of these plots, consider the meaning of the straight line representing the Subgroup of straight plate, Class U, discolored wheels from Figure 4.35. We see that 73% of these wheels have a net rim force less than 100 Kips.

An estimate of the accuracy of the second method for predicting the rim force was made by comparing the results with

TABLE 4.4
DISTRIBUTION OF RIM FORCES FOR SAW-CUT SERVICE WHEELS

*TYPE/DISCOLORATION OF WHEEL
CODE: 1st digit - 1 = curved plate
                  2 = straight plate
       2nd digit - 1 = nondiscolored
                   2 - discolored

WHEELS CODE*/CLASS		TOTAL WHEELS	% OF WHEELS <0 kips	% OF WHEELS 0-100 kips	% OF WHEELS >100 kips	% WHEELS WHICH CRACKED DURING SAW-CUTTING
12	U	82	30.5	40.2	29.3	4.9
22	U	48	41.7	31.2	27.1	14.6
12	C	135	89.6	9.7	0.7	0
22	C	13	84.6	0	15.4	0
12	B	6	66.7	33.3	0	0
11	U	108	51.9	45.3	2.8	0
21	U	73	67.1	24.7	8.2	1.4
11	C	21	95.2	4.8	0	0
21	C	35	74.3	14.3	11.4	8.6
21	B	21	66.7	19.0	14.3	4.8
22	B	5	100.0	0	0	0
11	B	5	100.0	0	0	0

Class C, Discolored, Straight Plate
Net Rim Force (KIPS)
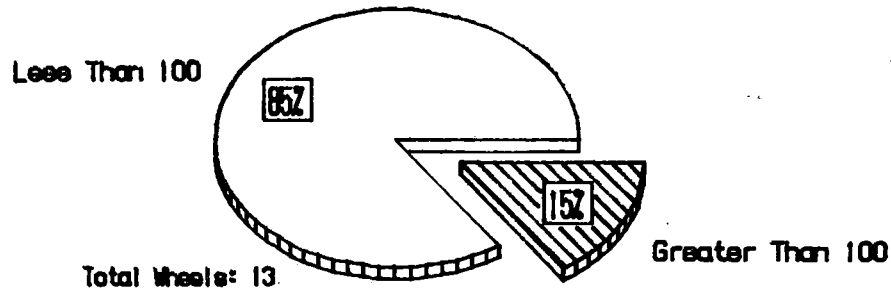
Less Than 100

85%

Total Wheels: 13

15%

Greater Than 100

Class C, Discolored, Curved Plate
Net Rim Force (KIPS)

99%

1%

Greater Than 100

Less Than 100

Total Wheels: 136

Class C, Nondiscolored, Straight Plate
Net Rim Force (KIPS)

Less Than 100

81%

8%

11%

Fractured

Total Wheels: 35

Greater Than 100

Class C, Nondiscolored, Curved Plate
Net Rim Force (KIPS)

100%

Less Than 100

Total Wheels: 21
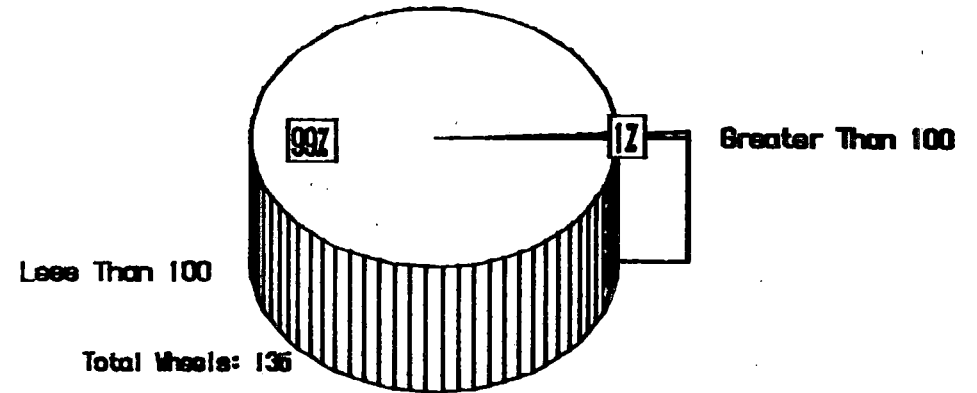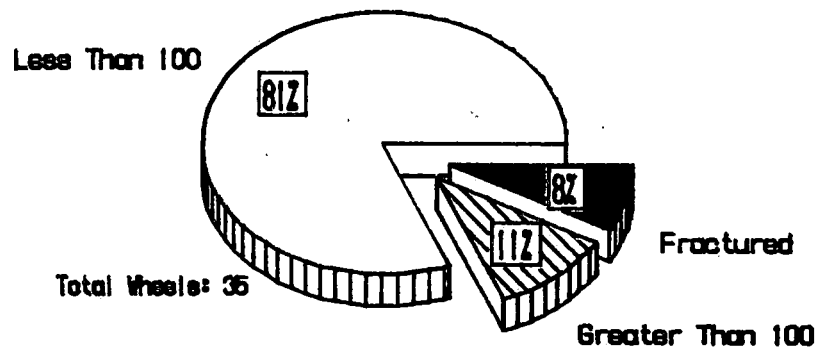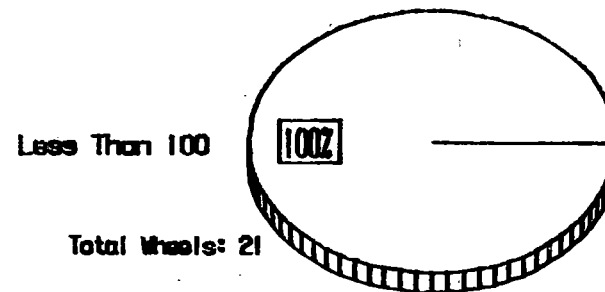
FIGURE 4.32   NET RIM FORCE BEHAVIOR OF CLASS C WHEELS FROM RAILROAD SERVICE

Class U, Discolored, Straight Plate
Net Rim Force (KIPS)
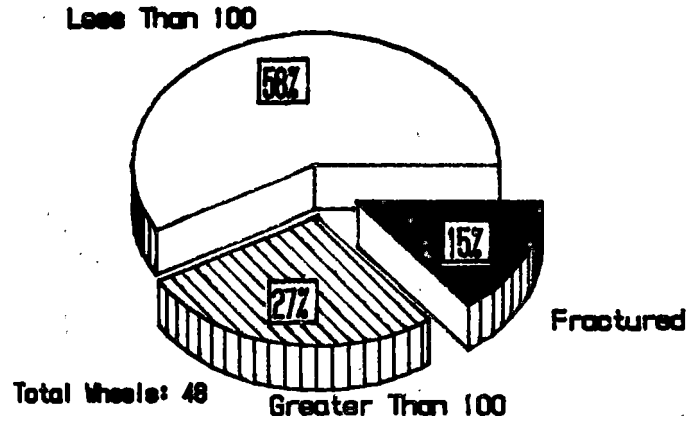
Less Than 100

58%

15%

27%

Fractured

Total Wheels: 48   Greater Than 100

Class U, Discolored, Curved Plate
Net Rim Force (KIPS)

Less Than 100

66%

5%

28%

Fractured

Total Wheels: 82

Greater Than 100

4-65

Class U, Nondiscolored, Straight Plate
Net Rim Force (KIPS)

Less Than 100

90%

1%

8%

Fractured

Greater Than 100

Total Wheels: 73

Class U, Nondiscolored, Curved Plate
Net Rim Force (KIPS)

Less Than 100

97%

3%

Greater Than 100

Total Wheels: 108
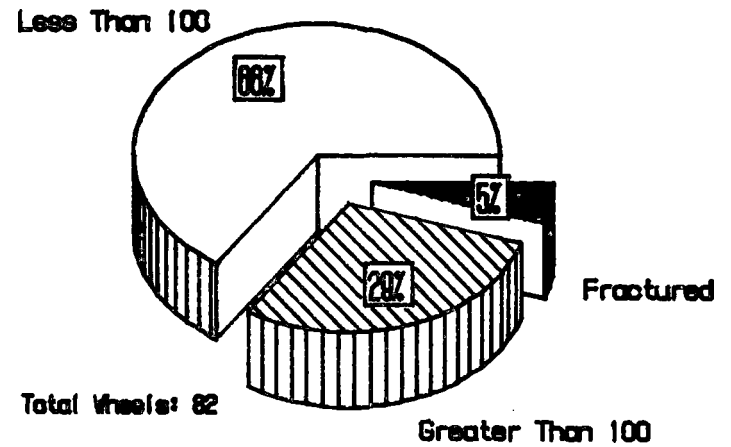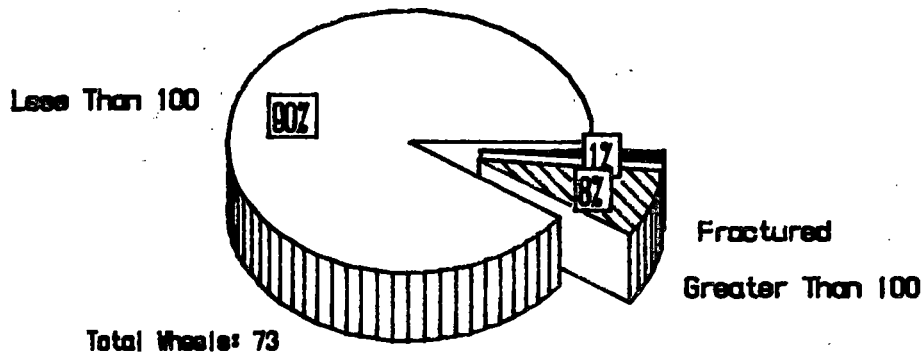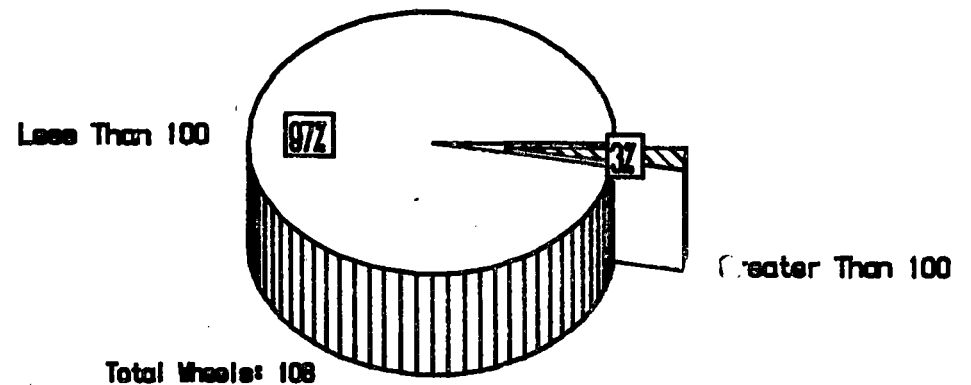
FIGURE 4.33   NET RIM FORCE BEHAVIOR OF CLASS U WHEELS FROM RAILROAD SERVICE
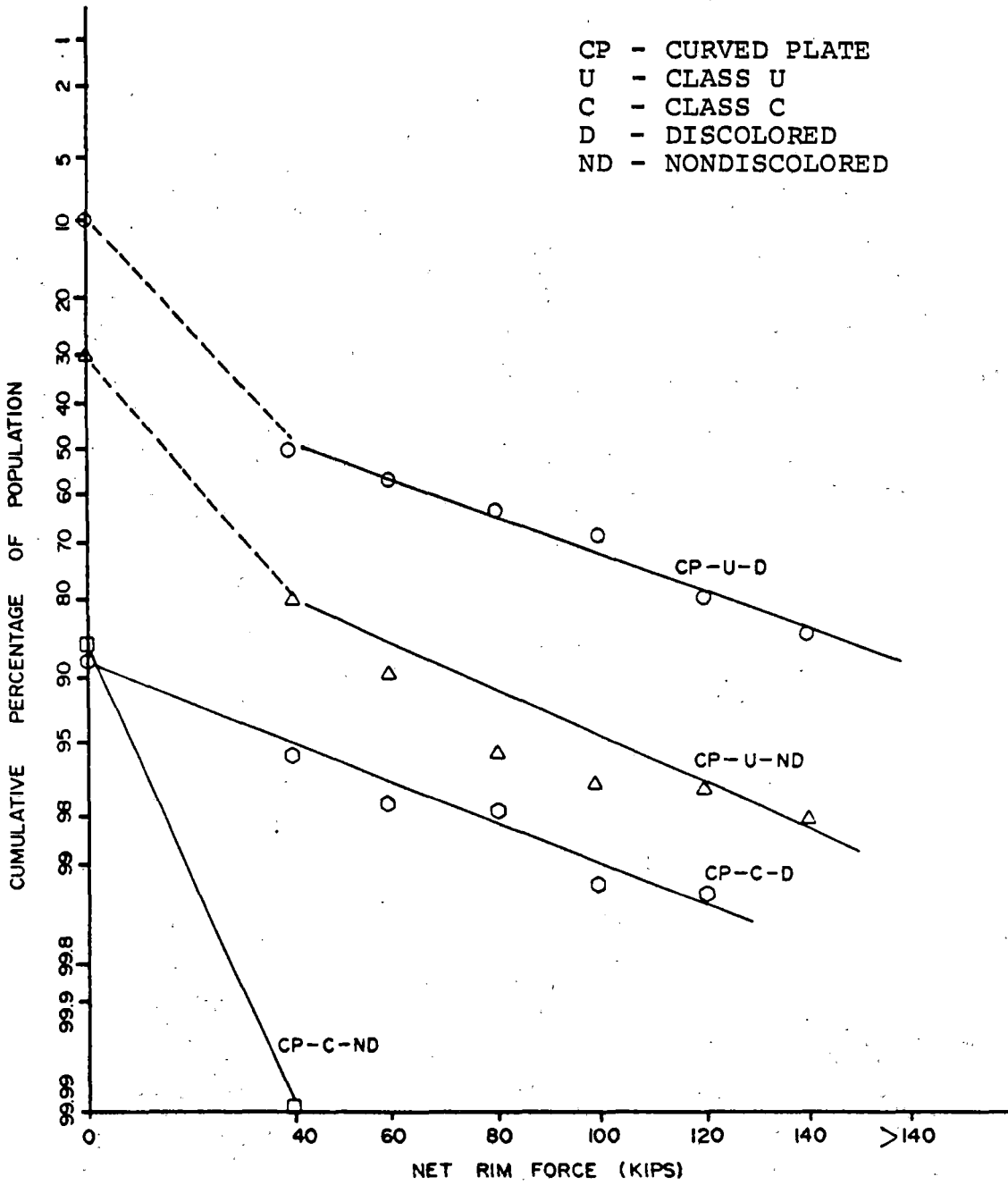
FIGURE 4.34 CUMULATIVE PERCENTAGE OF CURVED PLATE (SERVICE) WHEEL POPULATION VERSUS NET RIM FORCES COMPUTED FROM SAW-CUT DISPLACEMENT DATA
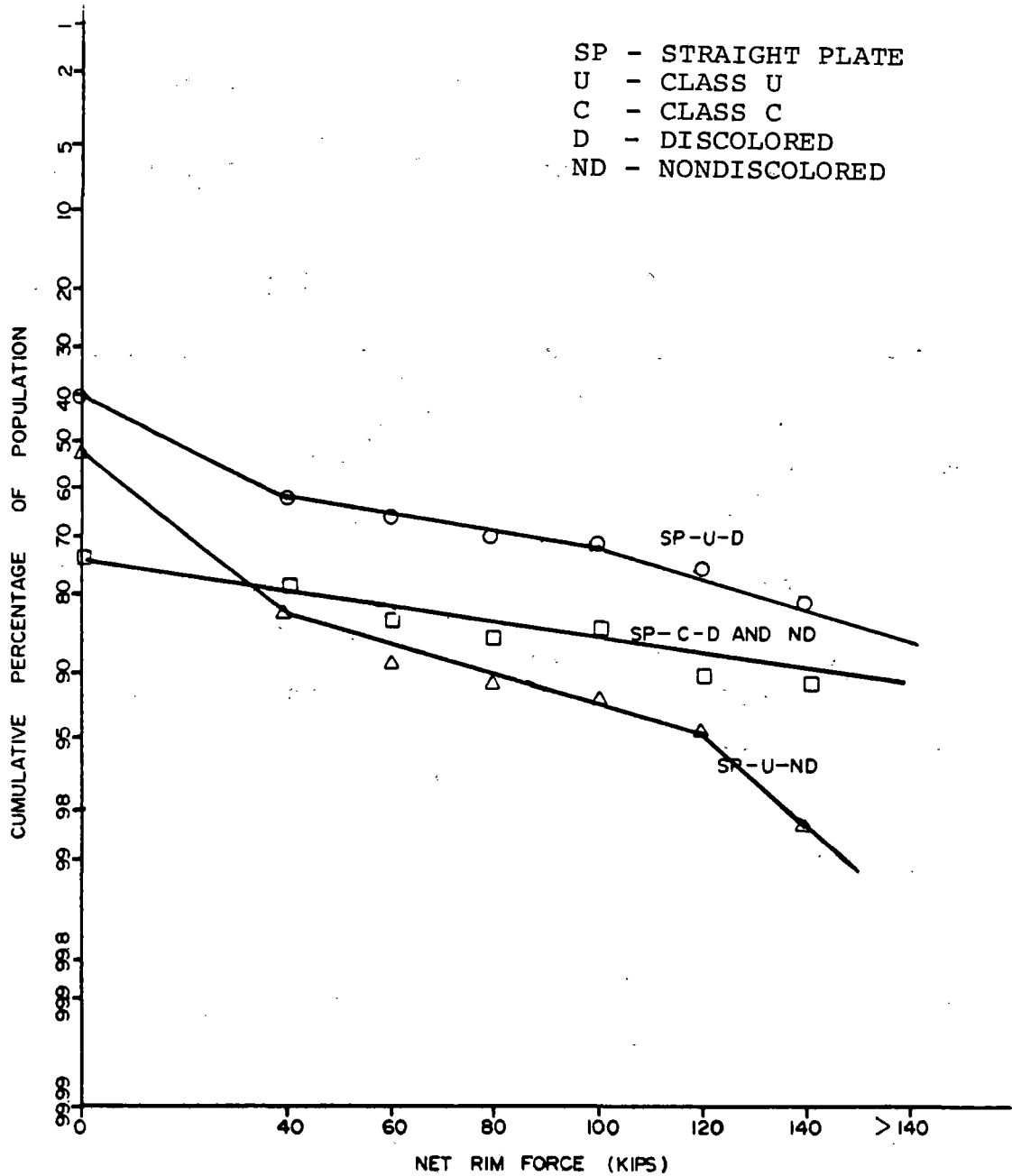
FIGURE 4.35 CUMULATIVE PERCENTAGE OF STRAIGHT PLATE (SERVICE) WHEEL POPULATION VERSUS NET RIM FORCES COMPUTED FROM SAW-CUT DISPLACEMENT DATA

TABLE 4.5
COMPARISON OF NET RIM FORCE COMPUTED FROM 3-D
FINITE ELEMENT ANALYSIS AND 2-D CLOSED FORM ANALYSIS

Wheel No.	Type	Class	Net Rim Force	
			3-D F.E. Analysis (Kips)	2-D Closed Form Analysis (Kips)
29	CH36	U	+156.5	+152.0
156	CJ33	U	+ 22.5	+ 18.0
30	CH36	U	+163.5	+167.0
72	H36	U	+ 43.2	+ 49.0
21	CH36	U	+ 72.5	+ 69.0
16	CH36	U	+ 15.3	+ 14.0
57	CH36	U	+ 4.6	- 10.0

those from a 3D-finite element analysis. The results were surprisingly close, as shown in Table 4.5, with the promise that the second method, though simple, does give reasonably accurate predictions of rim force.

Detailed presentations of saw-cut analysis by both the 3D-finite element analysis and simple analytical model are made in Section 11.0.

Illustration of a Rating Basis

After ascertaining the net rim forces for all the saw-cut wheels, analysis was performed for four types of responses (closed type, opened and mixed type, opened type, and fractured type) by prescribing three families of rating points which are described under Case I, Case II and Case III in Figures 4.36, 4.38, and 4.40, respectively.

The saw-cut wheels are divided into 12 categories as shown in Table 4.6. For each category of wheels that were saw-cut, the rating points are computed based on the net rim force levels and these results are presented in Figures 4.37, 4.39, and 4.41.

The most dominant category with the maximum performance rating is found to be for the curved plate, Class C wheel. The most dominant category with the minimum performance rating is found to be the discolored, Class U, curved or straight plate. It may be noted that in all but one order of ranking (wheel type 6 and 9 ranking), the relative performance rating of a given wheel category is found to be the same.

TABLE 4.6

	DESIGN CATEGORY	CLASS	DISCOLORATION DETAIL
1	CURVED	U	DISCOLORED
2	STRAIGHT	U	DISCOLORED
3	CURVED	C	DISCOLORED
4	STRAIGHT	C	DISCOLORED
5	CURVED	B	DISCOLORED
6	CURVED	U	NONDISCOLORED
7	STRAIGHT	U	NONDISCOLORED
8	CURVED	C	NONDISCOLORED
9	STRAIGHT	C	NONDISCOLORED
10	STRAIGHT	B	NONDISCOLORED
11	STRAIGHT	B	DISCOLORED
12	CURVED	B	NONDISCOLORED

CASE I

(Net rim force < 0 kips)
Y = 1.8 X − 80

Y = 0.2X
(0 < X < 50)

Y = 10 − 0.2 X
(Net rim force < 100 kips)

% WHEELS BY
CATEGORY

RATING POINTS

(Net rim force > 100 kips)
Y = − 2X

FRACTURED
Y = − 10X
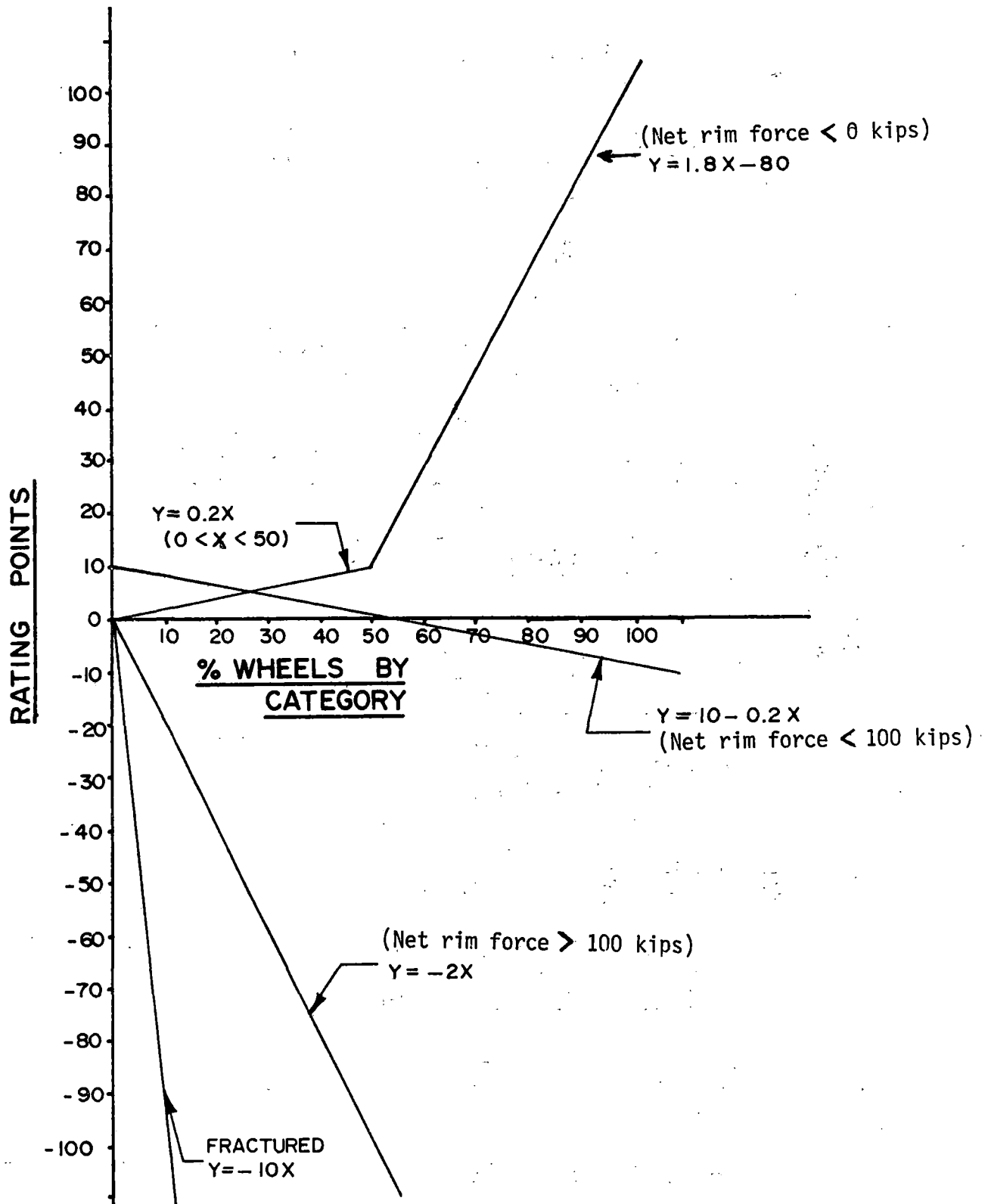
FIGURE 4.36   FIRST RATING OF FOUR TYPES OF SAW-CUT RESPONSES

4-71
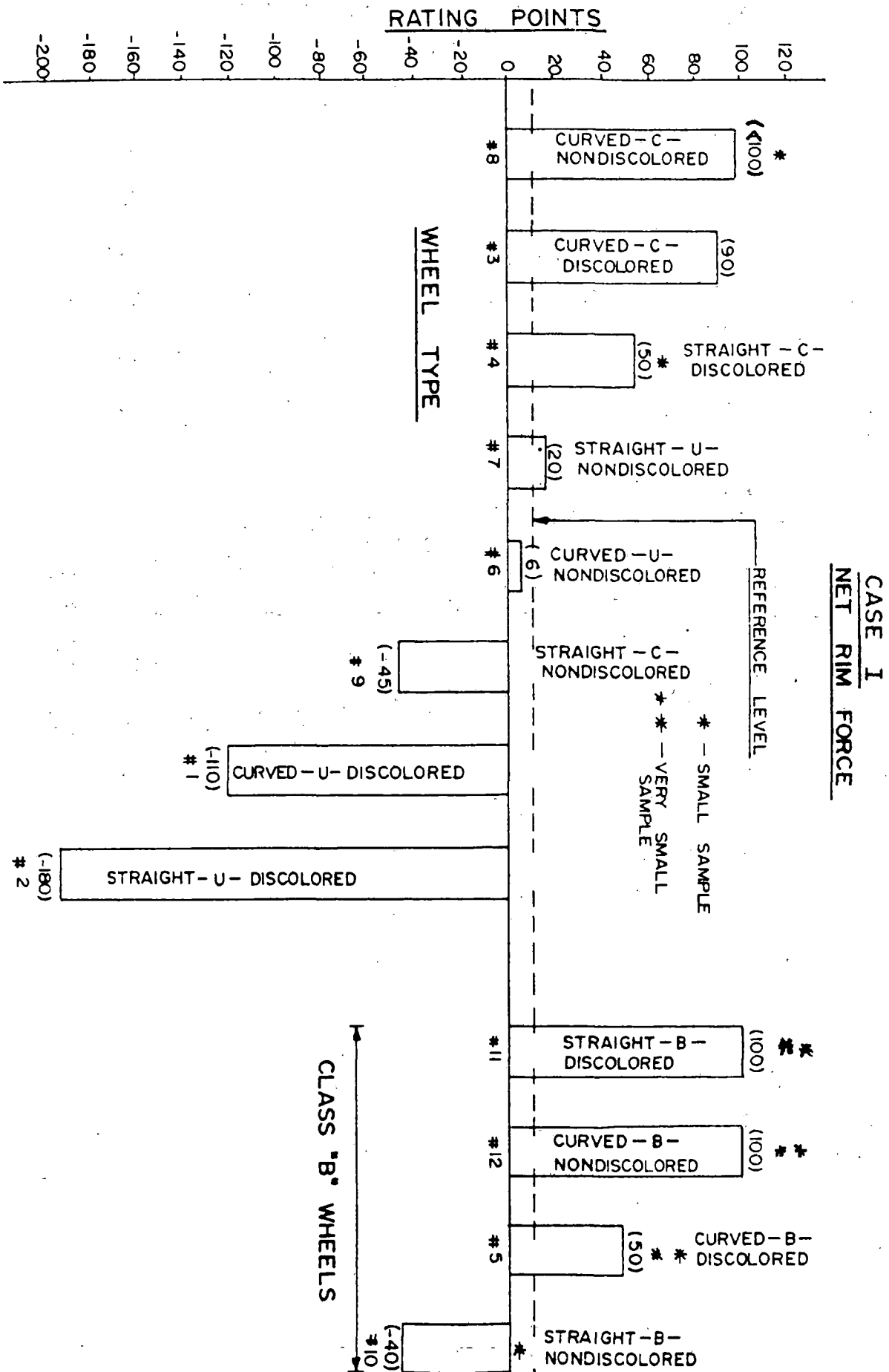
FIGURE 4.37   PERFORMANCE OF DIFFERENT WHEEL CATEGORIES ACCORDING TO FIRST RATING

4-72

CASE II

RATING POINTS

% WHEELS BY CATEGORY

Y = X
(Net rim force < 0 kips)

Y = 50 — X
(Net rim force < 100 kips)

Y = -X
(Net rim force > 100 kips)

Y = —2X
(FRACTURED)
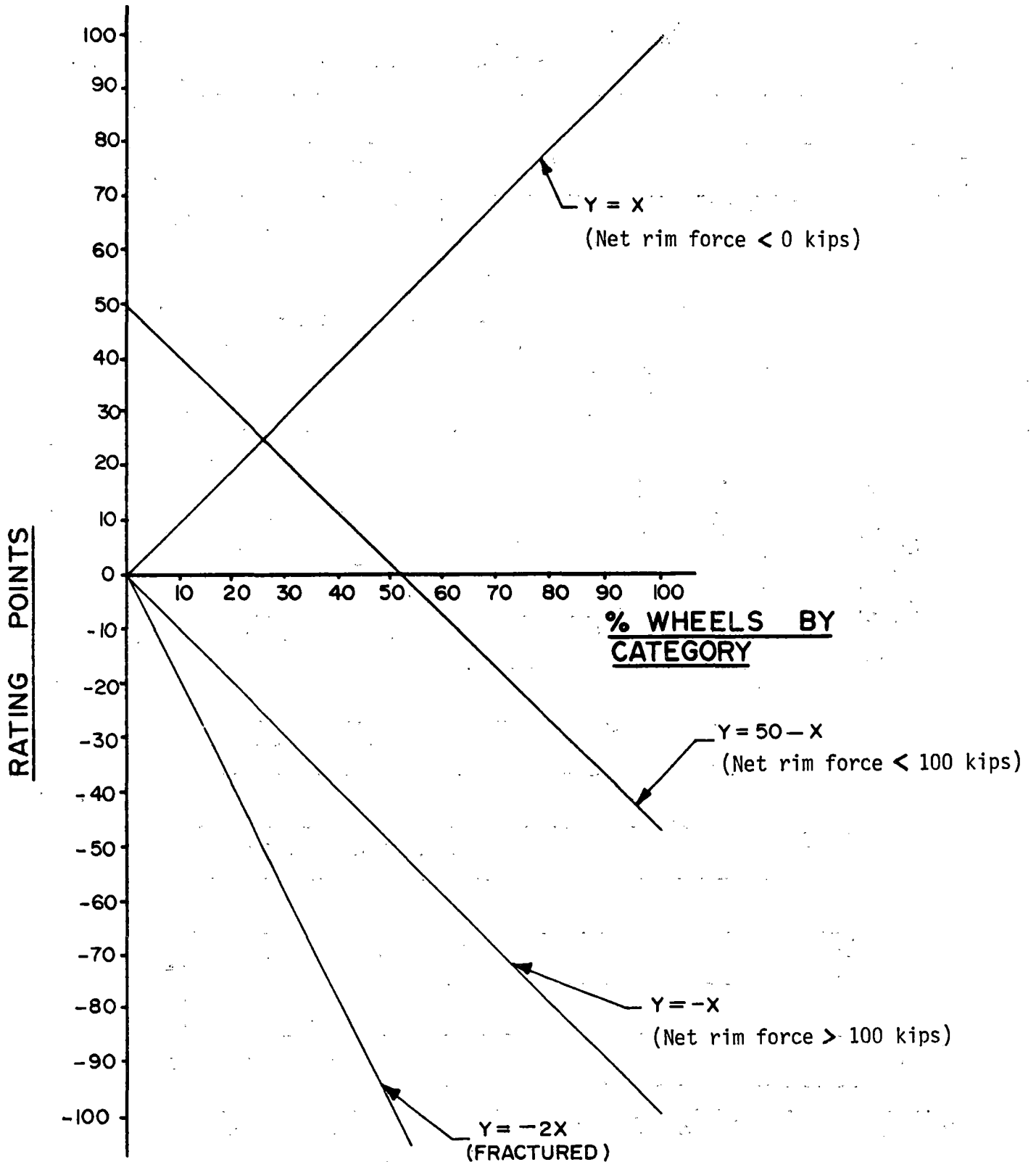
FIGURE 4.38   SECOND RATING OF FOUR TYPES OF SAW-CUT RESPONSES

4-73

RATING POINTS
4-74

#	Wheel Type	Rating
#8	CURVED – C – NONDISCOLORED *	(140)
#3	CURVED – C – DISCOLORED	(130)
#4	STRAIGHT – C – DISCOLORED *	(120)
#7	STRAIGHT – U – NONDISCOLORED	(85)
#9	STRAIGHT – C – NONDISCOLORED	(80)
#6	CURVED – U – NONDISCOLORED	(55)
#1	CURVED – U – DISCOLORED	(8)
#2	STRAIGHT – U – DISCOLORED	(7)
#12	CURVED – B – NONDISCOLORED **	(150)
#11	STRAIGHT – B – DISCOLORED **	(150)
#5	CURVED – B – DISCOLORED **	(85)
#10	STRAIGHT – B – NONDISCOLORED *	(80)

CASE II
NET RIM FORCE

* – SMALL SAMPLE
** – VERY SMALL SAMPLE

REFERENCE LEVEL

WHEEL TYPE

CLASS "B" WHEELS

FIGURE 4.39   PERFORMANCE OF DIFFERENT WHEEL CATEGORIES ACCORDING TO SECOND RATING

CASE III
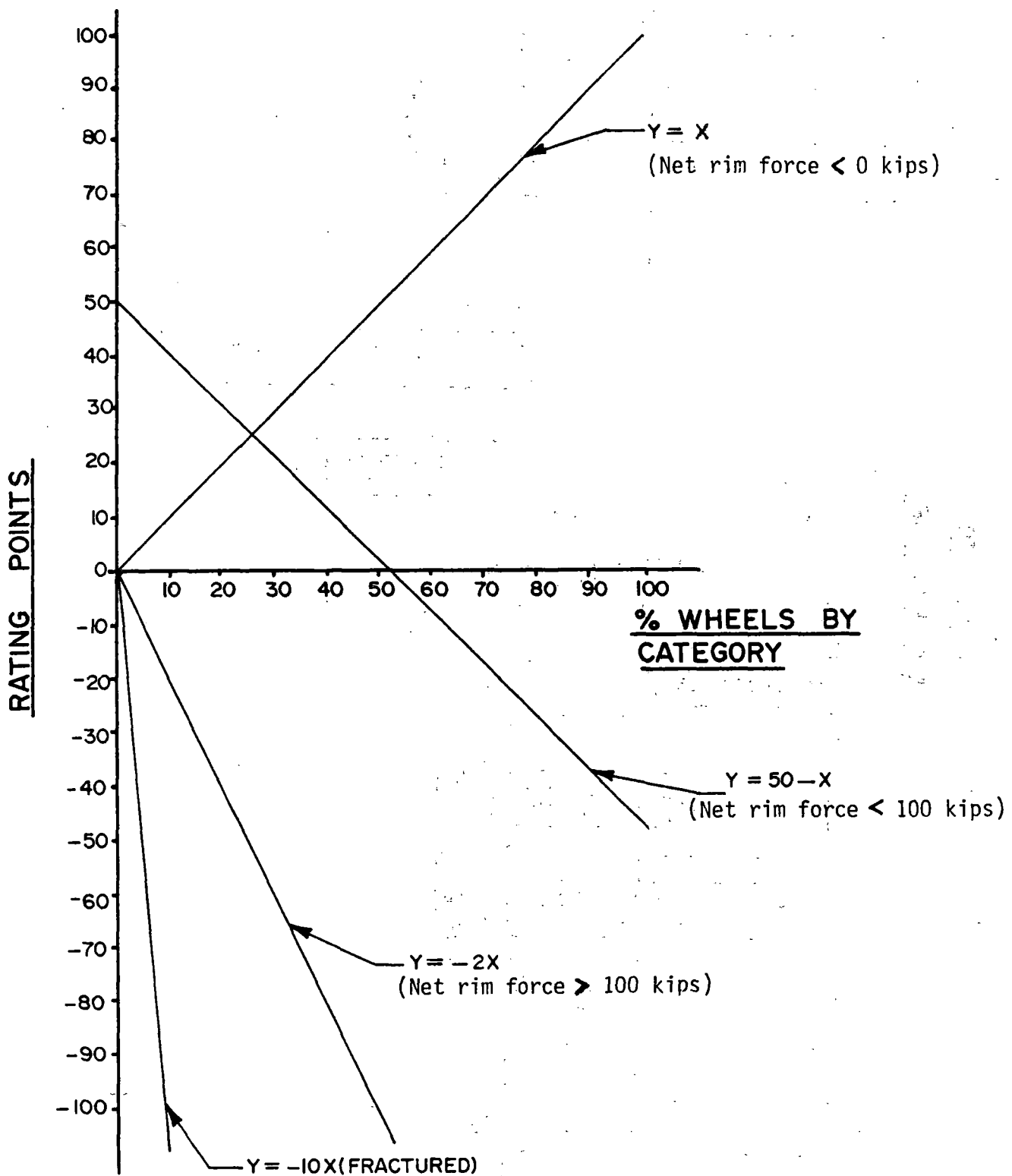
FIGURE 4.40 THIRD RATING OF FOUR TYPES OF SAW-CUT RESPONSES

4-75
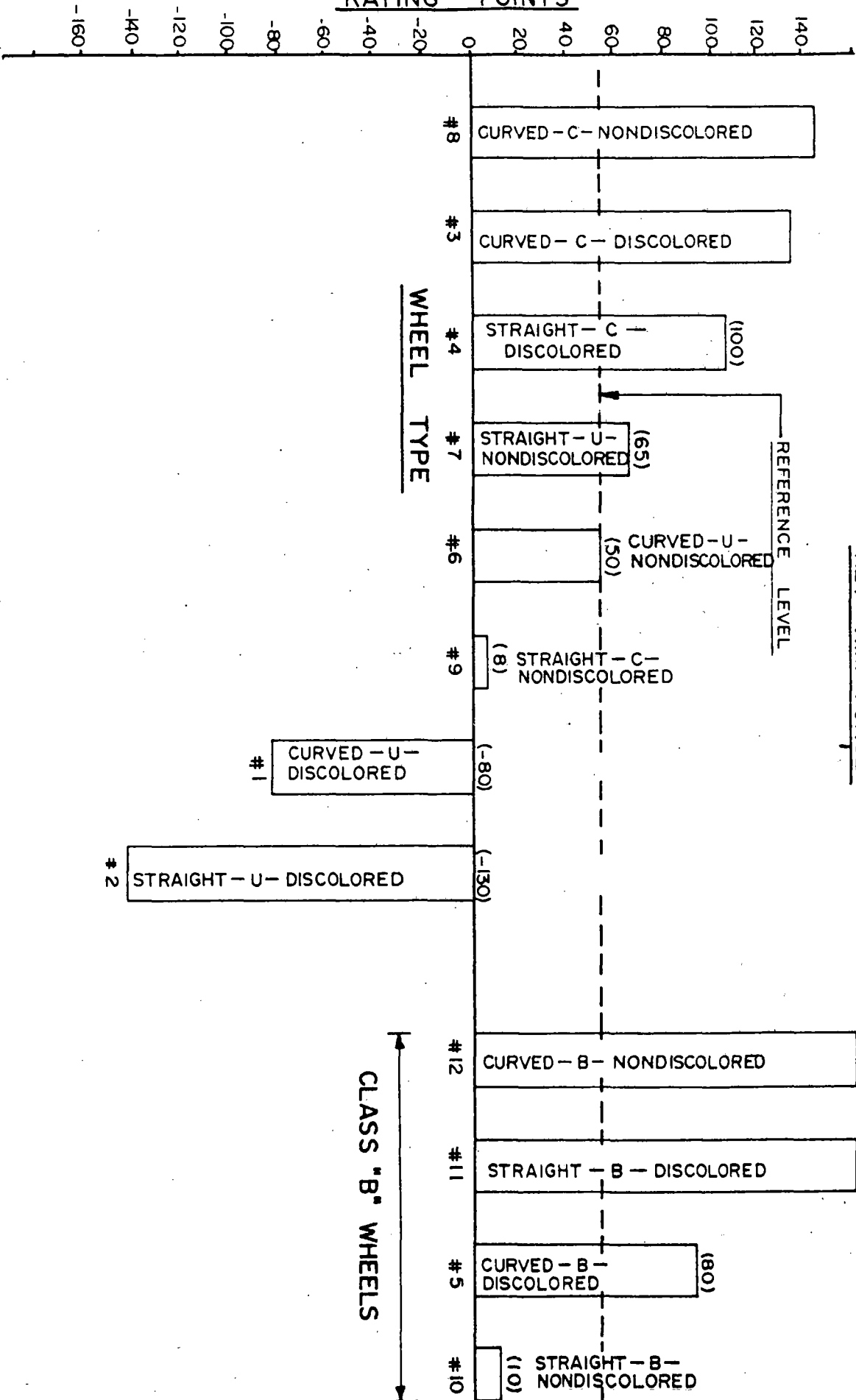
FIGURE 4.41 PERFORMANCE OF DIFFERENT WHEEL CATEGORIES ACCORDING TO THIRD RATING

4.5.7 Conclusions from Saw Cutting Analysis

1. The saw-cut opening displacement curve by itself is not a good representation of the residual stress in a wheel.

2. The net rim force calculated from a mechanic's model using the saw cut opening displacement curve _does_ correlate with the intensity of wheel residual stress and is proposed as an index or measure of wheel rim residual stress state (especially at a level of 100 kips or average rim tensile stress of about 10 KSI which may be a threshold level for unstable propagation of critical size cracks).

3. Based on this measure, the effect of discoloration, wheel class, and plate shape were

    a. Discolored wheels are more likely to have high residual rim tensile stresses.

    b. Generally, Class C steel wheels have lower residual tensile stresses.

    c. The rim tensile stresses are lower in curved plate wheels.

4. Sixty wheels with service induced thermal cracks (AAR Code 74) were saw cut (Appendix 4.3).

    None of these wheels displayed the presence of residual tensile stresses, indicating that crack

initiation and stress reversal are independent processes. Dynamometer and track tests failed to produce thermal cracks in all but one wheel. As all of the wheels tested had new wheel tread profiles, the crack initiation process lacked the necessary mechanical or metallurgical damage to proceed.

4.6 Overall Conclusions from Technical Task T-3

1. Elevated temperature fatigue tests indicate that heat treated wheel steels exhibit a higher resistance to fatigue than non-heat treated (high temperature fatigue).

2. Crack arrest tests show that heat treated wheels can arrest larger thermal cracks prior to unstable propagation than non-heat treated wheels.

3. There is no significant difference in crack initiation behavior of the various wheel heat treatments based on lab test results using a rotating wheel subjected to torch heating and subsequent cooling of the tread.

4. At higher temperature (752°F), there is significant (20%) reduction in flow stress of wheel steels (Class U) for very low strain rates ($2 \times 10^{-6} \text{sec}^{-1}$) that may occur during sustained drag braking. Higher residual rim tensile stresses on cooling are associated with lower hot compressive yield or flow stresses.

Therefore, lower stress-strain curves should be used in stress analyses of wheels during drag braking. Class C steels are expected to show similar behavior.

5. Analyses of wheel saw cutting data indicate that discolored wheels are more likely to have high rim tensile residual stresses than nondiscolored wheels, and that heat treated (Class C) wheels and curved plate wheels have lower rim tensile residual stresses.

REFERENCES

1. M. Fec and H. Sehitoglu, "Behavior of Railroad Wheel Steels Under Selected Thermal Histories", Proceedings of the Third International Heavy Haul Conference, Vancouver, 1986.

5.0 EFFECT OF HEAT TRANSFER AND RAIL LOADING - TECHNICAL TASK (T4)

The main objective of the Technical Task-T4 is to determine the effect of heat transfer at the rail contact through experimental study under controlled conditions using the Roll Dynamic Unit (RDU), Brake Dynamometer (BDU), and the Induction Heating Facility. The effect of rail load and heat transfer on the development/alteration of wheel residual stresses is investigated as a part of this technical task.

This section is divided into four major subsections: 1) Brake Dynamometer Testing, 2) RDU Testing, 3) Heat Transfer Analysis, and 4) Induction Heating Tests. Major test analysis results are presented at the end of each subsection. The overall conclusions of Technical Task T4 are summarized at the end of the section.

Status of Testing/Major Findings

5.1 Brake Dynamometer Testing

The Brake Dynamometer tests in support of Technical Task T4 were conducted and coordinated with Roll Dynamics Unit tests, track tests, induction heating tests, and analytical studies. The objective was met by conducting low and high speed drag-braking tests with composition brake shoes at different levels of brake force. The majority of tests were performed

loading. Limited testing was carried out (1) without vertical rail loading and (2) with both vertical and lateral loads. Post test evaluations included residual stress determination at certain strategic wheel locations by the hole-drilling strain gaging technique. Temperatures and surface strains at selected locations of the test wheels were monitored during the testing.

For Brake Dynamometer testing, a scheme was developed to combine both Technical Tasks T4 and T6 for convenience. The purpose of Task 4, with regard to the dynamometer tests, was twofold. First, it was desired, by way of temperature measurements, to determine the amount of heat lost from a heated wheel to the air, brake shoe, and rail.

In addition, it was desired to determine the effect of braking parameters (speed and brake force) and wheel parameters (diameter, rim thickness, heat treatment class, and plate shape) on residual stresses developed in wheels subjected to repeated drag-braking. This latter purpose is common with the objective of Technical Task T6 except that T6 covers additional types of test wheels. For this reason, Brake Dynamometer testing covered under both Technical Tasks T4 and T6 are presented in this section.

Because severe drag-braking (at constant speed) is known to produce residual tensile stresses in the rims of wheels, this type of test was chosen for this study. The general plan was to conduct 25 drag braking cycles of 45 minutes duration (with water cooling between cycles) on each wheel and then have the wheels saw-cut at Pueblo for the residual stress determinations.

Wheels and Instrumentation Used for Brake Dynamometer Testing

For this study, twenty-eight new one-wear freight-car wheels were obtained, Table 5.1. These wheels represented wheels with straight, parabolic, and "S" shaped plates, U and C classes, 33- and 36-inch diameters, new rim thicknesses, and rims machined to the reapplication limit. In addition, four of the Class U wheels were in a fully stress relieved condition.

The wheels were instrumented with thermocouples on the tread, back face of the rim, and on the front hub-plate fillet (Figure 5.1). One wheel had additional thermocouples on the rim and plate. The wheels also had one strain gage at the front-hub-plate fillet. Several wheels had high temperature strain gages on the back faces of the rims. All thermocouple and strain gage leads, except for the tread thermocouple, were connected to a slip ring. Temperatures were measured continuously with a multipoint strip chart recorder. Strains were measured with a static strain indicator at the beginning (cold) and end (hot) of each drag-brake cycle. In addition, some of the wheels were observed with an infrared thermography unit during testing. For selected tests, a hand-held Exergen 'microscanner' model D infrared thermometer was used to measure the wheel temperatures at the end of the tests. During certain limited tests, a Hughes Aircraft Probeye Model 4100 thermal video system was used to monitor temperature development during the test cycles.

TABLE 5.1
DRAG TESTS ON DYNAMOMETER FOR TECHNICAL TASKS T4 AND T6

Serial	Section	Class	Plate Type	Code Number	Speed	Brake Force	Vertical Load	Lateral Load
95409	CJ-33	U	P	5	20 mph	1500 lb	27 kip	0 kip
94783	CJ-33	C	P	9	20	1500	27	0
95403	CJ-33	U	P	7	40	1500	27	0
95526	CJ-33	U	P	6	20	3000	27	0
95400	CJ-33*	U	P	8	40	1500	27	0
43878	J-33	U	St	15	20	1500	27	0
47382	J-33	U	St	16	20	3000	27	0
43888	J-33	U	St	17	40	1500	27	0
42283	J-33	U	St	18	40	750	27	0
94787	CJ-33	C	P	10	20	3000	27	0
94777	CJ-33	C	P	11	40	1500	27	0
95393	CJ-33	C	P	12	40	750	27/0**	0
49543	J-33	C	St	20	20	1500	27	0
49549	J-33	C	St	21	20	3000	27	0
49544	J-33	C	St	24	40	1500	0	0
5174	J-33	U	S	25	40	1500	27	0
4907	J-33	C	S	++	40	1500	0	0
95401	CJ-33	U(ann)	P	3	40	1500	27	0
43905	J-33	U(ann)	St	13	40	1500	27	0
94561	CJ-33*	U(ann)	P	4	40	1500	27	0
43928	CJ-33*	U(ann)	St	14	40	1500	27	0
47371	J-33*	U	St	19	40	1500	27	0
49622	J-33	C	St	23	40	1500	27	13.5
4892	J-33	C	S	26	40	1500	27	0
49541	J-33	C	St	22	40	1500	27	0
46470	H-36	U	St	33	40	1800	33	0
507400	CH-36	U	P	27	40	1800	33	0
1755	H-36	U	S	29	40	1800	33	0

*Machined to reapplication limit

**Part loaded - Part unloaded

+TA (3-24), T6 (25-27, 29)

++Not in matrix of Table 8.1 of Sp-2

TABLE 5.1 (CONT.)
DYNAMOMETER DRAG TESTS

Section	Plate	Class	Rim	Vertical Load Kips	Lateral Load Kips	Speed B.F.	Wheel or Test No.			
							20 mph		40 mph	
							1500 lb	3000 lb	750 lb	1500 lb
J33	P	U(Ann)**	N***	27	0					3
CJ33	P	U(Ann)	R	27	0					4
CJ33	P	U	N	27	0		5	6		7
CJ33	P	U	R	27	0					8
CJ33	P	C	N	27	0		9	10	12+	11
J33	St	U(Ann)	N	27	0					13
J33	St	U(Ann)	R	27	0					14
J33	St	U	N	27	0		15	16	18	17
J33	St	U	R	27	0					19
J33	St	C	N	27	0		20	21		22
J33	St	C	N	27	13.5					23
J33	St	C	N	0	0					24
J33	"S"	U	N	27	0					25
J33	"S"	C	N	27	0					26
J33	"S"	C	N	0	0					++
CH36	P	U	N	33	0					27+++
H36	"S"	U	N	33	0					29+++
H36	St	U	N	33	0					33

*All tests 25 cycles. Each cycle 45 minutes braking followd by 15 minutes water cooling.

**U(Ann) = Class U wheel that was renormalized.

***N = New rim thickness.

R = Rim machined to reapplication limit prior to test.

+Wheel 12 tested without rail contact for 10 of 25 cycles.

+++1800 lb brake force instead of 1500 lb.

++Wheel not in original program.

SLIDING THERMOCOUPLE

THERMOCOUPLE

STRAIN GAGE & THERMOCOUPLE

PARABOLIC PLATE

SLIDING THERMOCOUPLE

THERMOCOUPLE

STRAIN GAGE & THERMOCOUPLE

STRAIGHT PLATE
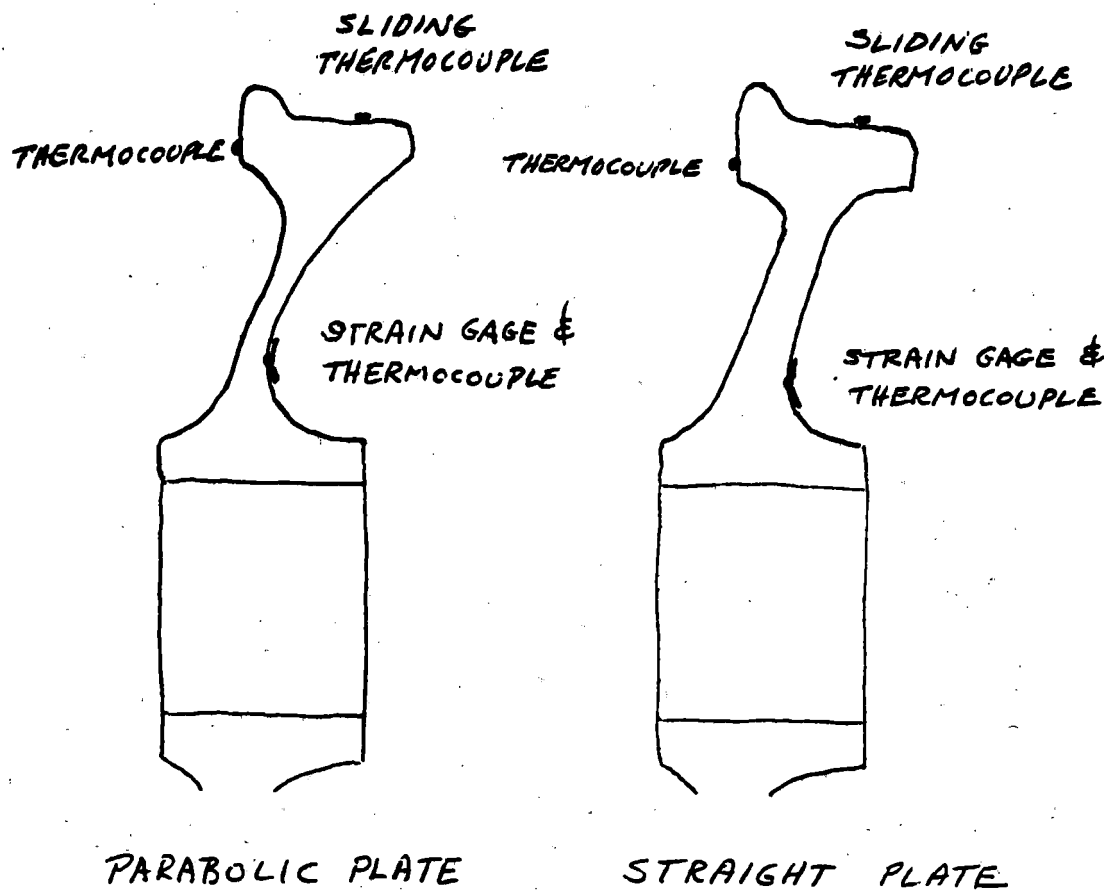
FIGURE 5.1   LOCATIONS OF THERMOCOUPLES AND STRAIN GAGES

5.1.1 Test Conditions

The tests were conducted as outlined in Table 5.1. For the 33-inch diameter wheels, brake forces of 1500 and 3000 lb. were used at a speed of 20 mph; brake forces of 750 and 1500 lb. were used at a speed of 40 mph. A brake force of 1800 lb. was used at 40 mph for the 36-inch diameter wheels. Most of the wheels were tested with the tread of the wheel in contact with the head of the 9-foot diameter rail wheel. The head profile was that of an AREA 136RE rail canted 1:40, the normal cant in track. With rail/wheel contact, the vertical load was 27 kips for most of the 33-inch diameter wheels and 33 kips for the 36-inch diameter wheels. Two of the 33-inch diameter wheels were tested without rail contact, and one was tested with vertical load for 6 cycles and without contact for 19 of the 25 cycles. In addition, one of the 33-inch diameter wheels was tested with a 27 kip vertical load and 13.5 kip lateral load.

5.1.2 Dynamometer Test Results

An important objective of these tests was to determine the relationship of the drag-braking conditions on the alteration of residual stresses in the wheels. Some observations were made on the relationships of speed, brake shoe force, and vertical load (wheel 5) to wheel temperature, apparent strain at the front hub-plate fillet, and heat transfer to the reaction rail.

Appendix 5.1 lists the strain and temperature data obtained

for wheels No. 5 through 17. These data are summarized in Table 5.2. Heat transfer studies conducted on wheel No. 5 are presented in Appendix 5.1, Table 1. With regard to the increase in wheel and rail temperatures during the tests, it appeared that both temperatures were markedly affected by the vertical load. For example, a preliminary observation of temperatures showed that tests with a vertical load of about 27 kips produced average wheel tread and rail temperatures of 487°F and 161°F, respectively. In contrast, tests with much lesser vertical load, such as 5 kips, produced average wheel tread and rail temperatures of 528°F and 106°F, respectively. Tests with an intermediate level of vertical load of 13.5 kips produced intermediate temperatures. Thus, increasing the wheel load decreased the wheel temperature and increased the rail temperature. This effect is probably caused by a corresponding increase in contact area.

The effects of wheel/rail contact on the strains and temperatures developed in the wheels from drag braking is further illustrated by the behavior of wheel 12 (Table 5.3 and Figures 5.2 and 5.3). This wheel was tested at 40 mph with a brake force of 750 lbs. (which corresponds to a Bhp level of 24), with a vertical load of 27 kips for the first six cycles, and then with no vertical load for the remaining 19 cycles.

With no vertical load, maximum temperatures increased by about 100°F on the tread and rim, and the hot wheel strain increased by about 1000   , compared to the results obtained with the application of vertical load, thus confirming that the

TABLE 5.2
TEMPERATURE AND STRAIN RESULTS

Wheel No.		Strain, με Cold	Hot	Temperature, °F Tread Cold	Hot	Rim Cold	Hot	Plate Cold	Hot
5	Max								
	Min								
	Avg			75	500				
6	Max	+164	+3242	100	845	–	–	95	220
	Min	-303	+2276	65	500	–	–	65	160
	Avg	- 41	+2556	83	573	–	–	81	191
7	Max	+282	+2574	95	700	95	535	95	205
	Min	- 77	+2013	50	525	50	420	50	150
	Avg	+ 99	+2385	74	579	79	485	78	184
9	Max	+143	+2440	100	590	100	490	100	195
	Min	- 43	+2180	60	530	55	430	60	155
	Avg	+ 47	+2259	76	565	76	446	82	184
10	Max	+123	+2592	95	795	95	580	95	205
	Min	- 87	+2128	75	550	80	520	80	155
	Avg	+ 30	+2399	85	623	85	543	85	185
11	Max	0	+1786	100	610	85	470	85	180
	Min	-129	+1215	75	370	75	400	75	150
	Avg	- 66	+1381	84	525	81	422	80	162
12	See Table 5.3 and Figures 5.2 and 5.3								
15	Max	-210	+3222	120	790	110	505	100	210
	Min	0	+2342	70	545	65	420	65	170
	Avg	+127	+2839	93	628	85	467	73	196
16	Max	+405	+3442	110	785	100	610	80	220
	Min	-500	+1902	70	490	50	460	60	145
	Avg	-258	+2533	79	620	77	532	70	186
18	Max	+ 56	+2760	100	595	80	515	85	170
	Min	-344	+2071	75	405	75	385	75	145
	Avg	-127	+2400	80	527	78	446	77	151
17	Max	+440	+3605	115	725	110	545	110	205
	Min	-205	+2184	60	450	50	390	50	140
	Avg	- 15	+2816	87	573	83	467	82	174

με = Micro inch/inch
"Max" and "Min" are the extreme values of strains measured when wheel was cold and when wheel was hot, "Avg" represents the average of 25 strain values.

TABLE 5.3
DYNAMOMETER DATA FOR WHEEL #12 (7/31/85-8/6/85)

Test #	Gage-Cold με	Gage-Hot με	Wheel Load Kips	Ambient Temperature F	Tread Temperature F	Rim Temperature F	Comments
1	0		27	80	495	450	
2			27	85	495	420	
3	-164	1653	27	75	500	450	
4	-205	1662	27	90	510	430	
5	-303	1756	27	90	530	440	
6	- 60	1951	27	75	530	425	
7	0	2740	0	80	675	515	Vert. load removed
8	- 39	2922	0	95	720	550	
9	-124	2816	0	90	720	525	
10	5	2855	0	80	730	560	47.7 min. test
11	7		0	95	760	520	
12	- 6	2794	0	80	750	525	47.39 min. test
13	- 96	2754	0	95	770	540	
14	-134	2621	0	95	650	500	
15	98	1760	0	80	435	395	New shoe aft. 25 min.
16	0	2186	0	90	510	430	
17	195	2370	0	85	560	480	
18	47	2492	0	90	620	495	
19	75	2780	0	95	690	545	
20	137	3074	0	80	680	580	
21	13	3080	0	95	620	580	
22	94	3028	0	85	600	560	
23	11	2958	0	90	630	550	
24	50	2951	0	95	630	520	
25	3	2755	0	80	650	545	

Avg 1-6	-146.4	1775.5	27.0	82.5	510.0	435.8	
Std 1-6	106.9	119.9	0.0	6.3	15.0	11.7	
Avg 7-14	- 48.4	2786.0	0.0	88.8	821.9	529.4	
Std 7-14	56.4	88.3	0.0	7.0	38.7	18.3	
Avg 15-25	65.7	2675.4	0.0	87.7	602.3	516.4	
Std 15-25	59.0	406.9	0.0	5.8	71.6	57.8	
Avg 7-25	17.7	2718.4	0.0	88.2	652.6	521.8	
Std 7-25	80.8	327.3	0.0	6.3	84.2	46.0	
Avg 1-25	- 16.5	2543.3	6.5	86.8	618.4	501.2	
Std 1-25	109.5	477.7	11.5	6.8	95.7	54.7	
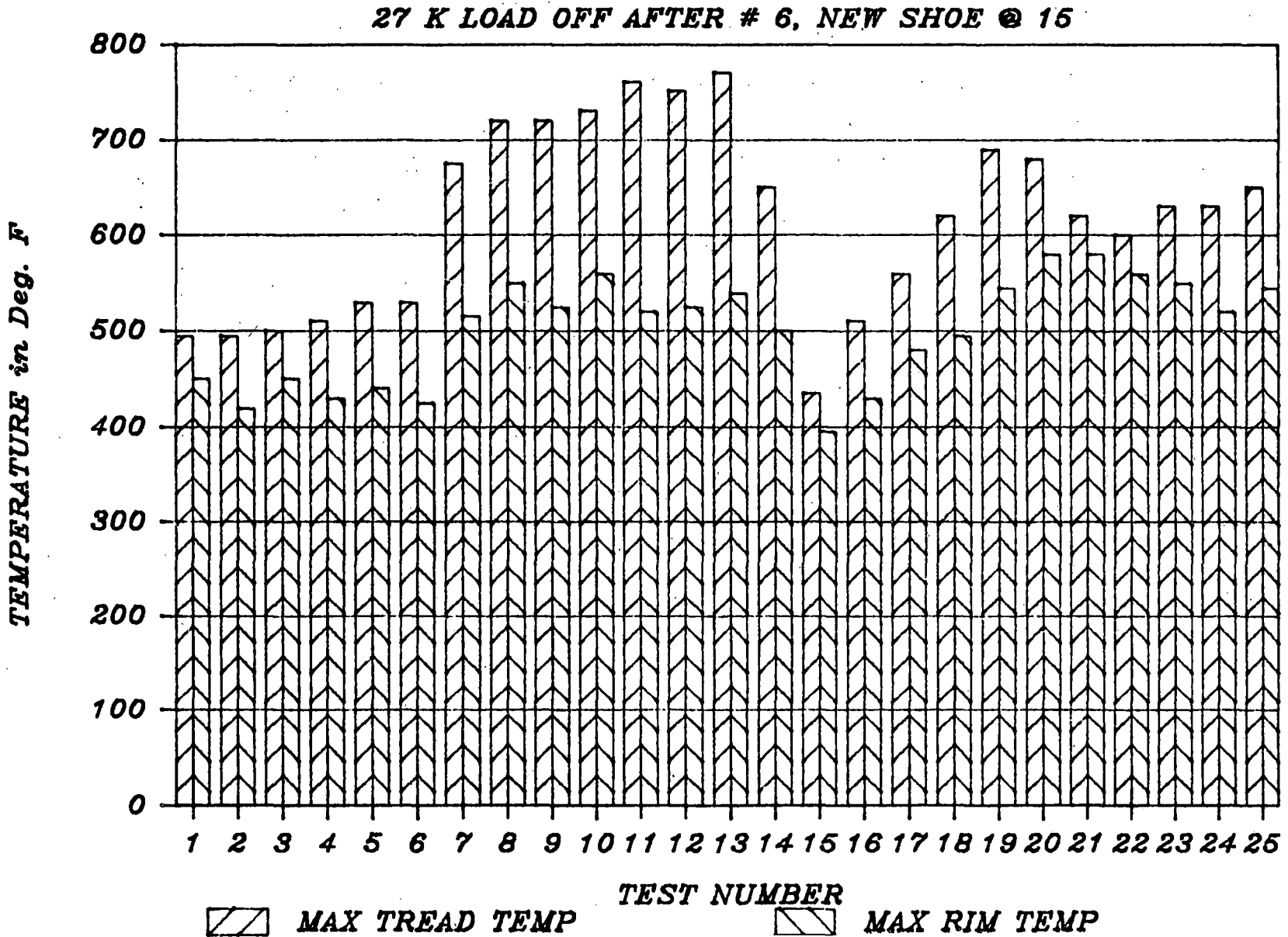
FIGURE 5.2   TEMPERATURE IN REPEAT DYNAMOMETER TESTS, CJ33 #12
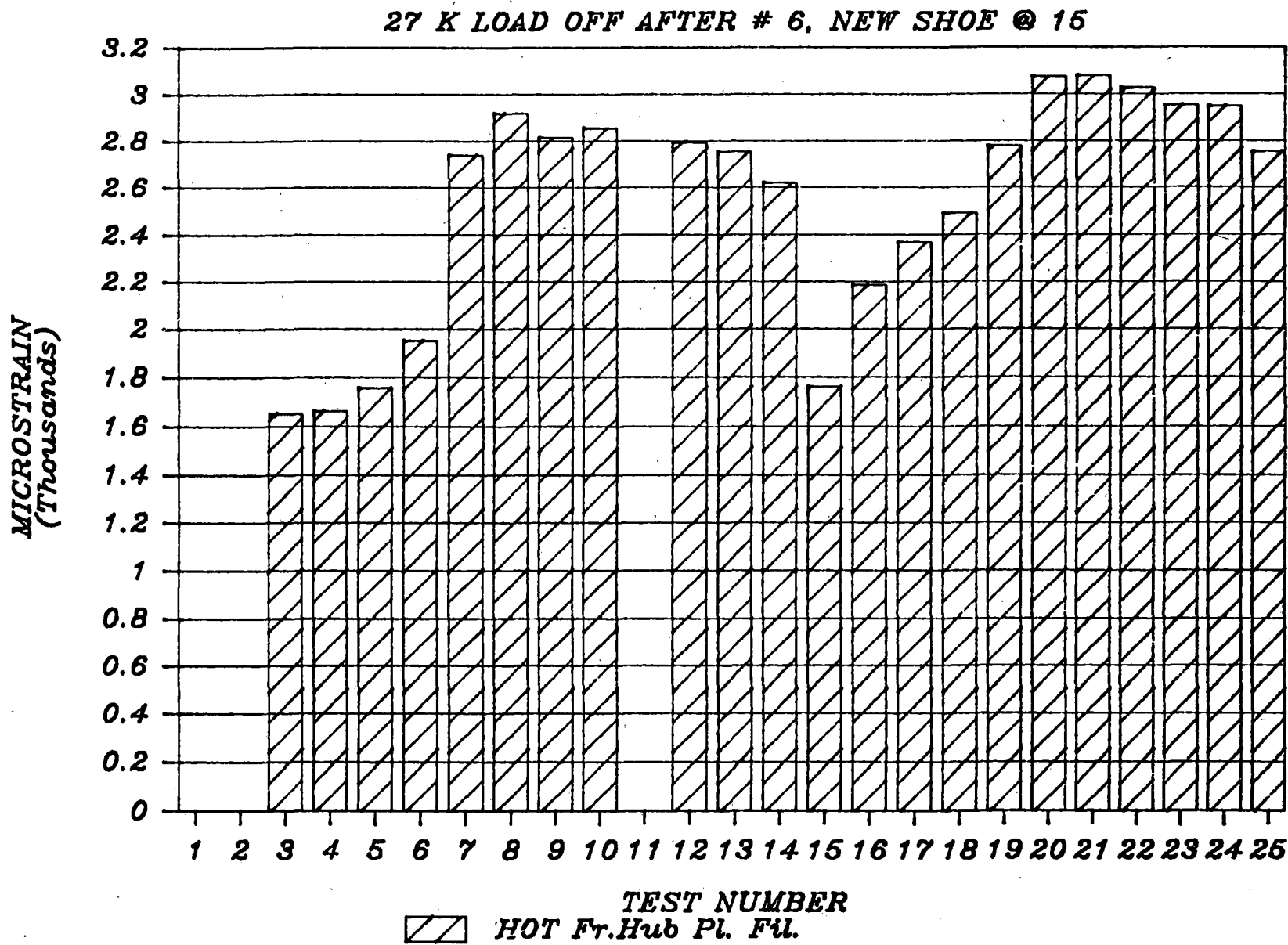
FIGURE 5.3   STRAIN IN REPEAT DYNAMOMETER TESTS CJ33-C #12

rail wheel and the associated vertical load remove a substantial amount of heat from the test wheel.

Table 5.2 shows the representative samples of the maximum, minimum, and average values of radial strain at the front hub-plate fillet as well as the temperatures for the tread, rim, and plate during the 25 tests. Strain and temperature values are shown at two points in time: (1) at the start, and (2) at the end of drag braking cycles. Strain values measured when the wheels are hottest indicate the relative expansion of the rim due to braking. High or low values of hot strain values appear to be associated with the corresponding high or low tread temperatures. For example, the highest strain value for wheel No. 6, + 3242 $\mu\varepsilon$, was associated with the highest tread temperature, 845°F. Rim temperatures were about 120°F below those of the tread. Front hub-plate fillet temperatures were even lower, being generally around 200°F or less.

The power input to the 33-inch diameter wheel is related to the brake force and speed by the following:

$$\text{Power Input (Bhp)} = \frac{\text{Brake Force (lbs) x Speed (mph)}}{375}$$

This equation gives power inputs of 24 and 48 Bhp for the combinations of speed and brake force used in these tests when the coefficient of friction, , is assumed to be 0.3. However, the coefficient of friction of AAR M926 high-friction composition brake shoe is not constant, but decreases with increasing temperature at the wheel/brake shoe interface. Other

factors affecting   are the contact area, wheel surface
roughness and possible changes in the friction characteristics
of the materials due to use. Therefore, when drag braking tests
are conducted with a constant brake force, the horsepower
changes (decreases) during the course of the 45 minute braking
cycle and is consistent from cycle to cycle. Furthermore,
because of the speed and force dependence of   , doubling speed
or brake force should not exactly double the horsepower. There
is a considerable variation of heating among wheels exposed to
essentially the same braking conditions. For example, wheels 7,
11, and 17 were exposed to 1,500 lbs. brake force at 40 mph, but
their average peak tread temperatures were 579°F, 525°F, and
573°F, respectively. Further, wheels 6, 10, and 16 were
exposed to 3,000 lb. brake force at 20 mph, with a corresponding
average peak tread temperatures of 573°F, 623°F, and
620°F.

The variation of the coefficient of friction during a
drag-brake heating cycle is illustrated by the torque curve
shown in Figure 5.4. Torque for two of the wheels, 9 and 10,
was measured with the strain gage torsion cell built into the
axle. These torque values represent a combination of torque or
retarding forces times radius, from two sources. These are
brake shoe friction and traction or rolling resistance between
the wheel and rail. Therefore, the values presented in Figure
5.4 do not reflect only the retarding forces due to braking. It
is possible that the rolling resistance also changes during the
test.

FIGURE 5.4.   SPEED AND TORQUE RECORD FOR SECOND DRAG BRAKE TEST,
              WHEEL #94783.

FIGURE 5.4   SPEED AND TORQUE RECORD FOR SECOND DRAG BRAKE TEST, WHEEL #94783

Inasmuch as the axle torque results from resistance of the track wheel, as well as from the braking forces, torsion values obtained without braking were subtracted from those obtained with braking to obtain the values caused by braking alone. In most of the tests, the axle torque was not measured; the tangential braking force was estimated by using a coefficient of friction value of 0.3, as described earlier.

The complete results of the temperature and strain measurements are listed in Lotus 1-2-3 files. Because these data are ancillary to the main objective of this study, they will not be discussed further here. Also listed in the Lotus files are the saw-cut data obtained from Pueblo.

These results of Brake Dynamometer testing show that the Class C wheels have lower residual stresses after repeated drag brake testing than those of the Class U wheels. The data show generally that more severe braking conditions produce higher tensile stress levels in Class U wheels. In Class C wheels, this effect is less pronounced.

5.1.3 Conclusions from Saw-Cutting Results of Wheels Tested on Brake Dynamometer

The wheels tested on the Brake Dynamometer were saw-cut and net rim forces were computed from the saw cut displacement data. The following conclusions can be drawn from the results obtained (Table 5.3a).

1. All the Class C, 33-inch diameter wheels, both straight

TABLE 5.3A
WHEELS TESTED ON BRAKE DYNAMOMETER

Net Rim Force Computed from Saw-Cut Displacement Data

Total Number of Drag Braking Cycles = 25
Duration of each cycle = 45 minutes
Assumed Brake Shoe Coefficient of Friction = .25

St. Plate Class U 33" diam.			St. Plate Class C 33" diam.			Curved Plate Class U 33" diam.			Curved Plate Class C 33" diam.		
TTC I.D. No.	BHP	Net Rim Frc. (KIPS)	TTC I.D. No.	BHP	Net Rim Frc. (KIPS)	TTC I.D. No.	BHP	Net Rim Frc. (KIPS)	TTC I.D. No.	BHP	Net Rim Frc. (KIPS)
208	20	+39	211	40	-61	209	20	+20	224	20	-70
227	20	+43	417	40	-88	225	40	+31	233	20	-25
234	40	+75	423	20	-58	226	40	+129	210	40	+35
235	40	+158	435	40	-9	418	40	+84	228	40	-14
419	40	+80	230	40	+250	420	40	+180	229	40	-55
421	40	+250				422	40	+90			

--Assorted Test Wheels--

TTC I.D. No.	Wheel Diam. (Inches)	Plate Shape *	BHP	Net Rim Force (KIPS)
430	33"	S	40	+27
434	36"	P	48	+80
433	36"	St.	48	+40
432	36"	S	48	+8

* S = S Plate, P = Parabolic Plate, St. = St. Plate

plate and curved plate designs, showed net compressive rim forces after 25 drag cycles at 40 Bhp (assuming coefficient of friction 0.25), each cycle lasting for 45 minutes, simulating fully loaded 70-ton capacity car.

2. One Class C straight plate wheel without contact with the track wheel (which simulates rail) at the above braking severity fractured during saw-cutting. Due to the absence of track wheel contact, the wheel rim experienced higher levels of temperature leading to substantial stress reversal in the rim.

3. Lower levels of braking severity (20 Bhp, 25 cycles, 45 minutes duration) produced relatively lower levels of tensile rim forces in Class U, straight plate and curved plate wheels. Higher levels of braking severity (40 Bhp, 25 cycles, 45 minutes duration), produced higher levels of net tensile rim forces including unsafe ($\geq$ 100 Kips) levels of net tensile rim forces, in both the Class U, straight plate and curved plate wheels.

4. Under higher levels of braking severity (40 Bhp, 25 cycles, 45 minutes duration), a Class U, 33 inch diameter wheel with thin rim (which was machined to condemning limit before the start of the test), fractured during saw cutting, indicating dangerous levels of tensile rim forces.

5. There was no apparent difference between the

fully stress relieved and as-received, Class U wheels in their net rim forces after drag braking at higher levels of braking severity.

6. No distinct differences were observed between the net rim forces of Class U straight plate and Class U parabolic plate wheels at the 40 Bhp level. Class U, S-plate showed lower net rim forces compared to both straight plate and parabolic plate wheels.

7. 36 inch diameter, Class U wheels performed better than 33 inch diameter, Class U wheels (when compared at equivalent braking severity levels). 36 inch diameter, Class U, S-plate wheels showed the lowest net rim forces compared to Class U, 36 inch diameter, straight plate and parabolic plate wheels when tested under the same braking severity levels.

5.2 Testing on Roll Dynamic Unit

The objective of testing conducted on the RDU was to investigate the effects of brake force and speed on the alteration of residual stresses in 33-inch diameter wheels with wheel loading corresponding to a 70-ton capacity (loaded) car. The secondary purpose was to estimate the amount of heat transferred from the wheel to the roller during a few tests. The majority of tests were conducted in the drag braking mode for a sixty-minute duration while the rest were executed under the stop braking mode.

The test wheels selected for testing on RDU were restricted to Class U, 33-inch diameter and parabolic plate design. All the wheels were brand new before instrumentation.

With the test truck mounted on the Roll Module Unit of the RDU, necessary modifications were performed to provide longitudinal-restraint and vertical-loading systems.

The brake rigging for the test truck was retrofitted to be similar to the conventional rigging of a 70-ton car. Shop compressed air was admitted into the brake cylinder through a regulating valve (set at the required pressure) and a remotely controlled directional valve, so that braking loads were applied to the test wheels as if through a conventional brake rigging system.

A hydraulic power unit with related control hardware activated the vertical loading system, providing an axle load of 53,000 lbs, simulating the weight of a loaded 70-ton capacity car.

The Roll Module Unit of the RDU was reconfigured to provide approximately 40,000 ft-lb of rolling inertia per wheelset. The driving arrangement for each roller set consisted of one Lateral Actuator Thrust Assembly (LATSA), one gear box, one (No. 2) flywheel, and one 600-hp motor.

5.2.1 Truck Instrumentation

Figure 5.5 presents the description of Test Trucks 1 and 2. Truck 1 was provided with limited instrumentation (only

(RDU) TEST TRUCK I

1) ALL WHEELS: CLASS U,
   PARABOLIC PLATE, NEW,
   GRIFFIN CJ33

2) A&B — SLIP RINGS

WHEELS WITH
THERMOCOUPLES
AT LOCATIONS
B1, B2 & B3

DRILLED AXLE

AXLE AI

W1   W2

W3   W4
NON — DRILLED
AXLE

AXLE A2

WHEELS WITHOUT
THERMOCOUPLES
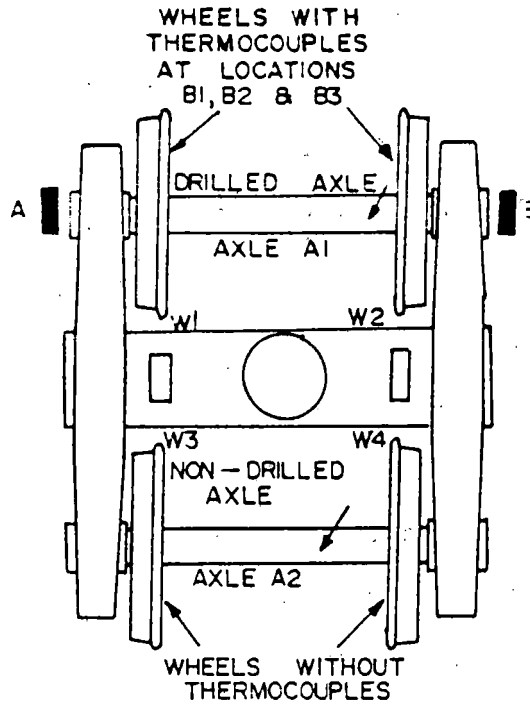
WHEEL I.D.	SERIAL NO.
W1	95554
W2	95551
W3	94552
W4	95528

(RDU) TEST TRUCK 2

1) ALL WHEELS: CLASS U,
   PARABOLIC PLATE, NEW,
   GRIFFIN CJ33

2) A, B, C, & D — SLIP RINGS

3) BOTH AXLES — DRILLED

4) ALL WHEELS STRAIN GAGED
   & THERMOCOUPLED AT
   LOCATIONS B1, B2, & B3

W5   W6

AXLE A3

W7   W8

AXLE A4
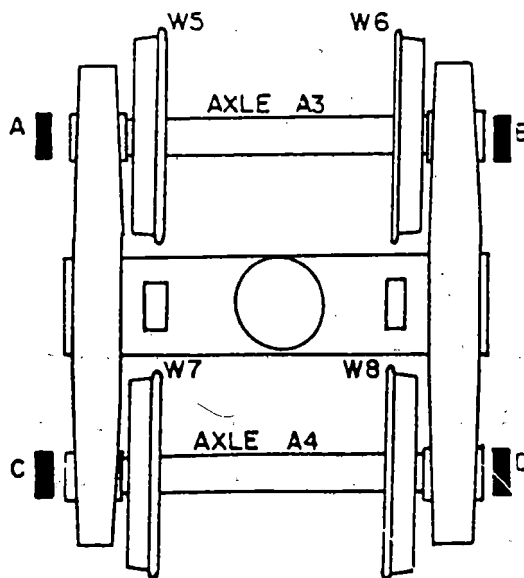
WHEEL I.D.	SERIAL NO.
W5	94559
W6	94550
W7	94565
W8	94566

FIGURE 5.5   WHEEL FAILURE MECHANISMS OF RAILROAD CARS TEST
              TRUCKS FOR RDU TESTING

thermocouples), while Truck 2 was heavily instrumented with high temperature strain gages and thermocouples.

The test trucks were provided with instrumented brake heads to monitor the tangential and normal brake loads that were applied during the test runs. The brake shoe load cells were strain-gaged and calibrated before they were fitted in the brake beams of the test truck.

The brake shoe normal force and the braking or tangential force for each test wheel were determined from the voltages developed across the strain-gage bridges and from the calibration factors unique to each load cell. The calibration factors were obtained by calibrating the brake shoe load cells individually in an MTS test setup.

A typical plot obtained for static brake shoe normal force versus brake cylinder pressure is shown in Figure 5.6. The brake shoes used were of high-friction composition type (AAR M926). They were centered on the wheel treads throughout the test run.

5.2.2 Test Conditions

A series of drag braking cycles, each usually consisting of 60 minutes of brake cylinder pressure (brake load) and speed followed by cooling to room temperature were conducted. The test wheels were subjected to thermal cycles of moderate horsepower levels (at the brake shoe-wheel interface) initially, followed by severe drag braking episodes (higher than 50 brake

STATIC GOLDEN SHOE TEST RESULTS
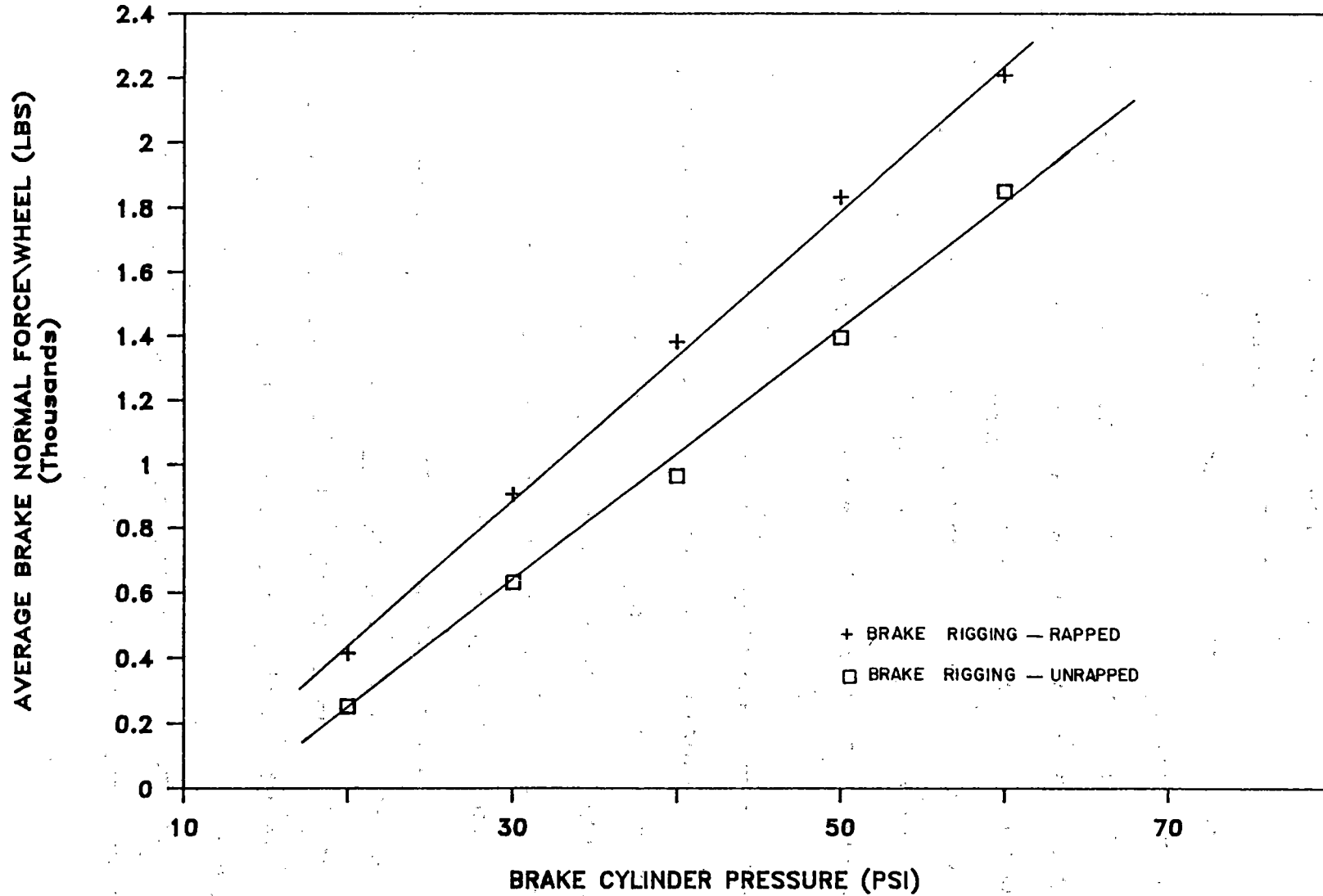
FIGURE 5.6   AVERAGE BRAKE NORMAL FORCE/WHEEL -VS- BRAKE CYLINDER PRESSURE FOR TEST TRUCK

horsepower levels at the brake shoe-wheel interface). After the wheels were cooled, hole drilling-strain gaging was used after every few thermal cycles to estimate residual stresses at certain critical locations on the wheels.

Tables 5.4 and 5.5 present relevant details pertaining to test parameters.

The performance of various transducers, slip rings, signal-conditioning equipment, and data collection methods were checked out during the first series of tests. Truck No. 2 was made ready with instrumented wheelsets, with a typical instrumentation layout as presented in Figure 5.7. Instrumentation scheme for RDU testing is presented in Figure 5.8.

5.2.3 Instrumentation of Wheels

All wheels were new (in "as received" condition). High temperature strain gages and thermocouples were installed on the test wheels at locations B1 (lower back side of rim), B2 (back side of rim fillet region), and B3 (front hub fillet region), as presented in Figure 5.9. The test wheels were heated to 1,100°F and slowly cooled to relieve the stresses induced in the strain gages during installation.

It is recognized that this thermal treatment also relieved the manufacturing stresses in the wheels and reduced their hardness.

Temperature data measured at locations B1, B2, and B3 were acquired through axle-mounted slip rings, while tread

TABLE 5.4
TESTING OF TRUCK #1 ON RDU (DRAG BRAKING)

WHEEL FAILURE MECHANISMS

Date	Run No.	Brake Cylinder Pressure (psi)	Speed (mph)	Duration (minutes)	Direction	Axle Vertical Load (kips)
02/25/85	2	30	30	60	West	44
02/26/85	3	30	30	60	East	44
02/27/85	4	40	40	30	West	52
02/28/85	5	40	40	40	East	52
03/01/85	6/7	40	45	30	West	52
03/04/85	8/9	45	40	30	East	52
03/05/85	10/11	50	30	60	West	52
03/06/85	12/13	50	30	60	East	52
03/07/85	14/15	60	20	60	West	52
03/08/85	16/17	50	40	60	East	52
03/18/85	18/19	45	40	60	West	52
03/18/85	20/21	50	35	60	East	52

Brake Cylinder Pressure (psi)	Average Normal Force/Shoe (lbs)
30	900
40	1400
50	1800
60	2200
45	1600

TABLE 5.4 (CONT.)

TESTING OF TRUCK #1 ON RDU (STOP BRAKING CYCLES)

WHEEL FAILURE MECHANISMS

Sl. No	Run.No.	Brake Cylinder Pressure (psi)	Initial Speed (mph)	Direction	Axle Vertical Load (Kips)
1	22	50	30	West	52
2	23	60	30	West	52
3	24	50	35	East	52
4	25	60	35	East	52
5	26	50	40	West	52
6	27	60	40	West	52
7	28	50	50	East	52
8	29	60	50	East	52

TABLE 5.5
TESTING OF (INSTRUMENTED) TRUCK #2 ON RDU

WHEEL FAILURE MECHANISMS

Average Vertical Load/Axle 52 Kips (Simulating Fully-Loaded 70-Ton Car)

Date	Run No.	Brake Cylinder Presure (psi)	Speed (mph)	Duration (minutes)	Direction	Remarks
4/2/85	30/31	20/60				Static Brake Shoe Tests
4/2/85	32/33	10/20	20	80	West	Cleaning of new tread surfaces
4/3/85	34/35/36	30	30	60	West	Four video cameras in position for observing front & back of wheels #6 & #8
4/3/85	37/38	30	30	60	East	"

(Hole Drilling Performed on Wheel #5 at B1, B2, B3 Locations)

Date	Run No.	Brake Cylinder Presure (psi)	Speed (mph)	Duration (minutes)	Direction	Remarks
4/4/85	39/40	40	30	60	West	"
4/4/85	41/42	40	30	60	East	"

(Hole Drilling Performed on Wheel #6 at B1, B2, B3 Locations)

Date	Run No.	Brake Cylinder Presure (psi)	Speed (mph)	Duration (minutes)	Direction	Remarks
4/8/85	43/44	50	30	60	West	"
4/8/85	45/46	50	30	60	East	"

(Hole Drilling Performed on Wheel #7 at B1, B2, B3 Locations)

Date	Run No.	Brake Cylinder Presure (psi)	Speed (mph)	Duration (minutes)	Direction	Remarks
4/9/85	47/48	50	25	60	West	"
4/9/85	49/50	50	25	60	East	"

(Hole Drilling Performed on Wheel #5 at B1, B2, B3 Locations)

Date	Run No.	Brake Cylinder Presure (psi)	Speed (mph)	Duration (minutes)	Direction	Remarks
4/10/85	51/52	40	25	60	West	"
4/10/85	53/54	40	25	60	East	"

(Hole Drilling Performed on Wheel #8 at B1, B2, B3 Locations)

TABLE 5.5 (CONT.)
TESTING OF (INSTRUMENTED) TRUCK #2 ON RDU

WHEEL FAILURE MECHANISMS

Average Vertical Load/Axle 52 Kips (Simulating Fully-Loaded 70-Ton Car)

Date	Run No.	Brake Cylinder Presure (psi)	Speed (mph)	Duration (minutes)	Direction	Remarks
4/11/85	55/56	45/60	42/50	60	West	a) " b) Severe sustained drag braking to hold 50 BHP for at least first 30 minutes
4/11/85	57/58	45	42	30	East	a) 4 video cameras b) Sustained drag braking (after this test, all video cameras removed)
(Hole Drilling Performed on Wheels #8 at B1, B2, B3 Locations)						
4/12/85	59/60	40/50	38	40	West	Tried to maintain 40 BHP throughout the test
4/12/85	62/63	40/48	38	55	East	"
(Hole Drilling Performed on Wheel #5 at B1, B2, B3 Locations)						
4/13/85	64/65	50/53	33/28/30/ 32/37	65	West	a) Fan cooling with 2 fans in front 1 fan in rear b) Tried to maintain 40 BHP throughout the test
4/13/85	66/67	50	33/31/28/ 33/32/35	65	East	a) Fan cooling b) Maintain 40 BHP throughout the test
(Hole Drilling Performed on Wheel #6 at B1, B2, B3 Locations)						
4/15/85	68/69	50	30		West	Stop Braking Test
"	"	60	30		"	"
"	"	50	35		"	"

TABLE 5.5 (CONT.)
TESTING OF (INSTRUMENTED) TRUCK #2 ON RDU

WHEEL FAILURE MECHANISMS

Average Vertical Load/Axle 52 Kips (Simulating Fully-Loaded 70-Ton Car)

Date	Run No.	Brake Cylinder Presure (psi)	Speed (mph)	Duration (minutes)	Direction	Remarks
"	"	60	35		"	"
"	"	50	40		"	"
"	"	60	40		"	"
"	"	50	45		"	"
"	"	60	45		"	"
"	"	50	50		"	"
"	"	60	50		"	"
"	"	50	55		"	"
"	"	60	55		"	"
"	"	50	60		"	"
"	"	60	60		"	"
4/15/85	70/71	40	40/42/45/ 49/51/53/ 55	60	West	a) Drag braking with fan cooling b) Maintained 40 BHP

(Hole Drilling Performed on Wheel #7 at B1, B2, B3 Locations)

Date	Run No.	Brake Cylinder Presure (psi)	Speed (mph)	Duration (minutes)	Direction	Remarks
4/16/85	72/73	40/45	35/32/30/ 34/43/45	65	East	a) Fan cooling b) Maintained 40 BHP
4/16/85	74/75	45/50	40/46/50	55	West	a) Fan cooling b) Maintained 50 BHP throughout the test

(Hole Drilling Performed on Wheel #8 at B1, B2, B3 Locations)

Date	Run No.	Brake Cylinder Presure (psi)	Speed (mph)	Duration (minutes)	Direction	Remarks
4/17/85	76/77	50	40		West	Stop Braking Test
"	"	60	40		"	"
"	"	50	45		"	"
"	"	60	45		"	"
"	"	50	50		"	"
"	"	60	50		"	"
"	"	50	55		"	"
"	"	60	55		"	"
"	"	50	60		"	"
"	"	60	60		"	"
"	"	50	40		East	"
"	"	60	40		"	"
"	"	50	45		"	"
"	"	60	45		"	"

TABLE 5.5 (CONT.)
TESTING OF (INSTRUMENTED) TRUCK #2 ON RDU

WHEEL FAILURE MECHANISMS

Average Vertical Load/Axle 52 Kips (Simulating Fully-Loaded 70-Ton Car)

Date	Run No.	Brake Cylinder Presure (psi)	Speed (mph)	Duration (minutes)	Direction	Remarks
"	"	50	50		"	"
"	"	60	50		"	"
"	"	50	55		"	"
"	"	60	55		"	"
"	"	50	60		"	"
"	"	60	60		"	"

(Intermittent Drag Braking and Free Running - With Fan Cooling)

Date	Run No.	Brake Cylinder Presure (psi)	Speed (mph)	Duration (minutes)	Direction	Remarks
4/17/85	78/79	45	35	13	West	Drag braking (50 BHP)
"	"	0	35	8	"	Free running
"	"	45	35/40	15	"	Drag braking
"	"	0	40	9	"	Free running
"	"	45	40/45	14	"	Drag braking
"	"	0	45	12	"	Free running
"	"	55	45	16	"	Drag braking
"	"	0	45	5	"	Free running
"	"	55	45	10	"	Drag braking

(Hole Drilling Performed on Wheel #5 at B1 and B2 Locations Only)

Date	Run No.	Brake Cylinder Presure (psi)	Speed (mph)	Duration (minutes)	Direction	Remarks
4/18/85	80/81	45/50	40/45/50/55	65	East	Drag braking - with fan cooling - Maintained 50 BHP

(Hole Drilling Performed on Wheels #8, at B1, B2, B3 Locations)

----

1) It may be noted that some of the Runs are assigned two numbers (viz., 78/79). This is simply because two data acquisition disks (Computer HP 9826) were needed from the start until the completion of each of those Runs.

2) " (Sign) under different Run numbers implies that, data for individual stop braking cycles was recorded on the same set of disks (Computer HP 9826).

WHEEL # 8

WHEEL # 6

WHEEL # 7

WHEEL # 5

_ BIC ⎫
−B2C ⎪
−B2R ⎬ HIGH TEMP. GAGES
−B3C ⎪
−B3R ⎭
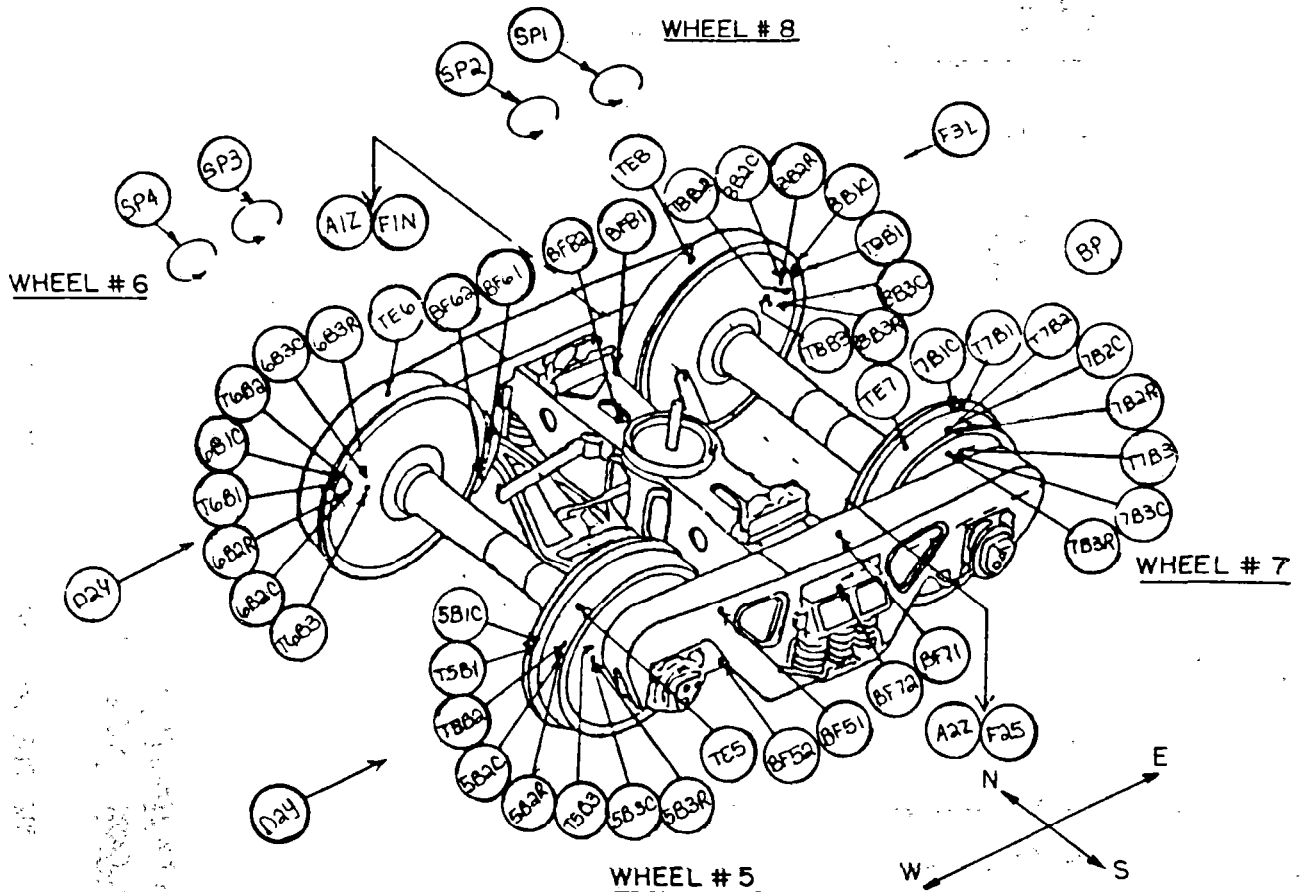
(ALL NUMBERS BEFORE GAGES INDICATE TEST WHEEL NUMBERS)

T − B1 ⎫
T − B2 ⎬ THERMOCOUPLES THROUGH SLIP RINGS
T − B3 ⎭

(NUMBERS AFTER 'T' INDICATE TEST WHEEL I.D.)

TE −⎫
TE −⎬ SLIDING CONTACT THERMOCOUPLES

(NUMBERS AFTER 'TE' INDICATE TEST WHEEL I.D.)

BF − 1 BRAKE FORCE STRAIN GAGE # 1
BF − 2 BRAKE FORCE STRAIN GAGE # 2
(NUMBERS AFTER 'BF' INDICATE TEST WHEEL I.D.)

FIGURE 5.7   INSTRUMENTATION SETUP FOR TEST TRUCK #2

5−31

WFM INSTRUMENTATION
LAYOUT BLOCK DIAGRAM
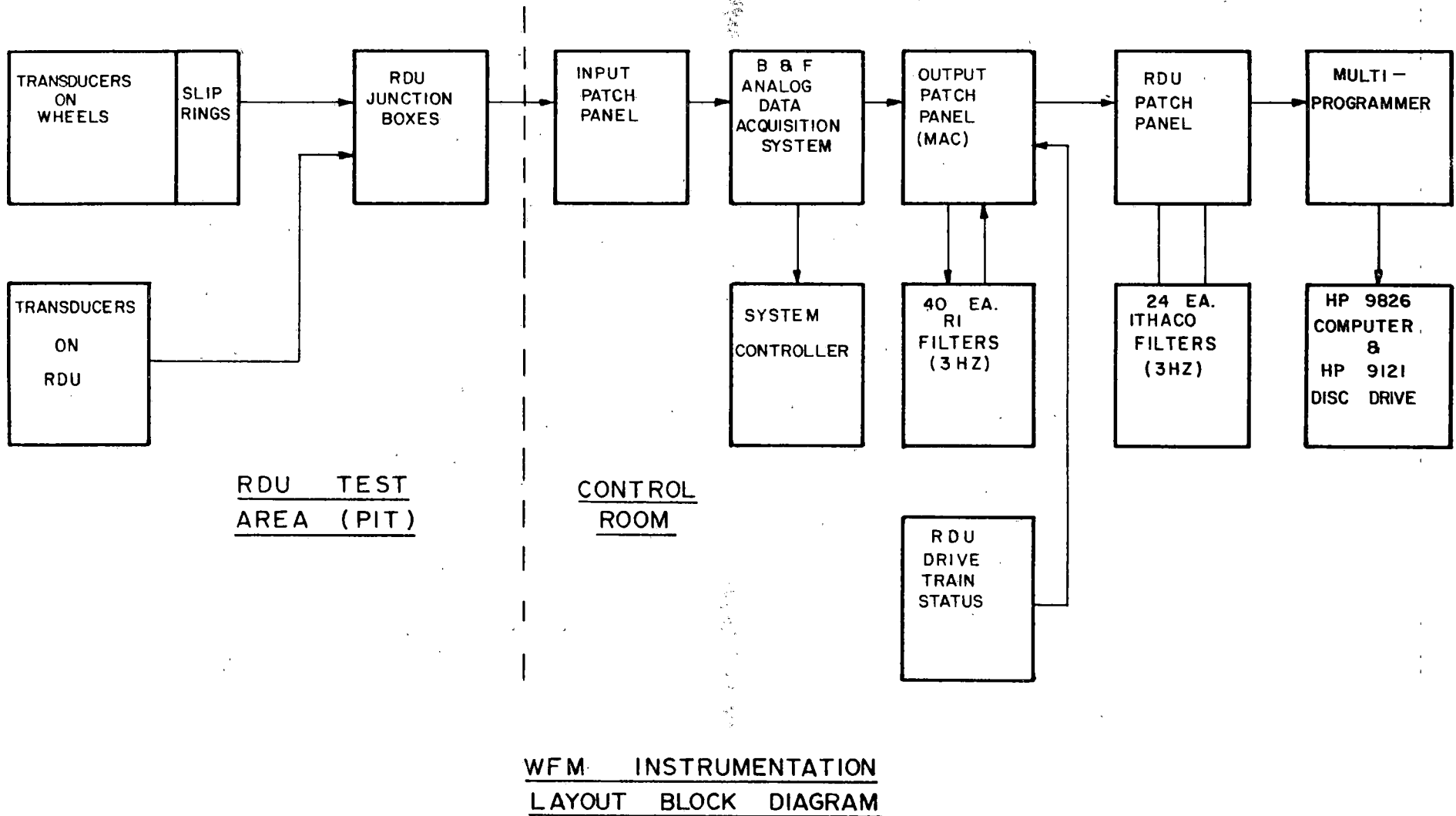
FIGURE 5.8   INSTRUMENTATION SCHEME FOR TEST SERIES #2
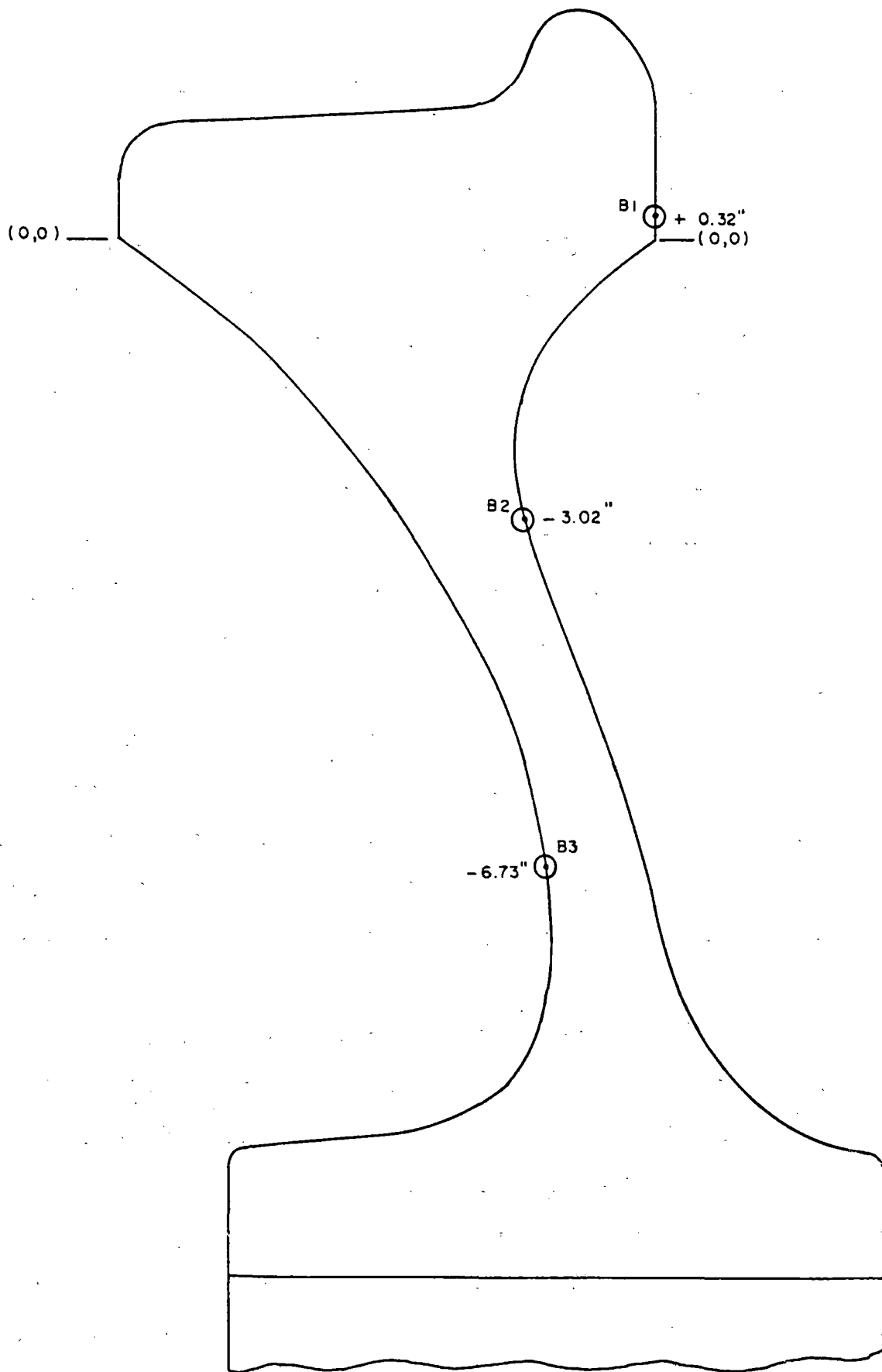
FIGURE 5.9   A TYPICAL 33 INCH (CURVED PLATE) TEST WHEEL,
SHOWING LOCATIONS (B1, B2, & B3) OF HIGH
TEMPERATURE STRAIN GAGES AND THERMOCOUPLES

temperatures were recorded by sliding contact probes.

5.2.4 Horsepower and Peak Wheel Temperatures

During drag braking tests, temperatures were monitored at the critical locations on the test wheels. The coefficient of friction and Bhp levels at the brake shoe-wheel interface were computed from the strain gage data from the instrumented brake heads.

Data were collected at the rate of 100 samples per second during 1 second of each minute of drag braking application. The data, which consisted of average, minimum, and maximum values for all test parameters including the computed items such as coefficient of friction and Bhp, were collected by a Hewlett-Packard 9826 microcomputer data acquisition system.

The most important results of the RDU testing were the significant wheel to wheel variation in the thermal input, the changes with time in coefficient of friction of the brake shoes, and the inability to hold a constant level of thermal input to the wheels.

During the drag braking tests, temperatures were monitored at three critical locations of the test wheels. The critical locations (B1, B2, and B3, Figure 5.9) were selected from previous finite element analysis, B1 being in the back rim region, B2 being in the back rim fillet region, and B3 being in the front hub fillet region. The coefficient of friction and Bhp levels at the brake shoe-wheel interface were computed from

the strain gage data of the instrumented brake heads. Table 5.6 presents the differences in maximum temperatures attained by the test wheels as observed at B1, B2, and B3 locations during the drag braking episodes for a given brake cylinder pressure and speed.

Details of changes in Bhp, as well as the coefficient of friction levels are presented. Maximum level of coefficient of friction, and hence Bhp, were attained during the start of the runs, and those values dropped (with increase in temperature) toward the end of the braking cycle.

Figures 5.10 and 5.11 show the maximum and minimum Bhp levels (at the beginning and end of the different braking cycles) attained during Truck #1 testing on the RDU for wheels 1, 2, 3, and 4.

Figure 5.12 and 5.13 show the maximum and minimum levels of Bhp attained during Truck #2 testing on the RDU for wheels 5 and 7.

After every two significant thermal (drag braking) cycles, and the test wheels were cooled to room temperature, the residual stress at critical locations of the test wheels was determined by the hole drilling strain gaging method. The hole drilling strain gaging method is fully described in Section 11.2.5 (Failure Model).

At the B1 location, the hoop stress, $_H$, changed eventually from compressive to tensile stress of varying magnitudes for different test wheels as shown in Figures 5.14 and 5.15. These figures also present equivalent unidirectional

TABLE 5.6
WHEEL FAILURE MECHANISMS, TECHNICAL TASK T4
RDU TESTING (TRUCK #2)

Run #	Wheel #	Max. Temp. Attained (°F) at Locations			B.H.P. at Brake Shoe Wheel Interface		Coefficient of Friction	
		B1	B2	B3	Max	Min	Max	Min
32/33	5	263	228	---	3.5	3.1	.38	.36
20 mph	6	---	249	169	3.1	2.9	.31	.28
10/20 psi	7	238	197	135	---	---	.36	.32
	8	256	195	168	---	---	.45	.27
37/38	5	450	375	250	15.5	11	.28	.16
30 mph	6	390	350	230	12.5	9	.22	.15
30 psi	7	436	355	220	16	13	.28	.22
	8	390	345	236	16	10.5	.24	.16
39/40	5	433	377	---	31	20	.26	.18
30 mph	6	388	392	203	29.9	18.5	.24	.18
40 psi	7	468	369	209	20.7	13.9	.16	.12
	8	493	397	226	32	17	.24	.12
43/44	5	464	---	---	47	23.5	.30	.16
30 mph	6	---	397	198	44.5	23.3	.30	.19
50 psi	7	484	391	225	32.6	13.4	.26	.07
	8	461	234	219	45	18	.30	.11
49/50	5	512	415	250	26	15	.20	.10
25 mph	6	477	426	248	27.5	16.5	---	---
50 psi	7	455	424	228	27	20	.19	.16
	8	395	350	235	30	19	.22	.12
55/56	5	605	495	320	44	35	.22	.13
42/50 mph	6	496	480	270	57	25	.26	.15
45/60 psi	7	624	560	310	45	27	.18	.10
	8	705	520	350	95	30	.24	.11
57/58	5	550/600	445	255	50	---	---	---
42 mph	6	611	511	278	50	30	---	---
45 psi	7	490	460	245	62	40	.34	.25
	8	660	370	295	---	---	---	---
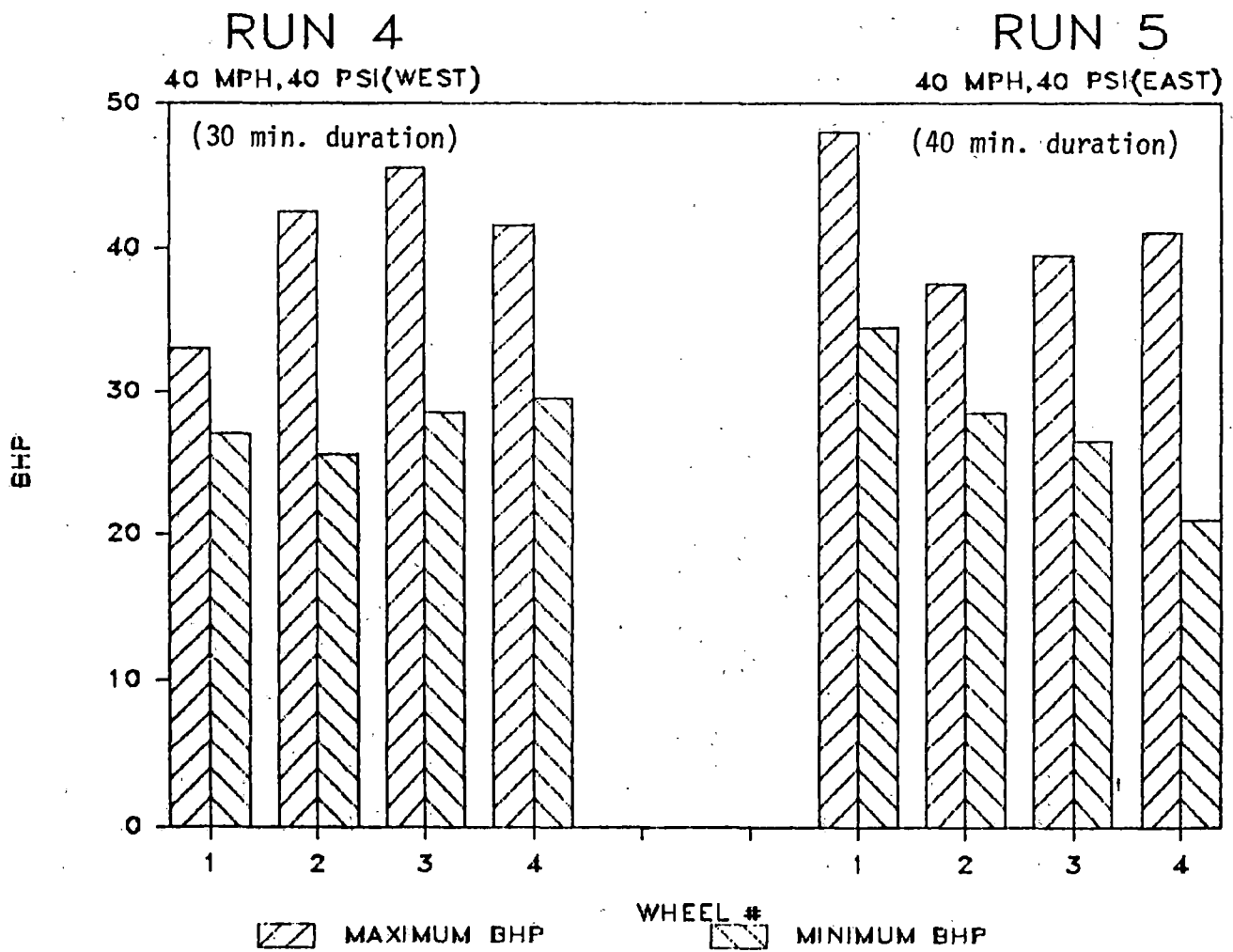
FIGURE 5.10   MAXIMUM VALUES OF BHP AT BRAKE SHOE/WHEEL
               INTERFACE FOR WHEELS # 1, 2, 3, AND 4 DURING DRAG
               BRAKING CYCLES

FIGURE 5.11   MAXIMUM AND MINIMUM VALUES OF BHP AT BRAKE
SHOE/WHEEL INTERFACE FOR WHEELS # 1, 2, 3, AND 4
DURING DRAG BRAKING CYCLES

RUNS 43/44
30 MPH,50 PSI(WEST)

RUNS 45/46
30 MPH,50 PSI(EAST)

60 MIN. DURATION

60 MIN. DURATION

BHP

WHEEL #

MAXIMUM BHP   MINIMUM BHP

FIGURE 5.12   MAXIMUM AND MINIMUM VALUES OF BHP AT BRAKE
                SHOE/WHEEL INTERFACE FOR WHEELS # 5 AND 7 DURING
                DRAG BRAKING CYCLES

RUNS 62/63   RUNS 64/65   RUNS 66/
38 MPH,40/48 PSI(EAST)   28/37 MPH,50/53 PSI(WEST)   28/35 MPH, 50 PSI

(ALL RUNS 60 MINUTE DURATION)

BHP

WHEEL #

▨ MAXIMUM BHP   ▨ MINIMUM BHP
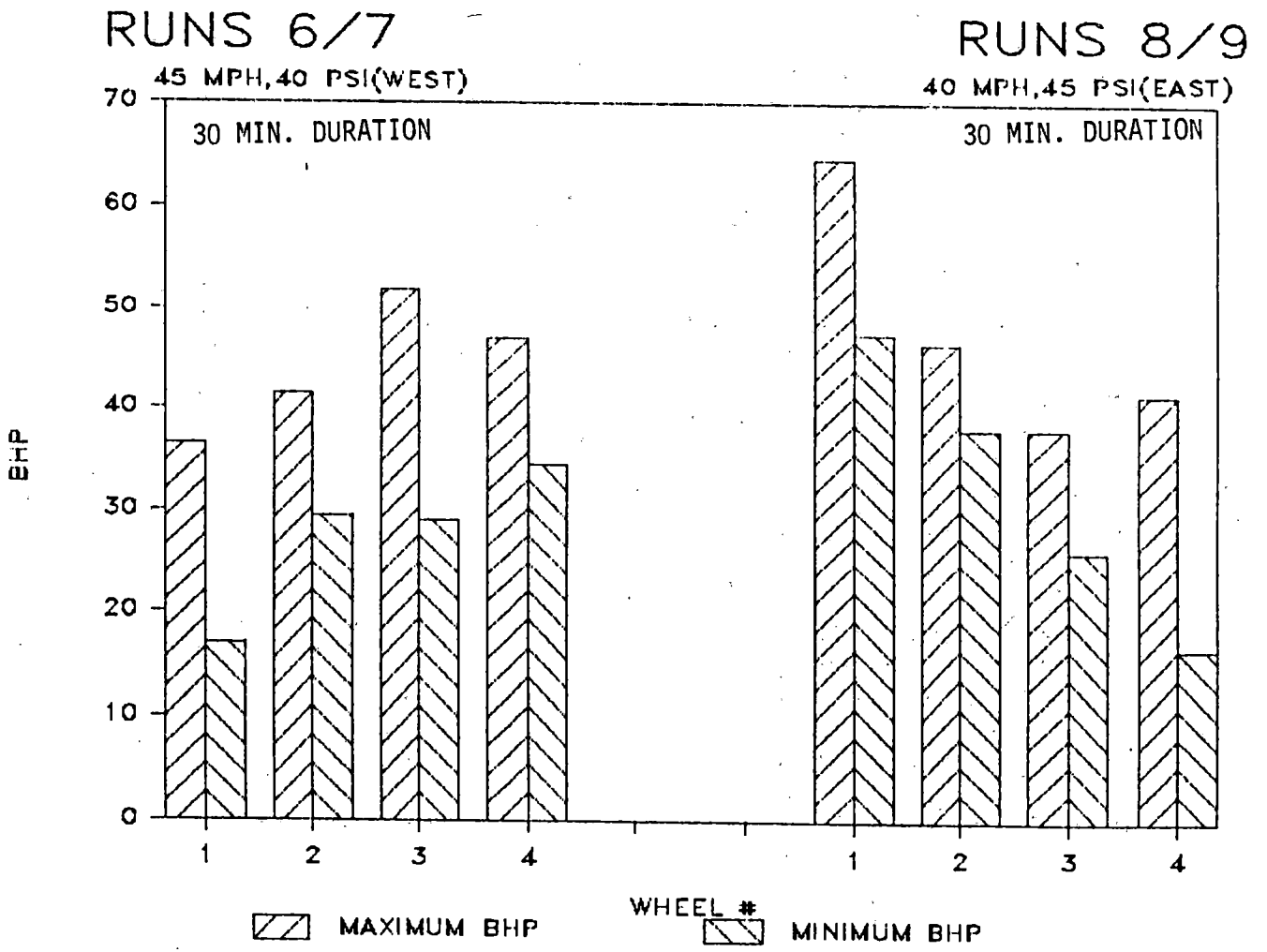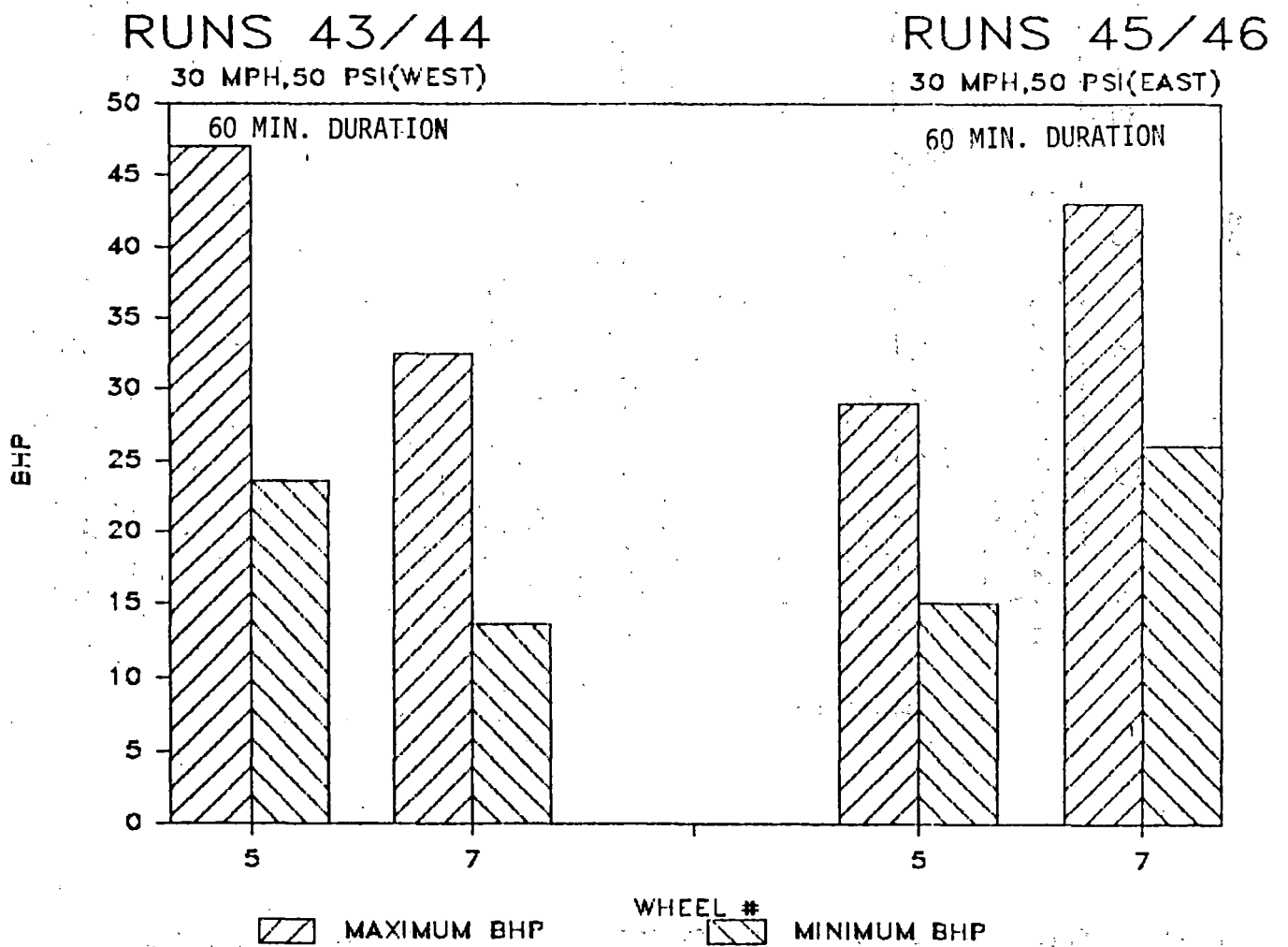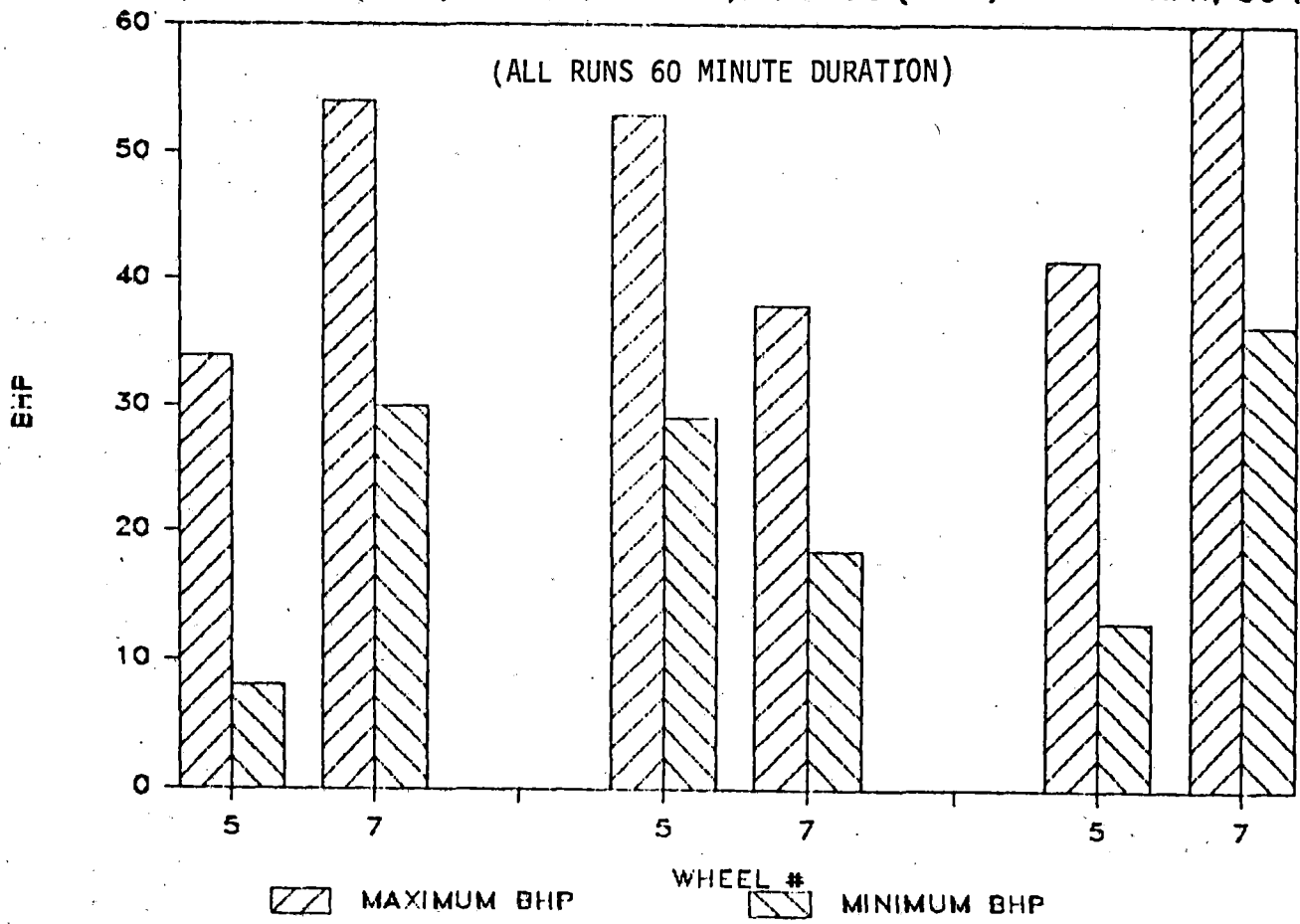
FIGURE 5.13   MAXIMUM AND MINIMUM VALUES OF BHP AT BRAKE
                SHOE/WHEEL INTERFACE FOR WHEELS # 5 AND 7 DURING
                DRAG BRAKING CYCLES

5-40
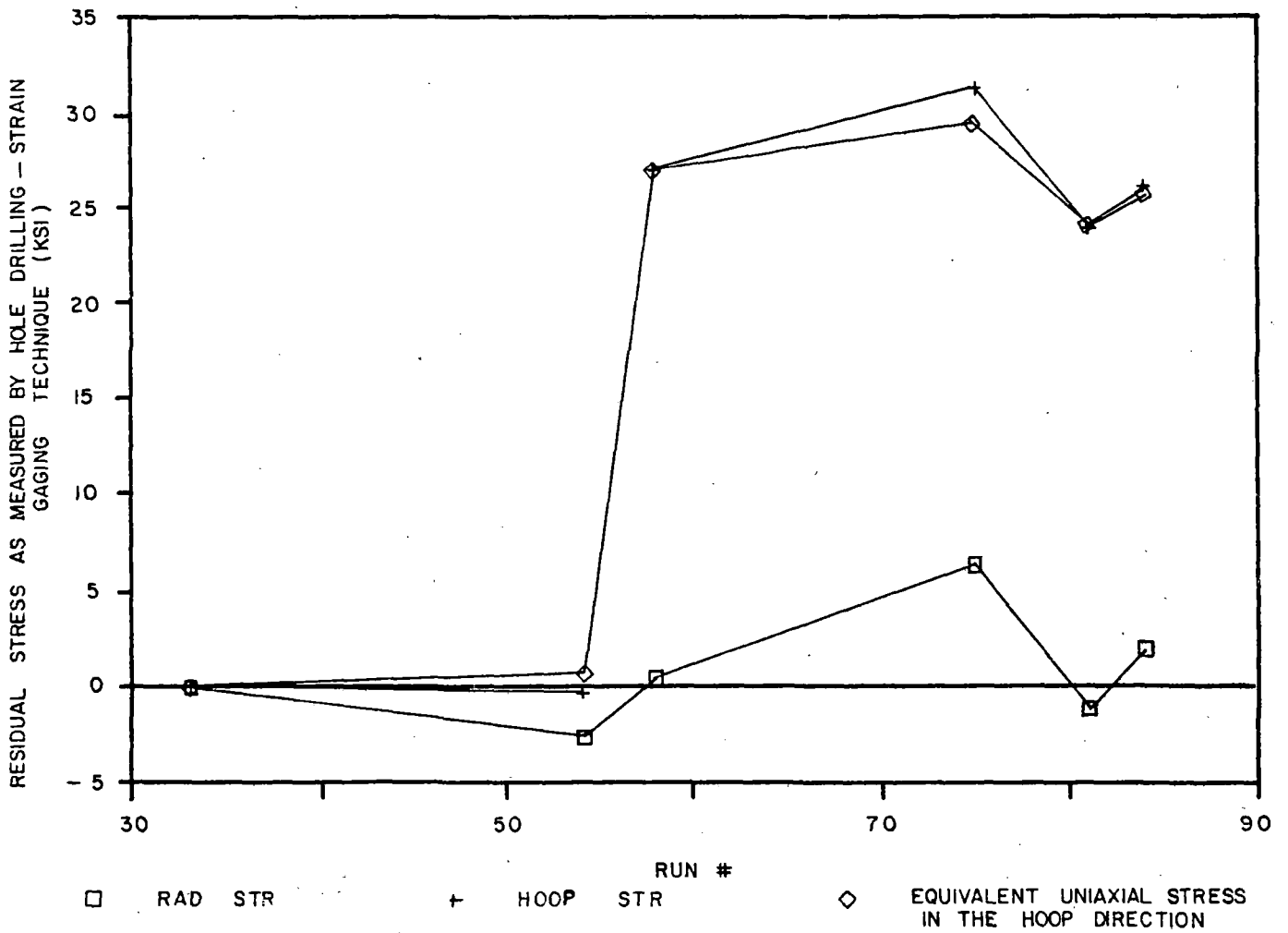
FIGURE 5.14   RESIDUAL STRESS AT B1 LOCATION, WHEEL 8

WHEEL 7

LOCATION B1
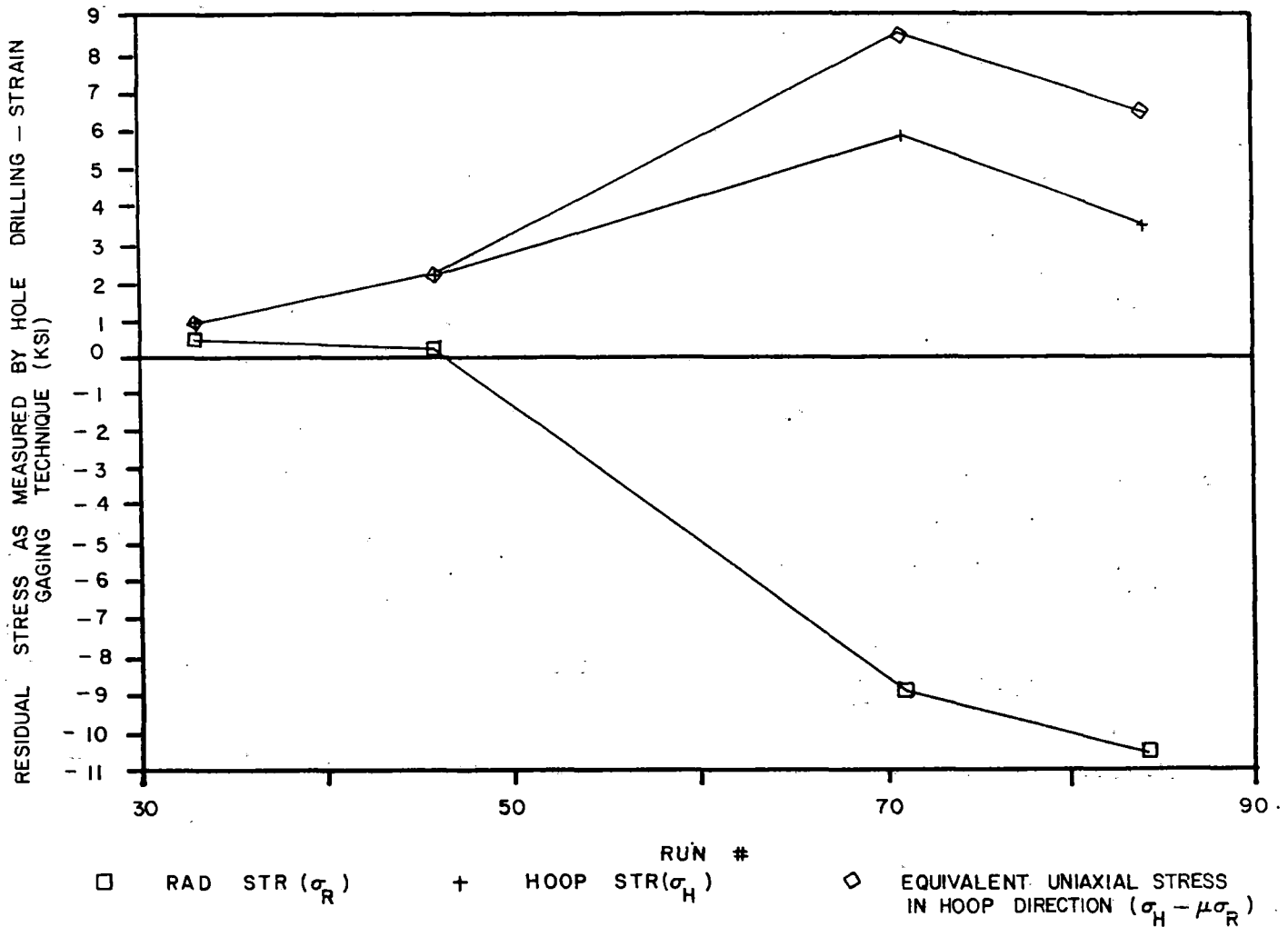
FIGURE 5.15   RESIDUAL STRESS AT B1 LOCATION, WHEEL 7

stress versus number of drag braking cycles.

It was observed that the residual stress (σ_R) at B1 locations became more compressive, making the equivalent uniaxial stress in the hoop direction ($\sigma_h - \sigma_r$) more tensile.

Similar trends were noticed at B2 and B3 locations except that the radial stress component (which is increased in the compressive direction) showed a more dominant effect resulting in an equivalent uniaxial stress in the hoop direction, pushed toward zero or the tensile direction (Figures 5.16 and 5.17).

5.2.5 Wheel Strains and Temperature Histories

In addition to temperatures, wheel surface strains were monitored at the three specified wheel locations. From these data, it was possible to reconstruct the actual mechanical strain and temperature cycles corresponding to the braking cycles imposed on the wheels. The temperature and rim hoop (mechanical) strain cycles corresponding to the most severe pair of braking cycles imposed on wheel No. 8 are illustrated in Figures 5.18 and 5.19.

5.2.6 Peak Elastic Stress, Temperature and Horsepower
       Correlation

During braking tests on the RDU, apart from the evaluation of residual stresses by the hole drilling-strain gaging method after regular intervals, the thermal and residual strains were
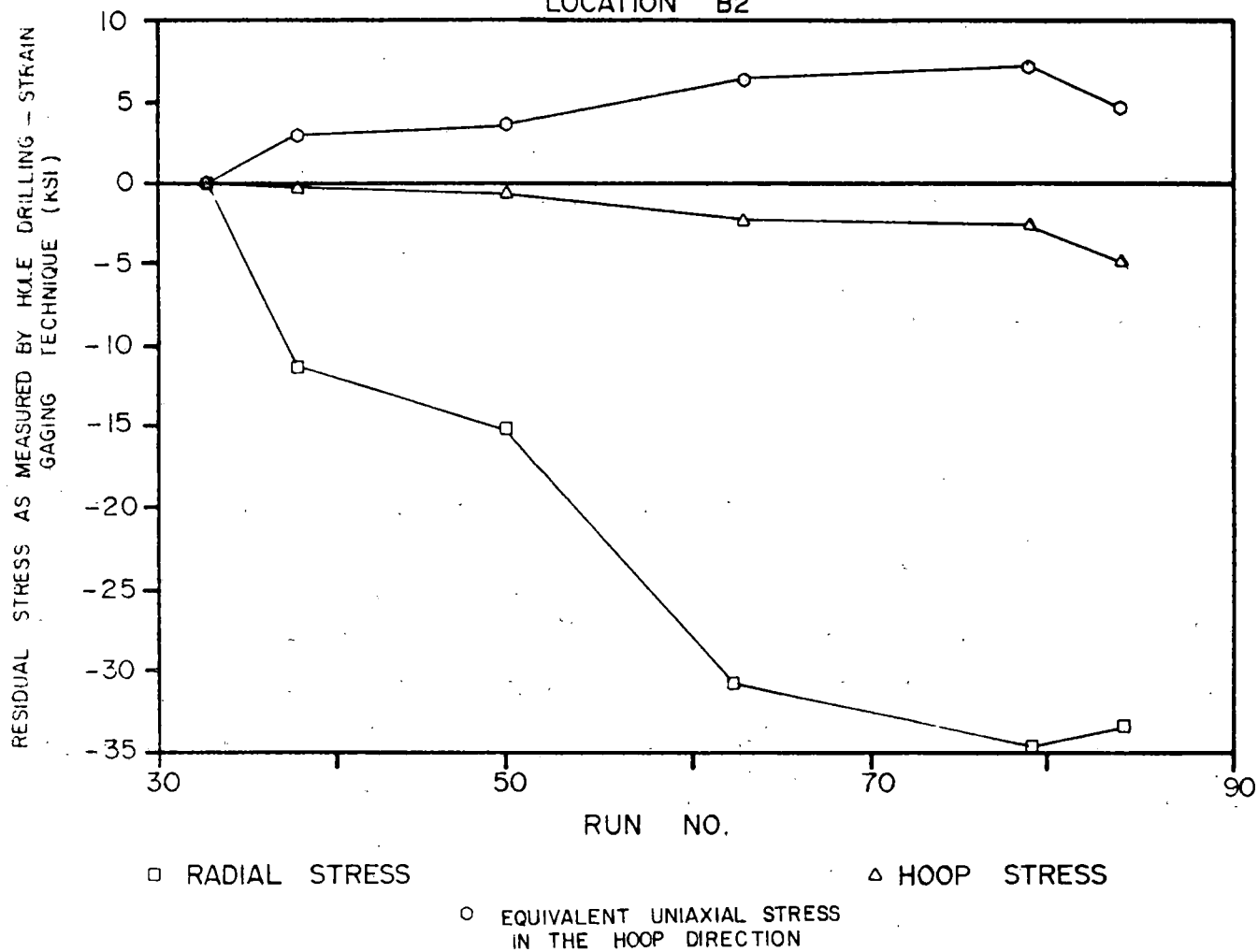
FIGURE 5.16   RESIDUAL STRESS AT B2 LOCATION, WHEEL 5

WHEEL 6

LOCATION B2
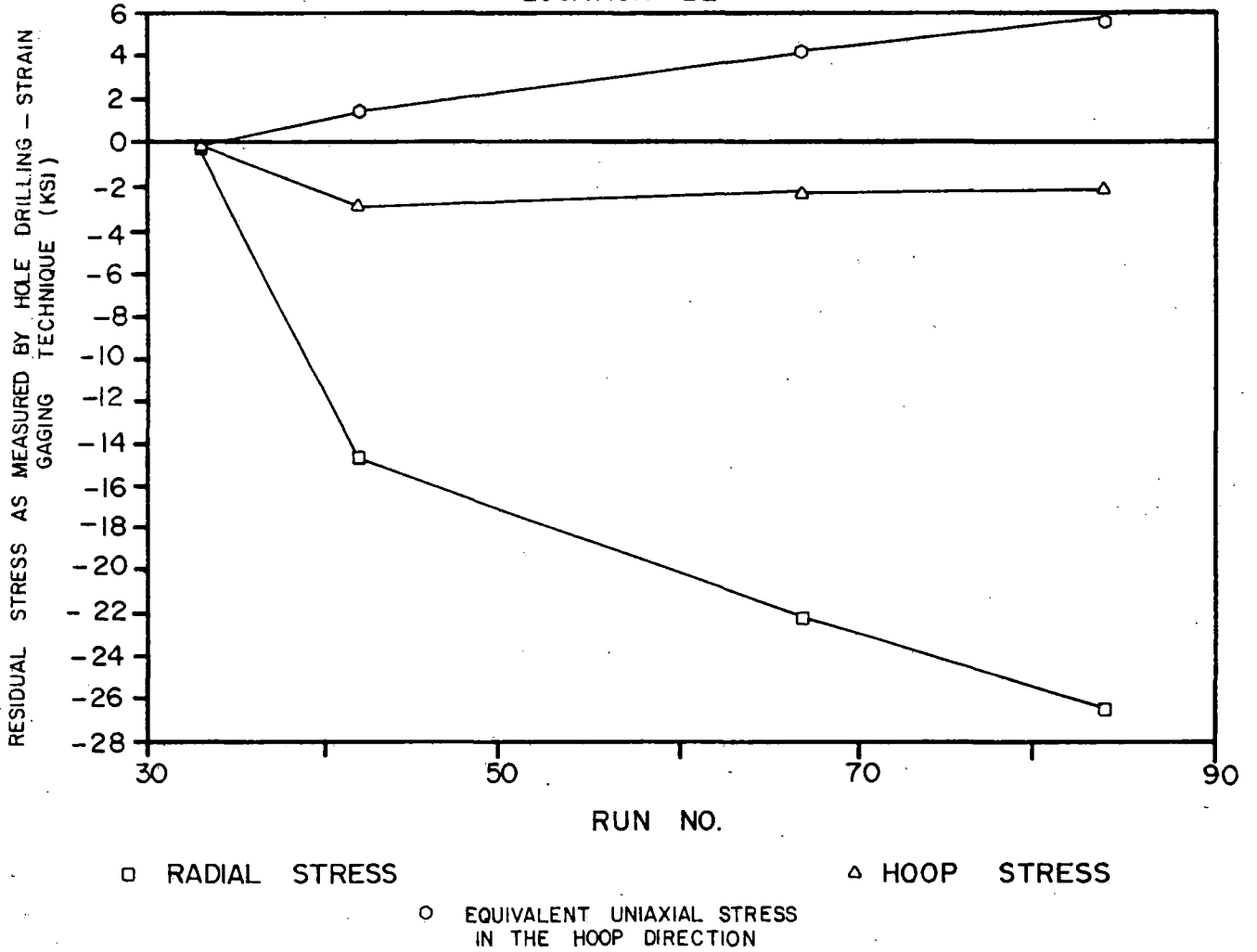
FIGURE 5.17   RESIDUAL STRESS AT B2 LOCATION, WHEEL 6

TIME HISTORY OF TEMPERATURE
RUNS 55/56 & 57/58, WHEEL 8 B1 LOCATION
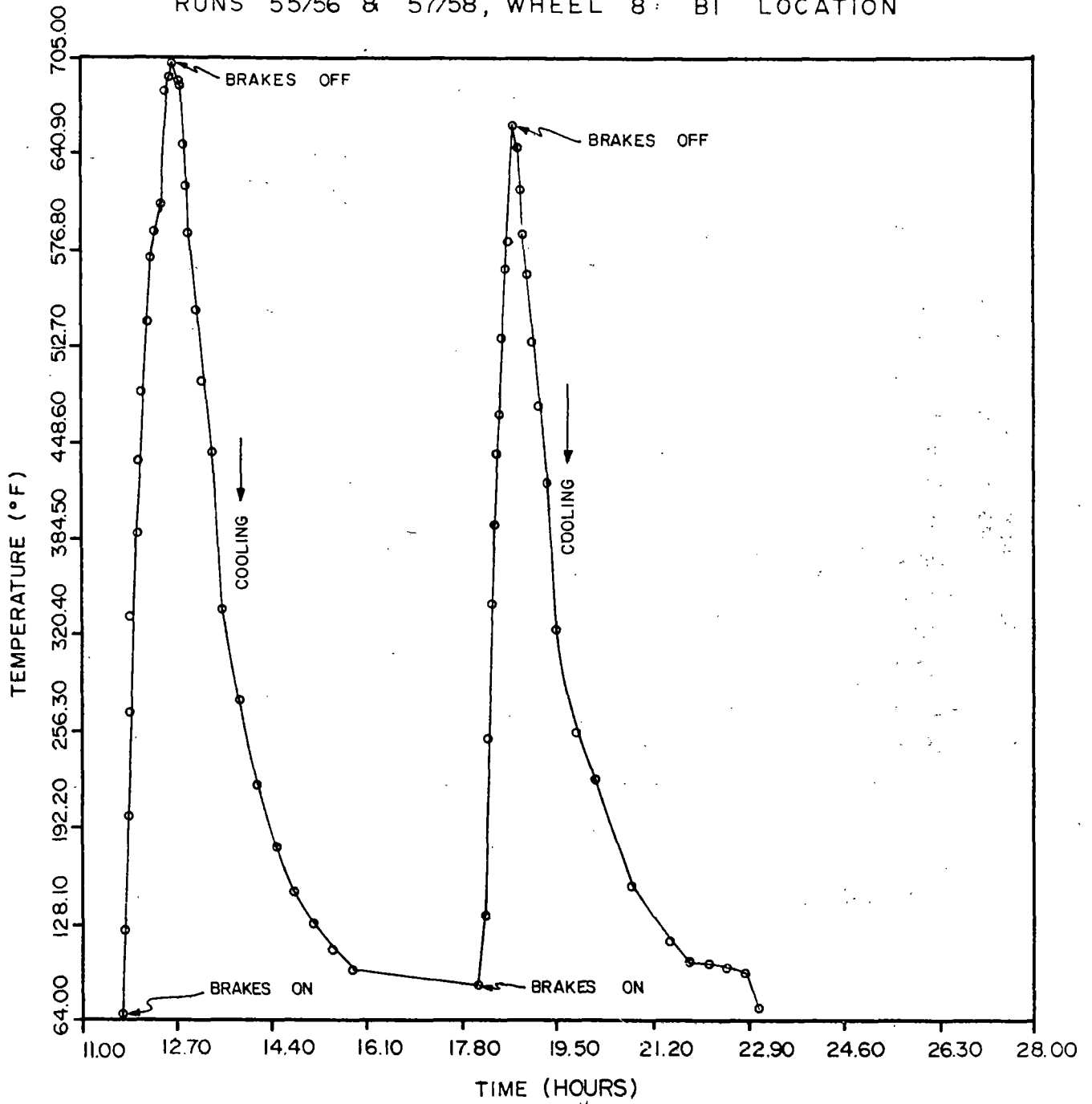
FIGURE 5.18   TIME HISTORY OF TEMPERATURE MEASURED AT BACK FACE
RIM (B1) LOCATION DURING SEVERE DRAG BRAKING ON
RDU

TIME HISTORY OF ACTUAL MECHANICAL STRAINS
RUNS 55/56 & 57/58, WHEEL 8: B1 LOCATION
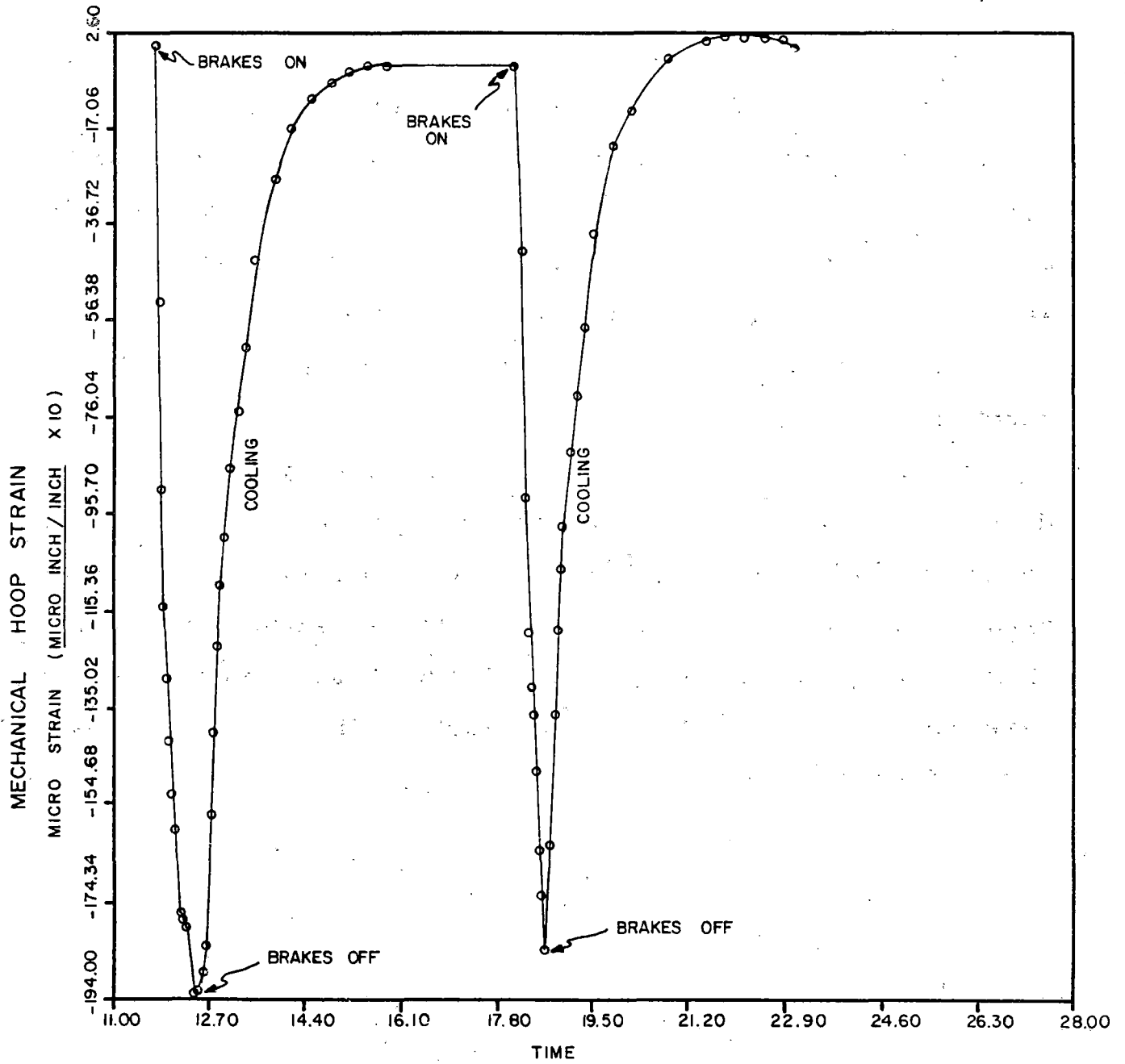
FIGURE 5.19   TIME HISTORY OF MECHANICAL HOOP STRAIN MEASURED AT
BACK FACE RIM (B1) LOCATION DURING SEVERE DRAG
BRAKING ON RDU

monitored by high temperature strain gages on a continuous basis during and after testing and were reduced for further stress analysis.

The strains monitored by high temperature strain gages at locations B1, B2, and B3 during the heating portions of drag braking cycles were converted into actual mechanical strains by applying the required corrections. The apparent strain measurements made by the weldable high temperature strain gages were converted into actual mechanical strains after applying lead wire resistance and temperature dependent gage factor corrections.

At B1, strain was measured only in the tangential (hoop) direction. At B2 and B3 strains were measured in both tangential and radial directions. The information at B1 was treated as if it were a uniaxial stress situation and the elastic tangential stress was calculated. Locations B2 and B3 were treated as biaxial stress fields. The elastic stresses were calculated from:

$$\sigma_R^E = \frac{E}{(1-\upsilon^2)} (\epsilon_R + \upsilon \epsilon_T)$$

$$\sigma_T^E = \frac{E}{(1-\upsilon^2)} (\epsilon_T + \upsilon \epsilon_R)$$

From these, an elastic effective stress was calculated from:

$$\bar{\sigma}^E = \sqrt{\sigma_T^{E2} + \sigma_R^{E2} - \sigma_T^E \sigma_R^E}$$

The magnitude of elastic effective stress is a measure of the thermal severity to which the wheel has been subjected. If its magnitude is more than the material's yield strength at the temperature, the effective stress (though fictitious in character) provides a potential for predicting the onset of plasticity during thermal cycle.

The brake shoe-wheel interface forces were continuously monitored and the Bhp for each wheel was computed and acquired. The temperature levels attained by different locations of the test wheels were recorded so that the actual strains, temperatures, and Bhp's could be interrelated.

The data were analyzed assuming the indices of braking severity to be parameters such as average Bhp dissipated at the brake shoe-wheel interface and elastic effective stresses computed at various critical locations of the wheel. The indices were correlated with the maximum temperatures attained at different critical locations of the wheel.

Correlations between elastic effective stress computed at a given critical location and average Bhp at the corresponding wheel-brake shoe interface are presented in Figures 5.20 through 5.25. The nonlinearity in the relationship seems to be on account of the limitation in the Bhp levels that can be sustained in the brake shoe-wheel interface.

Typical correlations between elastic effective stress and maximum temperatures attained at a given location are presented in Figures 5.26 through 5.31. Maximum temperatures attained at the back side of the rim and back side of the rim fillet region

$$\sigma_{max} = 8.04 \sqrt{BHP}$$
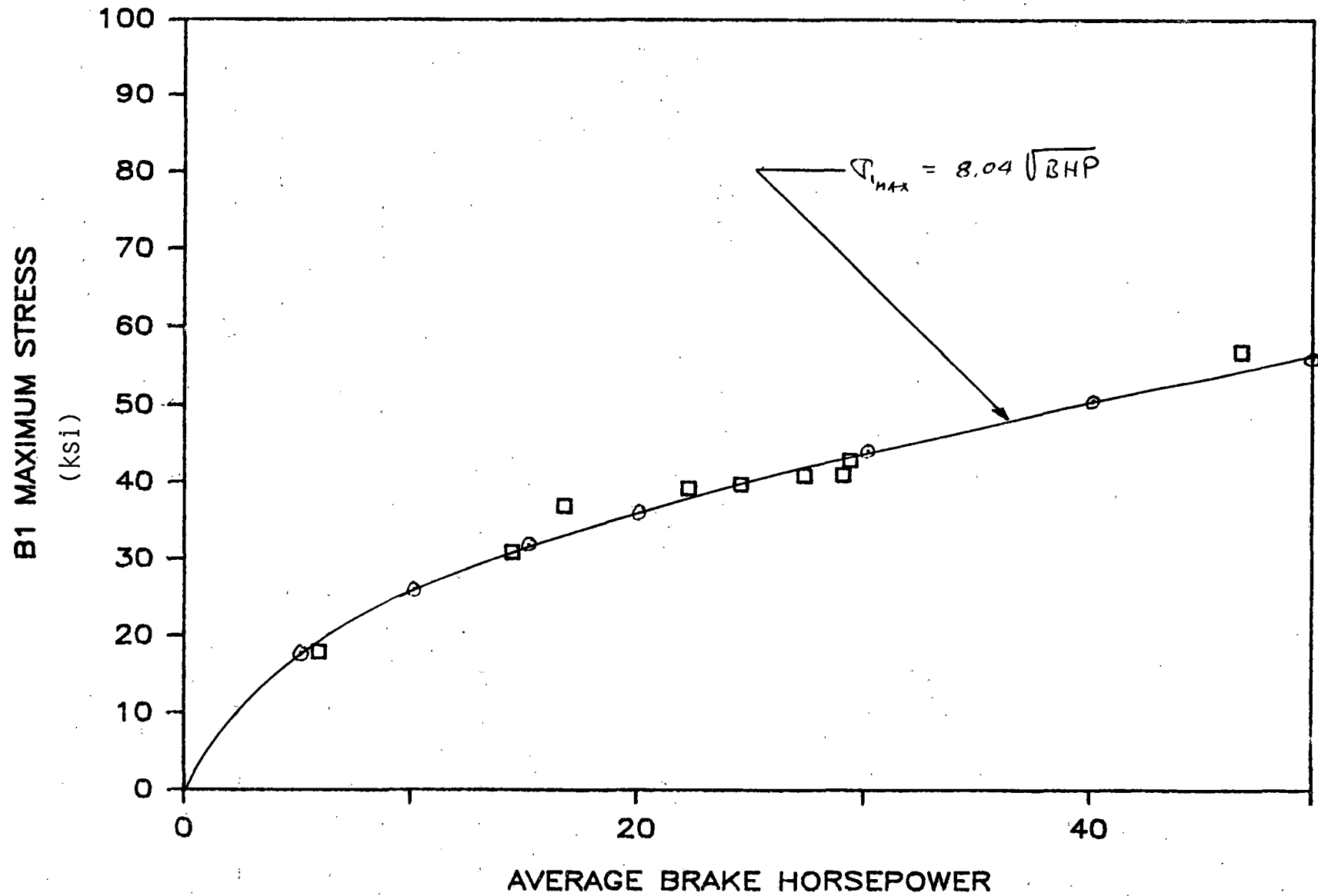
FIGURE 5.20 MAXIMUM ELASTIC STRESS (B1) -VS- AVERAGE BHP, WHEEL #8
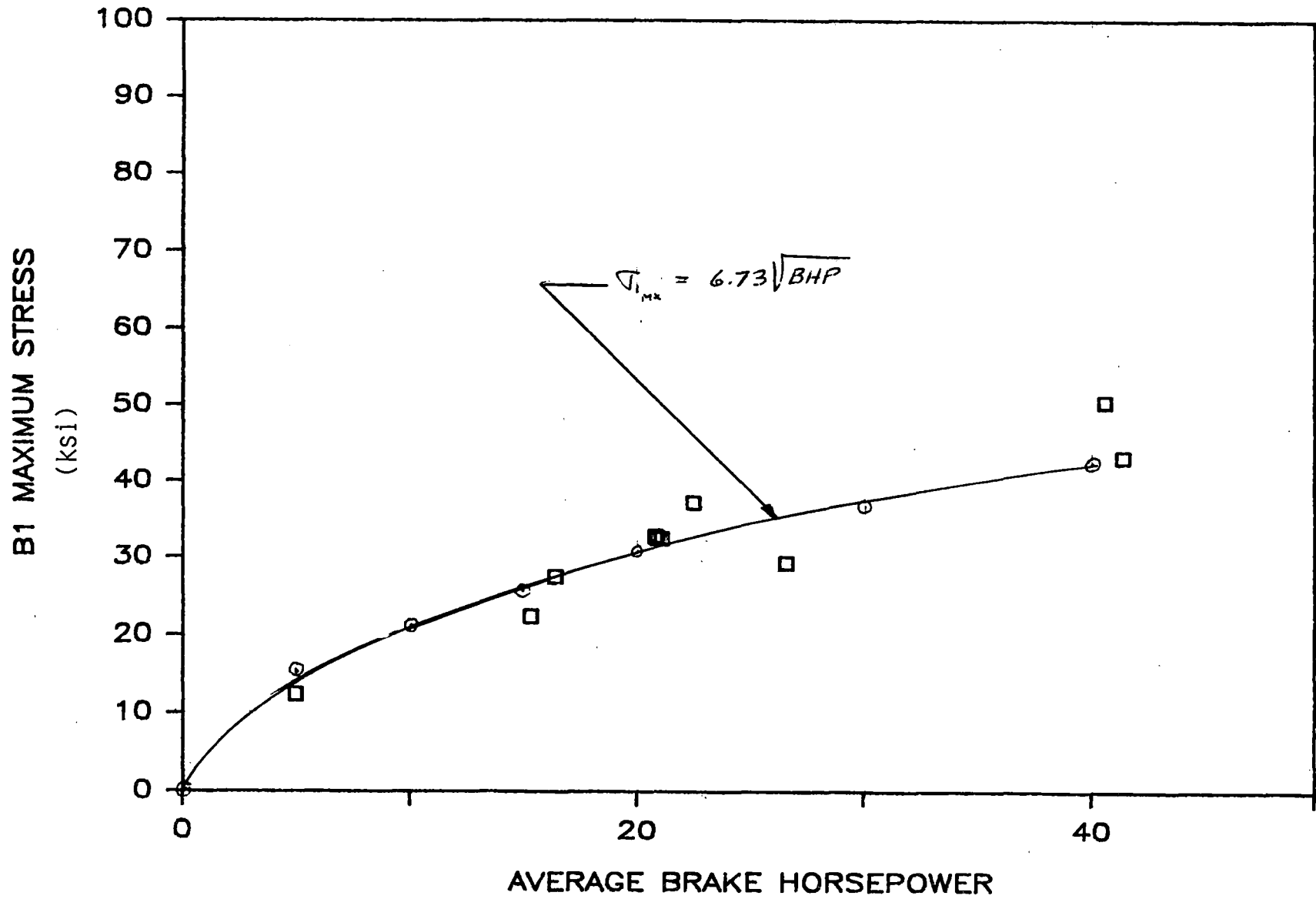
FIGURE 5.21   MAXIMUM ELASTIC STRESS (B1) -VS- AVERAGE BHP, WHEEL #5

$$\sigma_{2_{EFF_{MAX}}} = 10.83 \sqrt{BHP}$$
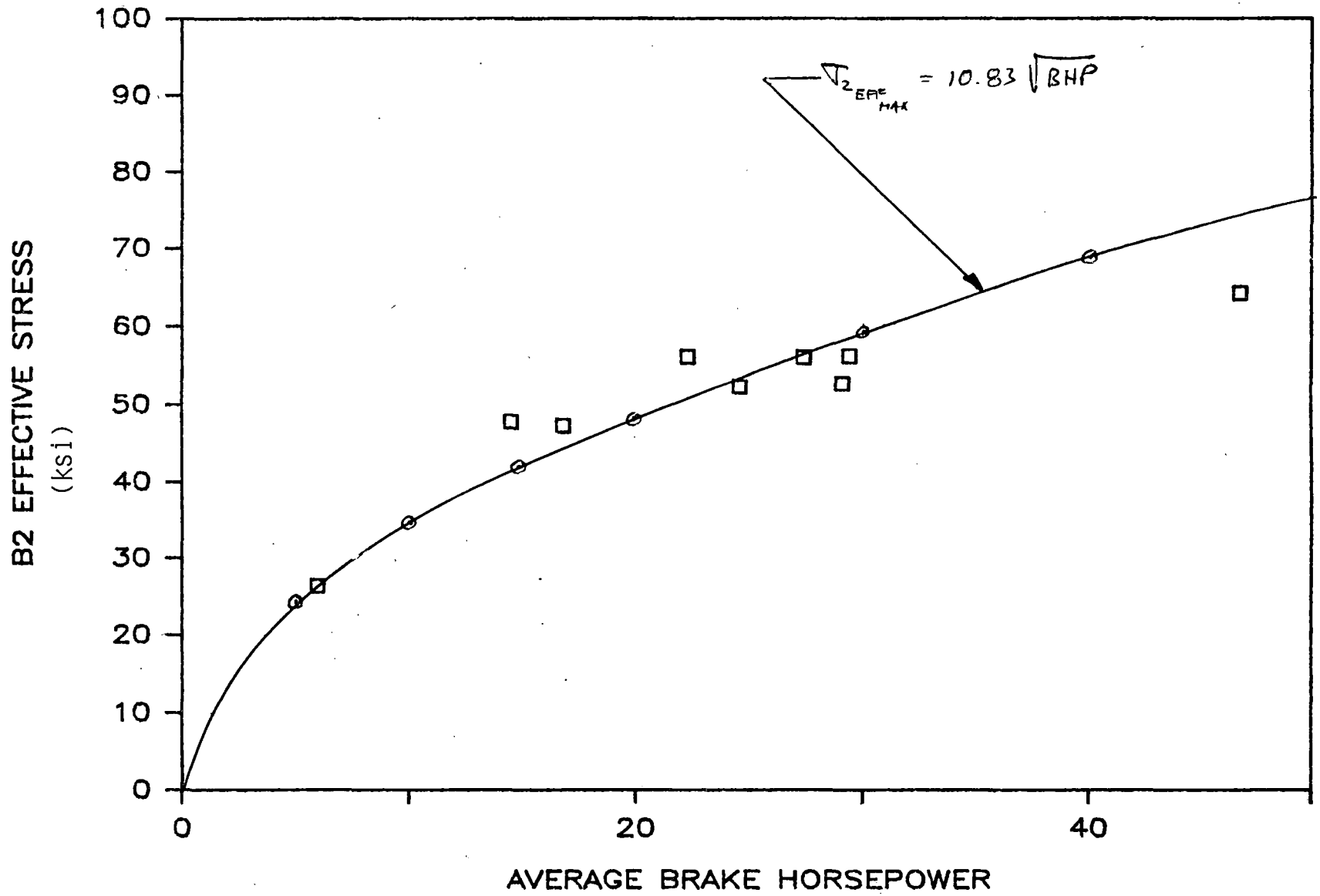
FIGURE 5.22   EFFECTIVE ELASTIC STRESS (B2) -VS- AVERAGE BHP, WHEEL #8

$$\sigma_{2_{eff_{MAX}}} \simeq 11.73\sqrt{BHP}$$
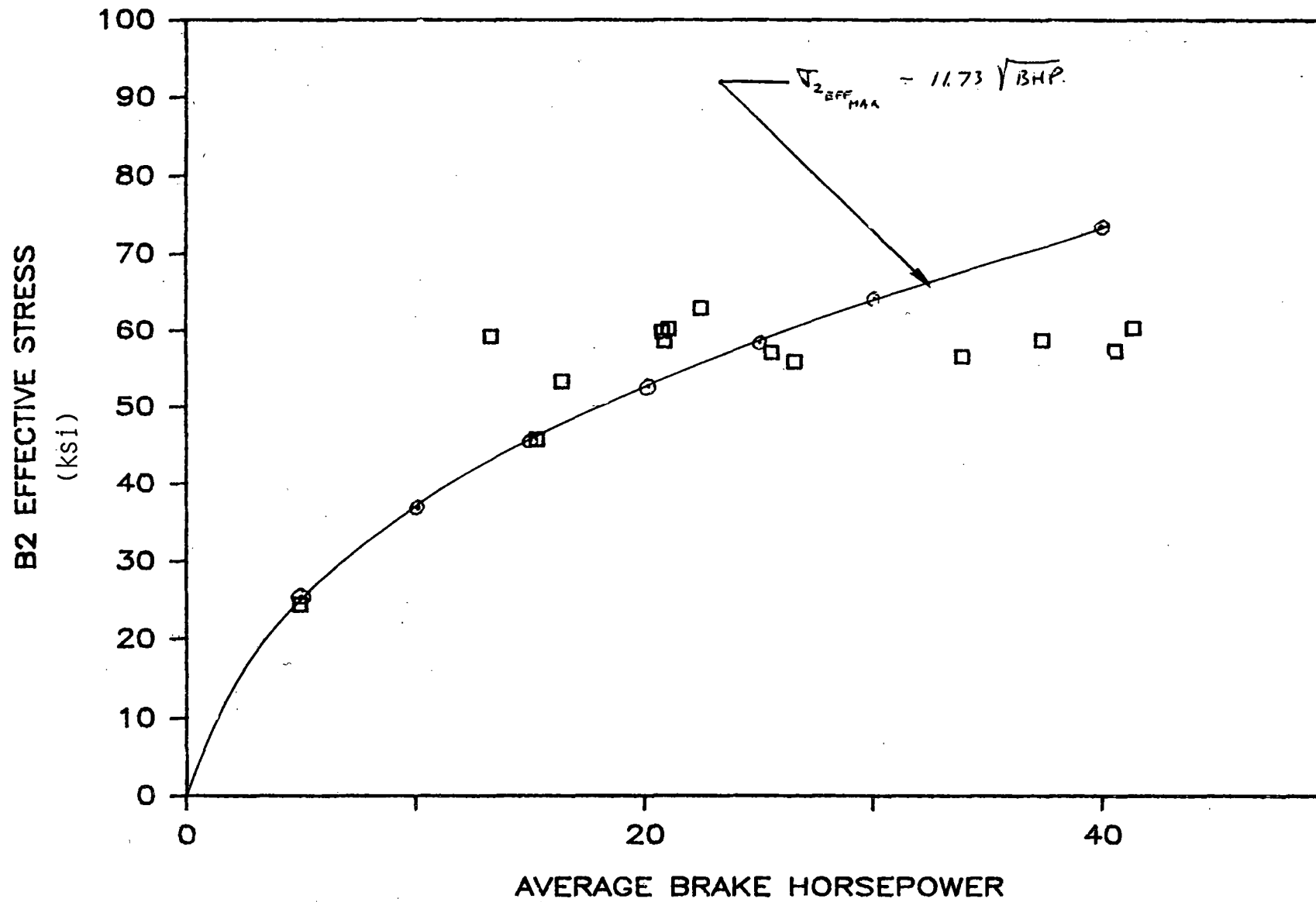
FIGURE 5.23   EFFECTIVE ELASTIC STRESS (B2) -VS- AVERAGE BHP, WHEEL #5

$$\sigma_{3_{EFF\ MAX}} = 12.89 \sqrt{BHP}$$
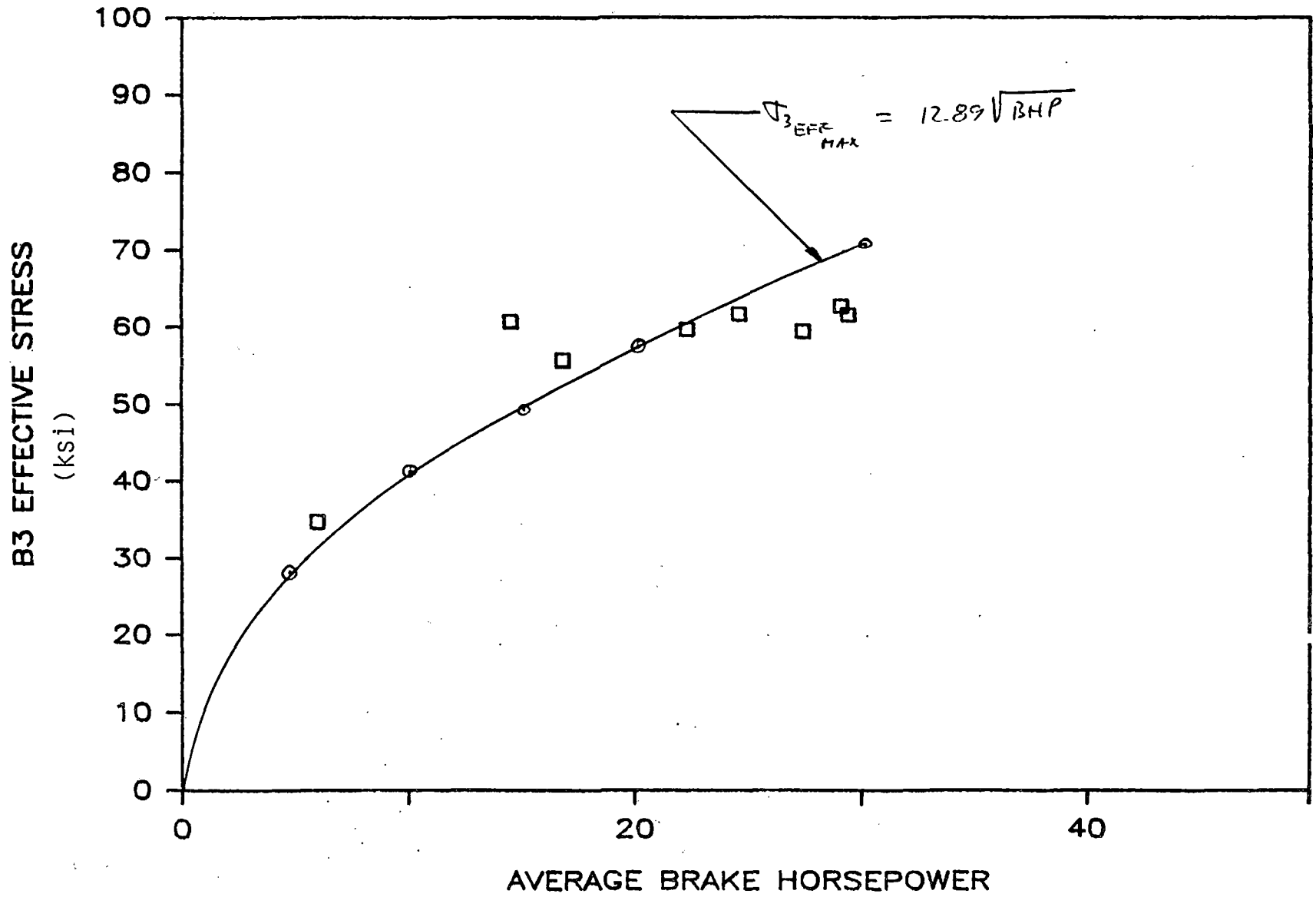
FIGURE 5.24   EFFECTIVE ELASTIC STRESS (B3) -VS- AVERAGE BHP, WHEEL #8
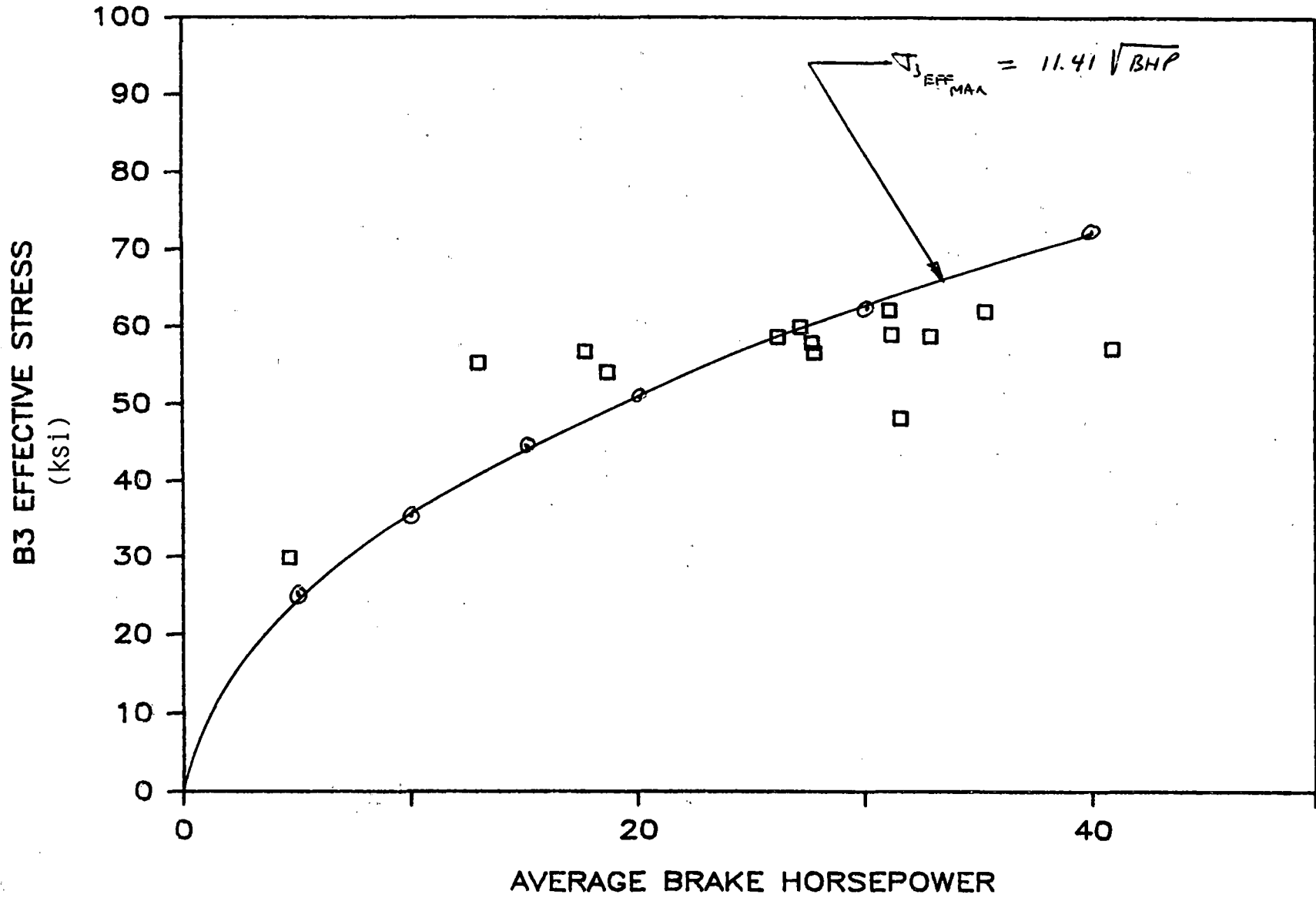
FIGURE 5.25   EFFECTIVE ELASTIC STRESS (B3) -VS- AVERAGE BHP, WHEEL #7
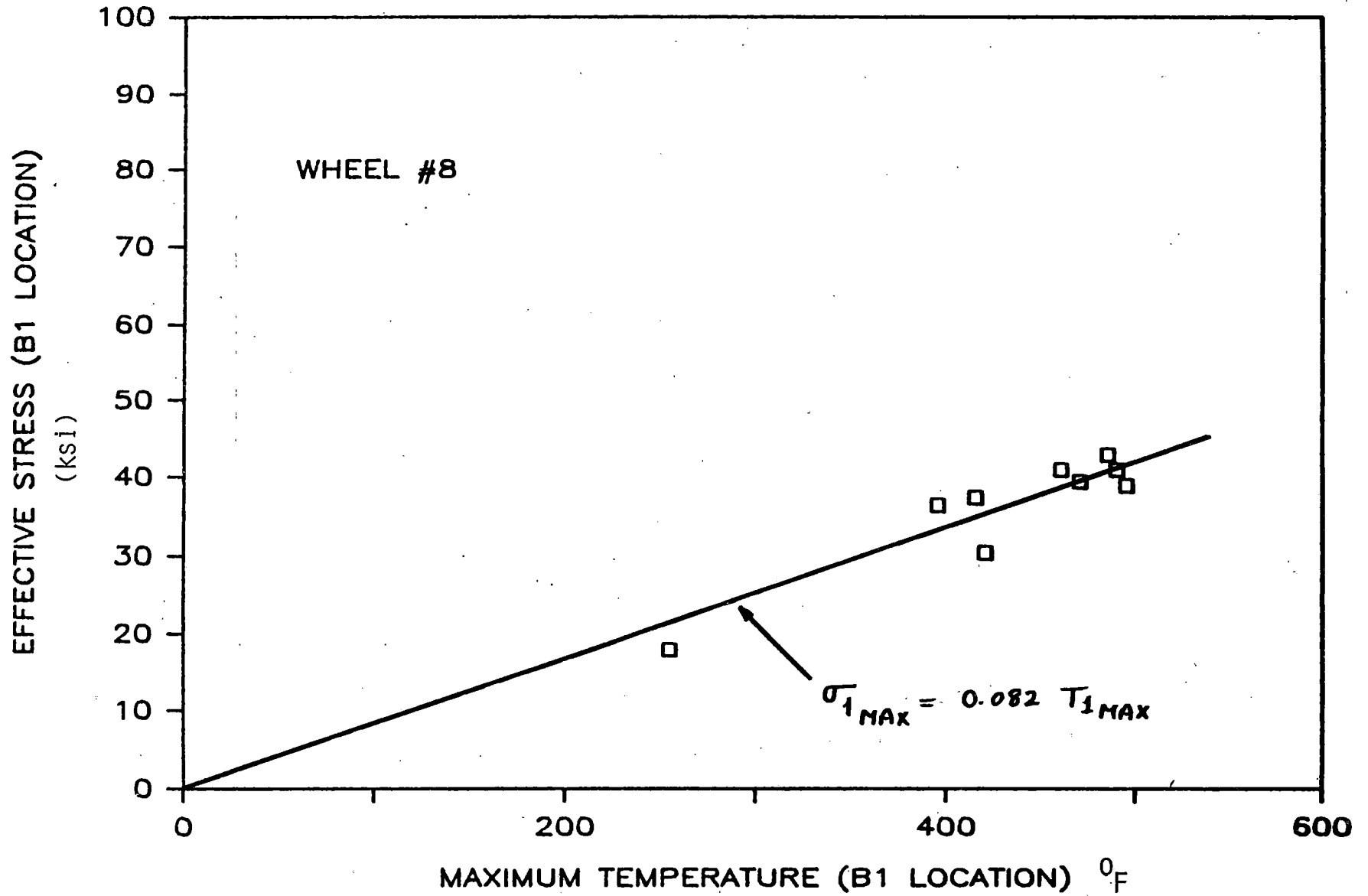
FIGURE 5.26   EFFECTIVE ELASTIC STRESS (B1) -VS- TEMPERATURE (B1), WHEEL #8
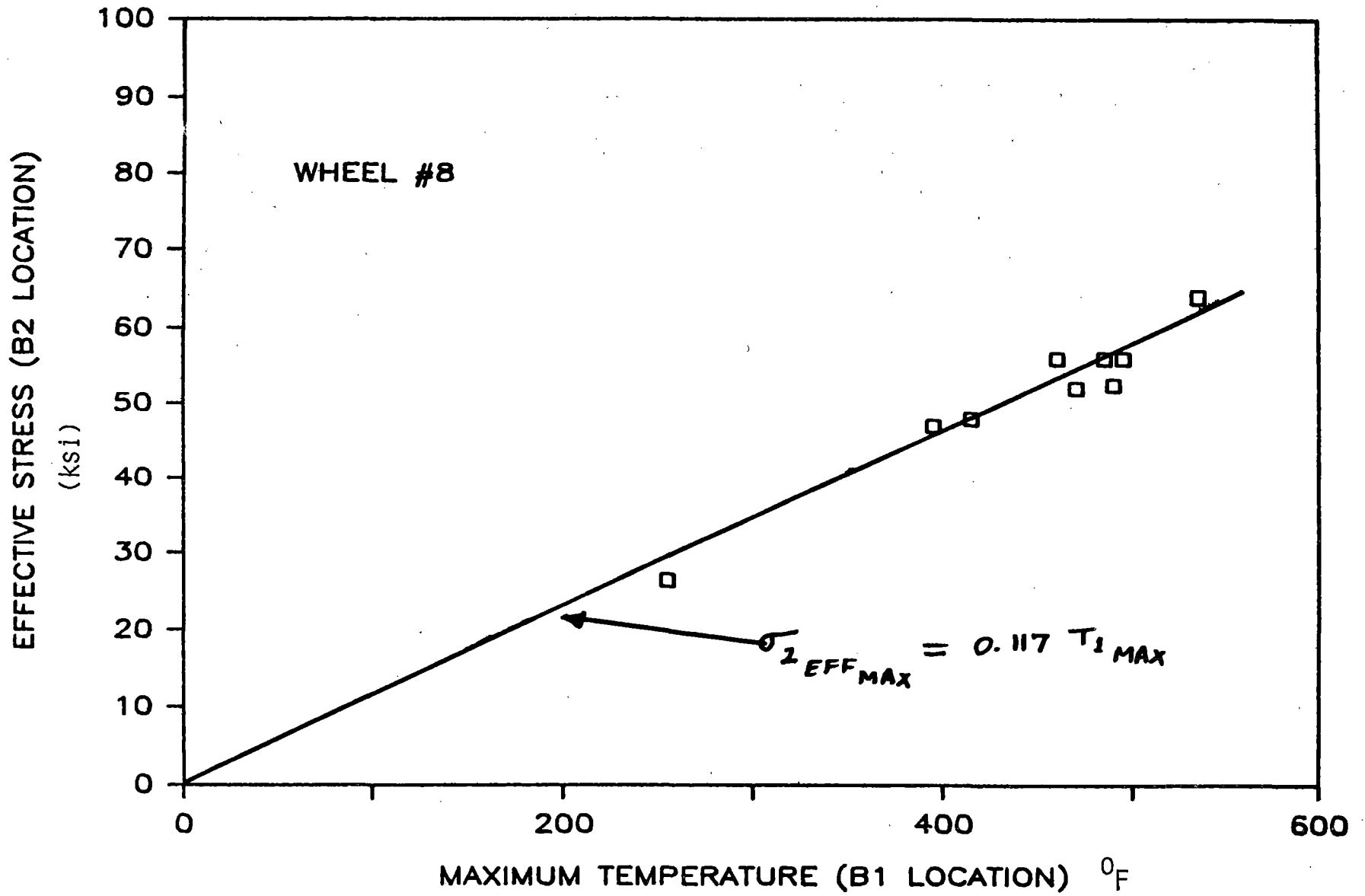
FIGURE 5.27   EFFECTIVE ELASTIC STRESS (B2) -VS- TEMPERATURE (B1), WHEEL #8

The plot is labeled WHEEL #8 with a linear relationship shown:

$$\sigma_{2_{EFF_{MAX}}} = 0.137 \; T_{2_{MAX}}$$

Y-axis: EFFECTIVE STRESS (B2 LOCATION) (ksi)

X-axis: MAXIMUM TEMPERATURE (B2 LOCATION) ^0F
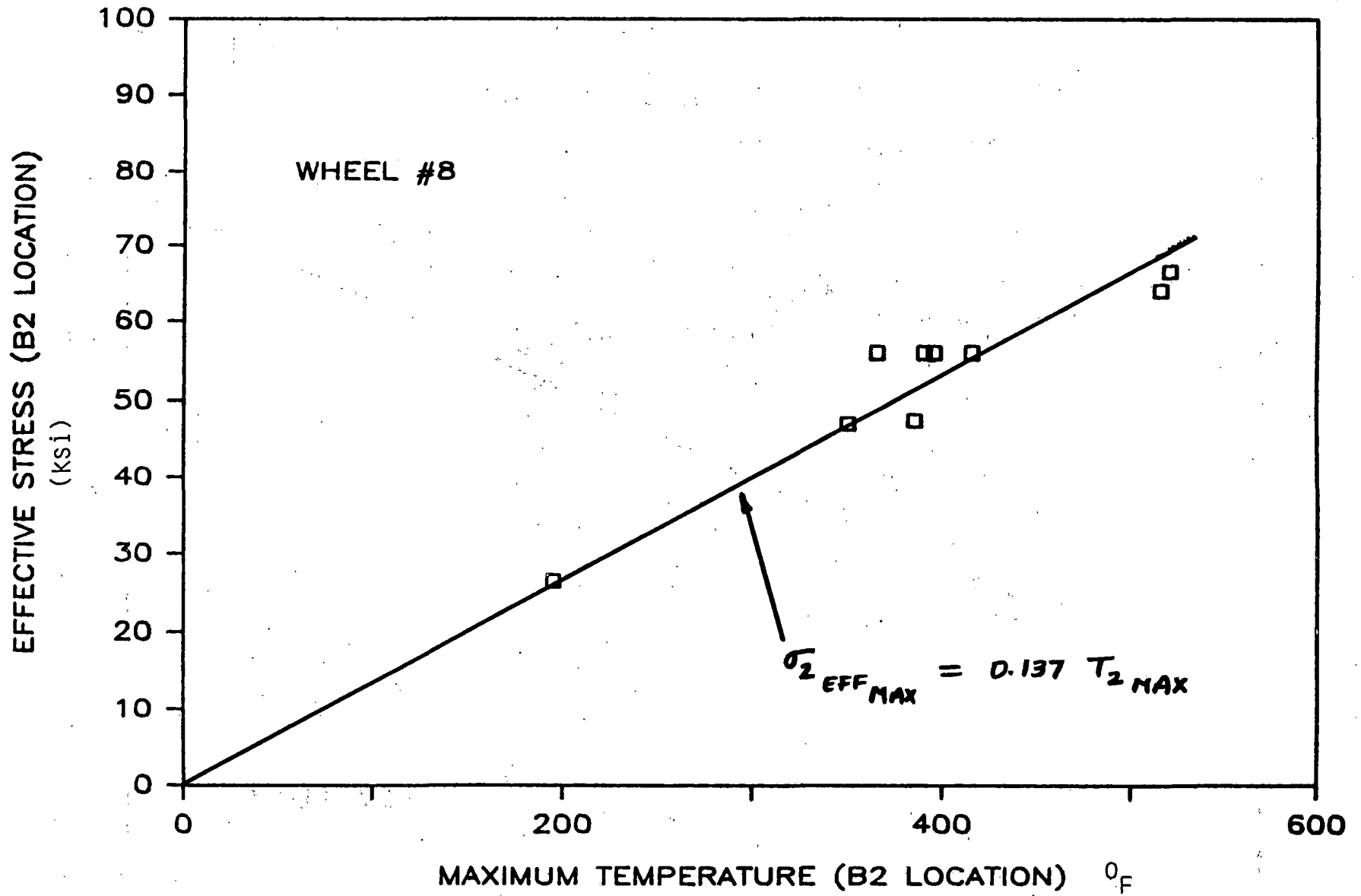
FIGURE 5.28   EFFECTIVE ELASTIC STRESS (B2) -VS- TEMPERATURE (B2), WHEEL #8
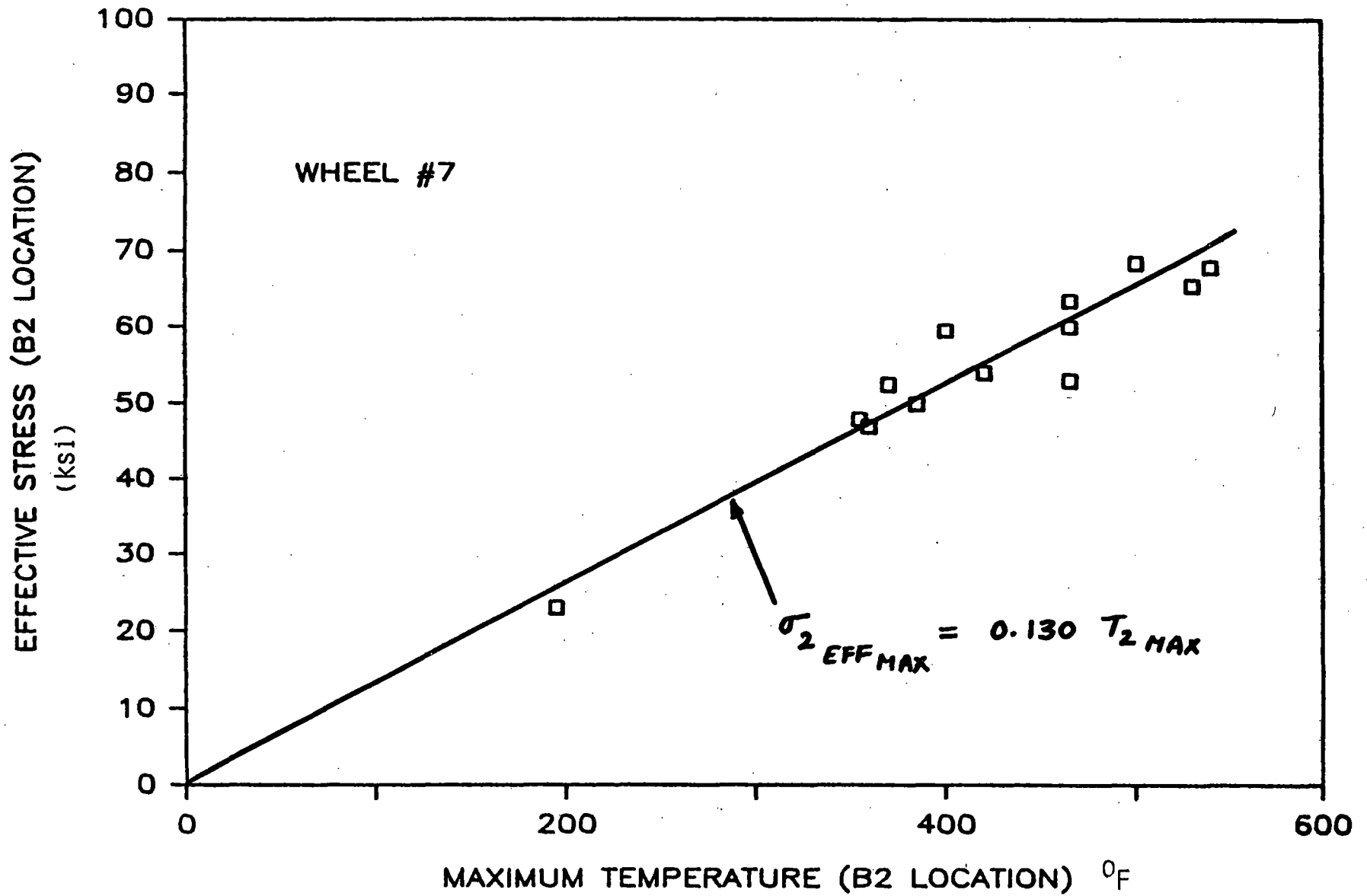
FIGURE 5.29   EFFECTIVE ELASTIC STRESS (B2) -VS- TEMPERATURE (B2), WHEEL #7
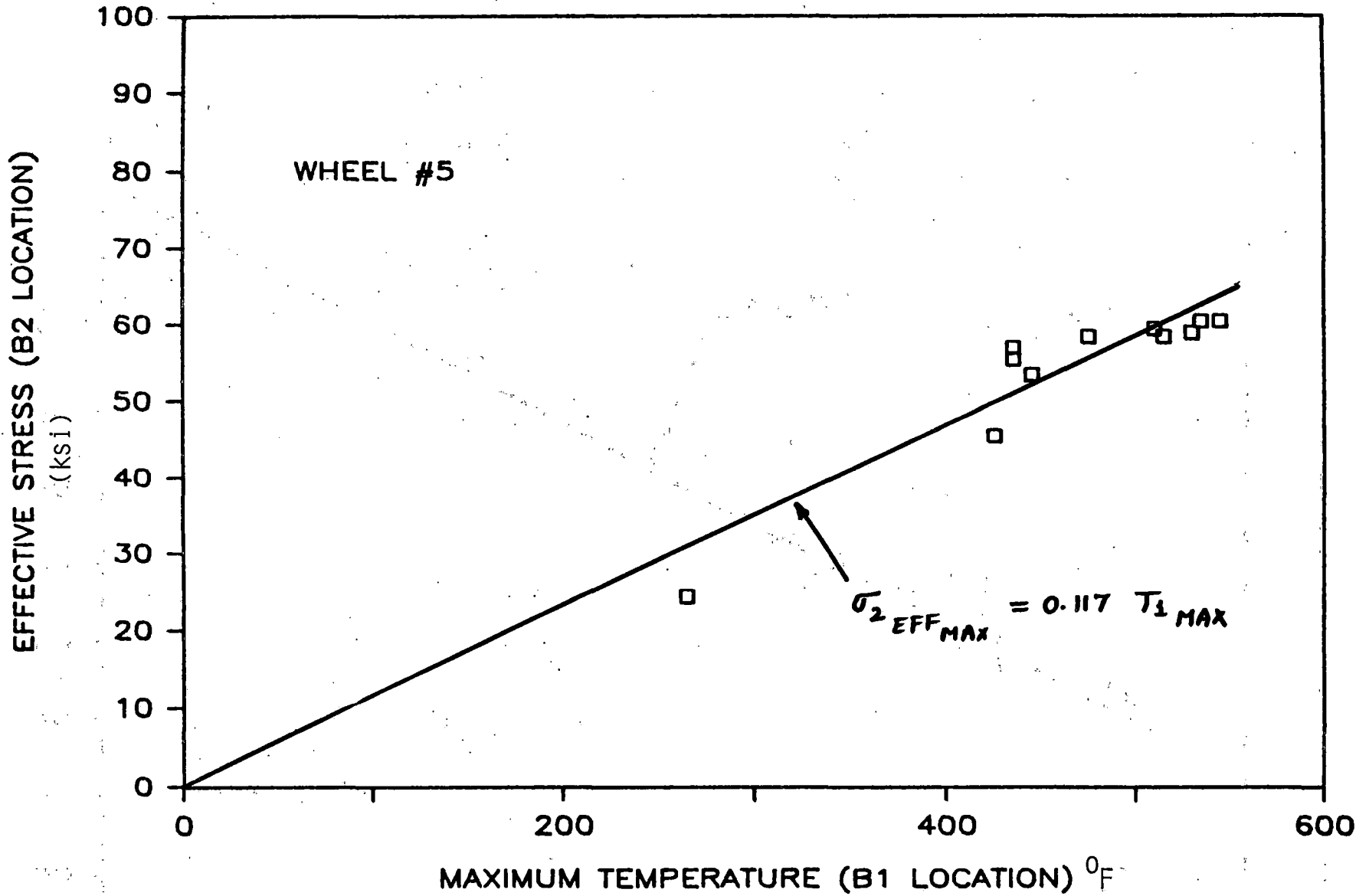
FIGURE 5.30   EFFECTIVE ELASTIC STRESS (B2) -VS- TEMPERATURE (B1), WHEEL #5
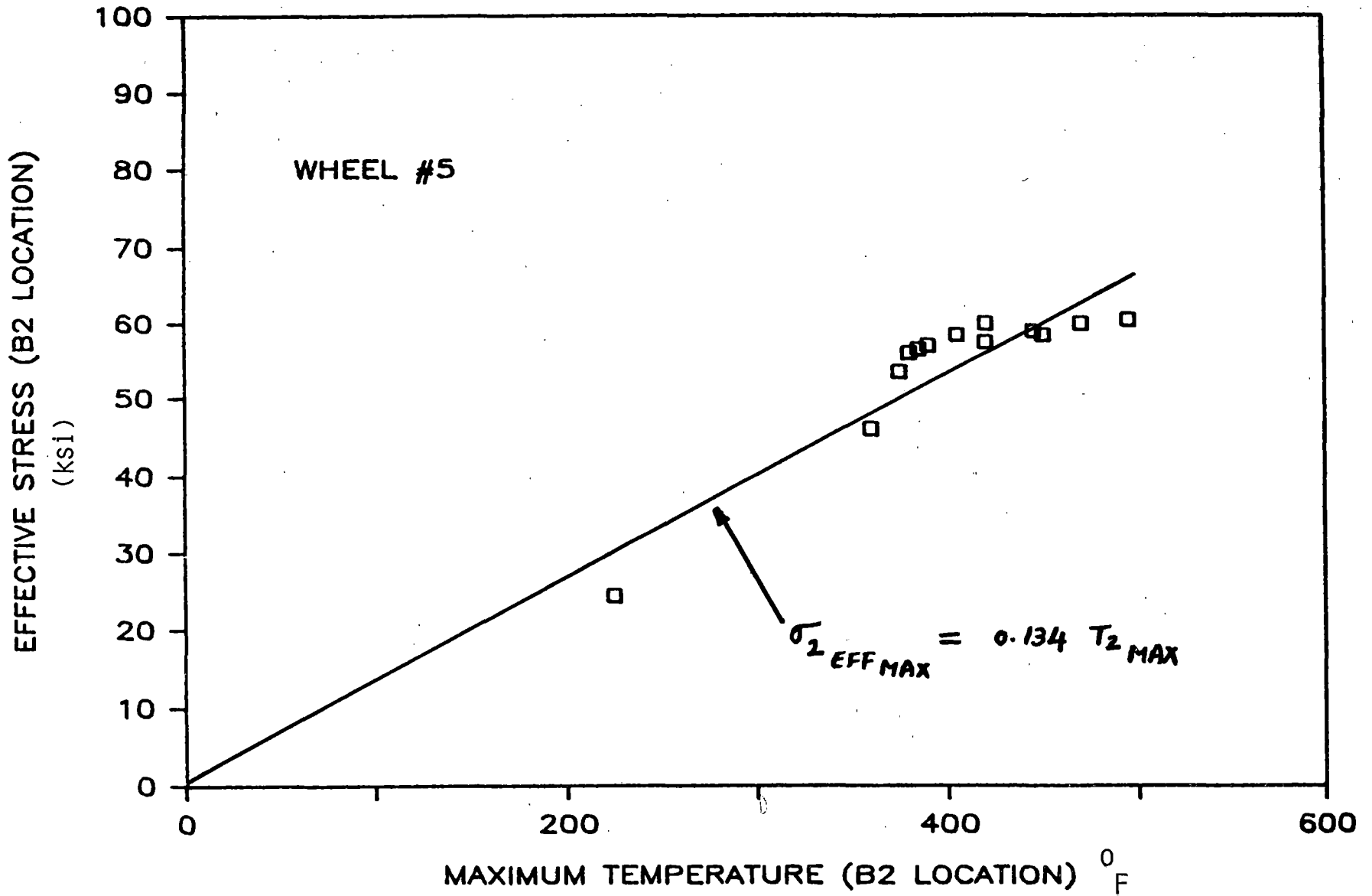
FIGURE 5.31   EFFECTIVE ELASTIC STRESS (B2) -VS- TEMPERATURE (B2), WHEEL #5

seem to have a linear relationship with the elastic effective stress attained in the corresponding locations.

5.2.7 Calculation of Derived Quantities

Lotus Data Base

Characteristic wheel temperature and strain data, brake force data, measured residual stresses, and test parameters were tabulated for each wheel and test cycle in the form of a Lotus data base (see Appendix 5.8). Selected analytical parameters, such as rim energy density, were also entered into the data base. Calculation of these analytical parameters is described below.

A number of columns in the RDU and Preliminary Data Bases contain values which were computed from data that was collected during the tests.

The column headings corresponding to derived quantities are:

1.   Average speed, Normal Brake Shoe Force, Tangential Shoe Force, and Brake Horsepower

2.   Rim Energy Density

3.   Estimated Bhp

4.   Energy Inputs above Threshold Bhp

5.   Effective Strain, Principal Stress, Effective Stress, Yield Ratio

The procedures used in calculating items 1 through 5 are described below.

Averages

Speed, Brake Force, and Horsepower averages were obtained by numerically integrating the quantity of interest with respect to time over the time of the test and dividing by the total elapsed time. Trapezoidal integration was used (see Figure 5.32).

Rim Energy Density

This was calculated from the following formula.

$$\text{Rim Energy Density} = \frac{\text{Total Energy Input During Test}}{\text{Weight of Rim}} \quad \text{Braking}$$

The total energy was computed by integrating the Bhp time history (which is done in the process of computing an average). The rim weight of the new test wheels was 438 lbs.[1]

[1]From Opinsky, Volume Considerations in Freight Car Wheels

Estimated Bhp

During the test, tangential brake shoe forces were computed (as the data were collected) from measured brake head strain gage voltages. Bhp's, in turn, were calculated from the train speed and tangential forces as follows:

Brake Power = Retarding Brake Force x Brake Shoe/Wheel Relative Velocity

FIGURE 5.32   CALCULATION OF TIME AVERAGE

$$\overline{Q} = \frac{\sum\limits_{i=1}^{n-1} \dfrac{Q(i) + Q(i+1)}{2} \times (T_{i+1} - T_i)}{T_n - T_1}$$

MEASURED
QUANTITY
Q

TEST
START
T_1

T_2

T_3

TEST
END
T_n

TIME

5-64

¹ Brake Horsepower is defined to be 550 ft. - lbs./sec. If the force is given in lbs. and the velocity in mph, then

Horsepower = Force (lbs.) x Speed (mph) x $\frac{5280 \text{ ft.}}{\text{mile}}$ x

$\frac{1 \text{ hr.}}{3600 \text{ sec.}}$ x $\frac{1 \text{ H.P. Sec.}}{550 \text{ ft.-lb.}}$ = .002666 x Force x Speed x 1 H.P.

For analysis purposes, the brake horsepower during each of the tests was estimated from the normal force and speed. The coefficient of friction,

$$f = \frac{\text{tangential force}}{\text{normal force}}$$

was assumed to be .18 for RDU tests, and .23 for preliminary and comprehensive track tests.

Energy Inputs Above Threshold Bhp

Another derived quantity, threshold energy, was used as an indicator of test severity. The threshold energy for a given test was computed by summing the total energy that was accumulated at a rate exceeding 30, 40, and 50 Bhp. As was done for averaging, a trapezoidal integration routine was used. In this routine, two consecutive points above the threshold Bhp level were required before an energy was counted in the summation (see Figure 5.33).

SHADED AREA = TOTAL ENERGY ACCUMULATED AT
A RATE EXCEEDING THRESHOLD BHP

$$= \sum_{i=1}^{n-1} \frac{BHP(i) + BHP(i+1)}{2} \times (T_{i+1} - T_i)$$

WHERE BHP(i), BHP(i+1) ARE TWO CONSECUTIVE
POINTS SUCH THAT BHP(i), BHP(i+1) $>$
THRESHOLD BHP

BRAKE
HORSE
POWER
(BHP)

THRESHOLD
BHP

TEST
START

T_1 T_2

ΔT_1

T_n

TEST
END

TIME
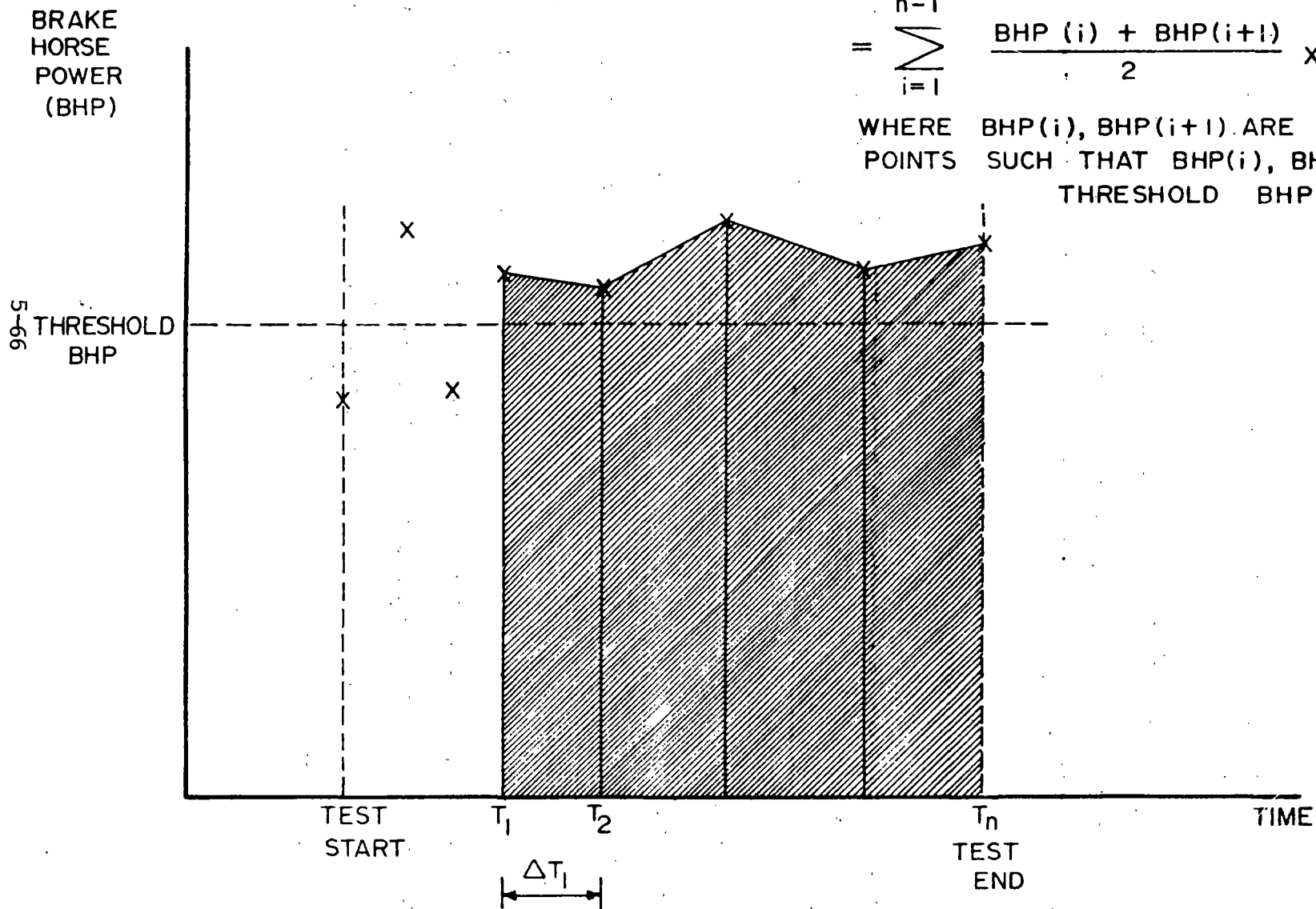
FIGURE 5.33   CALCULATION OF ENERGY ACCUMULATED AT RATE
EXCEEDING THRESHOLD BHP

Strains and Stresses

The equations used to calculate Effective Strain, Principal Stress, Effective Stress, and Yield Ratio are given in Figure 5.34.

Sample Test Data

Characteristic Test Data

Selected data (Bhp's, temperatures, strains, and stresses) from RDU testing has been extracted from the Lotus Database and is presented in Table 5.40. An important feature of the database is that it allows the user to 1) apply mathematical operations to selected parameters, and 2) extract only needed data for analysis.

5.2.8 Observations from RDU Testing

o   Satisfactory checkout of high temperature strain gages and thermocouples through slip rings and associated data collection software was achieved.

o   Preliminary estimates were made of braking cycle severity to cause wheel thermal damage, as measured by (positive) tensile stress field at the back face of the rim.

o   Wheel to wheel differences in temperatures and Bhp were observed under controlled conditions.

EFFECTIVE STRAIN $= \dfrac{2}{\sqrt{3}} \sqrt{\epsilon_H{}^2 + \epsilon_R{}^2 + \epsilon_H \epsilon_R} = \bar{\epsilon}$

WHERE ϵ_H = HOOP STRAIN

ϵ_R = RADIAL STRAIN

PRINCIPAL STRESS IN ϵ_1 DIRECTION $= \dfrac{1}{(1-\nu^2)} \times E(\epsilon_1 + \nu \epsilon_2) = \sigma_1$

WHERE ν = POISSON'S RATIO

E = YOUNG'S MODULUS

ϵ_1, ϵ_2 = PRINCIPAL STRAINS (HOOP OR RADIAL)

EFFECTIVE STRESS $= \sqrt{\sigma_H{}^2 + \sigma_R{}^2 - \sigma_H \sigma_R} = \bar{\sigma}$

YIELD STRESS
(IN KSI) $= 59.75 - .0325\ T$

WHERE T = TEMPERATURE IN °F

YIELD RATIO = EFFECTIVE STRESS / YIELD STRESS AT TEMPERATURE OF MEASURED STRAIN

FIGURE 5.34   CALCULATION OF EFFECTIVE STRAIN, EFFECTIVE STRESS, AND YIELD RATIO

TABLE 5.40
SAMPLE DATA FROM RDU TESTS
MINIMUM AND MAXIMUM DATA FOR WHEELS 5, 6, 7, AND 8

TEST NO.	SPEED (MPH)	BCP (PSI)	DURATION OF TESTING (MIN)	AVERAGE POWER (HP) MIN	(HP) MAX	PEAK POWER (HP) MIN	(HP) MAX	<--B1 LOCATION PEAK HOOP STRAIN (E-6) MIN	(E-6) MAX	PEAK HOOP STRESS (KSI) MIN	(KSI) MAX	PEAK MEASURE TEMPERATURE (DEGREES F) MAX	B2 LOCATION--> PEAK RADIAL STRAIN (E-6) MIN	(E-6) MAX	PEAK MEASURED TEMPERATURE (DEGREES F) MAX
32-33	20	20	65	4.3	5.5	5.9	7.4	-602	-602	-19.8	-19.8	263	787	937	249
34-36	30	30	64	12.1	15.9	16.5	23.1	-740	-1028	-24.0	-33.9	457	383	1562	386
37-38	30	30	50	10.6	15.2	13.0	16.7	-819	-1229	-27.0	-40.5	447	347	1818	373
39-40	30	40	59	16.6	26.3	20.8	32.0	-983	-1286	-32.0	-42.4	493	1761	1849	397
41-42	30	40	60	20.3	25.8	26.1	33.5	-905	-1365	-30.0	-45.0	472	1718	2141	408
43-44	30	50	59	18.5	30.5	32.5	47.3	-1083	-1395	-36.0	-46.0	484	1867	1903	397
45-46	30	50	61	19.8	31.7	29.2	43.0	-1085	-1401	-36.0	-46.2	483	1917	2031	406
47-48	25	50	60	19.8	26.6	25.8	43.7	-1088	-1359	-36.0	-44.8	500	1845	2062	421
49-50	25	50	59	19.6	24.8	26.0	29.7	-1095	-1322	-36.0	-43.6	512	1782	2144	426
51-52	25	40	59	18.0	24.7	28.7	33.8	-1059	-1311	-35.0	-43.2	473	1731	1863	407
53-54	25	40	52	19.7	27.8	25.9	37.6	-1083	-1366	-36.0	-45.0	541	1796	2080	492
55-56	46	53	53	31.0	48.5	43.5	94.7	-1460	-1935	-48.0	-63.8	701	2019	2335	564
62-63	38	44	50	15.6	38.4	33.8	53.3	-1274	-1274	-42.0	-42.0	690	1964	2335	426
64-65	32	52	57	25.4	38.5	37.2	51.5	-1511	-1511	-49.8	-49.8	580	1926	2254	496
66-67	32	50	62	19.2	43.1	28.6	58.5	-1247	-1247	-41.0	-41.0	480	1903	2007	393
70-71	47	40	53	34.4	36.2	40.4	48.3	-1217	-1217	-40.1	-40.1	581	1701	2023	500
72-73	37	43	59	25.9	38.8	37.4	49.1	-1269	-1269	-41.8	-41.8	730	1802	2212	566
74-75	45	48	49	31.2	40.9	38.5	56.6	-1627	-1627	-53.6	-53.6	647	1825	2273	531
80-81	48	48	59	25.0	42.7	58.8	68.6	-1833	-1833	-60.4	-60.4	574	1942	2198	414

o   Significant decay of the coefficient of brake shoe friction was observed with increasing temperature at the brake shoe-wheel interface.

o   Measurement of heat transfer at wheel/roller interface was consistent with similar observations at the Brake Dynamometer Unit.

o   Residual stress development in the test wheels as determined by the hole drilling - strain gaging method showed a definite trend with increased braking cycle severity. The residual stress field at the back face of the rim changed from compressive to tensile and subsequently increased value of tensile stress.

o   Established the basis for comparison of residual stress estimates by the hole drilling - strain gaging method and mechanical analysis of strain/temperature history.

5.3   Heat Transfer Analysis During Brake Dynamometer and RDU Testing (Technical Task T4)

5.3.1 Introduction to Brake Dynamometer Heat Transfer Analysis

An important part of this task is to estimate the "amount" of heat transfer at the wheel/rail contact patch based on appropriate measurements. As described above, one approach was to measure the rail wheel temperature rise before and after passing through the hot wheel tread contact patch. It would

then be theoretically possible, using transient thermal analyses such as those adapted to Brake Dynamometer Unit (BDU) application in Appendices 5.2 and 5.3, to estimate the "strength" of the heat source or power transmitted through contact. On the average, a measurable increase in temperature was observed from "lead-to-trail" position of the test wheel. It is significant to note that a temperature rise of only 15°F (measured 16 inches trailing contact) would indicate a heat transfer rate of 7.75 HP for typical test conditions described and computed in Appendix 5.3.

The other approach used to estimate the amount of heat transfer is to measure the slow rise in average rail temperature over time and use the first law of thermodynamics. This is illustrated in Appendix 5.4. A heat transfer rate of 7.3 HP was calculated based on measurements made (4/26/85) on a 40 mph nominal 50 Bhp run. A typical analysis of heat transfer at wheel rail contact using the above two approaches for Brake Dynamometer as well as RDU testing is presented in Section 5.2. Since convection heat losses were ignored, this would be a "lower" estimate of at least 14.7% of the nominal power input at brake shoe.

5.3.2 Estimate of Convection Heat Loss

Measurements of the rate of cool-down of the rail wheel following a braking test while the wheel is still turning at test speed but under reduced (minimum) load have also been made

in order to provide data for analysis of convection losses.

Although an analysis of these transient cool-down data is not complete, a rough estimate of the convection heat loss from the rail wheel as it heats up during the test may be obtained by using a nominal value of convection coefficient such as that given in AAR Standard S-660-83 of 4 Btu/hr-sq ft-F. The basic equation for convection heat loss rate is:

$$q_c = hA \quad T \quad (Btu/HR)$$

where

    h   is the convection coefficient having units of Btu/hr-sq ft-F

    A   is the rail head area

    T is the surface average temperature differential relative to ambient air in $^\circ$F

In order to appreciate how "h" would depend, for example, on relative air speed, a literature search was conducted for applicable data and theory. The results of this search are presented in Figure 5.35, which, on logarithmic coordinates, presents "h" versus speed in m.p.h.

The highest values of "h" were obtained from an Illinois Institute of Technology plain-bearing "hotbox" research project performed for the AAR and reported in 1954.[1] In this case, a full-scale three-piece truck assembly with rotating wheels had its journals heated electrically and cooled in a forced-air stream. The wheel-temperature distribution was "inverted" in this case relative to the brake-heating problem.

KEY

1. WHL. SET WITH HOT BOX, REF. (1)
2. ROTATING DISK IN AIR STREAM, REF. (2)
3. ROTATING CYLINDER IN AIR STREAM, REF. (3)
4. ROTATING DISK IN STILL AIR, REF. (2)
5. AAR S—660—83

CONVECTION COEFFICIENT IN BTU / (HR·FT^2·°F)

MILE PER HOUR
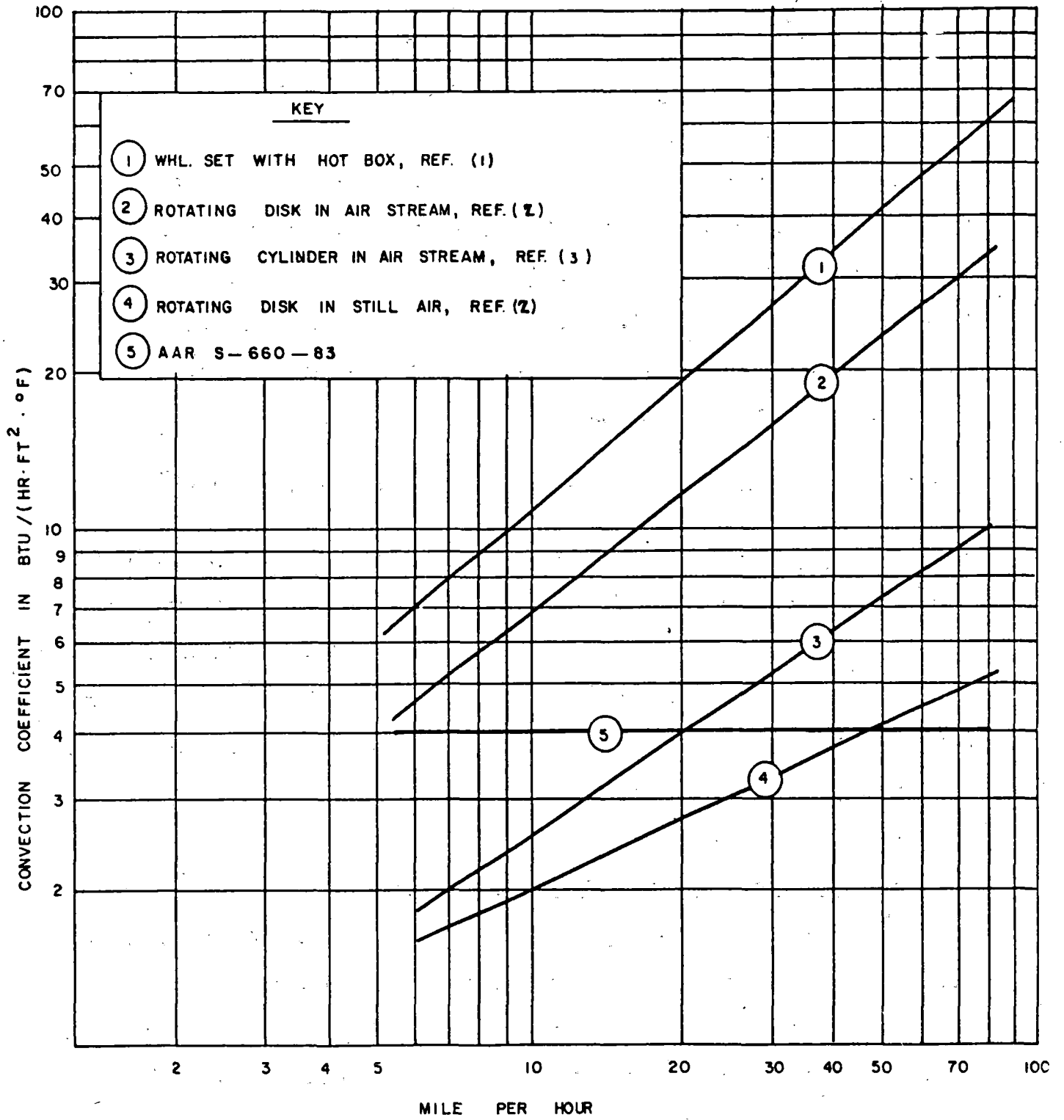
FIGURE 5.35   HEAT CONVECTION COEFFICIENT -VS- SPEED

Results of heat-transfer experiments with rotating disks are summarized by Newcomb, et al[2], and are presented in Figure 5.35 for a rotating disk in an air stream (line No. 2) and in still air (line No. 4) where speed refers to the equivalent wheel rotational speed.

Perhaps the experimental study most pertinent to the wheel "tread" is the work on rotating cylinders published by Kays and Bjorklund in 1958.[3] Their results are shown as line No. 3 in Figure 5.5. An empirical expression that embodies their research is expressed in terms of the Nusselt (N_{Nu}), Reynolds (N_R), Grashof (N_{Gr}), and Prandtl (N_{Pr}) numbers:

$$N_{Nu} = 0.135 \ [(0.5 \ N_R^2 + N_{Rs}^2 + N_{Gr})N_{Pr}]^{1/3} \quad (1)$$

where "N_{Nu}" = hD/k; N_R = FV_p/v; N_{Rs} = DV_s/v; "D" is cylinder diameter (ft.); "V_p" is cylinder surface peripheral velocity (ft./hr.); "V_s" is cross-flow velocity (ft./hr.); "v" is air kinematic viscosity (ft.^{2}/hr.]; "k" is air thermal conductivity (Btu/ft.-hr.-deg. F]); and "h" is the heat-transfer coefficient (Btu/[ft.^{2}-hr.-deg. F]).

Adaptation of Prior Research to Wheel Tread

For practical wheel operating conditions, the Grashof number (ratio of buoyancy to viscous forces) is relatively small and is ignored. For the case of a cylinder rotating in an airstream of velocity equal to the peripheral speed (rolling wheel in still air) equation No. 1 may be simplified. For a Prandtl number of

0.685 (applicable to a range of practical test conditions) equation No. 1 can be solved for the heat-transfer coefficient:

$$h = (0.136k/v^{2/3})(v^{2/3}/D^{1/3}) \qquad (2)$$

where the ratio of air viscosity to density, "v" is the kinematic air viscosity near the wheel surface. This may be obtained from tables as illustrated, for example, by Incropera.[4] As assumed previously in the radiation calculation, an exposed tread temperature of 820 deg. F and an ambient temperature of 70 deg. F will be used. For heated air at 445 deg. F, mean film temperature and atmospheric pressure, the kinematic air viscosity is found to be $39 \times 10^{-6} m^2$/sec. This may be converted to 1.511 ft^2/hr. The corresponding air conductivity is found to be 0.0409 w/m deg. K) or 0.0236 Btu/ (ft.-hr.-deg. F).

For a 33-in.-diameter wheel (D = 2.75 ft.), equation No. 2 becomes

$$h = 0.526(V)^{2/3} \qquad (3)$$

where speed is expressed in m.p.h. (1 mph = 5280 ft/hr) in this equation. At 50 m.p.h., "h" is 7.14 Btu/(hr.-$ft.^2$-deg. F), for example.

Now the convection heat flux from the tread may be calculated. For the 50-m.p.h. case, a tread temperature of 820 deg. F, ambient temperature of 70 deg. F. and a friction-heated tread area of 2.43 $ft.^2$, the heat flux is calculated to be

13,000 Btu/hr. or 5.1 h.p. At a friction horsepower input of 50 Bhp, this amounts to a 10.2% loss.

5.3.3 Estimate of Wheel Tread Radiation Losses

Another mode of heat loss from the friction-heated wheel-tread surface is thermal radiation, which, according to the Stefan-Boltzmann law, depends on the fourth power of the absolute temperature of the surface.[5] For radiative exchange between the wheel tread at absolute temperature, T_t (degrees Rankine), and its ambient surroundings at absolute temperature T_a, the heat flux in Btu/hr. is

$$q_R = A e S (T_t^4 - T_a^4) \qquad (4)$$

where "A" is the area of the tread in contact with the shoe in ft.^{2}; "e" is the dimensionless emissivity of the tread surface; and "S" is the Stefan-Boltzmann constant having the value of 0.1713×10^{-8} Btu/(ft.^{2}-h-deg. R^4).

Values of emissivity vary from 0.28 for polished wrought iron to 0.95 for strongly oxidized steel. Some experimentation at the AAR with matching thermographic temperature readings and contact-pyrometer measurements on the polished tread indicate that a value of 0.6 may be satisfactory for calculational purposes. It should be noted that an emissivity of 0.95 is applicable to the other rusted wheel surfaces.

The average tread temperature under the brake shoe, based on the track tests listed in Table 1, is 1,280 deg. F. As

discussed above, the corresponding exposed tread temperature may be 820 deg. F. A typical calculation may now be made for radiative heat flux from the tread for the following values:

T_t = 1,280 deg. R (820 deg. F);

T_a = 530 deg. R (70 deg. F);

A = 2.43 sq. ft.;

e = 0.6.

When these values are substituted into equation No. 4, a heat flux of 6,507 Btu/hr. is obtained. This flux may be expressed as 2.56 h.p. For a friction horsepower input of 50, this amounts to about a 5.1% loss. Of course, such radiation losses are strongly dependent on maximum tread temperature.

5.3.4 Effect of Rail Load on Heat Transfer

The effect of rail load on the estimated heat transfer rate has also been estimated based on temperature measurements under three load levels. The results are shown in Figure 5.36. The calculated contact areas are also given below the graph for each test load. The rate of heat transfer appears to be roughly proportional to contact area.

5.3.5 Estimates Based on Steady Temperature Rise Across Contact

Using transient thermal analyses such as those of Rosenthal for moving heat sources over various conducting spaces, it is
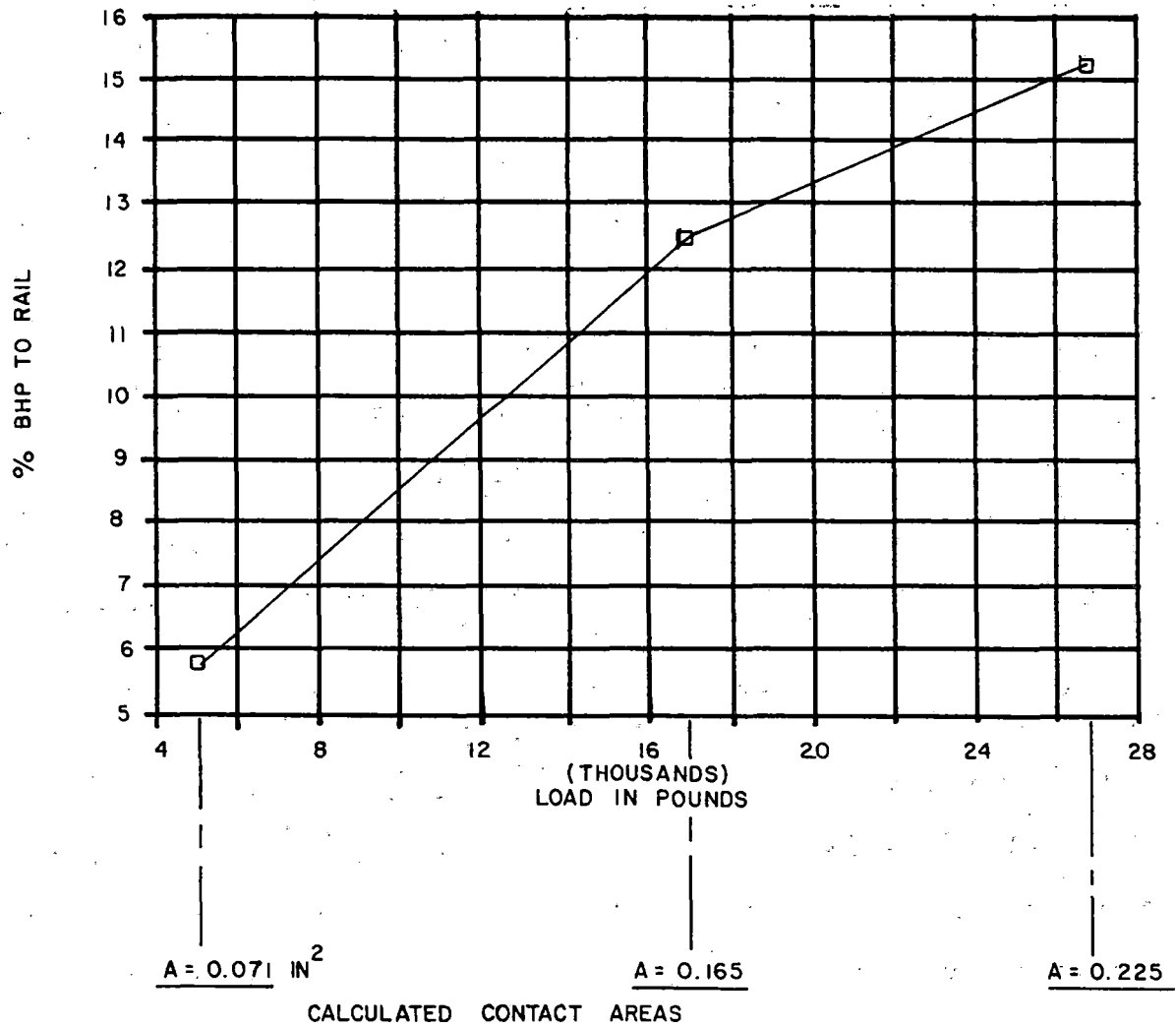
FIGURE 5.36   EFFECT OF LOAD ON HEAT TRANSFER TO RAIL IN BRAKE
DYNAMOMETER TEST 20 MPH, 25 BHP, 45 MINUTES TEST
DURATION

possible to estimate the "strength" of the heat source or power transmitted through contact based on a measurement of the leading and trailing surface temperatures.[6] For this purpose, sliding thermocouples were mounted on the running surface of the reaction wheel. An infrared pyrometer was also used for some tests.

Although experimental difficulties with sliding thermocouples were experienced that so far have prevented reliable application of the approach based on Rosenthal's transient analysis (see Figure 5.37), a review of Table 5.5 suggests that there is, on the average, a measurable increase in temperature from "lead-to-trail" position. It is significant to note that a temperature rise of only 15 deg. F (measured 16 in. trailing contact) would indicate a heat-transfer rate of 7.75 h.p. for the typical test conditions described below. Similarly, a rise of 11 deg. F at 40 m.p.h. (test A) indicates a heat-transfer rate of 7.5 h.p.

The theoretical solution for the surface temperature difference from leading (inlet) to trailing (outlet) position relative to a heat input source, idealized as a line source across the width of the contact, may be obtained from Rosenthal.[6]

From this solution, the "strength" of the heat source may be shown to be:

$$q = \frac{g \, (T_O - T_I) \, (V)^{1/2} \, (s)^{1/2}}{21.63} \tag{5}$$

BRAKE
SHOE

FORWARD

WHEEL

A

TC 5
RAIL
TC 10

A

16"   16"

CJ — 33
WHEEL

136   RE   CONTOUR
1/40   CANT

SECTION A — A
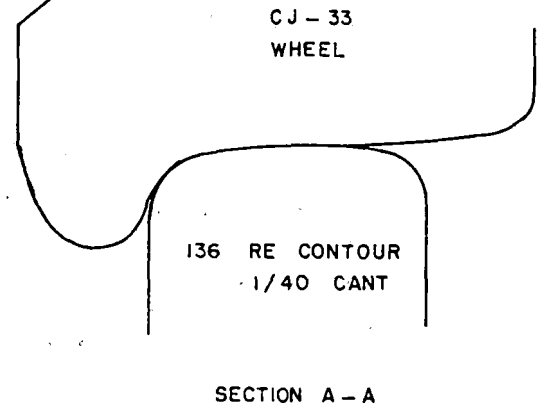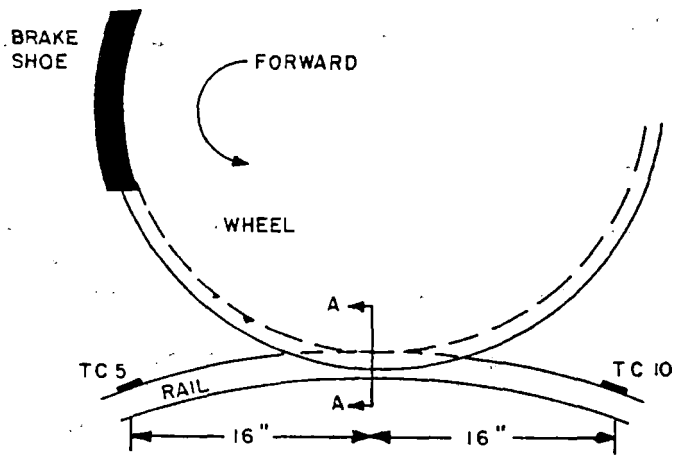
FIGURE 5.37   ARRANGEMENT OF WHEEL, RAIL AND THERMOCOUPLES FOR
HEAT TRANSFER TESTS OF WHEEL 5 ON BRAKE
DYNAMOMETER UNIT

TABLE 5.5
DYNAMOMETER "RAIL" WHEEL SURFACE TEMPERATURES
BEFORE AND AFTER WHEEL CONTACT

| Test | Direction | Test Conditions | | | | Thermocouple Readings (Deg. F) | |
		Speed (Mph)	Brake Shoe Force (Lb)	Vertical Load (Lb)	Time (Min)	TC5	TC10
1		0	0	0	0	65	65
2	Forward	20	1500	26,800	45	153	180
3*	Forward	20	0	26,800	30	95	105
4**	Forward	20	0	26,800	15	88	105
5	Reverse	20	0	26,800	18	90	105
6	Reverse	20	1500	26,800	45	145	130
7*	Reverse	30	0	26,800	22	85	83
8	Reverse	30	1500	26,800	20	150	135
A	Forward	40	1500	26,800	30	116***	127***

*After wheel was cooled with water
**Next day after one stop from 20 m.p.h.
***Measured with Exergen infrared pyrometer at 14 in.; not corrected for emissivity

If we assume the following typical values: "g" = 0.625 in. (width of contact); "s" = 16 in. (distance from contact to surface temperature measurement); "T_O" = temperature at outlet (deg. F); T_I = temperature at inlet (deg. F); "T_O-T_I" = 15 deg. F; and "V" = 20 m.p.h. (wheel speed).

The estimated heat-transfer rate would be:

$$q = \frac{0.625 \ (15) \ (20)^{1/2} \ (16)^{1/2}}{21.63} = 7.75 \text{ h.p.}$$

5.3.6 Estimates Based on Slow Temperature-Rise of Rail Rollers

The other approach used to estimate the amount of heat transfer is to measure the slow rise in average rail temperature over time and calculate the increase in internal energy, then determine from the first law of thermodynamics the average heat flux at wheel contact for that time period. The application of this approach to temperature measurements made on the rail wheel of the brake dynamometer and on the RDU support roller follows.

5.3.6.1 Internal Energy Increase of Dynamometer Rail Wheel

The 110-in.-diameter rail wheel on the wheel dynamometer unit shown in Figure 5.38 heats up during the course of wheel braking. The 33-in.-diameter test wheel was pressed against this reaction rail wheel with a 27,000-lb. force. For a nominal
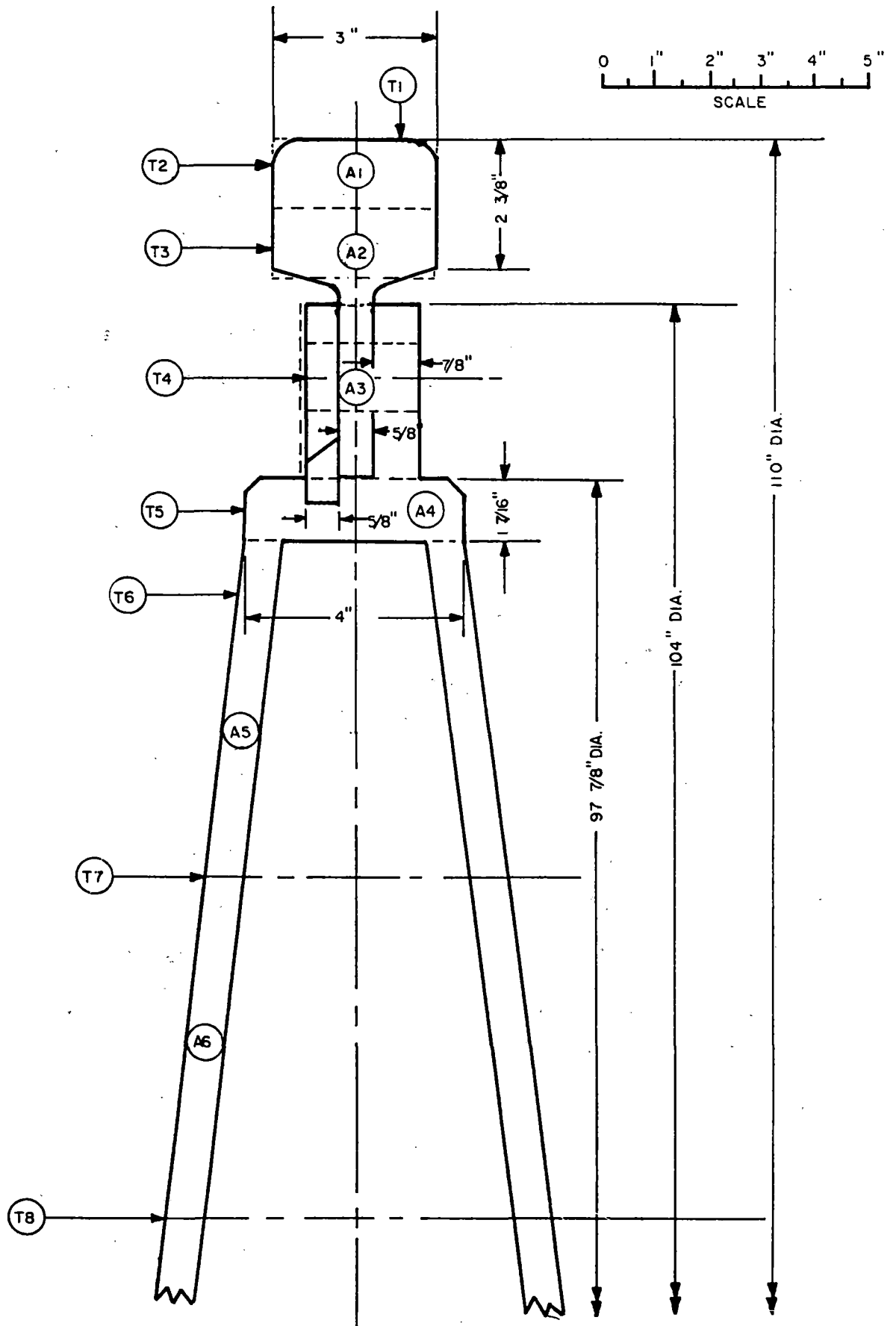
AAR BRAKE DYNAMOMETER UNIT

FIGURE 5.38   RAIL WHEEL DIMENSIONS AND TEMPERATURE
MEASUREMENT RADII

50 Bhp braking cycle (40 m.p.h. with 1,500-lb. normal brake shoe force) of 46 minutes duration (and subsequent cool-down), temperature measurements were made using an Exergen D-series digital infrared thermometer on the dynamometer rail wheel surface, which had been sprayed with flat black paint where shiny metal was exposed.

Wheel and rail temperatures were also recorded by a Hughes Aircraft Co. Probeye Thermal Video Series 4000 system.

A chronological listing of these temperatures is provided in Table 5.6.

Since the increase in internal energy or heat of the rail wheel (ΔI) equals the heat transfer into the rail wheel at wheel contact (ΔQ) during braking (ignoring convection losses):

Also, $\Delta I = \Delta Q =$

$$2,544.5 \; [Btu/(hr \; hp)] \; q \; time \; (hr) \qquad (6)$$

Therefore, the heat transfer rate in terms of horsepower is

$$q = (\Delta I \; Btu) / (2544.5t \; (hr)) \qquad (7)$$

The internal energy increase of the rail wheel may be determined by summing the energy increases of several "rings", each having an internal energy increase expressed as:

$$I_i = D_i \; A_i \; w \; c \; (T_i - T_a) \qquad (8)$$

where D_i is the average diameter of the ring in inches; A_i is the cross-section area of the ring in in.^{2}; T_i is the current temperature of the ring in deg. F; T_a is the initial or ambient temperature in deg. F; w is steel density (lbs./in.^{3}); and c is specific heat capacity (Btu/lb. deg. F).

TABLE 5.6
TEMPERATURE MEASUREMENT HISTORY FOR HEAT-UP AND COOL-DOWN
OF DYNAMOMETER "RAIL" WHEEL, APRIL 26, 1985

Time	Temperatures (Deg. F)								
	T1	T2	T3	T4	T5	T6	T7	T8	Ambient
9:01:00	75	75	75	75	75	75	75	75	75
9:35:30	(Start brake application)								
9:54:00	160		146						
10:19:00	205	192	185		94	88			
10:21:00	204	200	184		93	89			
10:21:30	(Brake off; slow track wheel to few r.p.m.; reduce vertical load to minimum after brief stop for temperature measurement)								
10:24:00	(Increase wheel back to 40 m.p.h.)								
10:25:30	(Set up thermal video in track wheel pit)								
10:31:30	149		141*	109	93	85			
10:35:49	140		134*	98	90	82			
10:40:00	132		130*	96					
10:44:58	122		120*	94	85	80			
10:48:20	117		110*	90	82	80			75

*Measured at location between T2 and T3

The basis of calculations for the rail wheel internal energy is given in Table 5.7. The sum of these ring energy-increases is thus found to be 15,008.3 Btu. Therefore, for t = 0.766 hrs. the average heat flux into the rail wheel may be obtained from:

$$\dot{q} = 15,008.3/(2,544.5 \times 0.766) = 7.7 \text{ h.p.} \tag{6}$$

A minimum heat-transfer rate into the rail wheel equivalent to 7.7 h.p. is estimated, ignoring convection heat losses. This amounts to 15.4% of the nominal Bhp applied.

A rough estimate of the convection heat loss from the rail wheel as it heats up during the test may be obtained by using a nominal value of convection coefficient, such as that given in AAR Standard S-660-83, of 4 Btu/hr.-ft.^{2}-deg. F).

The basic equation for convection heat loss is:

$$q_c = hA \quad T(\text{Btu/hr}) \tag{10}$$

where h is the convection coefficient taken as 4 Btu/hr.-ft.^{2}-deg. F); A is the rail head area in ft.^{2}, and T is the surface average temperature differential relative to ambient air in deg. F.

If a simple linear temperature-buildup during the test is assumed, the rate equation above may be integrated for the following simple results:

$$Q_c = (hA \quad T_{max}t)/2 \tag{11}$$

where T_{max} is the maximum temperature differential reached at the end of test period hours t. The average surface temperature of the dynamometer rail wheel head at the end of test (t = 0.766 hrs.) is taken as the average of

TABLE 5.7
BASIS OF DYNAMOMETER "RAIL" WHEEL INTERNAL ENERGY-INCREASE CALCULATION

Area No. Basis	Area (In^2)					Diameter (In)	Temp.
A1	3	x	1.25	=	3.75	108.75	(T1 + T2)/2
A2	3	x	1.25	=	3.75	107.50	T3
A3	2.25	x	3.125	=	7.03	100.88	(T3 + T5)/2
A4	1.43	x	4.00	=	5.72	96.44	T5
A5	0.625	x	6.00	=	3.75	89.00	(T6 + T7)/2
A6	0.625	x	6.00	=	3.75	77.00	(T7 + T8)/2

temperatures of the rail top surface (T1 = 160 deg. F and, lower side, T3 = 146 deg. F). Ambient air temperature was 75 deg. F. The convection heat loss during the test is then calculated to be:

$$Q_C = [(4 \times 24)/2][(160+146)/2-75]0.766 = 2,868 \text{ Btu}$$

The heat loss would require an additional average contact patch input:

2,868 Btu/0.766 hr/2544.5 Btu/hr/hp = 1.47 hp

This calculation suggests that the 7.7 hp contact patch heat-transfer rate estimate based on nonconvection losses is some 20% low. A "corrected" heat transfer rate of 9.2 h.p. is thus obtained. Since the nominal input for the test was 50 Bhp, the percentage loss through rail-wheel contact would be about 18.4%. Perhaps an even higher percentage may be expected if the actual average input was lower than 50 Bhp due to reduction in brake-shoe coefficient of friction below nominal.

5.3.7   Internal Energy Increase of RDU Roller

The 60-in.-diameter RDU support roller dimension and temperature-measurement radii are shown in Figure 5.39. Temperature measurements were made before and after the braking test using an Exergen D-Series digital infrared thermometer on the roller surface, which had been sprayed with flat black paint.

The temperature-change measured or extrapolated for each ring is listed in Table 5.8. The internal energy increase of

5-88
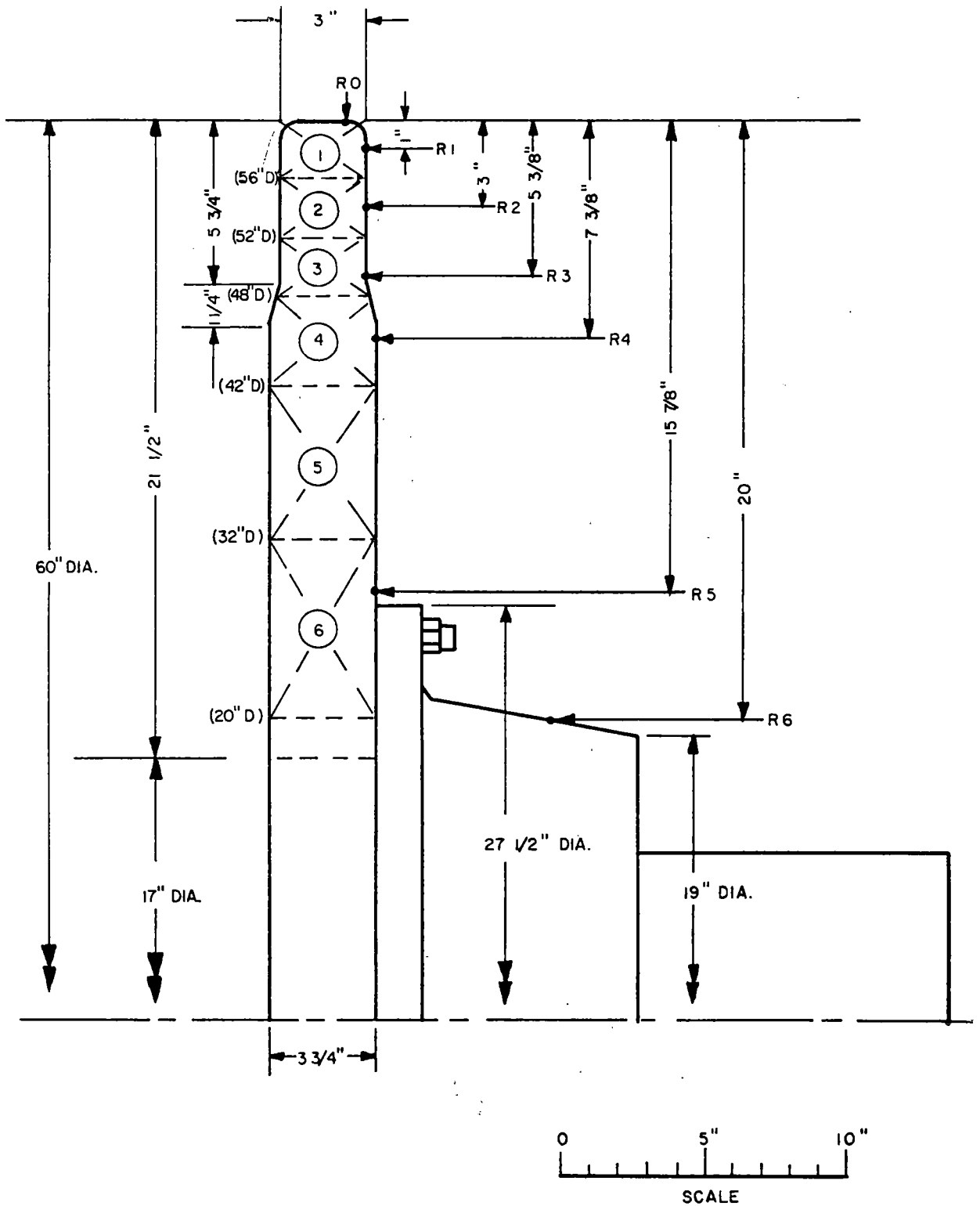
FIGURE 5.39   RDU ROLLER GEOMETRY AND RADIAL TEMPERATURE
MEASUREMENT POSITIONS

TABLE 5.8
RDU ROLLER TEMPERATURE CHANGE

Ring No.	Thickness (In)	H Outside Dia. (In)	Inside Dia. (In)	Ri Avg. Temp. Basis	Temp. Inc. (Deg. F)
1	3.00	60	56	R1	165
2	3.00	56	52	R2	137
3	3.00	52	48	R3	98
4	3.75	48	42	R4	77
5	3.75	42	32	(R4 + R5)/2	47
6	3.75	32	20	R5	17

the roller may then be calculated on the same basis as in the dynamometer rail wheel case discussed earlier. This energy is found to be 20,276 Btu for a one-hour drag-braking heat-input period. The equivalent heat flux through wheel contact is

$$q = \frac{20,276 \text{ Btu}}{2,544.5 \text{ (Btu/hr-hp) x } 1.0 \text{ (hr)}} = 7.97 \text{ hp}$$

The nominal brake-horsepower input was about 50. It actually decreased with time during the one-hour test as shoes heated up; there was no forced-air cooling in this particular test. Therefore, the heat transfer rate at the roller is at least (7.969/50) x 100 = 15.94% of the brake-shoe-to-wheel heat input rate, assuming that all braking power goes into the wheel and no heat is lost from the roller due to convection. A 27,000 lb. vertical load was maintained on the wheel during test and cool down.

5.4 Induction Heating

The induction heating tests were developed to simulate the effects of brake thermal loading on wheels. While the facility used for the test was not capable of simulating rail load and all brake shoe loading effects, it was easily accessible, and controlled, and made possible the development of instrumentation techniques, the examination of optimum gage placement locations, the application of various simulated braking cycles and the

exploration of residual stress measurement techniques. The induction heating test provided a controlled source of heat to simulate a brake application. The results could be compared with subsequent tests that included rail load and brake shoe effects. This comparison helped illuminate the issue of the contribution of rail loading effects to wheel failure mechanisms.

In setting up the tests, the uncertainty regarding the amount of friction generated heat which was actually transmitted into the wheel had to be considered. Preliminary thermal analyses were conducted where the same assumption was made that is used by the AAR in wheel design evaluation, namely, that 70% of the heat generated by friction is conducted into the wheel. One objective of the tests was to compare results from the induction heating tests with results from the brake dynamometer tests in order to determine equivalent thermal inputs.

The induction heating test program included:

o   an instrumentation subtask to develop optimum procedures for the measurement of strain and temperature at selected locations on the wheel,

o   an analytical subtask where finite element analyses were used to obtain an understanding of the response of the freight car wheel to thermal loading, and

o   a data evaluation subtask where the data generated during the induction heating test were compared with data obtained from dynamometer and track tests.

5-92

5.4.1 Wheels

Two one-wear 36-inch diameter wheel designs were included in the tests. The first wheel was a CH-36 wheel, with curved-plate design. The second wheel was a wrought straight-plate wheel design with fairly sharp rim-plate fillets. Differences in the development of residual strains in the two designs were to be investigated along with differences in the temperature distributions. The wheels were stress-relieved before instrumentation. Finite element analyses were made, using the best available estimates of thermal and mechanical properties to obtain predictions of circumferential residual stresses at the locations where strain gages were installed.

5.4.2 Instrumentation

The instrumentation used on the first test wheel (CH36) is shown in Figures 5.40 and 5.41. For the second test (H36), the strain gages and thermocouples were installed at the base (B) locations.

Both of the test wheels were sent to a special machine shop in Denver, Colorado, for precise drilling of holes for the installation of subsurface thermocouples at selected locations within the rim.

The test wheels were then prepared for the installation of high temperature strain gages at the designated locations. The strain gages used were the AILTECH weldable type, SG

THERMOCOUPLES

2, 6, 10 are mounted on tread surface.

3, 7, 11 are imbedded within 1/8" of 2, 6, 10.

4, 8, 12 are in another slice imbedded 1/4" from tread, 5° displaced under 3, 7, 11 (See plan view).

16 is located over 8, on the tread, analogous to 6.

STRAIN GAUGES

B's are basic strain gauge locations.

Others are additional gauges for this wheel only.

• Thermocouple location

✗ Strain gauge location (back face)

⊗ Strain gauge location (front face)

CH-36 WHEEL

FIGURE 5.40   INSTRUMENTED WHEEL FOR INDUCTION WHEEL TEST (FIRST WHEEL)
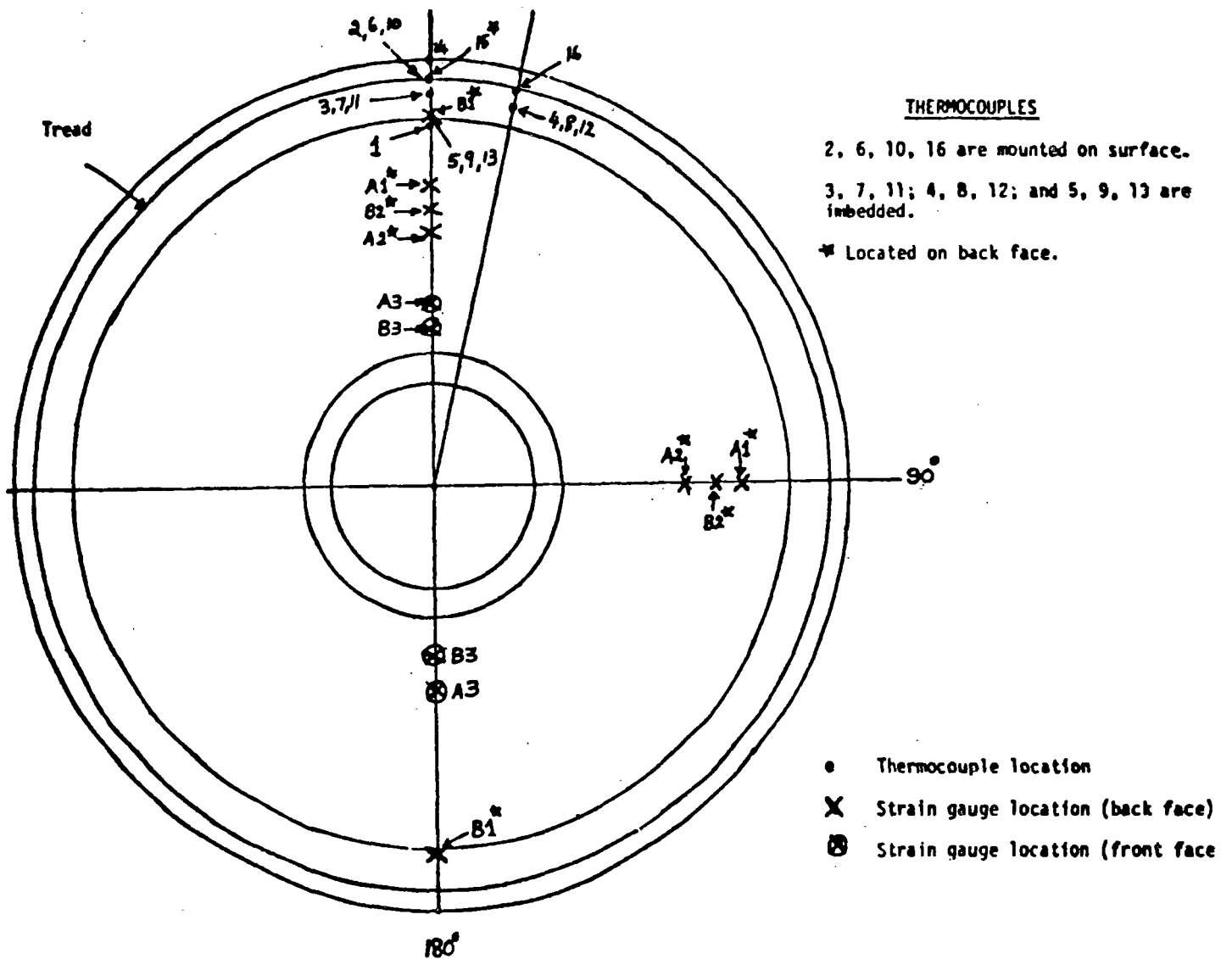
FIGURE 5.41   INSTRUMENTED WHEEL FOR INDUCTION WHEEL TEST
(PLAN VIEW)

5-95

425-08-05-06S. This gage has a platinum-tungsten alloy designed for use in static measurements up to 1200°F. The gage also has a 5-foot stainless steel tube welded to it to protect the lead to 1500°F. It also required extension leads to the signal conditioning equipment. Bridge completion networks consisting of temperature compensation and balance resistors were also prepared.

A data acquisition system with 42-channel capability was used. It made use of a Campbell Scientific CR7 data logger with new excitation and input cards for acquiring data during temperature cycling and induction heating. The system uses a modular approach to combine precision measurement capabilities with multiple processors in a single battery-operated system. Some of the functions of the system included data linearization, engineering unit conversion, programmed data processing, and data storage. The system was configured to measure 24-four wire half bridges and 28 thermocouples. The sample rate was set for 20 differential samples per second. The system was rugged, but portable, weighing approximately 30 pounds.

The thermocouple (TC) wire used was 20-gage, ANSI type K premium gage wire. The accuracy specification for this premium gage wire was $\pm$ 2°F. or 0.4%. Each TC was welded to the wheel with the same welding unit used for strain gages.

The thermocouples and strain gages were located to provide a good description of the temperature and stress distributions developed in the wheel. The locations of strain gages and thermocouples were determined after preliminary finite element

calculations were completed, so that the strains and temperatures could be compared with the calculated values at strategic locations.

Both wheels were sent to Maxcar Corporation in Colorado Springs where they were cycled up to temperatures of 1100°F. to relieve welding stresses. They were held at the high temperature for 2 hours and then allowed to cool uniformly to room temperature. On the last cooling cycle, an apparent strain curve was generated for each gage. These data were used to correct the data acquired during each of the induction heating tests (Appendix 5.6).

5.4.3 Test Conditions

After the temperature cycling, the wheels were sent to AMSTED Research Laboratories in Bensenville, Illinois, for the induction heating tests. The induction heating facility consists of a 100 kW induction coil and a high frequency generator (2500-2900 Hz). There is a 3/4 inch clearance between the coil, which surrounds the wheel and the wheel tread. The following induction heating cycles were used:

Test No.	Test Wheel	Thermal Cycle (Drag Brake Simulation)
1	CH36	30 kW, 12 minutes
2	CH36	40 kW, 15 minutes
3	CH36	30 kW, 25 minutes
4	CH36	40 kW, 30 minutes
5	CH36	40 kW, 30 minutes (repeat test)
6	H36	30 kW, 8 minutes
7	H36	30 kW, 16 minutes
8	H36	40 kW, 12 minutes
9	H36	40 kW, 24 minutes
10	H36	40 kW, 24 minutes (repeat test)

Data were acquired at prescribed intervals during heating and cooling using the CR7 Campbell Scientific data logger.

5.4.4   Test Results

5.4.4.1 Analysis of Temperature Data

The first step in the analysis and evaluation of the temperature data was to compare data from the thermocouples with predictions. The principal uncertainties in the analyses were the selection of the appropriate assumption for the transmission of power into the wheel, and the selection of values for the convection coefficient and emissivity. The material thermal properties from AAR S-660 (1) were used. These are:

Specific Heat

$$C_p = 0.102 + 0.000052T \text{ (Btu/lb-}^\circ\text{F.)}$$

Thermal Conductivity

$$k = 28.1 - 0.0060T \text{ (Btu/hr-ft-}^\circ\text{F.)}$$

It was found that the use of these properties, a convection coefficient 30% of that listed in S-660, radiation with an emissivity of 0.8 (there is no provision for radiation loss in S-660), and assuming a thermal input efficiency of 91%, yielded a fairly good fit of the CH-36 curved-plate wheel data at 12 and 25 minutes. The H-36 straight-plate wheel data also fit fairly well at 8 and 16 minutes (test nos. 6 and 7) with the assumption

of 91% efficiency.

The results are summarized for the CH-36 wheel in Table 5.9 and for the H-36 wheel in Table 5.10. The results for the CH-36 wheel suggest that thermocouples 3, 4, and 15 were not responding properly because the deviations for these thermocouples are significantly off the trends shown for the other thermocouples. Similarly, the results for the H-36 wheel suggest that thermocouple 18 is not responding properly.

5.4.4.2   Analysis of Thermal Strain Data

The data from the strain gages were analyzed by preparing plots of the mechanical component of strain versus temperature for each of the tests. Typical results are presented in Figures 5.42 and 5.43. Figure 5.42 shows results for the B1 strain gage on the first test with the H-36 wheel. Figure 5.43 shows results for the B1 location on the second test with this wheel. The plots show the large strain ranges that are associated with tests of this type.

Table 5.11 summarizes the strain data for the B1 location and Table 5.12 summarizes the strain data for the B3 location for each of the tests. Note that there is a progressive, but diminishing, accumulation of residual strain at the B1 location. The accumulation of residual strain at the B3 location is much more erratic.

TABLE 5.9
INDUCTION HEATING CURVED PLATE CH36 WHEEL
30 KW FOR 12 AND 25 MINUTES

25 Minutes, η = .91

T/C No.	Observed Temperature	Calculated Temperature	Deviation
1	637	636	1
2	735	716	19
3	670	704	-34
4	653	685	-32
5	649	633	16
6	714	696	18
7	672	677	- 5
8	673	658	15
9	607	596	11
10	634	641	- 7
11	615	624	- 9
12	604	611	- 7
13	559	564	- 5
14	598	612	-14
15	528	575	-47
16	710	696	14
17	553	549	-16
18	416	417	- 1
19	180	178	2

12 Minutes, η = .91

T/C No.	Observed Temperature	Calculated Temperature	Deviation
1	428	398	30
2	511	474	37
3	438	462	-24
4	424	443	-19
5	423	394	29
6	477	453	24
7	433	436	- 3
8	435	417	18
9	373	359	14
10	401	402	- 1
11	379	385	- 6
12	367	373	- 6
13	325	330	- 5
14	374	375	- 1
15	313	340	-27
16	472	453	19
17	312	316	- 4
18	218	219	- 1
19	95	98	- 3

TABLE 5.10
INDUCTION HEATING OF STRAIGHT PLATE H36 WHEEL
30 KW FOR 8 AND 16 MINUTES

8 Minutes, η = .91

T/C No.	Observed Temperature	Calculated Temperature	Deviation
1	358	349	9
2	274	425	
3	407	416	- 9
4	401	401	0
5	359	348	11
6	378	390	-12
7	369	377	- 8
8	358	358	0
9	300	298	2
10	325	339	-14
11	307	317	-10
12	303	308	- 5
13	264	268	- 4
14	297	276	21
15	266	261	5
16	390	390	0
17	251	250	1
18	143	185	-42
19	72	78	- 6

16 Minutes, η = .91

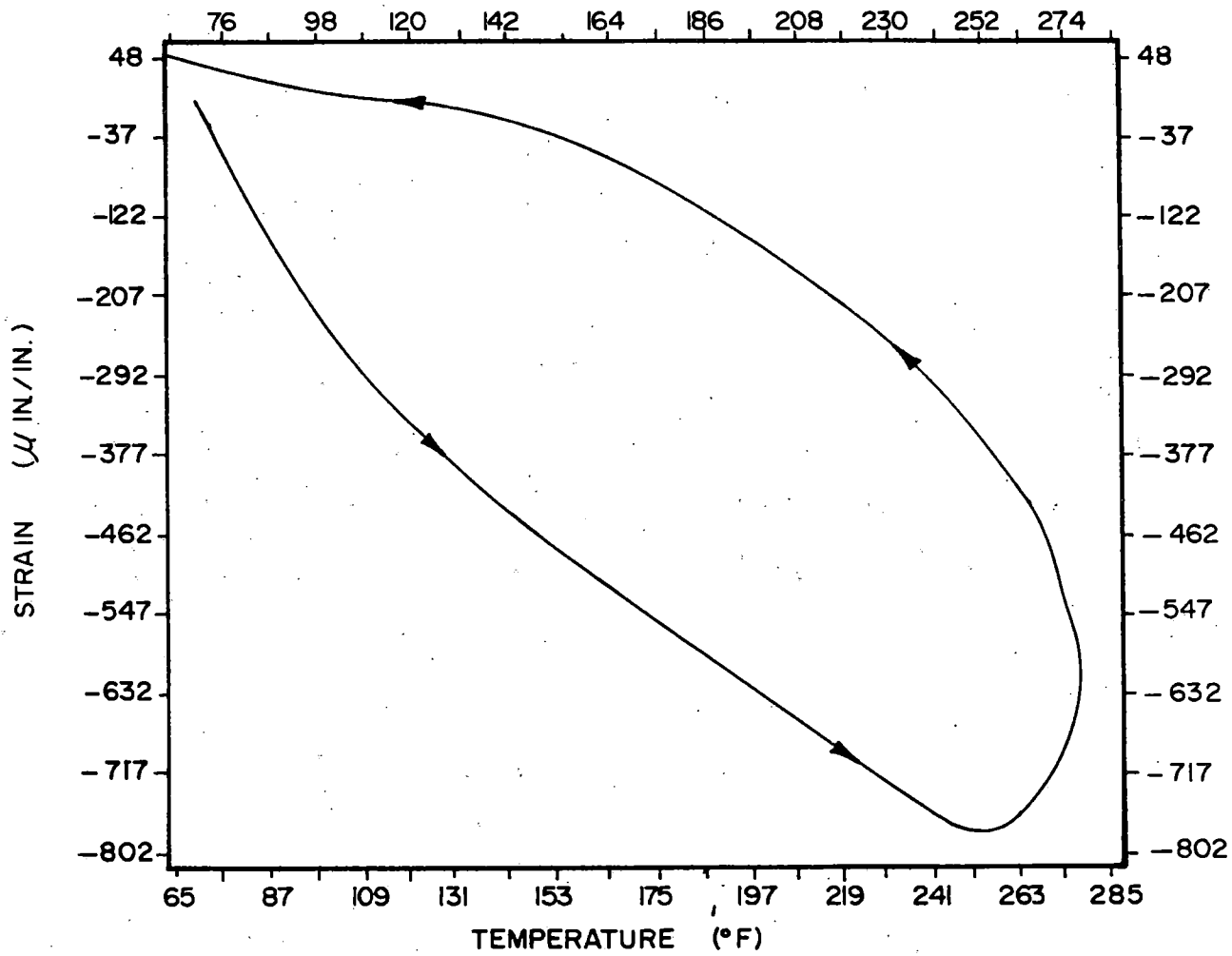| T/C No.	Observed Temperature	Calculated Temperature	Deviation
1	532	540	- 8
2	457	620	
3	599	610	-11
4	592	594	- 2
5	544	539	5
6	576	581	- 5
7	562	568	- 6
8	551	549	2
9	487	484	3
10	517	528	-11
11	500	505	- 5
12	494	496	- 2
13	451	453	- 2
14	473	462	11
15	429	447	-18
16	587	581	6
17	427	434	- 7
18	272	333	-61
19	101	103	- 2

FIGURE 5.42   STRAIN -VS- TEMPERATURE AT B1 LOCATION TEST NO. 6,
H36 WHEEL, 30 KW, 8 MINUTES
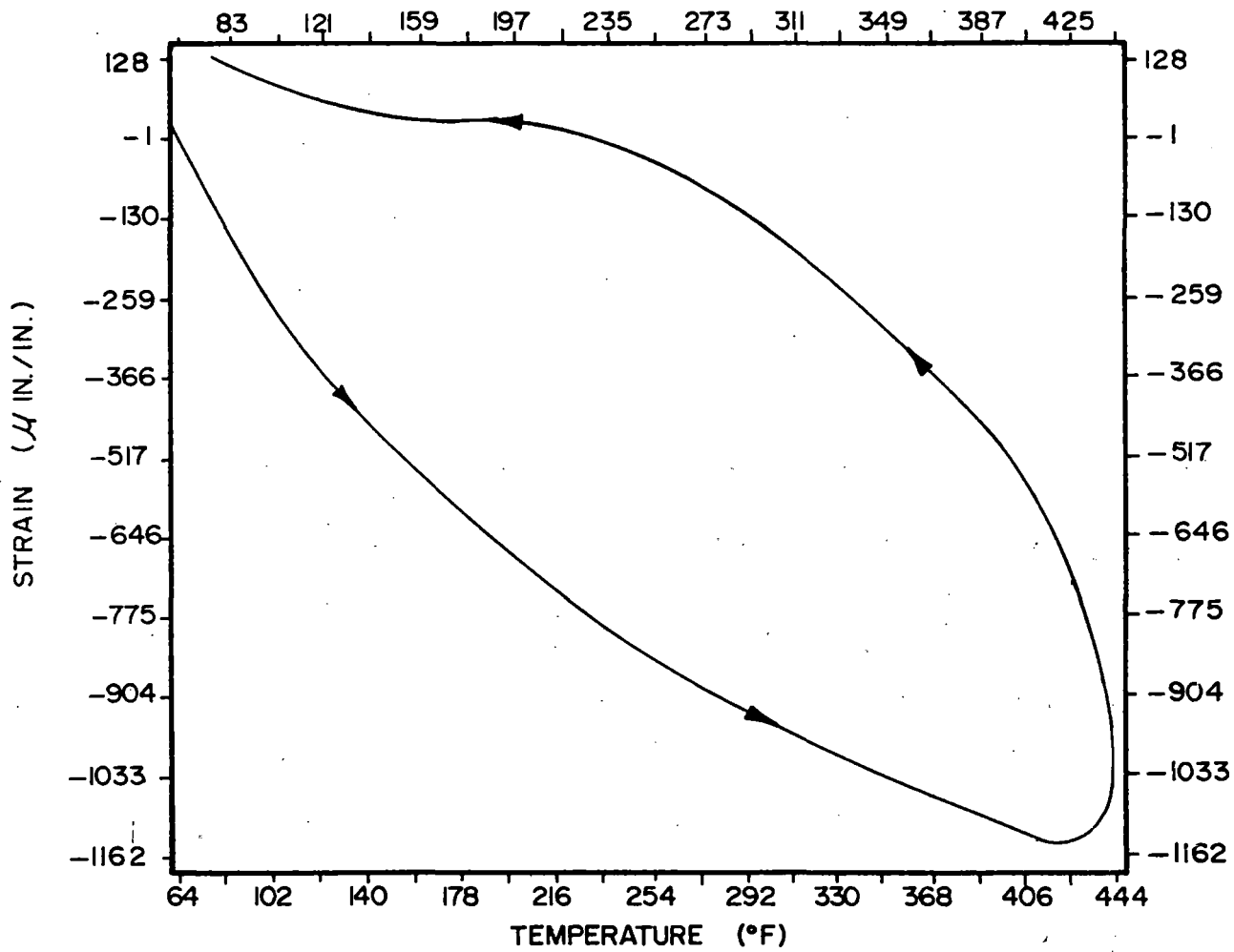
FIGURE 5.43   STRAIN -VS- TEMPERATURE AT B1 LOCATION TEST NO. 7,
H36 WHEEL, 36 KW, 16 MINUTES

TABLE 5.11
B1 LOCATION STRAIN DATA (CIRCUMFERENTIAL)

Thermal Load (kW) and Time (min)	Strain at End of Heating (μin/in)	Residual Strain (μin/in)
Curved-Plate		
30-12	-1048	73
40-15	-1677	70
30-25	-1848	19
40-30	-2586	25
40-30	-2577	11
Straight-Plate		
30-8	-801	48
30-16	-1161	123
40-12	-1401	17
40-24	-1875	55
40-24	-1903	32

TABLE 5.12
B3 LOCATION STRAIN DATA (RADIAL)

Thermal Load (kW) and Time (min)	Strain at End of Heating (μin/in)	Residual Strain (μin/in)
Curved-Plate		
30-12	1567	-88
40-15	2834	144
30-25	3436	185
40-30	5116	258
40-30	4730	-45
Straight-Plate		
30-8	1608	-56
30-16	4159	666
40-12	3661	38
40-24	6455	-209
40-24	6570	-19

5.4.4.3 Prediction of Residual Stresses

Prof. H. Sehitoglu of the University of Illinois has made an independent evaluation of some of the results of the induction heating tests. He conducted finite element analyses (using ANSYS) to simulate the tests on the curved-plate CH-36 wheel. His major interest was the calculation of residual circumferential stresses at the back face rim position (B1) using mechanical properties which had been derived from tests conducted at the University of Illinois. A major objective of their work has been to develop a model which provides the mechanical properties as a function of strain rate. The properties used in his simulation were representative of those predicted in the 10^{-3}/sec to 10^{-4}/sec range.

The analyses included the prediction of temperatures from the heat input for each of the induction heating thermal loads. The calculations spanned a period of about 40 hours and included the heating and cooling cycles of each of the 5 thermal loads. The results of these calculations are summarized in the following table:

PREDICTED TEMPERATURES AND RESIDUAL STRESSES
AT THE B1 LOCATION, CH36 WHEEL

Thermal Load	Predicted Maximum Temperature (^{O}F)	Observed Maximum Temperature (^{O}F)	Predicted Residual Circumferential Stress (ksi)
30 kW-12 min.	320	320	0.0
40 kW-15 min.	445	480	1.0
30 kW-25 min.	477	540	1.0
40 kW-30 min.	673	710	13.2
40 kW-30 min.	673	710	13.2 (no change)

The predicted residual stress following the last test is in good agreement with the stress derived from a hole-drilling test on this wheel, which was about 10 ksi.

5.5 Overall Conclusions for Technical Task T4

1.   Wheel-rail contact and convection heat-transfer mechanisms are of comparable significance and jointly account for a major (perhaps 28%) reduction in effective friction heat input to the wheel tread in track testing.

2.   Dynamometer testing in still air without rail contact will result in greater effective friction heat flux into the wheel than will "equivalent" track testing. A 30% greater flux is possible at the same level of friction horsepower, based on computations made on the basis of data and theory presented here.

3.   Residual stress development in the test wheels as determined by the hole drilling-strain gaging method showed a definite trend with increased braking-cycle severity. The residual stress field at the back face of the rim changed from compressive to tensile and subsequently increased in value of tensile stress.

4.   A change of residual stress from near 0 to 27 k.s.i. tensile was measured at the lower rim back face of a 33-inch Class U parabolic-plate wheel after two severe drag-braking cycles of 1 hour and 1/2 hour duration

respectively at average friction horsepowers that varied between 40 and 50 h.p.

5. Linear relationships were established between effective stress calculated elastically from measured strains and the peak temperature. Also, effective stress and applied horsepower showed a non-linear relationship.

6. Some of the most important findings of the RDU testing were the significant wheel-to-wheel variation in the thermal input, the changes with time in the coefficient of friction of the brake shoes, and the inability to hold a constant level of thermal input to the wheels. Even repeat braking tests on the Brake Dynamometer showed significant variation in heating.

REFERENCES

1. "Railroad Freight Car Hotboxes," Project No. L524 Final Report, Vol. II, Appendix E, Armour Research Foundation, Illinois Institute of Technology, 1954.

2. Newcomb, T. P.:   "Thermal Aspects of Railway Braking," International Conference on Railway Braking, University of York, September 26-27, 1979.   Institution of Mechanical Engineers Conference Publications, 1979-11; London, The Institution of Mechanical Engineers, 1979.

3. Kays, W. M., and Bjorklund, I. S.:   "Heat Transfer From a Rotating Cylinder With and Without Crossflow," Transcript, ASME, 1958, pages 70-78.

4. Incropera, F. P.:   " Fundamentals of Heat Transfer," John Wesley & Sons, Inc., 1981, page 333 and Table A4.

5. Marks' Standard Handbook for Mechanical Engineers, edited by T. Baumeister, et al, eighth edition, McGraw-Hill 1978, pages 4-70.

6. Rosenthal, D.; "Theory of Moving Sources of Heat and its Application to Metal Treatments", ASME Transactions, Volume 68, 1946, pages 849-866.

6.0 PRELIMINARY TRACK TESTING (TECHNICAL TASK T5) AND STUDY OF BRAKE SHOE TEMPERATURE DISTRIBUTION (TECHNICAL TASK T7)

Technical Task T5 required monitoring the development and/or shake down of wheel strains during drag braking, and change in strain field after cooling. The development of wheel plate temperatures during a series of drag braking track tests was monitored with two instrumented test trucks of a 70-ton capacity loaded hopper car.

During the course of preliminary track testing, the effects of a 2-inch flat ground on the tread of an instrumented wheel were studied.

The objective of Technical Task T7 were also fulfilled by instrumenting the brake shoes of test truck #2 and monitoring the temperature distribution at different depths within the brake shoes during the second series of preliminary track testing.

6.1 <u>Test Conduct</u>

Preliminary track testing Technical Task (T5) included measurement of wheel temperatures and strains during prescribed braking tests on rail car wheels of the same size, shape, and metallurgy, keeping the wheel-related variables to a minimum. The test wheels selected for preliminary track testing were of

Class U, 33-inch diameter as shown in Figure 6.1. Truck #1 was fully instrumented with high temperature strain gages, thermocouples, and slip rings (exactly like the trucks tested on RDU as described in Section 5.0). A series of drag braking cycles was performed on truck #1 and residual stresses at strategic locations were measured by the hole drilling-strain gaging method after each cycle to ascertain the stress buildup. Typical drag/stop braking cycles were selected from the test data already acquired during RDU testing in order to introduce significant stress reversals in the wheel.

High friction composition type shoes produced by one manufacturer were used throughout preliminary track testing.

All the track tests covered under Technical Task T5 and Technical Task 7 were conducted on the Transit Test Track (TTT) at TTC.

The TTT is a 9.1 mile loop composed of three tangent and three curved sections. The tangent sections include track that lies on 0%, 0.69%, and 1.47% grades. The curved sections include two 1-degree, 30-minute curves with 4.5-inch superelevation and one 0-degree, 50 minute curve with 2-inch superelevation. The transit loop, which is built for speeds of up to 100 mph, has six different track constructions that are representative of those used by transit authorities in the United States.

Track tests were conducted in two stages. In the first or preliminary track tests, the same extensively instrumented standard brake rigged 70-ton capacity truck was used that was

WHEEL FAILURE MECHANISMS OF RAILROAD CARS
PRELIMINARY TRACK TESTING

(TRACK) TEST TRUCK 1

(Instrumented Wheelsets
with Slip Rings)

1) All Wheels: Class U,
   Parabolic Plate, New,
   Griffin CJ33

2) A,B,C,& D- Slip Rings

3) Both Axles-Drilled

4) All Wheels Strain Gaged
   and Thermocoupled at
   Locations B1,B2 & B3

Diagram labels: W9, W10, AXLE-A5, A, B, W11, W12, AXLE-A6, C, D
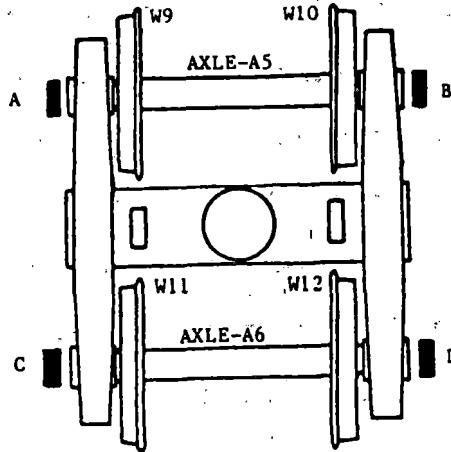
WHEEL I.D.	SERIAL NO.
W-9	94551
W-10	94554
W-11	94545
W-12	94562

NOTE: Truck 1 and Truck 2 are tested separately under two series of tests. These tests will be conducted in conjunction with thermocoupled composition brake shoes to study brake shoe thermal input effects covered under Technical Task T7.

(TRACK) TEST TRUCK 2

(With Limited Instrumen-
tation)

1) All Wheels: Class U,
   Parabolic Plate, New,
   Griffin CJ33

2) A&B - Slip Rings

Diagram labels: W13, W14, DRILLED AXLE, A, B, AXLE A7, W15, W16, NON-DRILLED AXLE, AXLE A8, WHEELS WITHOUT THERMOCOUPLES
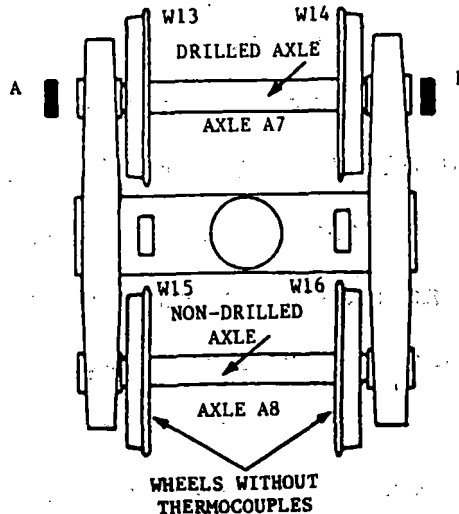
WHEEL I.D.	SERIAL NO.
W-13	95543
W-14	95531
W-15	95536
W-16	95553

FIGURE 6.1   TEST WHEELS FOR PRELIMINARY TRACK TESTS COVERED UNDER TECHNICAL TASK T5

tested on the RDU.

The test consist consisted of a locomotive followed by an instrumentation car and test car. A fully loaded 70-ton capacity open hopper car was used as the test car, with conventional brake rigging. The typical braking arrangement for the test truck (#1) is presented in Figure 6.2. The instrumentation car (211) brake reservoir was tapped into, to provide the compressed air supply for the test truck brake cylinder. The test truck was also provided with instrumented brake heads to monitor the normal and tangential forces at each brake shoe/ tread interface on a continuous basis. Measurement of the tangential braking force allowed computation of brake horsepower directly. The brake cylinder pressure for the test trucks was independently controlled from a regulating valve in the instrumentation car. The signal conditioners for thermocouples (mounted on the test wheels and inside brake shoes) as well as for strain gages (mounted on the wheels and the brake heads) were housed in the instrumentation car. For tread surface temperature measurement, several styles of bow-type sliding thermocouples were used for RDU testing (Section 5.0). Due to excessive failures, these were replaced by thermocouples imbedded in the brake shoes during the track tests. There was an apparent difference in tread temperature as measured by a thermocouple imbedded in the brake shoe and bow-type thermocouple sliding on the exposed tread. To evaluate the differences between the two types of measurements, tests were conducted on the Brake Dynamometer with bow-type miniature

COOLING WATER FOR INSTR BRAKE HEADS OR WHEELS

B-END

PRESSURE REGULATOR

PRESSURE XDCR

TEST CAR BRAKE CYLINDER, ISOLATED FROM .9B VALVE, RESERVOIRS & TRAIN BRAKE LINE

211 CAR BRAKE RESERVOIR

A.S.A (GROUNDED AT FAR END)

TRAIN BRAKE LINE

INSTR. BRAKE HEADS WITH COOLING WATER FITTINGS
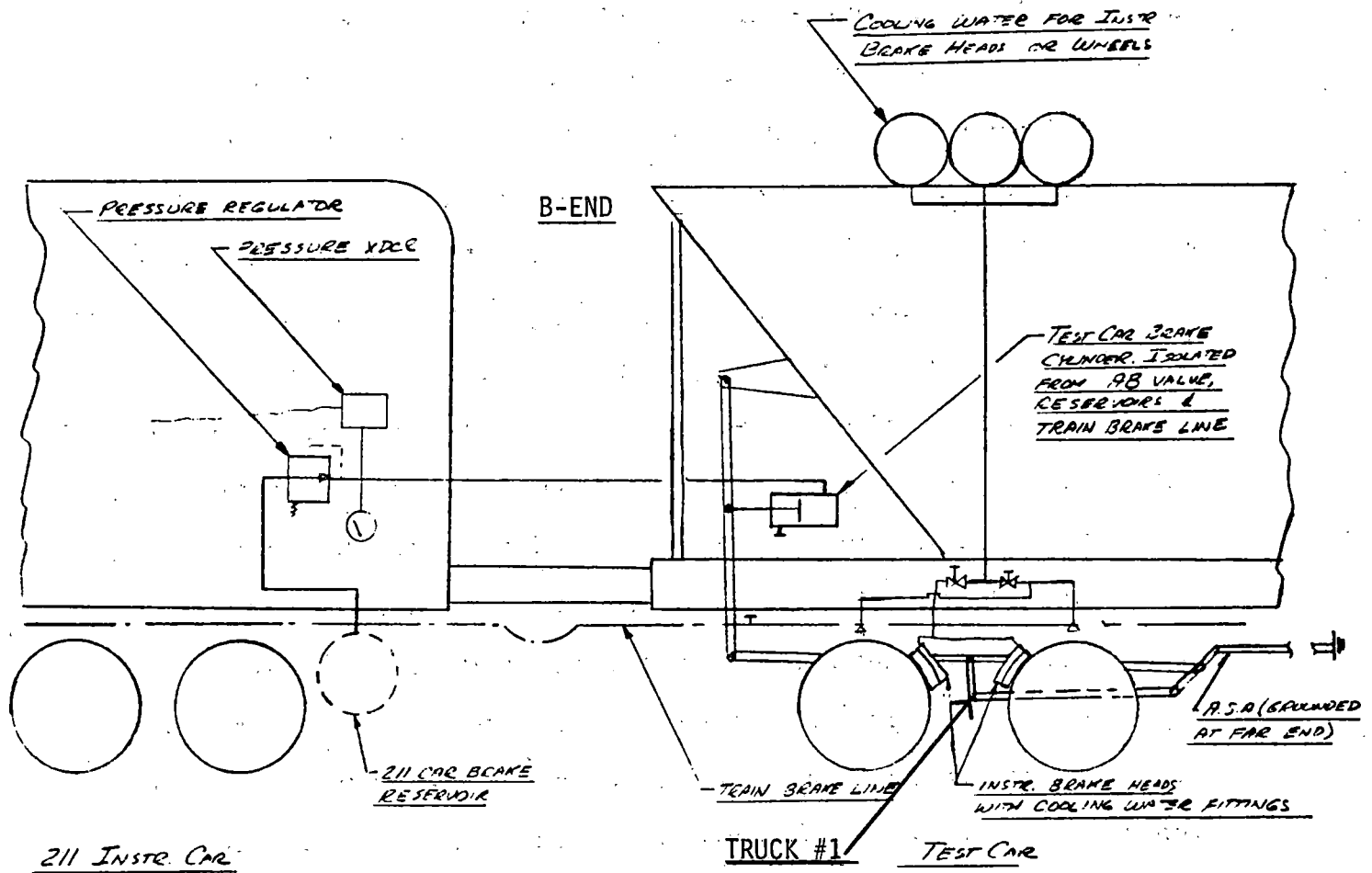
211 INSTR. CAR

TRUCK #1

TEST CAR

FIGURE 6.2   SCHEMATIC BRAKING ARRANGEMENT

6-5

thermocouples as well as with the thermocouple imbedded brake shoe. In these tests, a series of seven 45-minute drag brake cycles at 1,500 pounds of brake shoe force, the average temperature under the shoe was about 50% higher than was that measured by the bow-type thermocouple. Typically, if maximum tread temperature measured by the bow thermocouple was 600°F, then the temperature measured under the shoe was 900°F. Therefore, it is likely that tread temperature measurements made during track testing, which ranged from 1120°F to 1300°F, are significantly higher than were the average exposed tread temperatures. The corresponding exposed tread temperatures may be as low as 750°F to 870°F. Apart from monitoring wheel temperatures through slip rings by conventional thermocouples and signal conditioners, a special infrared thermographic unit (Hughes Probeye-Model 4100) was used to monitor and record temperature profiles of wheels #9 and #10 during the test mode. This thermography unit was also used for roll-by inspection of temperature distribution in the test wheels on one side of the test consist, immediately after the end of a few drag braking cycles. The Probeye unit was positioned at a wayside location for roll-by inspection. Wheel temperatures were also measured immediately after each thermal cycle at different locations on test wheels using hand held infrared microscanners. During the test run, data were collected at the rate of 100 samples per second during a period of one second after every minute of drag braking application. A Hewlett-Packard 9826 microcomputer data acquisition system was used and all test parameters including

the computed items such as friction coefficient and Bhp were printed out once a minute. A schematic of the instrumentation set-up is given in Appendix 6.1.

The first phase of preliminary track testing was completed after performing 13 drag braking cycles each of about 60 minute duration with varying brake cylinder pressures and speeds.

During the second phase of preliminary track testing, truck #2 was placed at the "A" end of the test car while retaining truck #1 at the "B" end, and a second series of thermal cycles was conducted. During the second series of testing, truck #2 was used for the brake shoe thermal effect study covered under Technical Task T7. Thermocouples were installed in the brake shoes at different depths from the contact surface as shown in Figure 6.3, five thermocouples were installed in brake shoes for wheels #14 and #15 to measure temperature profile within the brake shoes including the shoe surface contacting the wheel. Brake shoes for wheels #13 and #16 were provided with thermocouples to measure temperature at shoe-wheel interfaces. All the thermocouples of truck #2 brake shoes were monitored on an independent data logger. The test parameters of Phase 1 and Phase 2 are shown in Table 6.1.

6.2 Preliminary Track Testing Data Base

Characteristic wheel temperature and strain data, brake force data, measured residual stresses, and test parameters were tabulated for each wheel and test cycle in a Lotus data base
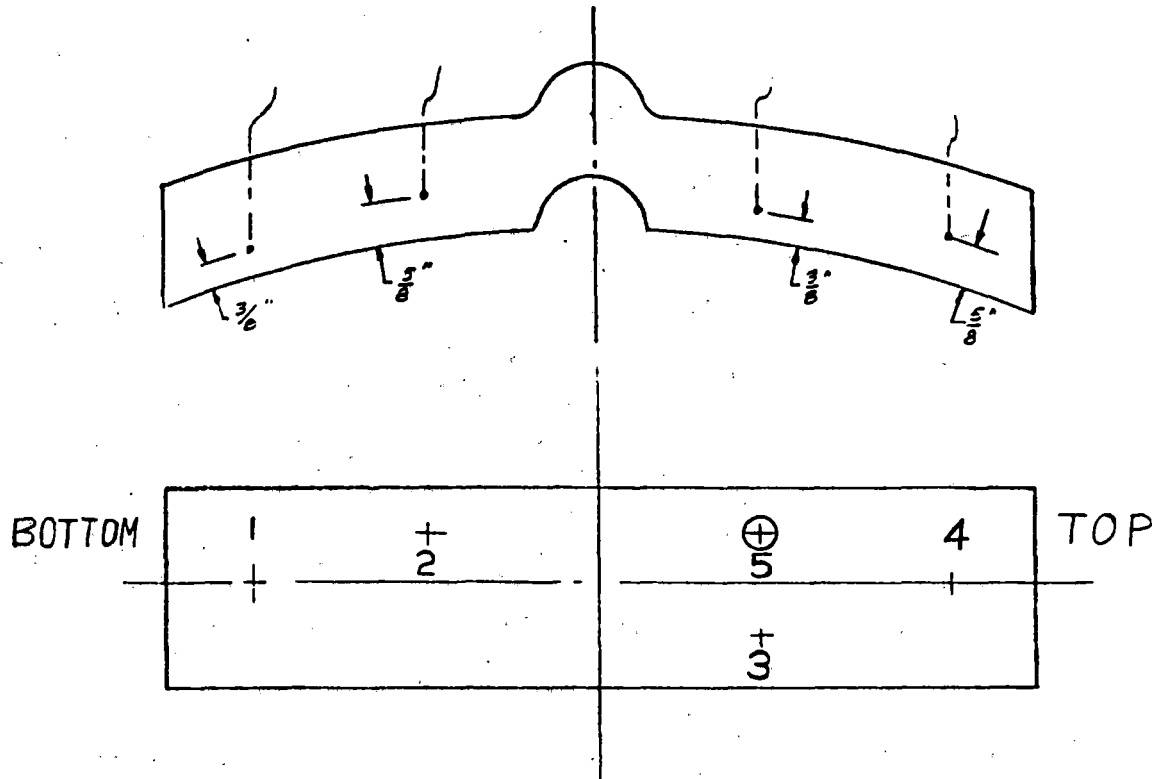
WHEEL # 14   BRAKE SHOE

FIGURE 6.3   THERMOCOUPLE LOCATION IN BRAKE SHOES FOR WHEELS
#14 AND #15, PRELIMINARY TRACK TESTING

TABLE 6.1

WHEEL FAILURE MECHANISMS
TESTING OF (INSTRUMENTED) TRUCK #1 ON TRACK
AVERAGE VERTICAL LOAD/AXLE = 54 KIPS

Date	Run No.	Brake Cylinder Pressure (psi)	Speed (mph)	Duration (minutes)	Direction	Remarks
09/04/85	1/2	20	20	2 laps		First run
09/04/85	3/4	30	30	40	CCW	45 min. between Runs 1 & 3
09/06/85	5	30	30	60	CCW	
09/10/85	6	40	30	60	CCW	
09/10/85	7	30	30	60	CW	3 hrs. between Runs 6 & 7
09/10/85	8	40	30	60	CW	1 hr. 45 mins. between Runs 7 & 8
09/12/85	9	40	30	30	CCW	
09/13/85	10	40	30	30	CW	
09/13/85	11	40	30	30	CW	1 hr. 12 mins. between Runs 10 & 11
09/17/85	12	40	30	10	CCW	
		45	30	11		
		45	40	48		
09/17/85	13	40	30	4	CW	2 hrs. between Runs 12 & 13
		45	30	3		
		45	35	10		
		45	40	26		
		45	35	2		
		50	35	14		
09/20/85	14	40	30	6	CCW	
		45	30	2		
		50	30	48		
09/20/85	15/16	40	30	6	CW	2 hrs. 30 mins. between Runs 10 & 11 Thermal video focused on WH9
		45	30	6		
		50	30	5		
		50	35	5		
		50	40	4		
		50	45	31		

TABLE 6.1 (CONTINUED)

Date	Run No.	Brake Cylinder Pressure (psi)	Speed (mph)	Duration (minutes)	Direction	Remarks
10/11/85	18/19	10	20	27	CCW	
		20	20	26	CCW	
		20	30	2	CCW	
		30	30	36	CCW	
10/14/85	20	30	20	63	CCW	Thermal video focused on WH10
10/14/85	21/22	30	30	66	CCW	1 hr. 26 mins. between Runs 20 & 21 Video focused on WH10
10/15/85	23	30	30	65	CW	Video focused on WH10
10/15/85	24/25	40	40	33	CW	1 hr. 3 mins. between Runs 15 & 16
		40	30	2		
		50	30	12		
		50	35	4		
		50	38	10		
		45	38	15		
		45	40	10		
		55	40	4		
		55	45	7		
10/16/85	26	50	30	20	CCW	Video focused on WH10
		50	40	8		
		55	40	34		
						Started 2 hrs. 15 mins. after preceding test Video on WH10
10/16/85	26/27	50	10	--	CCW	Stop braking test, no reduction*
		50	10	--	CCW	Stop braking test, 6 lb. reduction
		50	10	--		Stop braking test, 6 lb. reduction
		50	20	--		Stop braking test, no reduction
		50	20	--		Stop braking test, 6 lb. reduction
		50	30	--		Stop braking test, 6 lb. reduction
		50	40	--		Stop braking test, 10 lb. reduction
		50	50	--		Stop braking test, 10 lb. reduction

----

*With locomotive coasting

TABLE 6.1 (CONTINUED)

Date	Run No.	Brake Cylinder Pressure (psi)	Speed (mph)	Duration (minutes)	Direction	Remarks
10/16/85	27/28	50	30	5	CCW	Video on WH10
		50	35	3		
		55	35	4		
		55	40	13		
		55	45	26		
10/22/85	29	50	30	28		Video on WH10
		50	30	5		
		50	40	11		
		50	45	10		
		50	50	24		
10/22/85	30	50	40	49	CCW	2 hrs. 4 min. between Runs 29 & 30 Video on WH9 Wind 25 mph from SW
10/23/85	31	8-53	42	13	CCW	Speed, pressure varied to simulate RDU Runs 55 & 56
		55-60	45	12		
		60	50	20		
		50	43	6		
		53	42	2		
		55	40	3		
		56	45	3		
		59	45	6		
		60	47	18		
		59	50	11		
		50	40	5		
10/24/85	32	8	40	3	CW	Video on WH10
		46	42	4		
		50	42	6		
		53	43	3		
		55	45	7		
		59	44	4		
		60	45	9		
		60	50	17		
10/25/85	33	20	40	2	CCW	Video on WH10
		30	44	5		
		40	42	4		
		50	40	8		
		50	45	21		
		55	47	11		
		60	50	10		

TABLE 6.1 (CONTINUED)

Date	Run No.	Brake Cylinder Pressure (psi)	Speed (mph)	Duration (minutes)	Direction	Remarks
10/25/85	34	20	40	15	CW	2 hrs. 20 mins. between
		30	40	2		Runs 23 & 24
		40	40	8		Video on WH10
		45	50	5		
		55	45	4		
		55	50	10		
		60	50	20		
10/28/85	35	20	45	4	CCW	Video on WH10
		50	45	8		
		55	47	4		
		60	45	5		
		70	45	13		
		70	50	17		

(Appendix 6.2) similar to the one created for RDU test data. The following computed parameters (described in Section 5) were entered into the data base:

1. Average speed, Normal Brake Shoe Force, Tangential Shoe Force, and Brake Horsepower

2. Rim Energy Density

3. Estimated Bhp

4. Energy Inputs above Threshold Bhp

5. Effective Strain, Principal Stress, Effective Stress, Yield Ratio

Selected sample data (Bhp's, temperatures, strains and stresses) from Preliminary Track Testing are presented in Table 6.2. Typical time histories of B1 and B2 location strains and temperatures measured during Preliminary Track Testing are shown in Figures 6.4, 6.5, 6.6, and 6.7.

6.3 Friction Horsepower Measurements and Observations

One of the fundamental objectives of the FRA Wheel Failure Mechanisms project is to determine the effects of abnormal or extreme braking conditions on the residual stresses developed in representative freight car wheels when tested on various facilities. Accordingly, many of the tests were conducted with brake horsepower inputs exceeding those normally encountered in good railroad operating practice. For example, 50 Bhp per wheel was the aim of most of the tests. Therefore, some of the observations reported herein represent atypical, that is, more severe than in normal service operating conditions.

TABLE 6.2
SAMPLE DATA FROM PRELIMINARY TRACK TESTS
(MINIMUM AND MAXIMUM DATA FOR WHEELS 9, 10, 11, AND 12)

TEST NO.	SPEED (MPH)	BCP (PSI)	DURATION OF TESTING (MIN)	AVERAGE POWER* (HP)		PEAK POWER* (HP)		PEAK HOOP STRAIN (E-6)		PEAK HOOP STRESS (KSI)		PEAK MEASURED TEMPERATURE (DEGREES F) MAX	MICROSCANNER TEMPERATURES AFTER RUN (DEGREES F)		PEAK RADIAL STRAIN (E-6)		PEAK MEASURED TEMPERATURE (DEGREES F) MAX
				MIN	MAX	MIN	MAX	MIN	MAX	MIN	MAX		MIN	MAX	MIN	MAX	
18	20/30	10/30	108	18.8	20.3	25.7	28.6	-255	-627	-8	-21	354	-	-	1931	1931	309
20	20	30	61	20.6	24.0	25.7	34.3	-692	-692	-18	-18	365	406	573	1299	2222	358
21	30	30	66	26.2	30.1	35.3	41.1	-787	-787	-21	-21	371	348	532	1360	2336	349
23	30	30	65	28.4	30.3	42.4	47.8	-862	-862	-25	-25	364	421	550	1665	2301	370
26.7	30/45	50/55	62	37.1	48.5	53.4	77.4	-1167	-1167	-39	-39	531	560	661	2753	3340	503
27.3	40	50	60	22.0	54.3	59.6	92.3	-1266	-2983	-36	-98	635	482	625	2146	2931	472
29	30/50	50	78	41.4	52.3	73.5	82.8	-1331	-1331	-34	-34	452	-	-	1104	3219	436
30	40/50	50	50	48.1	66.8	70.9	87.6	-1514	-1514	-40	-40	559	424	549	2386	3343	444
31	40/50	45/60	60	47.7	54.2	72.5	97.7	-1229	-1229	-30	-30	411	450	517	2783	3790	488
32	40/50	45/60	55	50.1	60.4	79.1	102.5	-1345	-1494	-39	-44	468	474	499	3586	3586	448
33	40/50	40/60	62	46.3	58.0	75.2	103.5	-1284	-1538	-40	-51	658	400	507	2447	4211	498
34	40/50	40/60	60	40.4	52.5	74.4	101.1	-1350	-1904	-36	-63	527	475	532	1716	2506	503
35	45/50	50/70	51	47.0	62.0	94.2	108.9	-1502	-1858	-41	-61	537	476	579	2767	3864	520

*WHEEL 9 NOT INCLUDED BECAUSE OF FAULTY BRAKE FORCE INSTRUMENTATION

TIME HISTORY OF STRAIN B1C DURING RUNS 23 & 34 (PRELIMINARY TRACK TESTING)
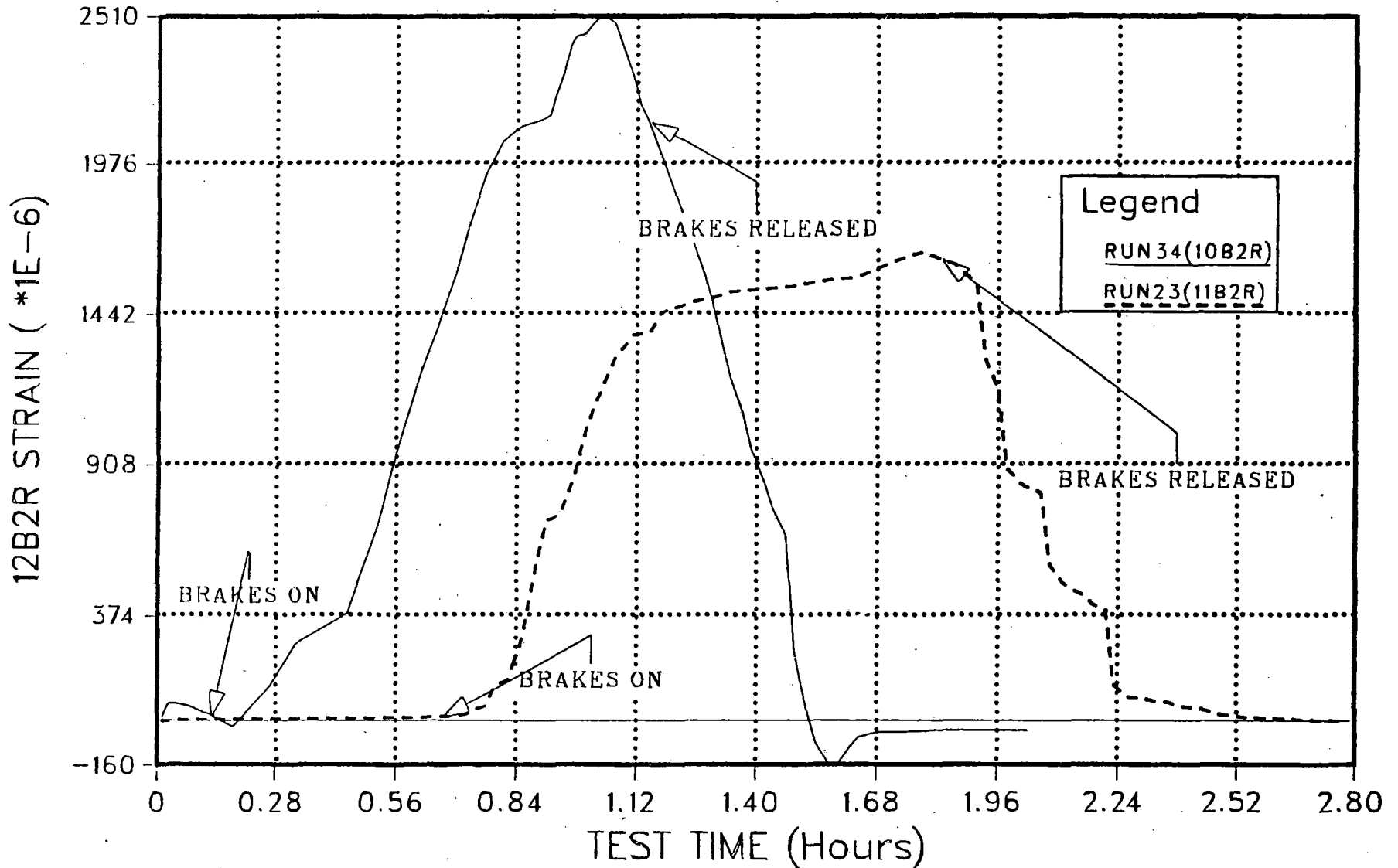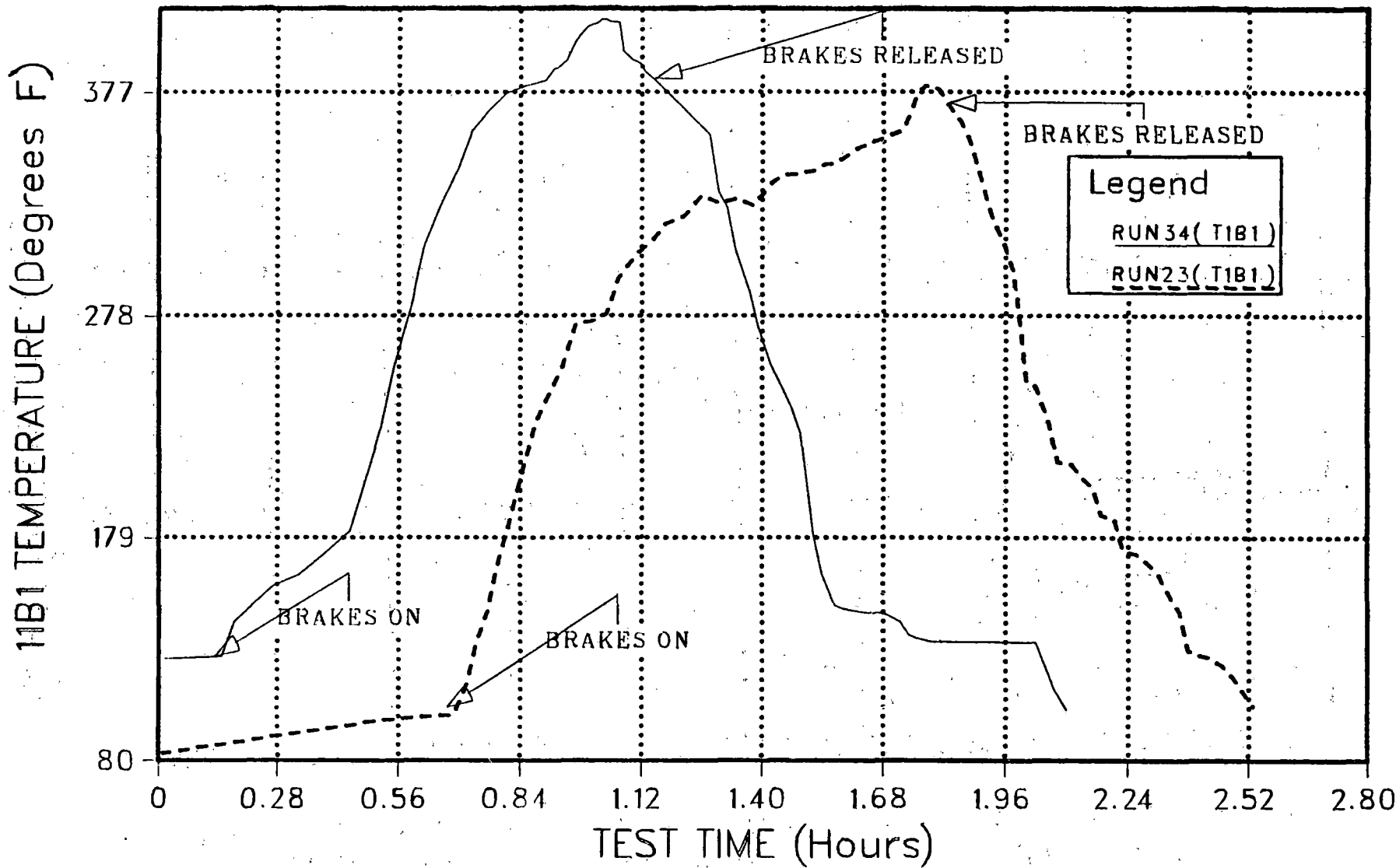(RUN 23: 30m.p.h,30p.s.i,70min; RUN 34: 40/50m.p.h,40/60p.s.i,61min)
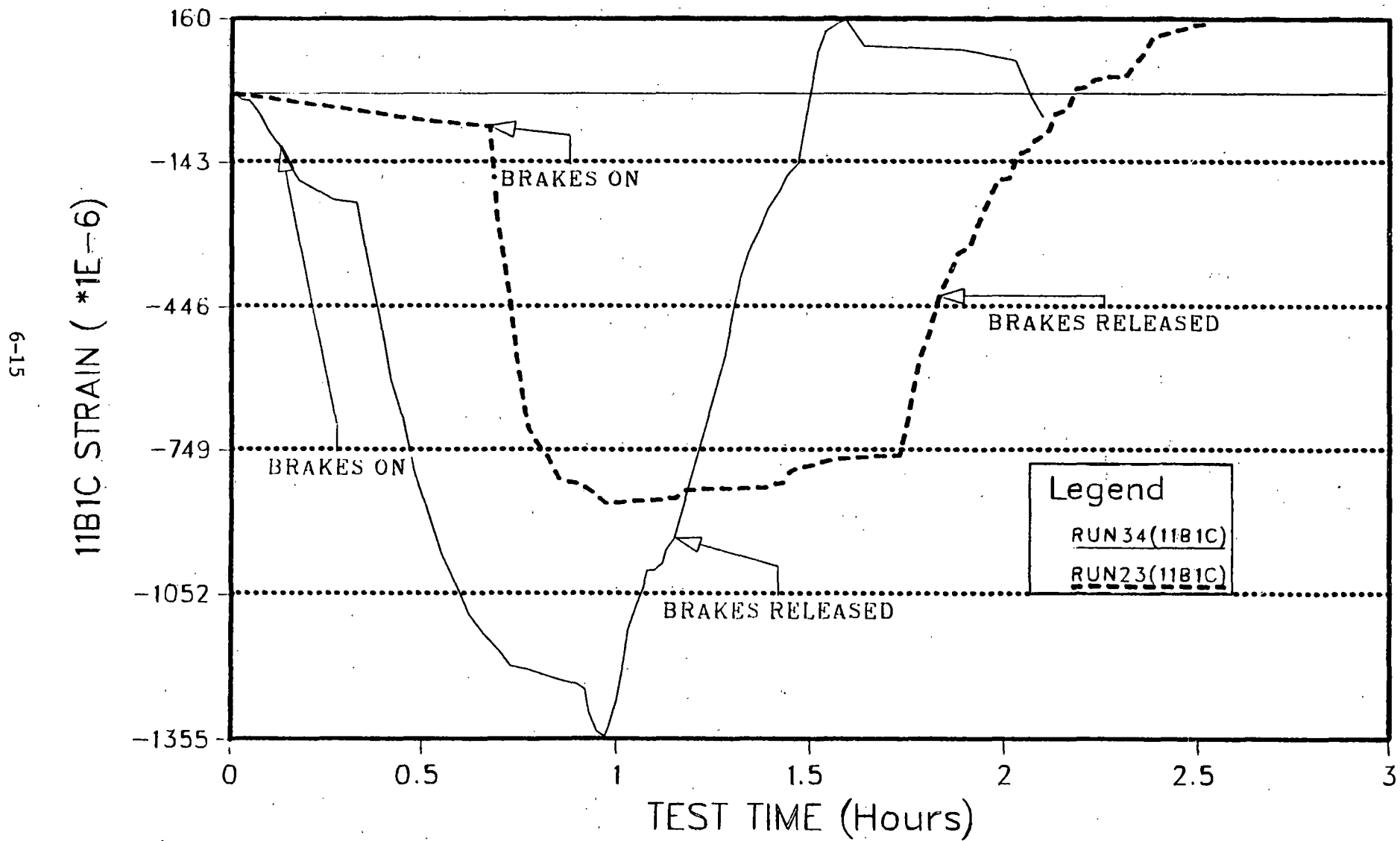
FIGURE 6.4   TIME HISTORY OF CIRCUMFERENTIAL STRAIN ON BACK RIM
FACE DURING TWO DRAG BRAKING TESTS

TIME HISTORY OF STRAIN B2R DURING RUNS 23 & 34 (PRELIMINARY TRACK TESTING)
(RUN 23: 30m.p.h,30p.s.i,70min; RUN 34: 40/50m.p.h,40/60p.s.i,61min)

FIGURE 6.5 TIME HISTORY OF RADIAL STRAIN AT RIM FILLET REGION OF
BACK RIM FACE DURING TWO DRAG BRAKING TESTS

TIME HISTORY OF T1B1 TEMPERATURE DURING RUNS 23 & 34 (PRELIMINARY TRACK TESTING
(RUN 23 30m.p.h,30p.s.i,70min; RUN 34: 40/50m.p.h,40/60p.s.i,61min)

FIGURE 6.6 TIME HISTORY OF TYPICAL CIRCUMFERENTIAL STRAIN ON BACK RIM FACE

TIME HISTORY OF B2 TEMPERATURE DURING RUNS 23 & 34 (PRELIMINARY TRACK TESTING)
(RUN 23: 30m.p.h,30p.s.i,70min; RUN 34: 40/50m.p.h,40/60p.s.i,65min)
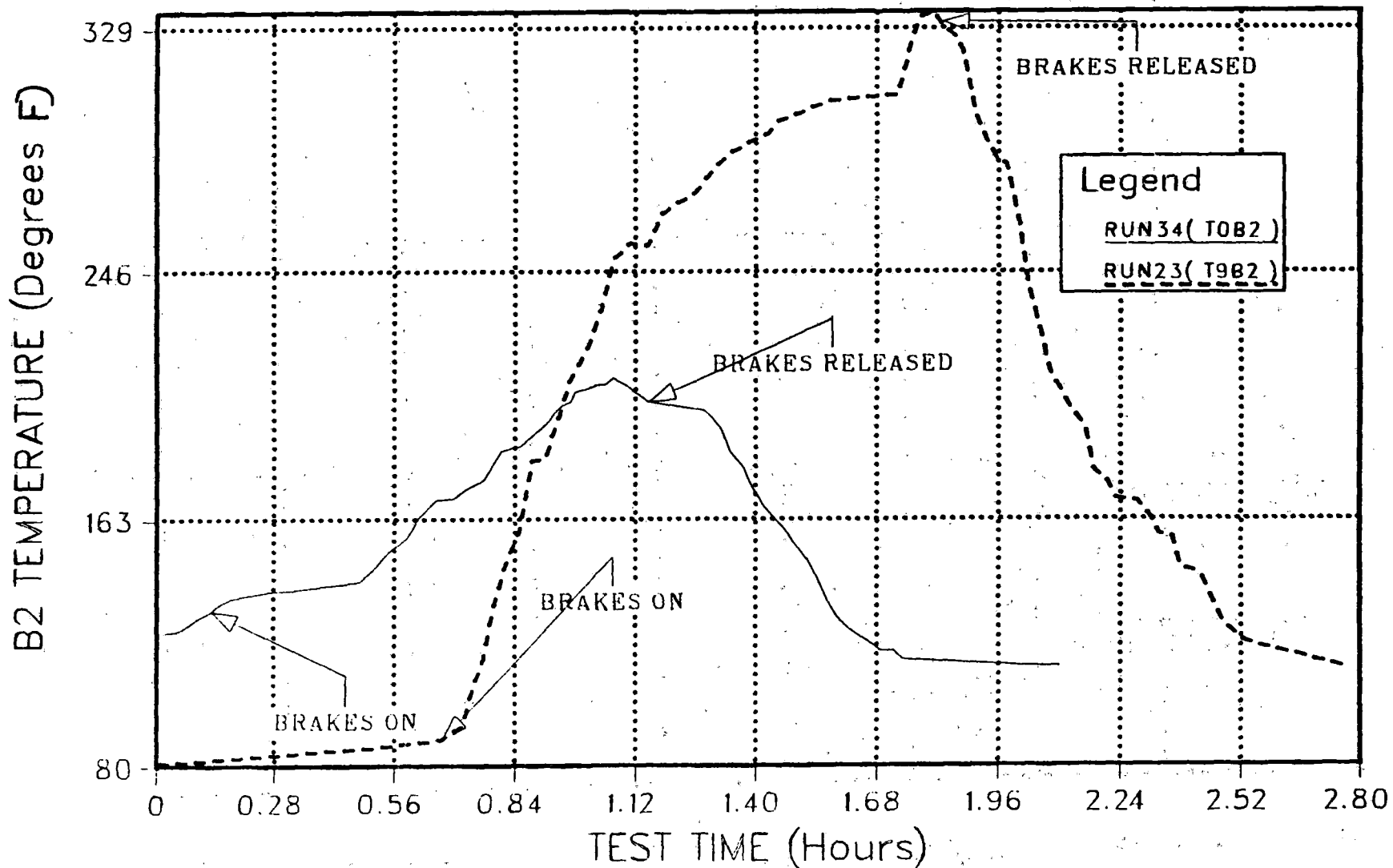
FIGURE 6.7 TYPICAL TIME HISTORY OF RIM FILLET REGION TEMPERATURE

Measurements of friction horsepower history and observations of the fundamental coefficient-of-friction behavior of the AAR M926 high friction composition brake shoe were included in the laboratory and track tests.

Braking conditions of speed and brake shoe force and resulting coefficients of friction, friction horsepower and wheel temperatures are presented in Table 6.3 for selected tests from three different facilities: dynamometer, RDU, and track. Because of varying test conditions and, in some cases, differences in instrumentation, a direct comparison of results may be misleading. Therefore, some discussion of relative test conditions is appropriate prior to considering brake shoe coefficient of friction, wheel temperatures, etc.

Moderately heavy braking test conditions under controlled conditions are illustrated by the dynamometer and special drag braking tests previously conducted by the AAR at Peotone, Illinois and at TTC.

In these tests, the speed and brake shoe force (bsf) was maintained virtually constant and at moderate levels (40 Bhp; 1,500 lbs. bsf for the dynamometer and 1,712 lbs. for the R-565A tests). In contrast, attempts were made during the RDU and track tests to sustain or increase the severity and duration of braking. As demonstrated in Figure 6.8, the speed was usually increased as testing proceeded. Also, the brake shoe force was applied at higher levels (overall averages exceeded 2,200 lbs.) and often increased toward the latter period of braking. This variation of brake shoe force for RDU test No. 55-56 and for

TABLE 6.3
COMPARISON OF HORSEPOWER AND TEMPERATURES
FROM VARIOUS WHEEL TEST FACILITIES

Facil.	Test No.	Wheel ID	Speed (MPH) Avg	Max	Brk. Shoe Force (LBS) Avg	Max	Brake Duration (Hrs)	Coef. of Friction Assum.	Measured Avg	Max	Brake Horsepower Nominal Avg	Max	Measured Avg	Max	Max Temp (F) Tread	BF Rim
Dyn.	1														585	345
	24	4892	40	40	1500	1500	0.75		0.32	0.36			51.6	57.9	475	475
R-565A (Ref4)		Avg of 8 Whls	40	40	1712	1712	0.5		0.23	0.38			42.5	68.5	550	
RDU	55/56	5	46.5	50.3	2141	2351	1.0		0.15	0.19			41.1	53.6		555
		6	46.5	50.3	2045	2178	1.0		0.16	0.26			41.7	58.1		
		7	46.5	50.3	2271	2571	1.0		0.11	0.17			31.0	43.5		502
		8	46.5	50.3	2466	3453	1.0		0.14	0.26			44.1	94.7		701
Prelim Trk.	29	9	34.2	49.6	2097	2252	1.3		0.16	0.27			34.0	67.5	1220*	
		10	34.2	49.6	2292	2596	1.3		0.20	0.28			40.0	73.2		
		11	34.2	49.6	2261	2454	1.3		0.25	0.35			51.3	76.8	1300*	439
		12	34.2	49.6		2493	1.3		0.22	0.37			46.8	62.4	1300*	581
Comp. Trk.	47	17	45		1690		0.5	0.2			40.5					
		18	45		1690		0.5	0.2			40.5				1120*	532**
		25	45		2257		0.5	0.2			54.1				1270*	
		26	45		2257		0.5	0.2			54.1				1170*	

*Measured by thermocouple imbedded in brake shoe
**Infrared thermal video
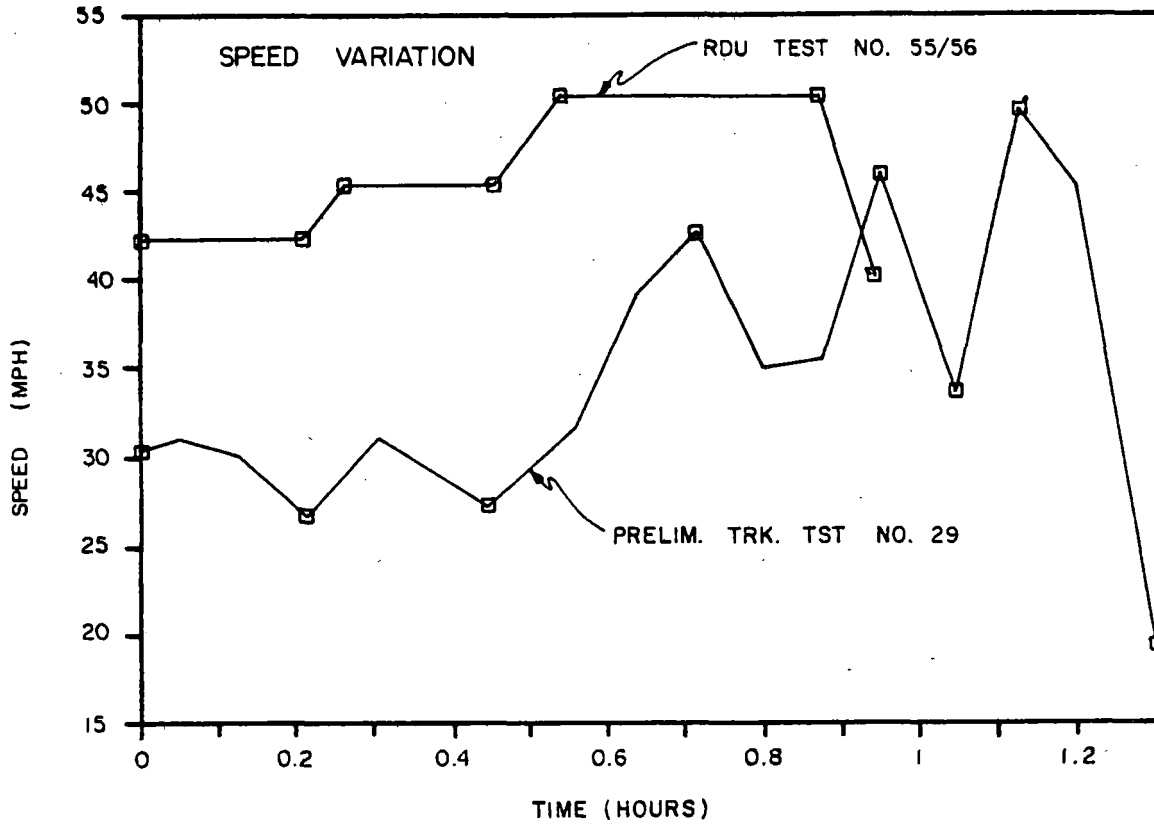
FIGURE 6.8   SPEED VARIATION DURING RDU AND TRACK TESTS

preliminary track test No. 28 is presented in Figure 6.9.

6.4 General Trends of Coefficient of Friction

The coefficient of friction of the composition brake shoe is not constant; it decreases with increasing brake force, speed, and temperature of wheel and/or brake shoe. Other factors affecting the coefficient are the contact area, wheel surface roughness, and possible changes in the friction characteristics of the materials due to use. Therefore, when repeated drag braking tests are conducted with a constant brake force, the horsepower changes (decreases) during the course of the braking test and may vary from test to test.

Furthermore, because of the speed and force dependence, doubling speed or brake force should not exactly double the horsepower.

Therefore, there can be a considerable variation of heating among wheels exposed to "equivalent" braking conditions.

The variation of brake shoe coefficient of friction with test time for the more moderate test conditions used in the dynamometer and drag braking tests (AAR R-565A) is illustrated in Figure 6.10. Note the reduction in the level of the friction coefficient with time, especially in the track test. The average coefficient for the dynamometer test is 0.32 and overall average for the R-565A track tests is 0.23.

At higher brake shoe forces applied in the RDU and preliminary track tests reported here, the average friction
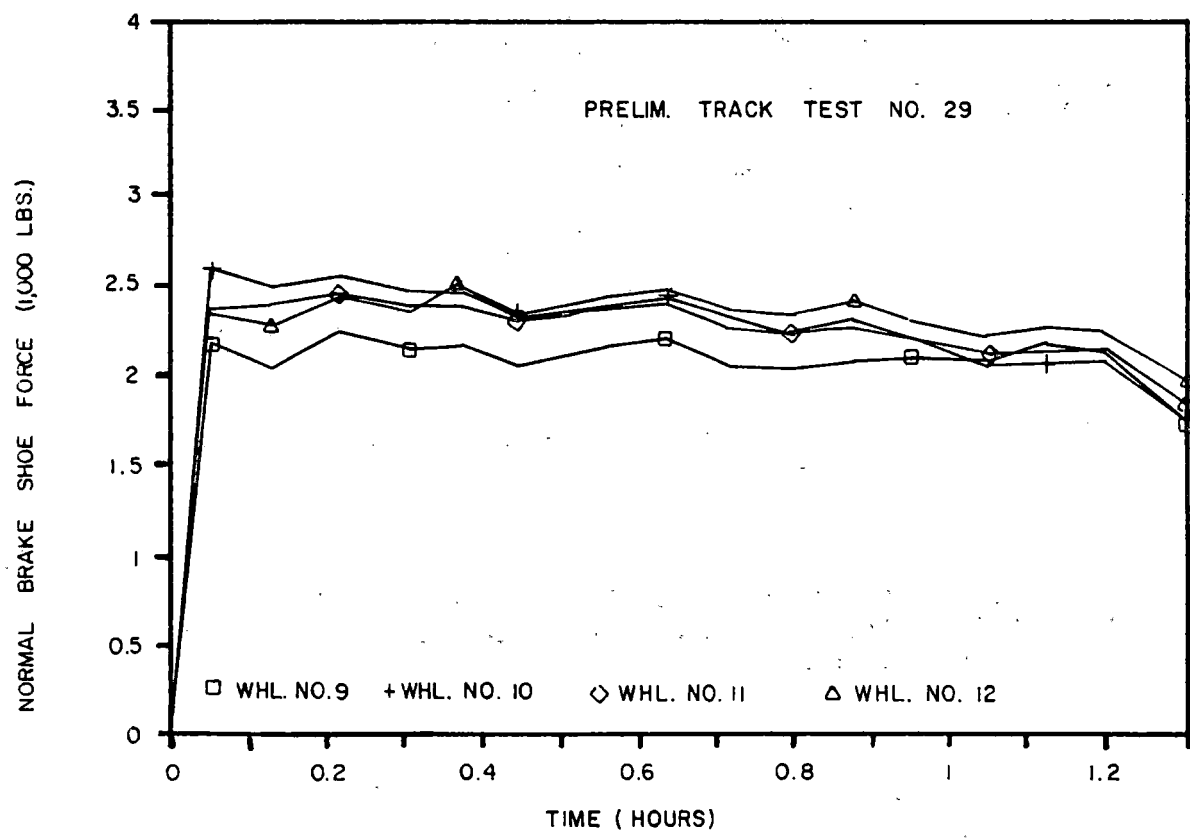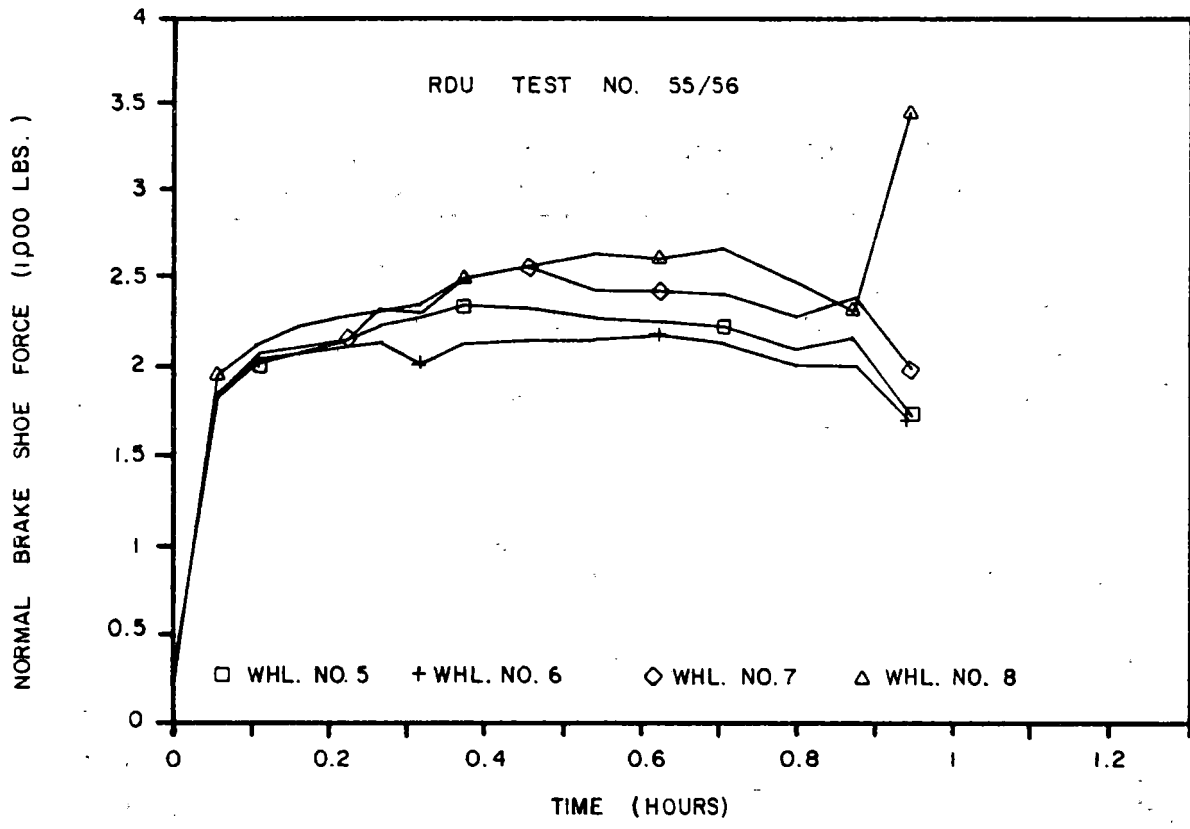
FIGURE 6.9   BRAKE SHOE FORCE VARIATION DURING
RDU AND TRACK TESTS

6-23

FRICT. COEFFICIENT — MODERATE BSF TESTS

40 MPH DYN NO. 24 AND TRACK TEST (AAR REPORT R-565A)

□ DYN NO. 24 BSF — 1500 LB.   + R565A   BSF — 1712 LB

TIME (HOURS)

FRICTION COEFFICIENT AT BRAKE SHOE/WHEEL INTERFACE
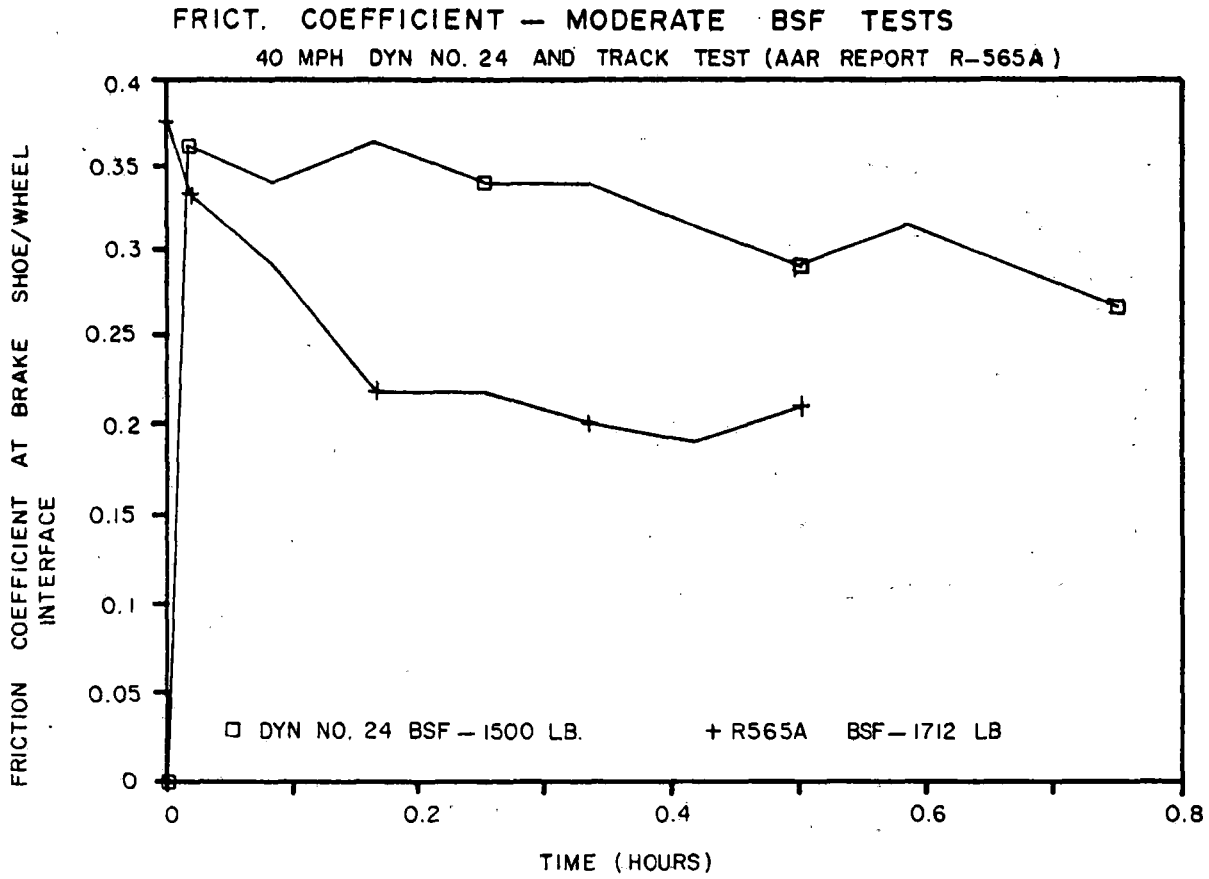
FIGURE 6.10   COEFFICIENT OF FRICTION VARIATION DURING
DRAG-BRAKING TESTS ON DYNAMOMETER AND PREVIOUS
TRACK TESTS

6-24

coefficients are lower and, with exception of notable spikes near the ends of tests, decrease markedly with test time. The time history of friction coefficients is shown in Figure 6.11. The overall average friction coefficients of 0.14 for the RDU test and 0.21 for the preliminary track test No. 29 are lower than those from the more moderate brake force level tests.

Typical Brake Horsepower Histories

The friction horsepower histories developed in the dynamometer and R-565A track tests are plotted in Figure 6.12. Brake horsepower histories for a severe braking cycle from the RDU and track test program are illustrated in Figure 6.13. These values were calculated from retarding force readings directly from the instrumented brake heads.

Such brake heads were not available for the dynamometer and some of the track tests. In these cases, the horsepower was estimated by use of assumed values of coefficients of friction and the equation

$$\text{power input} = bsf \cdot f \cdot s / 375$$

where the power input is expressed in Bhp; "bsf" is the brake shoe force in lbs.; "f" is the coefficient of friction; and "s" is the speed in mph.

For test cars that were not equipped with special instrumented brake heads, the brake shoe force was determined
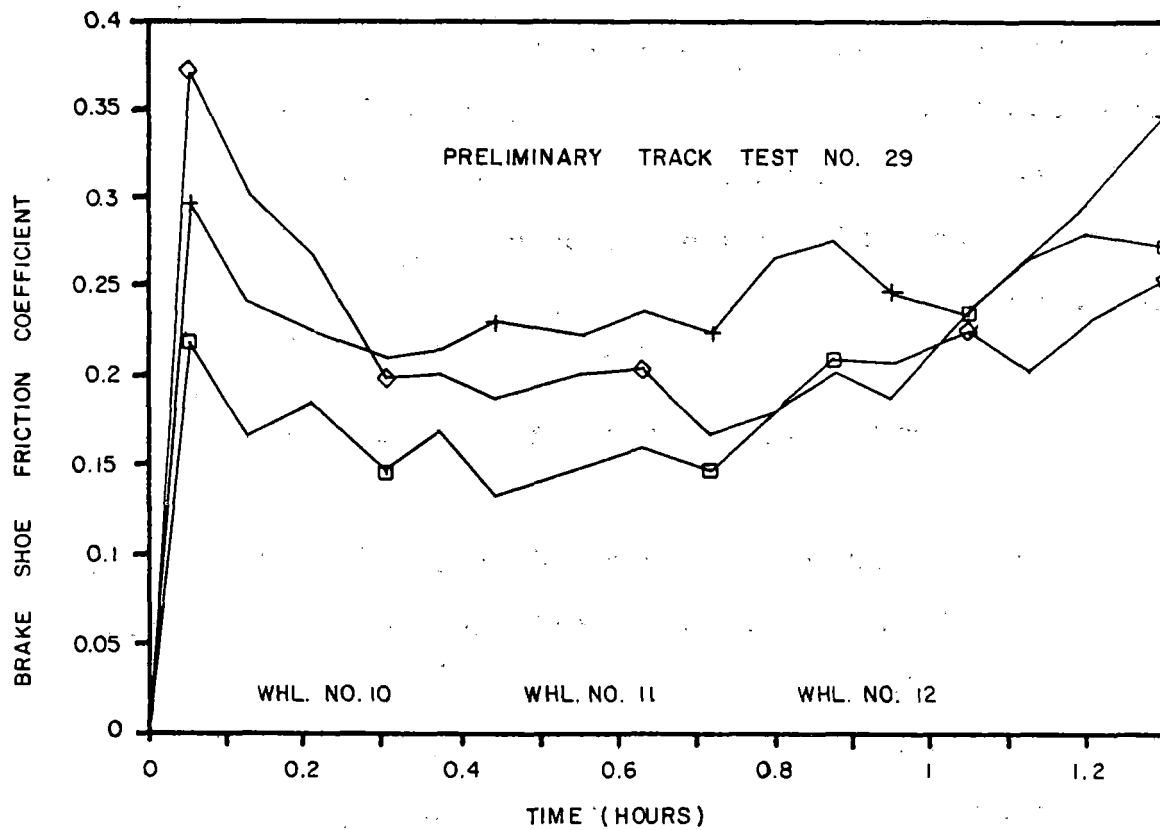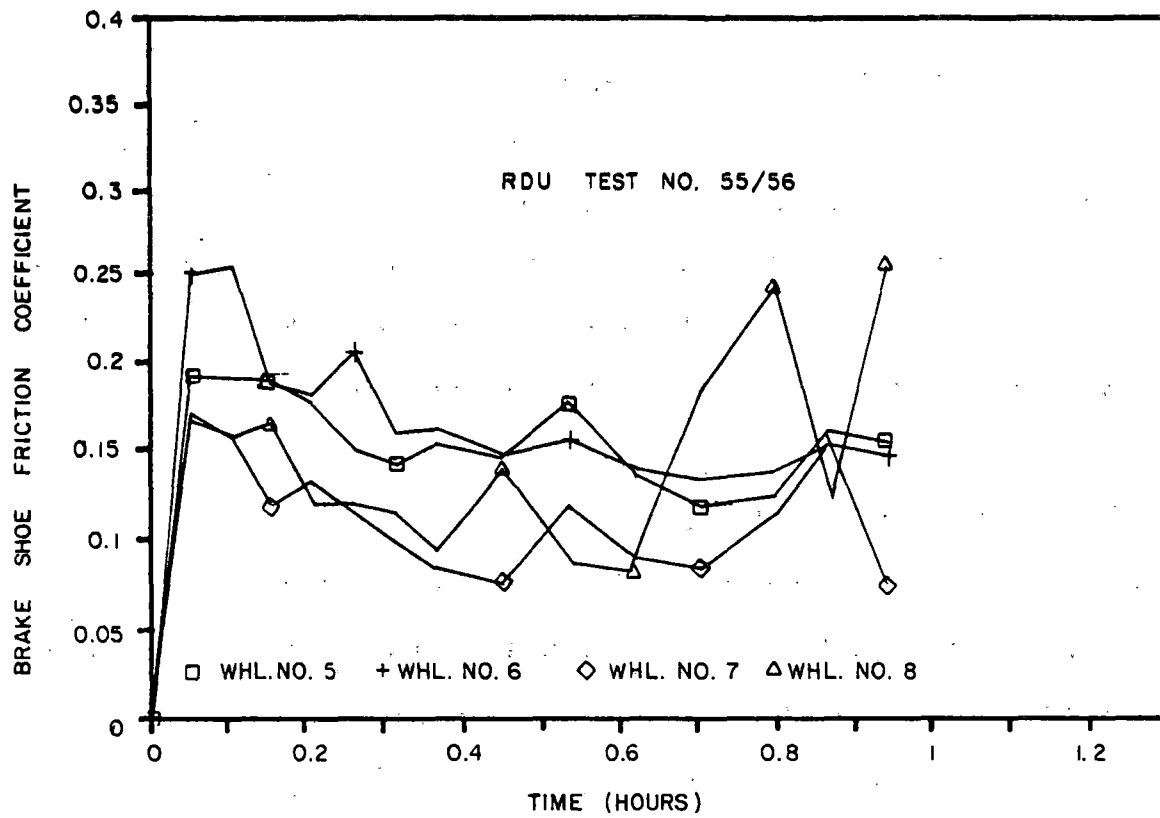
FIGURE 6.11   COEFFICIENT OF FRICTION VARIATION IN RDU AND TRACK
                DRAG BRAKING TESTS
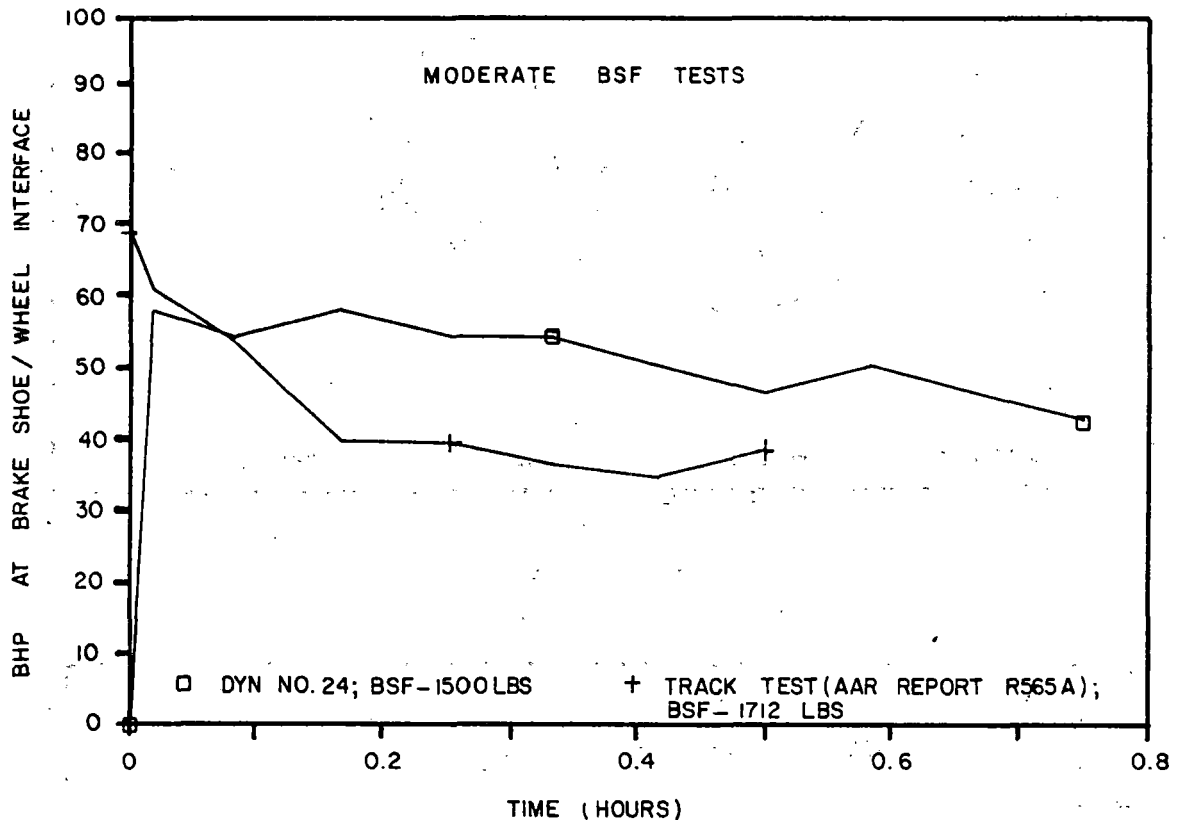
FIGURE 6.12   HORSEPOWER VARIATIONS IN DRAG TESTS AT
DYNAMOMETER AND PREVIOUS TRACK TESTS
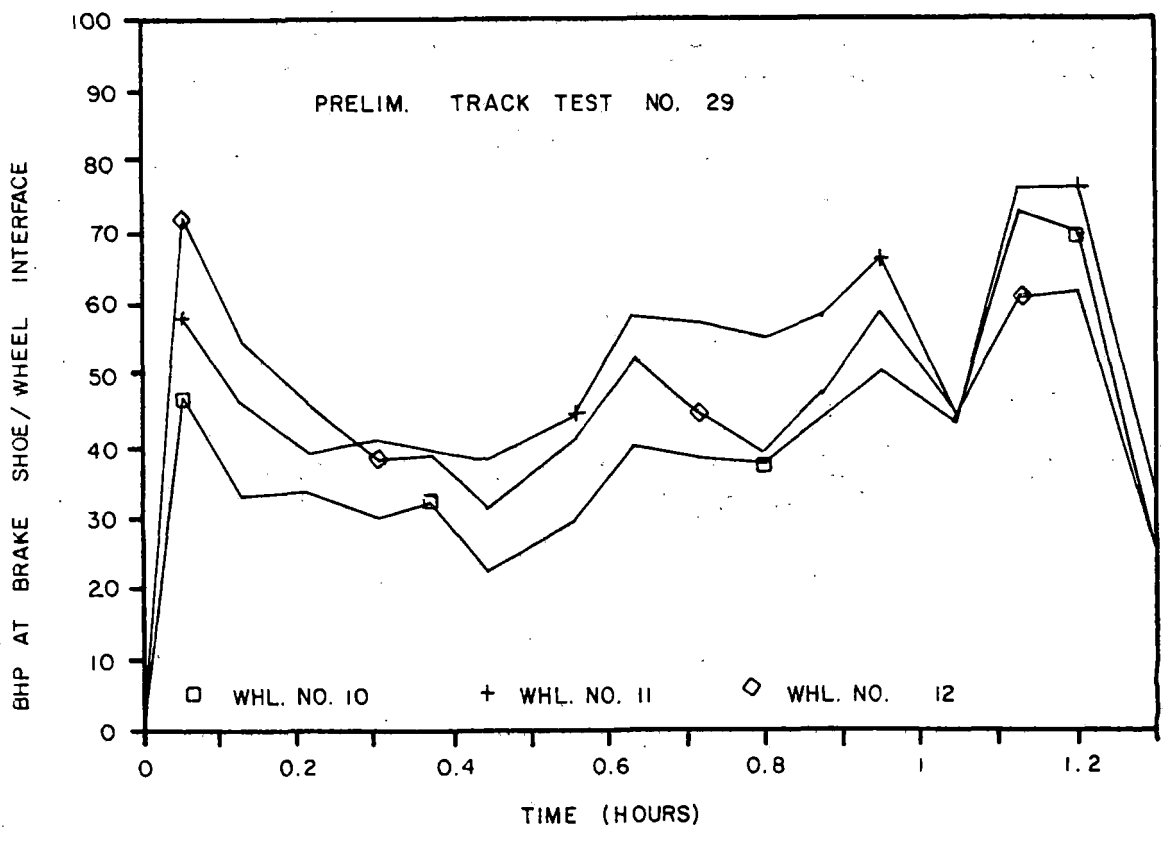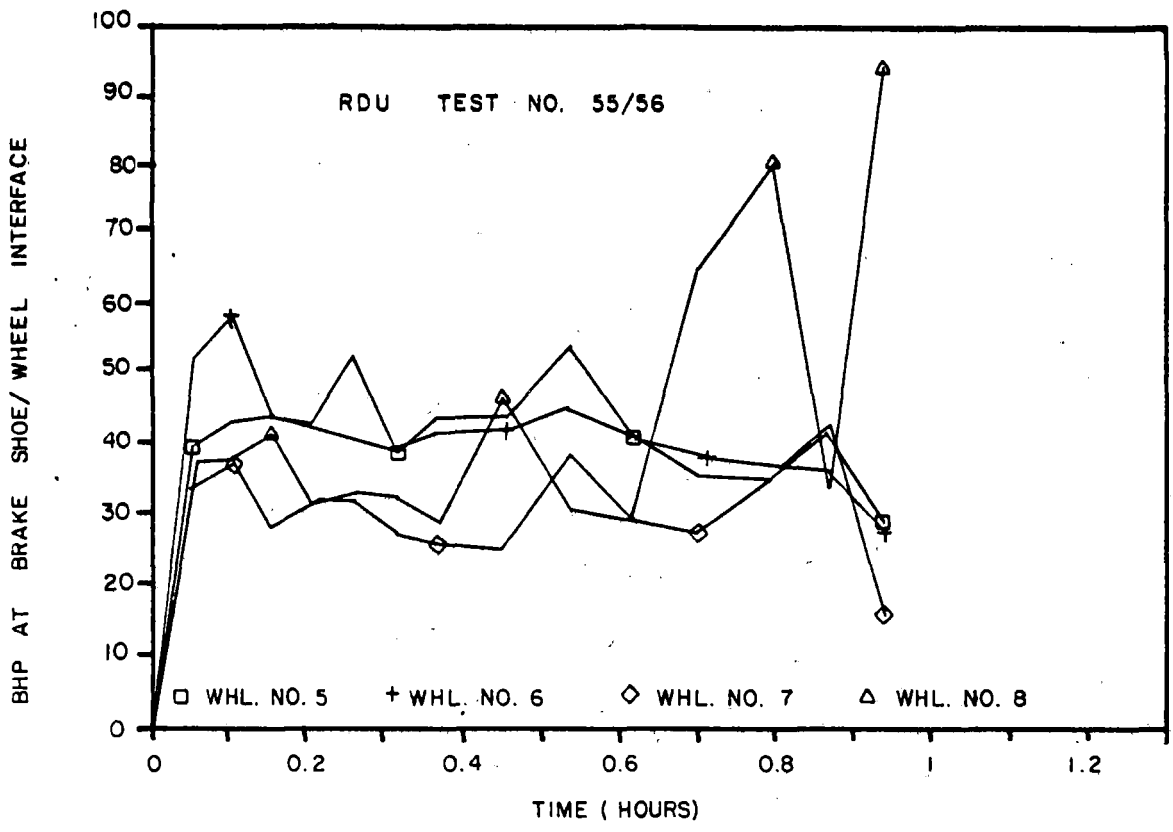
FIGURE 6.13   BRAKE HORSEPOWER VARIATIONS DURING DRAG BRAKING ON
               RDU AND TRACK

statistically with golden shoe calibration at various brake cylinder pressures.

6.5 Comparison of Dynamometer, RDU and Track Testing Wheel Horsepower and Temperatures

It would be desirable to make a direct comparison of input brake shoe friction horsepower and the resulting tread and rim temperatures for equivalent braking cycles. Although strict equivalence could not be maintained from one test type to another because of differences in instrumentation and operational constraints, some comparison of results is provided in Table 6.3 for selected test runs on the dynamometer, RDU, extensively instrumented preliminary track tests and subsequent comprehensive lightly instrumented track tests.

The wheel thermal responses to the severe RDU and preliminary track tests is indicated in Figure 6.14. The welded thermocouple readings plotted in these figures were taken from the lower back face rim location B1. All back rim temperatures reported in Table 6.3 were obtained this way with the exception of those for comprehensive track test No. 47, which did not have this instrumentation. In this particular case, a reading was available from the infrared thermal video system that was mounted under the test car. The details of Comprehensive Track Testing which was conducted under Technical Task T6, are presented in Section 7.

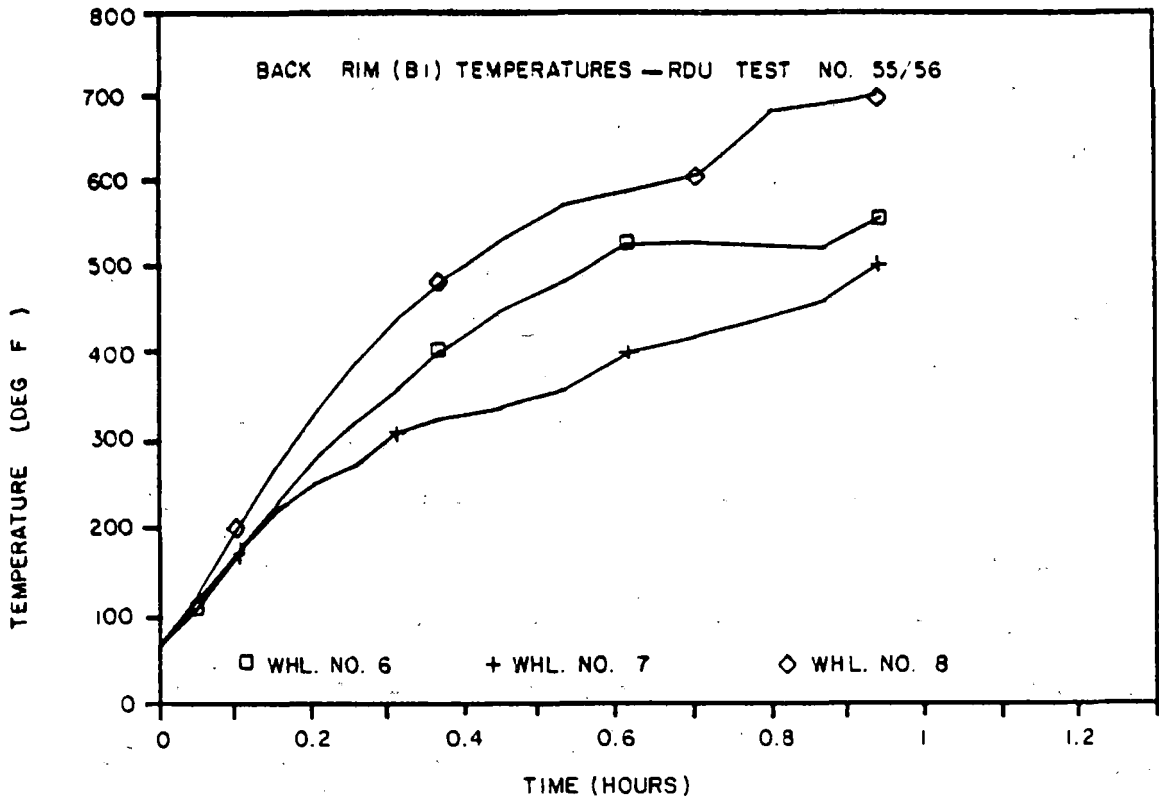The variability of wheel temperature from wheel to wheel in
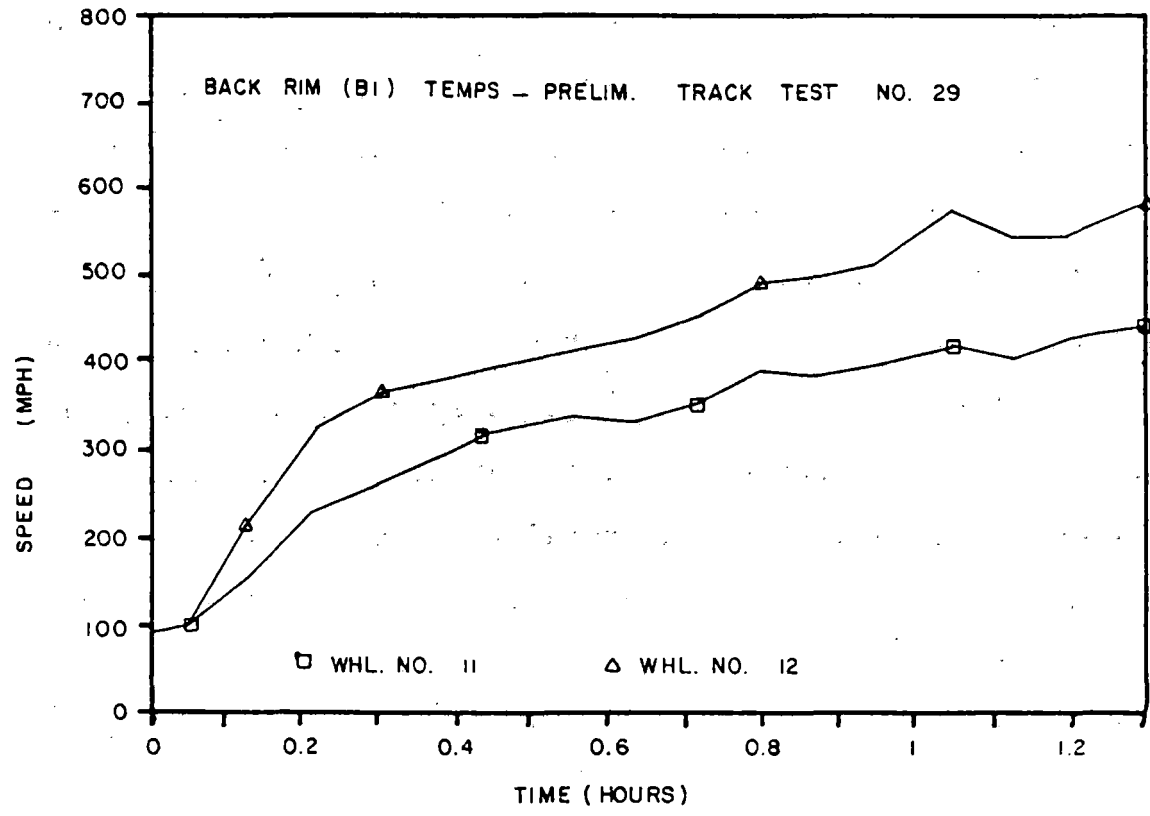
FIGURE 6.14 TEMPERATURE DEVELOPED ON BACK FACE OF RIM
DURING DRAG BRAKING ON RDU AND TRACK

the same truck and test reflects the variability illustrated previously in friction coefficient and horsepower. It may also reflect the fact that the data are based on a single thermocouple. The rotational asymmetry issue is discussed in Section 11. A typical variation of tread temperature with time is shown in Figure 6.15.

This tread temperature was obtained from thermocouples embedded in the brake shoe at the rubbing interface and were higher, as expected, than were temperatures obtained by bow-type thermocouples sliding on the exposed wheel tread. The exposed tread temperature as measured by bow-type thermocouples is usually taken as more representative of the average tread temperature. For study of heat flow in brake shoes, the embedded thermocouple reading may be the appropriate one to use. These differences are discussed in Section 7.1.3.

Miniature bow-type thermocouples were used in the RDU tests and initially in the track tests, but they were replaced by thermocouples imbedded in the brake shoes for preliminary and comprehensive track tests because they were mechanically unreliable.

6.6 Wheel-Brake Shoe Heat Transfer Study

Brake shoe thermal effects covered under Technical Task T7 were combined with the implementation of Technical Task T5 during the preliminary track testing. Data obtained from the composition brake shoes of wheels #14 and #15 were used for this
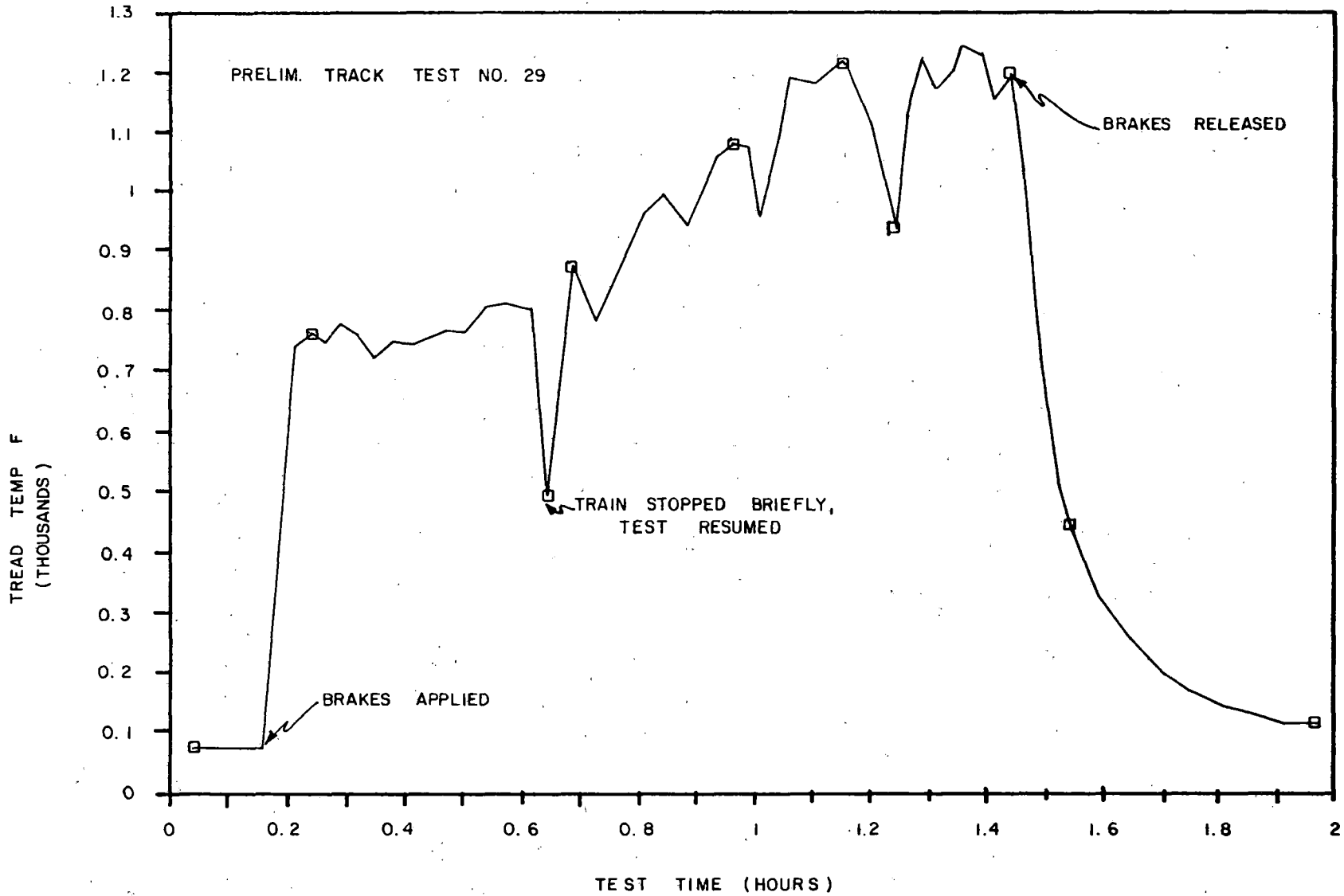
FIGURE 6.15   TREAD/BRAKE SHOE TEMPERATURE MEASUREMENT DURING DRAG BRAKING
IN TRACK TEST

analysis. Thermocouples were installed at different depths in the brake shoes of wheels #14 and #15.

The percentage of friction generated heat that flows into a composition brake shoe during sustained braking has been stated to vary between 3% and 10%. However, most of the test analysis appears to be for short stop braking cycles.[2] The theoretical work is based on early solutions of Carslaw and Jaeger.[3] The proportion of heat entering the wheel during longer braking cycles is given by Newcomb[1] as:

$$\left[1 + \left(\frac{d_1}{d_2}\right)^{\frac{1}{2}} \frac{K_2}{K_1} \frac{A_2}{A_1}\right]^{-1}$$

where d is the thermal diffusivity; k is thermal conductivity; and A is area of rubbing path. Subscript 2 refers to the brake shoe.

For the material constants from Larson, et al[2], reproduced in Table 6.4 and the brake shoe and wheel tread rubbing areas of 0.27 and 2.43 ft[2], respectively, "B" becomes 0.986. This means that 1.4% of the heat generated by friction would flow into the brake shoe.

Some evaluation of this theoretical relative heat flow into the brake shoe may be made on the basis of a few special observations with thermocoupled brake shoes made during one series of drag braking tests on track in this program. For these special tests, thermocouples were located at the surface and at depths of 3/8 inch and 5/8 inch below the shoe surface, as shown in Figure 6.16.

The temperature histories of four selected thermocouple

TABLE 6.4
THERMAL PROPERTIES (FROM LARSON, ET AL[2])

Material	Specific Heat c Btu/(Deg F-lb) [Btu/(Deg F-lb)]	Density w lb/in^3 [lb/ft^3]	Thermal Conductivity k Btu/in-sec-deg F [Btu/ft-hr-deg F]	Thermal Diffusivity $d_2 = k/(wc)$ in^2/sec [ft^2/hr]
Composition Shoe	0.239 [0.239]	0.076 [131.33]	0.000019 [0.821]	0.001046 [0.02615]
Wheel Steel	0.118 [0.118]	0.278 [480.38]	0.000604 [26.09]	0.018412 [0.4603]

channels from these shoes on one of the drag braking tests (preliminary track test No. 26) are given in Figure 6.16. For this test, which lasted slightly more than one hour, the speed was increased from 30 to 40 mph after 20 minutes. The nominal average brake horsepower developed was about 50 Bhp.

The change in brake shoe thickness during the test is also indicated in Figure 6.16, based on final shoe thicknesses measured after the test. This estimate assumes a linear wear rate for the shoe that may be misleading, since a disportionately higher rate would be expected near the end of the test when the tread temperature has risen from about 750° to $1150^{\circ}F$. Therefore, it is difficult to determine temperature gradient reliably. Nevertheless, for the purpose of making an approximate comparison to theory let us ignore shoe wear during the first 0.1 hour. Although this time is short in terms of shoe wear it should be long enough to approach steady-state heat transfer conditions in the shoe.

For a time of 0.1 hour, an average temperature difference between the surface (channel 5) and 3/8 inch below the surface (channel 3) is about $600^{\circ}F$. The corresponding gradient is $1093^{\circ}F$ per inch. The average gradient between the 3/8 inch depth and the 5/8 inch depth (channel 3 minus channel 4) is only about 103° at this time. The corresponding gradient would be $412^{\circ}F/inch$. The nonlinear gradient may be expected to reflect the fact that the heat flow into the shoe is not one-dimensional. That is, lateral heat flow is expected.

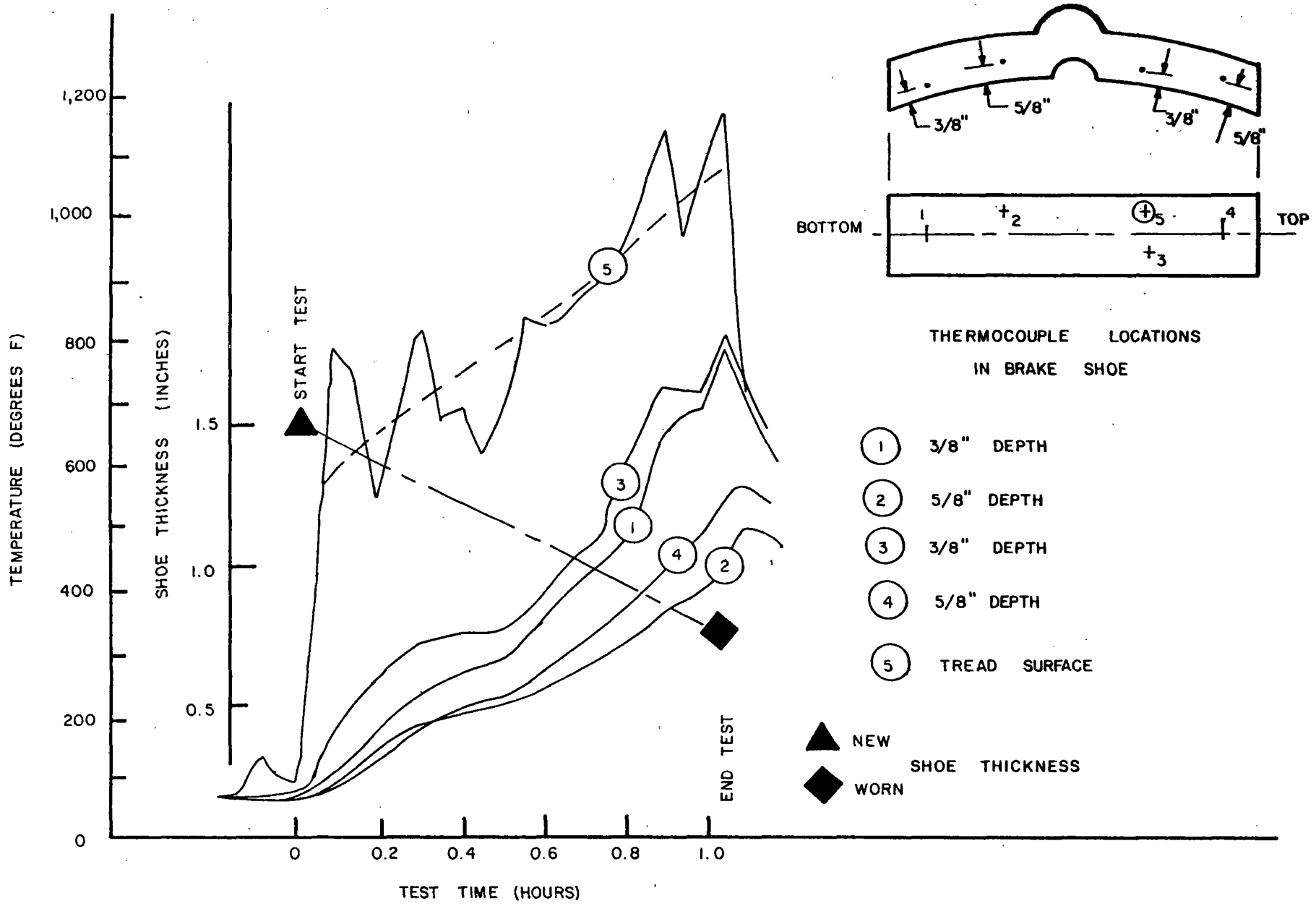No data from directly applicable tests of thermal

FIGURE 6.16   BRAKE SHOE TEMPERATURES DURING RUN 26 OF TRACK TESTS

conductivity on the particular composition shoe material used in these tests are available. However, values for three composition shoes are available from earlier AAR tests.[4] The value of 0.82 Btu/(ft-hr-^{o}F) from Larson, et al, is on higher end of the AAR range. These earlier AAR values range from 0.35 to 0.85 Btu/(ft-hr-^{o}F) for virgin material at 392°F to 0.19 to 0.42 Btu/(ft-hr-^{o}F) at 754°F for material baked at 1138°F.

An estimate may now be made of the heat flux into the brake shoe using the temperature gradients, the thermal conductivity value of 0.82 Btu/(hr-ft-^{o}F) from Larson and the fundamental heat conduction equation:

$$q = -k \ A \ dT/dx \qquad\qquad (2)$$

where q is the heat flux in Btu/hr; k is conductivity in Btu/(hr-ft-^{o}F); T is temperature in ^{o}F; x is distance in feet; and A is brake shoe rubbing area in feet^2.

For a gradient of 1093°F/inch, and a brake shoe contact area of .282 ft^2, the heat flux is 3033 Btu/hr. This amounts to 1.2 hp or 2.3% of the horsepower developed during the early stages of the test. The corresponding calculated heat flux based on the gradient between the 3/8 inch deep and 5/8 inch deep measuring points is 1,141 Btu/hr (0.45 hp) or 0.9% of a hypothetical 50 Bhp input.

It should be emphasized that these are only approximate computations or rough estimates that are intended to explore the

relative magnitudes of the several tread heat transfer mechanisms. Nevertheless, it is encouraging that this preliminary empirical rate of perhaps 1% to 2.5% of friction horsepower is comparable to the theoretical value of 1.4% based on the study by Newcomb[1].

6.7 Asymmetry of Heating Observations

Special infrared thermographic studies were made of the distribution of heating and cooling temperatures around the rim and plate of wheels tested on the TTC tracks.

Heretofore, it was believed that heating a wheel by brake shoe friction would result in an axisymmetric distribution of temperature around the wheel, except for localized transient "hot spots" on the tread surface. However, we noted in our studies that in several cases the temperature was not uniform around the circumference of the wheels. For example, temperature differences around the tread of up to 200°F were observed during drag braking.

Temperature Variation Around Wheel Rim and Plate

After a one-hour drag brake test on TTC tracks at 40 mph with a consist of two cars of 70-ton capacity and one of 100-ton capacity, the train was brought to a stop using locomotive brakes after the car brakes had been released, and was slowly rolled past the infrared thermographic camera stationed at

trackside. Significant variation in temperature was noted around the rim of several wheels including the wheel on the trailing axle of the last car (the car of 100-ton capacity). The wheel came to a stop at the camera location and a typical image is shown in Figure 6.17 obtained within seconds of wheel stop. Note that the crosshair was moved around the front face rim in a time period of less than one minute at a radius approximately equal to that for the B1 reference location on the back face rim. The highest digital temperature recorded was 642.5°F at about the 9 o'clock position on the rim while the lowest was 502.5°F near the 5 o'clock position.

Therefore, the temperature varied 140°F over this rim sector of about 120°. This 36 inch parabolic plate wheel was on an axle of a car with individual brake cylinders for each axle and should have received a nominal 2,600 lbs. of brake force.

The cause of the nonaxisymmetric heating is not known at this time. However, future research is being directed toward an evaluation of the effects of brake system dynamics, wheel rim-bore concentricity, bore straightness, and rim out-of-roundness on temperature distribution.
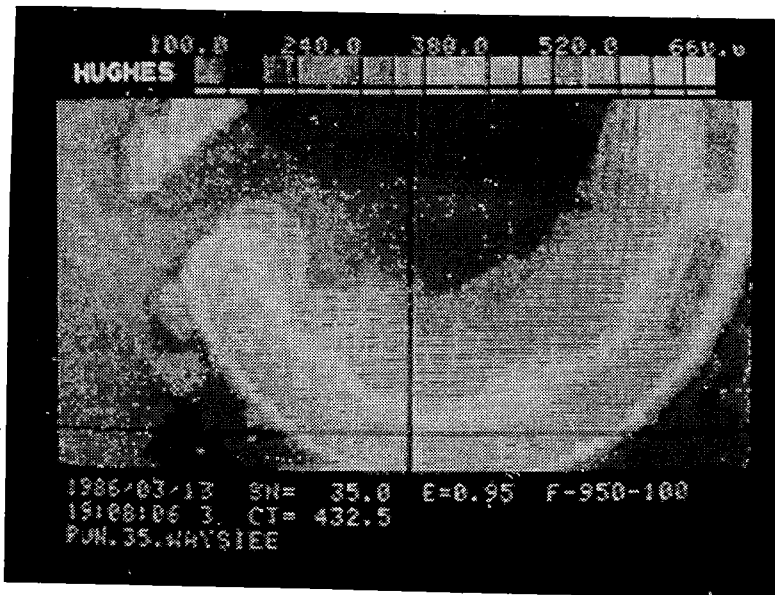
FIGURE 6.17   TYPICAL THERMAL IMAGE OF A WHEEL
                IN ROLL-BY MODE

6.8 Residual Stress Measurements by Hole Drilling Method and Subsequent Evaluation of Net Rim Forces from Saw-Cut Displacement Data

6.8.1 Test Procedure

During Preliminary Track Testing, residual stresses at the B1 location (back rim face) were periodically measured with the hole-drilling technique (a description of the technique is given in Section 4). At the conclusion of testing, each of the test wheels was saw-cut and the resulting flange tip displacements were used to estimate the total circumferential rim force existing in the test wheels prior to saw-cutting.

The two test trucks of the 70-ton test car were tested under separate operating conditions. In the first phase of testing, 12 drag braking cycles were applied to the B-end truck wheels. During this phase of testing, the A-end truck wheel brakes were not applied.

Prior to the second phase of testing, the rims of the second axle wheels of each test truck (wheels 11, 12, 15, and 16) were machined to condemning limits. A series of 14 drag braking cycles were then applied to all test wheels during the second phase.

The B-end truck wheels were partially annealed at the start of testing to relieve strain gage bonding stresses. The A-end truck wheels were not annealed. Hence, these four wheels had more compressive rim stresses to start with, compared to that of

B-end truck wheels.

The development of residual stresses (as measured by the hole drilling technique) in each wheel during Preliminary Track Testing is shown in Figures 6.18 - 6.21. The B1 circumferential residual stresses measured at the end of testing, as well as rim forces computed after saw-cutting, are given in Table 6.5.

6.8.2 Discussion

As seen in Figures 6.18 and 6.19, tensile circumferential B1 location residual stresses were produced in B-end truck wheels during the first phase of testing. At the end of the second phase of testing, wheels 11 and 12 (with thin rim cross sections) exhibited slightly higher B1 circumferential residual stresses than wheels 9 and 10 (with normal rim cross sections).

The A-end truck wheels all exhibited compressive B1 circumferential residual stresses of various magnitudes at the conclusion of testing.

All rim forces computed for the B-end truck wheels approached or exceeded the level of 100 Kips. As discussed in Section 11, 100 Kips is considered to be an unsafe level of rim force. The highest rim force (184 KIPS) was computed for wheel 12, which also had the highest tensile residual stress on the back rim face as determined by hole drilling. Wheel 12 had a thin rim cross section.

Among wheels in A-end truck, the highest computed rim force

RESIDUAL STRESS HISTORY
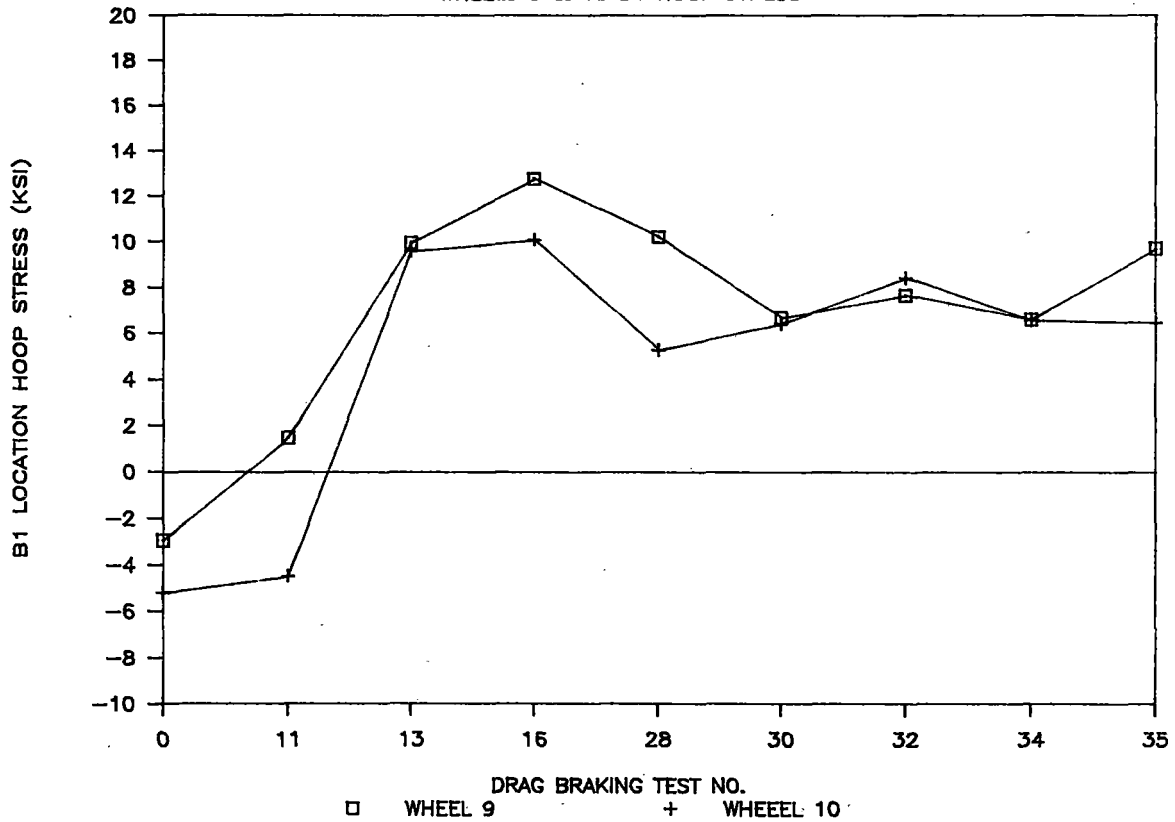## WHEELS 9 & 10 B1 HOOP STRESS

FIGURE 6.18   RESIDUAL STRESS HISTORY WHEELS 9 & 10
B1 HOOP STRESS

RESIDUAL STRESS HISTORY
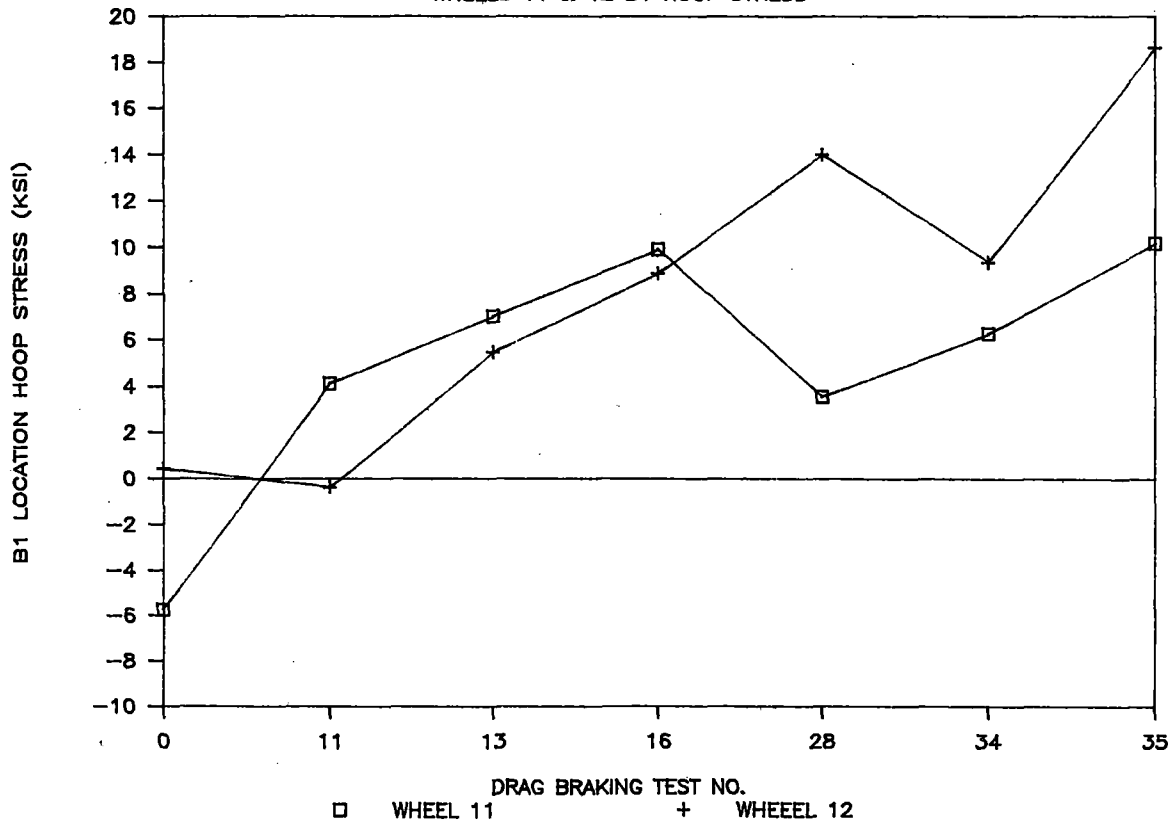## WHEELS 11 & 12 B1 HOOP STRESS

FIGURE 6.19   RESIDUAL STRESS HISTORY WHEELS 11 & 12
B1 HOOP STRESS

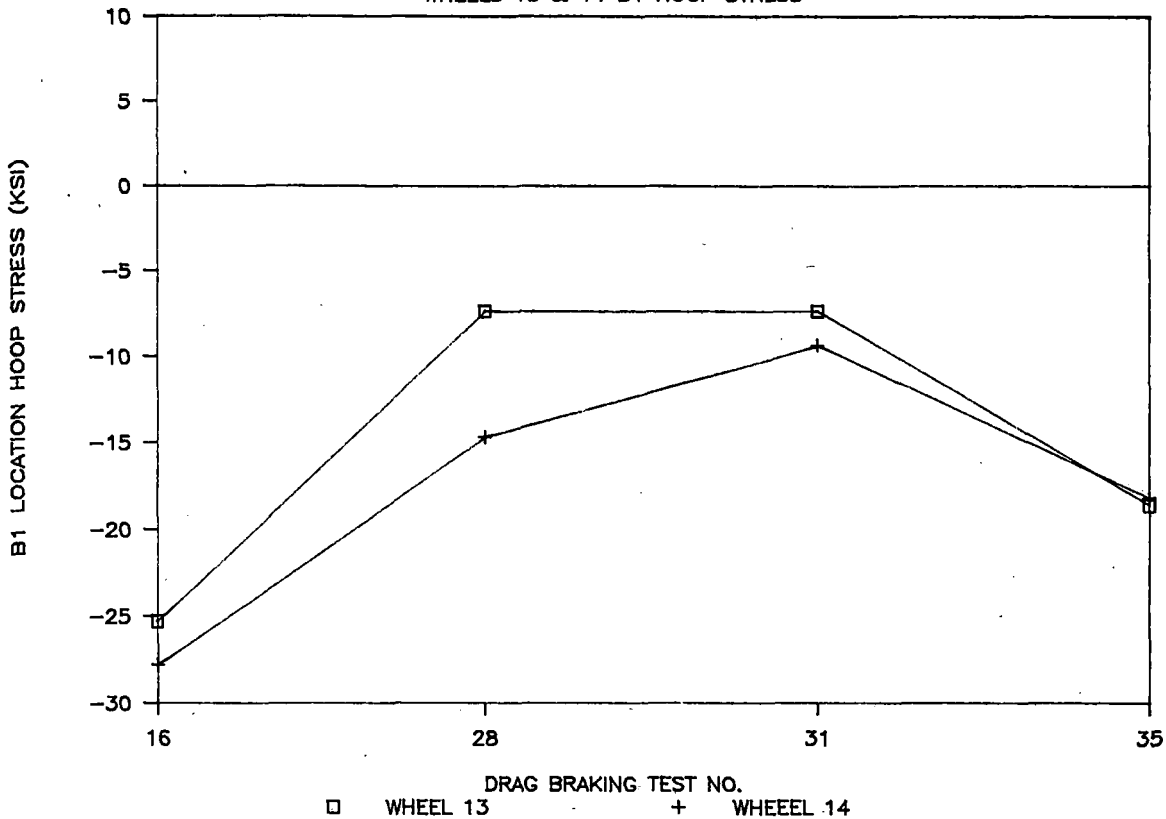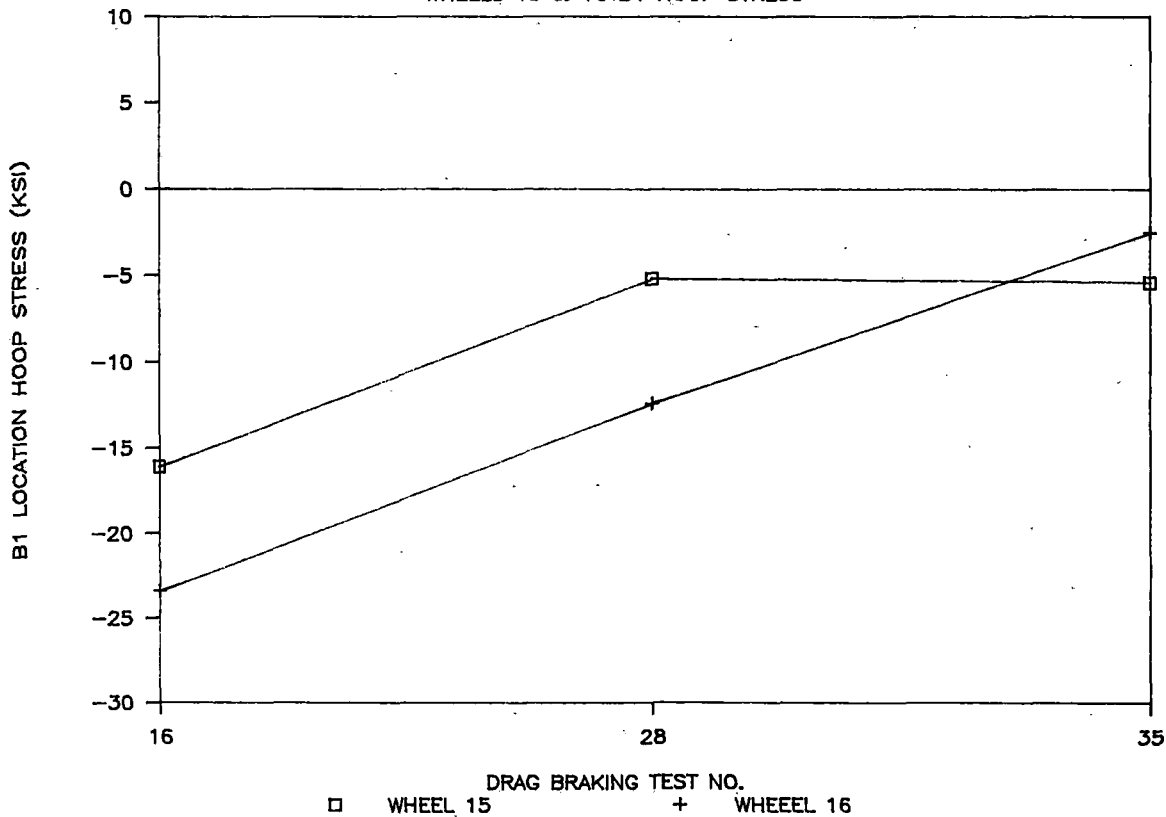## RESIDUAL STRESS HISTORY
WHEELS 13 & 14 B1 HOOP STRESS

FIGURE 6.20   RESIDUAL STRESS HISTORY WHEELS 13 & 14
          B1 HOOP STRESS

RESIDUAL STRESS HISTORY
WHEELS 15 & 16 B1 HOOP STRESS

FIGURE 6.21   RESIDUAL STRESS HISTORY WHEELS 15 & 16
          B1 HOOP STRESS

6-44

TABLE 6.5
RESIDUAL STRESSES AND COMPUTED RIM FORCES
AT THE CONCLUSION OF TESTING

Wheel #	Rim Thickness	Residual B1 Circumferential Stress (KSI)	Computed Rim Force (KIPS)
9	Normal	9.7	125
10	Normal	6.4	129
11	Thin	10.2	92
12	Thin	17.4	184
13	Normal	-18.6	53
14	Normal	-18.1	21
15	Thin	- 5.4	57
16	Thin	- 2.5	107

(107 KIPS) occurred in wheel 16, which also had a thin rim cross section.

6.8.3 Summary

o Tensile residual stresses were measured at the B1 location in B-end truck wheels, and compressive residual stresses were measured in A-end truck wheels.

o Estimated rim forces were tensile for all test wheels. The B-end truck wheels had more tensile rim forces compared to A-end truck wheels. B-end truck wheels received approximately twice the cycles of A-end wheels.

o Test wheels with thin rims in trucks A and B exhibited more tensile (or less compressive) B1 location residual circumferential stresses and rim forces than test wheels with normal rim cross section.

6.9 Conclusions of Technical Tasks T5 and T7

1) Higher levels of Bhp were expended at the brake shoe/wheel interface during track testing, compared to RDU testing, to achieve equivalent wheel temperatures and strains.

2) Higher Bhp's were maintained during Preliminary track testing due to more heat losses from the test wheel in the form of convection, radiation, and conduction into the rail resulting in lesser wheel temperatures whereby the coefficient of friction at the brake shoe/wheel

interface did not reduce at the same rate as on the RDU.

3. Tensile residual stresses of various magnitudes were measured on the back rim face of all B-end truck wheels of the test car. On the other hand, A-end truck wheels retained different magnitudes of compressive residual stresses on the back rim face. Two test conditions seemed to have contributed towards different levels of residual stresses in B-end and A-end truck wheels:

   i) B-end truck wheels were annealed (to relieve strain gage bonding stresses) where as A-end truck wheels were not.

   ii) B-end truck wheels were subjected to approximately twice as many drag braking cycles as the A-end truck wheels.

4. B-end truck wheels categorically exceeded the unsafe level of rim forces (100 KIPS) as computed from the saw-cut displacement data. Among B-end truck wheels, wheel #12 contained highest tensile rim forces and this result is consistent with the wheel temperatures and strains attained by wheel #12 (Appendix 6.1).

5. Among the A-end truck wheels, wheel #16, with thin rim cross section, exhibited the highest tensile rim force (107 KIPS). It was observed during testing that wheel #16 tread temperatures (as measured by brake shoes with embedded thermocouples) were consistently higher than

wheel #15 tread temperatures (wheel #15 also had thin rim cross section).

6. Within B-end truck wheels, wheel #12 which exhibited highest tensile rim force, had a thin rim cross section. It was observed during testing that rim temperatures and Bhp levels of wheel #12 were consistently higher.

6.10 Wheel Flat Test

At the end of the second phase testing, the effect of a wheel flat on dynamic wheel strains and brake forces was investigated. The existing consist (Figures 6.1 and 6.2) was utilized for the test. The objectives of the wheel flat test were:

1. To measure the dynamic wheel strains in the vicinity of a wheel flat as well as at a location 60° from the flat.

2. To gather normal and tangential force data at the brake shoe/wheel interface for the wheel with a flat under selected combinations of speeds and brake cylinder pressures.

In preparation for the test, a 2" flat was machined into the tread of wheel #11. The rim of wheel #11 had previously been machined (for Phase II testing) to a 15/16" tapeline thickness to simulate a worn wheel. Dynamic strain and brake force data were then collected for wheels 10 and 11 at speeds ranging from

10 to 50 mph, and brake cylinder pressures of 10 to 50 psi on three types of track construction.

6.10.1   Instrumentation

A Kiowa analog recorder was used to continuously record signals from strain gages 10B0C, 10B1C, 11B1R, 11B1C, 11B2R, and 11B1C60, as well as the signal from an accelerometer.

Simultaneously, signals from strain gages 11B1R, 11B1C, 11B2R, 11B1C60, the instrumented brake heads, and the accelerometer were recorded digitally with an HP 9826 data collection computer at a sample rate of 2000/sec. with 1 sec. of data recorded at selected points on the track. Locations and specifications of the strain gages on wheels #10 and #11 appear in Figure 6.22. Gages 11B1R, 11B1C, and 11B2R on wheel #11 were placed on a radial line coincident with the trailing edge of the flat. The accelerometer, which was located on the bearing adapter wheel of wheel 11, provided a positive time history of the wheel flat impacting the rail.

6.10.2   Test Conditions

Prior to the test, the contact portion of the tread was established by coating the tread with a blue dye and running the consist on a tangent section of track. A 2" x .03" deep flat, centered on the wheel contact area, was then machined into the tread.
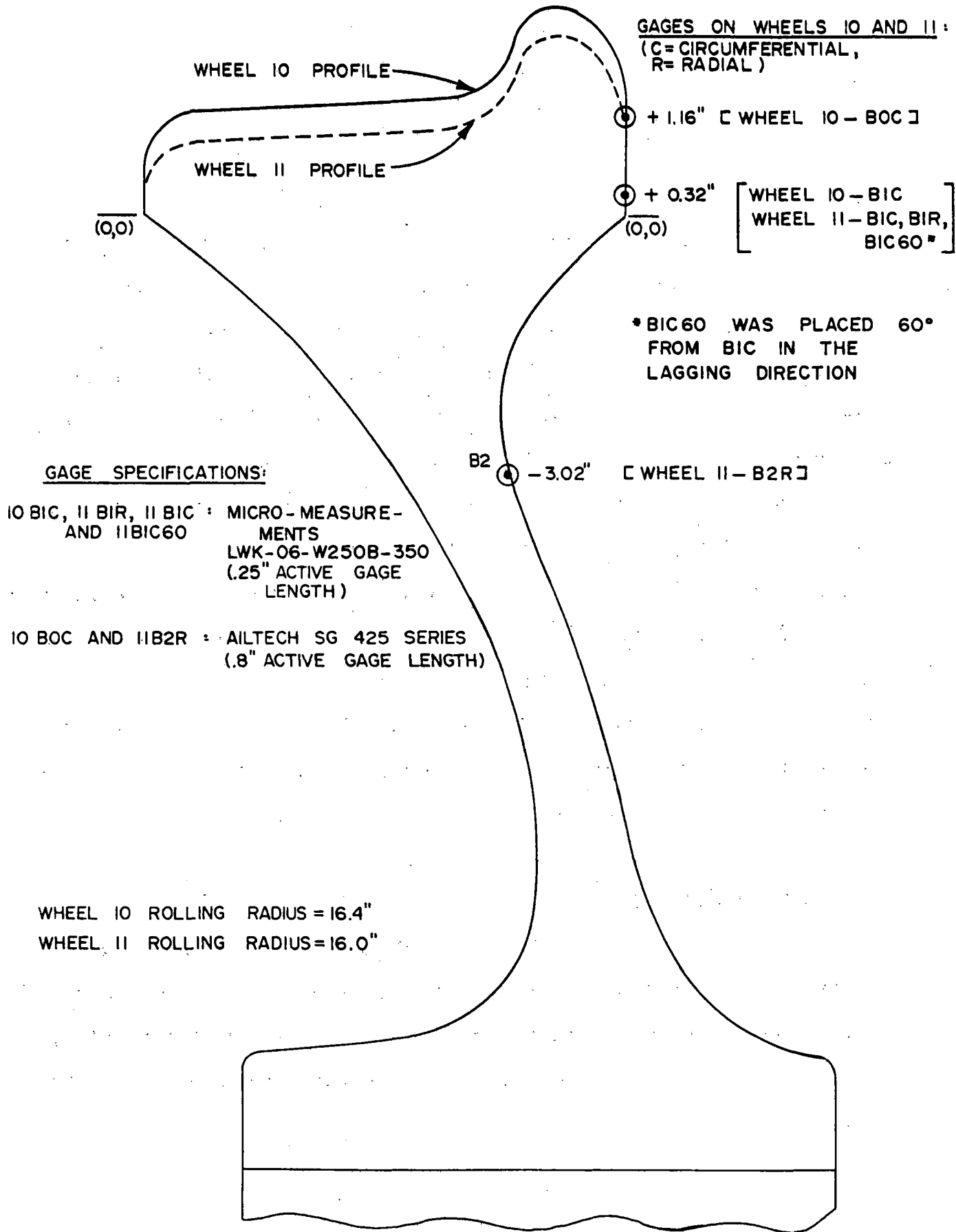
WHEEL 10 PROFILE

WHEEL 11 PROFILE

+ 1.16" [WHEEL 10 — BOC]

(0,0)

+ 0.32" ⎡ WHEEL 10 — BIC
         ⎢ WHEEL 11 — BIC, BIR,
         ⎣   BIC60 * ⎤

(0,0)

* BIC 60 WAS PLACED 60°
FROM BIC IN THE
LAGGING DIRECTION

GAGE SPECIFICATIONS:

B2 ⊕ — 3.02"   [WHEEL 11 — B2R]

10 BIC, 11 BIR, 11 BIC : MICRO - MEASURE -
    AND 11BIC60   MENTS
                          LWK - 06 - W250B - 350
                          (.25" ACTIVE GAGE
                               LENGTH)

10 BOC AND 11B2R : AILTECH SG 425 SERIES
                    (.8" ACTIVE GAGE LENGTH)

WHEEL 10 ROLLING RADIUS = 16.4"
WHEEL 11 ROLLING RADIUS = 16.0"

FIGURE 6.22   CROSS SECTIONAL PROFILES OF TEST WHEELS 10 AND 11,
               SHOWING STRAIN GAGE LOCATIONS B0, B1, AND B2

The test consist was operated on a tangent section of track under the following conditions:

Speed (mph)	Brake Cylinder Pressure (psi)
10-50	0
10	10, 25, 50
20	10, 25, 50
30	10, 25, 50

At each speed, data were recorded on two types of track construction. The first type was 100-lb. jointed rail with wood ties spaced at 24"; the second was 119-lb. welded rail with concrete ties spaced at 30".

In what follows, data reduction, results, and conclusions are presented separately for the (i) wheel strain measurements and for the (ii) brake force measurements.

6.10.3   Wheel Strain Measurements

Data Reduction

After the test, both digital and analog strain data were plotted. The analog data were used for analysis since they were available for both wheel 10 and 11. Analysis was restricted to strain measurements which were made while the consist was operating _without_ applied brakes (wheel temperature data, needed to compute apparent strains, were not available during braking episodes). For each test condition, peak-to-peak (P-P) strains were measured directly from the plots, as shown in Figure 6.23.
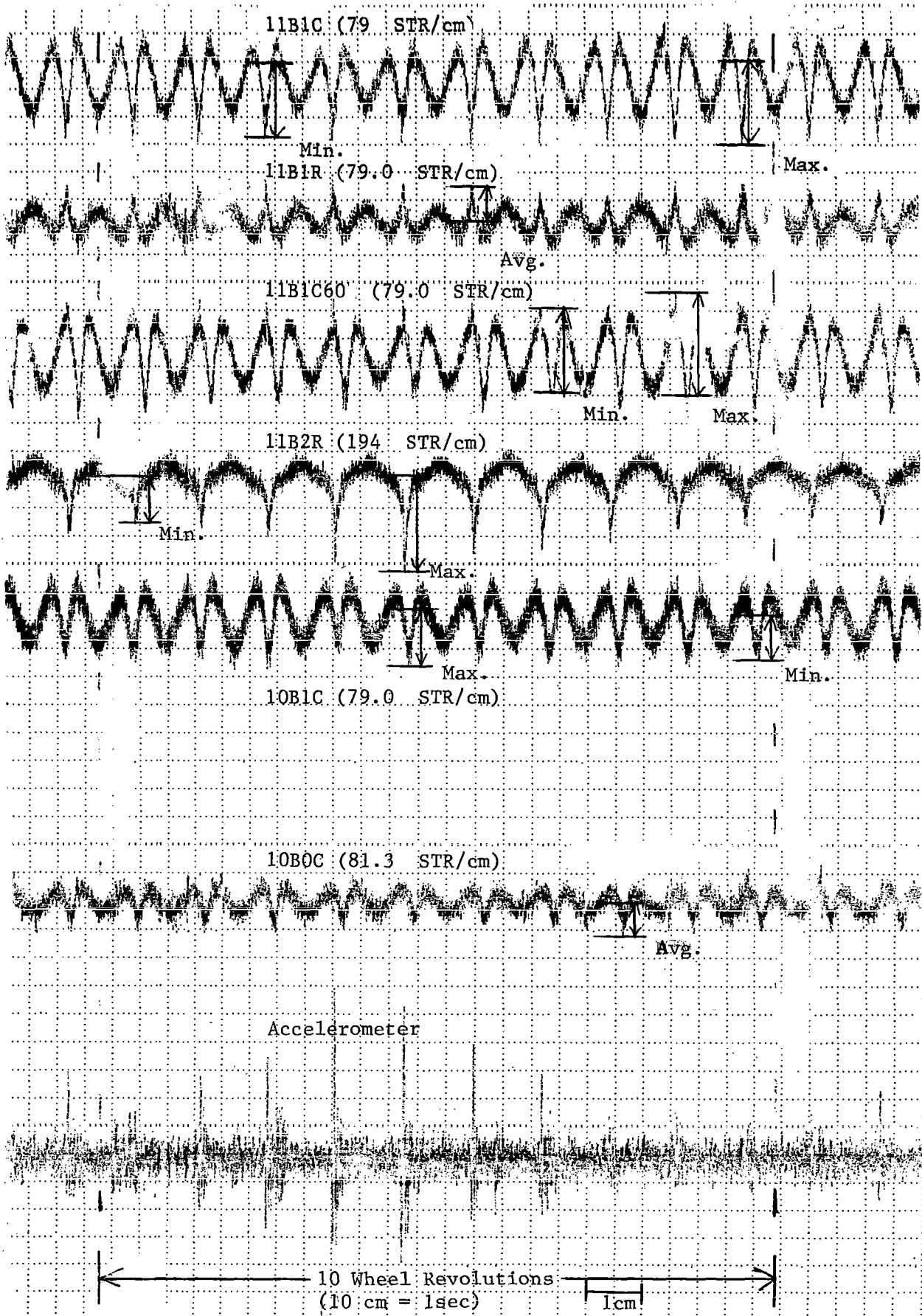
FIGURE 6.23   MEASUREMENT OF PEAK TO PEAK STRAIN AMPLITUDE

The maximum and minimum peak to peak strains occurring in 10 revolutions were tabulated. Selected data from run 35, the last run of preliminary track testing, were also reduced in this manner.

In certain cases, a roughly sinusoidal variation in peak to peak strain amplitude was observed (see Figure 6.23, Strain Channel 11B2R). In those cases, the frequency of the amplitude oscillation was noted.

Unfortunately, there was a rather large noise component in each channel of the measurement system. This was due to the fact that strain circuits were designed to measure low frequency, large strain cycles associated with temperature changes in the wheel rather than the high frequency, relatively small strains occurring during each revolution of the wheel. In measuring peak to peak strain amplitudes, care was taken to exclude the noise component of each signal.

Results (Wheel Strain Measurements)

The main results from the flat test are summarized in Figure 6.24 and Tables 6.6 through 6.8. Figure 6.24 shows the circumferential locations corresponding to extreme strains measured during one revolution of wheel 11. Table 6.6 contains maximum and minimum peak to peak strains measured during the flat test. Table 6.7 contains peak to peak dynamic stresses which were calculated from the peak to peak strains measured during testing. The strain components were measured at B1
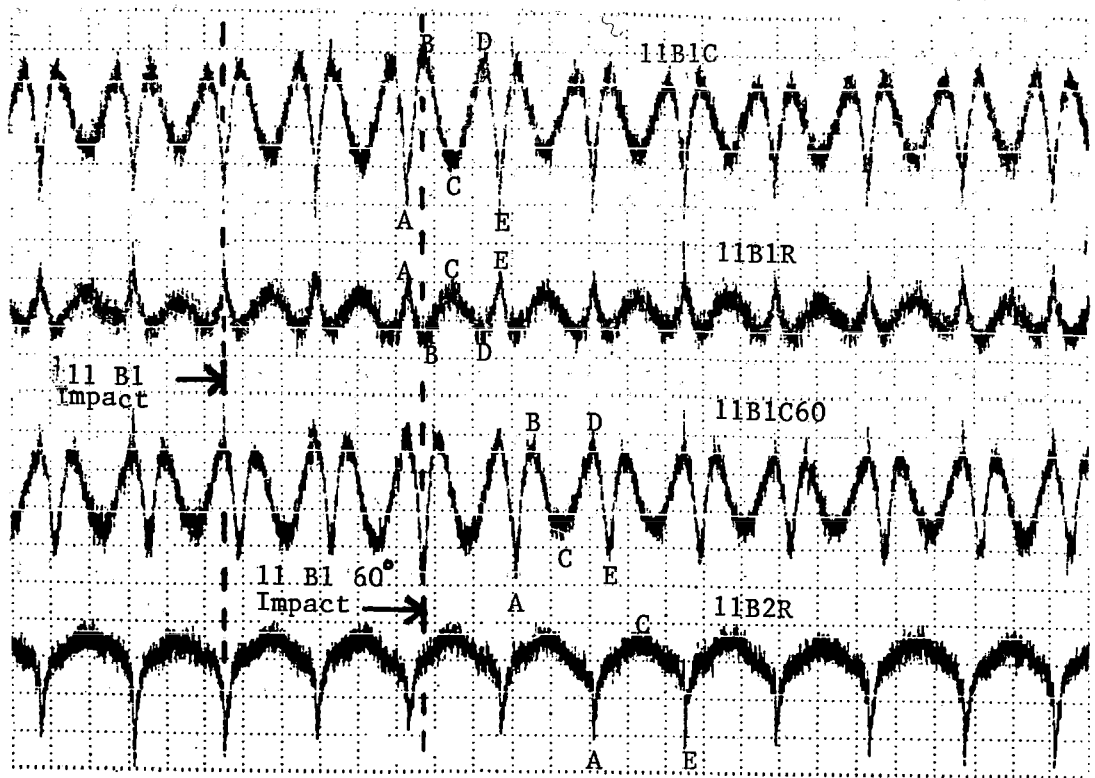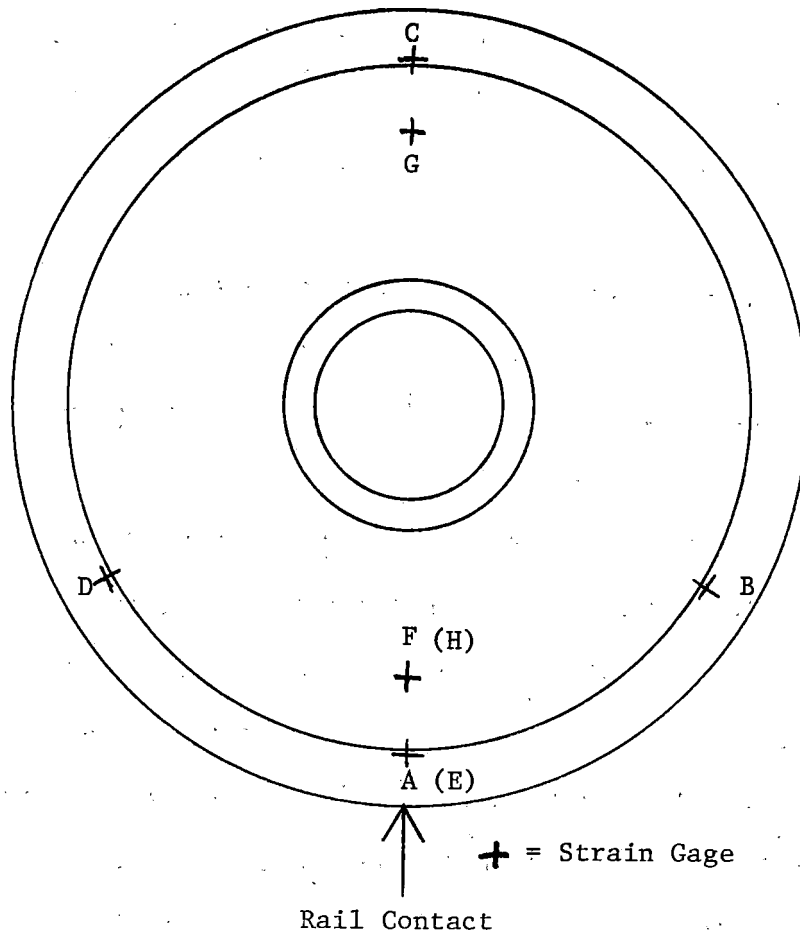
FIGURE 6.24   CIRCUMFERENTIAL LOCATION OF EXTREME STRAINS

TABLE 6.6.
DYNAMIC STRAIN AMPLITUDES FROM TRACK TESTING (RUN 40)

Test Parameters

Wheel 10 - New, CJ-33 Class U, 1 5/16" rim
Wheel 11 - New, CJ-33 Class U, rim machined to 15/16", 2" flat spot ground on tread

Track Type I - 100 lb jointed rail, wood ties spaced at 24"
Track Type II - 119 lb welded rail, concrete ties spaced at 30"

Speed (mph)	Track Type	Max/Min Strain Amplitude (in μ STR) in Ten Wheel Revolutions						Amplitude Ratio 11B1C Max / 10B1C Max
		11B1C	11B1R (Avg)	11B1C60°	11B2R	10B1C	10B0C (Avg)	
10	I	141/74	48	127/105	242/153	78/54	33	1.81
30	I	121/58	40	151/82	375/163	88/52	39	1.38
30	II	131/109	38	119/109	281/168	82/68	37	1.60
40	I	117/90	46	117/92	345/92	80/74	37	1.46
40	II	133/108	54	131/98	330/153	76/58	43	1.75
50	I	141/76	44	131/84	276/192	82/52	43	1.72
50	II	121/105	48	145/117	330/163	80/64	46	1.51

TABLE 6.7
CALCULATED PEAK TO PEAK DYNAMIC STRESSES
AT B1 LOCATION WITH AND WITHOUT FLAT

RUN	SPEED	TRACK TYPE	DYNAMIC HOOP STRAIN	DYNAMIC RADIAL STRAIN	DYNAMIC HOOP STRESS	DYNAMIC RADIAL STRESS
35 (WITHOUT FLAT)	40	I	-96	46	-2,700	600
40 (WITH FLAT)	40	I	-117	46	-3,300	400

location both in circumferential and radial directions.

Estimation of Wheel Load Variation During Flat Test

The 11B2R peak to peak strain was by far the largest strain amplitude that was measured during the flat test. In earlier experiments by Bruner, et al[5], a 33-inch diameter wheel was subjected to incremental normal loads and the corresponding strains were measured at several locations in the plate. The following strains were measured at B2 locations for incremental vertical loads of 10,000 lbs. (the strains were calculated from the author's published stresses):

LOAD	RADIAL STRAIN	TANGENTIAL STRAIN
10,000	128	-13
20,000	234	-29
30,000	327	-50
40,000	435	-58

During the flat test, the largest 11B2R, peak to peak strain was observed to occur at 30 mph where a 11B2R peak to peak strain of 375 micro strain was recorded. Using Bruner's measured load/strain relationship, this strain would correspond to a wheel load of 34,400 lbs. which exceeds the nominal static load of 27,000 lbs.

Observations/Conclusions

The dynamic strain data collected during the flat test and during the last run of preliminary track testing point towards a number of important conclusions.

The rim thickness, and track construction parameters were also considered independently on dynamic strains variations occurring in the test wheels.

Wheel Flat Effect

Introduction of a wheel flat was observed to increase the peak to peak strain amplitude measured in the B1 location. At 40 mph the peak to peak B1 hoop strain on wheel 11 was 22% larger with the flat than without.

Rim Thickness

The B1 location peak to peak hoop strains occurring in wheel 11 (1" rim, prior to machining) were observed to be approximately 20% larger than those in wheel 10 (1-15/16" rim) at a speed of 40 mph.

Combined Rim/Flat Effect

During run 40, dynamic strain measurements were made concurrently for wheel 10 (normal rim thickness) and 11 (thin

rim). The strains measured in wheel 11, were due to the combined effect of thin rim section and the presence of 2" flat on the tread. At 40 mph, wheel 11B1 peak to peak strains were 46% larger than wheel 10, B1 strains.

Distribution of Circumferential Strain During Impact

During the playback of strains from testing, it was observed that in the absence of a flat in the B1C location, the extreme compressive strain occurred at the wheel/rail contact, while the tensile extreme occurred at two positions approximately 60 degrees from the rail contact. After the flat was introduced, the impact at the rail was seen to produce a tensile strain at the 60-degree location which added to the tensile strain which normally occurs at that position (see Figures 6.23 and 6.25). The net result was that peak to peak tensile strain occurring at the B1C60 location when the wheel flat impacts the rail increased in magnitude.

Summary (Wheel Flat Test)

In conclusion, the magnitude of peak-to-peak strains occurring in a rolling wheel were affected by the presence of a wheel flat, and by rim thickness variation. At 40 mph, on jointed rail supported by wood ties, B1 peak to peak strains of 80, 96, and 117 micro strains were measured for a normal rim, a thin rim, and a thin rim with a flat, respectively. Peak-to-peak

TRAILING END OF 2" FLAT
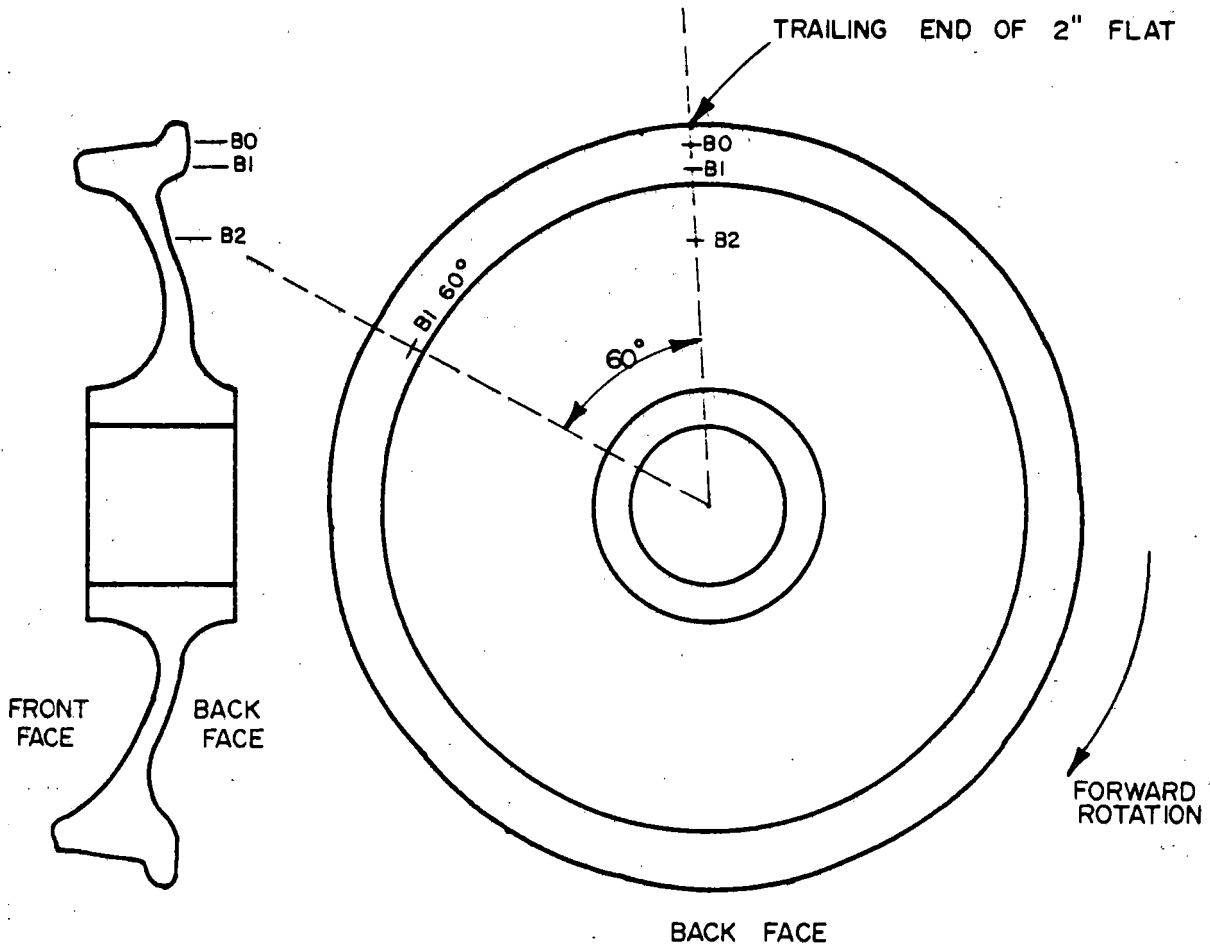
FIGURE 6.25   LOCATION OF WHEEL 11 STRAIN GAGES

6-60

dynamic stresses on the order of 4 ksi were computed for the B1 location.

Finally, it was demonstrated that there are 3 points (0 degrees, -60 degrees, +60 degrees) on the back rim fillet region of the wheel (Figure 6.25) which experienced an augment in the cyclic strains due to the impact of the wheel flat on the rail.

6.10.4   Brake Force Measurements

The second portion of the wheel flat test consisted of evaluating brake force variations due to the impact forces between the wheel flat and rail. At various speeds, data were collected at 2,000 samples/second, once every minute in one second bursts. The normal and tangential brake shoe forces were computed from the instrumented brake head output signals measured during the test.

In addition to monitoring minimum and maximum brake shoe forces, acceleration levels of wheel 11 bearing adapter were used to determine the moment of impact between the wheel flat and rail. Figure 6.26 presents a typical plot of wheel bearing adapter acceleration and brake force voltages.

Since, for any given data burst of a 1-second duration there was more than one wheel revolution (a 33-inch wheel at 10, 20, or 30 mph, performs 1.7, 3.4, and 5.1 revolutions/second), brake force variation from one wheel revolution to the next was examined by generating brake force statistics for each revolution of the wheel as well as for the entire burst.
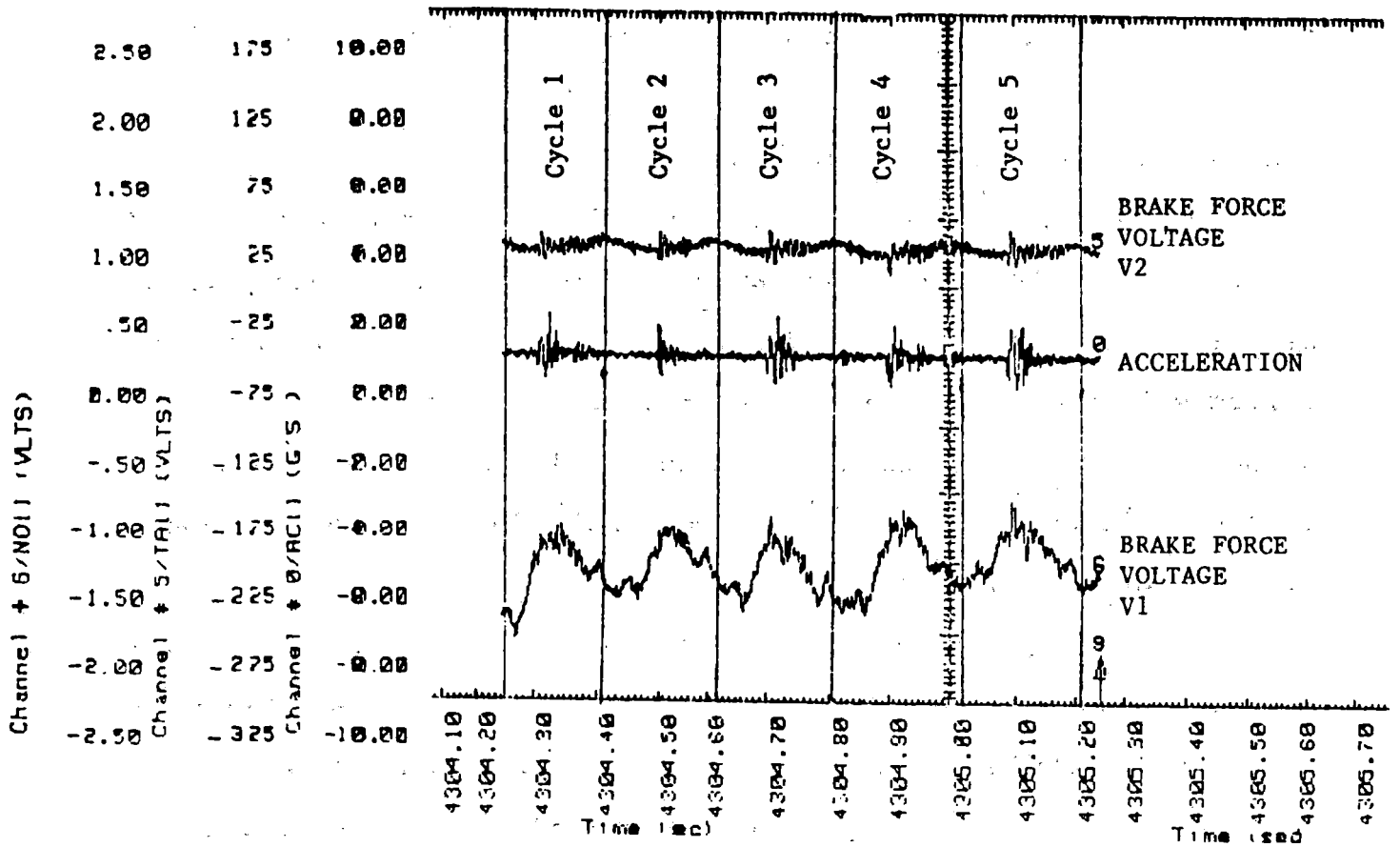
**FIGURE 6.26   TYPICAL PLOT OF WHEEL BEARING ADAPTER
ACCELERATIONS AND BRAKE SHOE FORCE VOLTAGES**

As an example, the table below contains force statistics for each of five revolutions of a wheel that occurred during a data burst that was collected at 30 mph and 25 psi. Also shown are statistics for the entire burst.

Time Period		Mean Brake Force (lb)	Maximum Brake Force (lb)
1st Revolution	Normal	1207	1547
	Tangent	282	361
2nd Revolution	Normal	1144	1341
	Tangent	272	344
3rd Revolution	Normal	1196	1401
	Tangent	282	347
4th Revolution	Normal	1155	1411
	Tangent	271	350
5th Revolution	Normal	1091	1285
	Tangent	257	323
Entire Burst	Normal	1159	1547
	Tangent	273	361

Results

Brake force data and completed statistics obtained for a wheel with 2-inch machined flat at brake cylinder pressures 10, 25, and 50 psi and speeds of 10, 20, and 30 mph are presented in Tables 6.8 - 6.10.

Table 6.8 shows data collected at Station #31 of TTT (wood ties with 24-inch spacing); Table 6.9 shows data collected at Station #33 (wood ties with 24-inch spacing); Table 6.10 presents data collected at Station #35 of TTT (concrete ties

TABLE 6.8

BRAKE FORCE STATISTICS FOR WHEEL #11 WITH 2-INCH MACHINED FLAT

(Data Collected at Station #31, Transit Test Track,
Wood Ties Spaced at 24-Inches

Speed (mph)	B.C.P. (psi)	Mean Normal Force (lb)	Max. Normal Force (lb)	Mean Tangential Force (lb)	Max. Tangential Force (lb)
10	10	460	593	143	200
20	10	401	581	100	317
30	10	347	489	94	201
10	25	1198	1407	444	534
20	25	1065	1342	281	458
30	25	1159	1547	273	361
10	50	2536	2868	699	781
20	50	2486	2804	460	550
30	50	2584	3045	496	635

TABLE 6.10

BRAKE FORCE STATISTICS FOR WHEEL #11 WITH 2-INCH MACHINED FLAT

(Data Collected at Station #35, Transit Test Track,
Concrete Ties Spaced at 30-Inches)

Time	Speed (mph)	B.C.P. (psi)	Mean Normal Force (lb)	Max. Normal Force (lb)	Mean Tangential Force (lb)	Max. Tangential Force (lb)
137	10	10	471	583	134	231
724	20	10	327	530	92	269
908	30	10	421	560	119	240
2562	10	25	1153	1234	413	446
3147	20	25	1088	1330	294	445
4212	30	25	1190	1471	282	435
4786	10	50	2347	2703	650	734
5379	20	50	2477	2846	414	507
5606	30	50	2498	2871	469	570

TABLE 6.9

BRAKE FORCE STATISTICS FOR WHEEL #11 WITH 2-INCH MACHINED FLAT

(Data Collected at Station #33, Transit Test Track,
Wood Ties Spaced at 24-Inches

Time	Speed (mph)	B.C.P. (psi)	Mean Normal Force (lb)	Max. Normal Force (lb)	Mean Tangential Force (lb)	Max. Tangential Force (lb)
274	10	10	449	575	131	184
648	20	10	354	544	94	274
951	30	10	369	568	103	281
2698	10	25	1132	1351	404	514
3074	20	25	1085	1413	287	437
4257	30	25	1268	1555	283	363
4952	10	50	2447	2742	638	715
5311	20	50	2486	2977	454	557
5651	30	50	2498	2897	459	559

with 30-inch spacing).

For purposes of comparison, brake force data for the same wheel (#11), with flat, collected at random on TTT appears in Table 6.11.

Observations (Brake Shoe Force Variations Due to Wheel Flat Impacts on Rail

o   Examination of Tables 6.8 - 6.10 reveals that the introduction of 2-inch machined flat on the tread of a 33-inch wheel did not result in any unusual change in the normal or tangential brake force under selected speeds and brake cylinder pressures.

o   The extreme values of normal and tangential brake forces occurred mostly at the time of impact between the wheel flat and rail. (The occurrence of impact was correlated with the extreme acceleration levels attained by the wheel 11 bearing adapter.)

o   The fluctuations in the normal and tangential force with and without flat were comparable, implying that the introduction of a 2-inch flat did not appreciably change the magnitude of brake shoe forces.

TABLE 6.11

BRAKE FORCE STATISTICS FOR SAME WHEEL WITHOUT FLAT SPOT

(Data Collected at Random Locations on Transit Test Track
at a Rate of 100 Samples/Second Over One-Second Periods)

Speed (mph)	B.C.P. (psi)	Mean Normal Force (lb)	Max. Normal Force (lb)	Mean Tangential Force (lb)	Max. Tangential Force (lb)
19	12	319	409	69	92
17	12	301	360	88	114
20	12	284	432	81	128
22	22	826	1120	250	335
20	22	897	1353	290	405
30	22	855	1433	200	346
31	22	860	1446	202	344

REFERENCES

1. Newcomb, T.P.: "Thermal Aspects of Railway Braking," International Conference on Railway Braking, University of York, September 26-27, 1979. Institution of Mechanical Engineers Conference Publications, 1979-11; London, The Institution of Mechanical Engineers, 1979.

2. Larson, H.; Huntress, H.; and Haley, M.: "Distribution of Heat Between Wheel and Brakeshoe," Fourth International Wheelset Congress, 1972, page 75.

3. Carslaw, H.S., and Jaeger, J.C.: "Conduction of Heat in Solids," second edition, Oxford, Clarendon Press, 1959.

4. Lagedrost, J.F.; Eldridge, E.A.; and Stone, D.H.: "Thermal Property Measurements of Brake Shoe Materials," AAR Report R-345, December, 1978; and in International Conference on Railway Braking, University of York, September 26-27, 1979, Institution of Mechanical Engineers Conference. Publications, 1979-11, page 111; London, The Institution of Mechanical Engineers, 1979.

5. Bruner, J.P.; Benjamin, G.N.; and Bench, D.M.; "Analysis of Residual Thermal, and Loading Stresses in a B33 Wheel and Their Relationship to Physical Damage". ASME 66-WA/RR-3, December, 1966.

7.0 COMPREHENSIVE TRACK TESTING – TECHNICAL TASK T6

The objective of Technical Task T6 was to determine the effects of wheel design/material/size and brake application history on the development and/or shakedown of residual stresses. The demonstrated methodology of Technical Task T5 was used to determine the test conditions for Comprehensive Testing. Track testing was conducted with reduced instrumentation but with a wider variety of test wheels.

7.1 Test Description

7.1.1 Brake Rigging

Since earlier RDU and preliminary track testing measurements revealed a substantial wheel to wheel brake force variation within a truck fitted with conventional brake rigging, cars with Wabcopac rigging were selected for use in the comprehensive phase of testing. The Wabcopac design (see Figure 7.1) features two pneumatic cylinders with pushrods that act directly on the brake beams, resulting in a more even distribution of forces than is possible with conventional rigging.

Three cars were selected for testing, which included two 70-ton boxcars and a 100-ton tank car, all with the Wabcopac brake rigging. Prior to testing, static brake shoe normal forces, under rapped and unrapped conditions, were measured as a function of brake cylinder pressure for each car (see Figures 7.2 through 7.4). The forces were measured for each wheel with
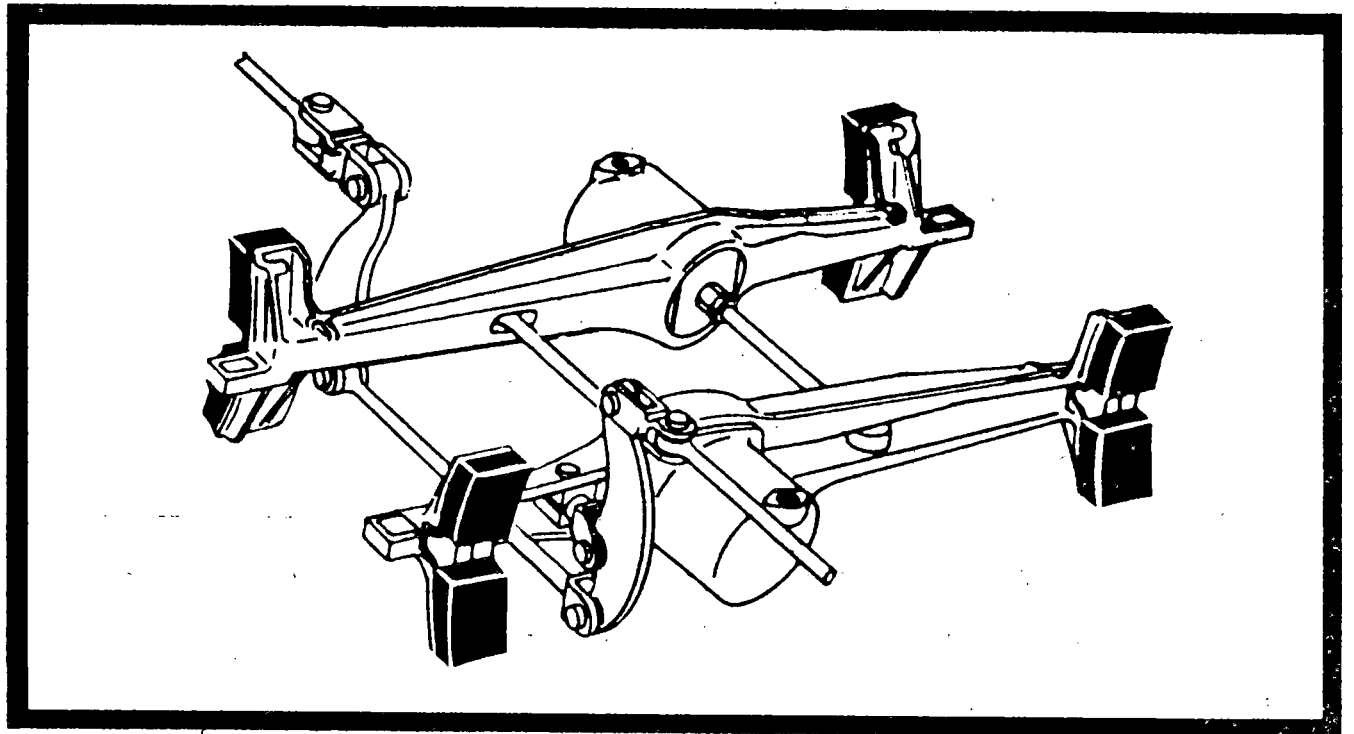
FIGURE 7.1   WABCOPAC BRAKE RIGGING ARRANGEMENT

STATIC GOLDEN SHOE CALIBRATION RESULTS

CAR NO. 20457 A—END & B—END
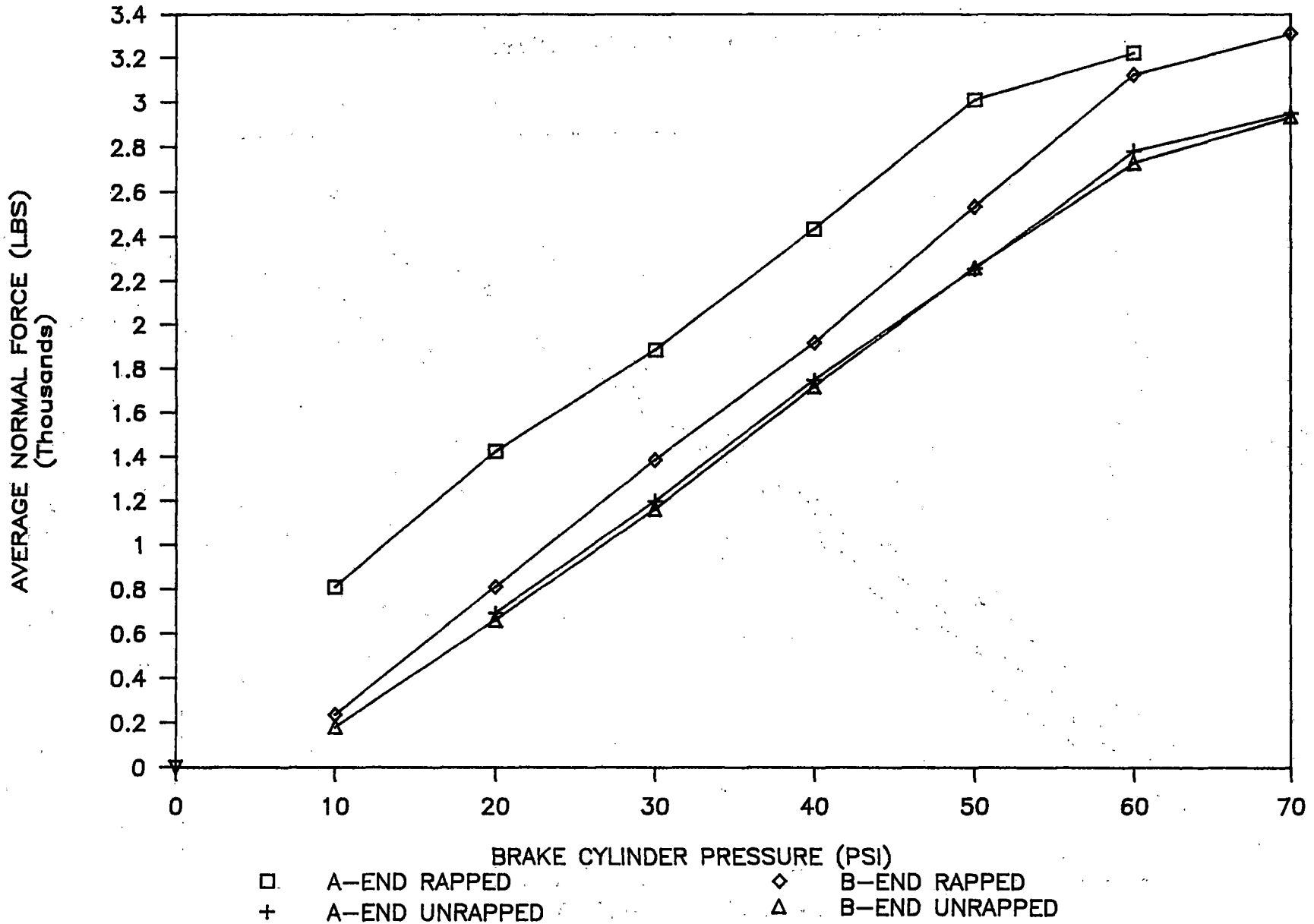
FIGURE 7.2   STATIC GOLDEN SHOE CALIBRATION RESULTS

STATIC GOLDEN SHOE CALIBRATION RESULTS

CAR NO. 520049 A—END & B—END
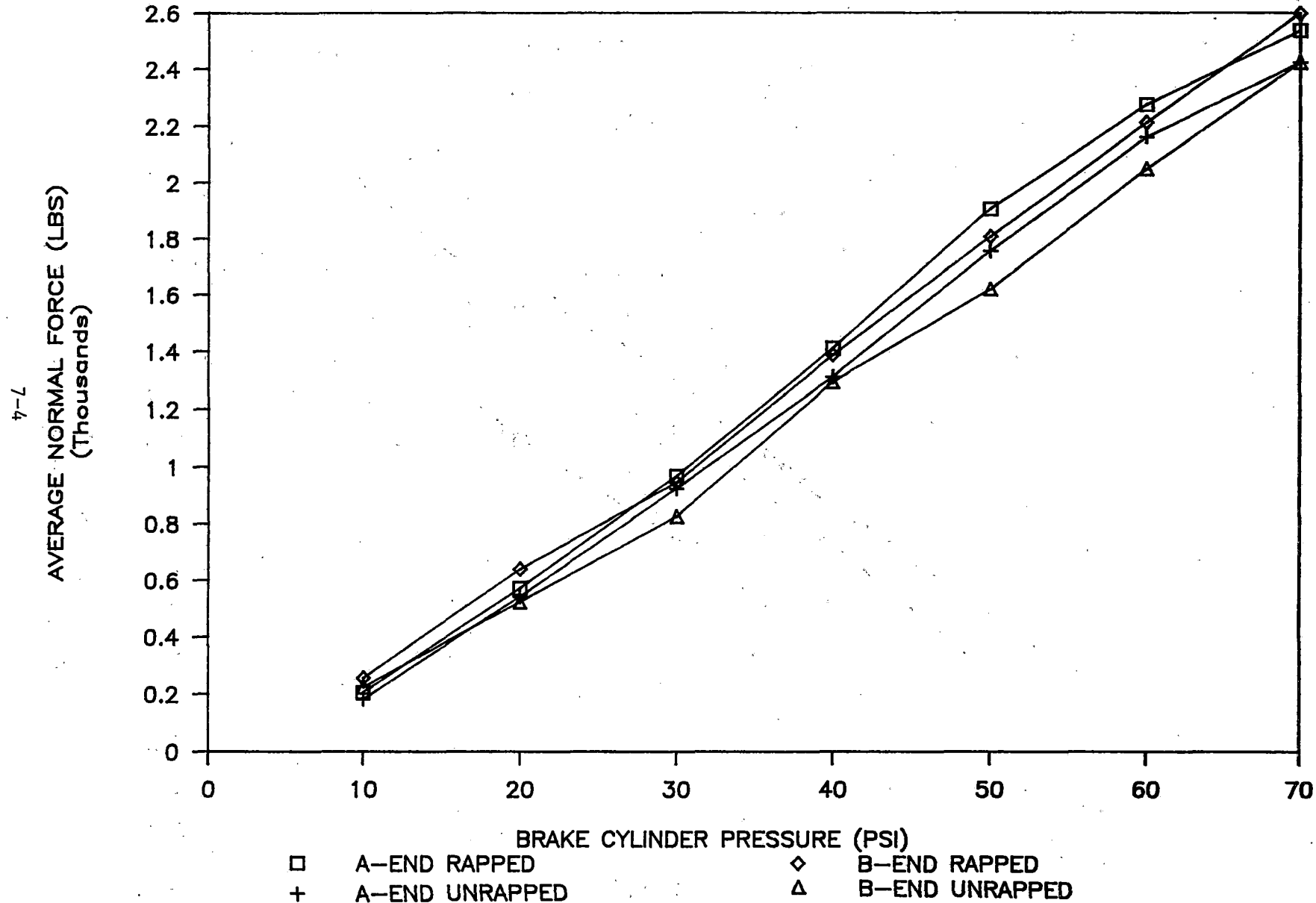
FIGURE 7.3   STATIC GOLDEN SHOE CALIBRATION RESULTS

STATIC GOLDEN SHOE CALIBRATION RESULTS

CAR NO. 520203 A—END & B—END
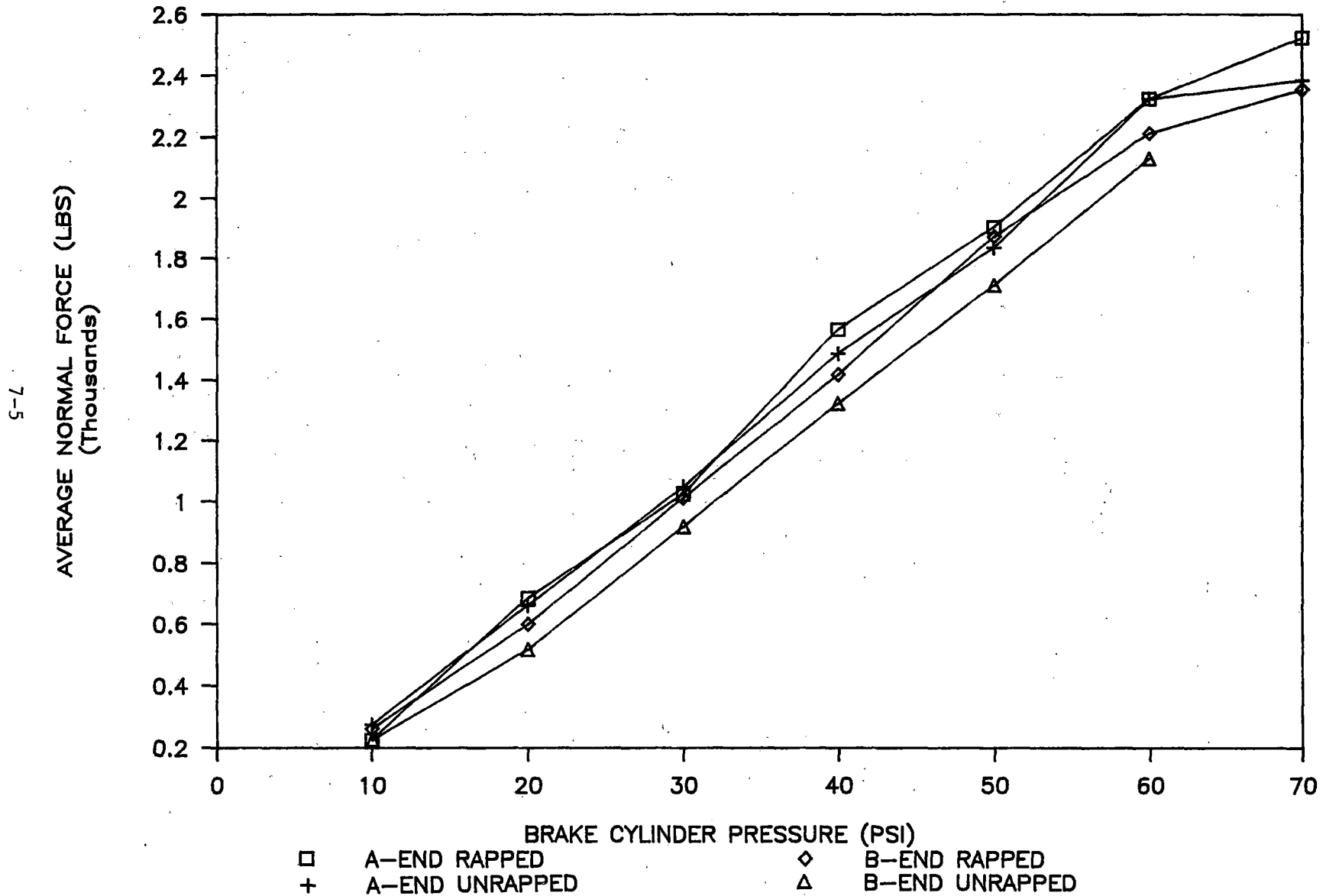
FIGURE 7.4   STATIC GOLDEN SHOE CALIBRATION RESULTS

golden shoe load measuring equipment. With Wabcopac brake
rigging it was noticed that the brake shoe thermal force
variations between rapped and unrapped conditions were minimal,
compared with conventional brake rigging system.

7.1.2 Operating Conditions

Comprehensive Track Testing consisted of a series of 51 drag
brake cycles which were applied to 24 wheels of different plate
shapes, heat treatment, and sizes. The test consist included a
locomotive, an instrumentation car, two 70-ton boxcars, and a
100-ton car. The brake cylinder pressure of the first car,
which was controlled from the instrumentation car, was
maintained at 10-15 psi lower than the brake cylinder pressure
of the second two cars, which was controlled by brakeline
pressure reductions applied directly from the locomotive by the
locomotive engineers. A diagram of the test consist, and a
descriptive history of the enforced test parameters appears in
Figure 7.5 and Table 7.1, respectively. A description of the
test wheels showing the plate design and heat treatment details
is presented in Table 7.2.

7.1.3 Instrumentation

A number of methods were used to measure wheel temperatures
during braking. K-type thermocouples, embedded in the brake
shoes, were used to measure the temperature at the tread/brake

WFM
TECHNICAL TASK — T6
COMPREHENSIVE TRACK TESTING

PNU SNU -NU SRU PNU PRU—RU -NU SNC -NU -NU PNC

| LOCOMOTIVE | 211 INSTRUMENTAT-ION CAR | B-END | I | | | | B-END | II | | | | B-END | III | | | |

I 18 20 22 24 17 19 21 23

II 26 28 30 32 25 27 29 31

III 34 36 38 40 33 35 37 39

PNC SNC -NC SRC PNC PRC —RC -NC PNC -NC -NU SNC

BCP CONTROL

BRAKE CYLINDER PRESSURE (BCP) CONTROLLED FROM LOCOMOTIVE
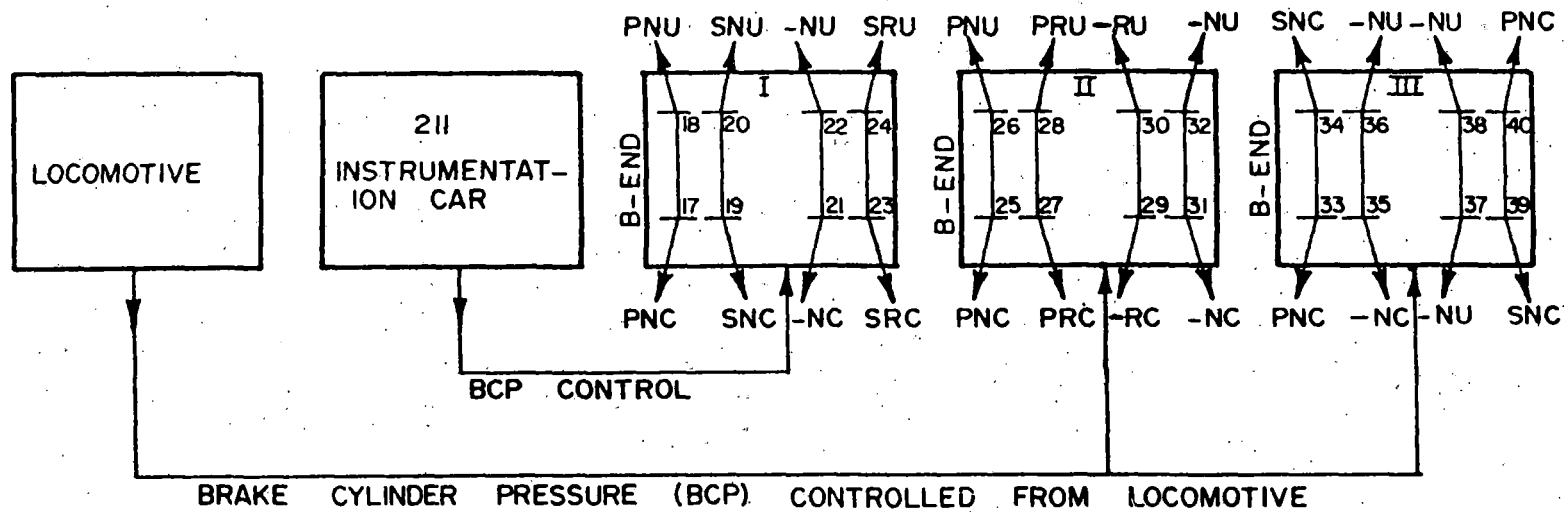
TEST CAR I, NO. 520049 (70 T) ⟶ LESS SEVERE BRAKING CYCLES (30—40 BHP)

TEST CARS II, NO. 520203 (70 T) & III, NO. 20457 (100 T) ⟶ SEVERE BRAKING
CYCLES (40—50 BHP & ABOVE)

ALL TEST CARS WITH WABCOPAC BRAKE RIGGING

ALL BRAKE SHOES WITH TEMPERATURE PROBES FOR MONITORING TEMPERATURES
AT WHEEL / SHOE INTERFACE

24 CHANNEL DATA ACQUISITION SYSTEM FOR CONTINUOUS WHEEL/SHOE
INTERFACE TEMPERATURE RECORDING WITH BRAKE SHOE EMBEDDED
THERMOCOUPLES

AT A GIVEN TEST SPEED, BCP OF CAR I IS MAINTAINED AT A LOWER
LEVEL (CONTROLLED FROM 211 CAR), THAN THE BCP OF CARS II
& III (CONTROLLED FROM LOCOMOTIVE)

— STRAIGHT PLATE

P PARABOLIC PLATE

S S-SHAPED PLATE

R REAPPLICATION LIMIT

WHEEL TYPE	MANUFACTURER
33 INCH STRAIGHT	CANADIAN STEEL
33 INCH PARABOLIC	GRIFFIN
33 INCH S-SHAPED	STANDARD STEEL
36 INCH STRAIGHT	CANADIAN STEEL
36 INCH PARABOLIC	ABEX
36 INCH S-SHAPED	STANDARD STEEL

FIGURE 7.5   COMPREHENSIVE TRACK TESTING CONSIST

TABLE 7.1
COMPREHENSIVE TRACK TESTING

DATE	DRAG BRAKING CYCLE NO.	Speed (mph)	BCP* (psi)	DURATION (min)	START TIME	END TIME	REMARKS
2/12/86	1	30	20/35	30	10:58	11:29	Hole drilling at B1 location for
2/12/86	2	30	30/30	60	14:01	15:01	all 24 wheels
2/13/86	3	30	30/40	120	09:15	11:13	performed, before start of testing
2/13/86	4	30	35/35	45	11:15	12:00	
2/13/86	5	30	30/30	60	13:20	14:24	Photos taken after 5th Cycle
2/18/86	6	30	30/40	70	13:27	14:37	
2/19/86	7	35	30/40	100	09:37	11:16	
2/19/86	8	35	30/40	60	12:38	13:42	
2/19/86	9	40	35/45	75	14:45	16:00	
2/19/86	10	40	40/50	60	16:59	18:03	1) Photos taken after 10 cycles 2) Hole drilling performed for all 24 wheels at B1 locations.
2/25/86	11	40	35/45	65	14:10	15:17	
2/25/86	12	40	35/45	60	16:44	17:44	
2/25/86	13	40	40/50	60	18:48	19:47	
2/26/86	14	35	40/50	60	10:58	11:58	
2/26/86	15	35	40/50	60	13:17	14:17	
2/26/86	16	35	45/55	60	15:40	16:38	
2/26/86	17	35	45/60	60	17:35	18:32	
2/27/86	18	30	45/60	60	13:20	14:22	
2/27/86	19	30	45/60	60	15:30	16:30	
2/27/86	20	30	45/60	60	17:30	18:30	

---
*30/35 ---- 30 psi in car #520049
           35 psi in car #520203 and car #20457

TABLE 7.1 (CONT.)
COMPREHENSIVE TRACK TESTING

DATE	DRAG BRAKING CYCLE NO.	Speed (mph)	BCP* (psi)	DURATION (min)	START TIME	END TIME	REMARKS
3/05/86	21	30	45/60	60	10:31	11:32	
3/05/86	22	30	45/60	60	13:15	14:16	
3/05/86	23	30	45/60	60	15:19	16:19	
3/05/86	24	30	45/60	60	17:41	18:41	
3/06/86	25	30	45/60	60	10:24	11:25	
3/06/86	26	30	45/60	60	13:17	14:17	
3/06/86	27	30	45/60	60	15:43	16:43	
3/07/86	28	30	45/60	60	10:15	11:15	
3/07/86	29	30	45/60	60	12:28	13:28	
3/07/86	30	30	46/60	60	14:52	15:53	1) Photographs of wheels taken after 30 cycles 2) Hole drilling performed on all wheels 3) Infrared Viewer System set up to view wheels from a) wayside at the conclusion of the test, or b) when attached to the first test car to view wheel 17 or 18 throughout the test and during cool down
3/12/86	31	35	50/60	60	18:27	19:27	VIEWER FOCUS: Odd wheels
3/13/86	32	35	50/60	60	10:32	11:27	Even wheels
3/13/86	33	35	50/60	60	13:48	14:50	Even wheels
3/13/86	34	35	50/60	55	16:10	17:11	Odd wheels
3/17/86	35	35	50/60	60	18:09	19:04	Odd wheels, wheels 37, 39, 40 inside and outside

TABLE 7.1 (CONT.)
COMPREHENSIVE TRACK TESTING

DATE	DRAG BRAKING CYCLE NO.	Speed (mph)	BCP* (psi)	DURATION (min)	START TIME	END TIME	REMARKS
3/17/86	36	35	50/60	60	9:59	10:59	Odd wheels
3/17/86	37	35	50/60	60	12:34	13:34	Odd wheels
3/17/86	38	35	50/60	60	14:49	15:49	Even wheels
3/17/86	39	35	50/60	60	16:35	17:31	Even wheels
3/17/86	40	35	50/60	60	18:20	19:18	Odd wheels
							1) Photos taken after 40 cycles 2) Hole drilling performed on all wheels 3) All brake shoes fitted with brake shoe thermocouples Wheels 39 and 40 fitted with spring loaded thermocouples
3/17/86	40	35	50/60	60	18:20	19:18	Odd wheels
3/21/86	41	35	50/60	60	11:53	12:54	Wheel 17
3/21/86	42	35	50/60	60	14:26	15:27	Wheel 17
3/21/86	43	45	50/65	30	17:22	17:54	Wheel 17
3/24/86	44	45	50/65	30	9:37	10:04	Wheel 17
3/24/86	45	45	50/65	35	12:30	13:06	Wheel 18
3/24/86	46	45	50/65	30	14:37	15:09	Wheel 18
3/25/86	47	45	50/65	30	10:32	11:04	Wheel 18
3/25/86	48	45	50/65	30	13:29	14:00	Wheel 17
3/25/86	49	45	50/65	30	16:04	16:34	Odd wheels
3/25/86	50	45	50/65	30	17:59	18:31	Odd wheels
3/25/86	51	45	50/65	35	19:44	20:19	Even wheels

TABLE 7.2
TEST WHEEL DESCRIPTION - COMPREHENSIVE TESTING

Wheel #	Wheel Type	Class	Manufacturer	Diameter (inches)	New (N) or Machined to Condemning Limit (R)
17	Parabolic	C	Griffin	33	N
18	Parabolic	U	Griffin	33	N
19	S-Shape	C	Standard Steel	33	N
20	S-Shape	U	Standard Steel	33	N
21	Straight	C	Canadian Steel	33	N
22	Straight	U	Canadian Steel	33	N
23	S-Shape	C	Standard Steel	33	R
24	S-Shape	U	Standard Steel	33	R
25	Parabolic	C	Griffin	33	N
26	Parabolic	U	Griffin	33	N
27	Parabolic	C	Griffin	33	R
28	Parabolic	U	Griffin	33	R
29	Straight	C	Canadian Steel	33	R
30	Straight	U	Canadian Steel	33	R
31	Straight	C	Canadian Steel	33	N
32	Straight	U	Canadian Steel	33	N
33	Parabolic	C	Abex	36	N
34	S-Shape	C	Standard Steel	36	N
35	Straight	C	Canadian Steel	36	N
36	Straight	U	Canadian Steel	36	N
37	Straight	U	Canadian Steel	36	N
38	Straight	U	Canadian Steel	36	N
39	S-Shape	C	Standard Steel	36	N
40	Parabolic	C	Abex	36	N

shoe interface. A sample plot of wheel tread temperature recorded during a test appears in Figure 7.6. The plot also contains the time history of a parameter termed as "severity index" which is defined as the product of brake cylinder pressure and speed.

It may be noted that there is a difference between the actual tread temperature and the temperature measured by the brake shoe embedded thermocouples. Tests conducted on the brake dynamometer revealed that the brake shoe embedded thermocouple will show temperatures $200^\circ F$ or more above temperatures measured by a bow type thermocouple which was placed in contact with the tread. Therefore, the brake shoes with embedded thermocouples were used to provide a relative measure of dissipated braking energy; the shoe thermocouples were not relied upon for absolute temperature measurements. Plots of peak measured tread temperature as a function of estimated Bhp are presented for selected wheels in Appendix 7.1. A correlation was observed between the peak tread temperature measured during a test and the Bhp maintained during the same test.

In a separate measurement, a hand held, infrared thermometer (Exergen Model D-500F) was used to measure B0, B1, B2, and B3 location wheel temperatures at the end of a test. These wheel locations are shown in Figure 5.11 of Section 5. Plots of B1 temperature (measured with the infrared thermometer) as function of test Bhp are superimposed on the plots of peak tread temperatures given in Appendix 7.1.

7-12
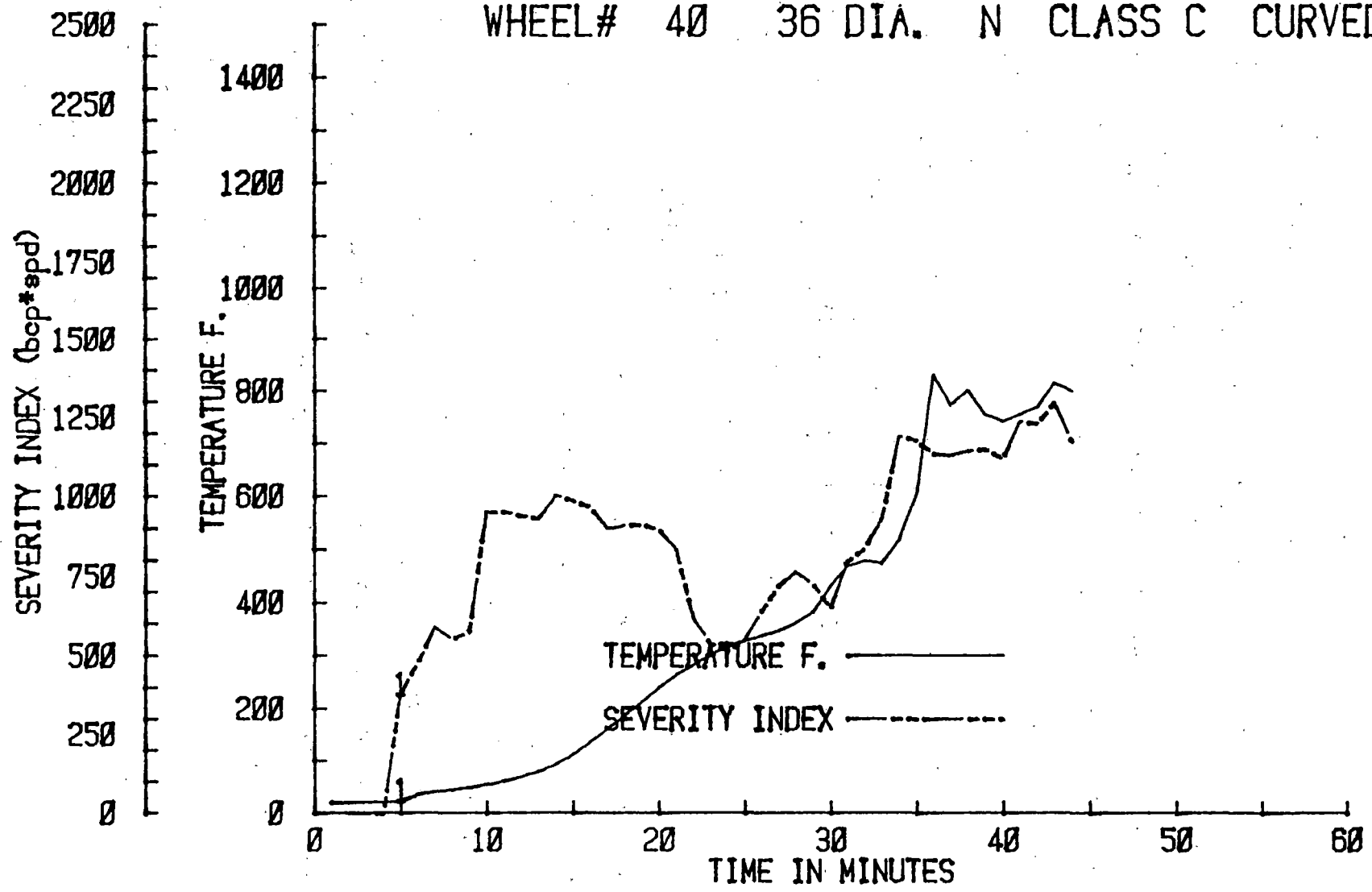
FIGURE 7.6 TYPICAL TIME HISTORY OF WHEEL TREAD TEMPERATURE DURING COMPREHENSIVE TESTING

A Hughes Probeye infrared camera was also used to record the distribution of temperatures on the test wheels. The camera was utilized in one of two ways: it could be attached to the underside of the first box car to view the front test wheels on (wheel #17 or #18) continuously during a test or, alternatively, the camera could be stationed adjacent to the test track to view all of the wheels at the conclusion of the test. A snapshot taken during playback of the infrared film appears in Figure 7.7.

7.1.4   Surface Stress Measurements/Saw Cutting of Test Wheels

The hole drilling technique of stress measurement was used to measure the surface stress at the B1 location (bottom of this back rim face) of each wheel prior to testing and after each set of 10 drag braking cycles. At the conclusion of testing, 22 of the 24 test wheels were saw-cut according to established procedures. The remaining two test wheels (39 and 40) were set aside for possible future testing.

7.2   Results

7.2.1   Data Base

All of the temperature measurements made during testing and residual stress measurements by hole-drilling technique after drag braking cycles have been compiled into a data base. The
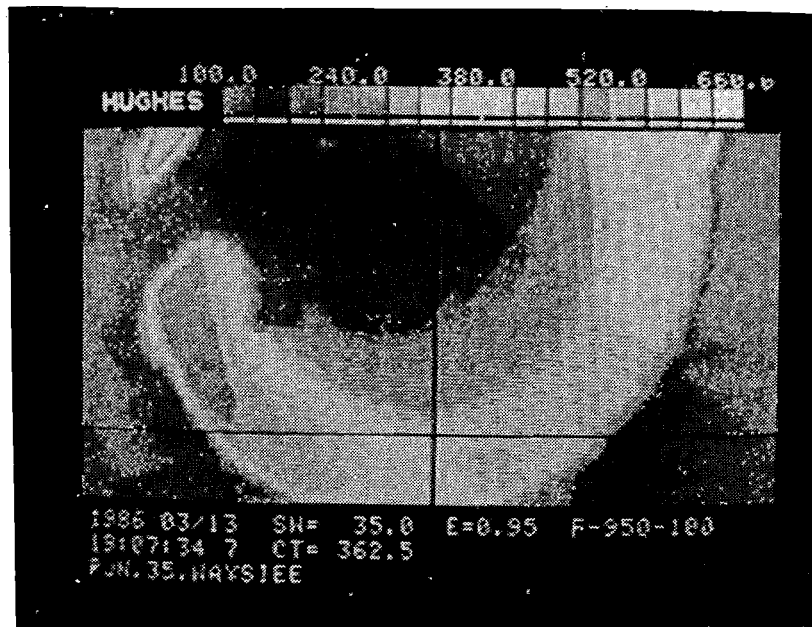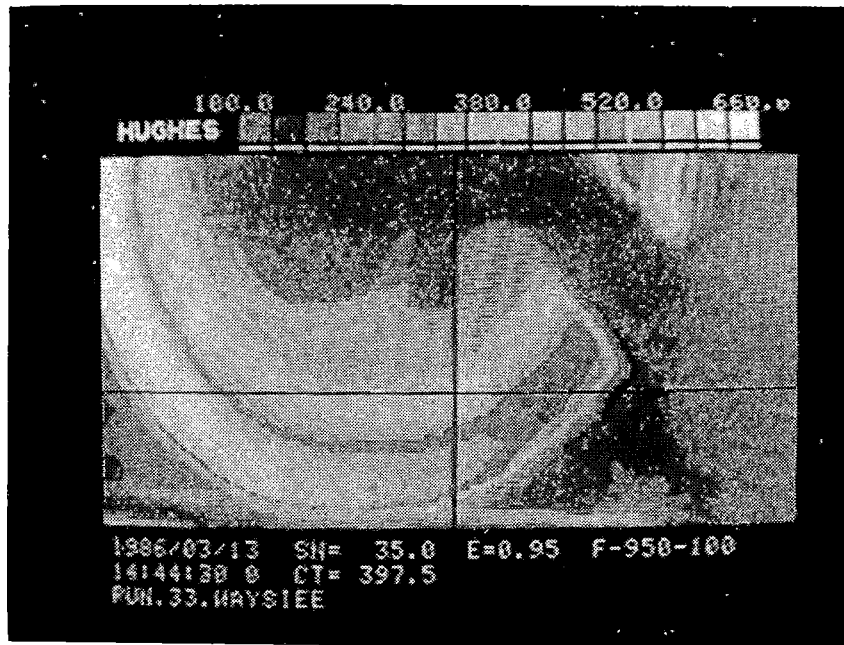
FIGURE 7.7   THERMAL VIDEO PICTURES OF TWO TEST WHEELS
              AT THE END OF A DRAG BRAKING TEST

data base, includes a descriptor of each wheel type, testing conditions (speed and brake cylinder pressure), estimated horsepower input, peak tread temperature, temperatures measured by the hand-held infrared thermometer, stresses measured by the hole drilling method, and the discoloration condition of all the test wheels at various stages during testing. All this information is compiled in the data base system at Pueblo. Appendix 7.2 presents the above data for selected test wheels from each test car.

7.2.2 Braking Energy Input

One objective of Comprehensive Track Testing was to determine the effect of service conditions on the development of residual stresses. To this end, the second two cars of the test consist were operated with brake cylinder pressures 10-15 p.s.i. higher than the first car. For each drag-braking cycle, average brake horsepower and cumulative braking energy input were calculated from test conditions of brake cylinder pressure, speed, and duration. Normal forces were computed from applied brake cylinder pressures and a coefficient of friction of .23 (based on the average coefficient of friction value obtained during Preliminary Track Testing) was assumed.

Average Bhp's for wheels in each test car and each series of drag braking cycles are shown in Figure 7.8. The total estimated braking energy input to each wheel during comprehensive testing is given in Figure 7.9. Average

AVERAGE BHP MAINTAINED IN TEST CARS
(COMPREHENSIVE TESTING)
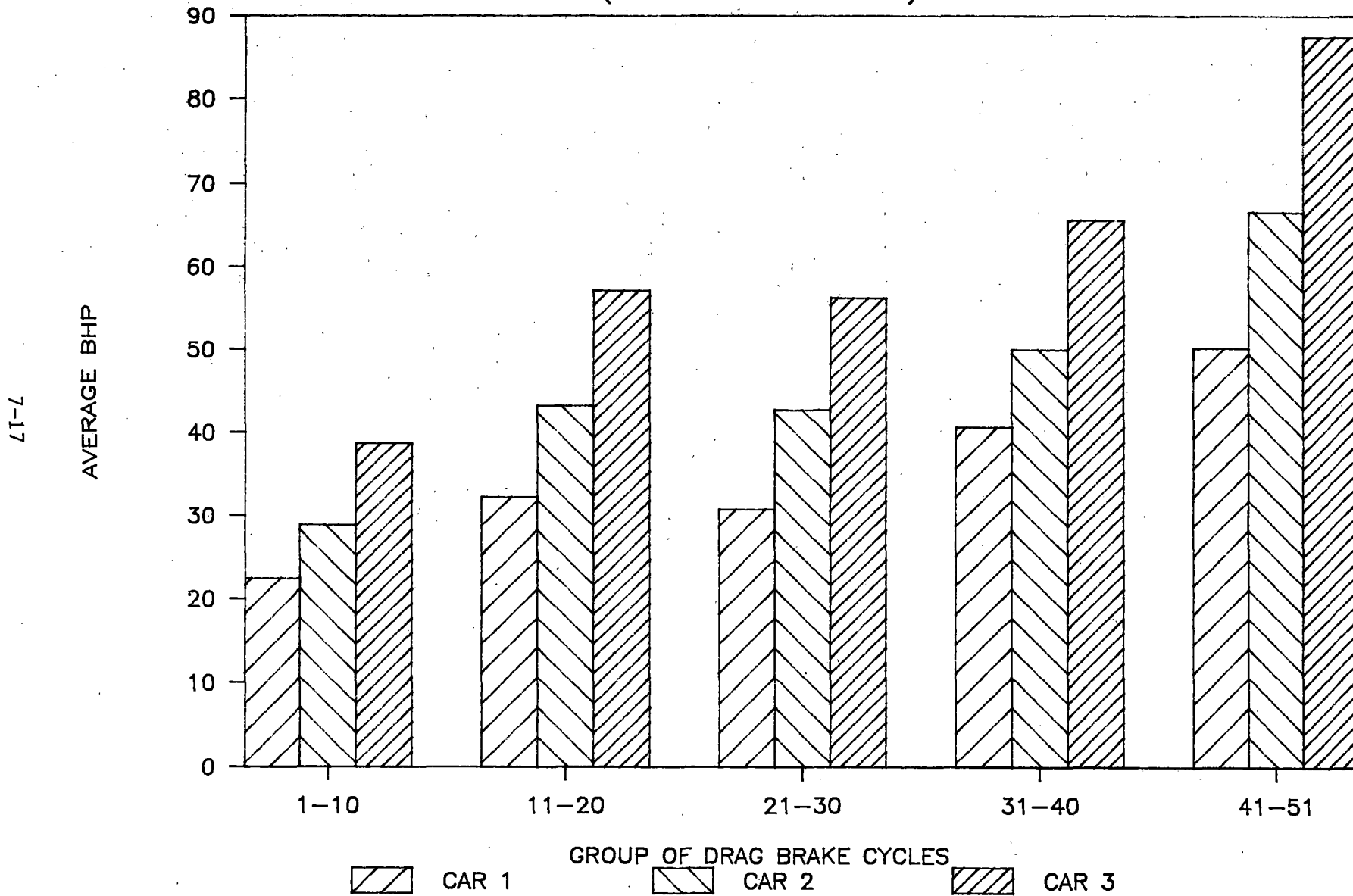
FIGURE 7.8   AVERAGE BHP MAINTAINED IN TEST CARS

ESTIMATED BRAKING ENERGY INPUT
AFTER 51 DRAG CYCLES
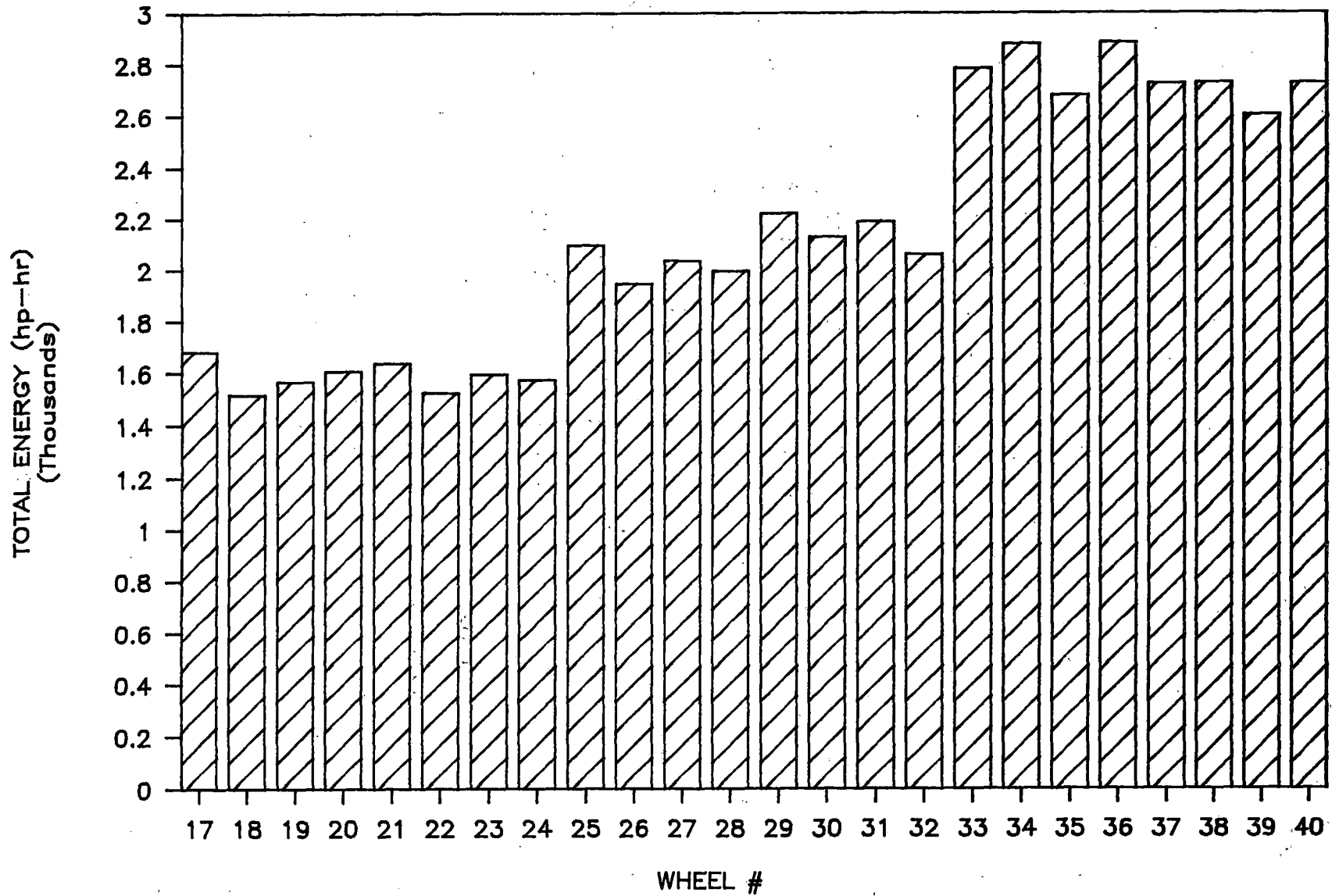
FIGURE 7.9   ESTIMATED BRAKING ENERGY INPUT AFTER 51 DRAG CYCLES-WHEELS #17-40

cumulative energy input for wheels in each car during testing is shown in Figure 7.10. Figure 7.11 shows the total amount of energy input to the test wheels during tests where the computed Bhp exceeded 40 Bhp.

For any given drag braking test, the amount of wear occurring in a given brake shoe may be used as a rough indication of the amount and/or rate of braking energy input to the corresponding test wheel. The total number of brake shoes that were worn out during Comprehensive Track Testing is shown in Figure 7.12. Wear of composition brake shoes has been found to be nonlinearly dependent on temperature (Reference 1).

It is seen from Figures 7.8 through 7.12 that substantially different rates of braking energy input were maintained in each of the three test cars.

7.2.3 Distribution of Wheel Temperatures

Temperatures measured at the brake shoe/wheel tread interface seem to indicate a wheel to wheel variation in tread temperatures developed within a given car. For example, during run 1, peak tread temperatures in the B-end truck of car 520049 ranged from 375° - 650° in Fahrenheit. During run 35, the same temperatures ranged from 800° to 1150°. Thus, despite the use of Wabco brake rigging, it would appear that within each car, there was a wheel to wheel variation in the amount of braking force applied and hence braking power.

ENERGY ACCUMULATED
DURING COMPREHENSIVE TESTING

TOTAL ENERGY (HP—HRS) (Thousands)

DRAG BRAKING CYCLE NUMBER

□   CAR 1   +   CAR 2   ◇   CAR 3
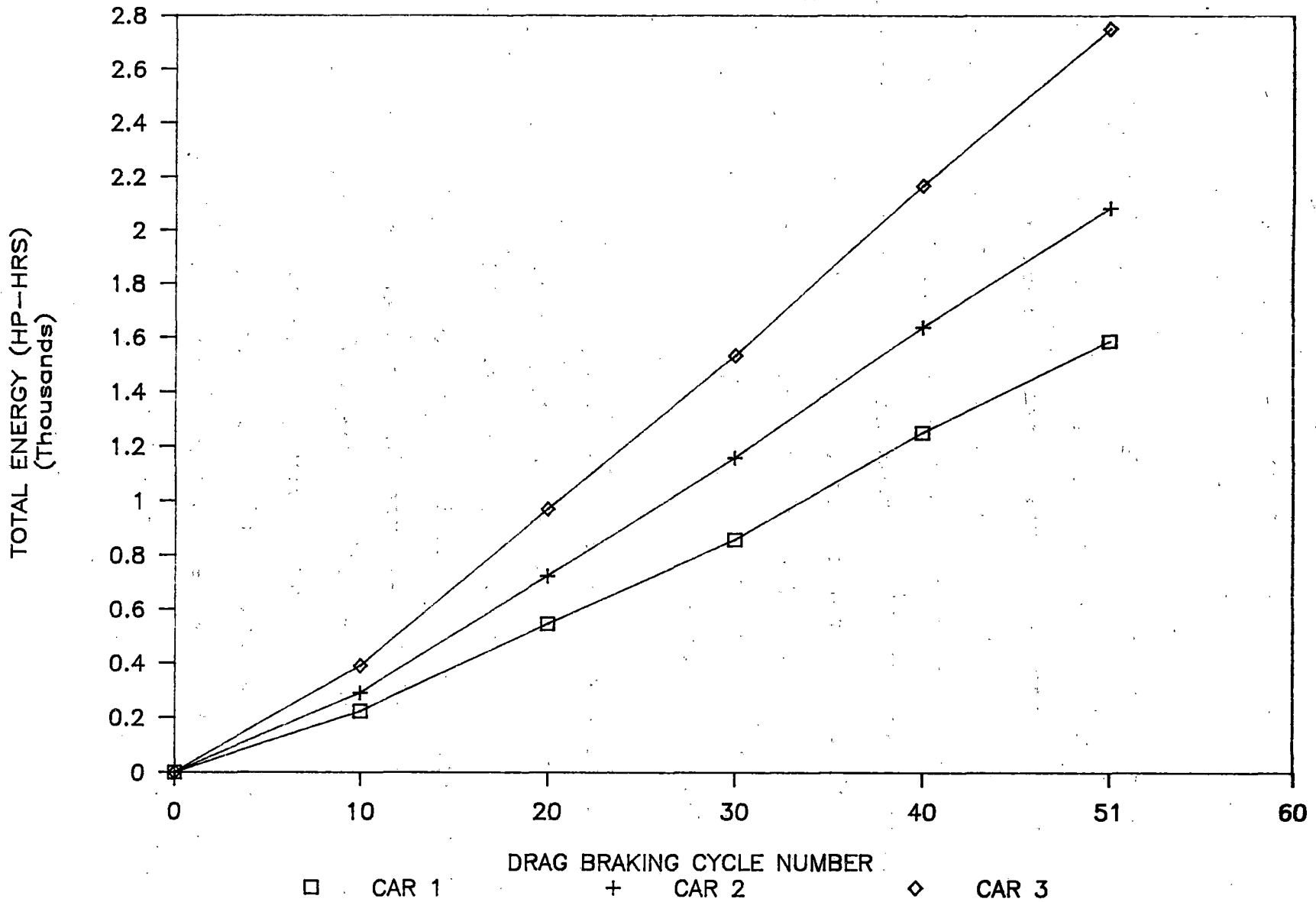
FIGURE 7.10   ENERGY ACCUMULATED DURING COMPREHENSIVE TESTING

FIGURE 7.11   CUMULATIVE ENERGY INPUT GREATER THAN 40 BHP-COMPREHENSIVE TESTING

NO. OF SHOES CONSUMED IN TESTING

(SHOES REPLACED WHEN 3/4 WORN)
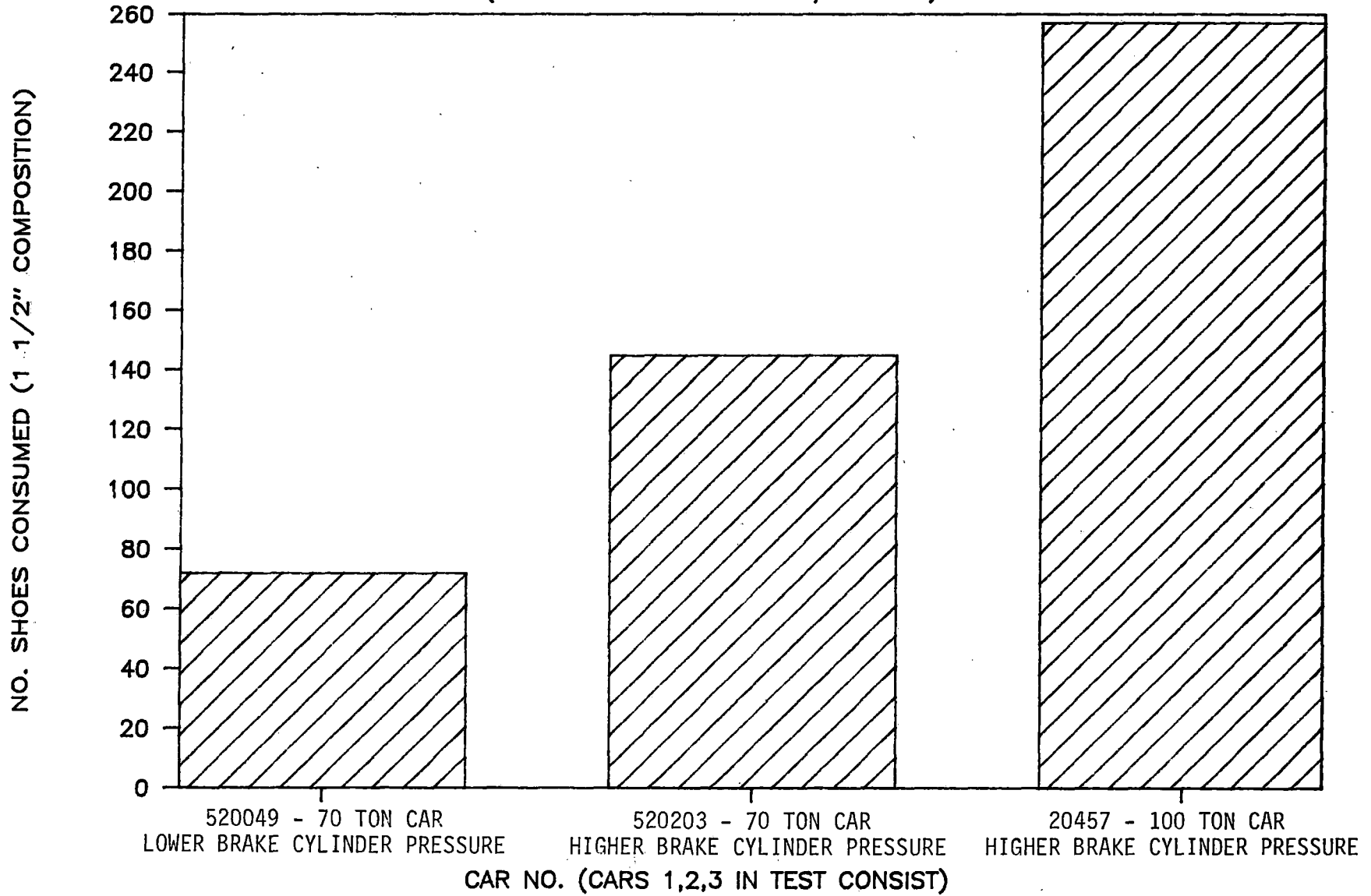
FIGURE 7.12   SHOES CONSUMED PER CAR IN TESTING

7.2.4 Development of Residual Stresses In Test Wheels

Hole Drilling Results

As was mentioned earlier, the hole drilling technique of stress measurement was used periodically during testing to provide a measure of surface residual stresses at the Bl location. The hoop and radial stresses calculated for each of the measurements are given in Table 7.3. As seen in this Table, the following six wheels underwent a compressive to tensile Bl location hoop stress reversal during comprehensive testing:

Wheel#	Shape	Class	Manufacturer	Diameter	New (N) or Remachined to Condem. Limit (R)
22	Straight	U	Canadian Steel	33"	N
24	S-Shape	U	Standard Steel	33"	R
26	Parabolic	U	Griffin	33"	N
29	Straight	C	Canadian Steel	33"	R
33	Parabolic	C	Abex	36"	N
40	Parabolic	C	Abex	36"	N

The measured residual stresses by hole drilling technique are shown in Figures 7.13 through 7.18.

The test conditions which preceded each of the stress reversals appear in Table 7.4.

TABLE 7.3
DEVELOPMENT OF B1 RESIDUAL STRESSES
IN WHEELS DURING COMPREHENSIVE TRACK TESTING

WHEEL #	WHEEL TYPE	CLASS	MANUFACTURER	DIAM (IN.)	NEW (N) OR MACHINED TO CONDEMNING LIMIT (R)	BEFORE TESTING		AFTER 10 CYCLES	
						HOOP (KSI)	RADIAL (KSI)	HOOP (KSI)	RADIAL (KSI)
17	PARABOLIC	C	GRIFFIN	33	N	-26.7	-29.4	-27.0	-30.1
18	PARABOLIC	U	GRIFFIN	33	N	-20.9	-26.6	-14.4	-26.2
19	S-SHAPE	C	STANDARD STEEL	33	N	-38.9	-39.8	-30.8	-32.9
20	S-SHAPE	U	STANDARD STEEL	33	N	-28.5	-33.2	-16.8	-27.9
21	STRAIGHT	C	CANADIAN STEEL	33	N	-38.9	-36.8	-28.9	-30.6
22	STRAIGHT	U	CANADIAN STEEL	33	N	-15.2	-23.0	-24.1	-28.2
23	S-SHAPE	C	STANDARD STEEL	33	R	-31.6	-34.8	-38.9	-40.7
24	S-SHAPE	U	STANDARD STEEL	33	R	-29.1	-33.2	-19.5	-30.1
25	PARABOLIC	C	GRIFFIN	33	N	-14.1	-17.2	-21.4	-29.7
26	PARABOLIC	U	GRIFFIN	33	N	18.2	4.4	5.0	-9.7
27	PARABOLIC	C	GRIFFIN	33	R	5.1	-1.7	2.2	-14.9
28	PARABOLIC	U	GRIFFIN	33	R	-10.4	-23.2	-5.4	-26.0
29	STRAIGHT	C	CANADIAN STEEL	33	R	-19.6	-10.7	-33.6	-43.5
30	STRAIGHT	U	CANADIAN STEEL	33	R	-21.8	-27.0	-44.5	-49.1
31	STRAIGHT	C	CANADIAN STEEL	33	N	-27.3	-19.8	-18.9	-24.8
32	STRAIGHT	U	CANADIAN STEEL	33	N	-17.9	-26.6	-19.5	-25.7
33	PARABOLIC	C	ABEX	36	N	-27.9	-26.8	-6.4	-26.4
34	S-SHAPE	C	STANDARD STEEL	36	N	-51.2	-47.8	-23.7	-31.7
35	STRAIGHT	C	CANADIAN STEEL	36	N	-44.2	-45.3	-44.4	-51.4
36	STRAIGHT	U	CANADIAN STEEL	36	N	-37.1	-40.2	-28.9	-43.7
37	STRAIGHT	U	CANADIAN STEEL	36	N	-32.0	-39.5	-34.3	-38.7
38	STRAIGHT	U	CANADIAN STEEL	36	N	-49.3	-58.4	-12.3	-41.8
39	S-SHAPE	C	STANDARD STEEL	36	N	-38.6	-43.4	-44.2	-46.9
40	PARABOLIC	C	ABEX	36	N	-21.0	-23.1	-10.7	-18.3

TABLE 7.3 (CONT.)
DEVELOPMENT OF B1 RESIDUAL STRESSES
IN WHEELS DURING COMPREHENSIVE TRACK TESTING

WHEEL #	AFTER 20 CYCLES HOOP (KSI)	AFTER 20 CYCLES RADIAL (KSI)	AFTER 30 CYCLES HOOP (KSI)	AFTER 30 CYCLES RADIAL (KSI)	AFTER 40 CYCLES HOOP (KSI)	AFTER 40 CYCLES RADIAL (KSI)	AFTER 50 CYCLES HOOP (KSI)	AFTER 50 CYCLES RADIAL (KSI)
17	-15.3	-22.0	-22.4	-28.8	-11.9	-20.4	-13.6	-24.3
18	-11.4	-25.5	-17.1	-34.7	-5.8	-23.1	-5.1	-29.5
19	-25.1	-27.1	-23.5	-28.5	-30.1	-33.8	-25.6	-31.4
20	-12.2	-20.3	-16.1	-24.7	-27.2	-37.3	-19.6	-26.2
21	-11.7	-27.2	-7.5	-24.4	-3.5	-21.1	-5.2	-25.3
22	-1.9	-20.1	-8.2	-19.5	-18.4	-30.7	1.0	-10.3
23	-24.1	-31.3	-30.7	-39.3	-30.3	-38.5	-17.6	-24.7
24	-28.8	-38.8	-25.8	-37.5	-21.3	-37.4	.9	-14.9
25	-22.5	-35.6	-23.6	-40.2	-16.9	-32.8	-2.8	-19.6
26	-4.2	-22.1	-6.2	-23.5	12.1	-11.4	18.5	-9.0
27	-25.0	-41.2	-10.6	-16.9	-9.6	-22.0	-9.3	-21.9
28	-8.4	-27.1	-8.3	-23.3	-1.1	-21.4	-11.7	-34.3
29	-12.4	-30.2	-8.0	-23.1	-0.5	-30.7	12.2	-23.1
30	-14.1	-27.8	-17.5	-27.2	-8.8	-40.6	-8.1	-22.8
31	-18.8	-23.4	-25.1	-26.2	-12.1	-17.1	-24.4	-28.8
32	-11.1	-29.6	-9.9	-31.2	-11.0	-29.6	-11.2	-29.8
33	10.0	-12.5	4.7	-16.2	2.0	-11.7	15.6	-2.2
34	-11.4	-22.9	-7.9	-28.8	-10.9	-28.6	-3.4	-19.7
35	-28.5	-43.5	-19.5	-36.8	-18.9	-28.6	-15.9	-36.8
36	-28.3	-45.1	-12.9	-27.6	-10.8	-24.7	-17.2	-28.8
37	-26.1	-38.8	-13.6	-23.3	-10.6	-24.4	-12.3	-29.5
38	-4.4	-38.8	-9.4	-45.5	- 0.5	-42.5	-10.6	-51.9
39	-35.3	-38.6	-23.1	-32.8	-35.9	-38.7	-19.0	-34.8
40	-1.8	-12.2	-6.2	-16.5	-4.2	-16.6	3.1	-11.8

WHEEL 22

33" STRAIGHT CLASS U
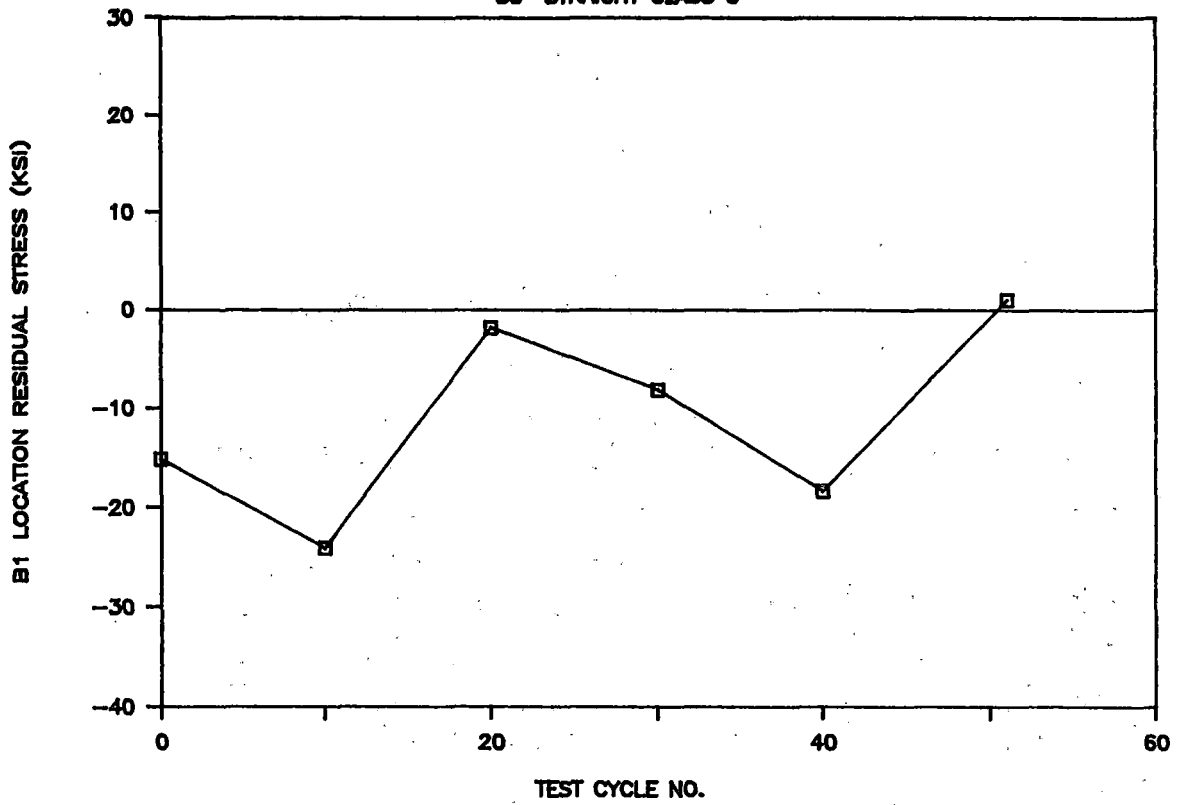
FIGURE 7.13   WHEEL #22 B1 LOCATION RESIDUAL STRESS HISTORY

WHEEL 24

33" S—SHAPE CLASS U
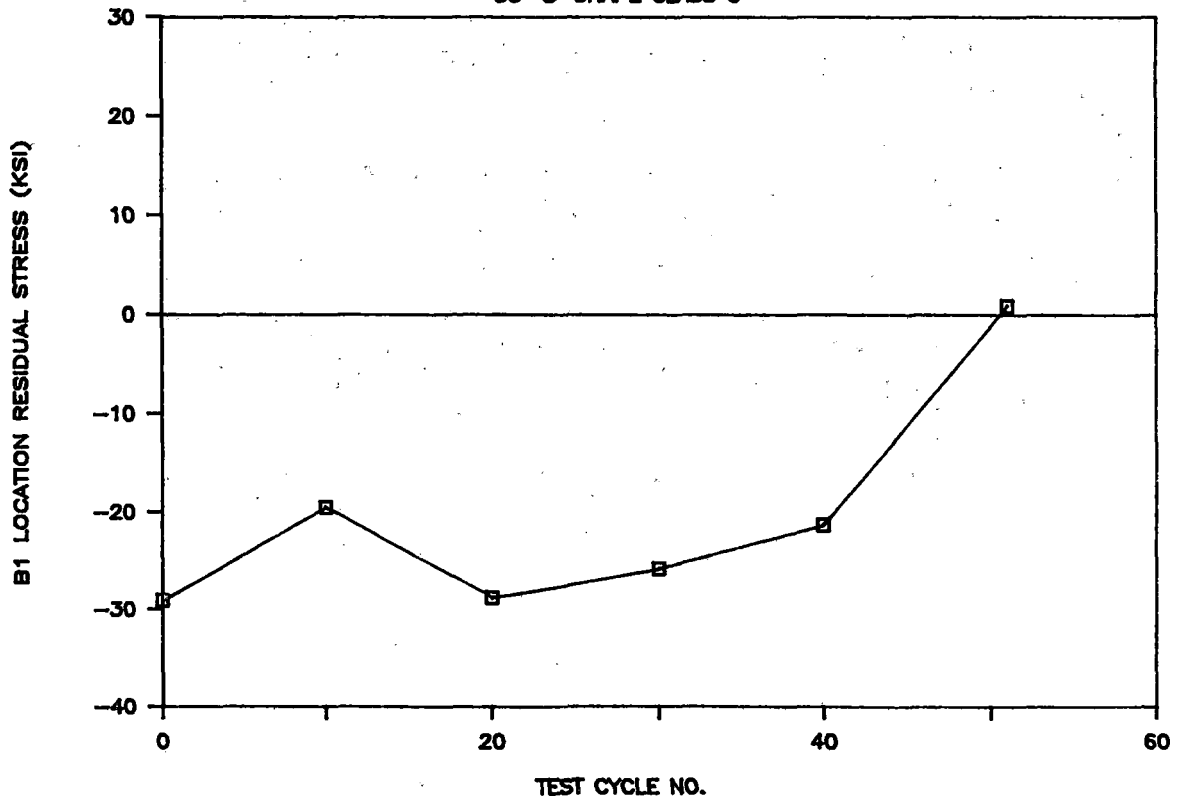
FIGURE 7.14   WHEEL #24 B1 LOCATION RESIDUAL STRESS HISTORY

WHEEL 26
33" PARABOLIC CLASS U
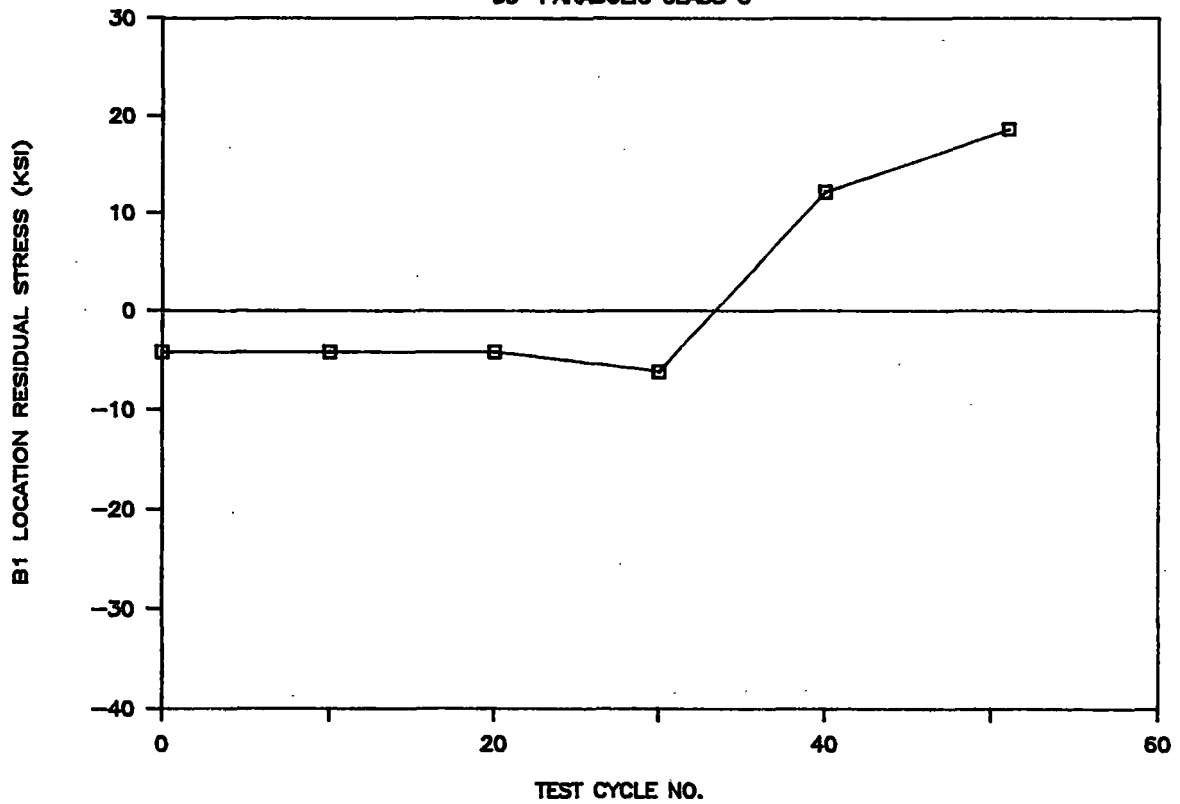
FIGURE 7.15   WHEEL #26 B1 LOCATION RESIDUAL STRESS HISTORY

WHEEL 29
33" STRAIGHT CLASS C
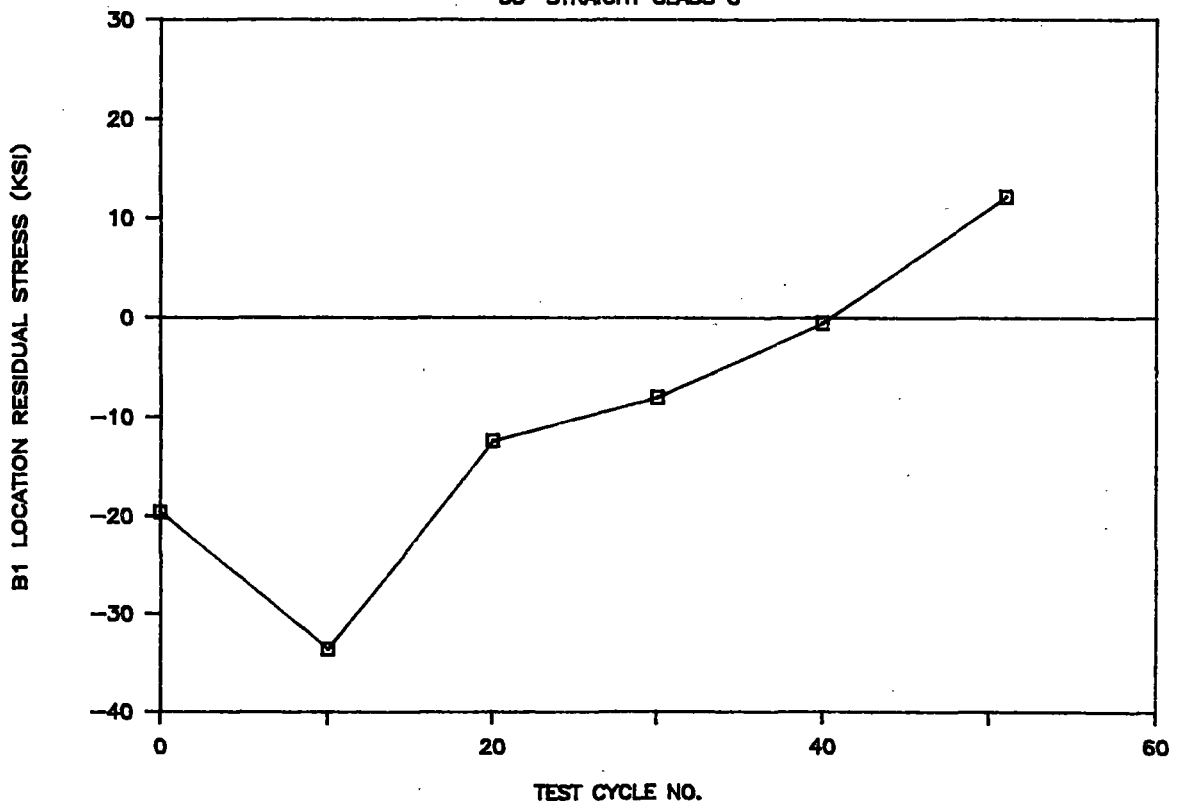
FIGURE 7.16   WHEEL #29 B1 LOCATION RESIDUAL STRESS HISTORY

WHEEL 33

36" PARABOLIC CLASS C
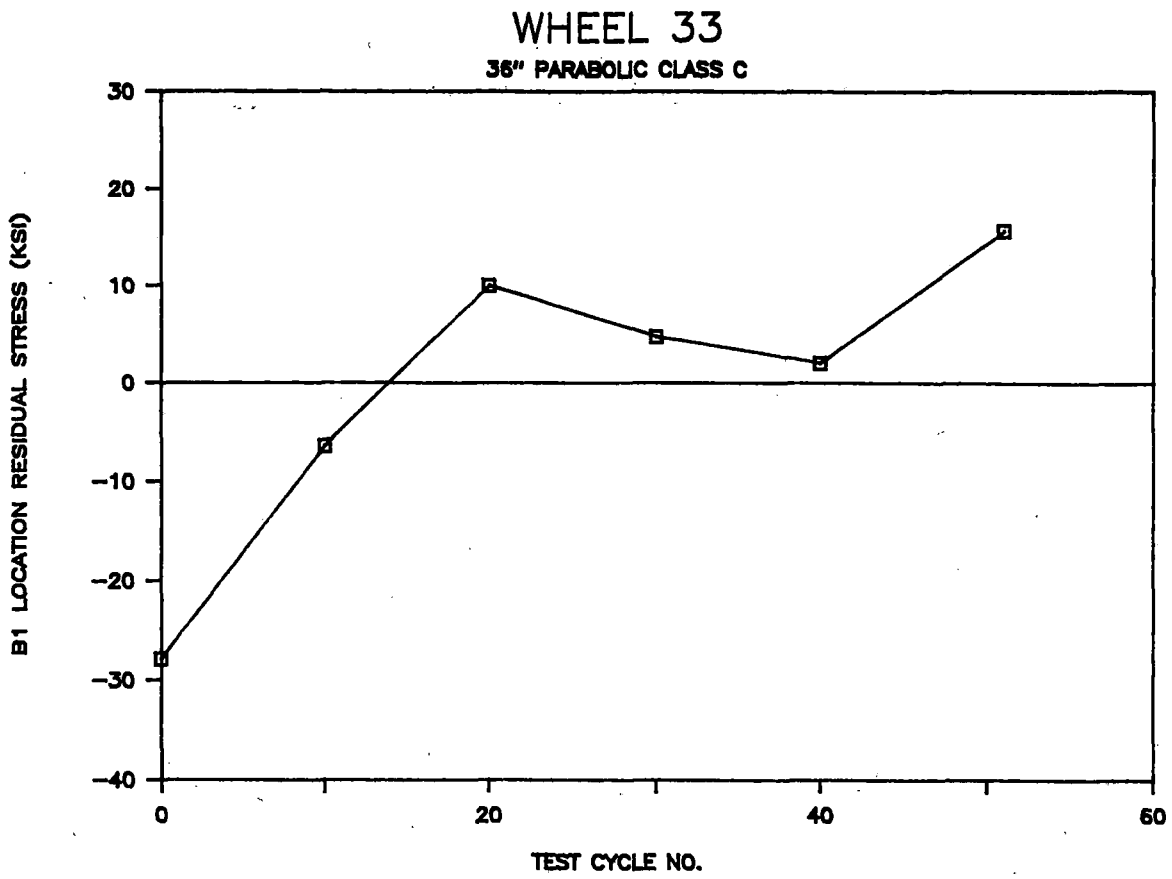
FIGURE 7.17   WHEEL #33 B1 LOCATION RESIDUAL STRESS HISTORY

WHEEL 40

36" PARABOLIC CLASS C
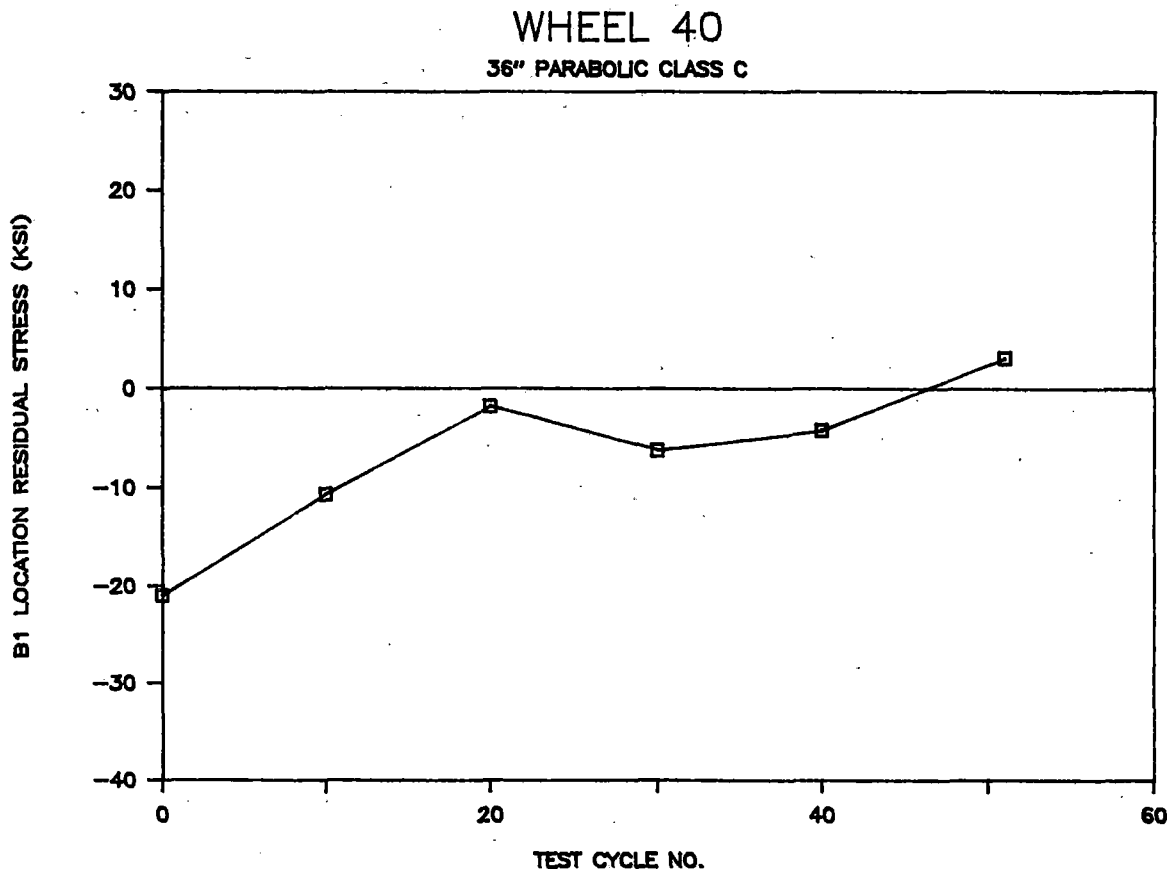
FIGURE 7.18   WHEEL #40 B1 LOCATION RESIDUAL STRESS HISTORY

TABLE 7.4
TEST CONDITIONS PRECEDING STRESS REVERSAL

WHEEL NO.	TYPE	CLASS	MOST SEVERE CONDITIONS (MAX. BHP, MAX. DURATION) IN TEST SERIES WHICH PRODUCED REVERSAL					MOST SEVERE CONDITIONS (MAX. BHP, MAX. DURATION) PRIOR TO TEST SERIES WHICH PRODUCED REVERSAL				
			TEST NO.	B.H.P.	DURATION (min)	SPEED (mph)	B.C.P. (psi)	TEST NO.	B.H.P	DURATION (min)	SPEED (mph)	B.C.P. (psi)
22	STRAIGHT	U	45	50.3	36	45	50	33	39.1	62	35	50
24	S	U	45	51.6	36	45	50	33	40.1	62	35	50
26	PARABOLIC	U	33	46.8	62	35	60	30	40.1	64	30	60
29	STRAIGHT	C	45	74.6	36	45	65	33	53.1	62	35	60
33	PARABOLIC	C	17	66.5	57	35	60	10	62.1	63	40	50
40	PARABOLIC	C	45	90.7	36	45	65	33	64.8	62	35	60

It may be noted that, for 4 of the 6 wheels, the stress reversal occurred in the last series of drag brake cycles. Furthermore, it may be noted that braking horsepowers in the series of tests which produced stress reversals were higher than those in previous test series.

If one examines the estimated maximum Bhp in the test series which preceded stress reversal (as measured by hole drilling-strain gauging method) it is seen that at least 46.8 Bhp (threshold value, see Section 11.4.1 for explanation) was required for stress reversal in 33" wheels. Similarly, at least an estimated 66.5 Bhp was required for stress reversal in 36" wheels. This increase in threshold Bhp is somewhat higher than would be expected from an extrapolation based only on increase in rim weight. (It may be noted that the Bhp computed for this series of tests, was based on an average coefficient of friction between brake shoe and wheel interface observed during RDU and Preliminary Brake Testing.)

7.2.5 Saw-Cutting Results

At the conclusion of testing, 22 of the 24 test wheels were saw-cut according to the established procedure (wheels 39 and 40 were set aside for future possible testing). Rim forces were computed for each the test wheels; the results are given in Table 7.5. As described in section 5, rim forces were computed from flange tip displacements measured during the saw-cutting process. For a given wheel, the rim force is an estimate of the

*1st DIGIT 1-CURVED PLATE
               2-STRAIGHT PLATE
 2nd DIGIT 1-NONDISCOLORED
               2-DISCOLORED

TABLE 7.5 SAWCUT DISPLACEMENT DATA FOR TEST WHEELS CUT AFTER COMPREHENSIVE TRACK TESTING

TEST WHEEL ID NO.	SERIAL NO.	* CODE	DISCOLORATION			CLOSED	OPENED	MAX OPENING (IN.)	CLASS	MANUF. DESIGN	CALCULATED NET RIM FORCE (kips)
			FRT	BACK	CODE 89						
17	95390	12	6.00	7.00		*			C	CJ 33 GK	-54
18	95556	12	6.00				*	0.0241	U	CJ 33 GK	71
19	4906	12	8.00	4.00		*			C	J 33 SW	-85
20	5033	12	4.00					0.0032	U	J 33 SW	-2
21	49621	22	5.00	4.00		*			C	J 33 ZW	-69
22	43841	22	4.50				*	0.035	U	J 33 ZW	78
23	4894	12	5.00			*			C	J 33 SW	-50
24	5177	12	5.00			*			U	J 33 SW	-19
25	94774	12	6.00	6.00				0.0057	C	CJ 33 GK	6
26	95525	12	6.50				*	0.0454	U	CJ 33 GK	149
27	94772	12	6.00	8.00				0.0051	C	CJ 33 GK	12
28	95555	12	6.00				*	0.0167	U	CJ 33 GK	68
29	49624	22	4.50	4.50			*	0.0334	C	J 33 ZW	171
30	43847	22	5.00				*	0.0372	U	J 33 ZW	115
31	49620	22	4.50	5.00		*			C	J 33 ZW	-97
32	43872	22	5.00				*	0.0138	U	J 33 ZW	36
33	108021	12	6.00					0.008	C	CH 36 SO	35
34	3453	12	5.00	5.50				0.021	C	H 36 SW	16
35	48976	22	5.00	7.00		*			C	H 36 ZW	-63
36	46466	22	4.00	7.00			*	0.0265	U	H 36 ZW	56
37	46465	22	4.50	6.00			*	0.0402	U	H 36 ZW	107
38	45311	22	5.00	6.50				0.017	U	H 36 ZW	55
39	3603	12	5.00	5.50	DID NOT SAW CUT THESE LAST				C	H 36 SW	
40	110209	12	5.00	5.50	TWO WHEELS				C	CH 36 SO	

total circumferential force existing in the rim of the wheel prior to saw-cutting.

7.2.6 Effect of Wheel Parameters and Braking History on Residual Stresses

The final goal of Technical Task T6 is to assess the effects of wheel design/material/size/rim thickness and brake application history on the development of residual stresses in railroad wheels. Rim forces were used as a means of estimating whether a given test wheel exhibited potential crack-opening stresses. By comparing rim forces for different wheels, it is possible to determine the effect of a given parameter on the tendency of a wheel to develop crack-opening stresses. A net rim force of 100 kips in a wheel considered as a limit beyond which the wheel is classified to be unsafe (see discussion of Rim Force in Section 11).

Computed rim forces and measured B1 hoop stresses for all of the test wheels are given in Table 7.6. In remaining sections, the effect of each test parameter on developed rim forces is discussed.

7.2.7 Plate Shape

The wheels which were tested in Comprehensive Testing were of three basic plate shapes: parabolic, S-shape, and straight. Examination of Table 7.6 reveals that all S-shape wheels (33"

TABLE 7.6
TEST WHEEL RIM FORCES AND B1 LOCATION HOLE DRILLING
STRESSES-COMPREHENSIVE TRACK TESTING

| DESIGN | | | | | | BEFORE TESTING | AFTER 51 CYCLES |
WHEEL TYPE	CLASS	DIAM (IN.)	TEST CAR	WHEEL #	RIM FORCE	HOOP (KSI)	HOOP (KSI)
PARABOLIC	C	33	1	17	-54	-26.7	-13.6
PARABOLIC	U	33	1	18	71	-20.9	-5.1
S-SHAPE	C	33	1	19	-85	-38.9	-25.6
S-SHAPE	U	33	1	20	-2	-28.5	-19.6
STRAIGHT	C	33	1	21	-69	-38.9	-5.2
STRAIGHT	U	33	1	22	78	-15.2	1.0
S-SHAPE *	C	33	1	23	-50	-31.6	-17.6
S-SHAPE *	U	33	1	24	-19	-29.1	.9
PARABOLIC	C	33	2	25	6	-14.1	-2.8
PARABOLIC	U	33	2	26	149	NA	18.5
STRAIGHT	C	33	2	31	-97	-27.3	-24.4
STRAIGHT	U	33	2	32	36	-17.9	-11.2
PARABOLIC *	C	33	2	27	12	5.1	-9.3
PARABOLIC *	U	33	2	28	68	-10.4	-11.7
STRAIGHT *	C	33	2	29	171	-19.6	12.2
STRAIGHT *	U	33	2	30	115	-21.8	-8.1
PARABOLIC	C	36	3	33	35	-27.9	15.6
PARABOLIC	C	36	3	40	NA	-21.0	3.1
S-SHAPE	C	36	3	34	16	-51.2	-3.4
S-SHAPE	C	36	3	39	NA	-38.6	-19.0
STRAIGHT	C	36	3	35	-63	-44.2	-15.9
STRAIGHT	U	36	3	36	56	-37.1	-17.2
STRAIGHT	U	36	3	37	107	-32.0	-12.3
STRAIGHT	U	36	3	38	55	-49.3	-10.6

* RIM MACHINED TO CONDEMNING LIMIT
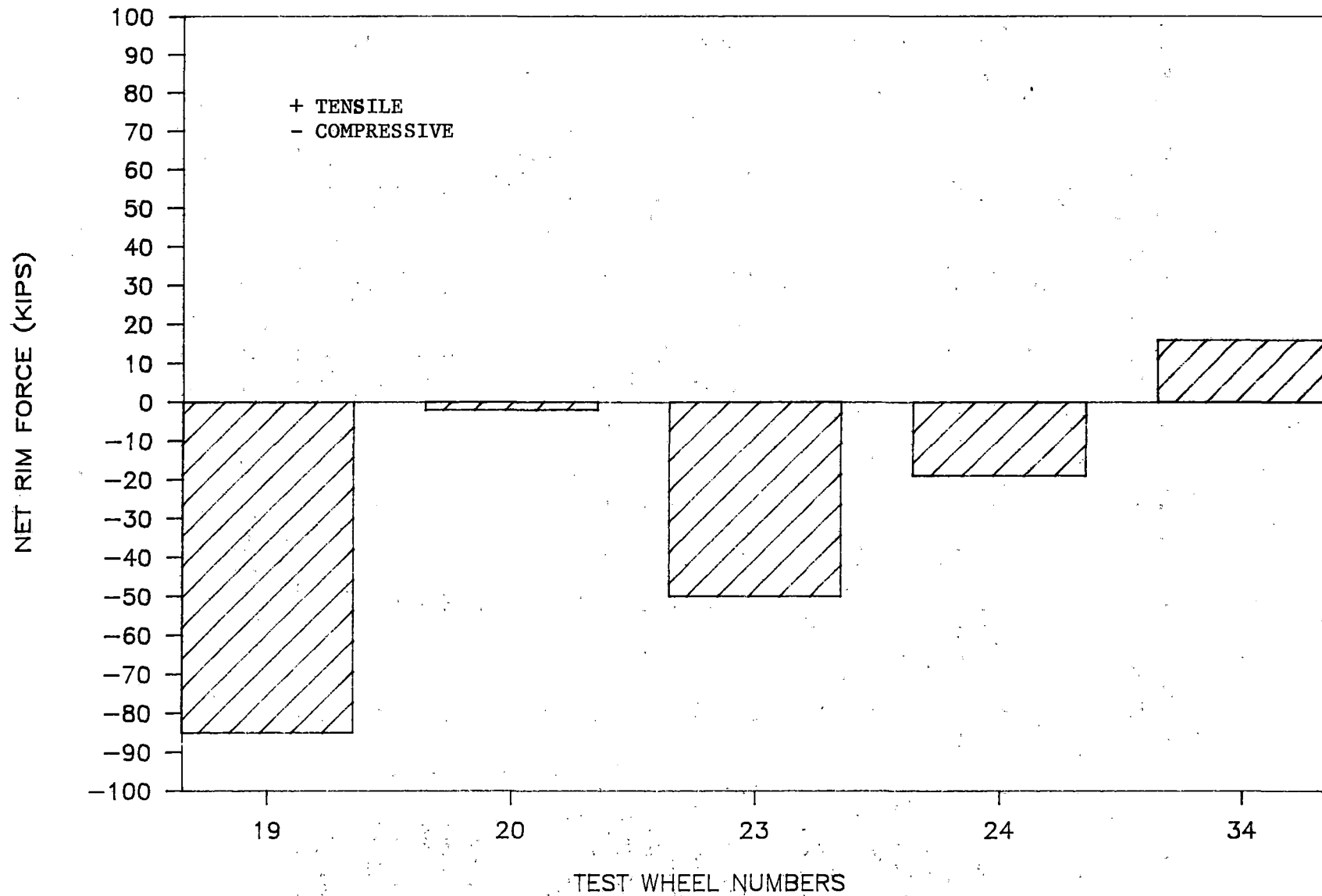
FIGURE 7.19 NET RIM FORCES IN S-PLATE WHEELS AFTER COMPLETION OF COMPREHENSIVE TESTING

Class U and C, 36" Class C) exhibited mostly net compressive rim force (see Figure 7.19). In one case, the S-plate wheel showed a small tensile rim force of 16 kips (which is considered to be safe). A comparison of rim forces for parabolic and straight plate test wheels is given in Table 7.7. The following observations can be made regarding the parabolic and straight plate wheels:

For parabolic and straight plate wheels, with the type of thermal loading corresponding to the wheel I.D. numbers in Table 7.7, there seems to be no significant difference in the net rim forces, for relatively new rim size. The thermal loading of individual wheels is shown at the bottom of the Table.

For the 33" Class U and C wheels with thin rims, however, computed rim forces for the straight plate wheels were more tensile than those for the parabolic plate wheels.

7.2.8 Wheel Class

Wheel Class was observed to have a pronounced effect on the development of residual rim stresses. With one exception, the Class U test wheels exhibited larger rim forces (more tensile or less compressive) than the Class C wheels. Computed rim forces for Class U and Class C wheels of the same design are shown in Figures 7.20, 7.21, and 7.22.

7.2.9 Wheel Size

The following wheel types were tested in 33" and 36" wheel

TABLE 7.7
DISTRIBUTION OF TEST WHEEL RIM FORCES

WHEEL DIAM.	TYPE CLASS.	RIM CONDITION	TEST WHEELS HAVING RIM FORCES <0 TO >100 KIPS					
			PARABOLIC WHEELS*			STRAIGHT PLATE WHEELS*		
			<0 KIPS	0-100 KIPS	>100 KIPS	<0 KIPS	0-100 KIPS	>100 KIPS
33"	C	New Rim	1(17)	1(25)		2(21,31)		
33"	U	New Rim		1(18)	1(26)		2(22,32)	
36"	C	New Rim		1(33)		1(35)		
33"	C	Thin Rim		1(27)				1(29)
33"	U	Thin Rim		1(28)				1(30)
36"	U	New Rim						1(37)

*Test Wheel #'s in Parenthesis

    For Wheel #'s 17-24, estimated total braking energy input per wheel=1600 HP-Hrs.
    For Wheel #'s 25-32, estimated total braking energy input per wheel =2100 HP-Hrs.
    For Wheel #'s 33-40, estimated total braking energy input per wheel =2800 HP-Hrs.

FIGURE 7.20 EFFECT OF HEAT TREATMENT ON WHEEL RIM FORCE CAR #520049 TEST WHEELS

EFFECT OF HEAT TREATMENT ON WHEEL R.F.

CAR # 520203 TEST WHEELS
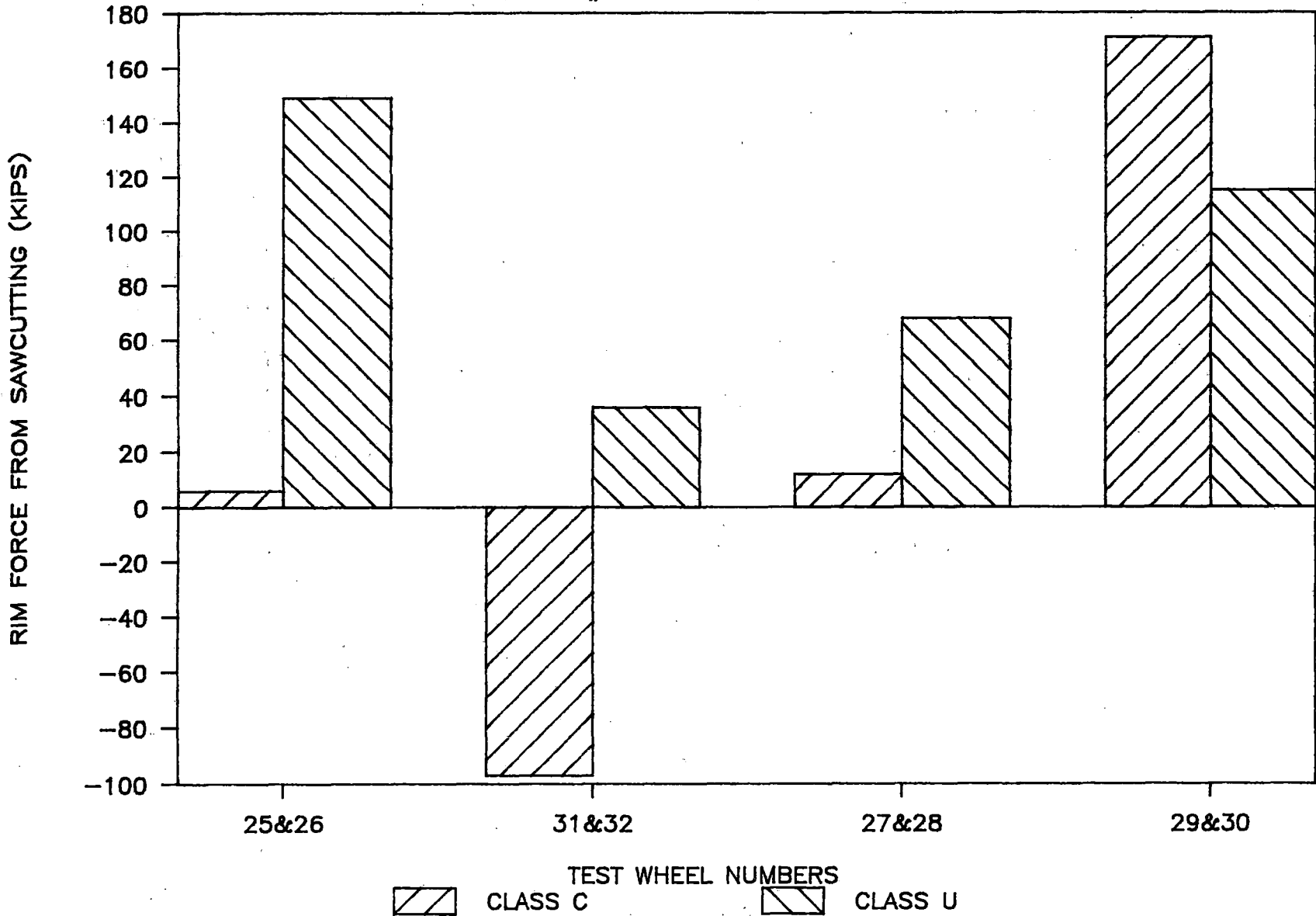
FIGURE 7.21 EFFECT OF HEAT TREATMENT ON WHEEL RIM FORCE CAR #520203 TEST WHEELS

EFFECT OF HEAT TREATMENT ON WHEEL R.F.

CAR # 20457 TEST WHEELS
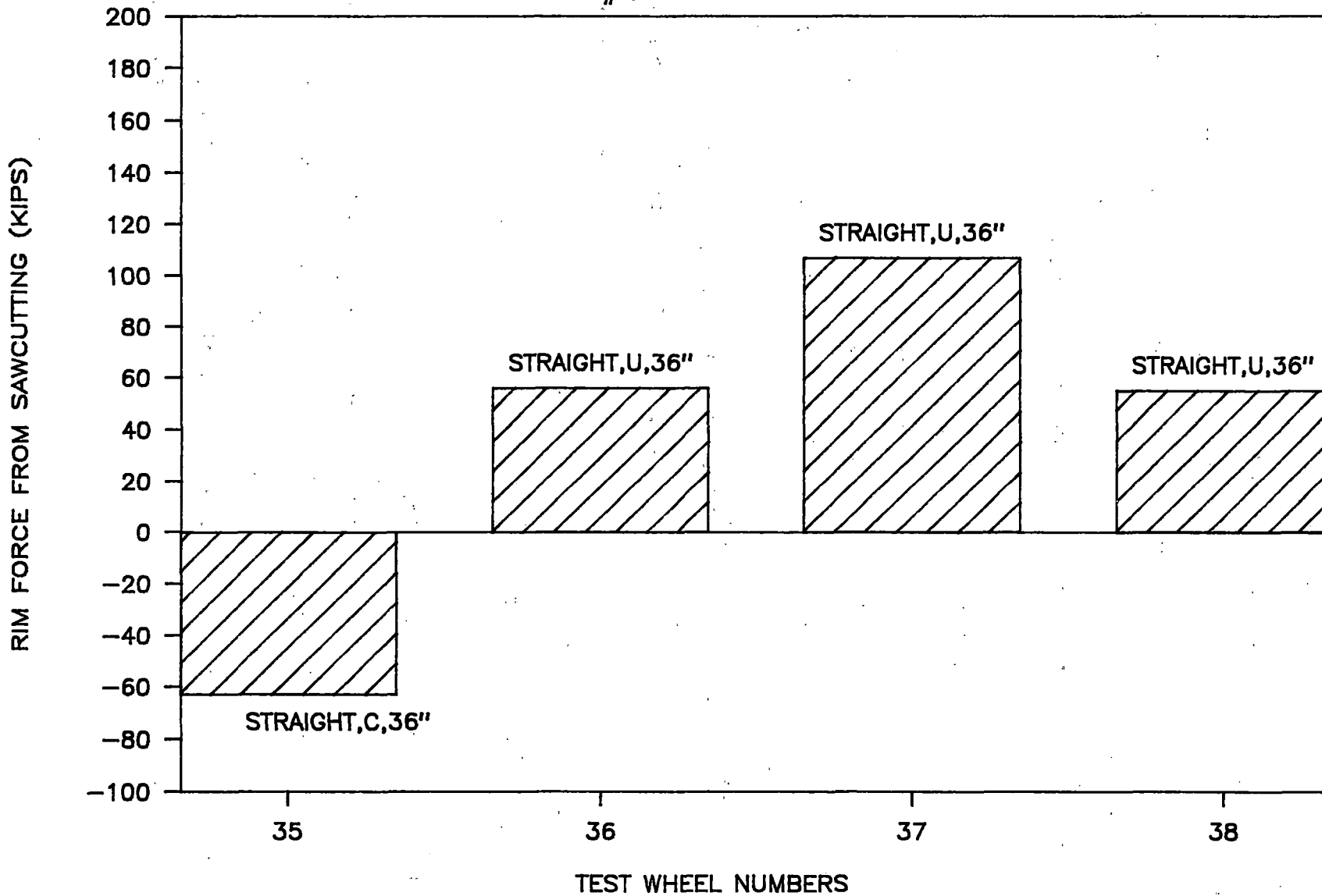
FIGURE 7.22 EFFECT OF HEAT TREATMENT ON WHEEL RIM FORCE CAR #20457 TEST WHEELS

diameters: 1) Parabolic, Class C

2) Straight, Class C

3) Straight, Class U.

No significant differences in rim forces were observed, between 33 and 36 inch wheel diameters for given brake cylinder pressure and speed conditions when compared between same shape and heat treatment with normal rim cross sections (Table 7.6).

7.2.10 Rim Thickness

Six different wheel types were tested with new rims and with thin (machined to the condemning limit) rims. The rim forces computed from saw-cut displacement data for these wheels are shown in Figure 7.23. The thin rim condition was observed to produce more tensile rim forces in the straight plate, Class U and C wheels, when compared with wheels subjected to the same test conditions. No appreciable differences in rim forces were observed for S-plate wheels (Class U and C) under the same braking conditions with normal and thin rim sections.

7.2.11 Brake Application History

Four wheel types (curved and straight section, Class U and C) were tested in both the first and second cars of the test consist (car # 520049 and car # 520203). Brake cylinder pressure in the second car was maintained at 10-15 psi higher than in the first car. Rim forces were computed from the saw-cut displacement data.

FIGURE 7.23   COMPUTED RIM FORCE -VS- RIM THICKNESS

As was shown in Figure 7.8, higher average Bhp was maintained in car two than in car one. The higher Bhp levels were seen to have significant effect on the computed rim forces for the Class U wheels, while no substantial effect was observed in the Class C wheels.

Comparisons of rim forces computed from saw-cut displacement data were also made between wheels of the same shape and class in cars 2 and 3, which were subjected to the same set of test conditions (see Table 7.6). Figure 7.8 shows average Bhp levels expended in cars 2 and 3. The average Bhp levels in car 3 (with 36-inch diameter wheels) were higher than the Bhp levels in car 2 (33 inch diameter wheels). The computed rim forces from the test wheel saw-cut displacement data showed that only Class U wheels (both 33 and 36 inch diameter) exhibited varied amounts of net tensile forces whereas Class C wheels had net comprehensive rim forces (or very low tensile forces). Only one Class C wheel (#29) with its rim machined to condemning limit, was an exception with high tensile rim force.

7.2.12 Growth of Wheel Discoloration During Comprehensive Track Testing

At intervals of 10 drag braking cycles, the extent of discoloration occurring on both sides of each wheel was measured. The bottom of the rim of each wheel was used as a reference and the extent of the discoloration in the plate towards the wheel hub was measured in inches. In several cases,

the boundaries of the discoloration were not sharply defined and it was necessary to make an estimate of the extent of discoloration.

Results

Measurements of front face discoloration for the test wheels are presented in Table 7.8. Front and back face measurements made at the conclusion of testing showed that the discoloration on back face of the wheel plate was similar to the extent of discoloration observed on the front face. The percentages of test wheels having various levels of discoloration after successive ten cycles of testing are presented in Table 7.9.

The following conclusions can be drawn from the wheel discoloration results:

* The 51 drag braking cycles applied during Comprehensive Track Testing produced discoloration which exceeded the FRA recommended limits for wheel removal from service.
* The level of discoloration in the test wheels increased gradually during testing.
* Discoloration may be used as a rough indicator of prolonged thermal input to the wheels during drag braking operations.

7.2.13 Nonaxisymmetric Heating of Test Wheels

During comprehensive track testing, wayside thermal video recordings were made of the test wheels in roll-by mode, at the

TABLE 7.8
GROWTH OF DISCOLORATION IN TEST WHEELS
FROM COMPREHENSIVE TRACK TESTING

Inches of Discoloration Measured (Front Face)

Wheel No.	After 10 Cycles	After 20 Cycles	After 30 Cycles	After 40 Cycles	After 50 Cycles
17	3	4	5	5	6
18	4	4	5	5.5	6
19	2	3	3.5	4	8
20	2.5	4	4	4	4
21	2	4	4	4	5
22	3	4	4	4.5	4.5
23	2	4	4	4.5	4.5
24	4	4	4	4.5	5
25	2	-	5	5.5	6
26	4	4	5.5	6.5	6.5
27	3	-	5	5.5	6
28	4	4	5.5	5.5	6
29	3	3.5	4	4	4.5
30	3	4	4.5	4.5	4.5
31	2.5	2.5	4	4	4.5
32	4	4.5	5	5	5
33	4	4	5	5	6
34	4	4	5	5	5
35	2.5	4	4.5	4.5	5
36	3.5	4	4	4	4
37	3	4	4	4	4.5
38	3.5	4	4.5	5	5
39	3	4	5	5	5
40	2	4	4.5	4.5	5

TABLE 7.9
LEVEL OF DISCOLORATION MEASURED ON THE FRONT FACE OF TEST WHEELS
(COMPREHENSIVE TRACK TESTING)

Number of Drag Cycles	% of Wheels $\geq 4''$	% of Wheels $\geq 5''$	% of Wheels $\geq 6''$
10	29	0	0
20	83	0	0
30	96	42	0
40	100	46	4
51	100	67	33

end of each test.   Nonaxisymmetric temperature distributions were observed in certain test wheels at the end of a given test. Figures 7.24 and 7.25 present the rim temperature variation measured along rim circumference by the infrared video camera during two runs (#33 and #34).   Of 24 test wheels, at least eight were observed to have rim temperature variations greater than 100°F around the circumference of the rim.

7.2.14   Wheel Runout Measurements

As discussed in Section 7.2.11, during portions of comprehensive track testing, observations made with the infrared viewer indicated that a few of the test wheels were developing nonaxisymmetric temperature distributions.   On the premise that this phenomenon might have been caused by irregular wheel geometry, the test wheels used in preliminary and comprehensive track testing were measured for radial and lateral runout.

Procedure

Prior to the measurements, each of the wheelsets was placed on a stand which restrained the roller bearings while allowing the wheels to rotate freely.   A dial gage with a portable mounting arrangement was then used to measure the radial and lateral runout of each wheel.   To obtain each runout dimension, the total variation in surface contour around the circumference

RIM TEMPERATURE VARIATION
(MEASURED AROUND RIM CIRCUMFERENCE)
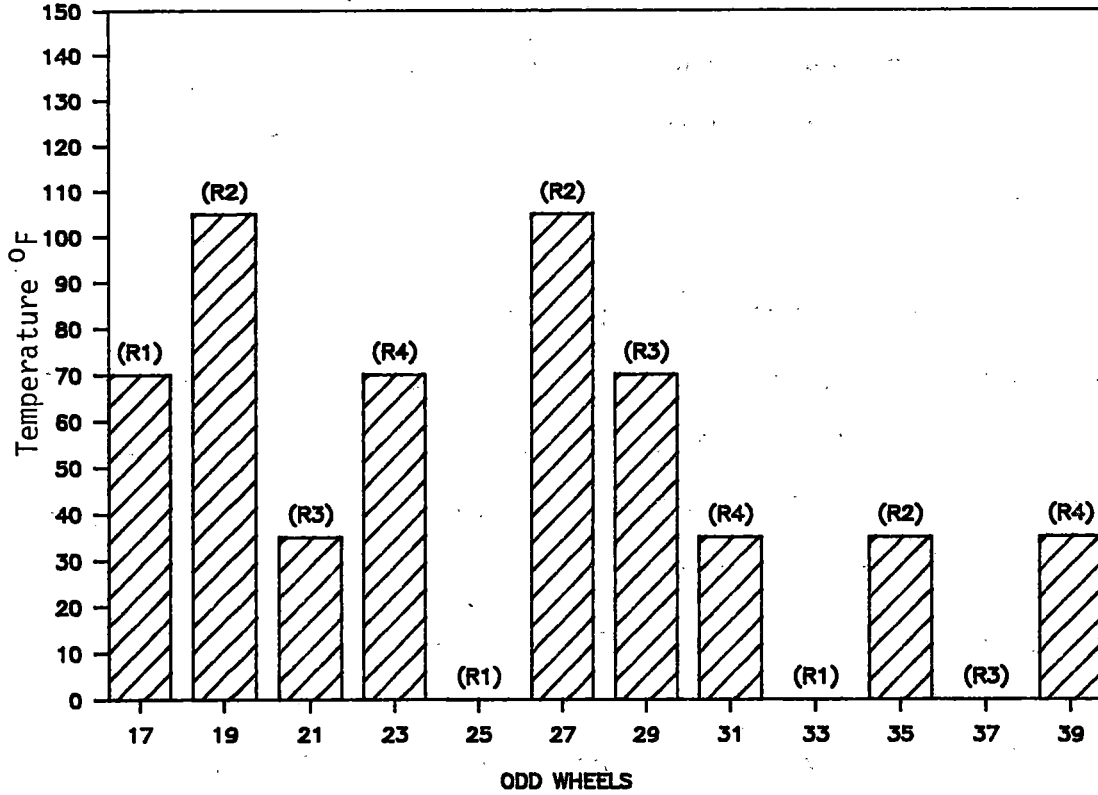
FIGURE 7.24   RIM TEMPERATURE VARIATION AROUND CIRCUMFERENCE

RIM TEMPERATURE VARIATION
(MEASURED AROUND RIM CIRCUMFERENCE)
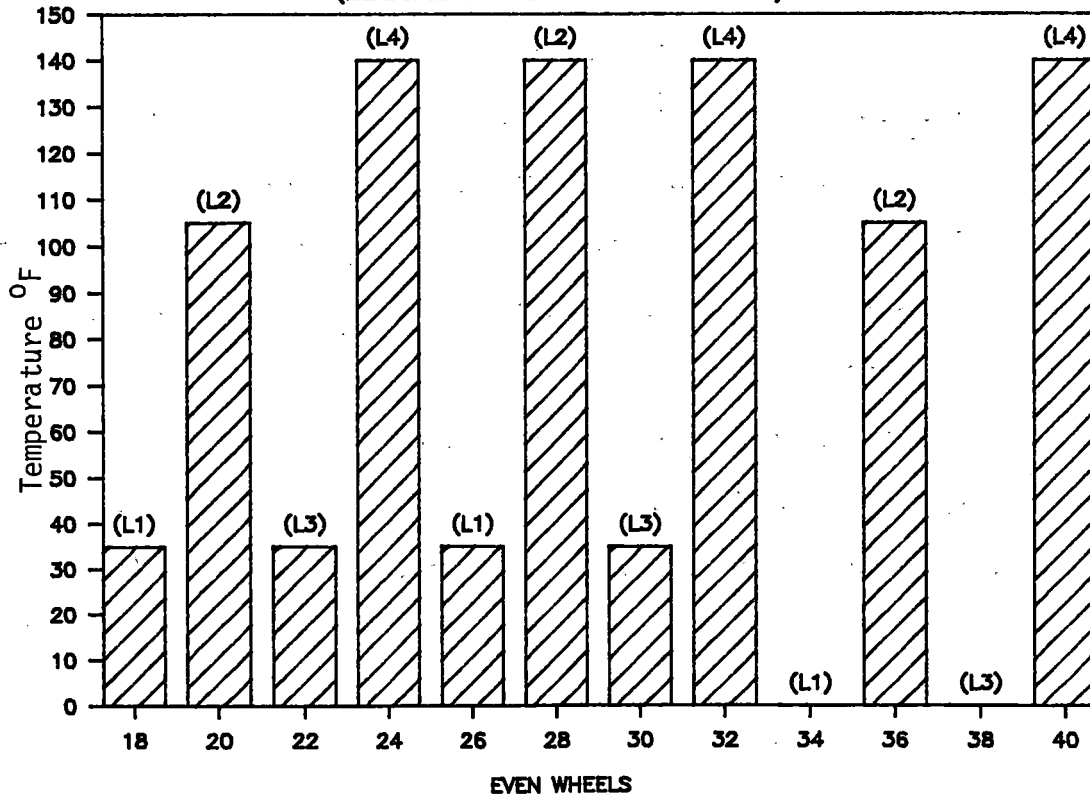
FIGURE 7.25   RIM TEMPERATURE VARIATION AROUND CIRCUMFERENCE

of the wheel was observed and recorded. Radial runout was measured at the tape line of the tread, and the lateral runout was measured at the center of the front rim face.

Results

Runout measurements for the test wheels, along with measurements for four randomly selected service wheels, are given in Table 7.10. The average radial runout for the test wheels was 0.0054" (0.0037" standard deviation); the average lateral runout was 0.0205" (0.0016" standard deviation). These statistics are in the neighborhood of those computed for the four service wheels: 0.0065" average radial runout (0.0026" s.d.) and 0.0213" average lateral runout (0.0108" s.d.).

Discussion

All of the radial runout measurements for the test wheels were well within the 0.030" tolerance specified in the AAR Wheel and Axle Manual. Although the current Manual does not specify an out-of-plane runout corresponding to the lateral runout measurements that were made, earlier Manuals specified a tolerance of 0.090". All of the test wheel lateral runouts fell within the 0.090" dimension.

In addition to a radial runout tolerance, the current manual specifies a 0.045" maximum runout for dial indicator measurements made at the throat of the flange. Although this

TABLE 7.10
RUNOUT MEASUREMENTS (IN 1/1000")

TEST WHEEL #	RADIAL RUNOUT (Measured at Tapeline)	LATERAL RUNOUT (Measured on Front Rim Face)
9	7	38
10	3	32
11	3	57
12	1	16
13	9	8
14	18	8
15	1	24
16	2	12
17	6	19
18	6	15
19	7	16
20	4	20
21	9	17
22	8	13
23	5	8
24	7	13
25	6	15
26	7	13
27	3	30
28	10	8
29	5	88
30	8	9
31	3	20
32	3	20

TABLE 7.10 (CONT.)
RUNOUT MEASUREMENTS (IN 1/1000")

TEST WHEEL #	LATERAL RUNOUT (Measured at Tapeline)	RADIAL RUNOUT (Measured on Front Rim face)
33	2	7
34	3	- 11
35	3	30
36	12	19
37	3	14
38	7	22
39	2	16
40	1	19

SERVICE WHEEL MEASUREMENTS (BR33 Wheels)

S-1	9	10
S-2	8	24
S-3	6	35
S-4	3	16

measurement was not taken, it is certain that the comprehensive test wheels met this requirement, since they were turned to an exact 1 in 20 profile prior to testing.

There does not appear to be a positive correlation between radial runout in the test wheels and the occurrence of non-axisymmetric heating as observed in thermal video recordings. For example, of the 8 test wheels which exhibited a $100^{\circ}F$ variation in temperature around the circumference of the rim (See Table 7.10), 5 were measured to have a radial runout of 0.004", or less. (The other 3 wheels had radial runouts of 0.007", 0.010", and 0.012".) Of the 16 remaining test wheels, 6 which were measured to have a radial runout of 0.015 or more exhibited circumferential temperature variations of less than $70^{\circ}F$.

This phenomenon of nonaxisymmetric heating will be addressed in the FRA funded program, entitled, "Improved Braking System" which is being undertaken by AAR.

7.3   Conclusions

Due to the (1) small number of test wheels involved, and (2) inevitable variations in braking energy input to the wheels of the same truck for a given set of operating conditions, it would be extremely difficult to establish an exact relation between each of the wheel variables and the development of residual stresses with different levels of thermal input during comprehensive track testing. It should be noted that unlike RDU

testing (Technical Task T4) and preliminary track testing (Technical Task T5), the brake shoe forces and wheel strains were not monitored continuously during testing. However, the following important observations can be made, with the above limitations in the conduct of the comprehensive track testing.

o   For a given wheel design, there appears to be some variation in the initial residual stress state as measured by the hole drilling-strain gaging method on a newly manufactured wheel. This was particularly evident for the 33", Parabolic, Class U wheels.

o   A minimum estimated 46 Bhp input at brake shoe/wheel interface for 33 inch Class U wheels was required to reverse the residual stress on the back rim face as measured by hole drilling-strain gaging method. The amount of stress change depends on the amount of braking energy absorbed by the wheel above this threshold Bhp (see Section 11.41). The 33 inch diameter Class U wheels sustained up to 40 Bhp level inputs without producing tensile stresses on the back rim face (Table 7.4).

o   Much higher levels of Bhp's were required for stress reversal on the back rim face as measured by hole drilling-strain gaging method for Class C wheels (Table 7.4).

o   The net rim forces computed from the saw-cut displacement

data showed that the most dominant parameter that controlled the performance of the wheel to withstand thermal abuse was heat treatment. For a given Bhp level expended at the brake shoe/wheel interface, Class U wheels resulted in varying amounts of net tensile rim forces whereas for the same amount of thermal input Class C wheels exhibited mostly net compressive rim forces and in a few cases very low levels of net tensile rim forces.

o   The next two significant parameters that changed or sustained the original (average) rim residual stress (as computed from the saw-cut displacement data) were the wheel shape and rim thickness. S-shaped wheels retained the original state of average rim stress better than other plate shapes.

o   The reduction of rim cross section (by machining to condemning size) did accelerate the change of average compressive rim stress to average tensile rim stress, for a given thermal input, in the straight plate wheels. The rim forces in S-shaped and parabolic plate wheels were not significantly affected by a reduction of rim cross section for a given set of operating conditions.

o   In some cases, nonaxisymmetric heating was observed in certain test wheels of the consist as viewed by the thermal video system at the conclusion of a given drag braking cycle.

o   No correlation was observed between the occurrence of non-axisymmetric heating and measurements of wheel out-of-roundness.

o   After 30 drag braking cycles, almost all the test wheels exhibited 4" or more discoloration. At that point in testing, only one of the twenty-four wheels showed tensile residual stress on back rim face as measured by the hole drilling method. However, the rim force computed from the saw-cut displacement of that particular wheel indicated that the wheel did not contain a net residual tensile stress.

REFERENCES

1. McGuire, M.   "Predicting the wear of composition brake blocks."   York Braking Conference, Inst. of Mech. Engin., 1979.

8.0 DETERMINE BRAKE SHOE THERMAL INPUT AND DISTRIBUTION (TECHNICAL TASK T7)

The main objective of this technical task was to perform a brake shoe heat transfer study by instrumenting the brake shoes to obtain complete temperature distribution within the brake shoes under a series of drag braking cycles, on track.

This task was accomplished along with preliminary track testing performed under Technical Task T5. The A-end truck of the 70-ton capacity open hopper car was used for this study. All the four brake shoes were thermocoupled, with two of the diagonally opposite shoes provided with five thermocouples (each), at different depths from the active surface of the shoe. The data were collected separately for the 12 channels on an analog as well as digital system. A complete report on the brake shoe heat transfer study is included in subsection 6.6, of this report.

9.0 INITIATE WHEEL CRACKS IN DYNAMOMETER AND TTC TRACK TESTS (TECHNICAL TASK T8)

This task requires that the conditions necessary for crack initiation or growth in rail car wheels be determined. Data and results from Technical Tasks T3 through T7 were used to produce initiation or growth of thermal cracks in three to five wheels on a dynamometer.

Crack growth under selected thermal and mechanical inputs were monitored using a quantitative ultrasonic technique developed for measuring the size of rail flaws.

Results from Tasks 3 through 7 and the results from the crack growth task on the dynamometer were used to produce initiation or growth of thermal cracks on 16 wheels of a representative wheel type and class in a test consist operating at two speeds at the TTC. The thermal cycles constituted a combination of drag and stop braking efforts.

9.1 Crack Growth Tests on Brake Dynamometer

9.1.1 Introduction

The objective of the dynamometer test portion of this task was 1) to define the conditions necessary to initiate thermal cracks and 2) to determine the relative propagation rates of thermal cracks in straight, S-shape, and parabolic plate (Class U) wheels.

The study was conducted in two phases on the AAR dynamometer. In the first phase, a straight plate J-33 Class C wheel was subjected to moderate and severe stop-braking until thermal cracks appeared on the tread surface. In the second phase, artificial cracks were machined in the rims of three 33-inch diameter, one-wear, Class U wheels (straight, S-shape, and parabolic). These wheels were tested on the dynamometer under alternating series of drag braking and stop braking conditions.

9.1.2 Materials and Experimental Work

The wheels used for this dynamometer study are listed in Table 9.1. The wheels for Phase II were prepared for testing by the following methods:

1. Seven slots were machined at tread, flange and back rim face locations where thermal cracks develop in service (see Figures 9.1 and 9.2).

2. A wheel steel shim was fitted into each slot and tack-welded on one side to hold it in place, and prevent closing of the slot during braking.

3. A welding arc burn was made on the tread surface of each wheel.

4. A one-inch diameter hole was drilled in the wheel plate beneath each of the eight artificial defects to prevent crack propagation further into the plate or hub.

9-2

TABLE 9.1
WHEELS FOR THERMAL CRACKING STUDIES

Serial Number	Section	Plate Shape	Class
	Phase I Crack Initiation		
49542	J-33	Straight	C
	Phase II Crack Propagation		
43992	J-33	Straight	U
95529	CJ-33	Parabobic	U
5530	J-33	S	U

FLANGE DEFECT

0°
A
2C
SLOT
A = 0.5
2C = 1.0

45°
SLOT
A = 0.5
2C = 2.5

90°
SLOT
A = 0.5
2C = 1.8

135°
SLOT
A = 0.5
2C = 2.2

180°
SLOT
A = 0.5
2C = 1.2

225°
SLOT
A = 0.5
2C = 1.2

270°
SLOT
A = 0.5
2C = 1.6

315°
ARC WELD BURN
2C = 2.0
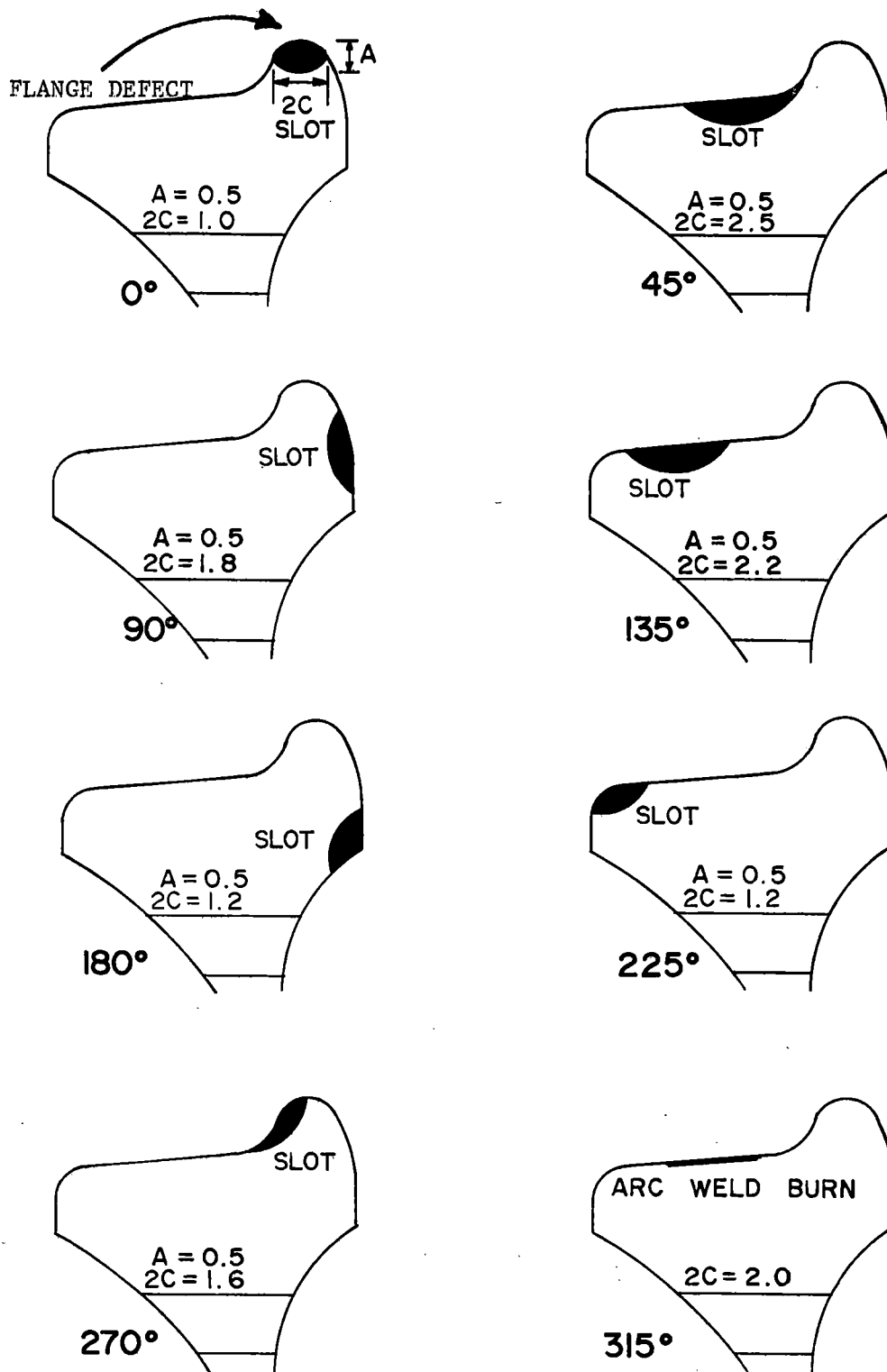
FIGURE 9.1   ARTIFICIAL CRACKS AT VARIOUS ANGLES AROUND THE WHEELS

9-4

SHEET METAL
TACK—WELDED
IN SLOT

R = 1 1/2"

1/2"

1/16"
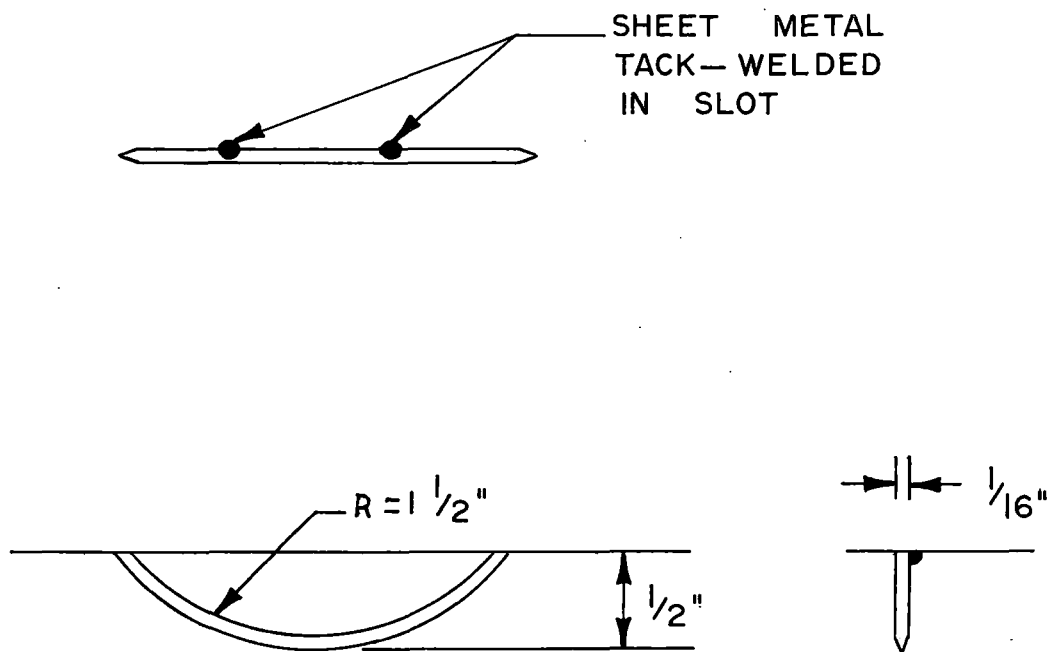
FIGURE 9.2   DETAILS OF AN ARTIFICIAL CRACK SHOWING SHEET METAL
PIECE INSERTED

The Phase I tests (Table 9.2) were stop-braking tests with rail contact and a vertical load of 27 kips. The inertia load, determined by the inertia of the flywheel and track wheel masses was set at 28,160 ft-lb. The first series of stops were from an initial speed of 60 mph with a brake force of 4,000 lbs. The second series was conducted with an initial speed of 80 mph and a brake force of 5,000 lbs. These brake forces are comparable to full-service and emergency braking forces, respectively.

The Phase II tests (Tables 9.3 and 9.4) consisted of alternating series of drag-braking and stop-braking. Generally, five drag-braking cycles were followed by 250 stop-braking cycles. The drag-braking cycles were for 45 minute duration at a speed of 40 mph with a brake force of 1,500 lbs. (about 50 Bhp). The stop-braking cycles were from initial speeds of 60 mph with a brake force of 4,000 lbs. The Phase II tests were conducted without rail contact to allow higher surface temperatures to be developed during braking and higher residual stresses to be developed on cooling. The inertial load for the stop-braking tests was 25,550 ft-lb.

In all of the tests, the wheel was cooled with water after each braking cycle: No test was started unless the temperature of the rim was below 125°F.

TABLE 9.2
DYNAMOMETER CONDITIONS
WHEEL 49542 J-33-C

Repeated Stops

Cycles   1-360

     Inertia Load   28,160 ft-lb

     Rail Load   27,000 lb

     Initial Speed   60 mph

     Brake Force   4,000 lb

     Cooling - 2.25 min. water
             .75 min. air

Cycles   361-796

     Inertia Load   28,160 ft-lb

     Rail Load   27,000 lb

     Initial Speed   80 mph

     Brake Force   5,000 lb

  Cooling - 5.15 min. water
         1.15 min. air

TABLE 9.3
DYNAMOMETER TEST CONDITIONS FOR WHEELS
43992, 95529, AND 5530

(No Rail Contact)

Drag Braking

    Speed - 40 mph

    Brake Force - 1500 lb

    Duration - 45 min.

    Cool - 15 min. to 100°F - Water on Tread and Back Plate

Stop Braking

    Speed - 60 mph

    Inertia Load - 25,550 ft-lb

    Brake Force - 4,000 lb

    Cool - 2 min., 15 sec. - Water on Tread and Back Plate

          - 45 sec. - Air to 100°F

TABLE 9.4
DYNAMOMETER TESTS FOR CRACK PROPAGATION STUDY

Test Sequence	Number of Drag	Test Stop	Total Drag	Test Stop
1	5		5	
2		312		312
3	7		12	
4		467		779
5	4		16	
6		225		1034
7	6		22	
8		251		1285
9	5		27	
10		250		1535
11	5		32	
12		410		1945
13	5		37	
14		250		2195
15	5		42	
16		250		2445
17	5		47	
18		250		2695
19	5		52	
20		1749		4444
21	63		115	

9.1.3 Results and Discussion

<u>Phase I</u>

These tests were intended primarily to determine the number of brake applications required to initiate thermal cracks in a Class C wheel. Because this information would be useful to plan track tests at Pueblo to determine the relative resistance to thermal cracking for about sixteen wheels of different designs and heat treatments, the tests were begun under braking conditions that could easily be obtained at Pueblo with the locomotive used for the drag-braking tests on the transit test track. Because these conditions (4,000 lbs. brake force and 40 mph inertial speed) did not produce cracking after 360 stops, the brake force was increased to 5,000 lbs. and the inertial speed was increased to 80 mph. These conditions represent the extreme level that can be attained with 33-inch diameter freight car wheels.

Incipient thermal cracks were observed on the tread surface after an additional 436 stops, at which time the testing was suspended on this wheel. This result (detection of thermal cracks after 360 moderate and 436 extreme stops) indicates that it is difficult to form thermal cracks in the wheel under normal service conditions in a reasonably short testing time.

Phase II

The purpose of this phase was to determine the relative resistance to crack propagation through the rim of wheels with straight, S-shape and parabolic plate designs. To provide samples, one 33-inch diameter, Class U wheel of each plate type was obtained. Seven artificial cracks and one thermally-stressed area (produced by an arc-welder) were introduced into the rim of each wheel to provide crack initiation sites. Further, a hole was drilled in the plate in line with each defect to limit the extent of crack propagation.

Alternating drag- and stop-braking series of tests were conducted on each wheel until a crack propagated into the plate or until it became clear that crack propagation was not imminent.

As shown in Tables 9.5, 9.6, and 9.7 a crack propagated into the plate of the straight-plate wheel after 21 drag and 1,034 stop-braking cycles. In contrast, after a considerably longer testing period (115 drag- and 4,444 stop-braking cycles) no cracks propagated into the plate of either the S-shape or parabolic-plate wheel. These latter wheels did, however, develop thermal cracks on the tread because of the greater number of stop-braking cycles.

Photographs of the artificial defects after testing are shown in Figures 9.3 through 9.30. For convenience, these photos are grouped together in a sequence. None of the flange or back rim face slots developed crack extension. Of the tread slots, those at 45° and 135° were most susceptible to crack extension. Thermal cracks are also shown in the photographs.

9-11

TABLE 9.5

DYNAMOMETER TESTS OF WHEEL 43992 (STRAIGHT PLATE)

Test Sequence	No. of Drag	Test Stop	Total Drag	Test Stop	Observations
1	5		5		
2		312		312	135° Shim Out
3	7		12		
4		468		779	45° 1/8" Long Crack
5	4		16		
6		225		1034	45° Crack Extends Across Tread, Sonic 1/4" Deep
7	5		21		45° Fracture to RPF*

* Rim Plate Fillet

TABLE 9.6

DYNAMOMETER TESTS OF WHEEL 95529 (PARABOLIC PLATE)

Test Sequence	No. of Drag	Test Stop	Total Drag	Test Stop	Observations
1	5		5		
2		312		312	
3	7		12		
4		467		779	135° 1/8" + 1/8" Long Cracks 315° 1/8" + 1/2" Long Cracks
5	4		16		
6		255		1034	45° 1/16" Long Crack 135° 1/4" + 1/4" Long Cracks 315° 1/8" + 1/2" Long Cracks
7	6		22		
8		251		1285	Same
9	5		27		
10		250		1535	Same
11	5		32		
12		410		1945	45° 1/4" + 1/4" Long Cracks 135° 1/2" + 1/2" Long Cracks 315° 7/8" Long Crack 45°-135° TC* on Tread Near Flange
13	5		37		Same
14		250		2195	Same
15	5		42		Same
16		250		2445	Same
17	5		47		
18		250		2695	
19	5		52		45° Shim Out 45°-135° More Extensive Thermal Cracking
20		1749		4444	
21	63		115		

* Thermal Crack

TABLE 9.7

DYNAMOMETER TESTS OF WHEEL 5530 ("S" PLATE)

Test Sequence	No. of Drag	Test Stop	Total Drag	Test Stop	Observations
1	5		5		
2		312		312	
3	7		12		
4		467		779	
5	4		16		
6		255		1034	135° 1/8" Long Crack
7	6		22		
8		251		1285	
9	5		27		
10		250		1535	45° 1/8" Long Crack & Shim Out 135° 1/4" Long Crack & T.C.
11	5		32		
12		250		1945	45° 3/16" Long Crack 135° 3/8" Long Crack
13	5		37		
14		250		2195	T.C.
15	5		42		
16		250		2445	T.C.
17	5		47		
18		250		2695	T.C.
19	5		52		
20		1749		4444	45° 1/4" Long Crack 135° 17/32" Long Crack & Shim Out
21	63		115		45° 1/4" Long Crack 135° 17/32" Long Crack
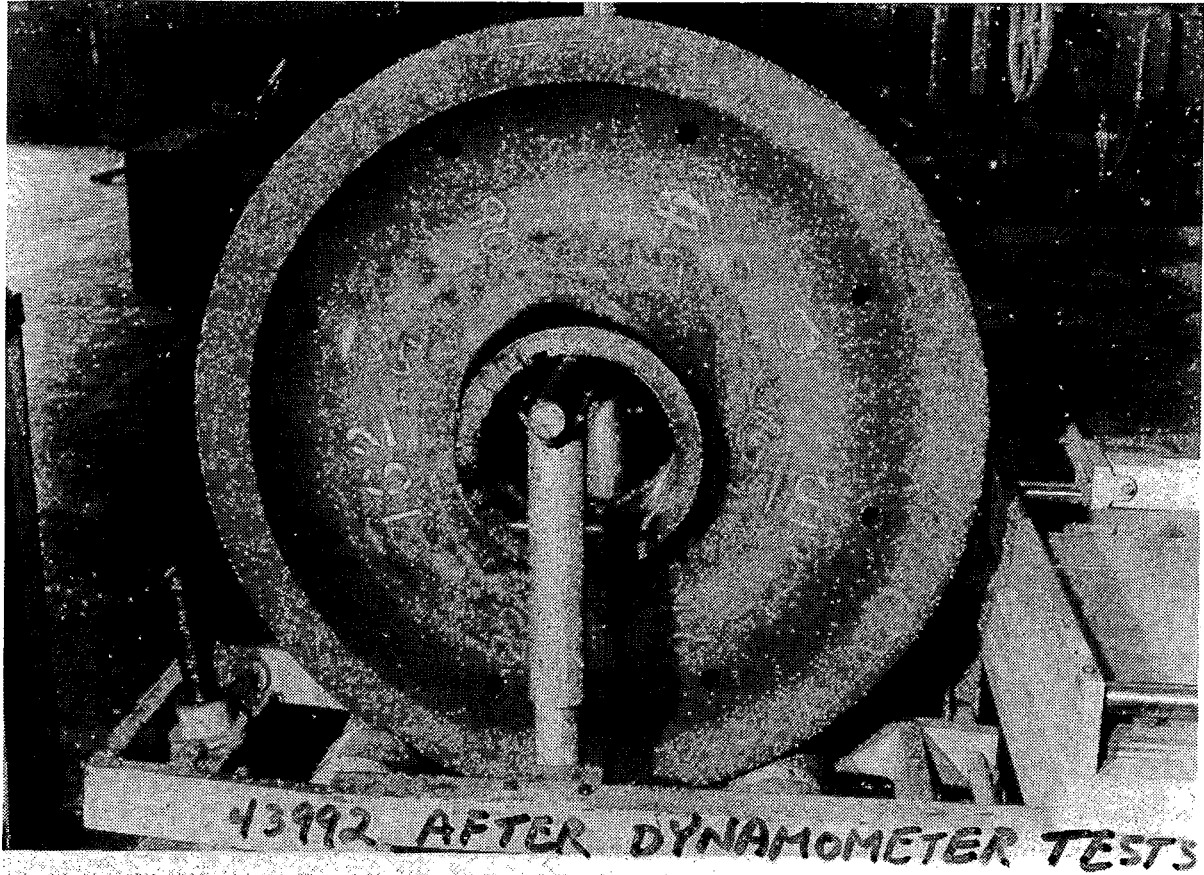
FIGURE 9.3   BACK FACE OF WHEEL 43992 AFTER DYNAMOMETER TESTS

FIGURE 9.4   FRONT FACE OF WHEEL 43992 AFTER DYNAMOMETER TESTS
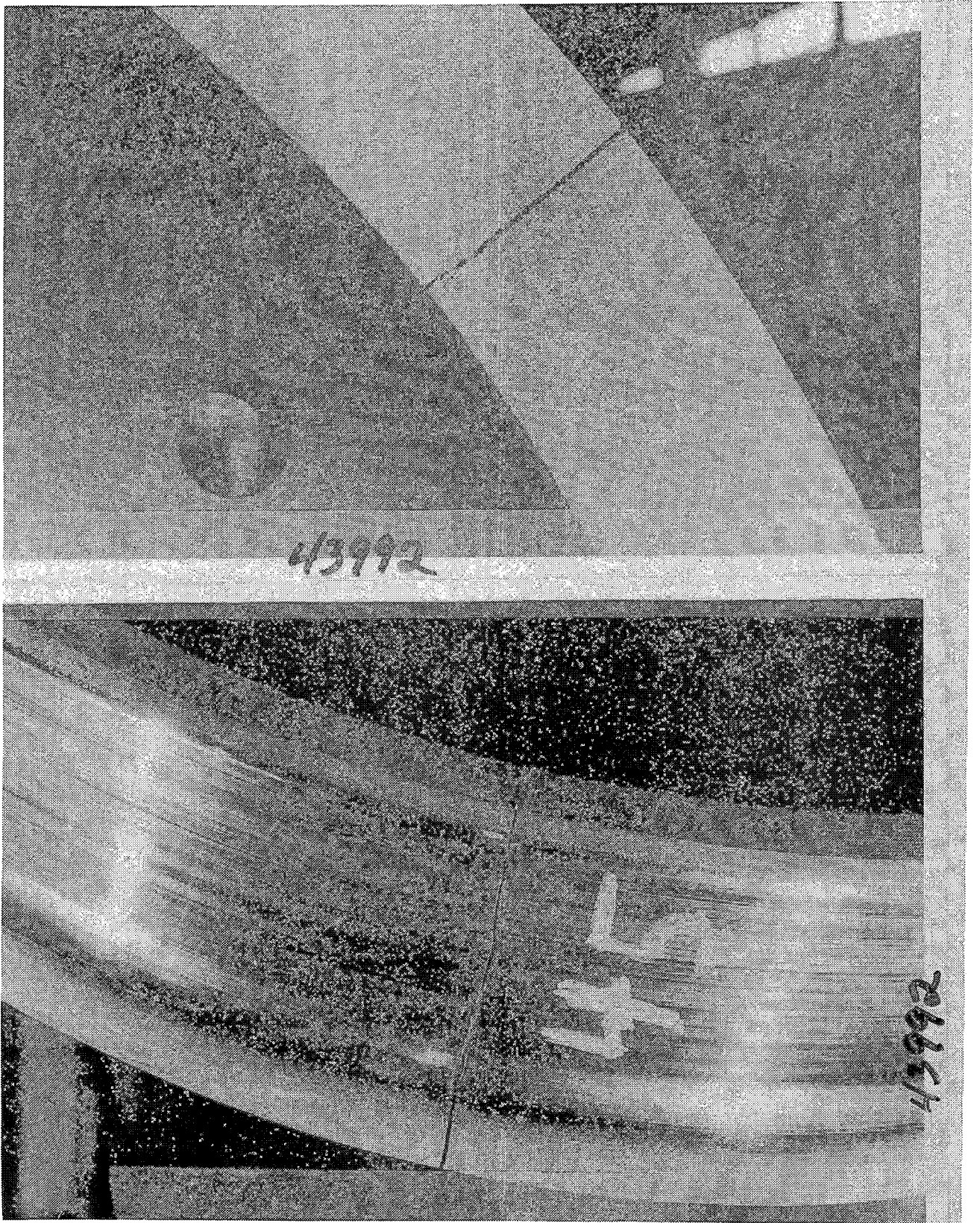
FIGURE 9.5   RIM OF WHEEL 43992 AT 45° POSITION AFTER
               DYNAMOMETER TESTS
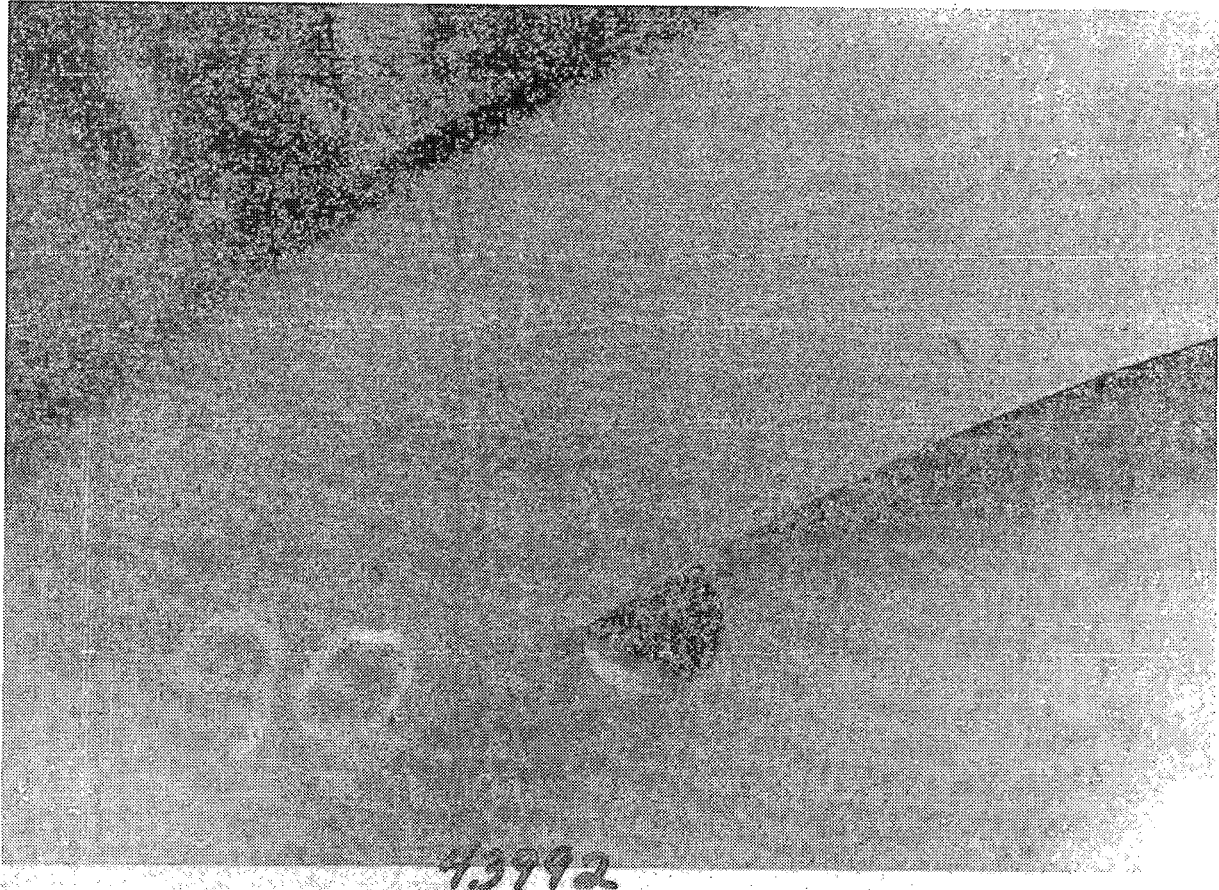
FIGURE 9.6   RIM OF WHEEL 43992 AT 90° POSITION AFTER
DYNAMOMETER TESTS

9-18
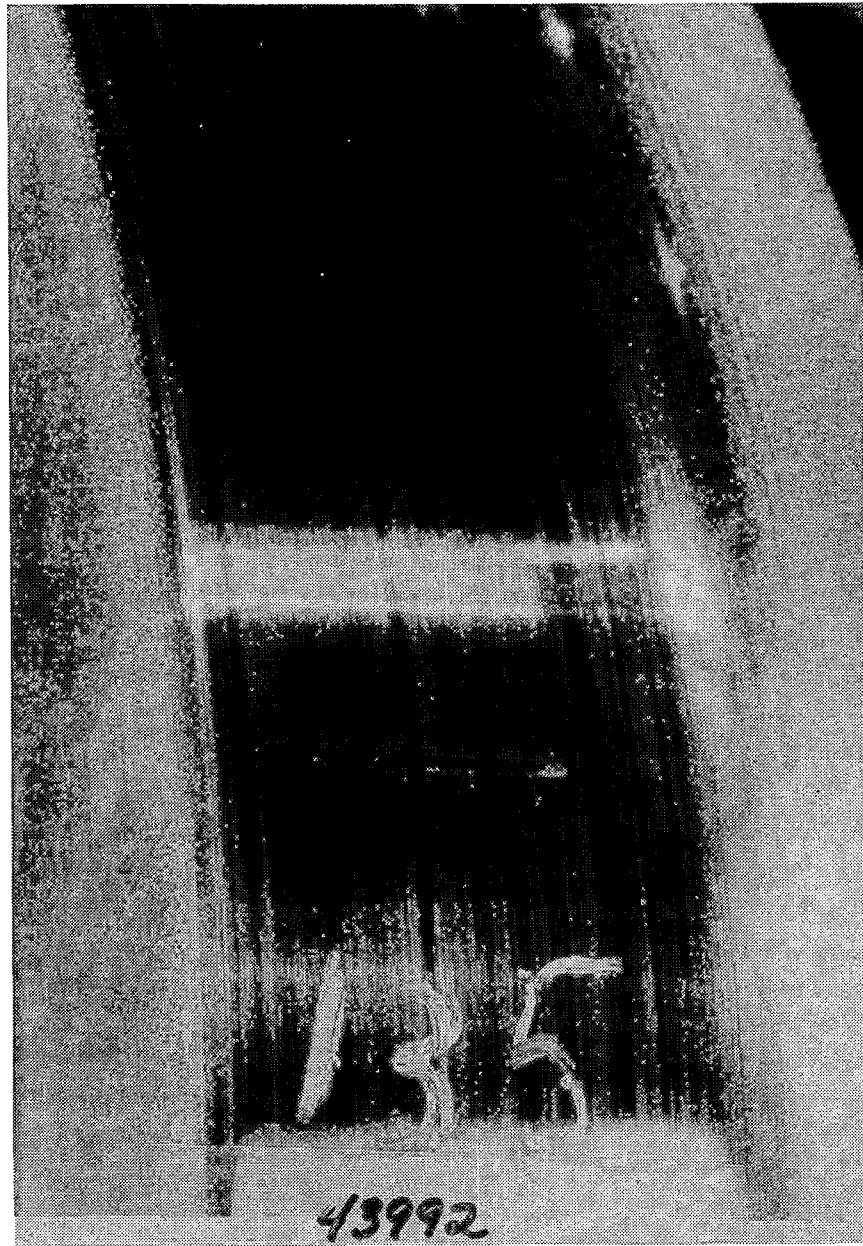
FIGURE 9.7   RIM OF WHEEL 43992 AT 135° POSITION AFTER
DYNAMOMETER TESTS
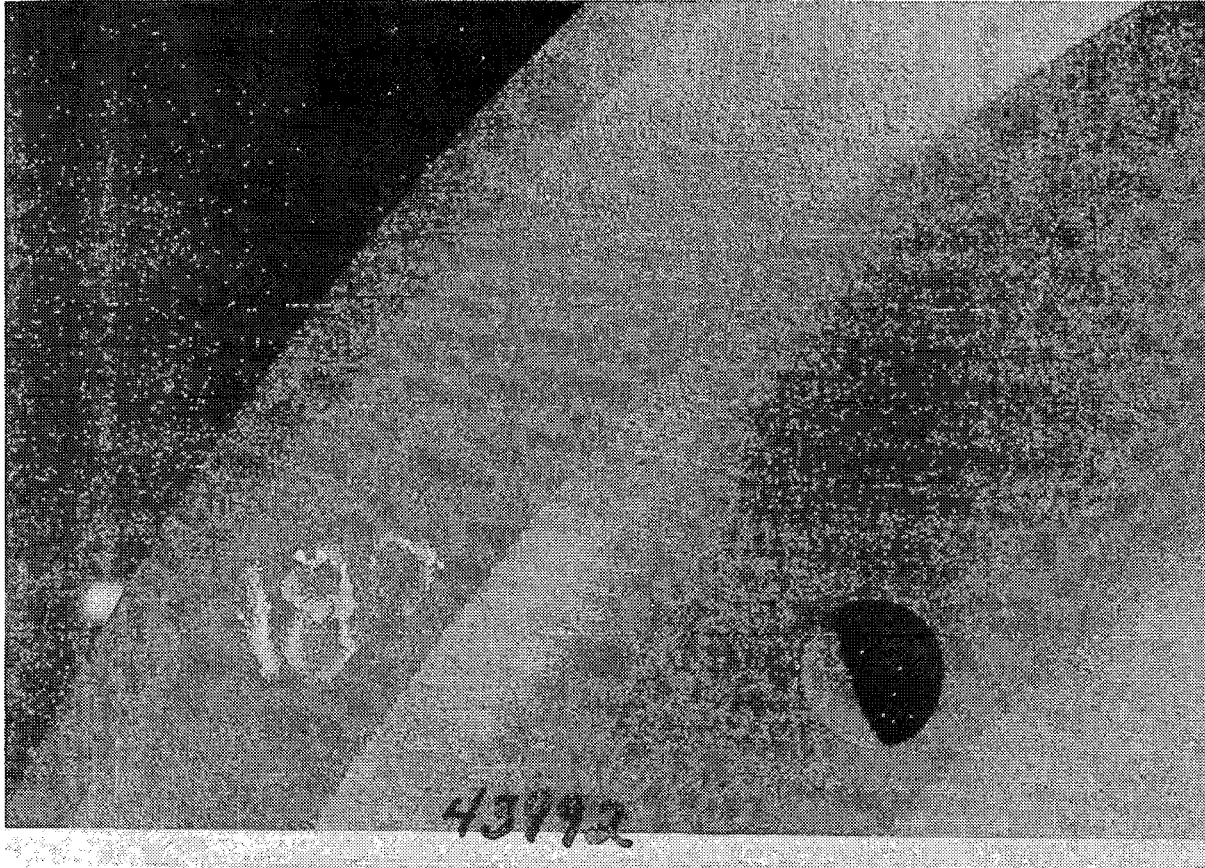
FIGURE 9.8   RIM OF WHEEL 43992 AT 180° POSITION AFTER
             DYNAMOMETER TESTS

9-20
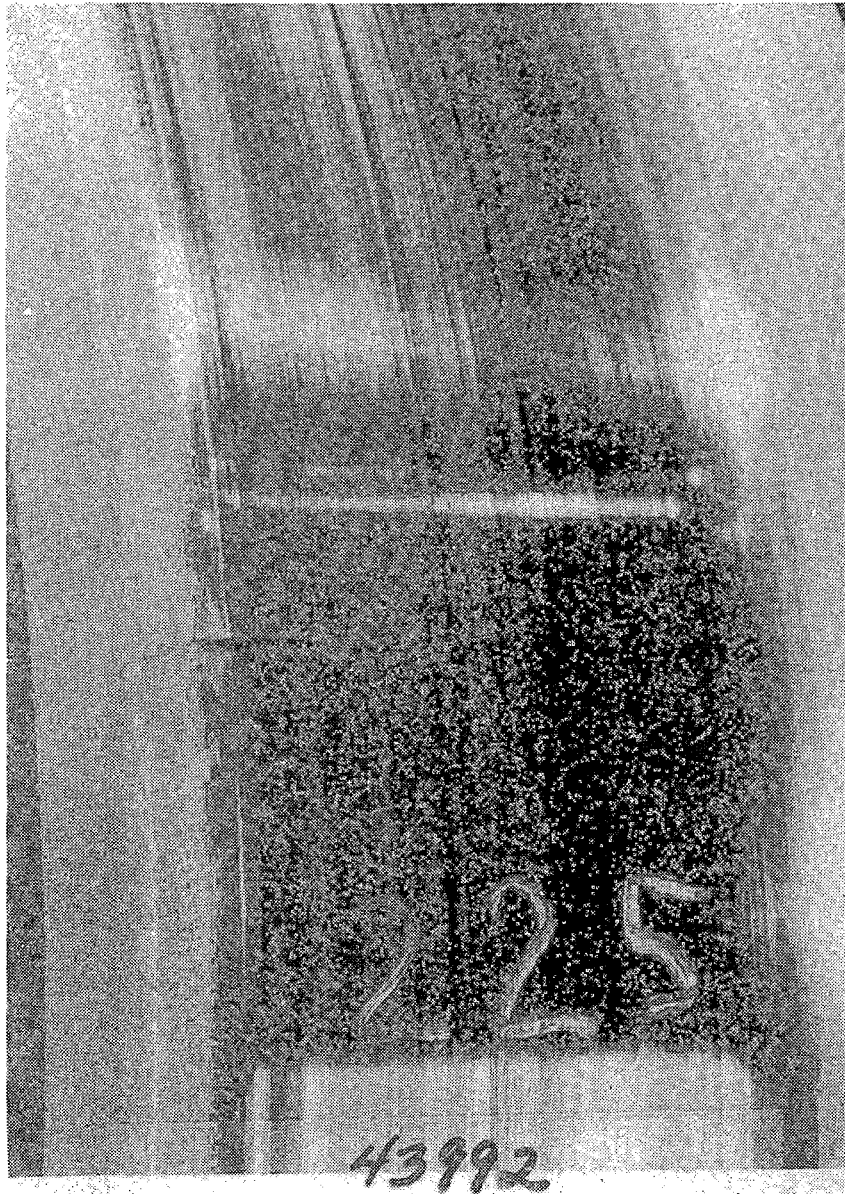
FIGURE 9.9   RIM OF WHEEL 43992 AT 225° POSITION AFTER
              DYNAMOMETER TESTS

9-21

FIGURE 9.10   RIM OF WHEEL 43992 AT 270° POSITION AFTER
DYNAMOMETER TESTS

FIGURE 9.11   RIM OF WHEEL 43992 AT 315° POSITION AFTER
               DYNAMOMETER TESTS
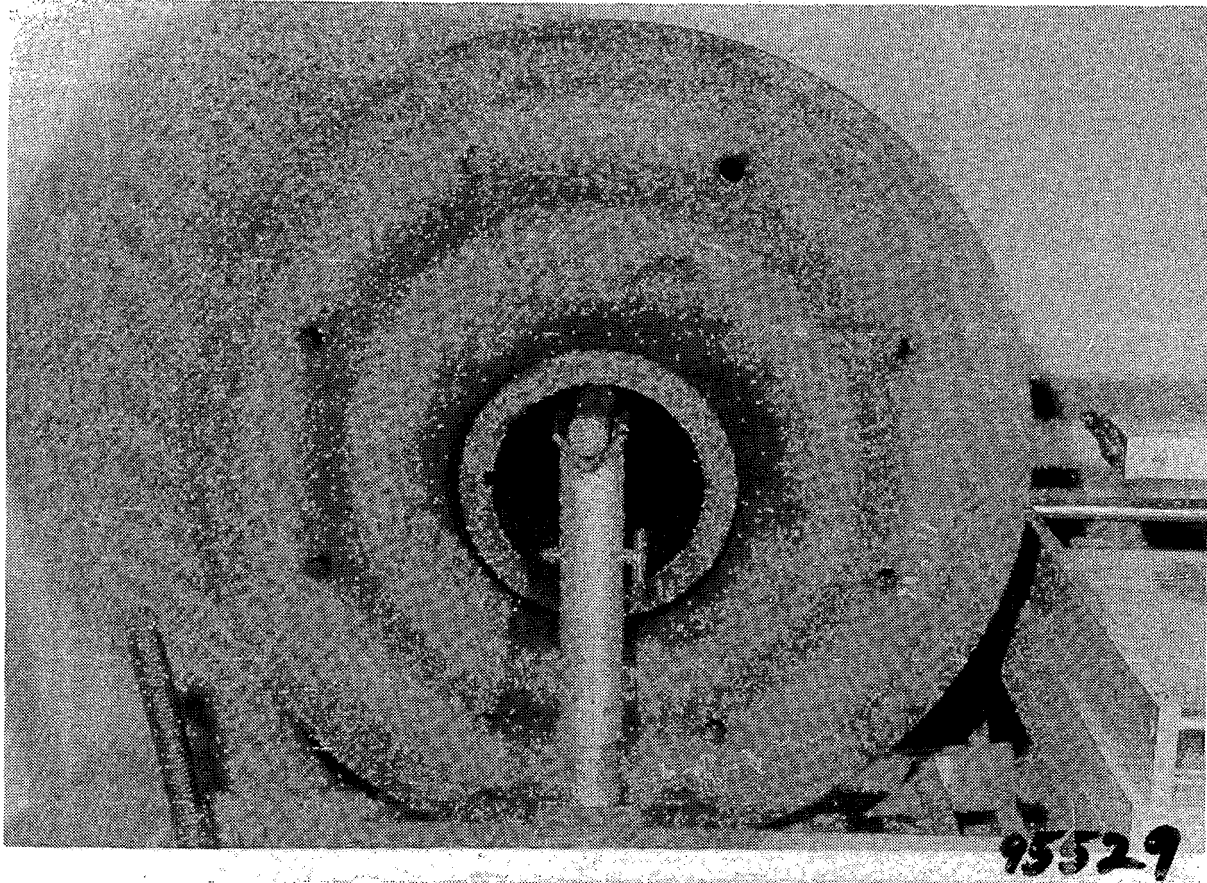
FIGURE 9.12   BACK FACE OF WHEEL 95529 AFTER DYNAMOMETER TESTS
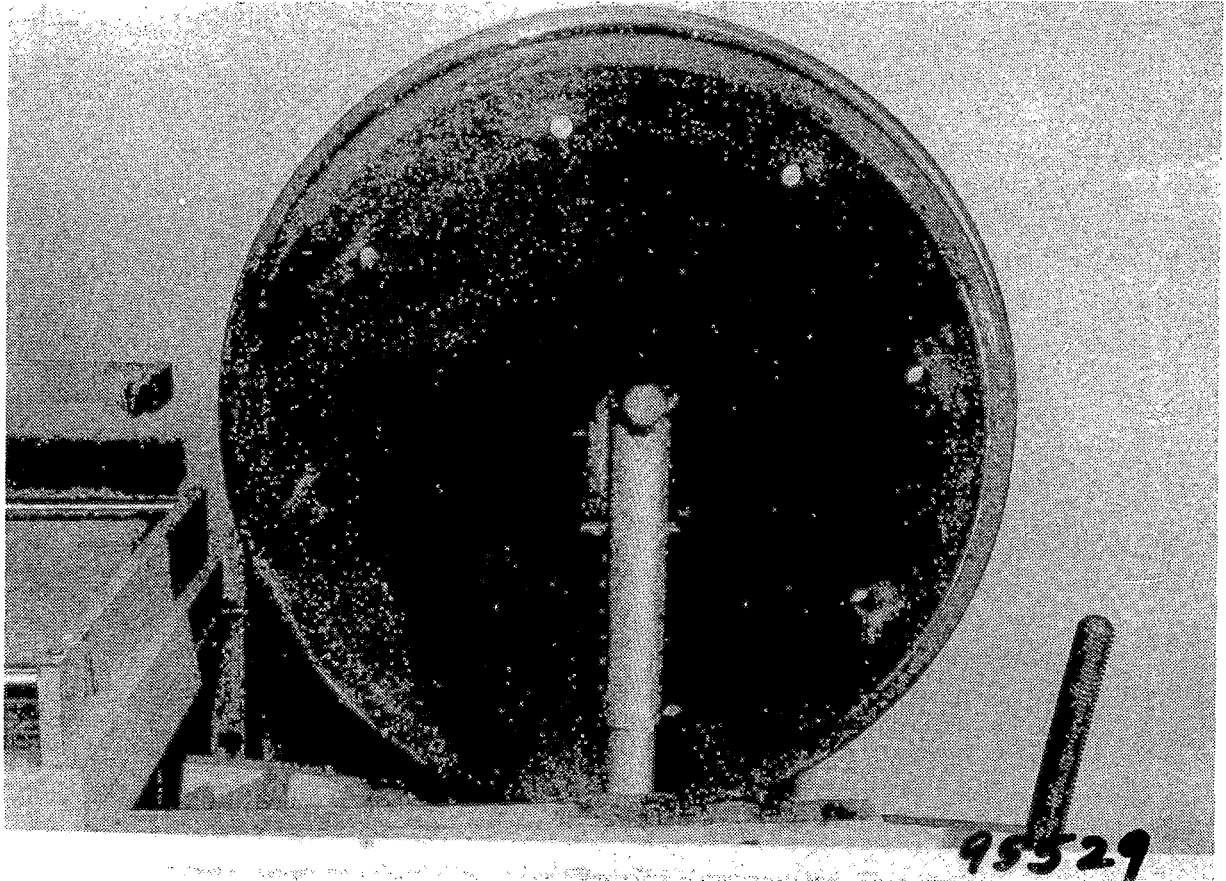
FIGURE 9.13   FRONT FACE OF WHEEL 95529 AFTER DYNAMOMETER TESTS
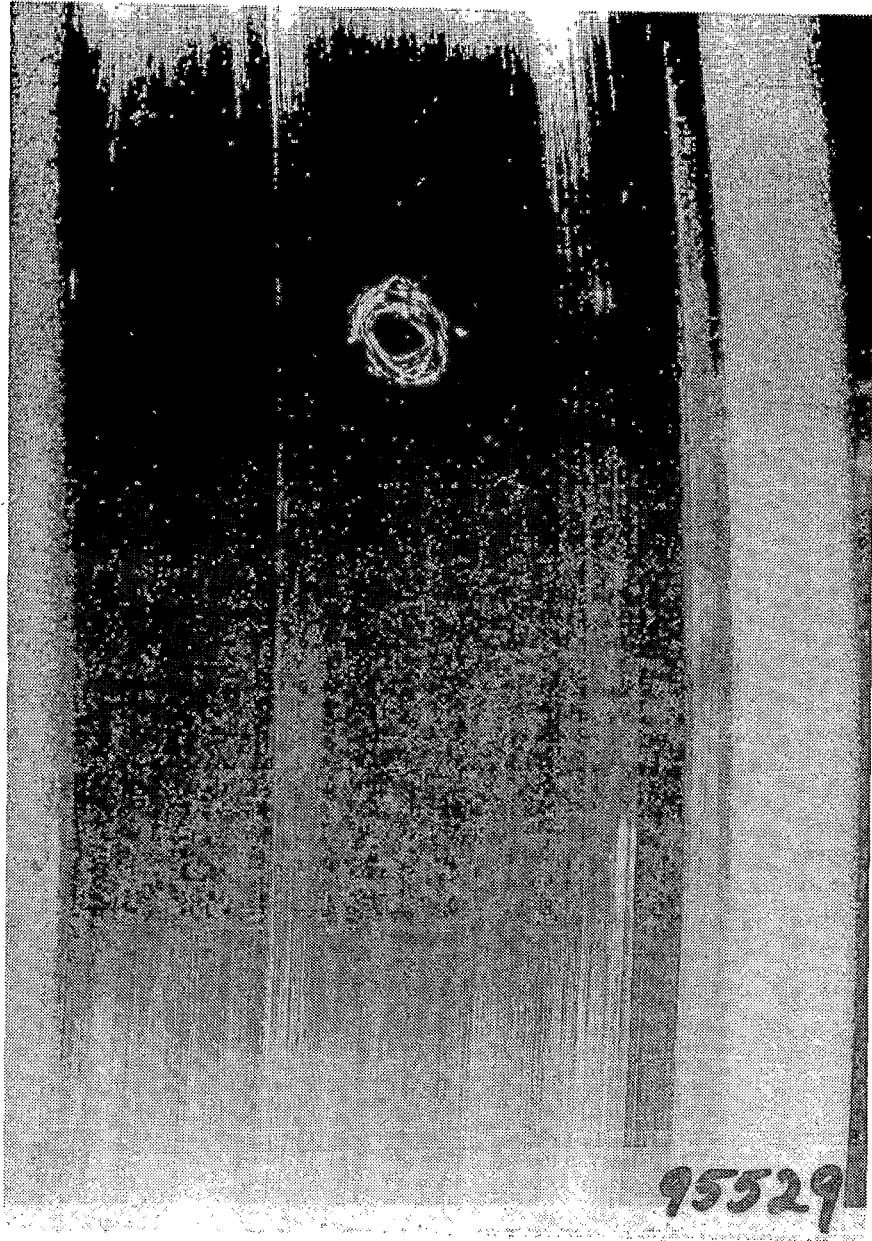
FIGURE 9.14   RIM OF WHEEL 95529 AT 0° POSITION AFTER
DYNAMOMETER TESTS
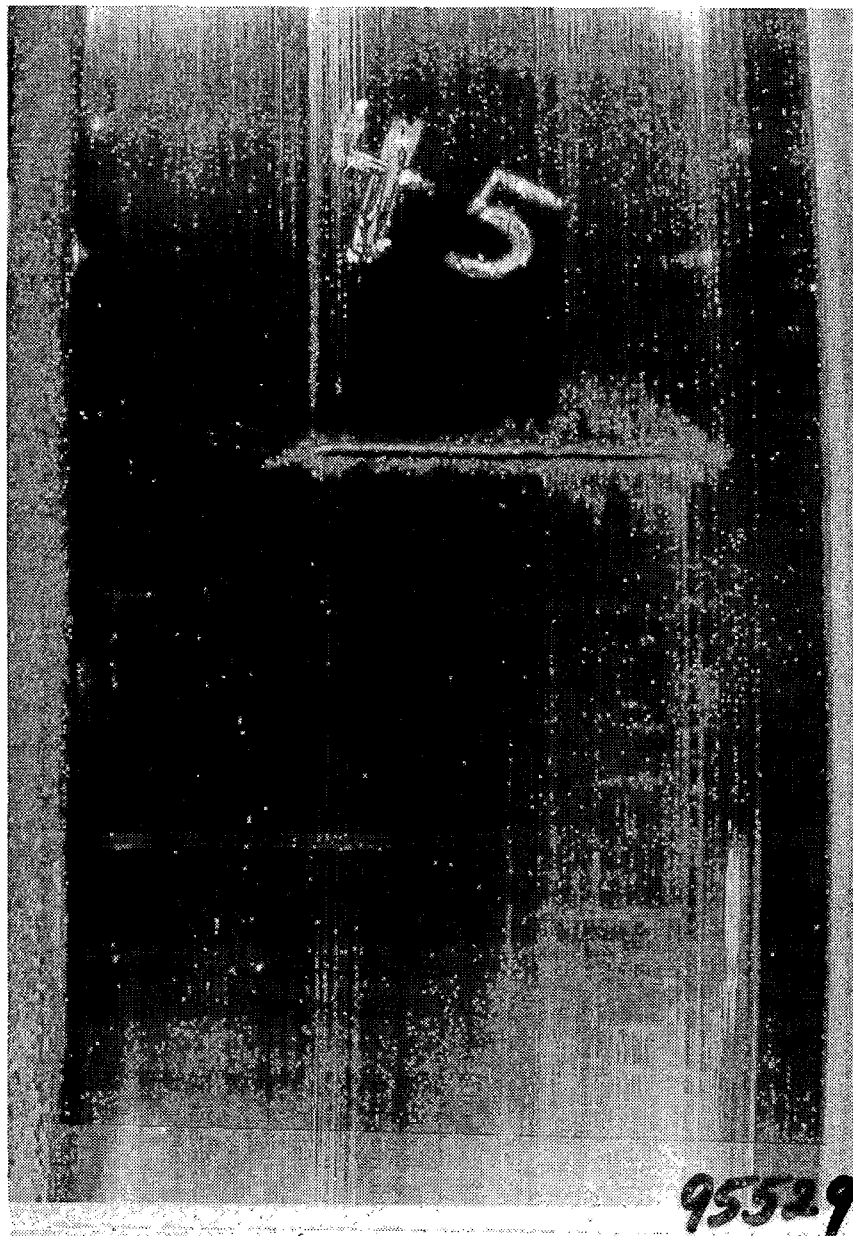
FIGURE 9.15   RIM OF WHEEL 95529 AT 45° POSITION AFTER
DYNAMOMETER TESTS
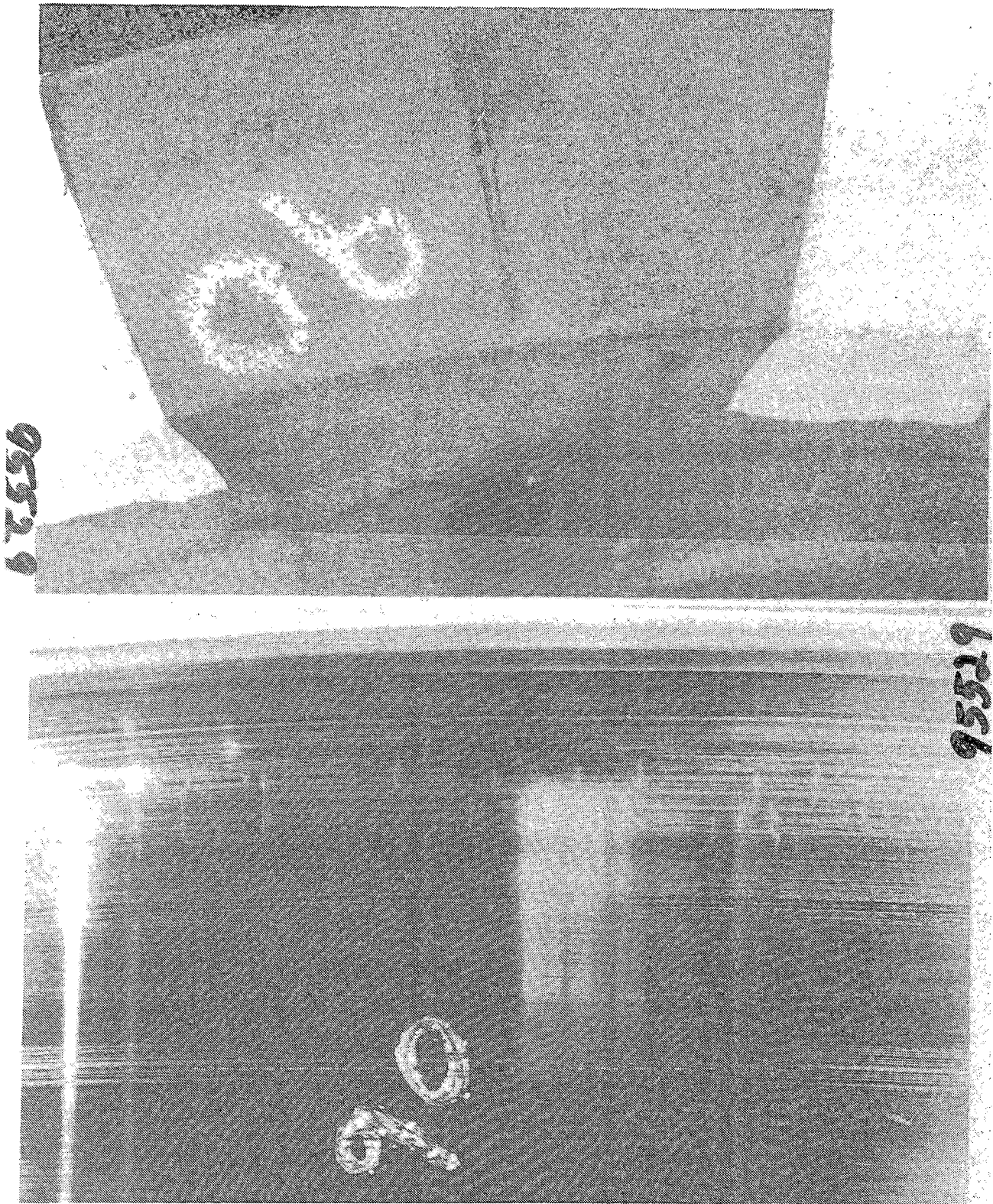
FIGURE 9.16   RIM OF WHEEL 95529 AT 90° POSITION AFTER DYNAMOMETER TESTS
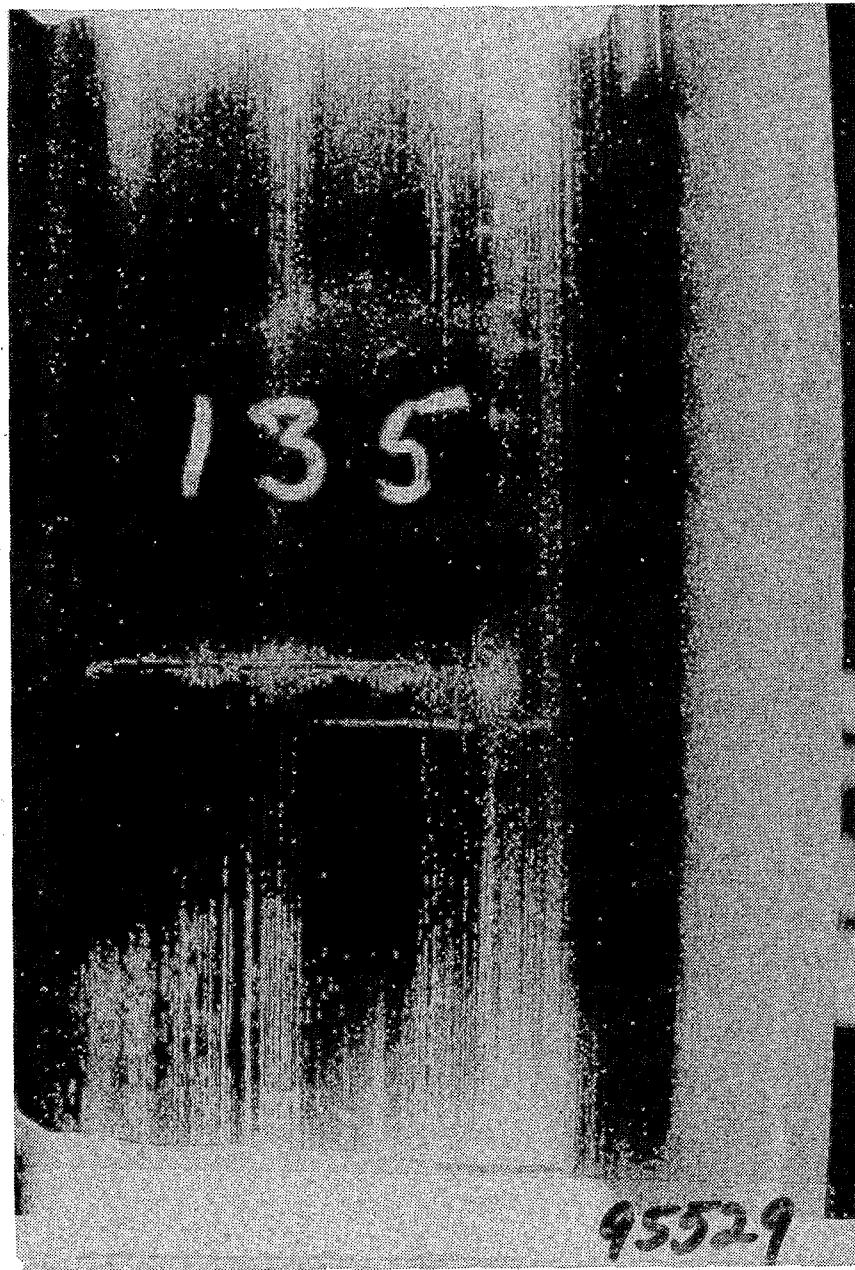
FIGURE 9.17   RIM OF WHEEL 95529 AT 135° POSITION AFTER
DYNAMOMETER TESTS
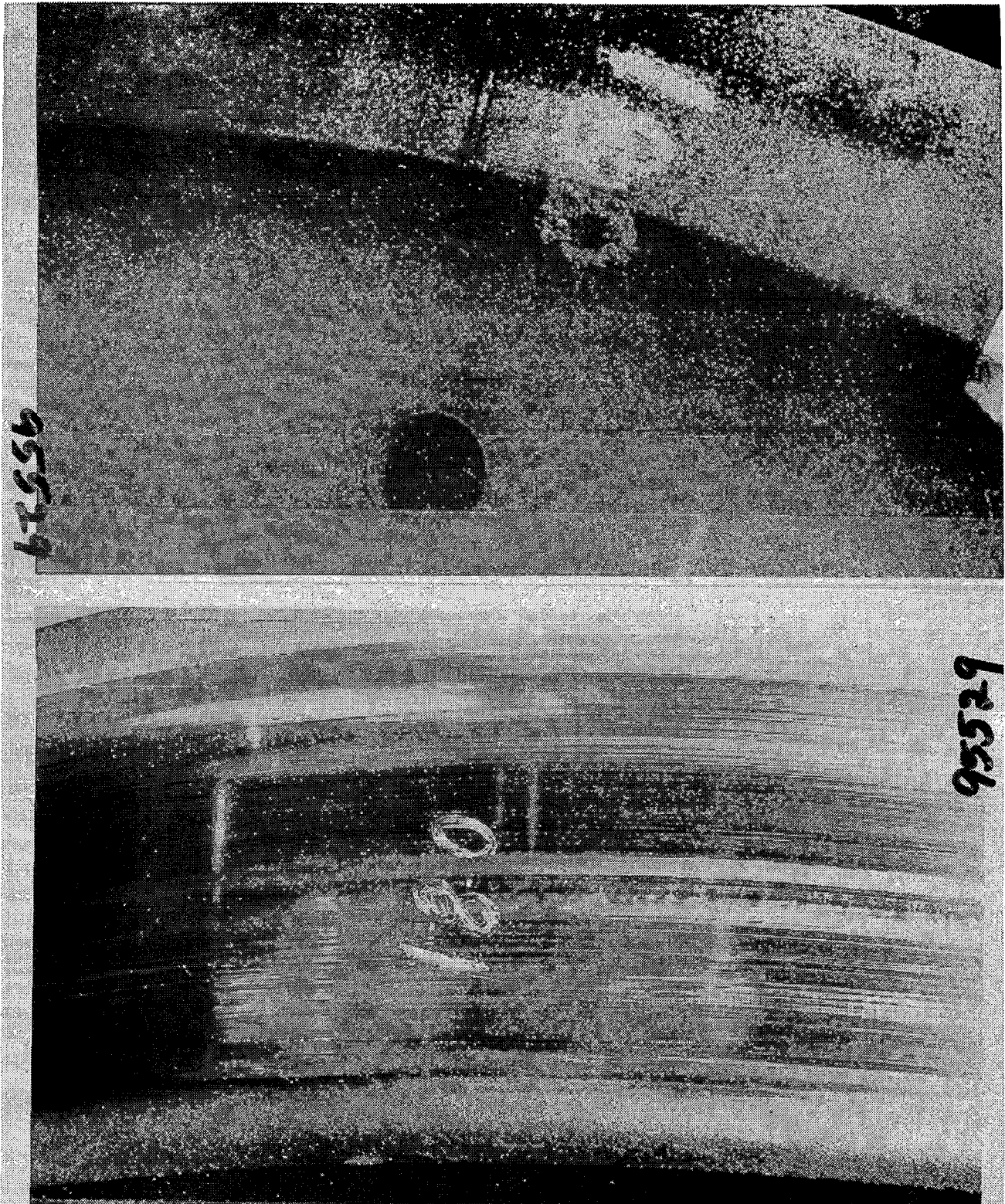
FIGURE 9.18   RIM OF WHEEL 95529 AT 180° POSITION AFTER
DYNAMOMETER TESTS
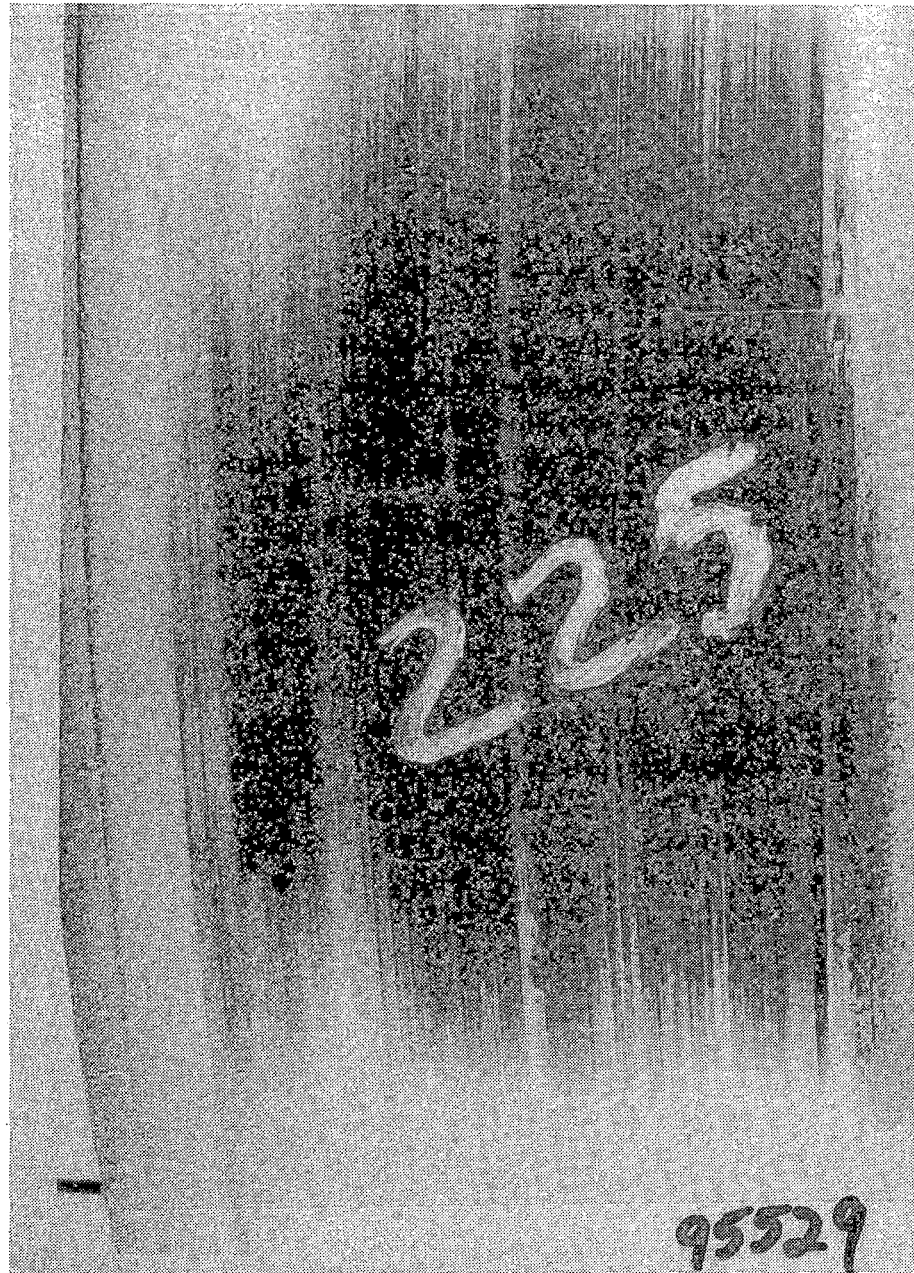
FIGURE 9.19   RIM OF WHEEL 95529 AT 225° POSITION AFTER
                DYNAMOMETER TESTS
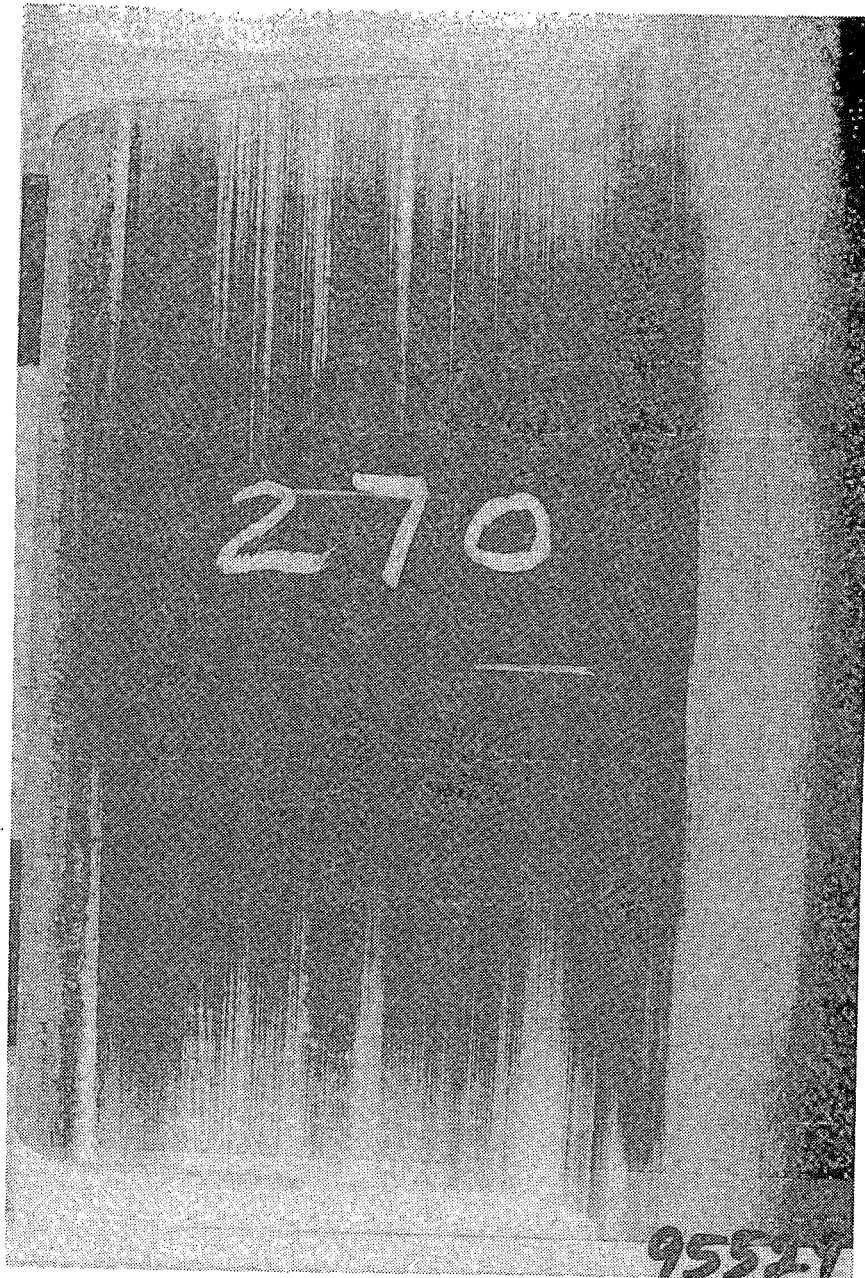
FIGURE 9.20   RIM OF WHEEL 95529 AT 270° POSITION AFTER
DYNAMOMETER TESTS
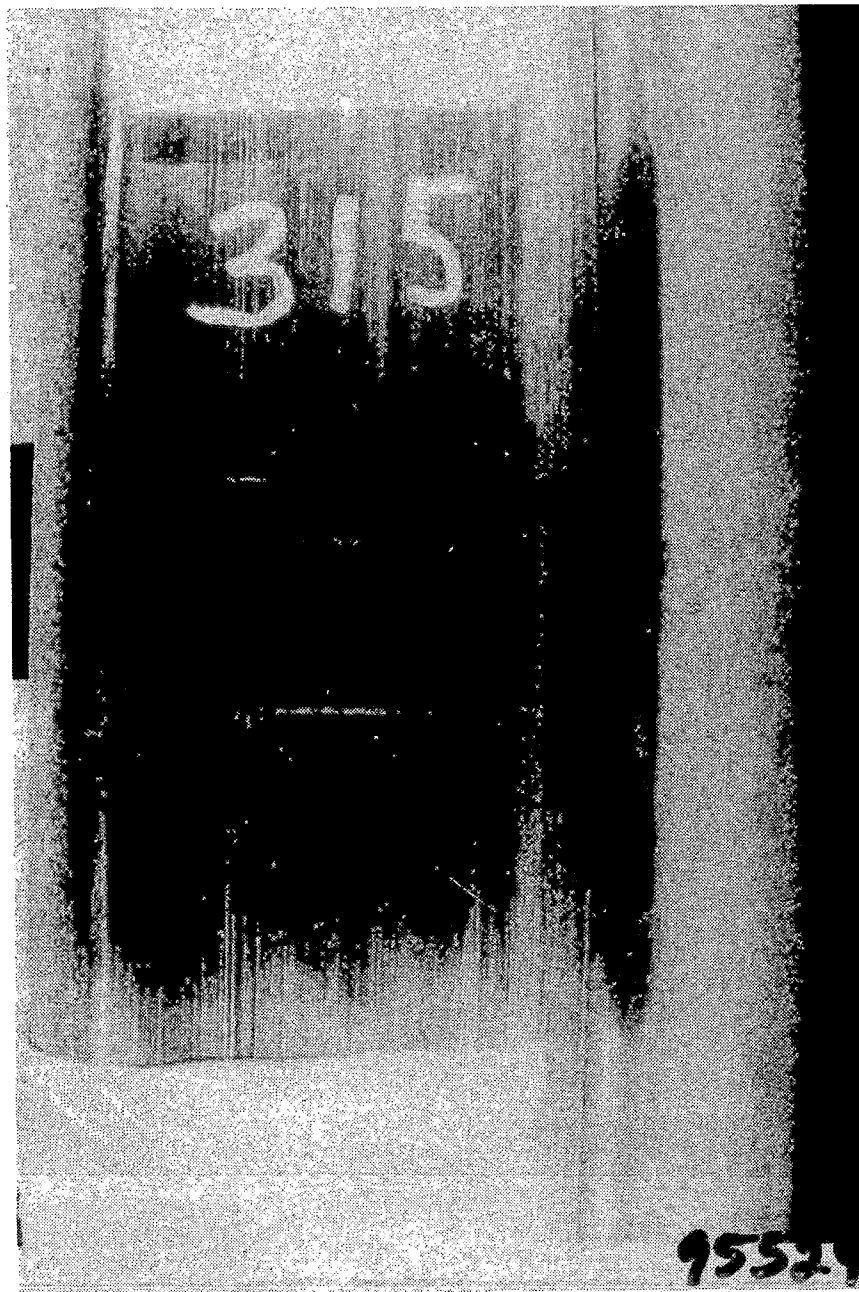
FIGURE 9.21   RIM OF WHEEL 95529 AT 315° POSITION AFTER
DYNAMOMETER TESTS
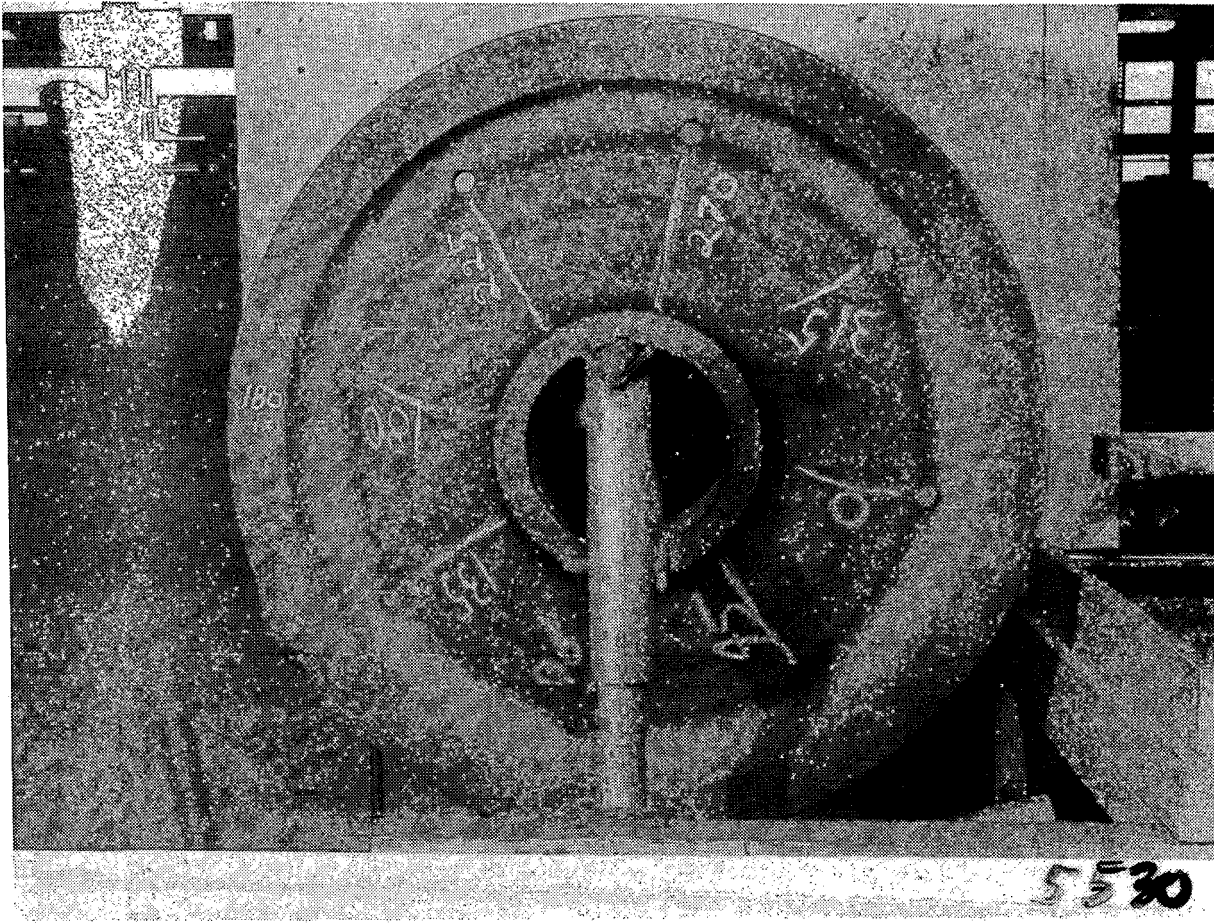
FIGURE 9.22   BACK FACE OF WHEEL 5530 AFTER DYNAMOMETER TESTS
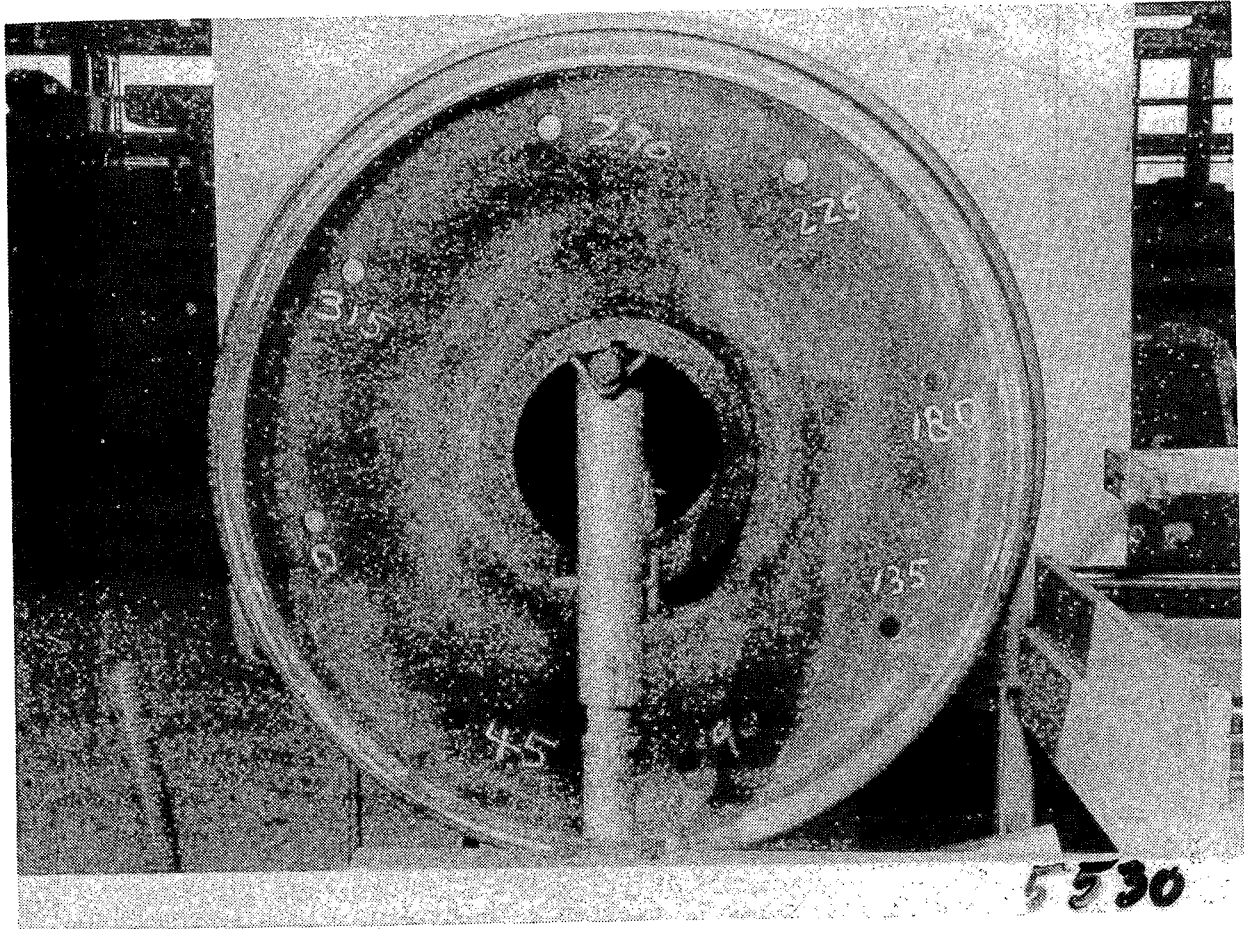
FIGURE 9.23   FRONT FACE OF WHEEL 5530 AFTER DYNAMOMETER TESTS
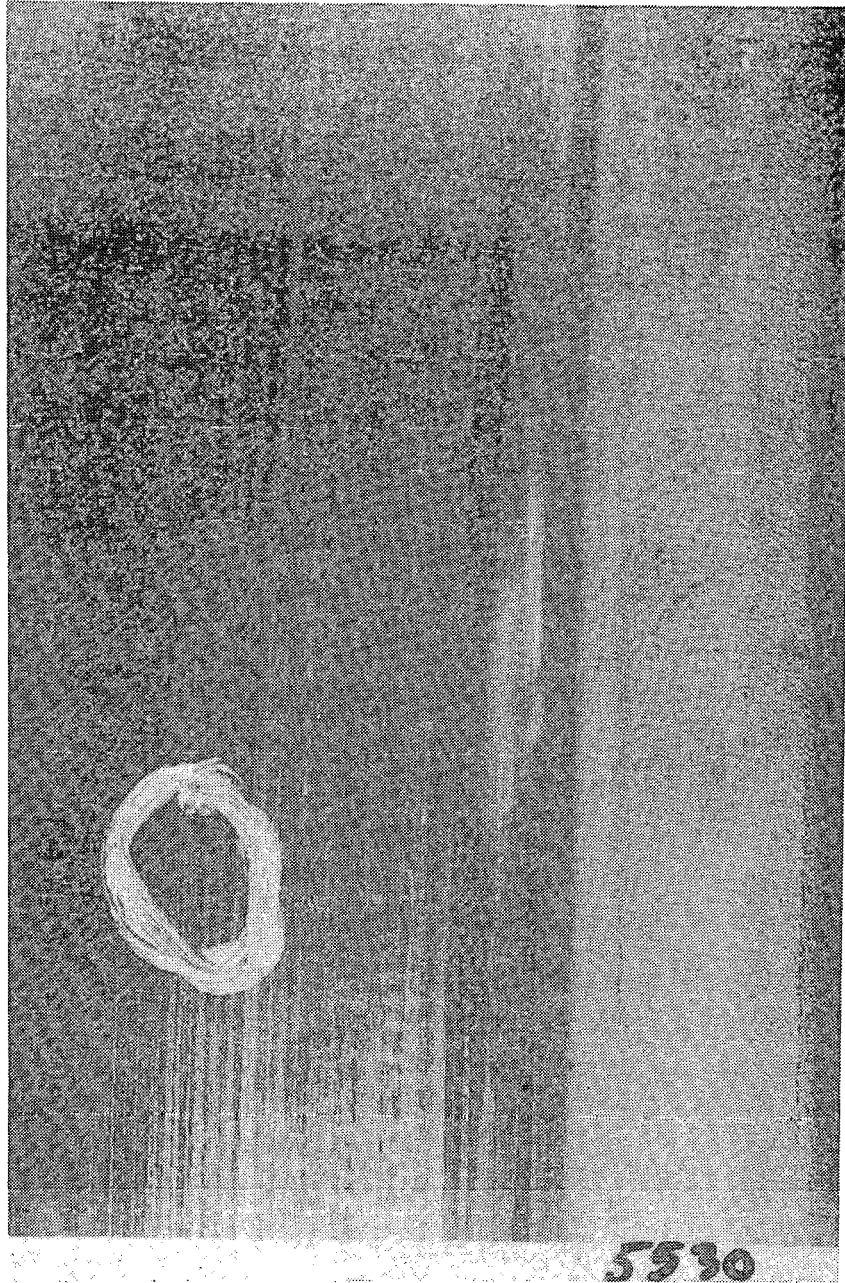
FIGURE 9.24   RIM OF WHEEL 5530 AT 0° POSITION AFTER
DYNAMOMETER TESTS
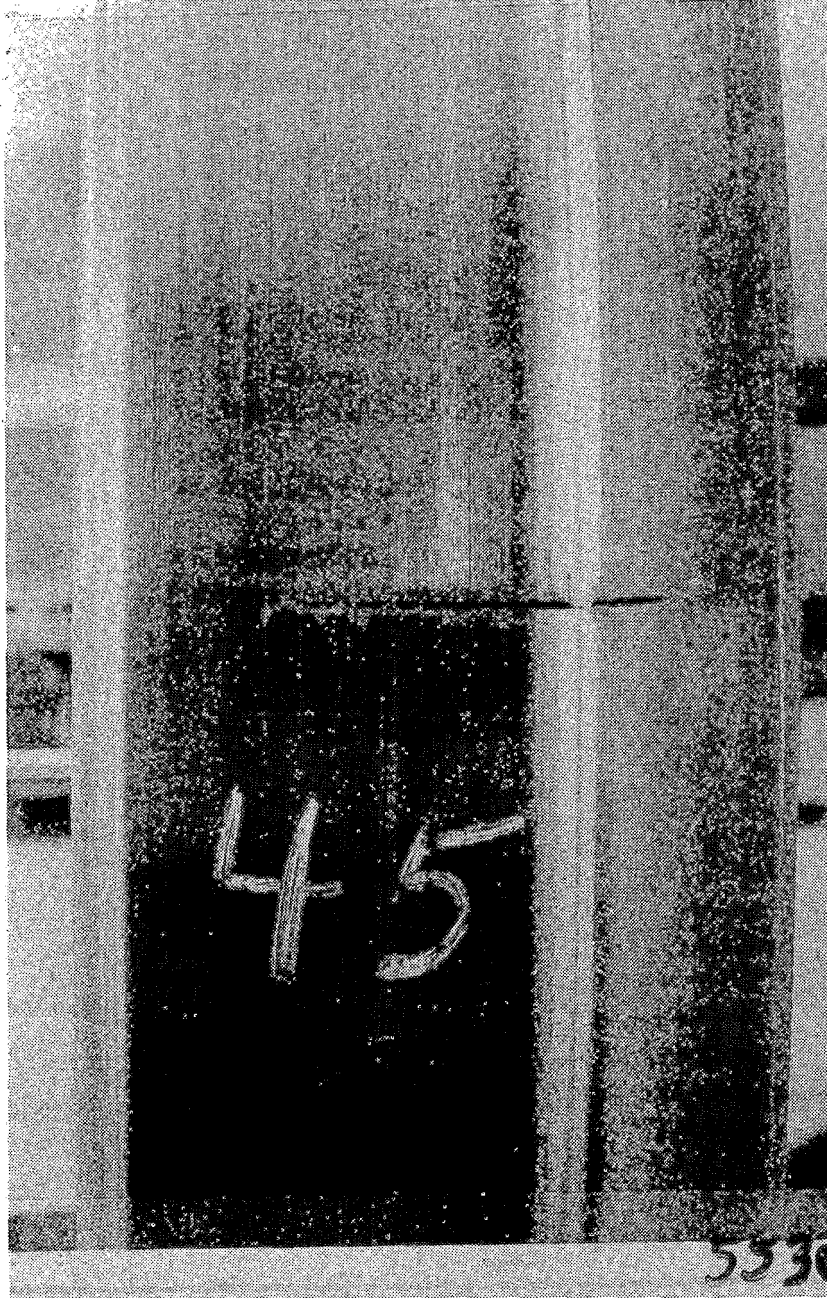
FIGURE 9.25   RIM OF WHEEL 5530 AT 45° POSITION AFTER
DYNAMOMETER TESTS

9-37
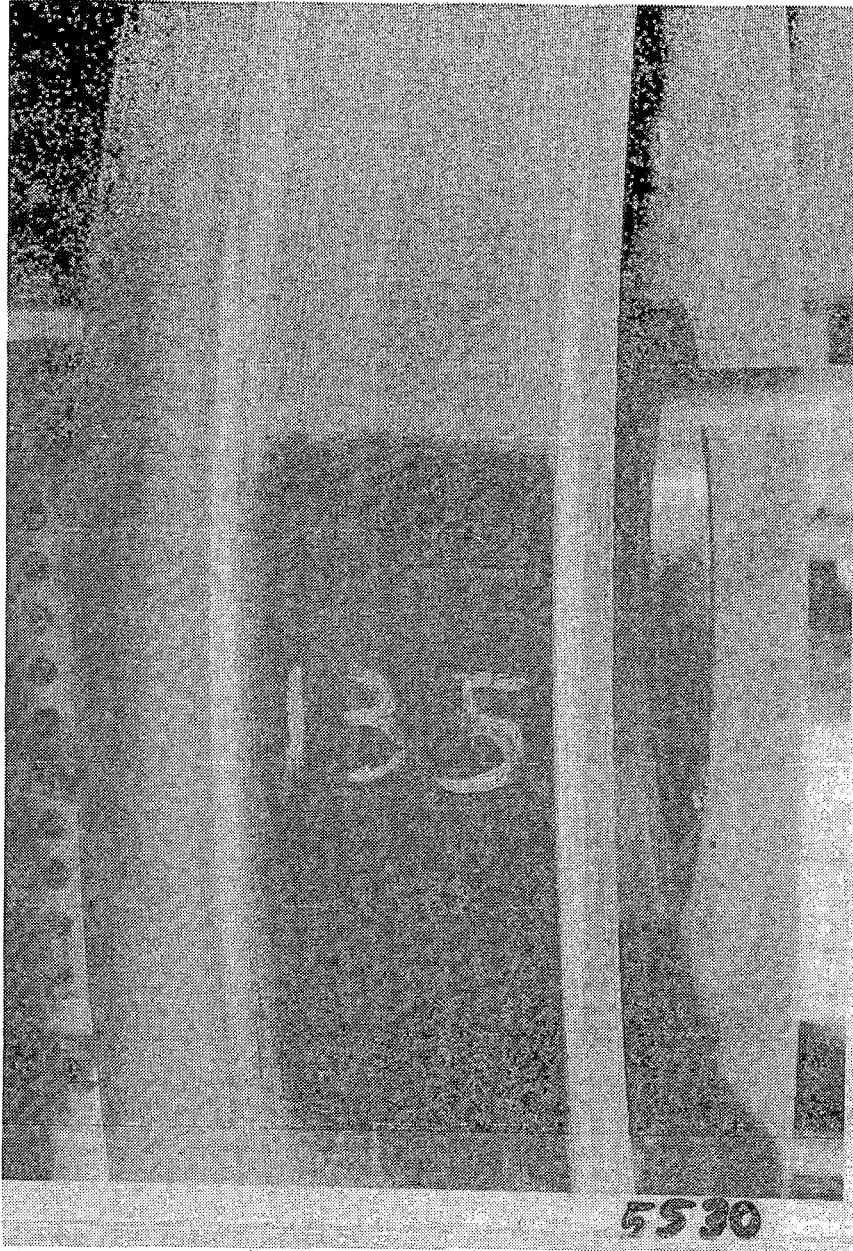
FIGURE 9.26   RIM OF WHEEL 5530 AT 135° POSITION AFTER
DYNAMOMETER TESTS
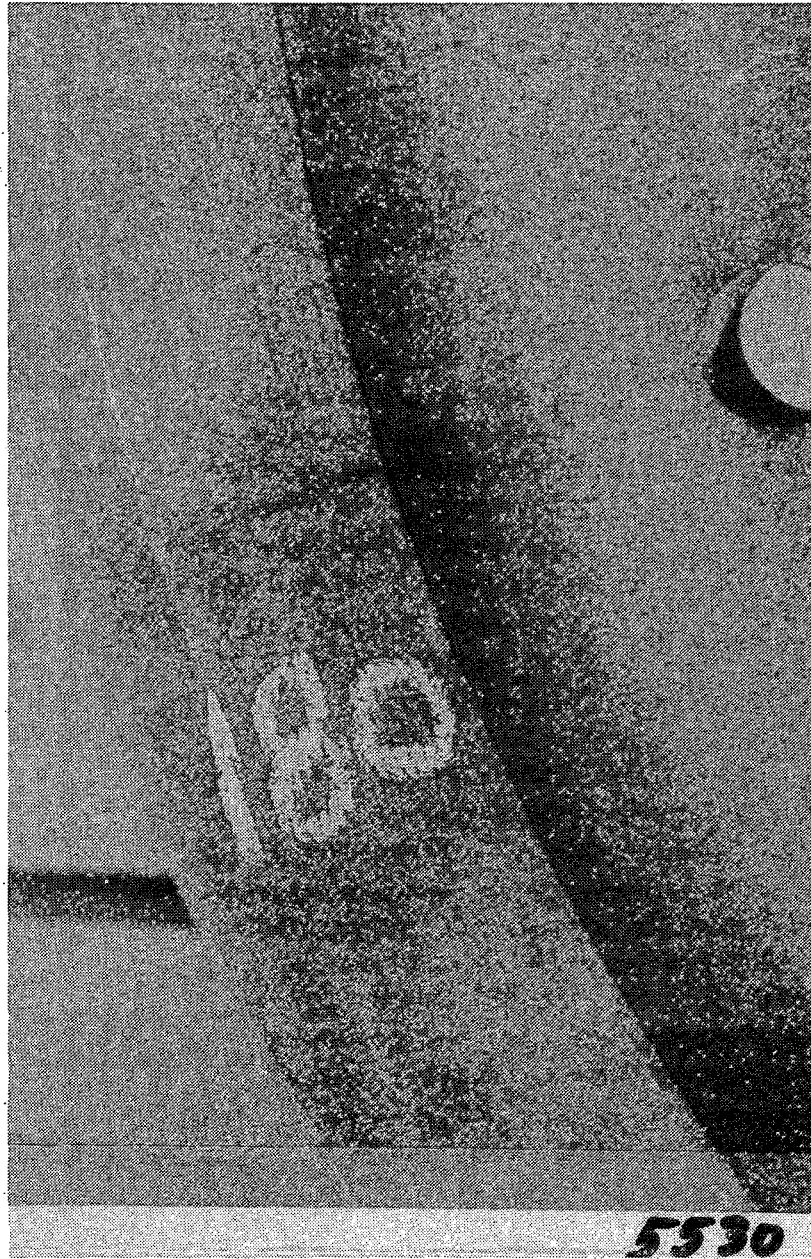
FIGURE 9.27   RIM OF WHEEL 5530 AT 180° POSITION AFTER
DYNAMOMETER TESTS
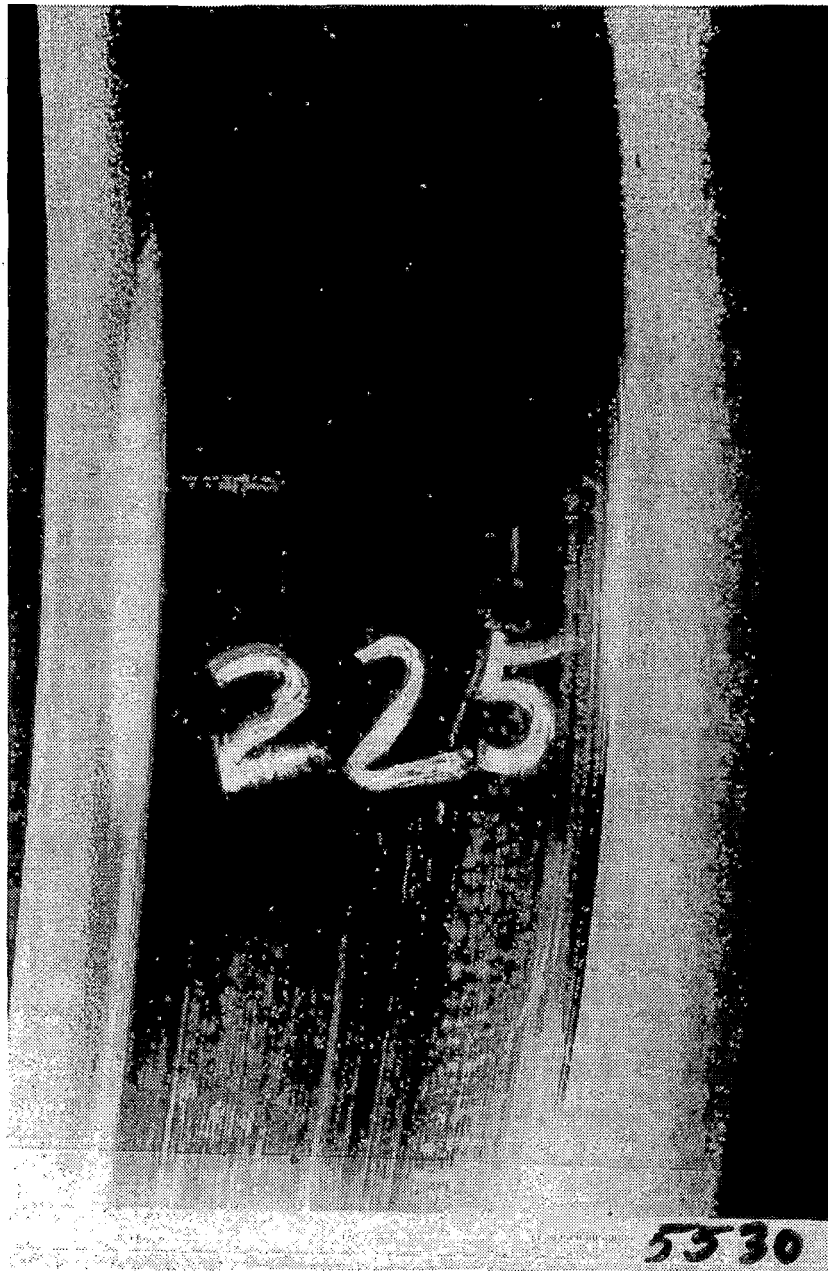
FIGURE 9.28   RIM OF WHEEL 5530 AT 225° POSITION AFTER
DYNAMOMETER TESTS
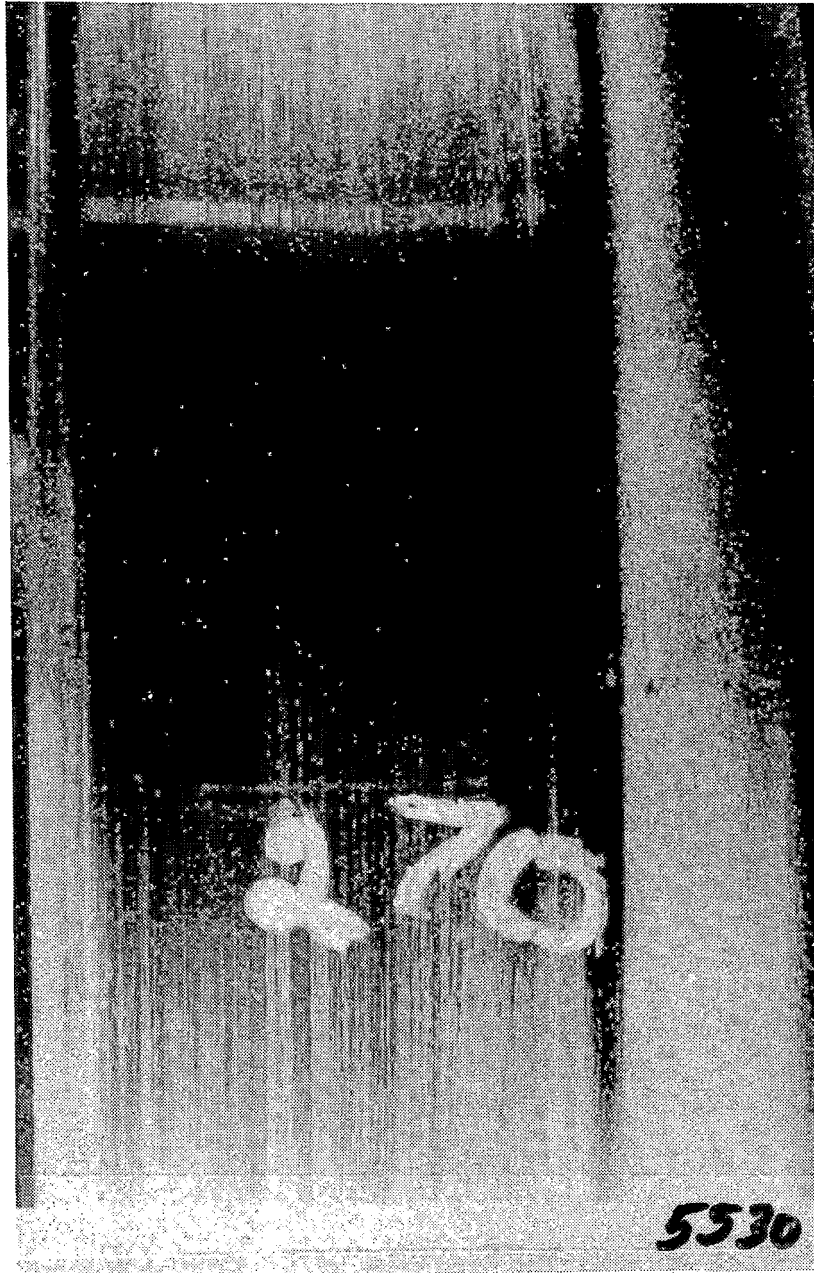
FIGURE 9.29   RIM OF WHEEL 5530 AT 270° POSITION AFTER
                DYNAMOMETER TESTS
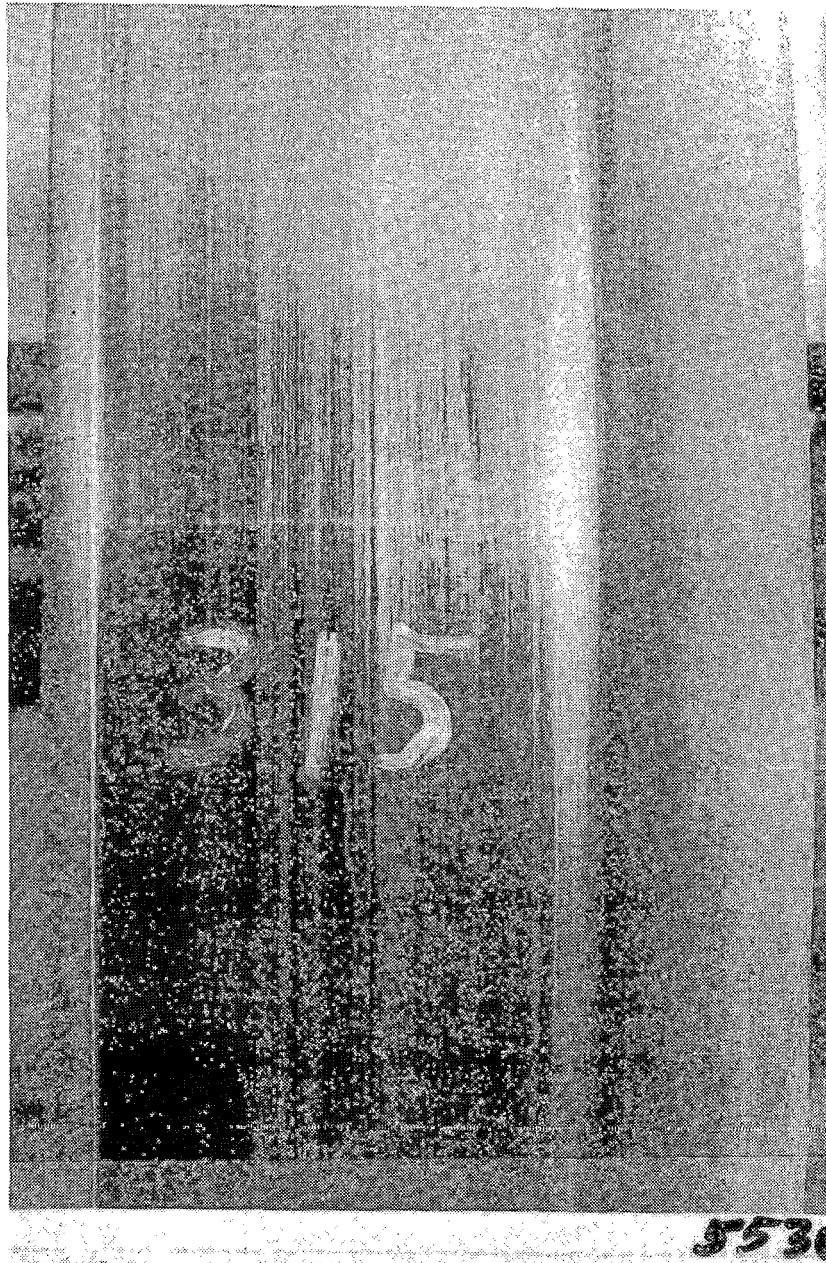
FIGURE 9.30   RIM OF WHEEL 5530 AT 315° POSITION AFTER
DYNAMOMETER TESTS

The welding arc burn in the straight-plate wheel developed a thermal crack. No cracks initiated at the arc-weld arc burns in the S-shape and parabolic plate wheels.

Visual examination of the fracture surface of the crack that propagated to the plate of the straight-plate wheel, Figure 9.31, showed that the crack extended from the slot by fatigue for a distance of about 1/16 inch. The fracture then proceeded from this front by cleavage in at least four steps with termination at the hole in the plate. Examination with the SEM (scanning electron microscope) failed to detect the fatigue portion of the fracture or the arrest and reinitiation lives of the cleavage fracture.

9.1.4 Summary

One J-33 Class C (straight plate) wheel was subjected to 360 full-service stops and 436 emergency stops on the dynamometer. Small thermal cracks were detected after this exposure. This result indicates the severity and number of stops required to initiate thermal cracks in this wheel.

Three J-33 (CJ-33) Class U wheels (straight, S-shape, and parabolic-plate) were prepared with seven artificial cracks and one arc weld burn in the rim. The wheels were subjected to alternating series of drag and full-service stop-braking cycles to determine the relative crack propagation tendencies of the artificial cracks for the three wheel types. A crack propagated into the plate of the straight-plate wheel from an artificial
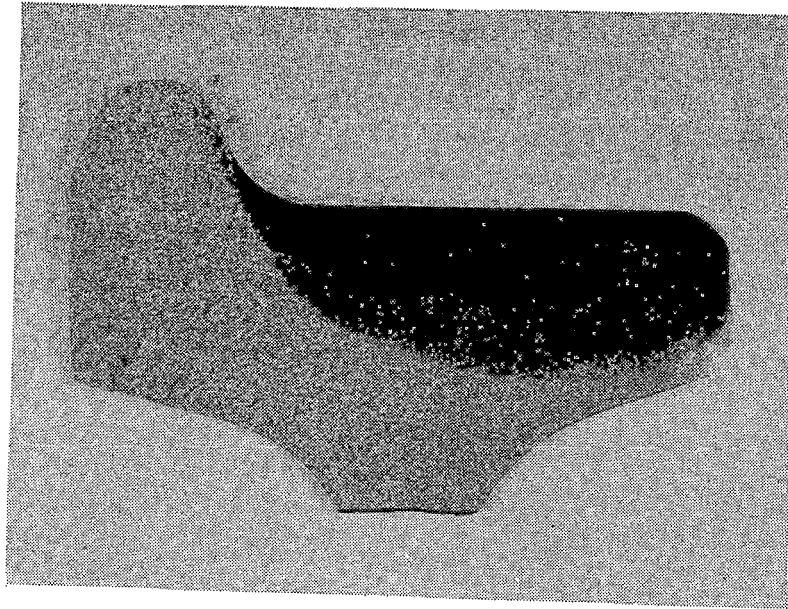
FIGURE 9.31   SURFACE OF FRACTURE IN WHEEL 43992 AT 45° POSITION

tread crack after 21 drag- and 1,034 stop-braking cycles. However, no cracks propagated into the plate of S-plate and parabolic-plate wheels after 115 drag- and 4,444 stop-braking cycles. These results indicate the superiority of the S-plate and parabolic plate wheels relative to that of the straight-plate wheel with regard to crack propagation through the rim. The relative thermal crack initiation tendencies of the S-plate and parabolic-plate wheels appeared to be about equal.

9.2   Crack Initiation/Propagation Study Report

9.2.1   Introduction

Subsequent to crack initiation/propagation tests on the brake dynamometer at Chicago, a series of track tests were conducted at Pueblo to evaluate the effects of thermal cycling due to drag and stop-braking applications on wheels with natural and artificial cracks. The wheels with natural cracks were chosen from wheels that had been taken out of service by a participating member railroad. With one exception, all of the natural cracks were transverse in the tread portion of the wheels. The one exception was a wheel, that was discovered at TTC, which had been used as a test wheel at the Facility for Accelerated Service Testing (FAST) in Pueblo, Colorado. This wheel had been removed from active testing at FAST due to the formation of several flange cracks. Apart from the above service wheels with natural cracks, additional test wheels were

made ready with specially designed artificial cracks. These artificial cracks were very similar to the ones in the wheels that were tested on the dynamometer in Chicago.

The test conditions were chosen based upon the results that were obtained from the dynamometer-tested wheels. The selected test conditions (speed and brake cylinder pressure) were much more severe than normally occurs in general freight service.

9.2.2 Test Setup

The test consist was made up of a locomotive, two test cars, (one 100-ton capacity tank car and a 70-ton capacity boxcar), and a buffer car. All the wheels of the 100-ton tank car (36 in. dia.) and the 70-ton boxcar (33 in. dia.) were regarded as test wheels which consisted of Class U, B, and C and straight, curved and S-plate wheels. The test cars were provided with Wabcopac trucks to minimize wheel-to-wheel differences of thermal input in the same truck for a given speed and brake cylinder pressure. The wheel configurations, wheel types, classes and types of cracks are given in Figures 9.32 and 9.33.

The test wheels consisted of new wheels (#43 and #44), wheels from comprehensive track testing (#25, #26, #27, #28, #39, and #40), and naturally-cracked wheels taken out of service (#41, #42, #45, #46, #47, #48, #49, and #50). One wheel (#43) was tested with all eight artificial cracks and defects as shown in Figure 9.1. Two wheels (#39 and #40) were tested where each
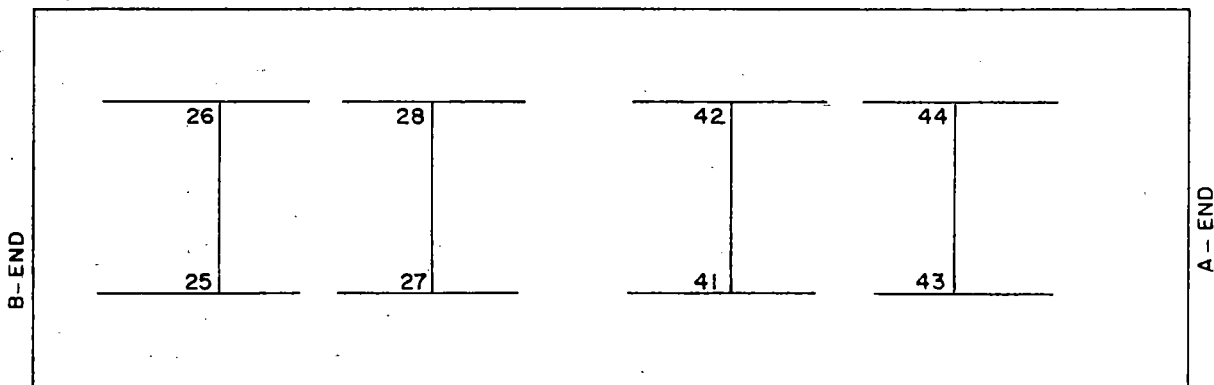
70 – TON   BOXCAR   (LOADED   WITH   54 TONS)

| WHEEL # | CLASS | PLATE TYPE | CRACK TYPE | | ORIGIN OF WHEEL |
			ARTIFICIAL	NATURAL	
25	C	CURVED	FLANGE	NONE	COMP. TRACK TEST
26	U	CURVED	FLANGE	NONE	"
27	C	CURVED	FLANGE	NONE	"
28	U	CURVED	FLANGE	NONE	"
41	C	CURVED	NONE	TREAD	UNION PACIFIC
42	C	CURVED	NONE	TREAD	"
43	U	CURVED	ALL	NONE	NEW
44	U	CURVED	NONE	NONE	NEW

FIGURE 9.32   WHEEL TYPES AND CONFIGURATION ON BOXCAR
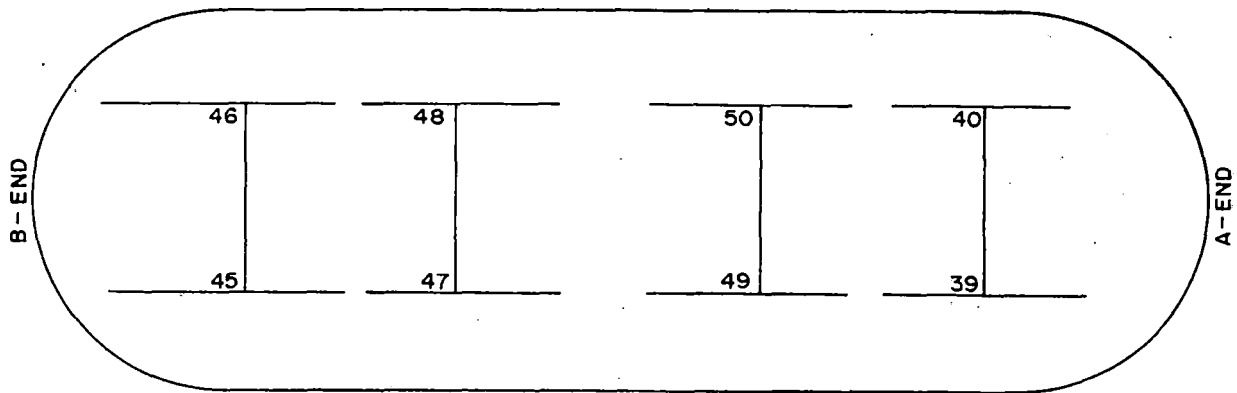
100 − TON TANK CAR (FULLY LOADED)

| WHEEL # | CLASS | PLATE TYPE | CRACK TYPE | | ORIGIN OF WHEEL |
			ARTIFICIAL	NATURAL	
45	B	STRAIGHT	NONE	TREAD	UNION PACIFIC
46	U	PARABOLIC	NONE	MULT. FLANGE	FAST
47	B	STRAIGHT	NONE	NONE	UNION PACIFIC
48	B	STRAIGHT	NONE	TREAD	"
49	B	CURVED	NONE	TREAD	"
50	B	CURVED	NONE	TREAD	"
39	C	"S"	FLANGE	NONE	COMP. TRACK TEST
40	C	CURVED	FLANGE	NONE	"

FIGURE 9.33   WHEEL TYPES AND CONFIGURATION ON TANK CAR

wheel had two artificial flange cracks as shown at the 0° position of Figure 9.1. The two cracks were cut at 60° apart from each other on each wheel. The last group of wheels that had artificial cracks (#25, #26, #27, and #28) had one flange defect in each wheel.

The artificial cracks were machined into the wheels using an abrasive cutting tool with a cutting wheel, 3 in. dia. and 1/16 in. thick. All of the slots simulating artificial cracks were machined at the various circumferential positions as shown in Figure 9.1 so that the greatest depth measured from the wheel surface to the bottom of the slots was 1/2 in. After the slots were made, 1 in. dia. holes were drilled in the wheel plates below each artificial crack in order to prevent the crack from propagating through the entire wheel plate. Finally, a 1/16 in. thick piece of sheet metal was inserted in the machined slot and tack-welded on one side of each slot. The sheet metal pieces prevented the slots from closing-in during track testing of the wheels, thus simulating natural cracks. Figure 9.2 shows various views of artificial cracks.

9.2.3 Test Procedure

Before any track testing began, static brake shoe forces on each test wheel were measured at various brake cylinder pressures, measured in the B-end tank car cylinder. These forces were then plotted as a function of the brake cylinder pressure. Figures 9.34 and 9.35 show how typical brake forces of the boxcar

BRAKE SHOE CALIBRATION-BOXCAR

WHEEL 44
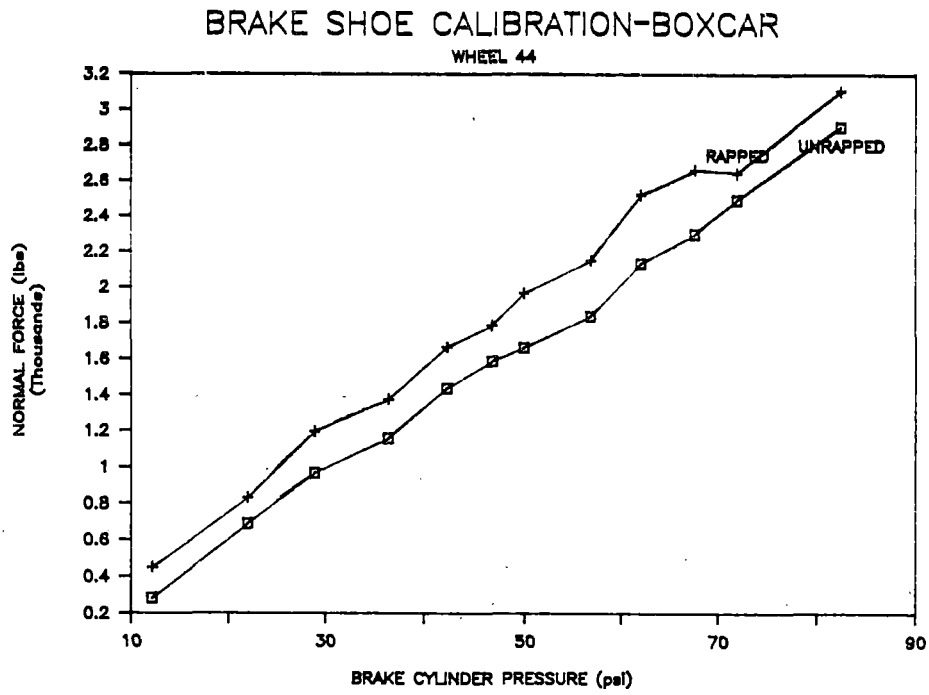
FIGURE 9.34   NORMAL BRAKE SHOE FORCES ON THE BOXCAR

BRAKE SHOE CALIBRATION—TANK CAR

WHEEL 50
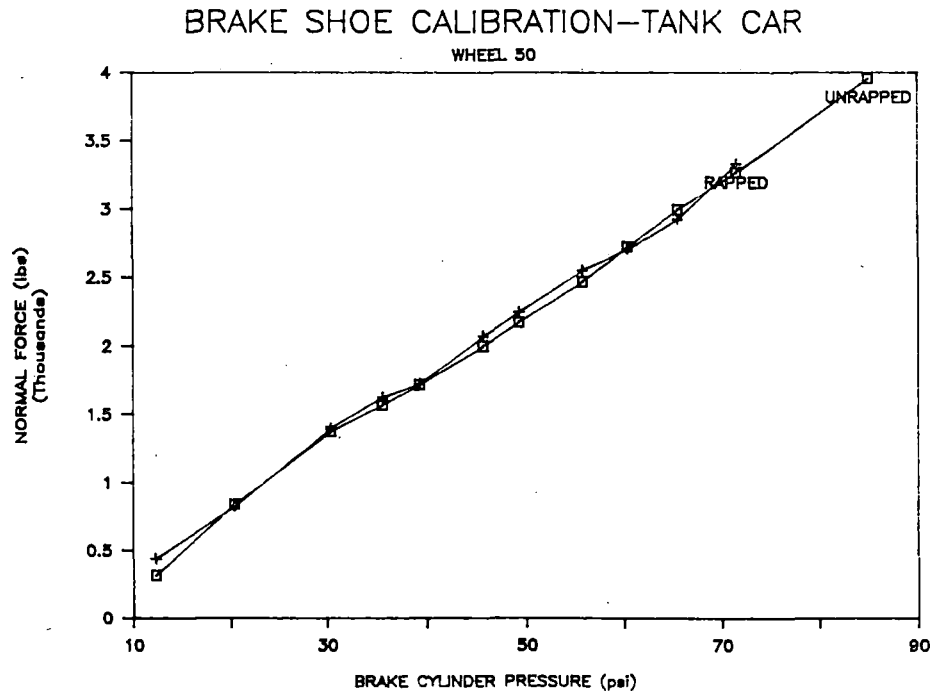
FIGURE 9.35   NORMAL BRAKE SHOE FORCES ON THE TANK CAR

and tank car varied. The rapped curves were obtained after tapping the brake beams with hammers to simulate the vibrations that occur on railroad track. These vibrations allow the brake rigging to move more easily at the hinged locations. In contrast to the rapped and unrapped data from the boxcar, the data from the tank car show little change in normal forces at a given brake cylinder pressures. In addition, these data show that the brake shoe forces were greater on the tank car wheels in comparison to the boxcar wheels.

Also before track testing began, each of the 16 wheels was inspected and the cracks (artificial and natural) were identified and measured. The depth of the natural cracks was measured using ultrasonic equipment and was found to be less than 1/16 in. for all of the cracks (surface cracks). The wheels were then inspected after 100 stop-braking cycles and again after an additional 100 stop-braking cycles and 3 drag-braking cycles. A total of 200 stop-braking cycles and 3 drag-braking cycles was accomplished on the RTT in Pueblo, Colorado at temperatures from 30° to 50°F.

The first 100 stop-braking cycles were run with the consist arrangement shown in Figure 9.36. The buffer car was used to ensure safety for the crew in the case where a wheel may have broken and caused a derailment. This consist was accelerated to a speed of 50 mph and only the brakes on the tank car and boxcar were applied to bring the consist to a complete stop. The measured brake cylinder pressure in the B-end of the tank car was 60 psi. Because the normal force for each brake shoe was
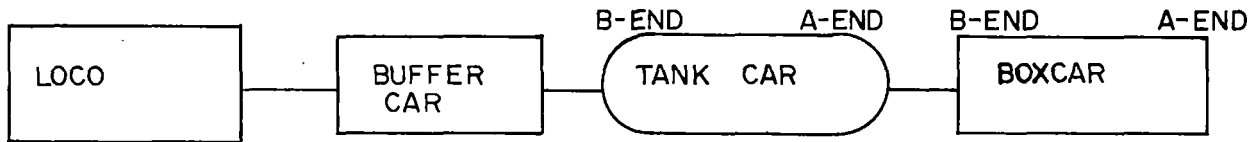
FIGURE 9.36   CONSIST DURING FIRST 100 STOP-BRAKING CYCLES

measured at given brake cylinder pressures immediately before the track testing, the brake shoe forces were known. The normal brake shoe forces for the tank car and the boxcar were 2600-2800 lbs. and 2100-2300 lbs., respectively.

After more confidence was gained in the safe operation of the test consist, a consist arrangement without the buffer car as shown in Figure 9.37 was used. This consist was accelerated to a speed of 80 mph and then the brakes were applied on the test cars to bring the consist to a near stop.

Three drag-braking cycles were accomplished after the 200 stop-braking cycles. With the consist arrangement as shown in Figure 9.37, each cycle lasted one hour at 45 mph with the brake cylinder pressure in the tank car at 45 psi. This brake cylinder pressure resulted in normal brake shoe forces of about 2000 lbs. and 1700 lbs. in the tank car and the boxcar, respectively.

After every 100 stop-braking cycles the wheels were inspected visually for gross cracks which could have caused a broken wheel. During this time brake shoes were inspected and replaced as needed. In addition, wheel temperatures were frequently measured after each test, using digital infrared microscanners.

A summary of the testing conditions is shown in Table 9.8.

B-END   A-END   B-END   A-END

```
+-----------+       +-----------+      +-------------+
|           |       |           |     /               \
|   LOCO    |-------|  BOXCAR   |-----|   TANK  CAR     |
|           |       |           |     \               /
+-----------+       +-----------+      +-------------+
```
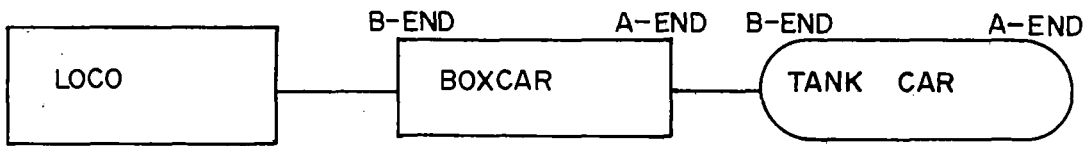
FIGURE 9.37   CONSIST AFTER FIRST 100 STOP-BRAKING

TABLE 9.8
TESTING CONDITIONS

	Speed (mph)	BCP (psi)	Normal Brake Shoe Forces		Duration (minutes)
			Boxcar	Tank Car	
0-100 Stop-Braking Cycles	50	60	2200	2700	--
101-200 Stop-Braking Cycles	80	60	2200	2700	--
3 Drag-Braking Cycles	45	45	1700	2000	60

The crack initiation/propagation track tests were the last series of tests conducted at Pueblo, under Wheel Failure Mechanisms Program.

9.2.4 Results and Discussion

No crack growth was observed from any artificial cracks after the completion of 200 stop-braking cycles and 3 drag-braking cycles. The artificial cracks were inspected using magnetic particles to be sure of crack growth detection.

The natural cracks in general did not grow significantly in any of the wheels. In fact, some cracks seemed to decrease in size. This is probably due to metal flow and the fact that the cracks were mainly transverse tread cracks. One wheel (36 in., Class U, parabolic plate, #46) did develop several cracks on its tread surface. A photograph of the tread of wheel #46 is shown in Figure 9.38. The cracks are outlined by magnetic particles. These were all surface cracks that probably would not have caused a catastrophic wheel failure. In addition to the tread cracks some minor pitting occurred after the braking cycles. The flange cracks that were in the wheel before testing did not appear to increase in size due to the braking cycles. A typical flange crack is shown in the photo in Figure 9.39.

The reason for the formation of cracks in wheel #46 may be due to strain hardening of the tread surface during previous running. Before the current study, this wheel underwent many miles of running on the FAST track which probably caused metal
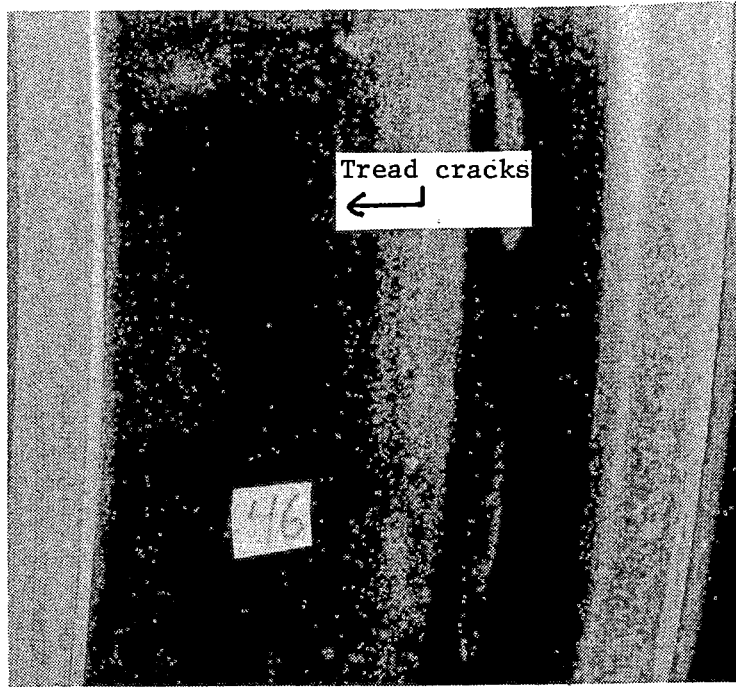
FIGURE 9.38   PHOTOGRAPH OF WHEEL 46 SHOWING THE TRANSVERSE TREAD
                CRACKS WHICH DEVELOPED AFTER 200 STOP-BRAKING CYCLES
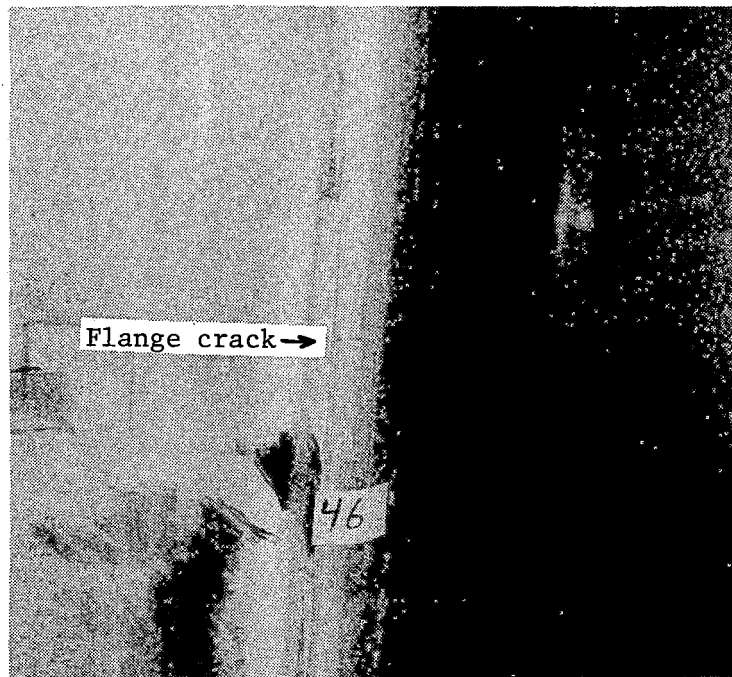
FIGURE 9.39   PHOTOGRAPH OF WHEEL 46 SHOWING A TYPICAL FLANGE CRACK.
                MAGNETIC PARTICLES WERE USED TO MAKE THE CRACK MORE
                OBSERVABLE

observable.   9-57

flow to occur resulting in strain hardening.

The remaining service wheels with natural cracks (selected from Union Pacific) of Class B type did not exhibit tread cracks. However, Wheel #46 (selected from FAST service), which did exhibit tread cracks, was of Class U type.

The wheel temperatures measured immediately after testing varied from 400° to 800°F. The temperatures were measured on the outside rim faces of the wheels. The temperatures varied due to the wheel location in the consist, the type of plate and the time lag between measuring the first wheel and the last wheel (about 5 minutes).

9.2.5 Conclusions from Crack Initiation/Growth Track Testing

1.   In order to cause the above specified artificial cracks in the prescribed test wheels to propagate, more than 200 stop-braking and 3 drag-braking cycles are required. According to the work done on the dynamometer more than 700 stop-braking cycles were required to propagate one artificial flange crack.

2.   After 200 stop-braking cycles and 3 drag-braking cycles no significant cracks developed in any of the wheels.

9.2.6 Recommendations

Even though the test conditions used for the brake dynamometer were also used on the track at Pueblo, the number of braking cycles required to propagate the natural and artificial cracks was not sufficient. More testing is required in the future to establish criteria during track testing which would initiate cracks in new as well as service wheels and propagate natural and artificial cracks in new and service wheels.

10.0 DETERMINE THE EFFECT OF WHEEL SLID FLATS ON TREAD SHELL PRODUCTION (TECHNICAL TASK T9)

Slid Flats and Tread Shelling studies were originally intended as a preliminary and limited approach in modeling and testing efforts to investigate the overall tread shelling problem. In view of its limited effort in addressing a complex problem like tread shelling, Technical Task T9 was eliminated in the revised scope of the Wheel Failure Mechanisms Program.

However, during the preliminary track testing (under Technical Task T5), a 2 inch flat was machined on the tread of an instrumented test wheel (#9). Additional series of tests were conducted to investigate the impact loads due to the machined wheel flat, and study their effect on the wheel strains and brake shoe forces. A complete report on this study is included in Section 6.0 under subsection 6.10.

11.0 DEVELOP A COMPREHENSIVE FAILURE MODEL (TECHNICAL TASK T10)

The objective of this task was the development of technically sound wheel removal criteria and guidelines for safe design and operation. To help achieve this objective, a comprehensive analytical effort was required to ensure thorough interpretation of data from various experimental tasks and to support the specific objectives of several other tasks.

This task included an analysis of all data accumulated and results of previous tasks and the following, Task 11. The analysis examined the combination of brake shoe force, time, and velocity which produce critical levels of residual stress in combinations of the two wheel designs and heat treatments. The data have been presented graphically for selected sets of wheel design and heat treatment. The methodology of producing the graphic results with velocity, brake force, and time inputs, has been developed so that plots were constructed using combinations of design and heat treatment of interest. The path dependence of thermally induced stress change caused by more than one braking cycle was investigated.

Organization Introduction

This section treats the modeling of stress change, failure sequence, and other analyses developed to support other program requirements.

11.1 Induction Heating Experiments

Work in this subtask has supported the proper placement of gages on test wheels in the induction heating, RDU, brake dynamometer, and track tests (Technical Tasks T4 and T5).

The induction heating experiments were conducted at the AMSTED Research Laboratories in Bensenville, Illinois. The induction heating facility consisted of a 100-kW induction coil and a high frequency generator (2500-2900 Hz). The following induction heating cycles were performed on CH36 (curved plate) and H36 (straight plate), Class U wheels:

Test No.	Test Wheel	Thermal Cycle (Drag Brake Simulation)
1	CH36	30 kW, 12 minutes
2	CH36	40 kW, 15 minutes
3	CH36	30 kW, 25 minutes
4	CH36	40 kW, 30 minutes
5	CH36	40 kW, 30 minutes (repeat test)
6	H36	30 kW, 8 minutes
7	H36	30 kW, 16 minutes
8	H36	40 kW, 12 minutes
9	H36	40 kW, 24 minutes
10	H36	40 kW, 24 minutes (repeat test)

Data were acquired at prescribed intervals during heating and cooling using the CR7 Campbell Scientific data logger.

11.1.1   Test Data

Analysis of Temperature Data

The first step in the analysis and evaluation of the temperature data was to compare data from the thermocouples with predictions. The principal uncertainties in the analyses were the selection of the appropriate assumption for the transmission of power into the wheel, and the selection of values for the convection coefficient and emissivity. The material thermal properties from AAR S-660 (1) were used. These are:

Specific Heat

$$C_p = 0.102 + 0.000052T \ (Btu/lb\text{-}^\circ F)$$

Thermal Conductivity

$$k = 28.1 - 0.0060T \ (Btu/hr\text{-}ft\text{-}^\circ F)$$

It was found that the use of these properties, a convection coefficient 30% of that listed in S-660, radiation with an emissivity of 0.8 (there is no provision for radiation loss in S-660), and assuming a thermal input efficiency of 91%, yielded a fairly good fit of the CH-36 curved plate wheel data at 12 and 25 minutes. The H-36 straight-plate wheel data also fit fairly well at 8 and 16 minutes (test nos. 6 and 7) with the assumption of 91% efficiency.

The results are summarized for the CH-36 wheel in Table 11.1 and for the H-36 wheel in Table 11.2. The results for the CH-36

TABLE 11.1
INDUCTION HEATING CURVED PLATE CH36 WHEEL, 30 KW FOR 12 AND 25 MINUTES

T/C No.	Observed Temperature	Calculated Temperature	Deviation
1	637	636	1
2	735	716	19
3	670	704	-34
4	653	685	-32
5	649	633	16
6	714	696	18
7	672	677	- 5
8	673	658	15
9	607	596	11
10	634	641	- 7
11	615	624	- 9
12	604	611	- 7
13	559	564	- 5
14	598	612	-14
15	528	575	-47
16	710	696	14
17	553	549	-16
18	416	417	- 1
19	180	178	2

12 Minutes, $\eta = .91$

T/C No.	Observed Temperature	Calculated Temperature	Deviation
1	428	398	30
2	511	474	37
3	438	462	-24
4	424	443	-19
5	423	394	29
6	477	453	24
7	433	436	- 3
8	435	417	18
9	373	359	14
10	401	402	- 1
11	379	385	- 6
12	367	373	- 6
13	325	330	- 5
14	374	375	- 1
15	313	340	-27
16	472	453	19
17	312	316	- 4
18	218	219	- 1
19	95	98	- 3

T/C No.	Observed Temperature	Calculated Temperature	Deviation
1	358	349	9
2	274	425	
3	407	416	- 9
4	401	401	0
5	359	348	11
6	378	390	-12
7	369	377	- 8
8	358	358	0
9	300	298	2
10	325	339	-14
11	307	317	-10
12	303	308	- 5
13	264	268	- 4
14	297	276	21
15	266	261	5
16	390	390	0
17	251	250	1
18	143	185	-42
19	72	78	- 6

16 Minutes, $\eta = .91$

T/C No.	Observed Temperature	Calculated Temperature	Deviation
1	532	540	- 8
2	457	620	
3	599	610	-11
4	592	594	- 2
5	544	539	5
6	576	581	- 5
7	562	568	- 6
8	551	549	2
9	487	484	3
10	517	528	-11
11	500	505	- 5
12	494	496	- 2
13	451	453	- 2
14	473	462	11
15	429	447	-18
16	587	581	6
17	427	434	- 7
18	272	333	-61
19	101	103	- 2

wheel suggest that thermocouples 3, 4, and 15 were not responding properly because the deviations for these thermocouples are significantly off the trends shown for the other thermocouples. Similarly, the results for the H-36 wheel suggest that thermocouple 18 was not responding properly.

Analysis of Thermal Strain Data

The data from the strain gages were analyzed by preparing plots of the mechanical component of strain versus temperature for each of the tests. Typical results are presented in Figures 11.1 and 11.2. Figure 11.1 shows results for the B1 strain gage on the first test with the H-36 wheel. Figure 11.2 shows results for the B1 location on the second test with the same wheel. The plots show the large strain ranges that are associated with tests of this type.

Table 11.3 summarizes the strain data for both the wheels at the B1 location and Table 11.4 summarizes the strain data for the B3 location for each of the tests. Note that there is a progressive, but diminishing, accumulation of residual strain at the B1 location. The accumulation of residual strain at the B3 location seems to be more erratic.

11.1.2   Prediction of Residual Stresses by Finite Element
         Analysis

Prof. H. Sehitoglu of the University of Illinois has made an
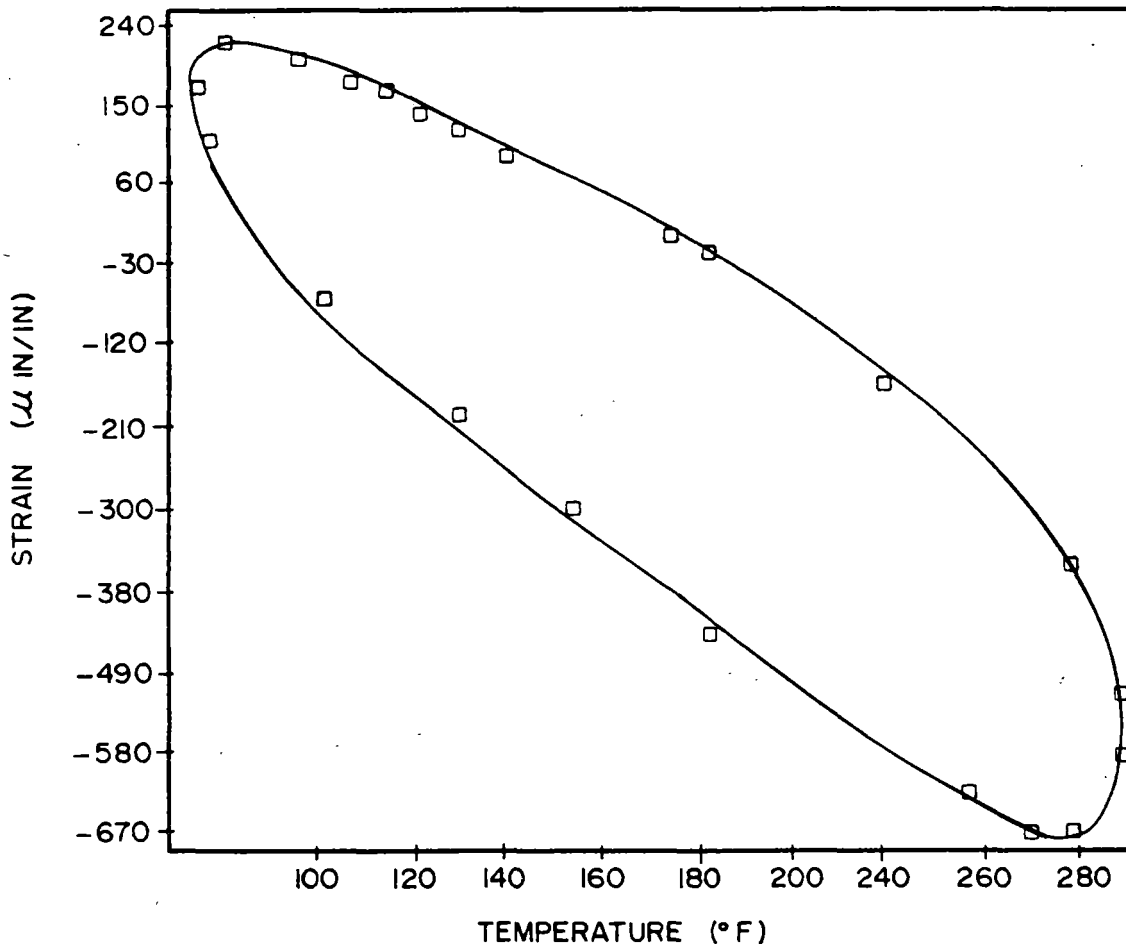
FIGURE 11.1   STRAIN -VS- TEMPERATURE AT B1 LOCATION,
TEST NUMBER 6, H36 WHEEL, 30 KW, 8 MINUTES

11-7
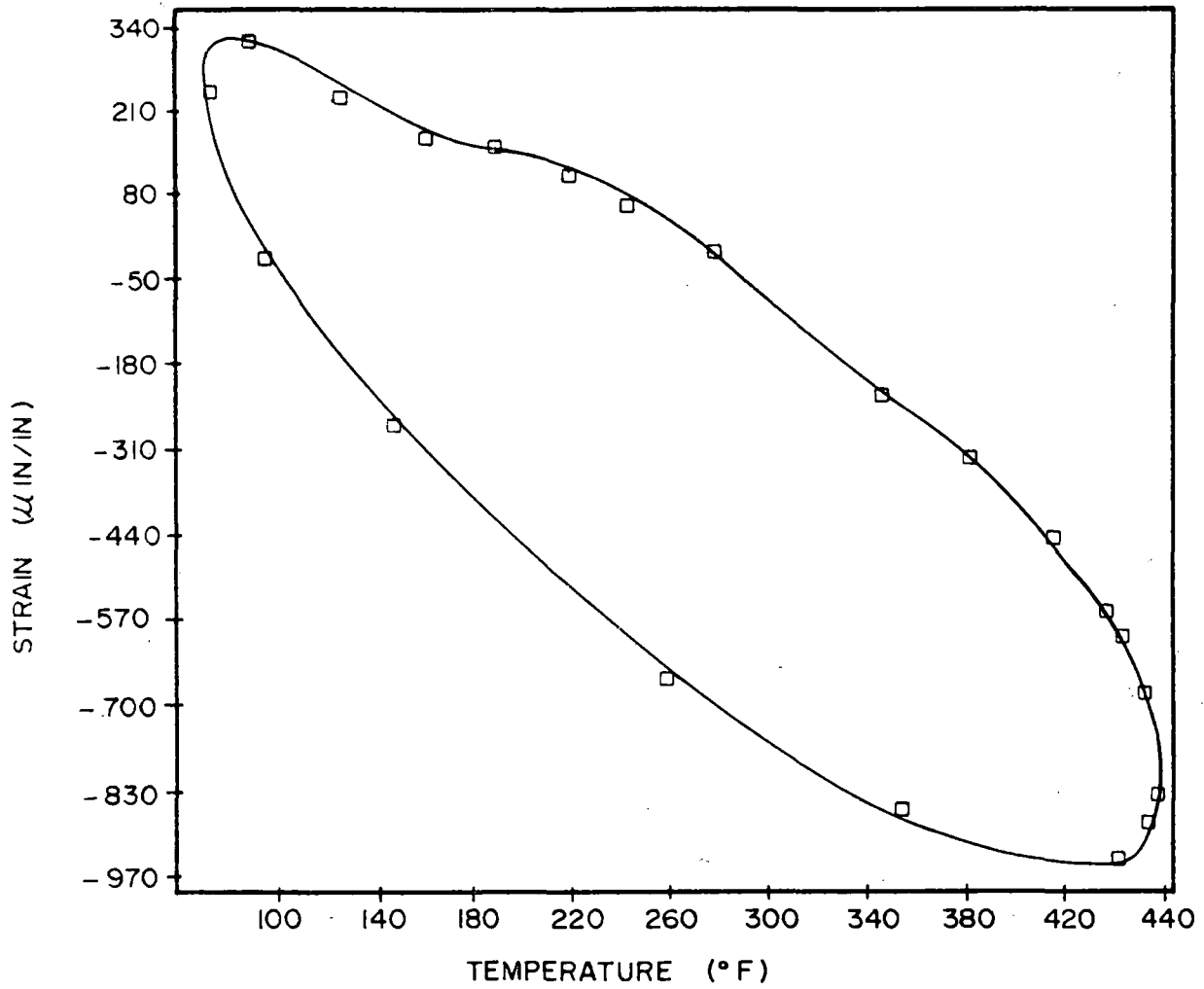
FIGURE 11.2   STRAIN -VS- TEMPERATURE AT B1 LOCATION,
               TEST NUMBER 7, H36 WHEEL, 30 KW, 16 MINUTES

TABLE 11.3

B1 LOCATION STRAIN DATA (CIRCUMFERENTIAL)

Thermal Load (kW) and Time (min)	Strain at End of Heating (μin/in)	Residual Strain (μin/in)
Curved Plate		
30-12	-1048	73
40-15	-1677	70
30-25	-1848	19
40-30	-2586	25
40-30	-2577	11
Straight Plate		
30-8	- 801	48
30-16	-1161	123
40-12	-1401	17
40-24	-1875	55
40-24	-1903	32

TABLE 11.4

B3 LOCATION STRAIN DATA (RADIAL)

Thermal Load (kW) and Time (min)	Strain at End of Heating (μin/in)	Residual Strain (μin/in)
Curved Plate		
30-12	1567	-88
40-15	2834	144
30-25	3436	185
40-30	5116	258
40-30	4730	-45
Straight Plate		
30-8	1608	-56
30-16	4159	666
40-12	3661	38
40-24	6455	-209
40-24	6570	-19

independent evaluation of some of the results of the induction heating tests. Finite element analyses (using ANSYS) were conducted to simulate the tests on the curved-plate CH-36 wheel. A major objective of this effort was the calculation of residual circumferential stresses at the back face rim position (B1) using mechanical properties which had been derived from tests conducted at the University of Illinois. An overall objective of this work has been to develop a model which provides the mechanical properties as a function of strain rate. The properties used in his simulation were representative of those predicted in the 10^{-3}/sec to 10^{-4}/sec range. The following material properties were used by Prof. Sehitoglu in his predictions.

1. Thermal Properties (1070 Steel)

   Thermal conductivity , K   2.9 $\dfrac{Btu}{hr-in-^{o}F}$

   Specific heat   , c_p 0.10357 $\dfrac{Btu}{lb-^{o}F}$

   Density   , ρ 0.283 $\dfrac{lb}{in^{3}}$

   Convection coefficient, h   0.06 $\dfrac{Btu}{hr-in^{2}-^{o}F}$

2. Mechanical Properties (1070 Steel Class U)

   $\dot{\varepsilon} = 2 \times 10^{-3}$ 1/sec

   Thermal expansion coefficient, $\alpha = 9.44 \times 10^{-6}$ 1/^{o}F

Temperature (^{O}F)	Plastic modulus (ksi)	Yield Stress (ksi)
68	2175.7	58.02
288	3162	56.71
514	3220	55.84
752	2683.3	50.33
1292	739.1	14.51
1472	435.1	11.60

Temperature (^{O}F)	Elastic modulus (ksi)
68	29245
392	28436
752	27537
932	24968
1292	16970
1472	11604

Material model: classical bilinear kinematic hardening

The analyses included the prediction of temperatures from the heat input for each of the induction heating thermal loads. The calculations spanned a period of about 40 hours and included the heating and cooling cycles of each of the 5 thermal loads. The results of these calculations are summarized in the following table:

PREDICTED TEMPERATURES AND RESIDUAL STRESSES
AT THE B1 LOCATION, CH36 WHEEL

Thermal Load	Predicted Maximum Temperature (^{O}F)	Observed Maximum Temperature (^{O}F)	Predicted Residual Circumferential Stress (ksi)
30 kW-12 min.	320	320	0.0
40 kW-15 min.	445	480	1.0
30 kW-25 min.	477	540	1.0
40 kW-30 min.	673	710	13.2
40 kW-30 min.	673	710	13.2 (no change)

11-11

The predicted residual stress distribution is shown in Figure 11.2A. The predicted residual stress following the last test is in good agreement with the stress derived from a hole-drilling test on this wheel, which was about 10 ksi.

11.2   Saw-Cut Openings Analysis - 3D Finite Element Method

The interpretation of wheel "saw-cut opening" behavior has been considerably clarified through application of nonaxisymmetric ANSYS analysis to calculate the residual stresses required to "close" the saw-cut displacements.

Typical saw-cut opening displacement curves are shown in Figures 11.3 through 11.5. These patterns are representative of those obtained by the saw-cutting procedure. Figure 11.3 shows closing of the saw-cut. When this behavior is observed, it is assumed that there is a state of compressive residual hoop stress within the rim of the wheel. This would be representative of a condition within the wheel which would inhibit crack growth and subsequent unstable crack propagation.

Figure 11.4 illustrates opening of the saw-cut as the saw moves into the wheel. This behavior is interpreted as an indication of residual stress in the wheel which are high tensile circumferential stresses that would promote the development, growth, and unstable propagation of radial thermal cracks.

Figure 11.5 illustrates an initial small opening and closing of the saw-cut, but then, as the cut becomes deeper, it opens.
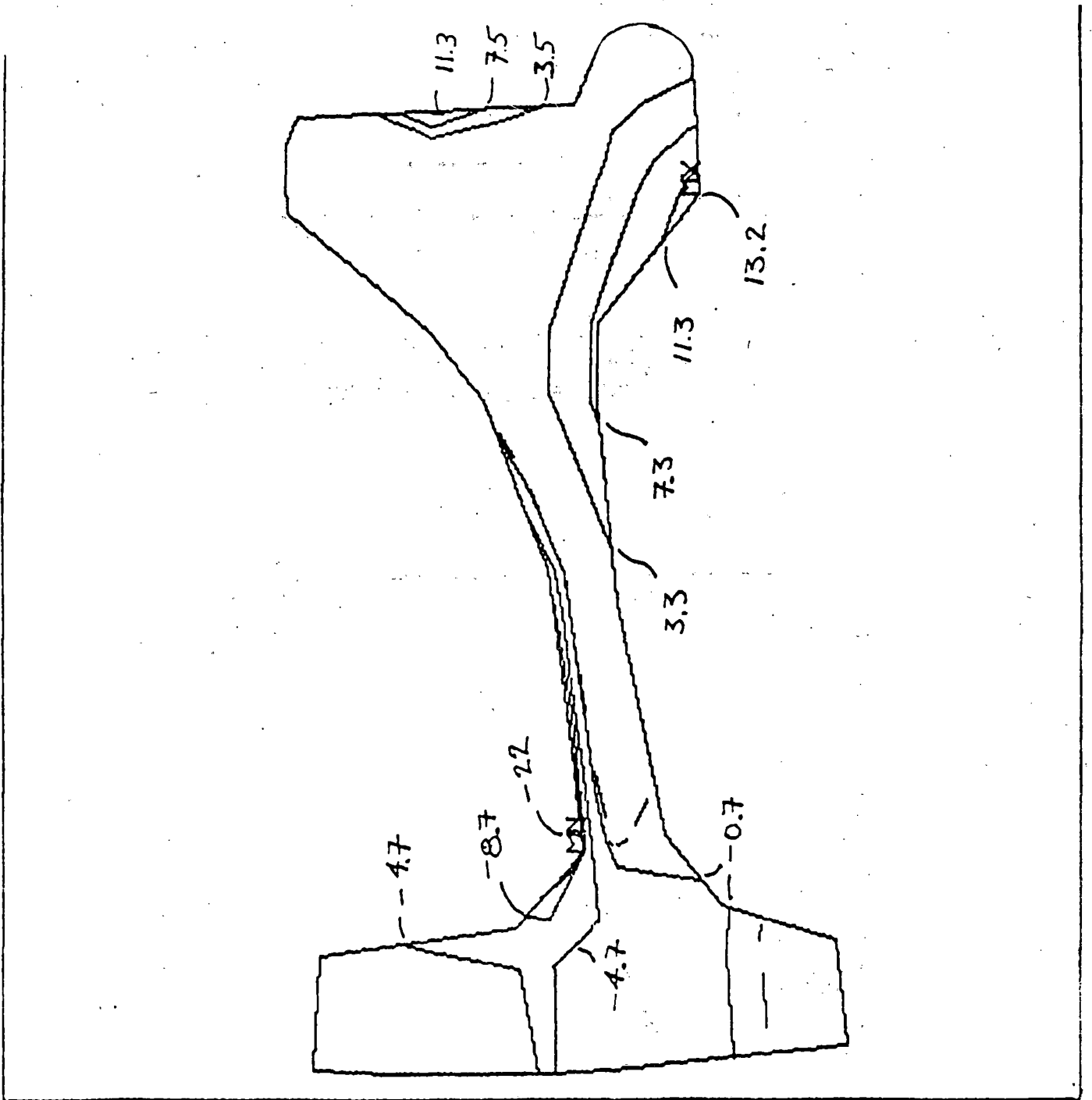
FIGURE 11.2A CONSTANT CIRCUMFERENTIAL RESIDUAL STRESS CONTOURS UPON
COOLING AT THE CONCLUSION OF THE HEATING AND COOLING CYCLES
OF FIVE THERMAL LOADS
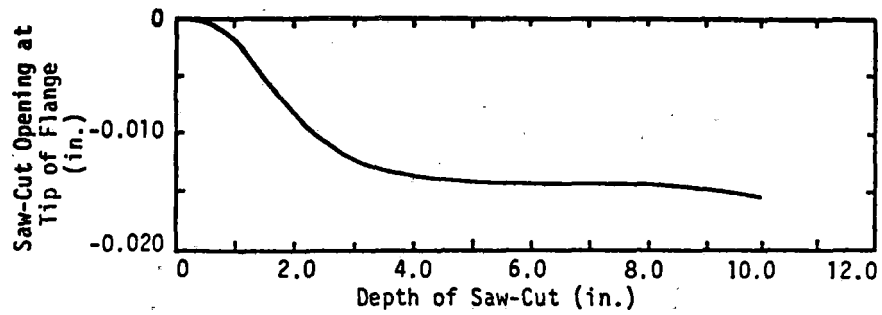
FIGURE 11.3 SAW-CUT OPENING AT TIP OF FLANGE AS FUNCTION OF
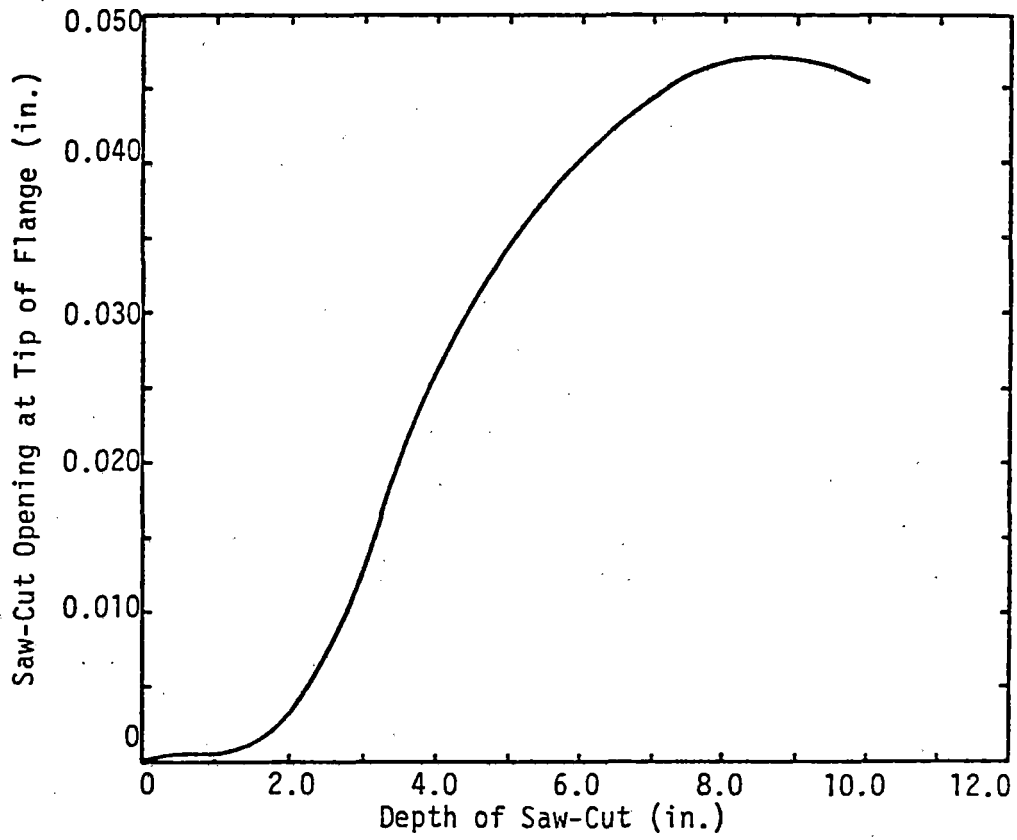DEPTH OF SAW-CUT, EXAMPLE OF SAW-CUT CLOSING
(NEGATIVE DISPLACEMENT VALUES)
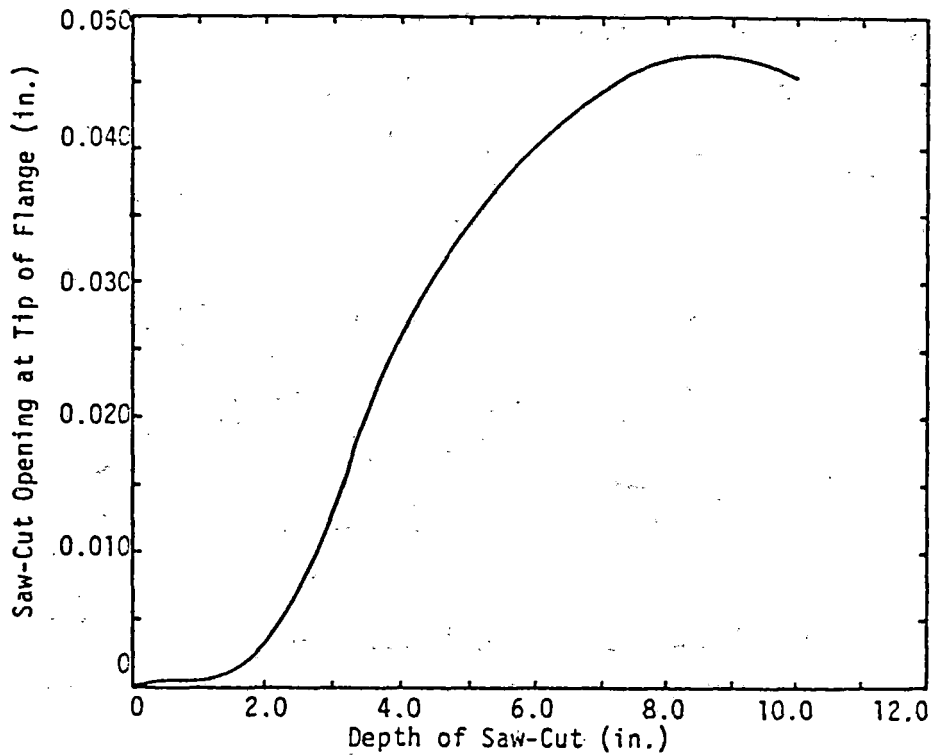
FIGURE 11.4 SAW-CUT OPENING AT TIP OF FLANGE AS FUNCTION OF DEPTH
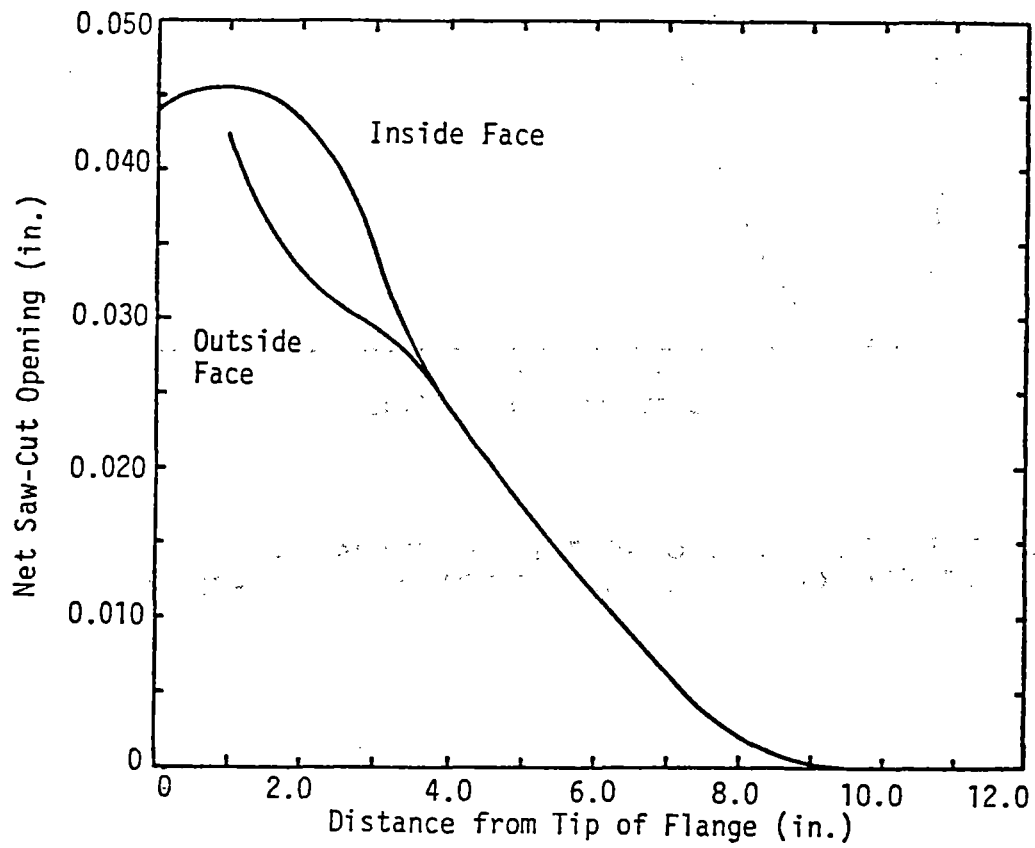OF SAW-CUT, 36-INCH DIAMETER CURVED-PLATE WHEEL

11-14
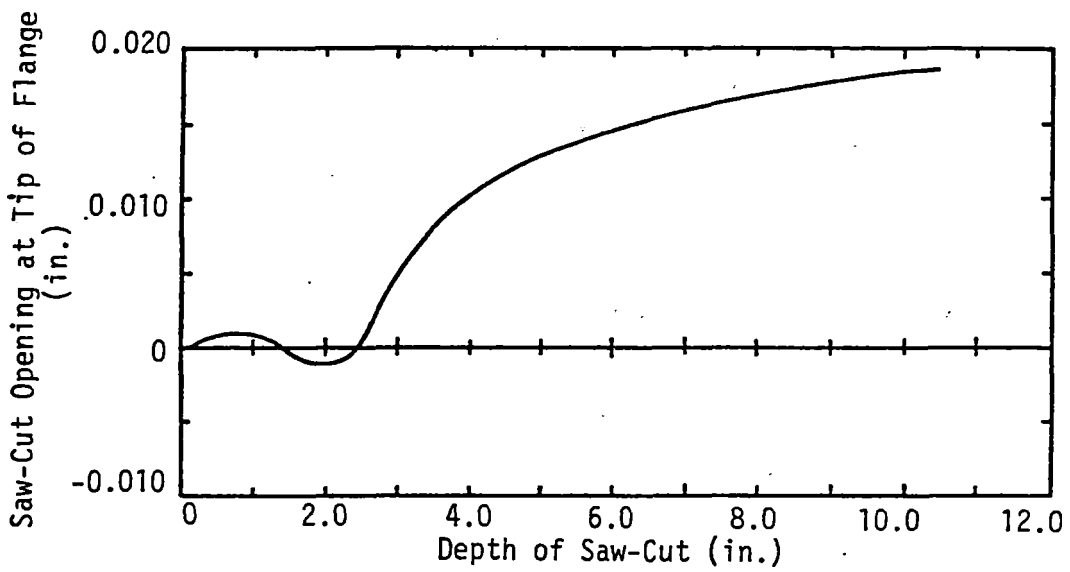
FIGURE 11.5 SAW-CUT OPENING AT TIP OF FLANGE AS FUNCTION OF DEPTH
OF SAW-CUT, 36-INCH DIAMETER STRAIGHT-PLATE WHEEL

The most obvious interpretation of this type of curve is that there are compressive hoop stresses on the periphery of the wheel, but residual tensile stresses deeper in the rim and plate.

11.2.1   Analytical Procedures

The data obtained by saw-cutting can be analyzed to obtain an indication of the magnitude and distribution of the residual stresses within a wheel. The saw-cut opening-displacement curve by itself will not yield a good indication of the distribution of the residual stresses in the wheel. However, additional data, easily obtained, can lead to a much better indication of the magnitude and distribution of the residual stresses within the wheel.

The problem can be approached in the following way. The saw-cut opening displacement is measured on both sides of the wheel along the entire length of a cut that has not severed the hub. Then a three-dimensional finite element analysis is performed to determine the stresses that result when the cut is closed (as a result of circumferential displacement loading on the free surface). The radial and transverse displacements, which occur along with the circumferential displacements when the saw-cut is made, are not presently included in the displacement loading, assuming the symmetry of the problem. The stresses that are calculated for the plane of the cut are then an indication of the stresses that existed before the wheel was cut.

A number of factors must be considered when this type of analysis is performed. First, since a three-dimensional analysis is employed, a large number of elements is required, which results in a substantial amount of computational time. It is desired to use the minimum number of elements that will give acceptable convergence of the solution.

Several analyses have been done to determine the minimum number of elements that are required for an acceptable solution. The number of angle planes in the mesh is an important factor in determining the number of elements. It has been found that the optimum mesh configuration is one where the spacing of the angle planes is small in the vicinity of the cut and increased as one moves away from the cut. It has also been found that the angle planes need not go beyond 90° from the saw cut.

The boundary conditions must also be considered. Little difference was found between calculations that utilized a model that spanned 180° and one that was fixed at 90°. The nodes at the bottom of the cut and the 90° boundaries were fixed circumferentially, but allowed to move radially.

Ideally, displacements generated by the cut should be measured on the inside surface of the rim. It is assumed for the present analysis that the interior surfaces are planar. No higher order approximation can be made with the present method of separation (saw-cutting).

11-17

11.2.2   Results from the Analysis of Saw-Cut Data

Three examples from the analysis of saw-cut data are initially presented. The primary objective of these analyses was to predict the residual circumferential stresses in the rim of the wheel before the wheel was cut.

"Thirty-six-Inch Diameter Curved-Plate Wheel". The first example is for a 36-inch diameter curved-plate cast wheel which gave indications of being overheated by plate discoloration. The saw-cut opening at the tip of the flange versus saw-cut depth curve is shown in Figure 11.6 for a 10-inch saw-cut in the wheel. The total opening is rather large. Figure 11.7 shows the net opening displacement of the 10-inch saw cut as a function of depth into the wheel. There are data for both the inside and outside surfaces of the wheel. Note that there is a significant difference between the two in the rim of the wheel.

Calculations have been made using two different finite element codes: SAP IV and ANSYS. The results were essentially the same. Figure 11.8 shows the circumferential residual stress that are calculated. The circumferential tensile residual stress on the back rim face is predicted to be approximately 35 ksi. The distribution of the residual stresses in the rim is quite similar to that predicted by inelastic finite element techniques for severe brake heating on the tread of the wheel.

"Thirty-six-Inch Diameter Straight-Plate Wheel". Figure 11.5 shows the saw-cut opening at the tip of the flange versus saw-cut depth for a 10.5-inch saw-cut into a 36-inch diameter

FIGURE 11.6   SAW-CUT OPENING AT TIP OF FLANGE AS FUNCTION OF DEPTH
OF SAW-CUT, 36-INCH DIAMETER CURVED-PLATE WHEEL

FIGURE 11.7   NET SAW-CUT AS FUNCTION OF DEPTH OF CUT INTO WHEEL,
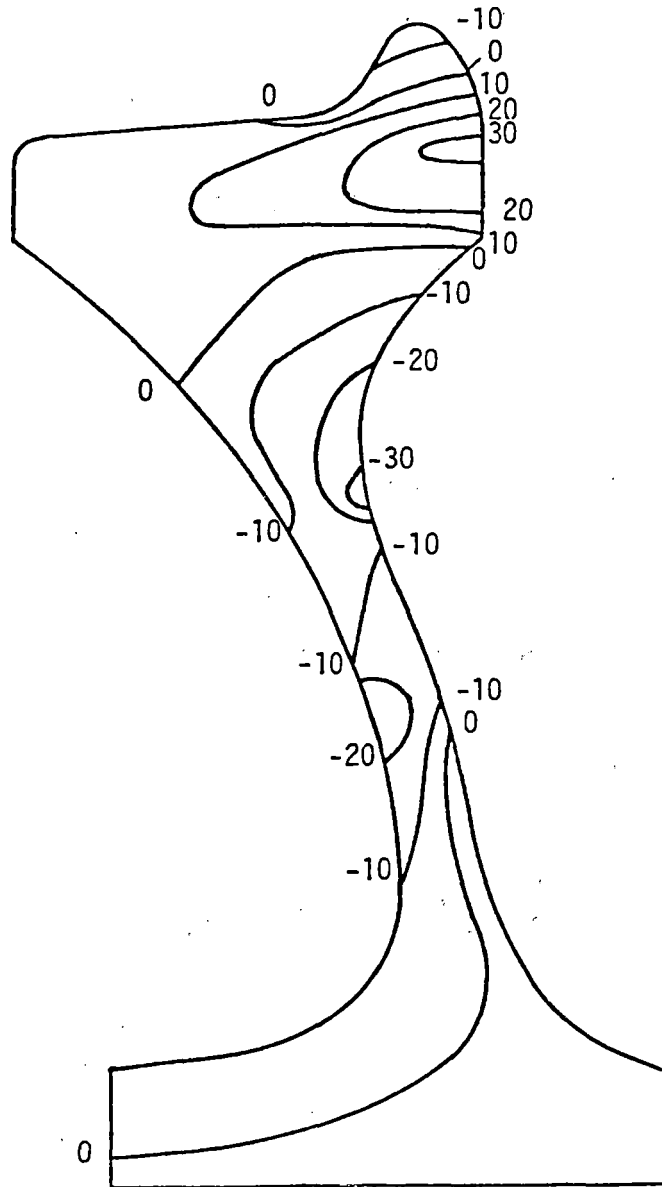36-INCH DIAMETER CURVED-PLATE WHEEL

11-20
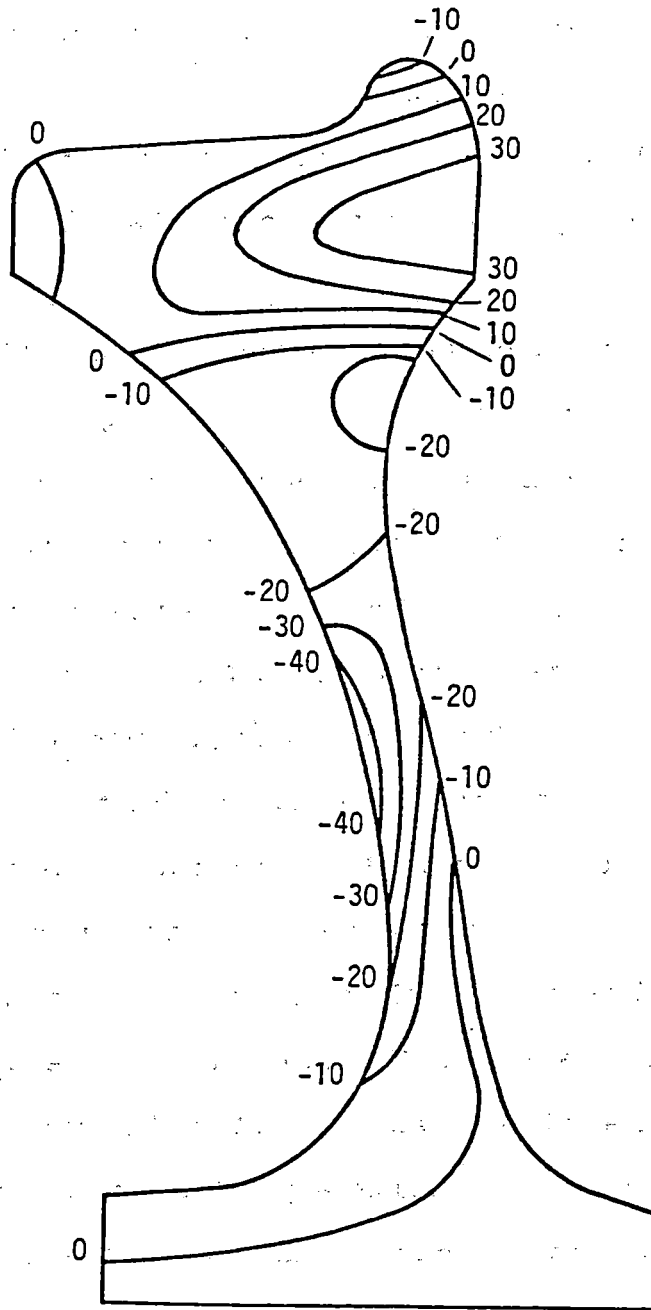
FIGURE 11.8 RESIDUAL CIRCUMFERENTIAL STRESS DISTRIBUTION PREDICTED
FOR 36-INCH DIAMETER CURVED-PLATE WHEEL FROM SAW-CUT
DISPLACEMENT DATA (STRESSES IN KSI)

11-21

straight-plate wheel. This wheel also gave evidence of being overheated (plate discoloration). The saw-cut opening for this wheel is less than that shown for the curved-plate wheel in Figure 11.4. Figure 11.9 shows the net opening displacement of the saw-cut as a function of depth of the 10.5-inch saw-cut into the wheel. Note that there is again a significant difference in the displacement data for the opposite sides of the rim of the wheel.

Results from the finite element calculation for closing the cut are shown in Figure 11.10. This figure shows the predicted circumferential residual stresses. The distribution in the rim is similar to that shown in Figure 11.8 except that the magnitudes are lower. The maximum stress is again on the back rim face and is predicted to be approximately 19 ksi.

"Thirty-three-Inch Diameter Curved-Plate Wheel". Figure 11.11 shows the saw-cut opening at the tip of the flange versus the saw-cut depth for an 8.5-inch saw-cut into a 33-inch diameter curved-plate wheel. This wheel was subjected to controlled braking cycles in tests conducted on the Roll Dynamics Unit at the Transportation Test Center in Pueblo, Colorado. The wheel was subjected to over 25 simulated drag braking cycles of approximately 60 minutes each at power levels from 25 to 50 Bhp. Figure 11.12 shows the net opening displacement of the 8.5-inch saw-cut as a function of depth into the wheel. Note again that there is a significant difference in the displacement data for the opposite sides of the rim of the wheel.
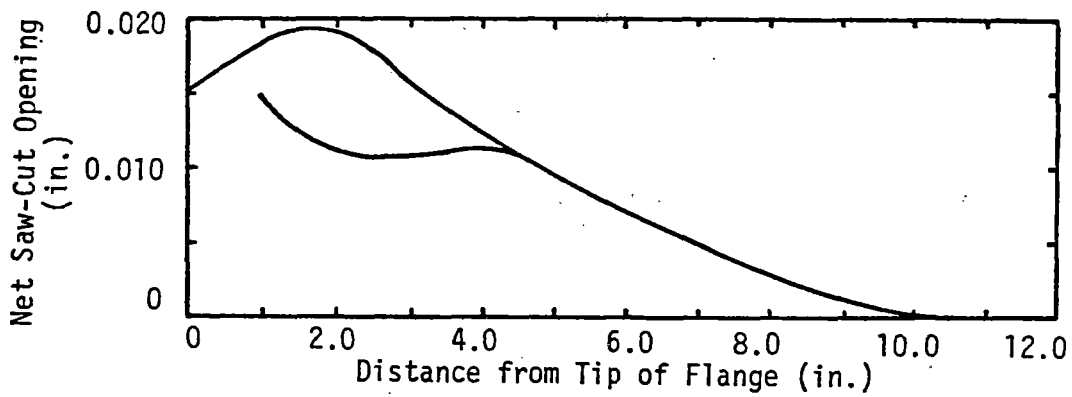
FIGURE 11.9   NET SAW-CUT OPENING AS FUNCTION OF DEPTH OF CUT INTO
WHEEL, 36-INCH DIAMETER STRAIGHT-PLATE WHEEL
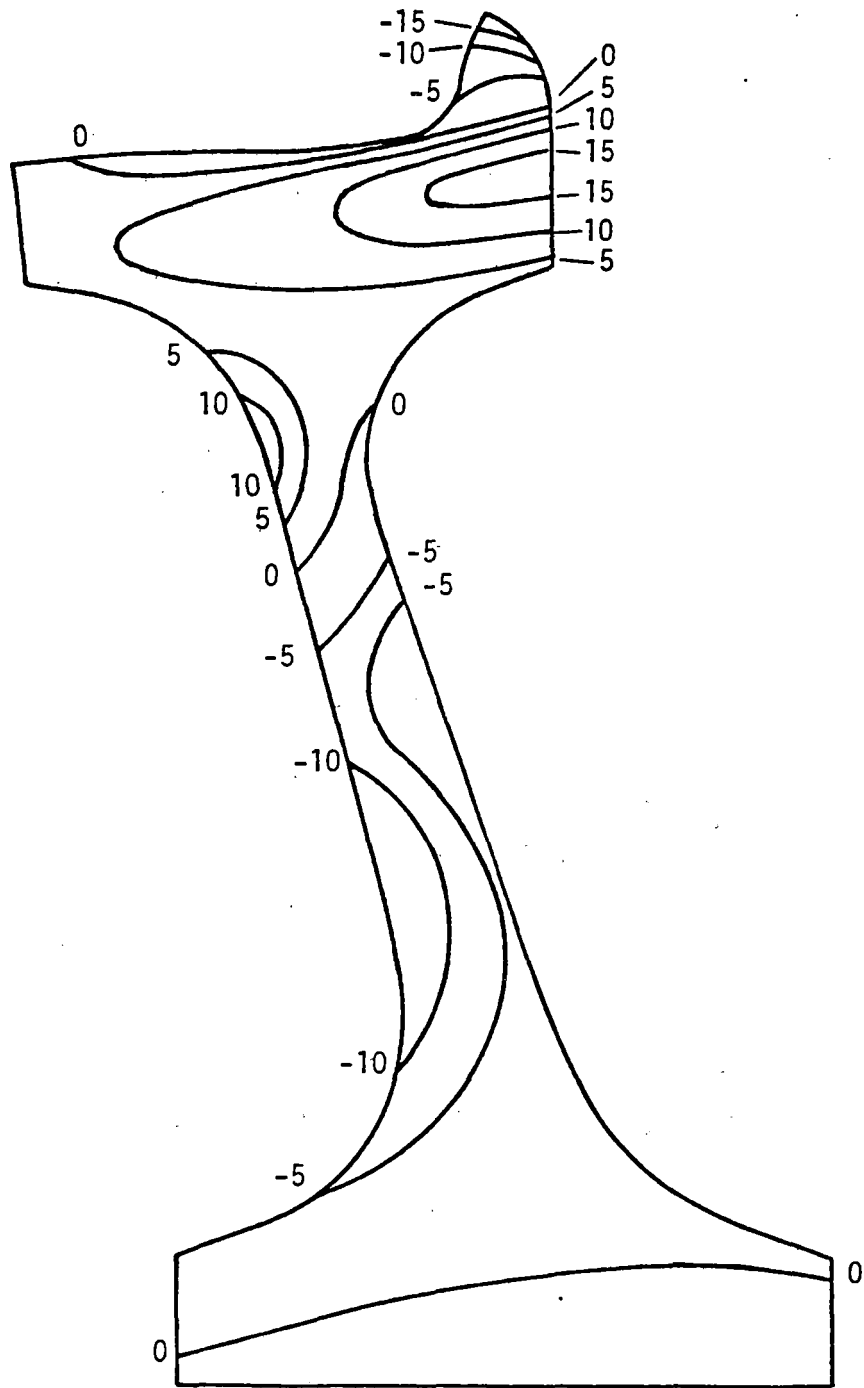
FIGURE 11.10   RESIDUAL CIRCUMFERENTIAL STRESS DISTRIBUTION
PREDICTED FOR 36-INCH DIAMETER STRAIGHT-PLATE
WHEEL FROM SAW-CUT DISPLACEMENT DATA
(STRESSES IN KSI)

11-24
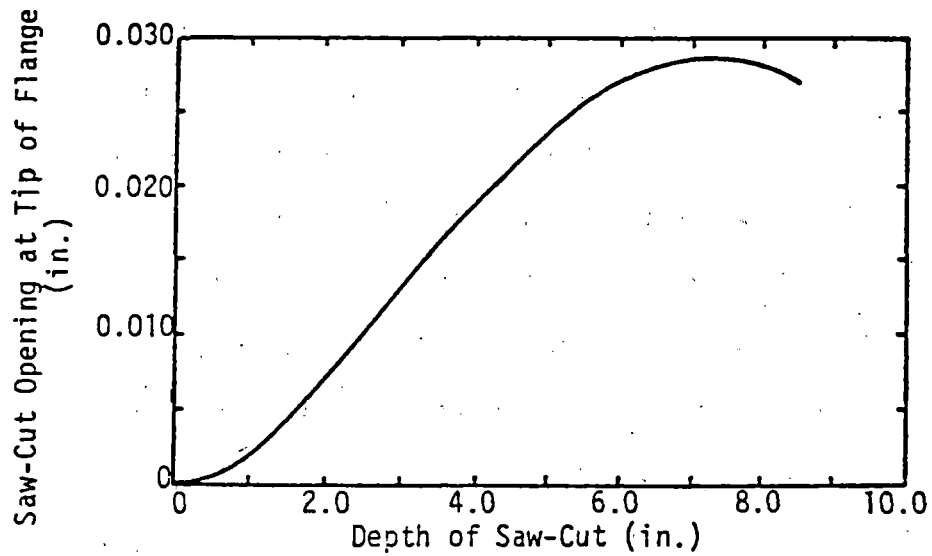
FIGURE 11.11   SAW-CUT OPENING AT TIP OF FLANGE
AS FUNCTION OF DEPTH OF SAW-CUT,
36-INCH DIAMETER, CURVED-PLATE WHEEL
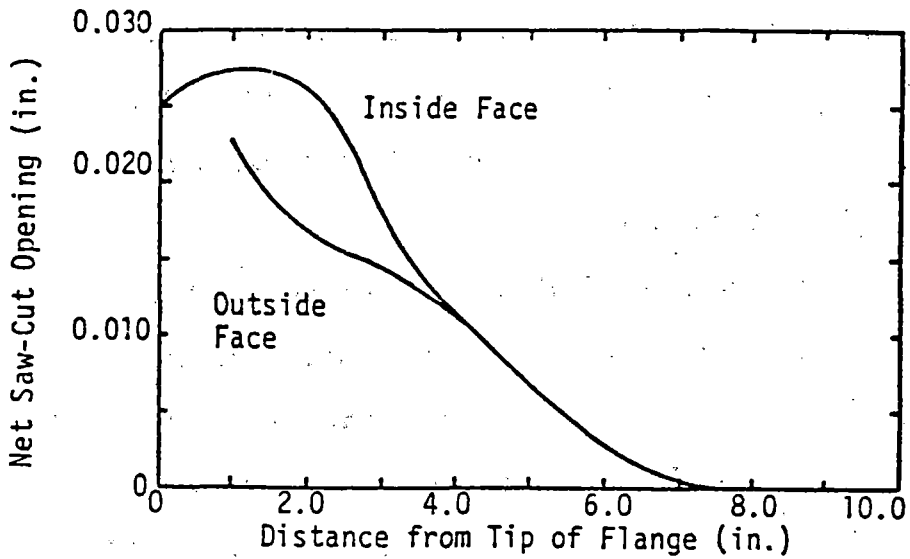
FIGURE 11.12   NET SAW-CUT OPENING AS FUNCTION OF
DEPTH OF CUT INTO WHEEL,
36-INCH DIAMETER, CURVED-PLATE WHEEL

11-25

Figure 11.13 shows the circumferential stresses that are predicted when the cut is closed. The stress distribution pattern in the rim is similar to those shown for the other wheels. The maximum circumferential residual stress predicted for the back rim face is approximately 30 ksi.

By the end of the Wheel Research Program, a large number of wheels had been saw cut in order to estimate the residual stress in the rims of these wheels. Thirty-one of the wheels, which were saw cut under the program, were designated for detailed finite element analysis. These wheels were selected to represent a variety of designs and prior usage. The wheels are listed in Table 11.5, which also summarizes the results of the work.

The first column in the table gives the identification number in the saw-cutting program. The next three columns indicate the wheel design, the class of heat treatment, and the manufacturer. The next column indicates the source of this wheel, whether received from a railroad or used on the program in a special test condition.

The next column indicates whether the finite element analysis is based on the first cut into the wheel or the second cut. A number of the wheels were saw-cut twice. The first cut was made with the clip gage in place to measure the saw-cut opening displacement. The next cut was made 180 degrees from the first saw-cut with no clip gage. This permitted detailed measurements all the way around the periphery of the cut. In most cases where wheels have been saw-cut twice, the cuts 180

FIGURE 11.13   RESIDUAL CIRCUMFERENTIAL STRESS DISTRIBUTION
PREDICTED FOR 36-INCH DIAMETER, CURVED-PLATE
WHEEL FROM SAW-CUT DISPLACEMENT DATA
(STRESSES IN KSI)

TABLE 11.5
WHEELS SELECTED FOR SAW-CUT ANALYSIS

No.	Type	Class	Mfr.	Source	1st or 2nd Cut Analysis	Max. Clip Gage Opening	Max. Opening Saw-cut	Max. Rim Stress & Location	Max. Back Rim Stress Analysis	Special Considerations
3	CJ33	U	Grif	RDU	1	29**	28	31BR	31	RDU 25 - 1 hr. drags
16	CH36	U	Grif	UP	2	13	11	20T	8	
21	CH36	U	Grif	UP	2	24	19	26BR	26	
29	CH36	U	Grif	UP	2	47	45	38BR	38	
30	CH36	U	Grif	UP	2	49	35	41T	39	
57	CH36	U	Grif	UP	2	7	4	11BR	11	
72	H36	C		UP	2	19	19	17BR	17	
132	CJ33		Grif	UP	2	6	0(-15)	22T/FR	15	
156	CJ33	U	Grif	NEW	2	11	0(-18)	12BR	12	New Wheel
208	J33	U	Cnd.Stl.	DYN	2	18	13	39BR	39	
209	CJ33	U	Grif	DYN	2	11	8	17FR	10	
210	J33	C	Std.Stl.	DYN	2	15	14	25T	10	
212	CH36	U	Abex	BN	2	12	10	29BR	29	
215	CH36	U	Abex	BN	2	19	15	15T	12	
216	CH36	C	Grif	BN	2	26	20	34BR	34	
219	CH36	C	Grif	BN	2	29	25	27BR	27	
230	J33	C	Cnd.stl.	DYN	1	40**	40(0') Fra(120')	100T	73	Unequal Heating Observed.
234	J33	U	Cnd.stl.	DYN	2	16	20	37FR	21	TL-1

(Continued...)

TABLE 11.5 (CONTINUED)
WHEELS SELECTED FOR SAW-CUT ANALYSIS

No.	Type	Class	Mfr.	Source	1st or 2nd Cut Analysis	Max. Clip Gage Opening	Max. Opening Saw-cut	Max. Rim Stress & Location	Max. Back Rim Stress Analysis	Special Considerations
235	J33	U	Cnd.Stl.	DYN	2	63	40	60BR	60	TL-2
249	J33	U	Sum	BN	1	NA	26	33FR	31	
275	CH36	C	Abex	BN	Fractured 1st cut - No analysis					
321	H36	U	Valdn.	BN	Fractured 1st cut - No analysis					
345	CH36	U	Abex	BN	1	NA	13	19BR	19	
361	CH36	U	Abex	BN	1	12*	12	35BR/FR	12	
363	CH36	U	Abex	BN	1	NA	37	54BR	54	Fractured but Analyzable
412	CH36	U	Grif	UP	1	NA	9	17BR	17	
418	CJ33	U	Grif	DYN	1	NA	15	19BR	19	T L - 1 Renormalized
419	J33	U	Cnd.Stl.	DYN	1	NA	25	42T	5	
420	CJ33	U	Grif	DYN	2	41	39	43T	39	TL-1 Machined
421	J33	U		DYN	Fractured 1st cut - No analysis					
422	CJ33	U	Grif	DYN	2	28	19	30T	20	T L - 1 Renorm & Machined

*2nd Cut used cup gage
**Meas. made at tip of flange every 1/2" of cut
T = Tread Crack
FR = Front Rimc
BR = Back Rim

TL-1 = Thermal load #1
    40 mph, 1500 lb. brake force, 25 cycles
TL-2 = Thermal Load #2
    20 mph, 3000 lb. brake force, 25 cycles
Machined = Machined to reapplication limit
NA = Not available

degrees apart, there has been little difference in the saw-cut opening displacement curve. In the later stages of the saw-cutting program, some wheels were cut without the clip gage in place. For these cases, the analysis was made from measurements on this first cut into the wheel, as indicated in the table.

The next column in the table indicates the maximum opening of the clip gage (in thousandths of an inch) where this information is available. The next column indicates the maximum opening of the saw-cut which was measured for the analysis. The next column indicates the maximum predicted residual circumferential stress in the rim of the wheel and its location. The next column gives the maximum predicted residual circumferential rim stress on the back rim face. The final column in the table indicates any special conditions which might be associated with the wheel.

The results from the analyses have also been summarized on two figures. Figure 11.14 presents results from all of the Griffin wheels. Figure 11.15 presents results from the remainder of the wheels. Three items of information are noted on these figures for each wheel. First, for every wheel, the maximum residual stress on the back rim is plotted as a function of the maximum measured opening of the saw-cut. This point is indicated by a small circle. Where the maximum opening of the clip gage was different from the maximum measured opening of the cut, this is indicated by a small triangle on the figure and the triangle is linked by a line to the corresponding circular
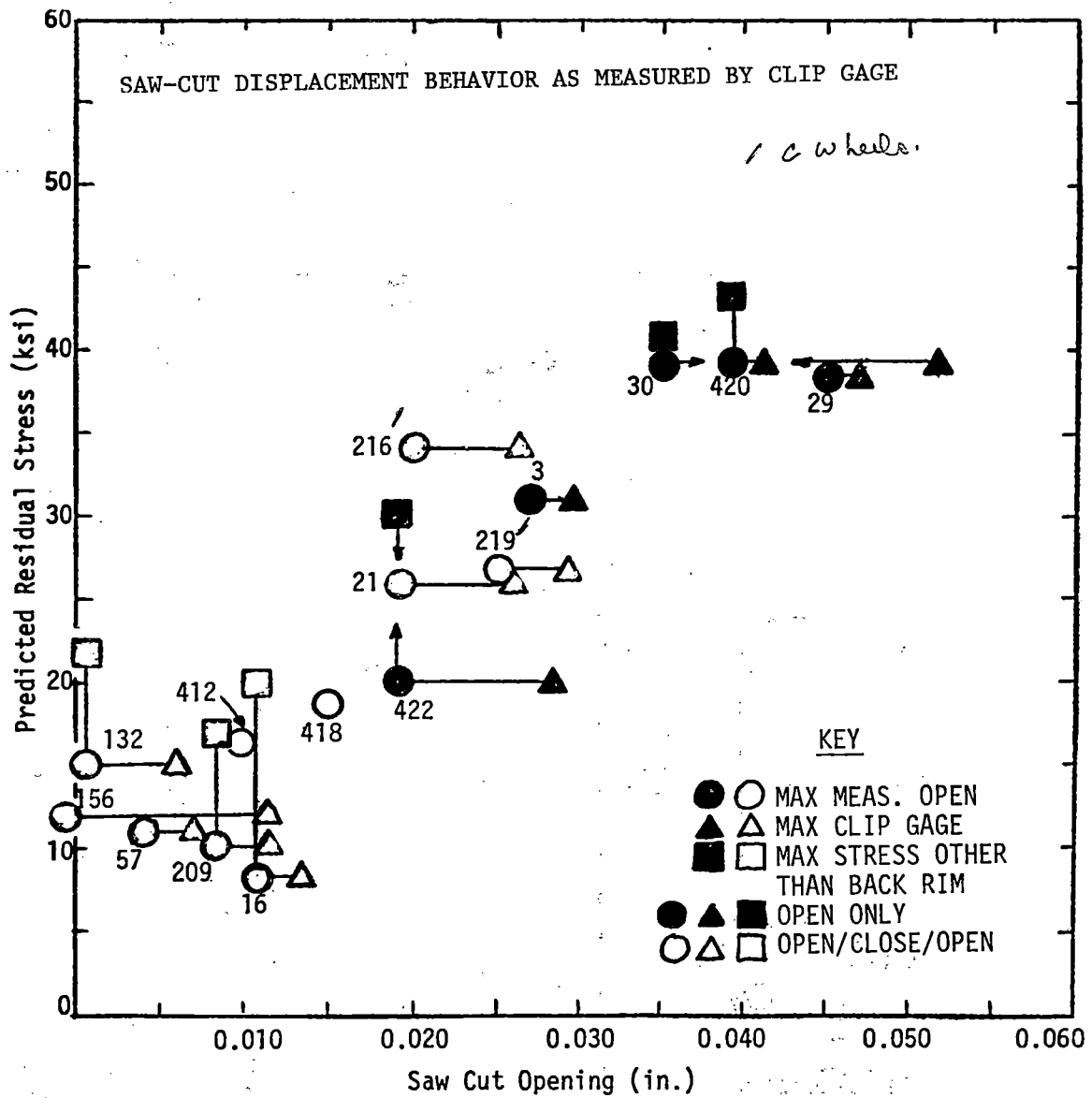
FIGURE 11.14   3D-FINITE ELEMENT ANALYSIS OF SAW-CUT
DISPLACEMENT DATA (FOR GRIFFIN WHEELS)

* 412 AND 418 HAD NO CLIP GAGE

SAW-CUT DISPLACEMENT BEHAVIOR AS MEASURED BY
CLIP GAGE
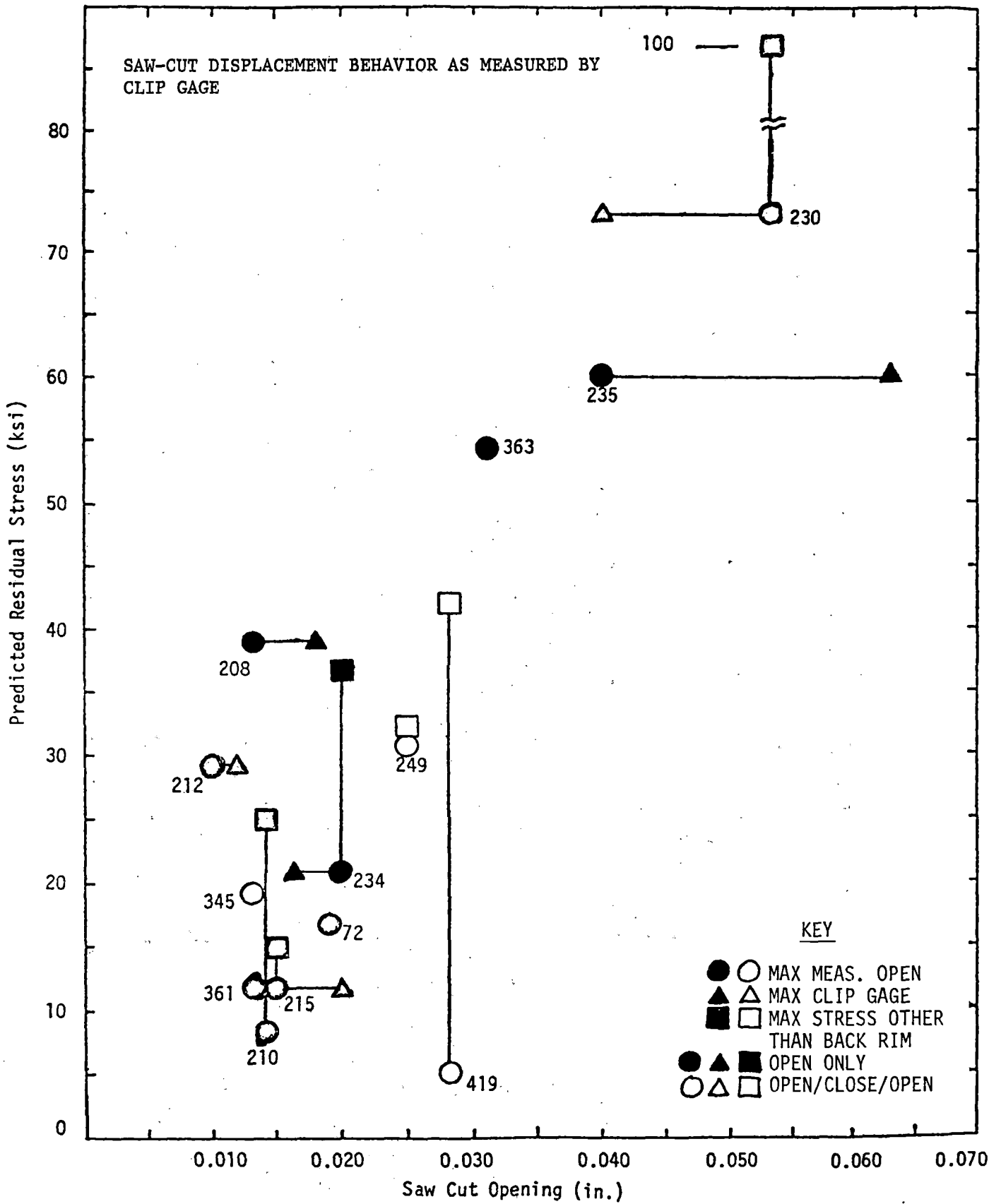
FIGURE 11.15   3D-FINITE ELEMENT ANALYSIS OF SAW-CUT
DISPLACEMENT DATA
(FOR WHEELS OTHER THAN GRIFFIN TYPE)

* 419, 249, AND 349 HAD NO CLIP GAGE

11-32

point. In those cases where the maximum stress was not on the back rim, this is indicated by a small square box. Again, this point is linked to the corresponding circular point.

It will be noted that each of these plots shows a general relationship where the maximum predicted stress in the wheel is a function of the maximum opening of the saw-cut.

11.2.3   Closed Form 2D Analysis of Saw-Cut Flange Tip Opening
         Behavior

The second approach in the evaluation of residual stresses from the saw-cut displacement data consisted of the development of a simple mathematical model for determining the average hoop stress distribution in a saw-cut wheel.

The model assumes that the cut portion of the wheel consists of several interconnected rings. Using the reverse saw-cut displacement response, the rings are brought to their original position. When the radial saw-cut is made, hoop and shear stresses are released on the cut surface, causing individual rings to displace circumferentially and radially. If the cut surfaces are subjected to the released stress distribution, they will merge and the wheel will be in its original position (before the saw-cut). During this process, radial and shear stresses are developed on the interface of adjacent rings, due to relative displacements. The hoop and shear stresses acting on the tip of an individual ring can then be determined as a function of the tip displacement and the stresses on the

interface. For this purpose, an individual ring is separated from the rest; and equations based on theory of elasticity are developed for determining stresses acting on the tip, which equilibrate with the stresses on the outer and inner interface, and are compatible with tip displacements. Finally, all the individual rings are reconnected. In the process, the complete hoop and shear stress distribution in the radial direction is generated for the depth of the saw-cut.

In this second approach, the results from the analyses were used to calculate the total circumferential force in the rim of the wheel and this force is suggested as a measure of the safety of the wheel. A typical average stress distribution and total circumferential force predicted by this model are presented in Figure 11.16. The complete details of the above analytical method for determining average residual stress in railroad wheels is presented in Appendix 11.4.

An estimate of the accuracy of the second method for predicting the rim force is made by comparing the results with those from a 3D-finite element analysis. The results were surprisingly close, with the promise that the second method, though simple, does give reasonable predictions of rim force.

Even though the simple analysis suggested in the second approach does not show the stress gradient across the cross section, it is indeed helpful in interpreting the saw-cut displacement data, and the computed average residual stress can be compared for a given family of wheels which exhibit varied degrees of opening, closing, or mixed behaviors. The net rim
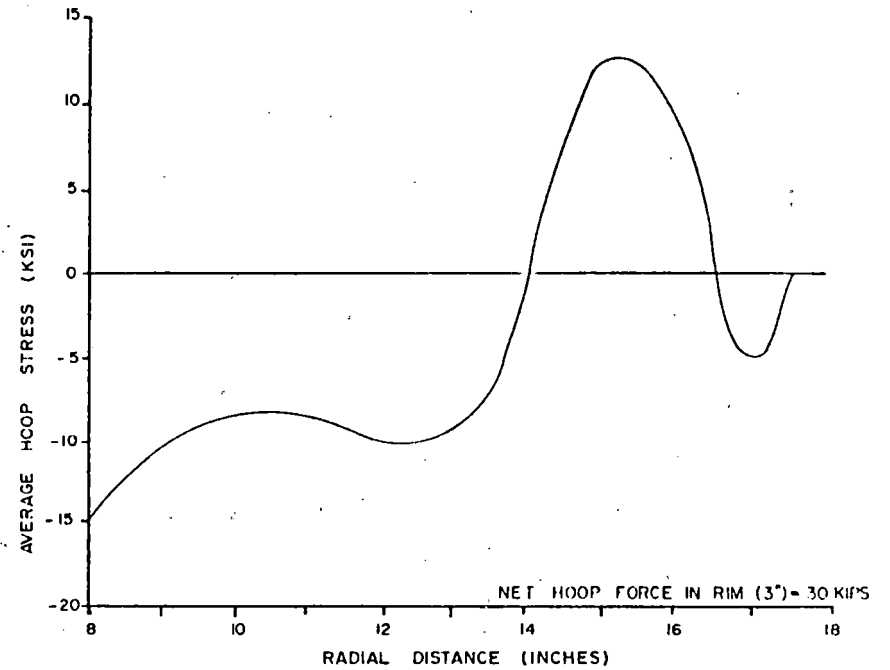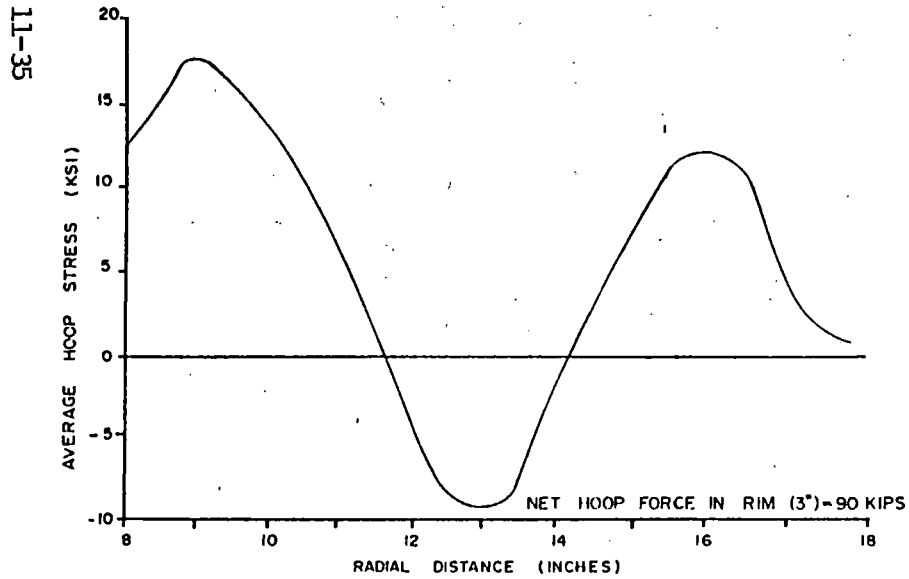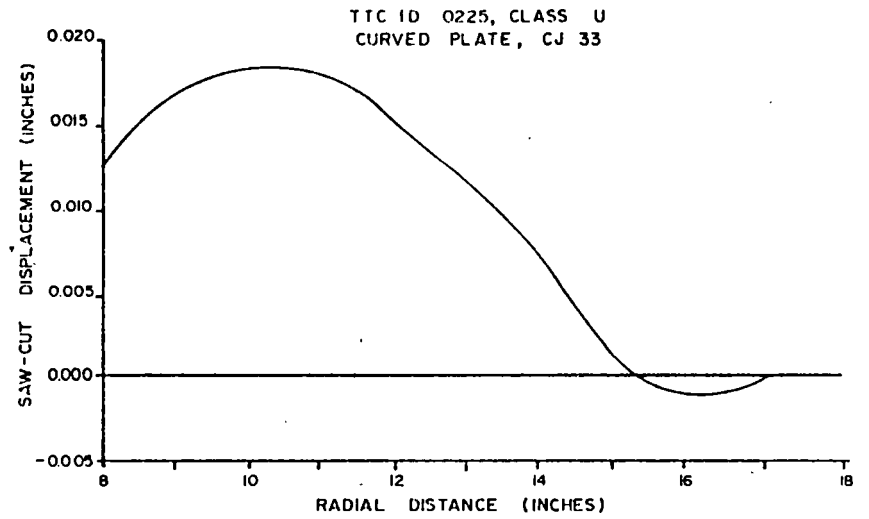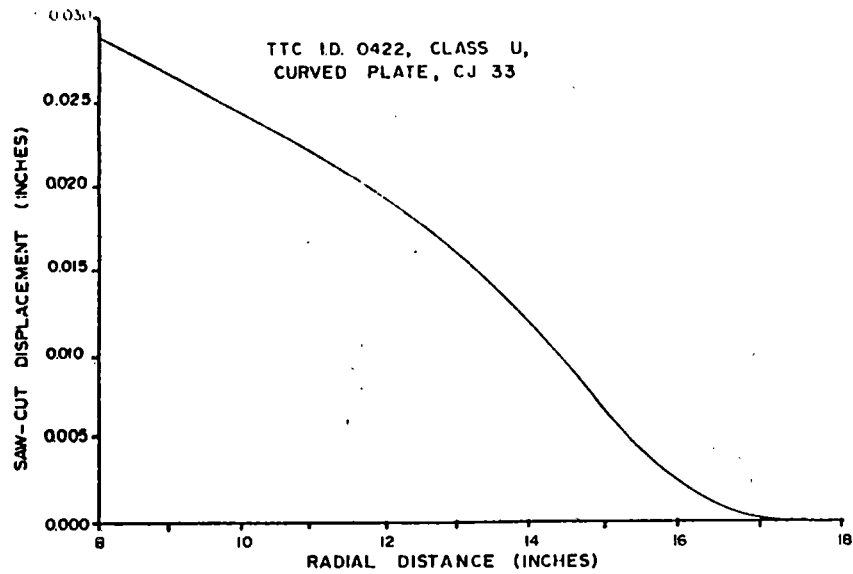
FIGURE 11.16   AVERAGE HOOP STRESS DISTRIBUTION AND NET RIM
FORCES FOR 33 INCH DIAMETER SAW-CUT WHEELS

force computed by the analysis can be compared to the rim force of fractured wheels during saw-cutting for the same family of wheels such that the "rim failure potential index" of the saw-cut wheel based on its saw-cut displacement behaviors can be evaluated.

Since finite element analysis for predicting residual stress state from detailed measurements of saw-cut opening is expensive, the suggested analytical procedure serves as an inexpensive and quick method to determine average residual stress distribution for a large number of wheels that were saw-cut at Pueblo. From a large data base of average residual stress distribution and net rim forces, a statistical analysis was performed for different classes and shapes of wheels that are discolored or nondiscolored.

11.2.4   Methodology of Analytical Procedure

This method assumes that the cut portion of the wheel is made up of several interconnected fictitious rings. Adjacent rings develop interactive shear and radial stresses on the corresponding interface, depending on the magnitude of relative displacement between them. When the radial saw cut is made, hoop and shear stresses are replaced on the cut surface (Figure 11.17), causing the rings to displace radially and circumferentially. The hoop and shear stresses on the tip of an individual ring can then be determined as a function of the tip displacement and the stresses on the interface.
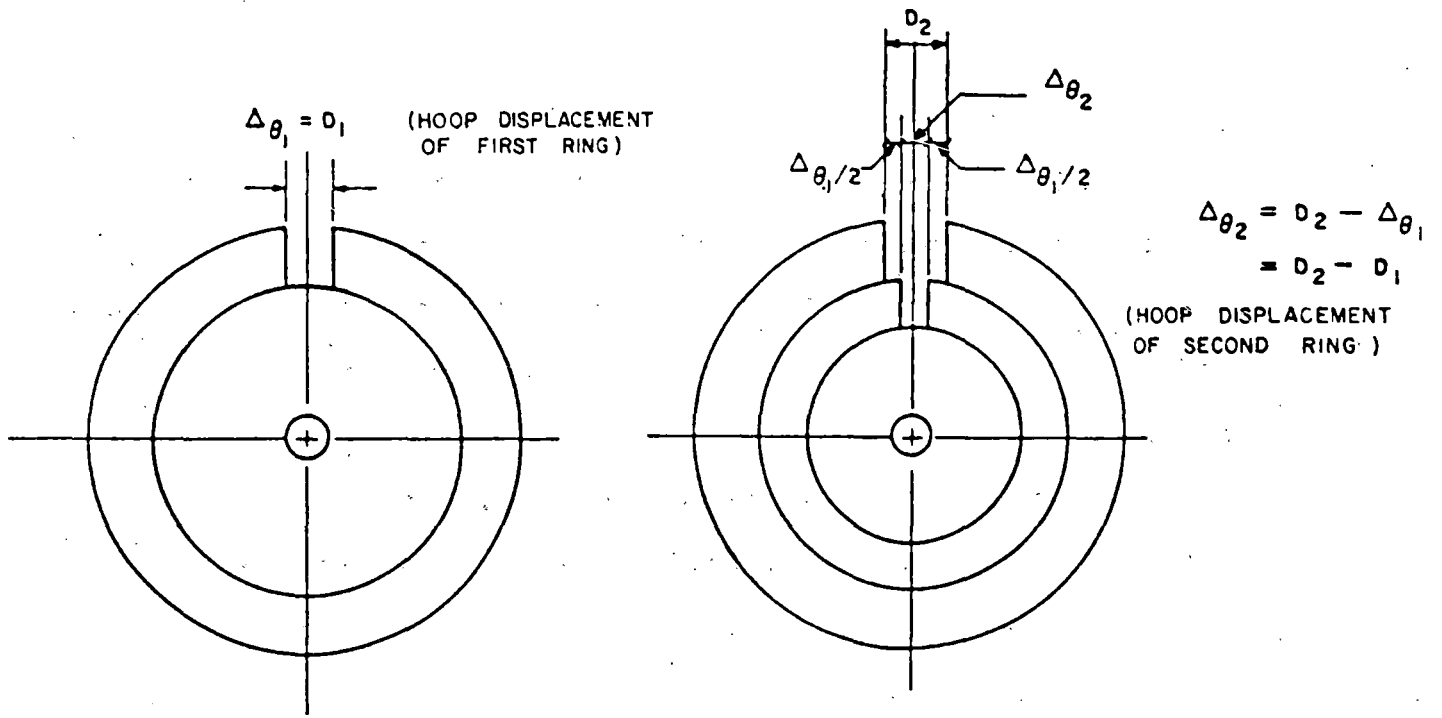
THE FIRST CUT

THE SECOND CUT

$\Delta_{\theta_2} = D_2 - \Delta_{\theta_1}$

$= D_2 - D_1$

(HOOP DISPLACEMENT OF SECOND RING)
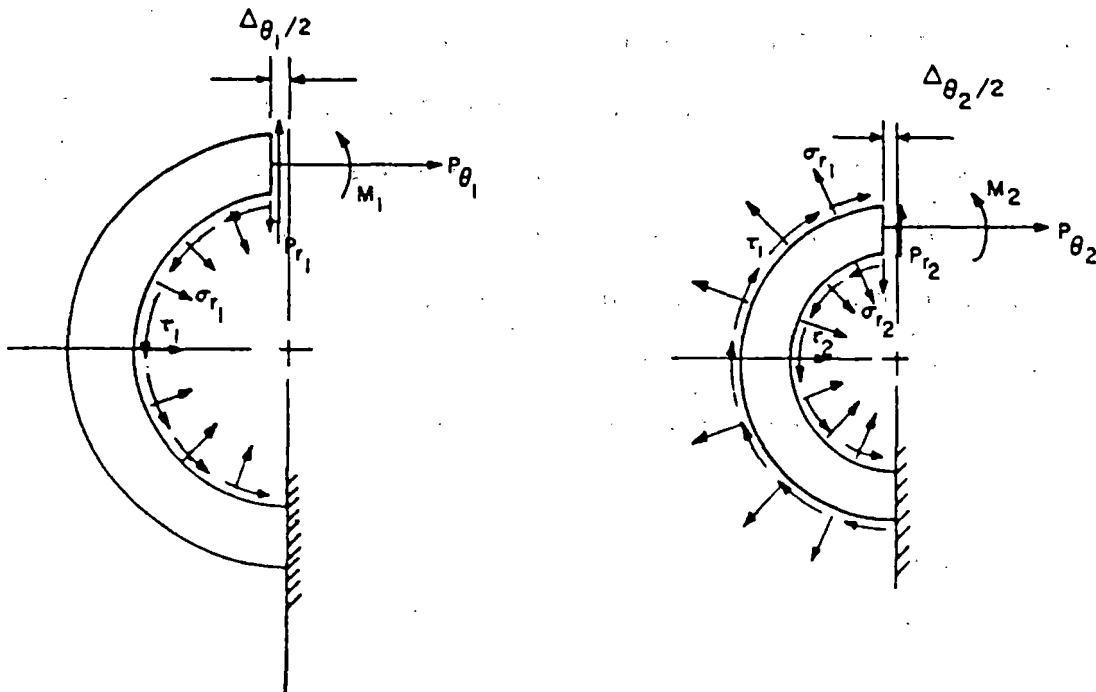
P_θ = HOOP FORCE ;   M = MOMENT ; P_r = SHEAR FORCE

τ & σ_r = SHEAR AND RADIAL STRESSES AT THE INTERFACE OF SUCCESSIVE RINGS

FIGURE 11.17   ANALYSIS OF RADIAL SAW-CUT IN TERMS OF INTERCONNECTED FICTITIOUS RINGS

11-37

For analysis, an individual ring is separated from the rest of the wheel. Equations based on the theory of elasticity are developed to determine stresses acting on the tip of individual rings which are in equilibrium with the stresses on the outer and inner interface, as well as compatible with the tip displacements.

A numerical procedure based on the above analytical method is set up with the use of a computer program which uses the clip gage displacement characteristic, against the depth of cut in the digitized form, as input.

At every incremental cut, the hoop force, shear force, and moment acting on the cut surface are computed. The nonuniformity in the thickness of the wheel in the radial direction is taken into account, and a special scheme of computations is set up to evaluate the hoop and shear stresses along the depth of the saw cut, for different wheel designs.

To test the performance of the numerical procedure, the general saw cut behavior of the wheel population was classified into a few categories based on the rate of opening during the saw cut. A family of hyperbolic tangent (tanh) curves were generated to simulate the categories of opening behavior with the general equation:

$$D = c_1 \tanh (c_2 \, x^n)$$

where

D = displacement in hoop direction

x = depth of cut

c_1, c_2 and n= constants selected to generate the curves with varied amounts of rate of opening.

Figure 11.18 presents typical straight opening and mixed opening behaviors. Mixed opening represents initial closing of the wheel during the saw cut, followed by opening. For the sake of convenience, the wheel radius is shown on the x-axis, with the depth of the cut initiated from the flange tip (right to left). In this specific evaluation, the maximum amount of opening at 8 inches depth of cut was limited to 0.05 inch. A one-wear, 36-inch diameter, curved plate wheel was used in the numerical procedure with the above simulated saw cut responses in the form of hyperbolic tangent curves.

The results, in the form of average residual hoop stress distribution across the cross section, starting from the flange tip to a depth of 10 inches, are presented in Figure 11.19.

It can be seen that the magnitude and distribution of average residual circumferential stress in the rim of the wheel is dependent on the rate of opening during the saw cutting operation, as well as on the maximum opening that occurs around 8 to 10 inches of depth of cut. With mixed behavior during the saw cutting operation (closing followed by opening), the hoop stress distribution in the rim is dependent on the depth of cut at which the saw cut begins to open from the initial closing, as
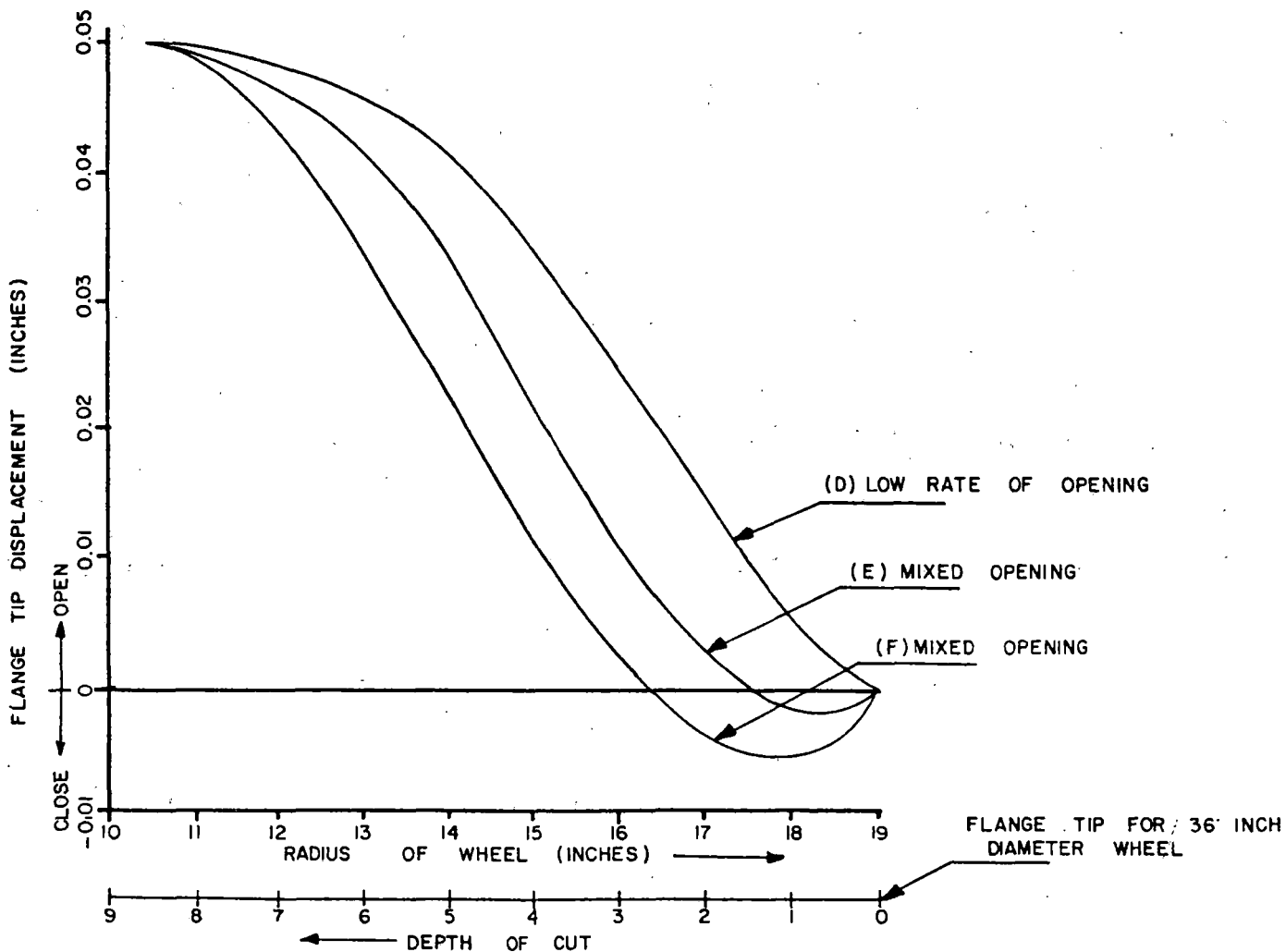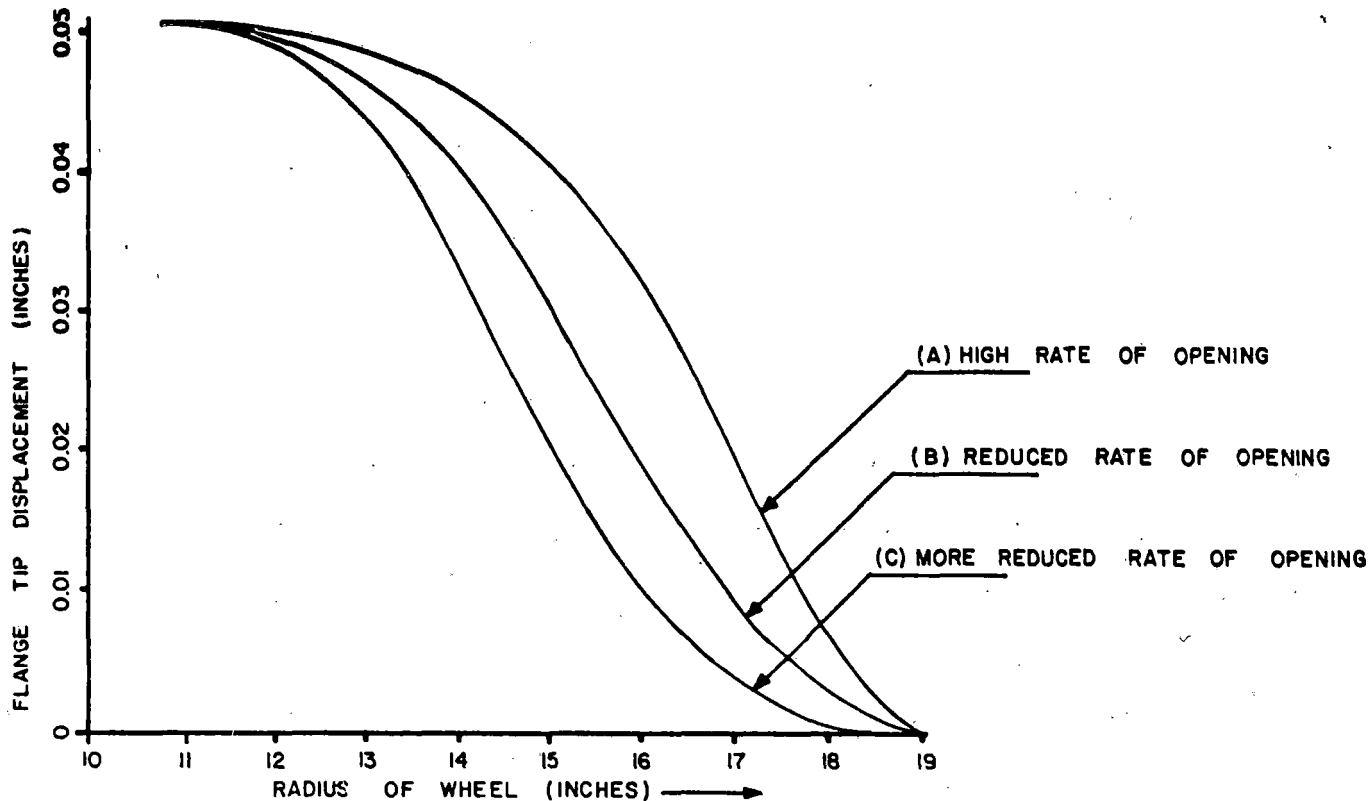
FIGURE 11.18   TYPICAL STRAIGHT OPENING AND MIXED OPENING
BEHAVIORS (DURING RADIAL SAW-CUT) REPRESENTED
BY TANGENT HYPERBOLIC (tanh) CURVES

11-40
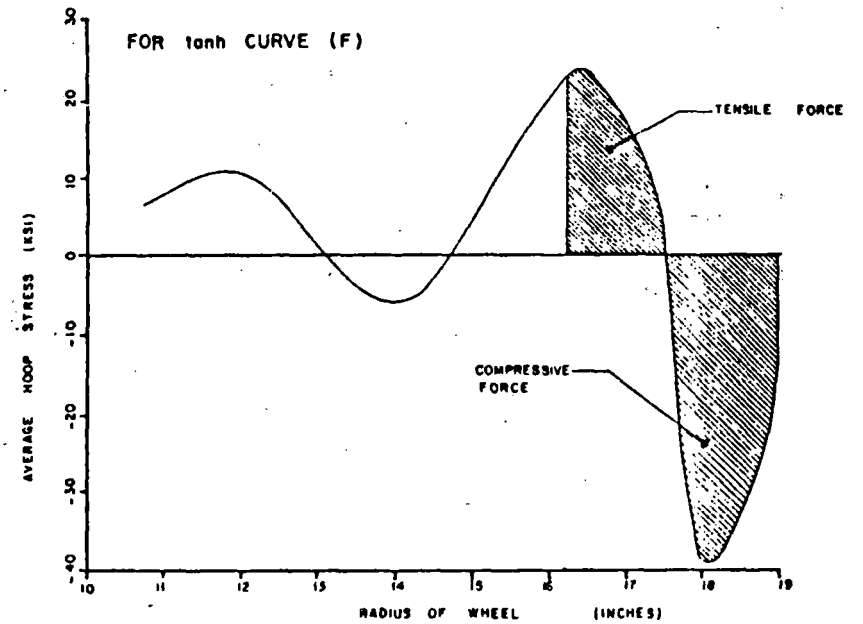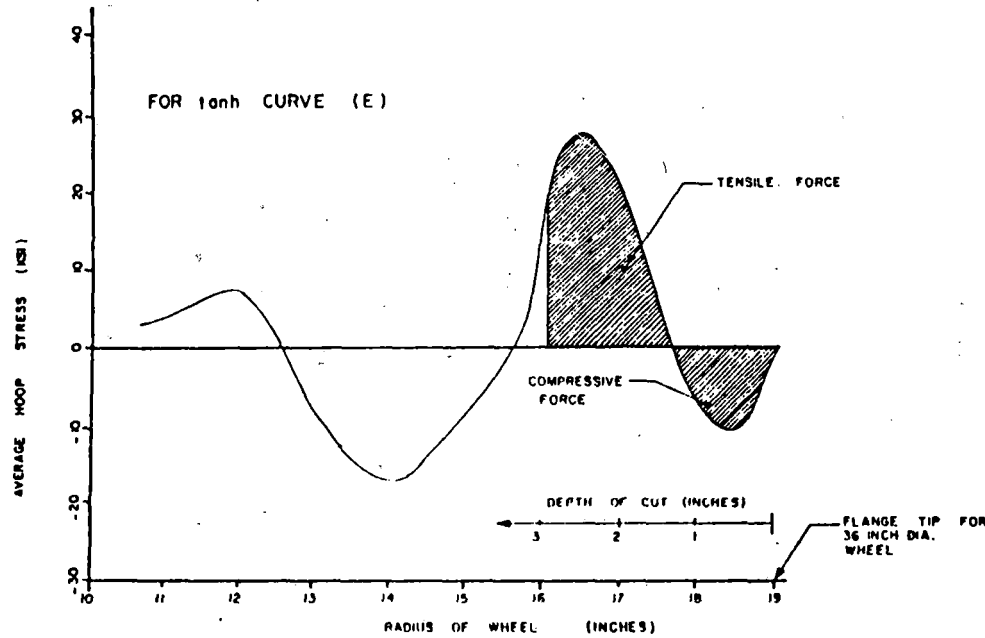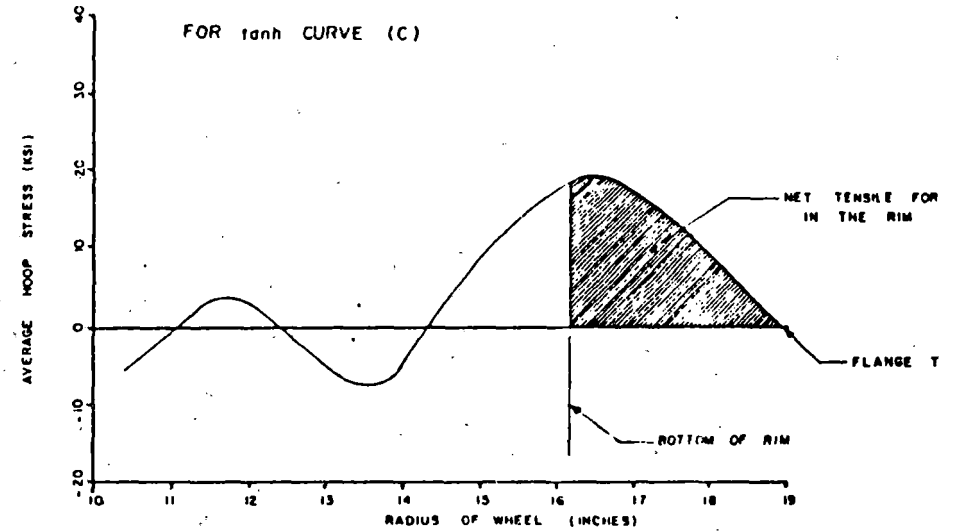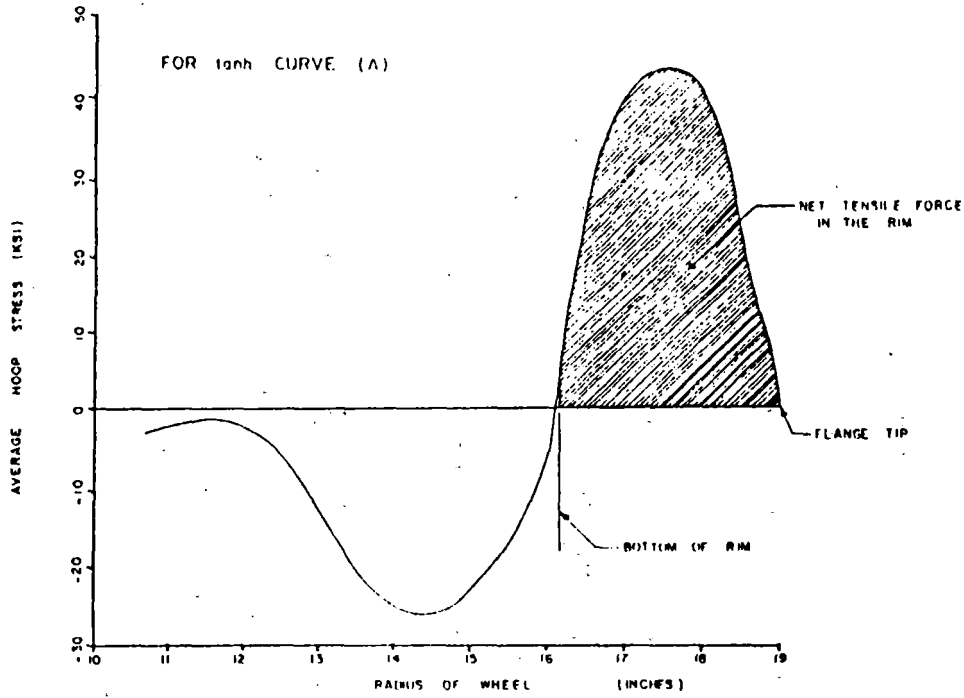
FIGURE 11.19   VARIATION OF AVERAGE HOOP STRESS FOR 36-INCH DIAMETER, CURVED PLATE, ONE WEAR WHEELS WHICH EXHIBITTED VARIOUS SAW-CUT OPENING BEHAVIORS

well as on the maximum amount of opening that follows. Figure 11.19 shows the variation of average hoop stress for 36-inch diameter, curved plate, one-wear wheels which exhibited various saw cut opening behaviors.

11.2.5   Analysis of Wheels from Saw Cut Displacement Data

After successful implementation of the newly developed analytical approach on hyperbolic tangent curves which simulated various types of wheel responses to radial saw cutting, this method was applied to actual wheel hoop displacement responses that were recorded during the radial saw cutting operation.

From the saw cut displacement data base of 612 service and test wheels, more than 300 wheels were analyzed by the proposed analytical method.

The saw cut displacement in the hoop direction, as recorded by the clip gage for each wheel, was used as input to the numerical procedure; and the average residual stress distribution in the wheel (before saw cut) was estimated.

An integration was performed from the flange tip to a depth of three inches, so as to evaluate the net force in the rim. (At each incremental depth, the force was determined from the average residual stress at that depth and the incremental area of wheel cross section.)

Saw-cut displacement responses which exhibited higher rates of opening resulted in higher levels of residual stresses, giving rise to larger tensile forces in the rim (Figure 11.20).
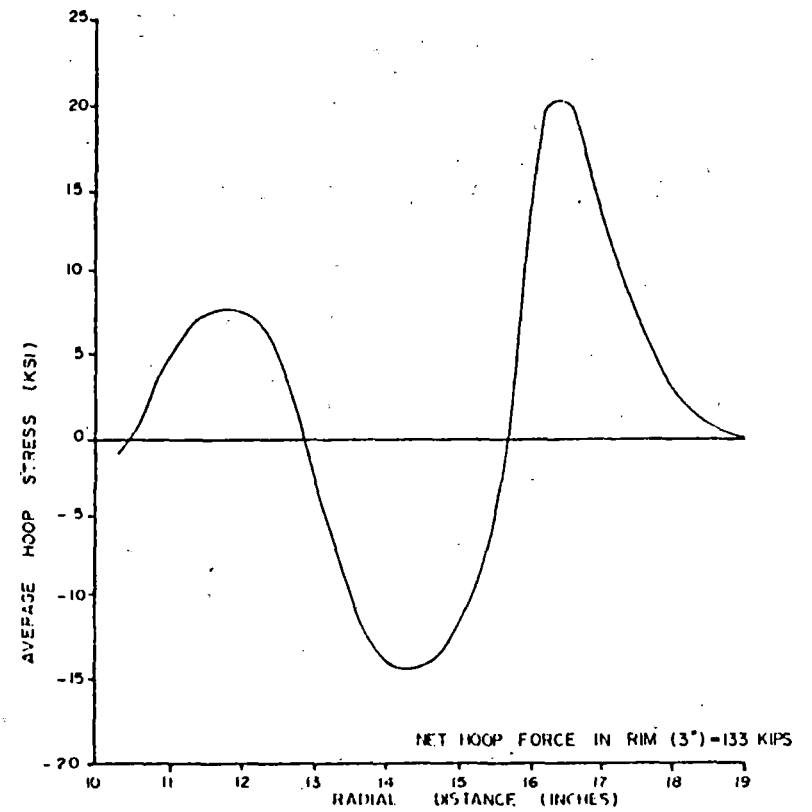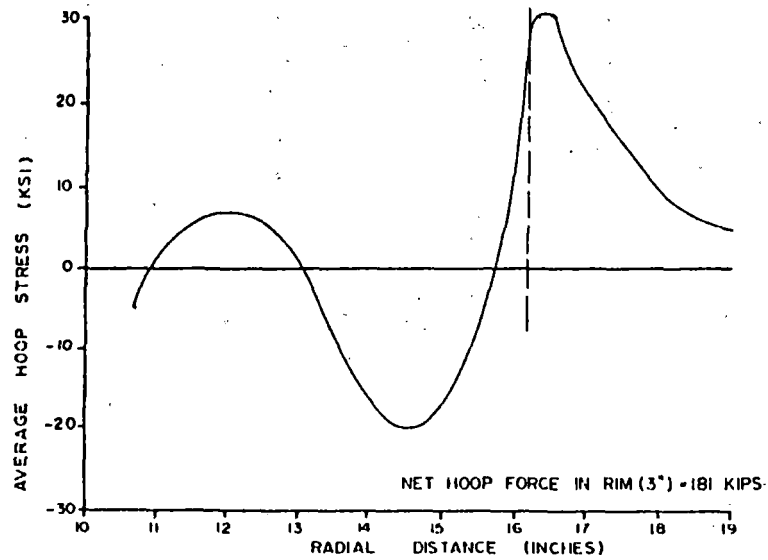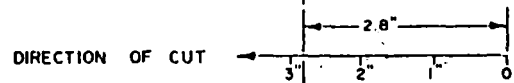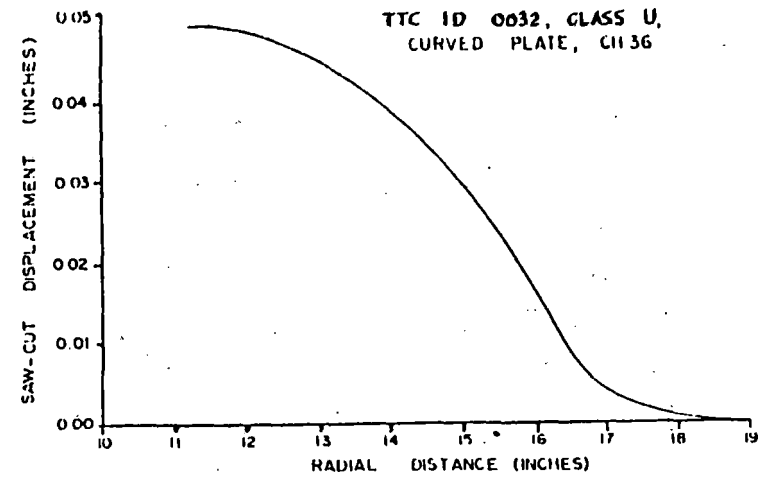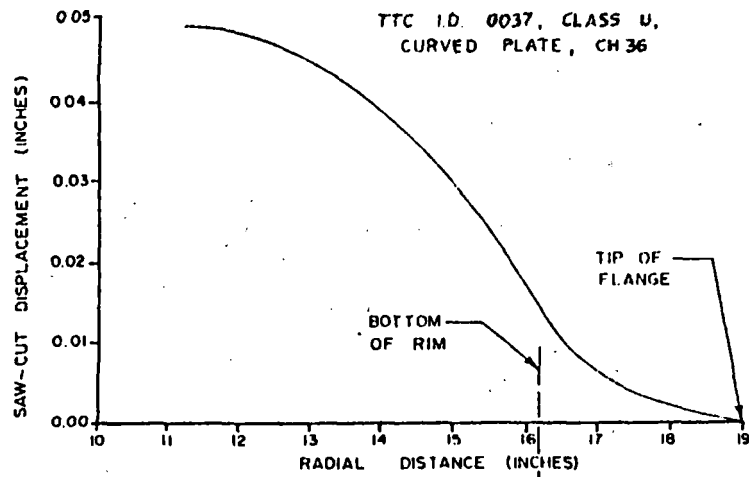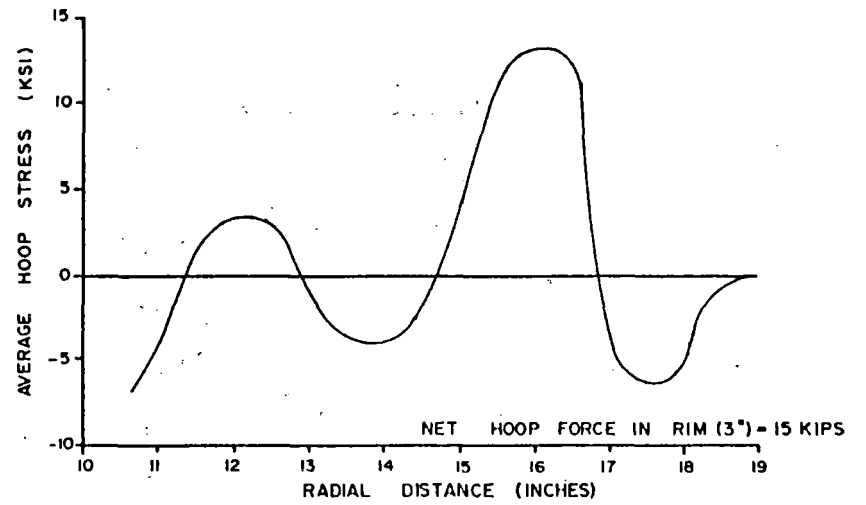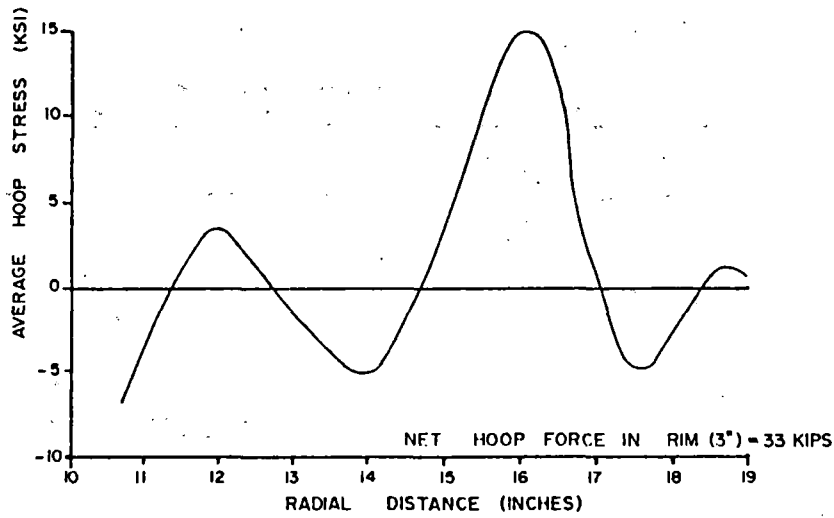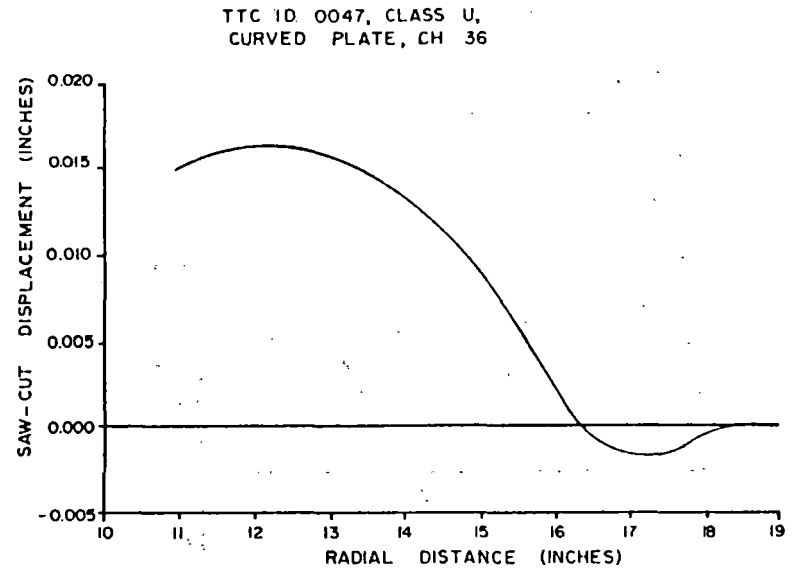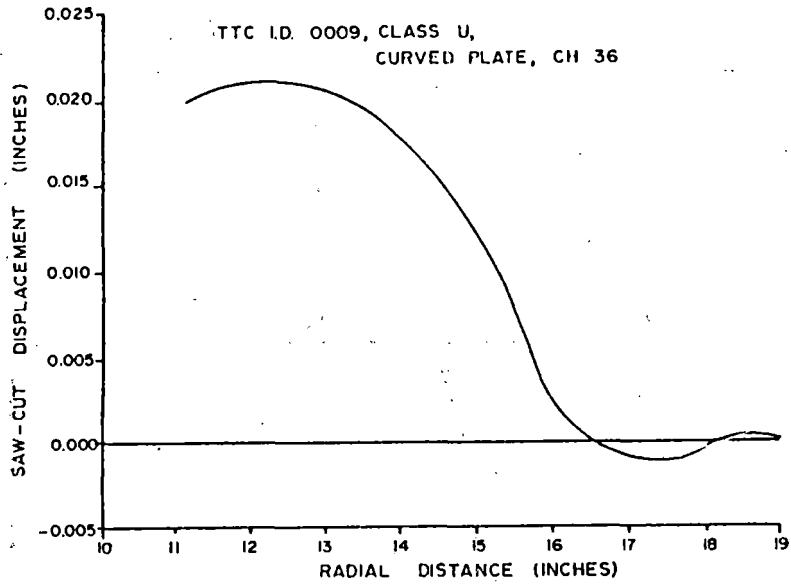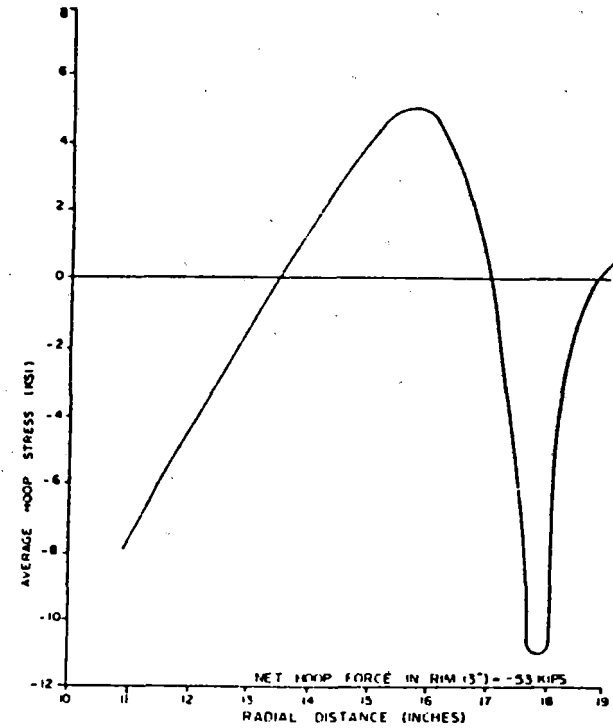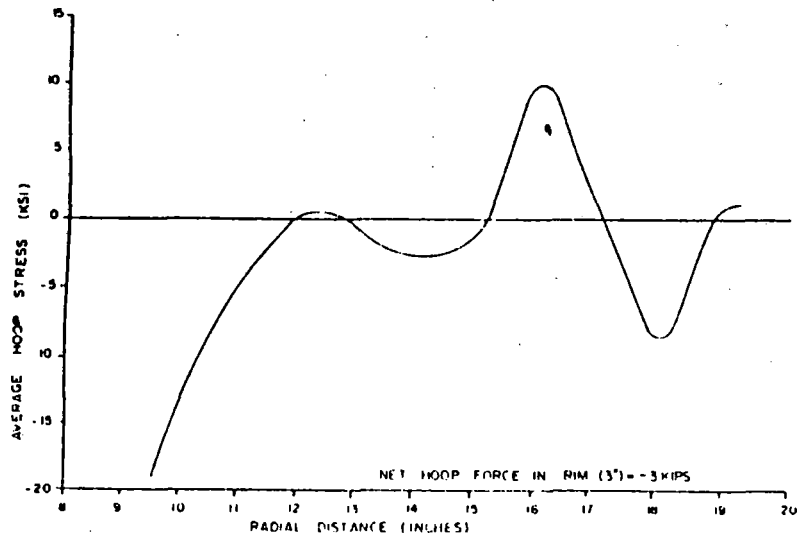
FIGURE 11.20   AVERAGE HOOP STRESS DISTRIBUTION AND NET RIM FORCES FOR 36-IN
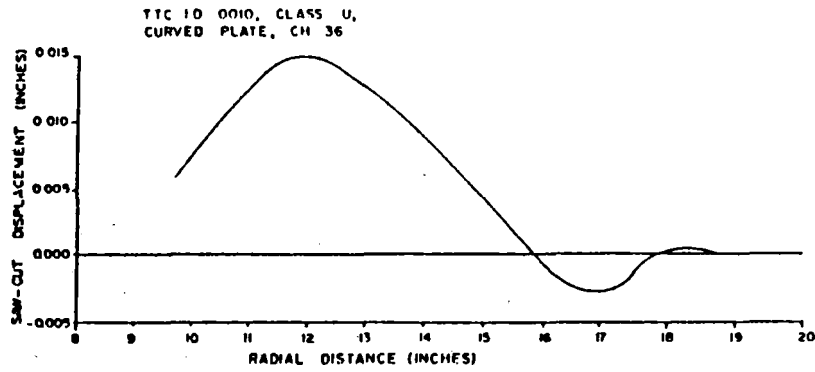DIAMETER SAW-CUT WHEELS

11-43

Responses of wheels to radial saw cutting exhibiting mixed behavior showed lesser amounts of residual stress levels and relatively lower levels of rim tensile forces (Figure 11.21). Figure 11.22 shows a typical mixed opening behavior which resulted in a net compressive force in the rim.

The closing behavior of a wheel to radial saw cutting resulted in net compressive forces in the rim. Definite trends were observed between the computed net rim forces and the saw cut opening behaviors for different categories of wheels analyzed. Figures 11.23 and 11.24 show typical trends of net rim forces for Class U, 36-inch diameter, curved plate and straight plate wheels. There seems to be a distinct difference in trends between the mixed opening behavior and straight opening behavior of the above two categories of wheels. Similar differences were also observed for 33-inch diameter, Class U, curved plate wheels, as shown in Figure 11.25.

During the saw cutting operation, a small percentage of wheels fractured. These wheels were also analyzed from the saw cut opening behavior recorded before the actual occurrence of fracture. Figures 11.26 and 11.27 show typical responses before fracture and the corresponding rim forces from analysis.

Typical tensile rim forces of 230 kips and more were evident in wheels that fractured during radial saw cutting.

For a given category of wheels, the net rim force before fracture was taken as the baseline data, and this parameter was compared with the rim force corresponding to various saw cut opening behaviors for the family of wheels. An index was

FIGURE 11.21   AVERAGE HOOP STRESS DISTRIBUTION AND NET RIM FORCES FOR 36-IN DIAMETER SAW-CUT WHEELS
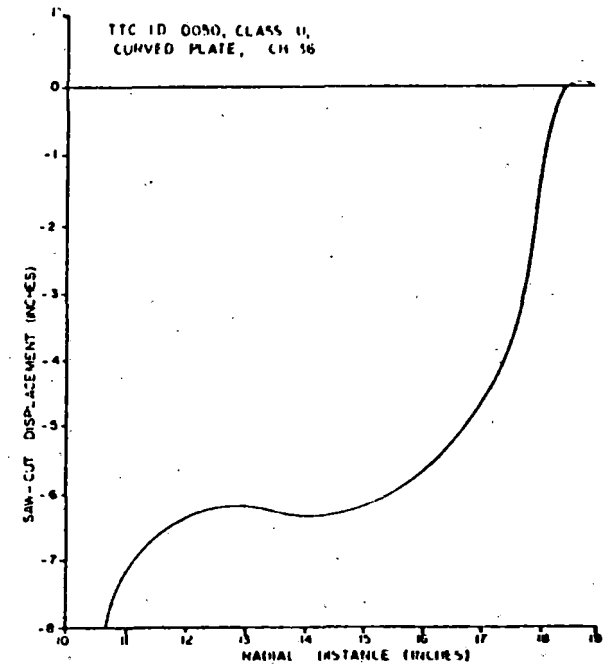
FIGURE 11.22   AVERAGE HOOP STRESS DISTRIBUTION AND NET RIM FORCES FOR 36-IN
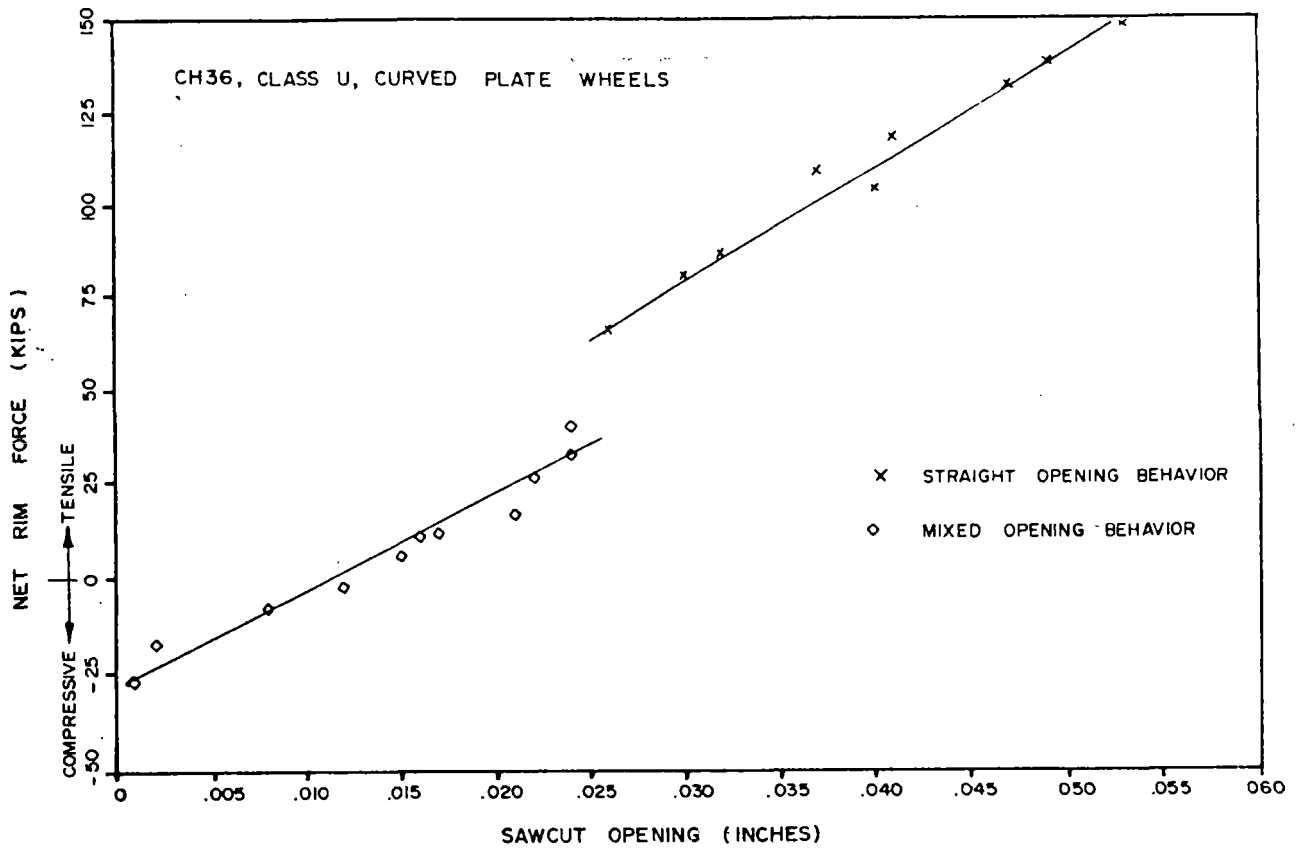DIAMETER SAW-CUT WHEELS

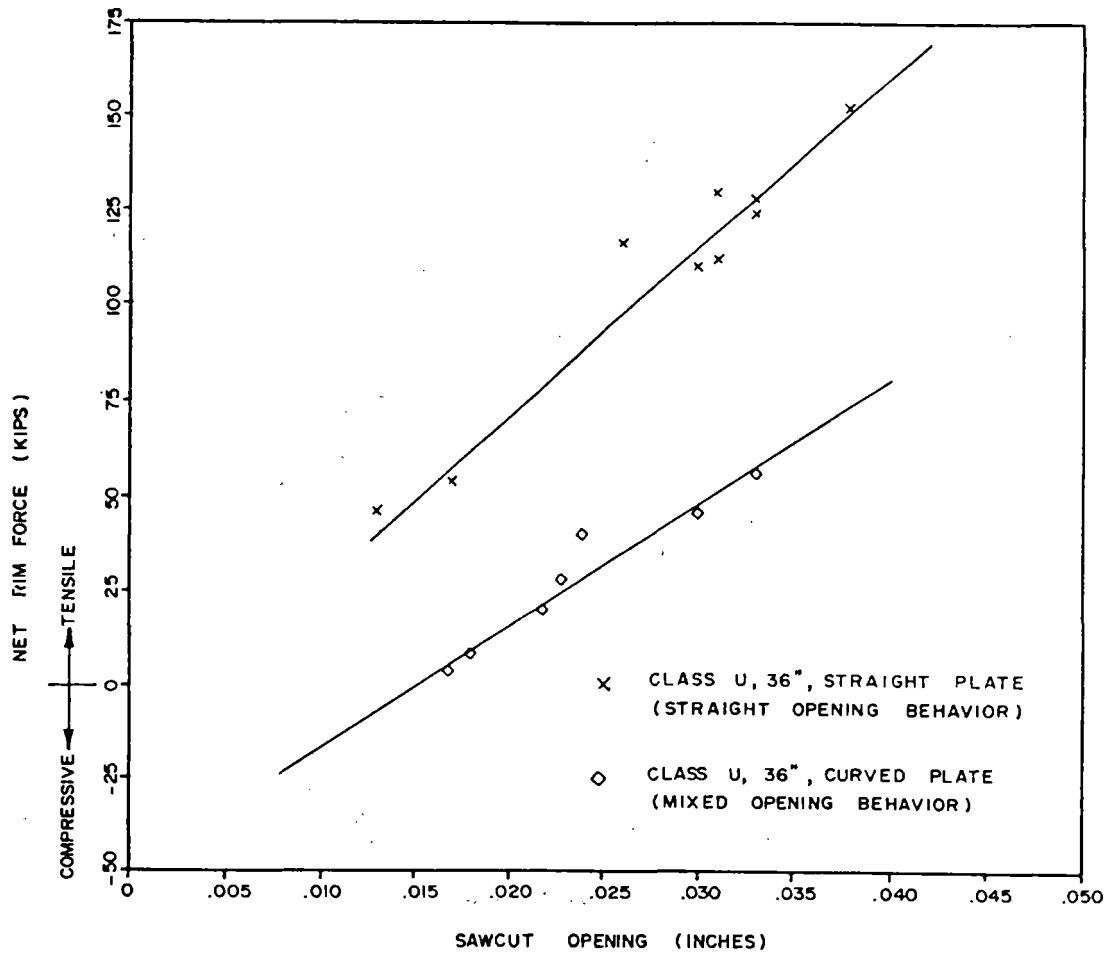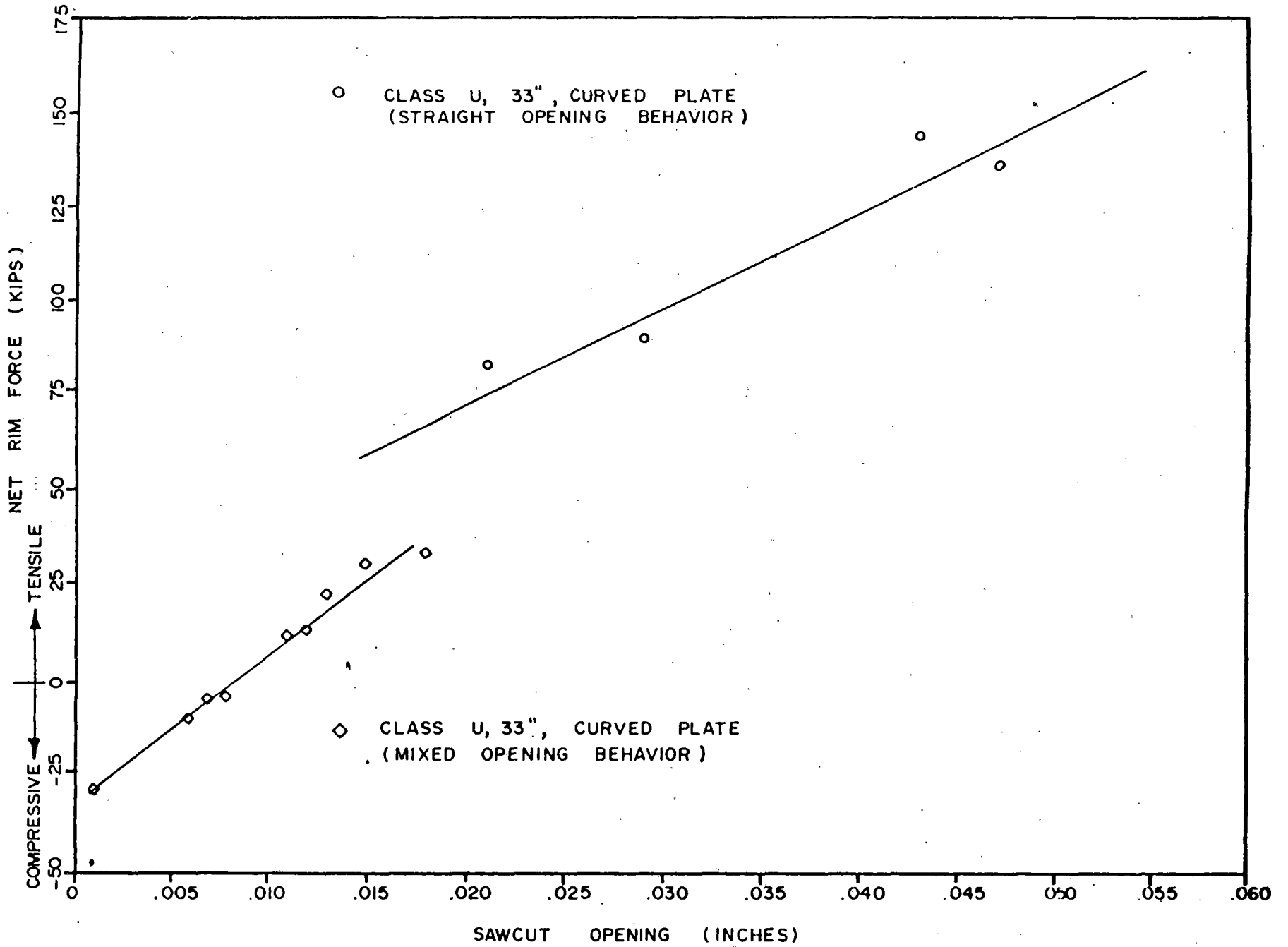FIGURE 11.23   NET RIM FORCES -VS- SAW-CUT OPENING

FIGURE 11.24   NET RIM FORCES -VS- SAW-CUT OPENING

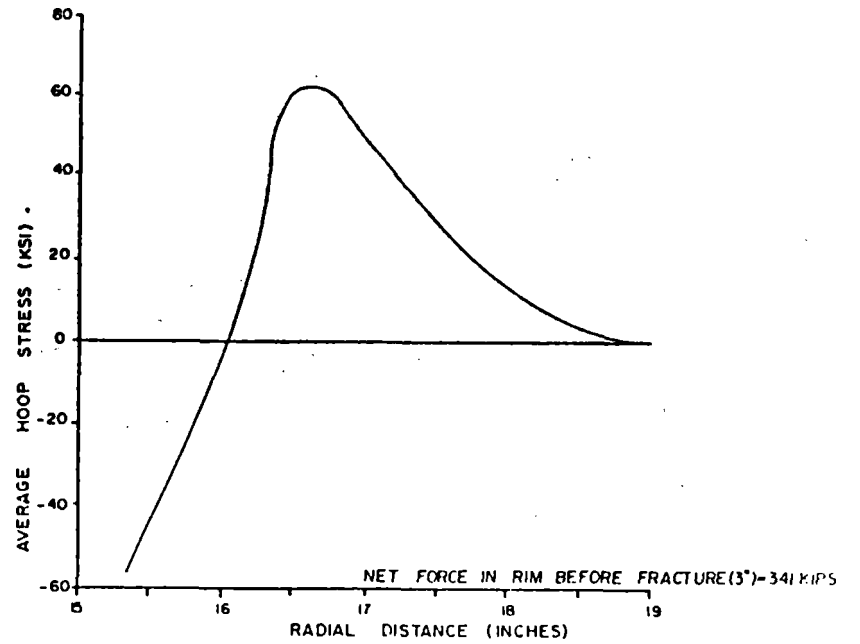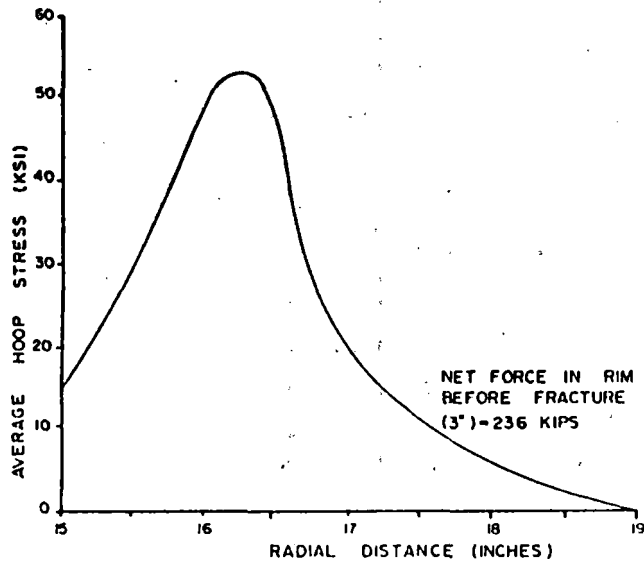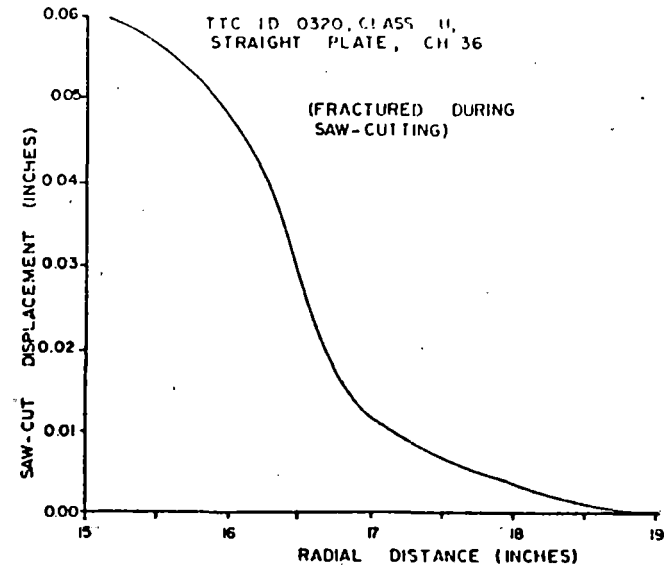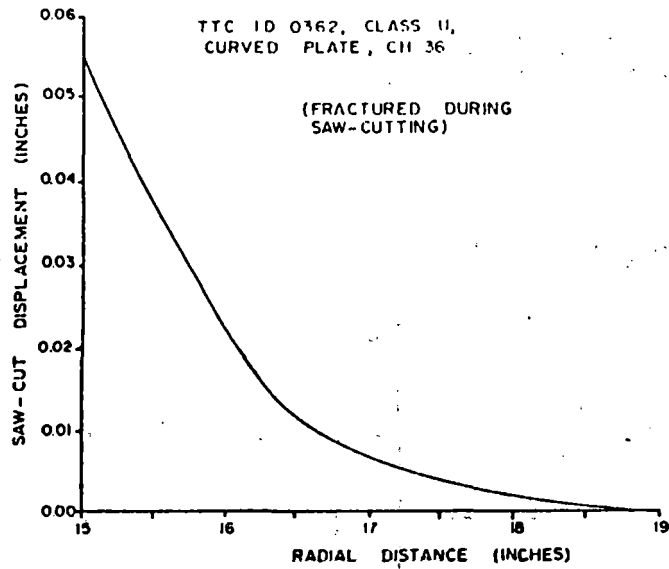FIGURE 11.25   NET RIM FORCES -VS- SAW-CUT OPENING

11-48

FIGURE 11.26   AVERAGE HOOP STRESS DISTRIBUTION AND NET RIM FORCES FOR
FRACTURED CLASS U WHEELS DURING SAW-CUTTING
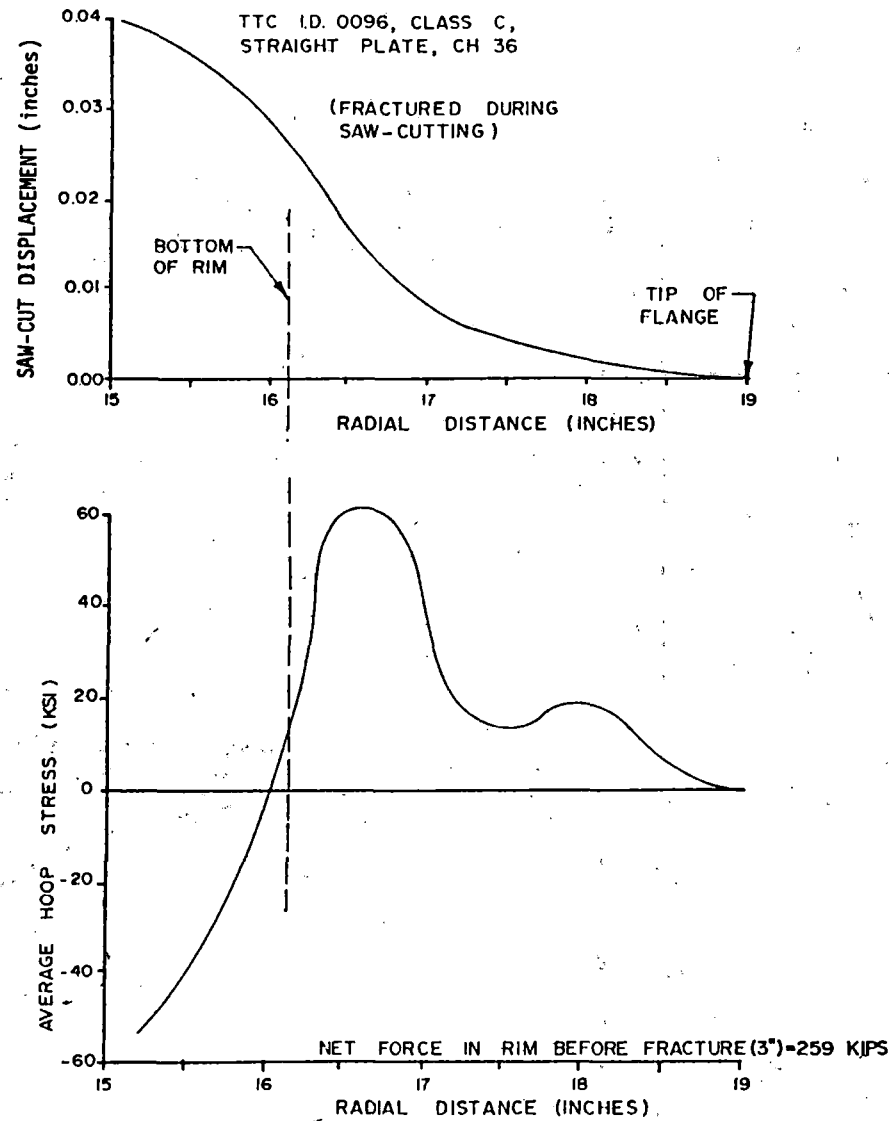
FIGURE 11.27 AVERAGE HOOP STRESS DISTRIBUTION AND NET RIM FORCES FOR FRACTURED CLASS C WHEELS

developed known as "Rim Failure Potential Index", which is the ratio of the net rim forces for a given wheel and the force corresponding to fractured wheels in that particular category.

Table 11.6 presents the typical representative values of this index for Class U, curved plate wheels. From this index, it is possible to interpret the failure potential of any wheel from its saw cut response behavior.

This type of index becomes very meaningful when a large population of wheels are analyzed by radial saw cutting and the relative failure potential between different categories of wheels such as Class U and Class C can be ascertained. For example, the effect of discoloration on the failure potential of a given category of wheels is more meaningful than its effect on the saw cut response behavior itself.

The second set of wheels that were saw cut and analyzed were previously subjected to systematic drag braking cycles of known thermal history on a brake dynamometer. Two categories of 33-inch diameter wheels were: (i) Class U, straight and curved plate, (ii) Class C, straight and curved plate design. All the wheels were subjected to 45-minute duration drag braking cycles at an optimum 35 Bhp level, accumulating a total of 25 cycles .

Before these wheels were saw cut, residual stresses were determined on the back rim face by "hole drilling/strain gaging" technique. Net rim forces in the test wheels were estimated from the saw-cut displacement behavior using the analytical procedure described in this section. Figure 11.28 shows the

TABLE 11.6
TYPICAL ANALYSIS OF NET RIM FORCE OF CJ36, CLASS U, CURVED PLATE WHEELS

$$\text{RIM FAILURE POTENTIAL INDEX} = \frac{\text{TOTAL RIM FORCE}}{\text{MINIMUM RIM FORCE REQUIRED FOR FRACTURE DURING SAW CUTTING}}$$

MINIMUM RIM FORCE (FOR WHEELS FRACTURED DURING SAW CUTTING) $\approx$ 230 KIPS

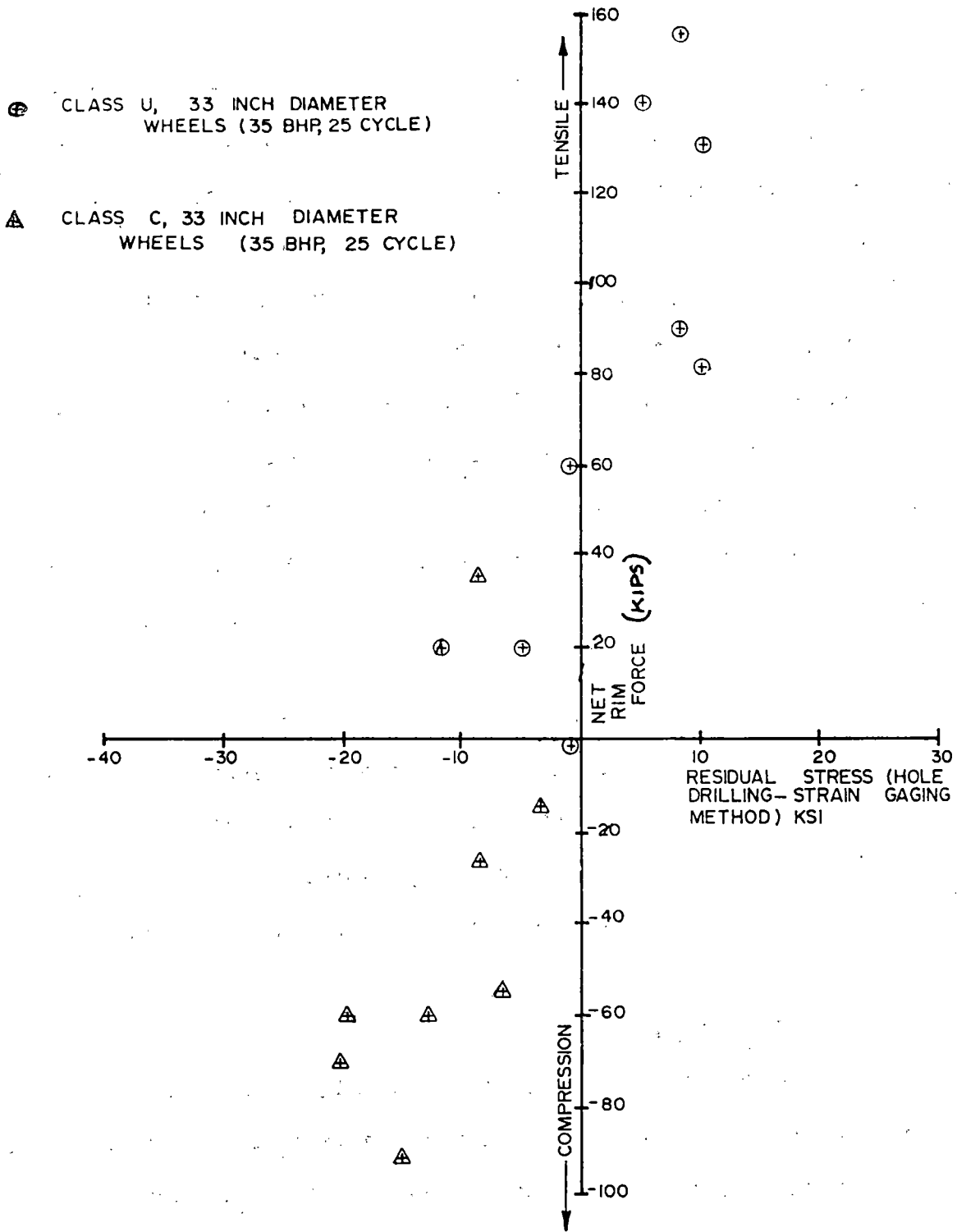| SAW CUT OPENING BEHAVIOR (INCHES)		NET RIM FORCE (AVERAGE OF MORE THAN 2 WHEELS) (KIPS)	RIM FAILURE POTENTIAL INDEX
MIXED OPENING	0.010	−14	—
"	0.015	6	0.025
"	0.020	20	0.087
"	0.024	30	0.130
"	0.030	45	0.200
STRAIGHT OPENING	0.020	50	0.218
"	0.030	80	0.350
"	0.040	100	0.440
"	0.050	120	0.520

FIGURE 11.28   RELATIONSHIP BETWEEN NET RIM FORCES
                (COMPUTED FROM SAW-CUT DISPLACEMENT DATA)
                AND RESIDUAL STRESS MEASURED ON BACK RIM
                FACE BY "HOLE DRILLING-STRAIN GAGING" METHOD

relationship between the residual hoop stress on the back rim face and the net rim forces computed using the suggested analytical approach described above. Two distinct trends can be seen for Class U and Class C wheels with the same level of thermal history. Class C wheels exhibit compressive residual stresses on the back rim face (determined by the hole drilling/strain gaging method) and net compressive rim forces; whereas, with the same level of thermal abuse, Class U wheels exhibit successively increasing levels of tensile stresses on the back rim face and higher magnitudes of net rim forces (in tensile direction).

11.3   Cyclic Path Dependence of Stress Change

Preliminary experimental inferences and material plasticity simulations of residual stress changes due to repetition of braking cycles have been made, primarily for the recently completed RDU tests. These efforts are described below.

Successive Hole Drilling

Measurement of residual stresses by the successive hole drilling method has been successfully tried and perfected during various facets of the program. Most of the test wheels during Technical Tasks T4, T5, and T6 have been analyzed using this method. Several rail car wheels prior to radial saw-cutting were also analyzed by this method. Careful consideration was

given to avoid any source of errors that may arise from operational practices and data reduction procedures.

In order to measure residual stress with standard sensors, the locked-in stress must be relieved in some fashion (with the sensor present) so that the sensors can register the change in strain caused by removal of the stress. This was usually done destructively in the past by cutting and sectioning the part, by removal of successive surface layers, or by trepanning and coring. With strain sensors judiciously placed before dissecting the part, the sensors measure the relaxed strains, from which the initial residual stresses can be inferred by conventional methods.

The most widely used modern technique for measuring residual stresses is the hole drilling strain-gaging method. With this method, after installing strain sensors on the part surface, a small shallow hole is drilled in the surface. After drilling, the change in strain in the immediate vicinity of the hole is measured, and the relaxed residual stresses are computed from these data. The hole drilling method can be described as "semidestructive", since the small hole will not, in many cases, noticeably impair the structural integrity of the part being tested [the hole is typically 1/16 to 1/8 inch (about 1.5 or 3.0 mm) in both diameter and depth].

When a hole of small diameter is drilled in a region initially containing residual stresses, the magnitudes of strain relieved at any point P are functions of the local principal stresses σ_x and σ_y, and of the geometric relationships

between the point and the hole, and the point and the principal axes.

The complete description of residual stress determination by the Hole Drilling strain-gaging method is already presented in Section 4.6.

Once σ_x and σ_y are determined, σ_1 and σ_2 (which can be hoop or radial stresses, depending on the orientation of gage #1 of the strain gage rosette on the wheel) can be calculated from the Mohr Circle relationships:

$$\sigma_{1,2} = \frac{\sigma_x + \sigma_y}{2} \pm \frac{\sigma_x - \sigma_y}{2} \; Cos2\beta \quad if \quad \beta = \beta_x$$

$$\& \; \sigma_{1,2} = \frac{\sigma_x + \sigma_y}{2} \pm \frac{\sigma_y - \sigma_x}{2} \; Cos2\beta \quad if \quad \beta = \beta_y$$

where β_x = angle between σ_x and gage No. 1 axis

β_y = angle between σ_y and gage No. 1 axis

The analysis of residual stresses on the back face of the rim (B1 location) revealed that the stress components in the hoop and radial directions were of the same order of magnitude resulting in a bi-axial state of stress.

After the evaluation of residual stress at the B1 location, the hole drilling strain-gaging method is applied at the B2 location in the rim fillet region about 5.5 inches radially down from the flange tip. The third (B3) location is in the hub fillet region about 10 inches radially down from the flange tip.

The development of residual stresses in a typical test wheel (Wheel No. 8) at the B1, B2, and B3 locations during drag braking simulation testing on RDU are presented in Figures 11.29, 11.30, and 11.31.

RESIDUAL STRESS AS MEASURED BY HOLE DRILLING – STRAIN
GAGING TECHNIQUE (KSI)

RUN #

□ RAD STR   + HOOP STR   ◇ EFF HOOP STR

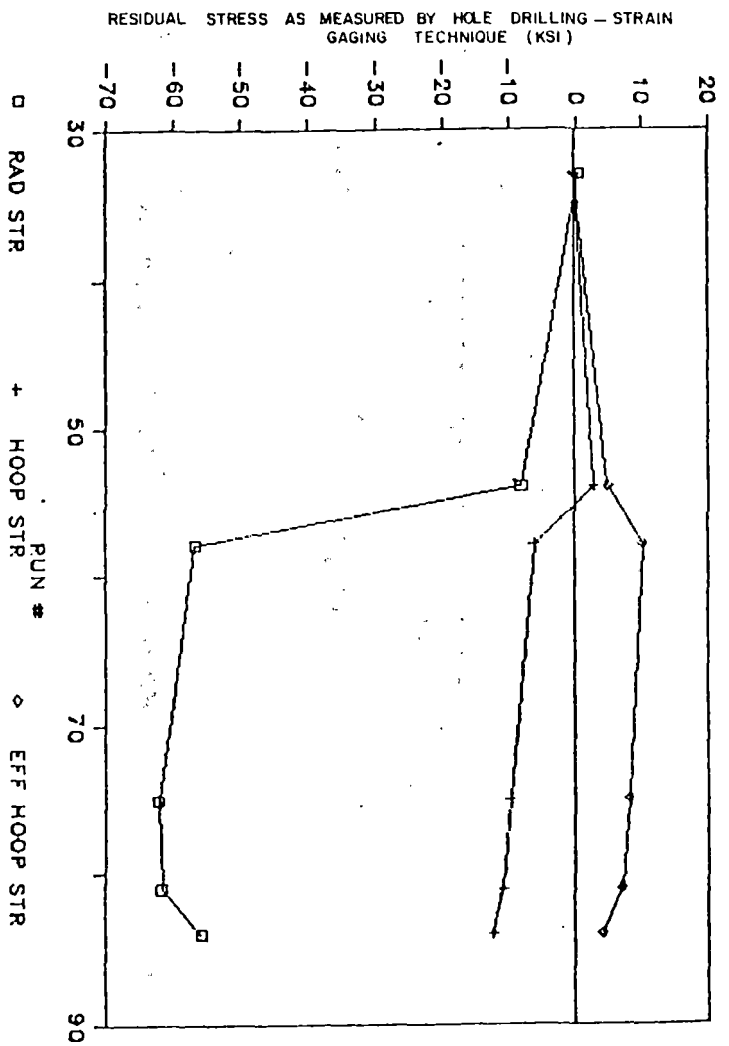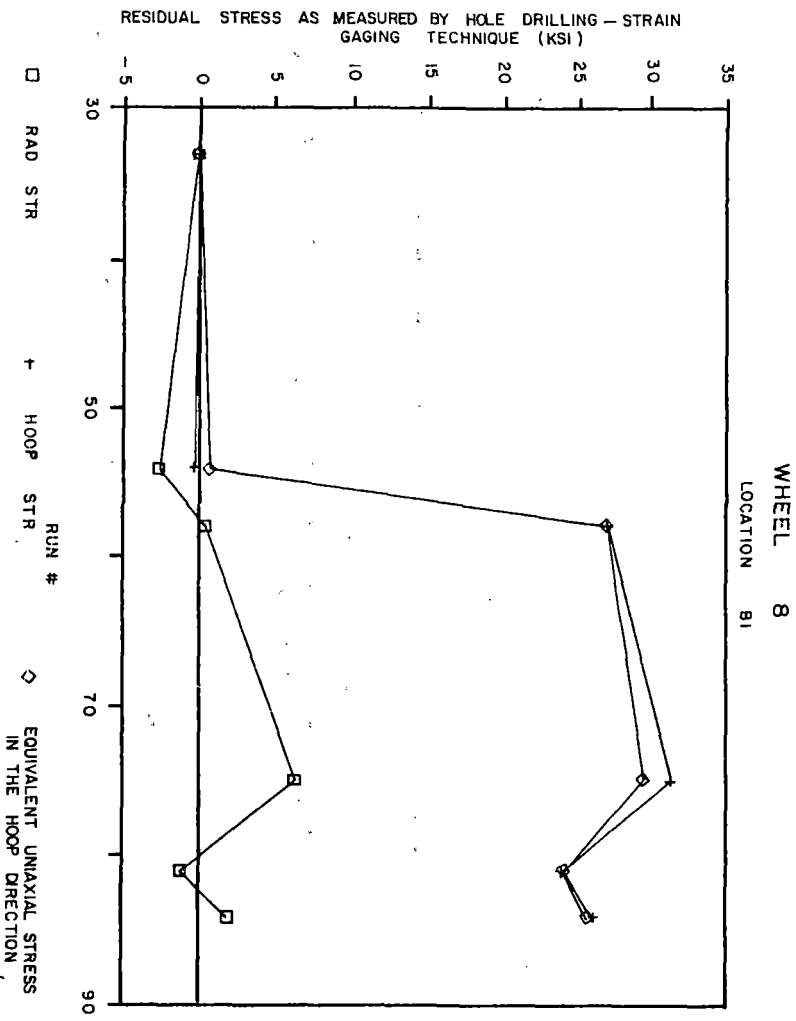FIGURE 11.30 HOOP STRESS AT B2 LOCATION, WHEEL #8

11-57

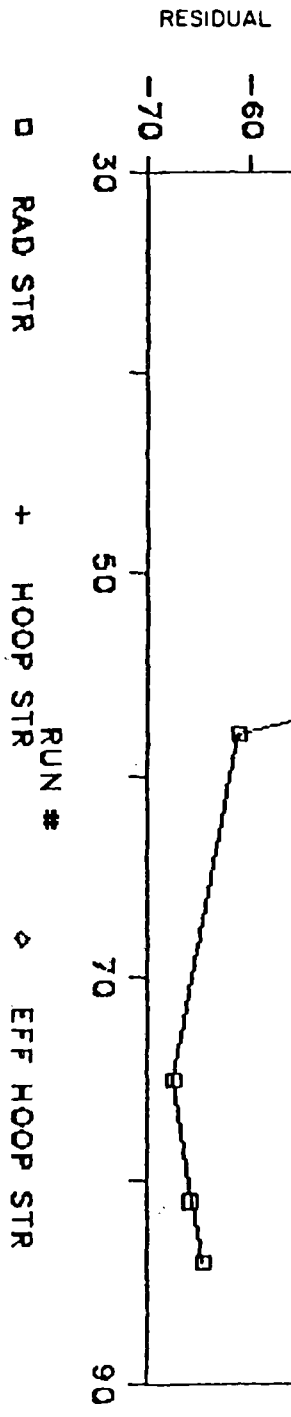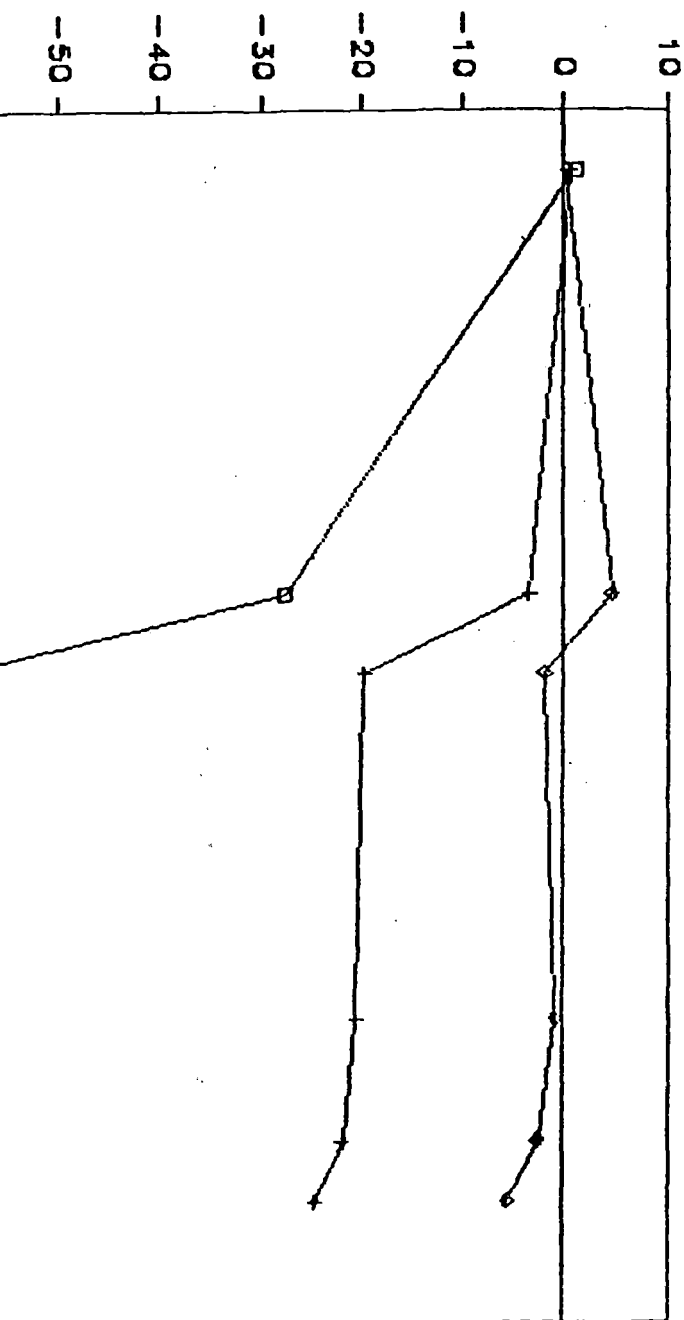FIGURE 11.29 HOOP STRESS AT B1 LOCATION, WHEEL #8

FIGURE 11.31 HOOP STRESS AT B3 LOCATION, WHEEL #8

STRESS AS MEASURED BY HOLE DRILLING — STRAIN
GAGING TECHNIQUE (KSI)

11.3.1   Computer Simulation Approach

A semi-empirical approach to the prediction of stress changes due to braking cycles is based on a material constitutive representation or computer simulation of the stress response for measured surface strains and temperatures. An initial application of the method based on the most elementary "flow model", (that is, perfect plasticity with a temperature dependent yield stress) is described in this section. The flow properties assumed in these analyses are illustrated in Figure 11.32. A best fit straight line temperature relationship is given for the conventional (fast rate) 0.2% and 0.02% plastic strain offset yield strengths for Class U steel. For the higher temperature and slower strain rates, lower flow stress values may be expected and the temperature dependent stress (corresponding to 0.02% yield) was assumed for uniaxial perfect plasticity model analysis as described below.

11.3.1.1   Uniaxial Model

This method may be illustrated in the most straightforward manner by use of a uniaxial model based on hoop strain measurements made at the back face, B1, location for the wheel induction heating experiment and the most severe braking cycles experienced on the Roll Dynamics Unit (RDU).

The brake horsepower input histories for the induction heating and RDU tests selected for analysis are shown in Figures 11.33 and 11.34, respectively. The measured temperature

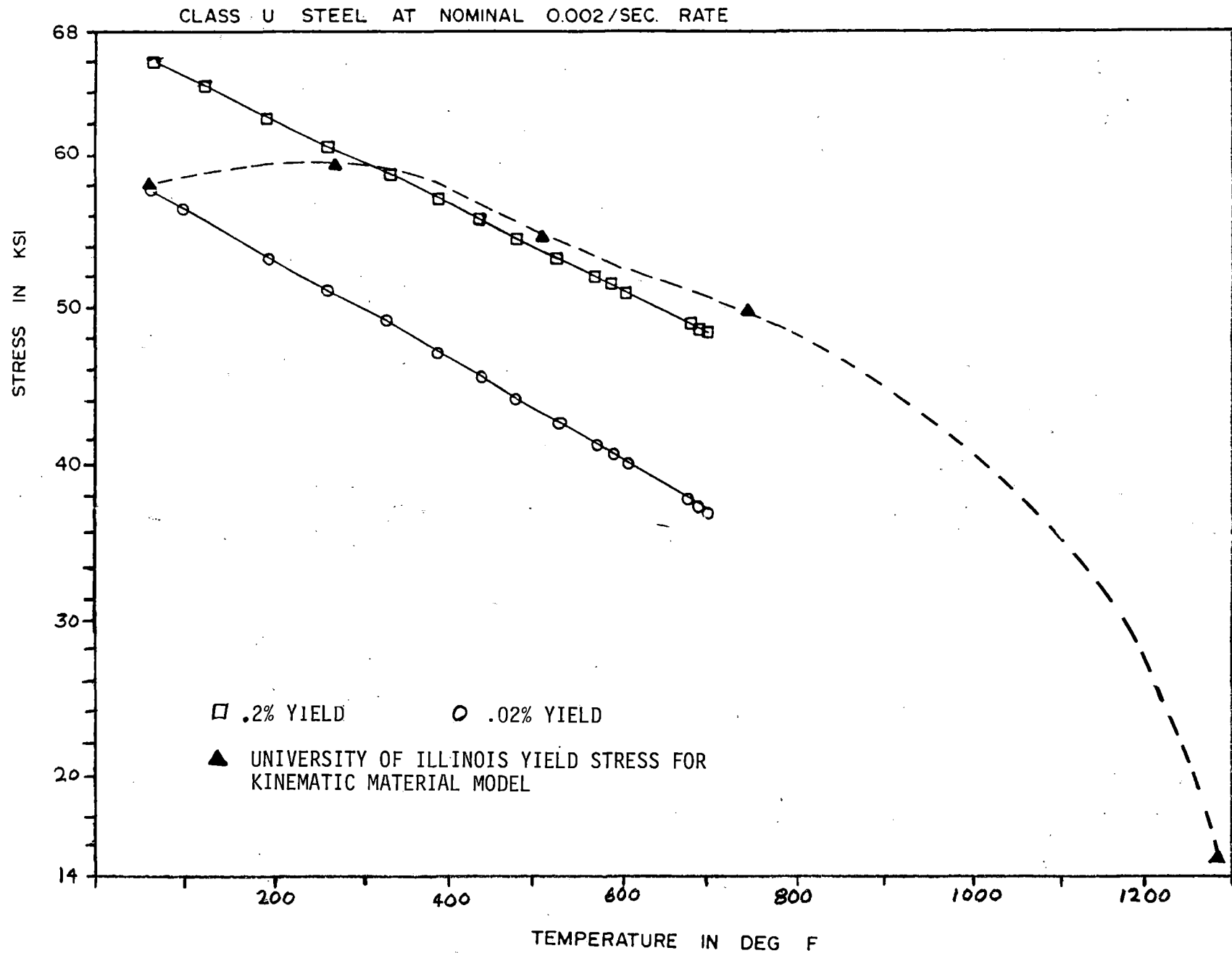FIGURE 11.32 ASSUMED EFFECT OF TEMPERATURE ON YIELD

FIGURE 11.33   HORSEPOWER HISTORY, INDUCTION HEATING
TESTS CP1-CP5

BHP HISTORY

FOR TEST 55/56   WHL. # 8
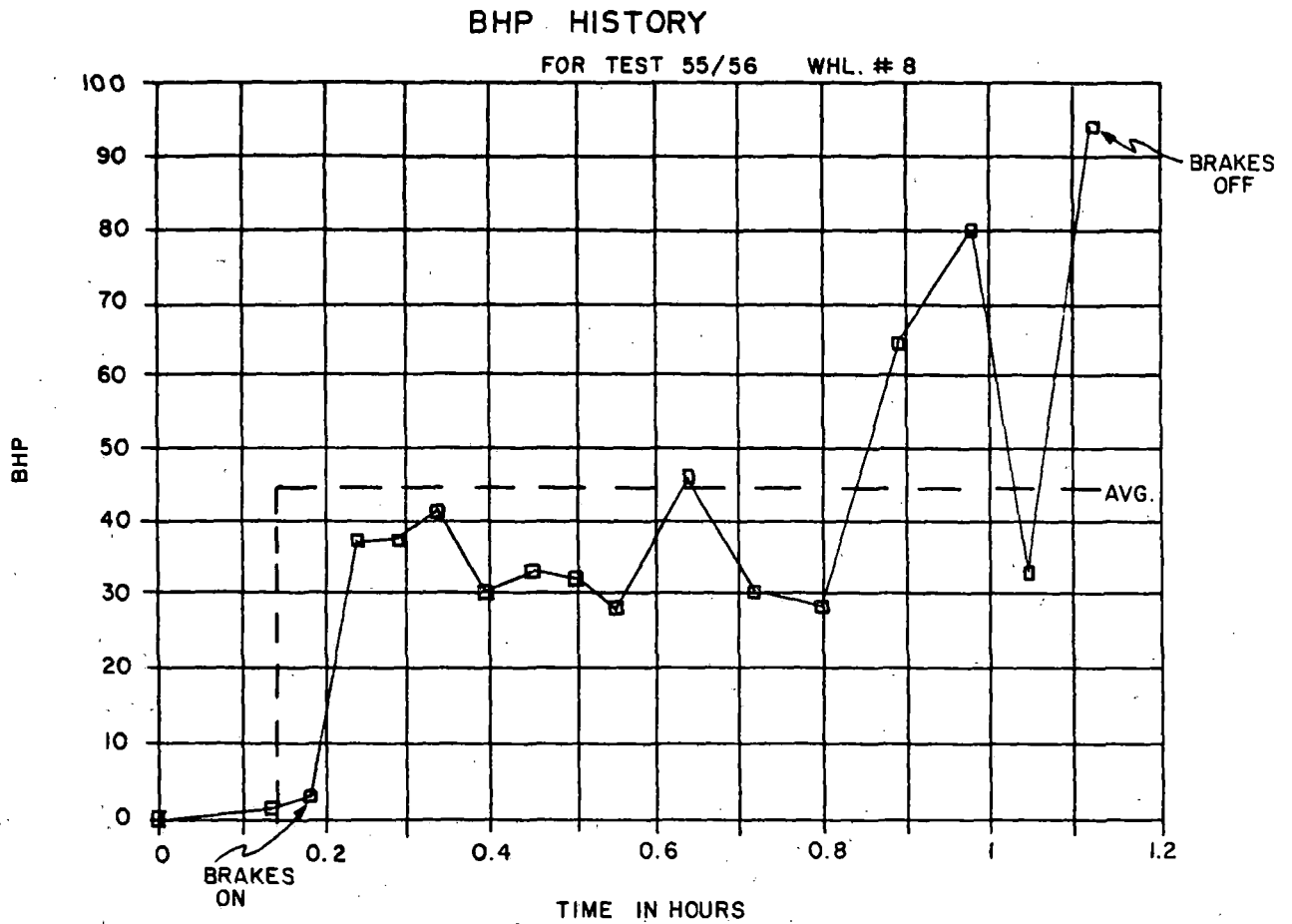
RUN	BRAKE CYL PRESS.(PSI)	SPEED (MPH)	DURATION (MINS.)	TARGET BHP	ACTUAL AVG. BHP	NOTE
55/56	45/60	42/50	60	50	43.8*	SHOE BURNED
57/58	45	42	30	----	NOT MEASURED AT WHL. NO. 8	

*INCLUDES POWER LOSS TO ENVIRONMENT
            AND ROLLER

FIGURE 11.34   BRAKE HORSEPOWER HISTORY, WHEEL #8 (TRUCK 2)

histories at the B1 location for these tests are given by Figures 11.35 and 11.36.

The corresponding hoop mechanical strain histories are provided by Figures 11.37 and 11.38.

Estimates of the associated stress histories were made by a typical computer spread-sheet analysis, assuming elastic response to the imposed strain until the current value of yield stress is reached at any temperature. Beyond initial yield, the stress remains at the value of yield stress corresponding to current temperature as long as straining continues in the same direction. When "unloading" occurs, the stress response is elastic for the change in strain. The results of following such a program for stress history are demonstrated in Figures 11.39 and 11.40. The corresponding stress-strain "loops" are shown in Figures 11.41 and 11.42.

It may be noted that the flow (yield) properties used by Prof. Sehitoghu in his analysis of Induction Heating experiments discussed earlier in this section and in Section 5.3 assumed higher strain rate (2×10^{-3} 1/sec), with higher strength properties, for the shorter time induction heating tests. (This contrasts with the strain rates of 10^{-6} and 10^{-7} 1/sec for the one-hour drag-brake tests on RDU.) The University of Illinois material model does indicate a rate dependence of wheel steel above 700°F. This rate sensitivity and temperature dependence of the flow properties have a strong influence on the residual stresses produced.

Prof. Sehitoghu predicted a circumferential residual stress

IND. HT. TEMPERATURE HISTORY at B1
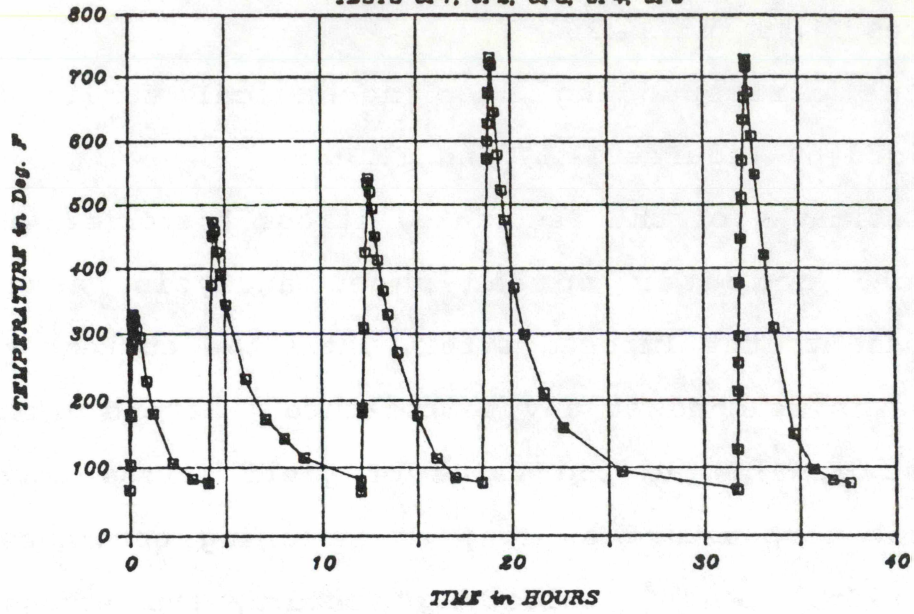
TESTS CP1, CP2, CP3, CP4, CP5

FIGURE 11.35   INDUCTION HEATING TEMPERATURE HISTORY AT B1,
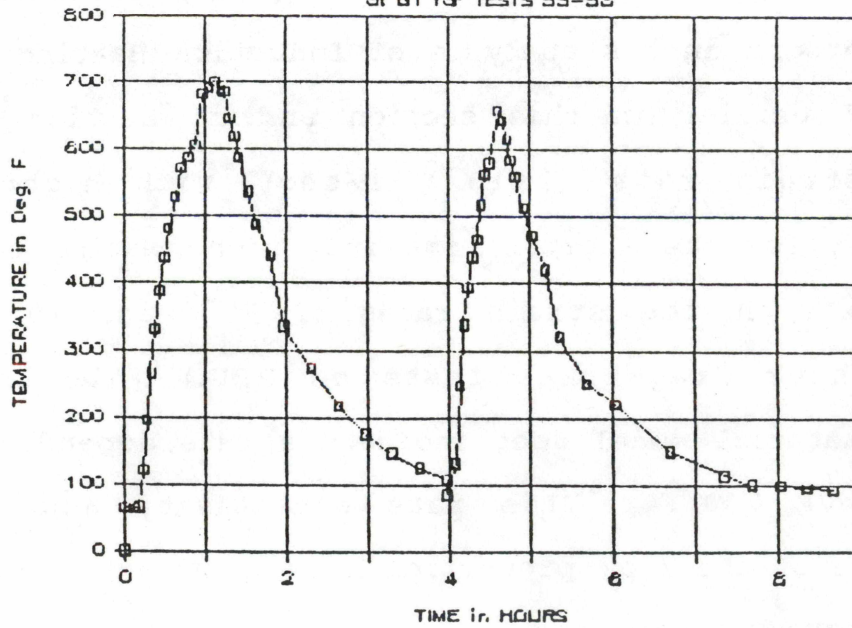TESTS CP1-CP5

RDU TEMPERATURE HISTORY

at B1 for TESTS S5-S8

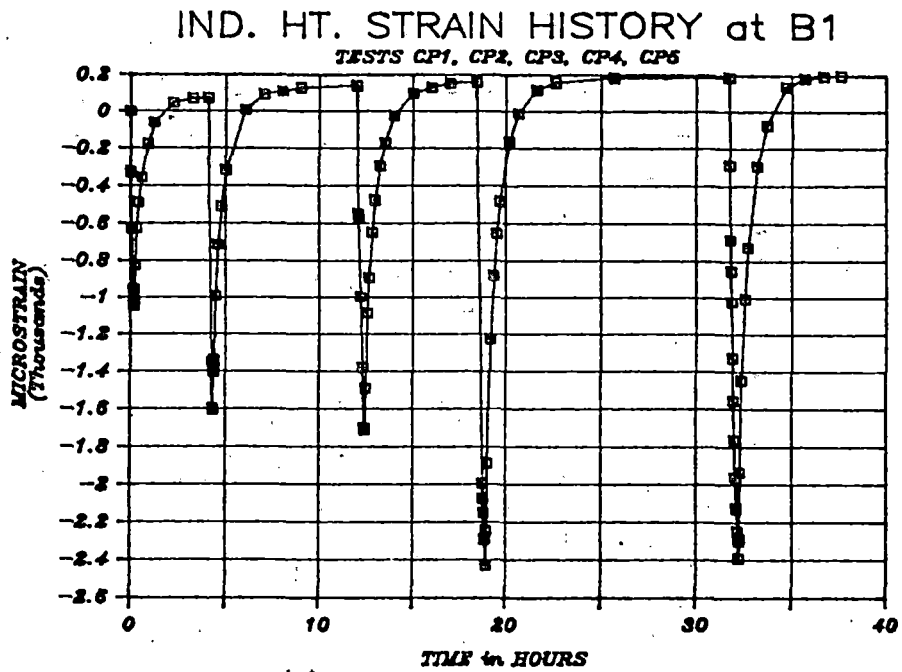FIGURE 11.36   RDU TEMPERATURE HISTORY

IND. HT. STRAIN HISTORY at B1

TESTS CP1, CP2, CP3, CP4, CP5

FIGURE 11.37 INDUCTION HEATING STRAIN HISTORY AT B1,
TESTS CP1-CP5

RDU STRAIN HISTORY

at B1 LOCATION for TESTS 5S-5S
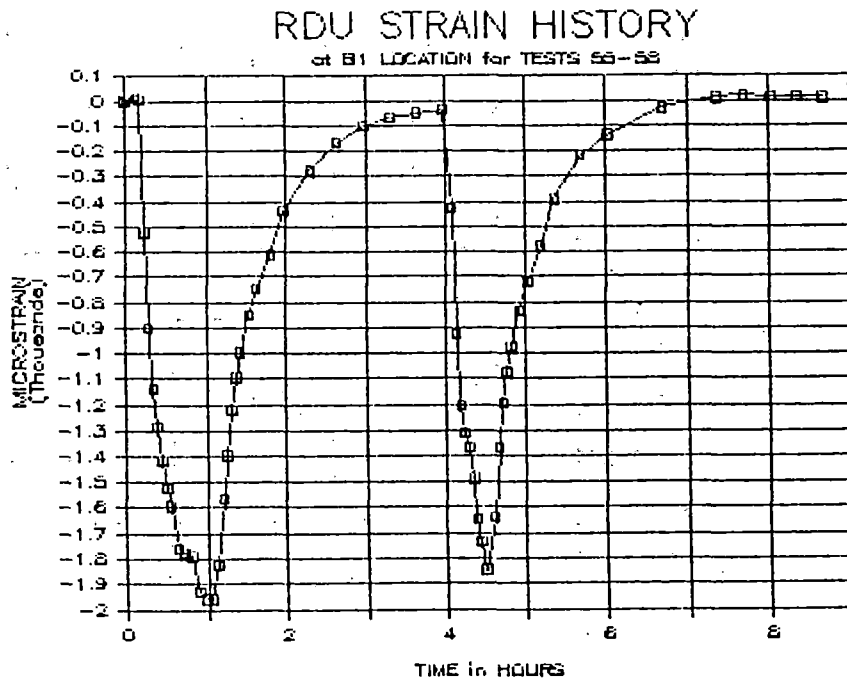
FIGURE 11.38 RDU STRAIN HISTORY

IND.HT. CALCULATED STRESS HISTORY

at B1 for TESTS CP1, CP2, CP3, CP4, CP6
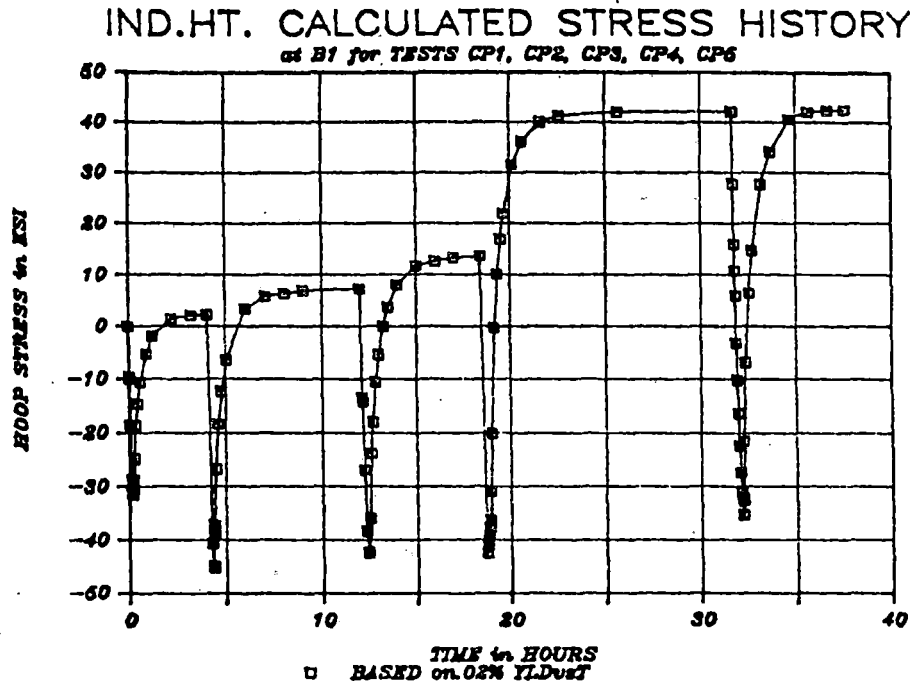
FIGURE 11.39   INDUCTION HEATING CALCULATED STRESS HISTORY

RDU   CALCULATED   STRESS   HISTORY

AT B1 LOCATION FOR TESTS 55-58

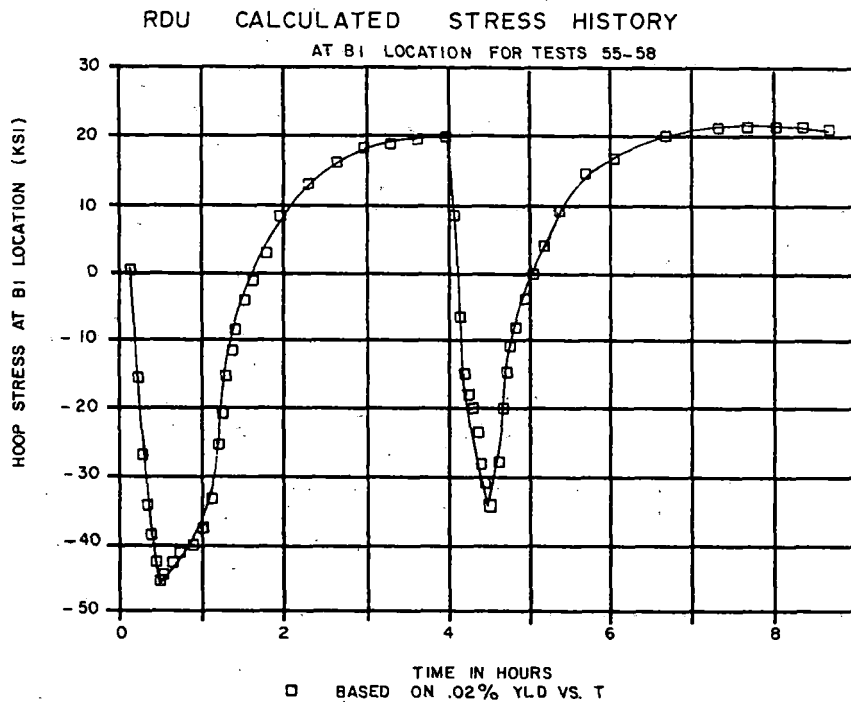FIGURE 11.40   CALCULATED HOOP STRESS HISTORY AT B1 LOCATION,
WHEEL #8, DURING TESTS 55-58

FIGURE 11.41   STRESS/STRAIN LOOPS AT B1 RIM LOCATION
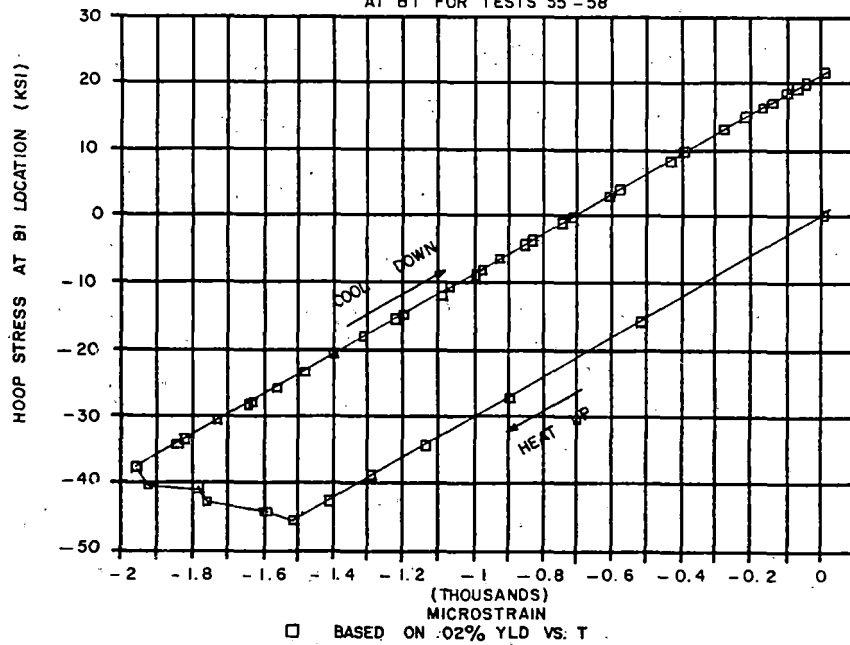

FIGURE 11.42   RDU STRESS/STRAIN LOOPS

of 13.2 ksi with a higher strain rate property which was in the same range of residual stress as determined by the hole drilling strain gaging method on the back rim face of the induction heating test wheel. The flow properties associated with the slower strain rate gave higher predictions of residual stresses on the back rim face, using the uniaxial model. Subsequently, bilinear material properties were used with the uniaxial model based on the actual measured mechanical strain and temperature histories of induction heating, which predicted a residual stress of 22 ksi on the back rim face. The above bilinear material properties were originally used by A. J. Opinsky, et al, in their paper "Effect of Brake Shoe Position on the Development of Residual Stresses in Freight Car Wheel", (Appendix 11.4). The importance of using the most realistic material properties can be revealed by this analysis.

However, with the lower strength properties, the uniaxial model predicted a residual stress on the back rim face comparable with hole drilling results for the most severe drag braking test on the RDU, as described below. This may be due to the fact that the RDU testing was of longer duration giving rise to stress relaxation while hot, and/or more nonuniformity in heating.

The value of about 22 ksi for hoop residual stress predicted for the RDU test is generally consistent with the value of 27 ksi predicted from hole drilling measurements after cycle #57/58. It is also interesting to compare the results of this simple uniaxial model to an inelastic finite element analysis

11-68

reported by Johnson, et al, in AAR Report R-580 in 1983. Their
results for "hot" and "cold" (or residual) hoop stresses at the
B1 location are plotted in Figure 11.43 for various 1-hour drag
braking input Bhp intensities. At 44 Bhp, the residual hoop
stress would be interpolated at about 32 ksi. Considering the
many material and loading history uncertainties, this
"theoretical" spread of 22 and 32 ksi is relatively encouraging,
especially in view of the intermediate hole drilling result at
27 ksi.

11.3.1.2   Biaxial Plasticity Model

During wheel braking tests (such as those conducted on the
RDU and on track at TTC), the surface biaxial strains and
temperatures were measured to estimate the associated stress
state. For this estimation, it is necessary to have a
satisfactory biaxial stress-strain constitutive relationship
which should be able to account for straining beyond the elastic
regime, the incremental nonproportional character of the strain
state (nonconstant strain component ratios) as well as the
effect of temperature on the current value of material yield or
flow stress.

The most elementary theory that satisfies these minimum
requirements is an extension of the uniaxial perfect plasticity
model described above.

In the biaxial (rotationally symmetric) case, the stress
components must satisfy both the yield condition as well as the

11-69

INELASTIC F.E.A. STRESS CALCULATIONS
AT BI FOR I HR. DRAG BRAKING

□ HOT STRESS   + COLD STRESS
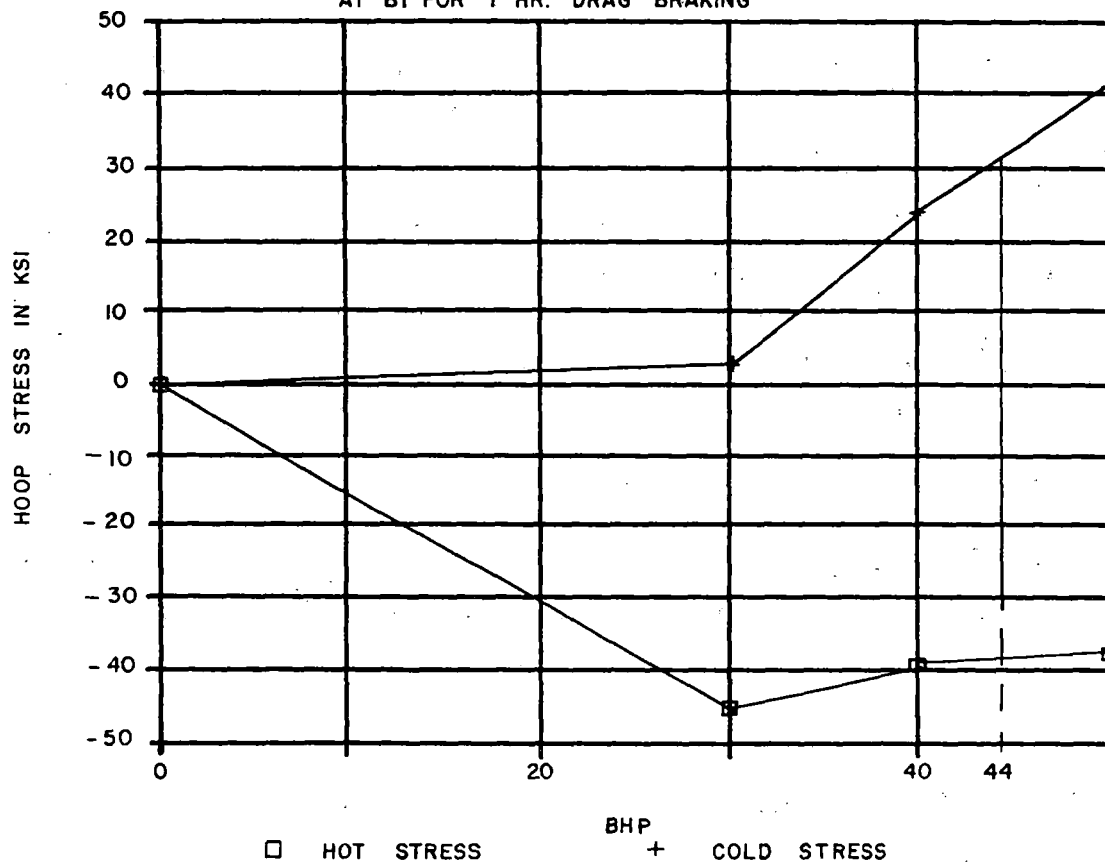
FIGURE 11.43   FINITE ELEMENT ANALYSIS
               INELASTIC STRESS CALCULATIONS

incremental plastic flow rule. The yield condition is taken as the Von Mises relationship which may be expressed in nondimensional form as the parabola:

$$x^2 + y^2 - xy = 1$$

where

> x is the ratio of radial stress to the current value of yield, and y is the corresponding ratio of circumferential stress.

The associated plastic flow rule requires that the increments in plastic strain be such that the vector formed by these strain components is normal to the yield surface. This condition leads to another second degree equation, a hyperbola in this case, that must be solved simultaneously with the parabolic yield condition for each time increment for which strains and temperatures change. Account must also be taken of the possibility of elastic unloading at some time after yielding has occurred.

This calculational scheme for taking the actual mechanical strain components and temperature histories (B1, B2, and B3) and predicting the stress components is described in Appendix 11.2. Provision is made in these computations for a yield or flow stress that decreases with increases in temperature. As in the simple uniaxial model, no account is taken directly of strain hardening or inherent cycle or rate dependency. Nevertheless, it is believed that this method provides an efficient and relatively simple but logical method of estimating the biaxial stress (applied and residual) as well as the "plastic" strain

components which will differ from the measured "residual" strain components in most cases.

This method was applied to most of the major tests conducted on the RDU, and the results are compiled in the Master Data Base Table at Pueblo. Some application of the form of results for selected data may be gained by reference to Figures 11.44 and 11.45.

They illustrate the complex radial and circumferential stress-strain loop calculated from the reduced strain and temperature data taken at wheel plate location B2 for the most severe RDU braking cycle (55/56) on Wheel #5.

An obvious limitation of the "perfect" plasticity material model described above is the inability to treat the known inherent material cycle and rate dependence of wheel steel. In order to gain some insight into the effect of repeated braking cycles on residual stress changes, ratchet effects and plastic "damage" accumulation, more realistic constitutive material models are required. The ANSYS finite element program includes a wide range of material options in addition to the special kinematic hardening selected for the wheel induction heating analysis attempt described earlier in this section.

Some exploratory studies of uniaxial cyclic material response with ANSYS special nonlinear material options have been conducted for certain hypothetical input total strain and temperature cycles. These examples have permitted comparison to, and qualification by, closed form independent solutions described in Appendix 11.3. As described earlier in this

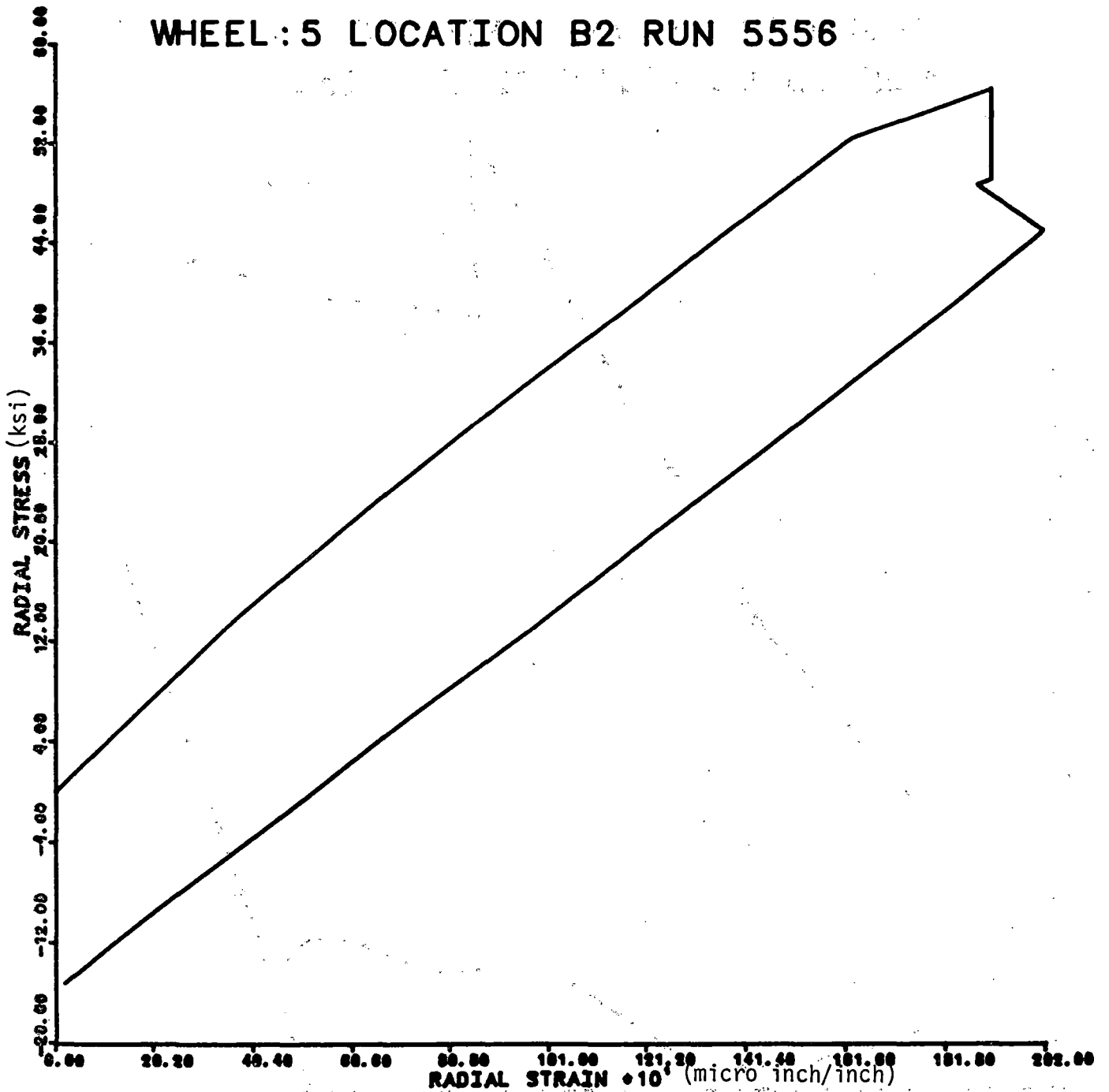RADIAL STRAIN AGAINST STRESS
WHEEL:5 LOCATION B2 RUN 5556

FIGURE 11.44   RADIAL STRESS-STRAIN LOOP CALCULATED AT B2
IN RDU TEST #55/56

TANGENTIAL STRAIN AGAINST STRESS
WHEEL:5 LOCATION B2 RUN 5556
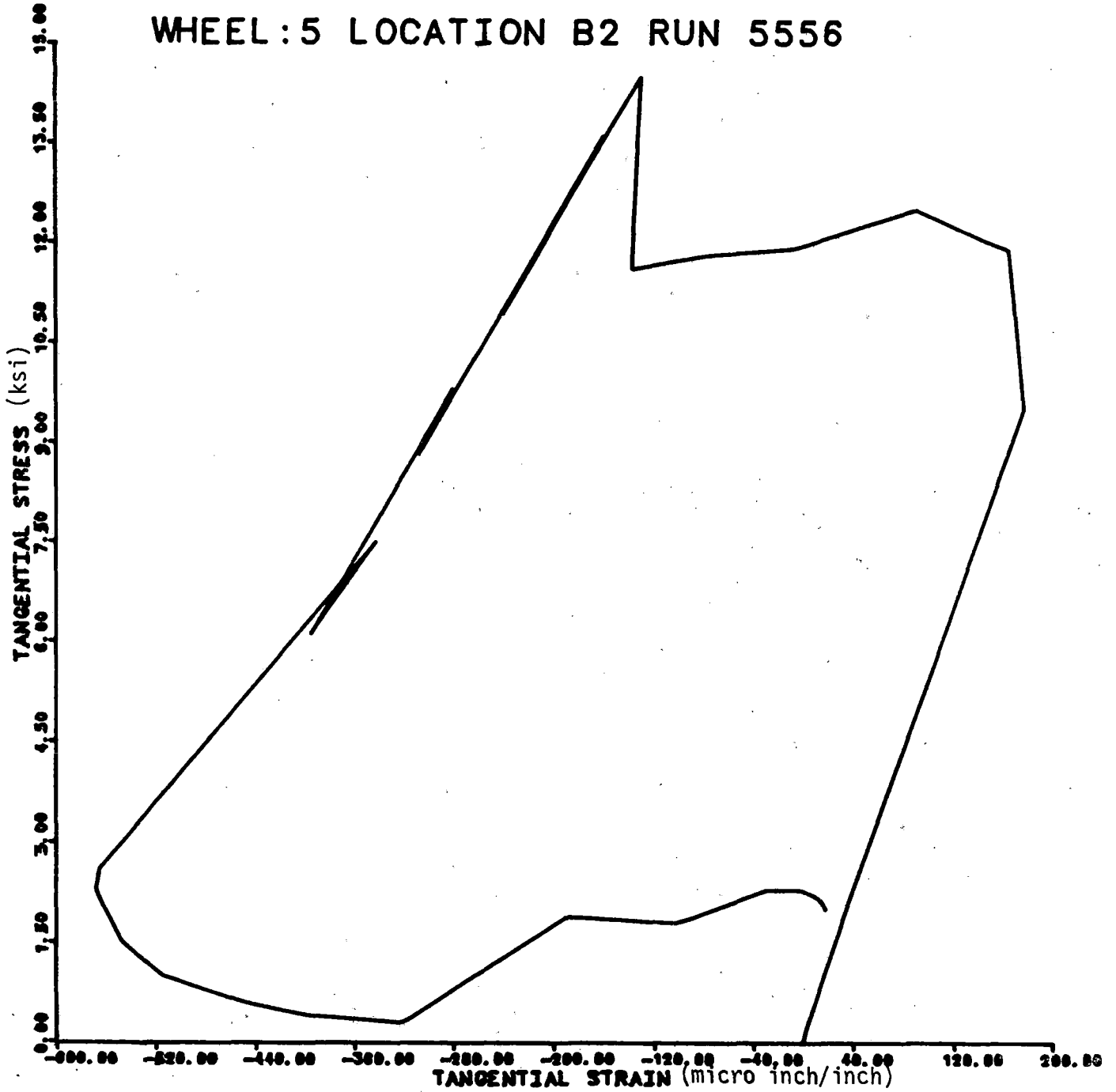
FIGURE 11.45   CIRCUMFERENTIAL STRESS-STRAIN LOOP CALCULATED
AT B2 IN RDU TEST #55/56

section by way of illustration, Figure 11.46 is the ANSYS produced stress-strain loops in temperature peaks to 800 degrees K (980 degrees F). The material behavior in this case features a second degree power creep law and classical kinematic plasticity with temperature dependent properties selected to roughly approximate Class U steel thermo-mechanical properties published by Sehitoglu in 1982. It is sufficient here to simply note the salient feature of such a stress-strain loop in contrast to the elastic unloading behavior predicted with the simple, perfectly plastic models. Reversed plastic strain and creep effects are apparent with this relatively simple nonlinear model. Closer simulation of actual uniaxial cyclic and variable rate behavior under way in Technical Task 3 is possible. Even if full finite element wheel model analyses with such properties do not prove to be cost effective, such ANSYS material options will be helpful in predicting stress states associated with measured uniaxial and biaxial strain and temperature cycles.

FIGURE 11.46   DEMONSTRATION ANSYS SOLUTION FOR
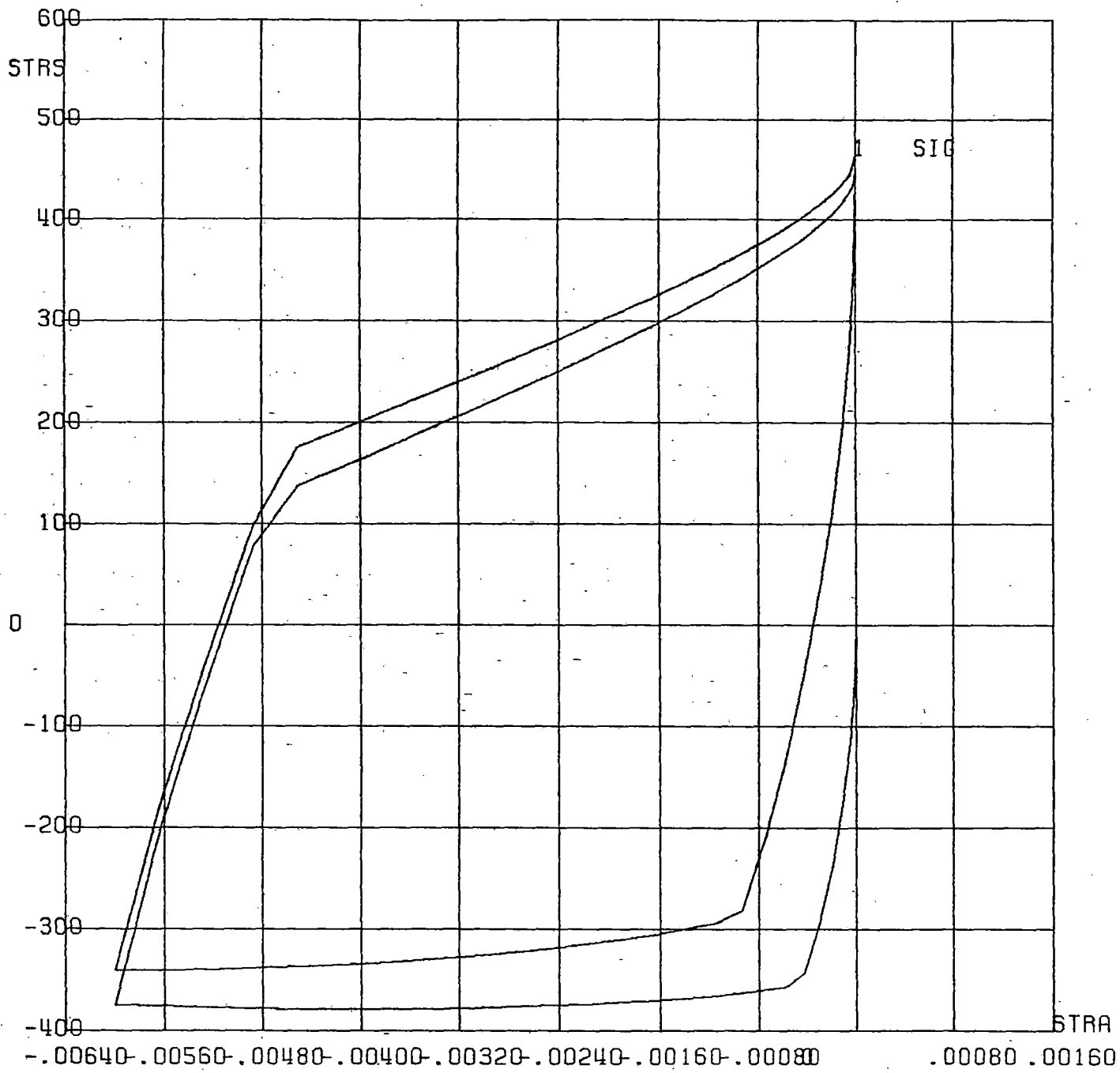STRESS/STRAIN LOOPS WITH RATE DEPENDENT
INELASTIC MATERIAL OPTION

11.4   Analysis of Data from Tests to Produce Residual Stress
        Changes in Test Wheels

The main emphasis of this program was to define operating
practices that contributed towards residual stress changes in
the wheels, as ascertained by semidestructive and destructive
means of residual stress determination. Information was
gathered in different test facilities such as the Brake
Dynamometer, Roll Dynamic Unit, and track testing, with
different levels of instrumentation. Although a relatively
small number of wheels were used in these tests, they were
subjected to closely controlled braking conditions so that
complete information on the braking history was available for
subsequent analysis. The test included the heavily instrumented
wheels tested on the RDU and in the Preliminary Track Test; the
lightly instrumented Comprehensive Track Tests and the Brake
Dynamometer Tests, wherein a range of wheel types were tested.

During RDU and Preliminary Track testing at Pueblo,
instrumented brake heads were used, which enabled monitoring of
tangential and normal forces at the brake shoe/wheel interfaces
on a continuous basis. During Comprehensive Track testing and
Brake Dynamometer testing, Bhp estimates were made with the
assumed average friction coefficient values.

A Braking Severity Index was defined as the cumulative
braking energy above threshold horsepower required to cause
residual stress changes. This index can be estimated for any
combination of speed, brake force, and duration of braking

11-77

history. It has been established primarily on the basis of the detailed tests and analyses of the reference CJ-33 Class U wheels.

A summary of the rationale and justification for this Braking Severity Index will be given below based on the data base correlation studies from the several test facilities. This will be followed by an application of the index to provide estimates of the regions of braking operation (speed, force, and duration) that would be expected to produce residual stress changes in various wheel types.

11.4.1 Development of Braking Severity Index

The brake operation threshold for rim residual stress change can be expressed generically in a Bhp versus time plot as shown in Figure 11.47. The representation is similar to that used by the Spanish Researchers, Meizoso and Sevillano, in 1985.[1] The Bhp history in the various test facilities was reviewed for the test wheels which showed significant residual stress change, and the horsepower-time thresholds were established for curved plate and straight plate wheels, making use of the RDU and track results.

The Bhp expended at the interface of brake shoe and wheel tread can be derived from the expression,

$$Bhp = \frac{(BSF)(f)(MPH)}{375} \tag{1}$$

11-78

LOCUS OF MINIMUM ENERGY (HP·HR$_c$)
ABOVE CRITICAL BHP (HP$_c$)

REGION OF OPERATING
CONDITIONS LEADING TO
RESIDUAL TENSILE STRESS
(IN THE RIM)

BHP

HP$_c$

REGION OF OPERATING
CONDITIONS FOR NO RESIDUAL
STRESS CHANGE

TIME
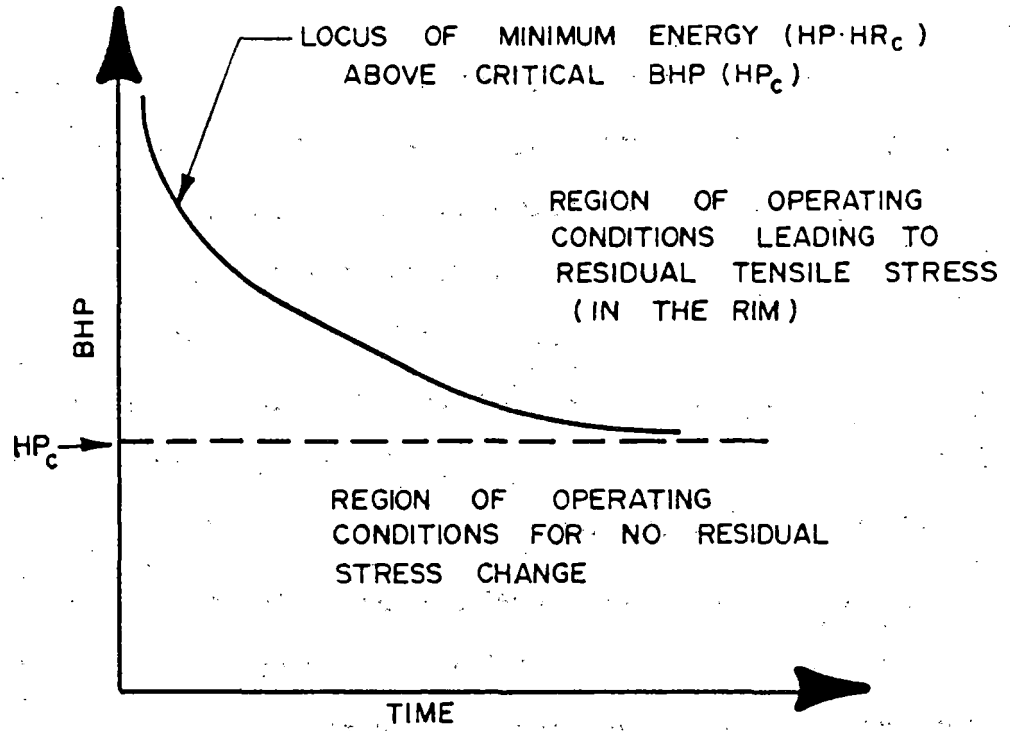
HP$_c$ = CRITICAL BHP LEVEL

FIGURE 11.47 GENERIC REPRESENTATION OF
BRAKING OPERATION SAFETY

where   BSF   =   Brake shoe normal force in lbs.

            f   =   Coefficient of friction between shoe and tread

A Braking Severity Index (BSI) can be developed which may be employed to estimate the "threshold" combinations of brake shoe force, speed, and duration of drag braking that may be expected to initiate significant change in the rim residual stress.

This Braking Severity Index is defined to be the energy above a critical brake horsepower level (HP_c) that exceeds a minimum required energy, (E_c), to cause residual stress change. E_c equals $(HP*HR)_c$.

$$BSI = (Bhp - HP_c) HR - E_c$$

Therefore, the "threshold" condition occurs when BSI = 0. The expression for horsepower at this threshold is:

$$Bhp = E_c/HR) + HP_c \qquad\qquad (2)$$

Analysis of the RDU and Preliminary Track Test Data for the Class U, CJ-33 Wheel

Table 11.7 presents the details of severe braking episodes which resulted in significant residual stress changes in the test wheels (all Class U, CJ-33, curved plate wheels) during RDU and Preliminary Track testing. The Table shows the maximum back rim temperatures attained, peak and average brake horsepower levels during (and prior to) the particular tests, peak hoop

TABLE 11.7
MEASURED BACK RIM FACE TEMPERATURES AND BHP'S FROM RDU AND PRELIMINARY TRACK TESTING

BI TEMPERATURES, PEAK AND AVERAGE BHP'S, AND PEAK HOOP STRESSES FROM RDU AND PRELIM TRACK TESTING

WHEEL NUMBER	RUN NUMBER	MAX. BI TEMP PRIOR TO TEST		MAX. BI TEMP DURING TEST		MEASURED BHP AVERAGE PRIOR TO TEST	DURING TEST	MEASURED BHP PEAK PRIOR TO TEST	DURING TEST	ESTIMATED BHP, AVERAGE PRIOR TO TEST	DURING TEST	PEAK HOOP HOT STRESS (KSI) (σ_H)	YIELD RATIO σ_H / σ_Y	ENERGY INPUT (HP-HRS) ABOVE 40 BHP	45 BHP	Δ HOLE DRILL STRESS (MEASURED)
		T.C.	M.S.	T.C.	M.S.											
5	55/56	541	—	555	—	31	41	47	53	30	49	—48	1.06	18.3		
	57/58	—	—	—	—	—	53	—	59	28	16	—41	.94	22.5		8
6	55/56															
	57/58															0
7	55/56	494	—	622	—	32	31	43	44	29	52	—	—	0		
	57/58	—	—	—	—	—	46	—	61	—	32	—	—	12.8		5
8	55/56	500	—	701	—	29	49	45	95	32	55	—64	1.53	19.4		27
	57/58	—	—									—60	1.35			
9	13	682	—	593	—	23	59	47	19	43	44	—	—	2.2		
	15	682	—	645	—	—	—	—	—	47	46	—	—	—		
	31—35	—	—	—	—	—	—	—	—	—		—41 —50	.89—1.06	5—10		
10	13	549	—	495	—	41	56	64	67	46	48	—	—	53	11	14
	15	593	557	611	522	—	48	—	73	—	51	—	—	28	3	0
	30—35	—	—	579	565	—	—	—	—	—	—	-50 — -63	1.07—1.3	35—46		0
11	13	570	—	521	—	37	41	56	58	47	49	—	—	27	1	4
	15	570	—	614	—	—	50	—	82	—	52	—	—	34	5	4
	30—35	—	—	507	—	—	—	—	—	—		-40 — -42	1.16—1.29	37—43		0
12	13	540	—	531	—	51	44	92	60	44	47	—	—	24	0	5
	15	635	—	682	—	—	50	—	72	—	53	—	—	45	5	5
	31—35	—	—	532	—	—	—	—	—	—		—	—	27—36		3

TC — THERMOCOUPLE
MS — MICROSCANNER

$\sigma_H / \sigma_{YIELD}$ — YIELD RATIO

WHEELS 5,6,7, & 8 : RDU TESTING
WHEELS 9,10,11, & 12 : PRELIMINARY TRACK TESTING

(hot) stress measured at the back rim face, the yield ratio at the peak hoop (hot) stress (ratio of peak hoop stress, and the yield stress of Class U steel at the corresponding peak temperature), energy input $(HP*HR)_c$ above 40 and 45 Bhp, and the change in the residual hoop stress at the back rim face as determined by hole drilling methods (after cooling).

As can be seen, high hoop (hot) stress and yield ratio occurred at high back rim temperatures, and they also reflect higher levels of Bhp expended at the brake shoe/wheel interface. Energy inputs (HP.HR) above 40 Bhp and 45 Bhp were computed for the most severe drag braking episodes during RDU and Preliminary Track testing. The effect of major drag braking cycles on residual hoop stress change at the back rim face was examined. The magnitude of critical Bhp was different for RDU testing and track testing. It was observed that a certain amount of energy over and above the critical Bhp was required to alter the rim residual stress, as ascertained by the hole drilling-strain gaging method conducted on all the test wheels. It was observed that higher amounts of Bhp levels were required during track testing than during RDU testing to alter the rim residual stresses. This was due to the fact that more heat was carried away due to convection during track testing than was possible during RDU testing.

The Braking Severity Index (BSI) developed in Section 3.3.1 may be employed to estimate the 'threshold' levels of brake shoe force, speed, and duration of drag braking that may be expected to alter the residual stress in the rim.

In terms of brake shoe force and speed, equation (2) can be rewritten as

$$Bhp = \frac{(BSF)(MPH)(f)}{375} = \left[(HP*HR)_c/HR\right] + HP_c$$

$$(BSF)(MPH) = \left[\frac{375}{f}(HP*HR)_c/HR\right] + HP_c \tag{3}$$

where HP_c =   Critical Bhp

          $(HP*HR)_c$ =   Minimum required energy over and above critical Bhp to initiate change in residual stress

The values for critical brake horsepower level (HP_c), and minimum required energy ($HP*HR_c$) were estimated from the evaluation of braking histories that caused residual stress changes in wheels tested under laboratory conditions (RDU) and on track (Preliminary Track testing) during the entire test series. A comprehensive tabulation of all the test parameters including HP_c and $(HP*HR)_c$ are presented in Appendices (Sections 5.8, 6.2, and 7.2).

After the complete evaluation of the test data for the 33 inch diameter, curved plate, Class U wheels, the values of critical brake horsepower level (HP_c) and minimum required energy above HP_c to initiate residual stress change appear to be:

$$HP_C \quad\quad = \quad 45$$
$$HP*HR_C \quad\quad = \quad 5$$

On Track

$$HP_C \quad\quad = \quad 40$$
$$HP*HR_C \quad\quad = \quad 5$$

On RDU

The corresponding values of brake shoe force and speed at various durations of drag braking that satisfy equation (3) can be easily computed by prescribing the threshold values of HP_C and $HP.HR_C$ for laboratory and track testing conditions.

It is best to initially express the brake operation threshold for rim residual stress change in a "Horsepower versus Time" plot similar to that used by Meizoso and Sevillano. Figure 11.48 presents a reasonable brake severity threshold in the form of "Horsepower-Time Thresholds for Stress Change". Curve B was estimated to fit the RDU test data, and curve D was estimated to fit Preliminary Track testing data for curved plate, Class U, 33 inch diameter wheels. The difference between curved plate wheels (D) and straight plate wheels (C) was established by judgment from the Comprehensive Track Test data. The critical Bhp (HP_C) for straight plate wheels seems to be 35, and the minimum required (threshold) energy over and above HP_C to initiate stress change in the rim is 5 HP-HR.

The corresponding values of brake shoe force and speed at various durations of drag braking were evaluated for the RDU with a criterion of 5 HP-HRS above a 40 (threshold) HP, to initiate a significant change in rim residual stress. The values of brake shoe force versus speed for four sets of drag braking durations are presented in Figure 11.49.

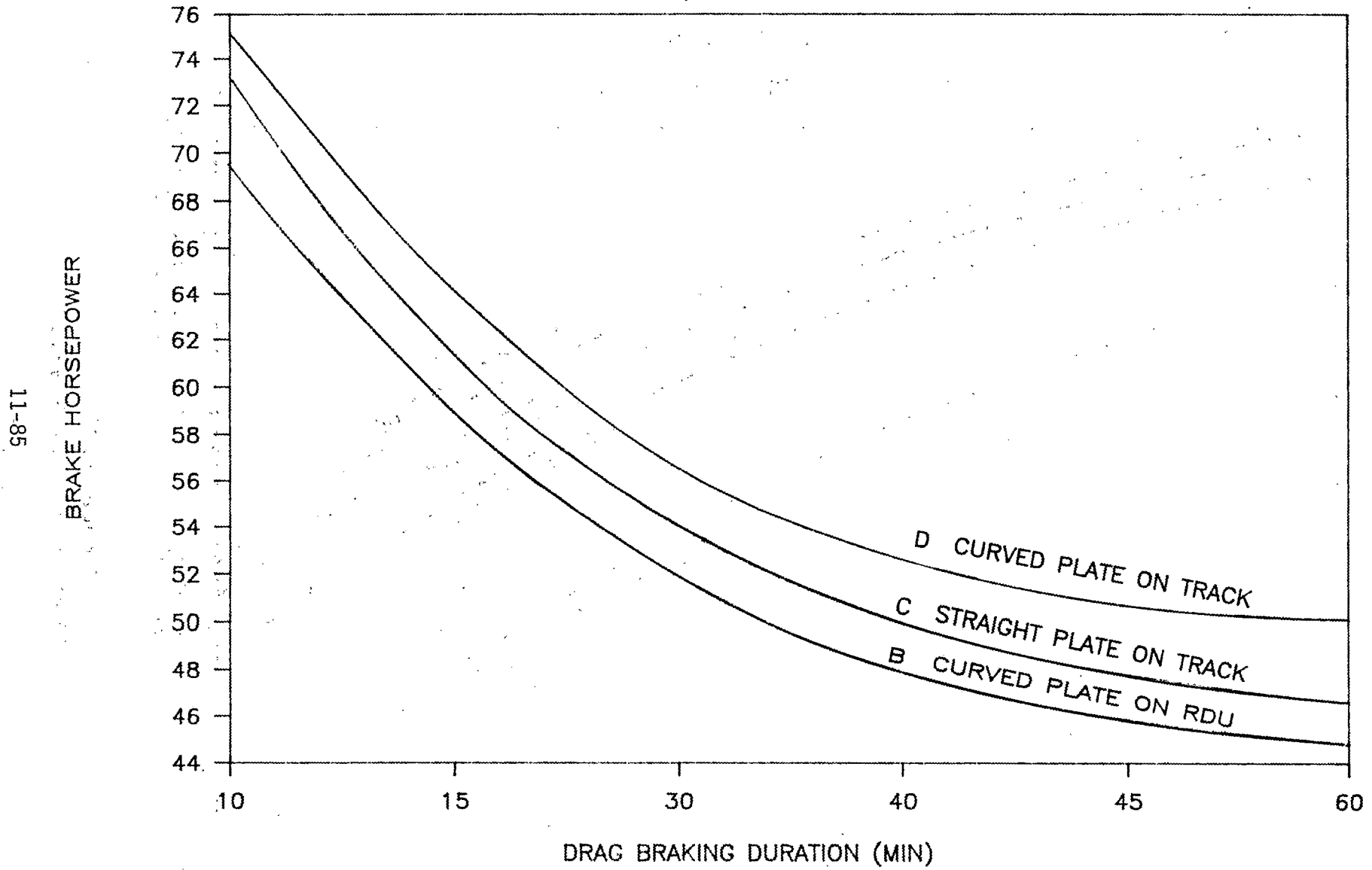HP — TIME THRESHOLDS FOR STRESS CHANGE

33 INCH, CLASS U WHEELS

FIGURE 11.48   HORSEPOWER-TIME THRESHOLDS FOR RIM RESIDUAL STRESS CHANGE

RDU DRAG BRAKING CYCLE THRESHOLDS

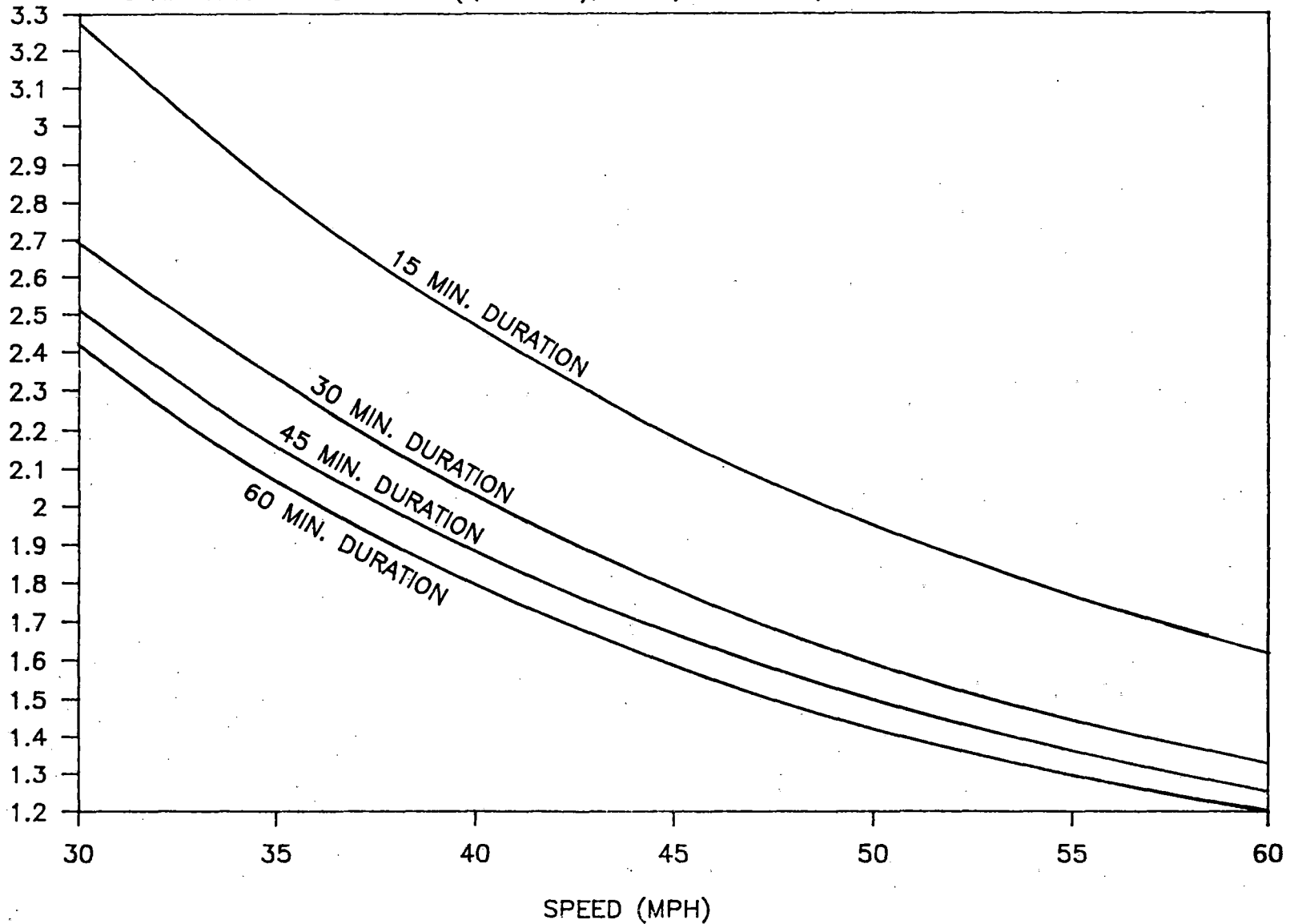## 5 HP-HRS ABOVE 40 HP (f = 0.23); CJ33, CLASS U, CURVED PLATE WHEELS

FIGURE 11.49   THRESHOLD DRAG BRAKING CYCLES ON RDU FOR RIM RESIDUAL STRESS
CHANGE IN CURVED PLATE WHEELS

Similar threshold braking cycles were evaluated for track testing conditions, with a criterion of 5 HP-HRS above a 45 (threshold) HP. The corresponding brake shoe forces versus speed at four drag braking durations are presented in Figure 11.50.

The threshold brake shoe forces versus speed for 33-inch, straight plate, Class U wheels on track, with a criterion of 5 HP-HRS above a 35 (threshold) HP are presented in Figure 11.51.

Figure 11.52 presents the threshold loci of Bhp versus braking duration for both curved plate and straight plate designs of Class U, 33 inch diameter wheels.

11.5 Effect of Brake Shoe Position on Residual Stress Change

An elasto-plastic finite element analysis has shown the brake shoe position has an important role in developing residual tensile stresses.[2]

The results of the calculations are summarized in Table 11.8, where the maximum temperatures and the circumferential stresses for the back rim face and the tread, both at the end of the 60-minute heating period and after the wheel has cooled, are tabulated.

From a practical standpoint, the high tread tensile residual stresses developed by braking would be modified on the surface by the action of the high contact stresses between the wheel and the rail. Wheels that roll on a rail eventually develop compressive circumferential stress on the tread. Hence, it is believed

TRACK TEST DRAG BRAKING CYCLE THRESHOLD

5 HP—HRS ABOVE 45 HP (f = 0.23); CJ33, CLASS U, CURVED PLATE WHEELS
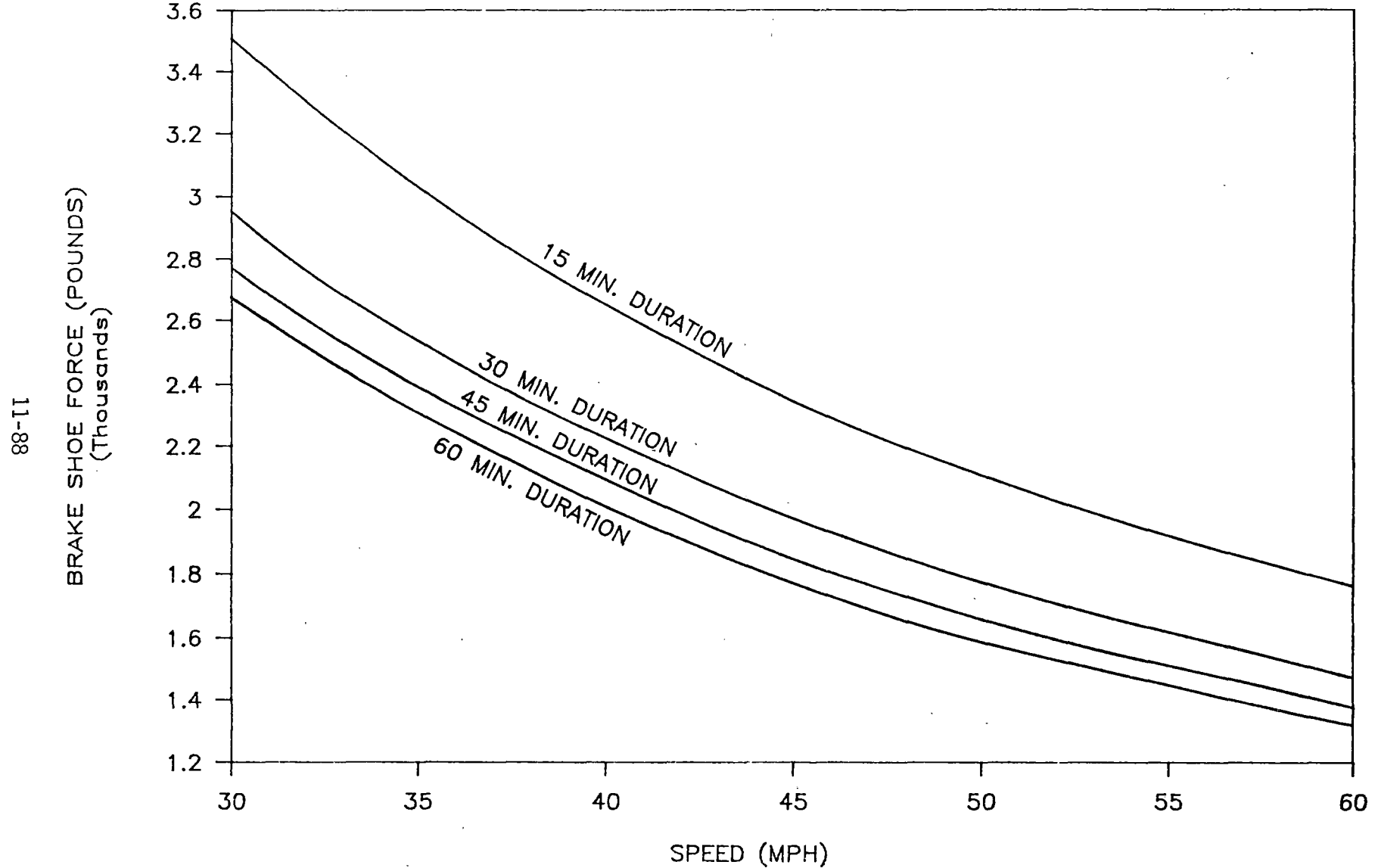
FIGURE 11.50   THRESHOLD DRAG BRAKING CYCLES ON TRACK FOR RIM RESIDUAL
STRESS CHANGE IN CURVED PLATE WHEELS

TRACK TEST DRAG BRAKING CYCLE THRESHOLD

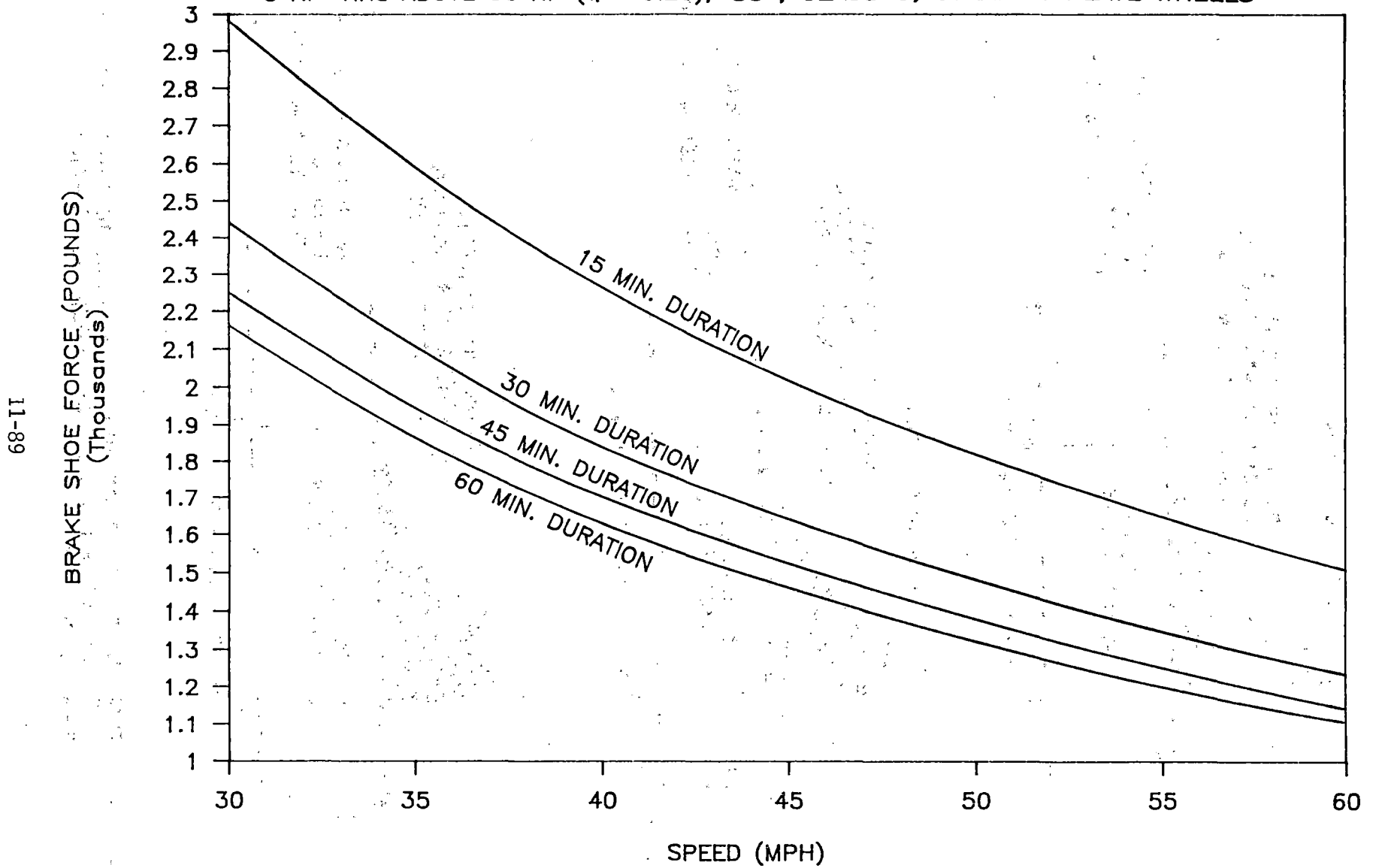## 5 HP–HRS ABOVE 35 HP (f = 0.23); 33″, CLASS U, STRAIGHT PLATE WHEELS

FIGURE 11.51   THRESHOLD DRAG BRAKING CYCLES ON TRACK FOR RIM RESIDUAL
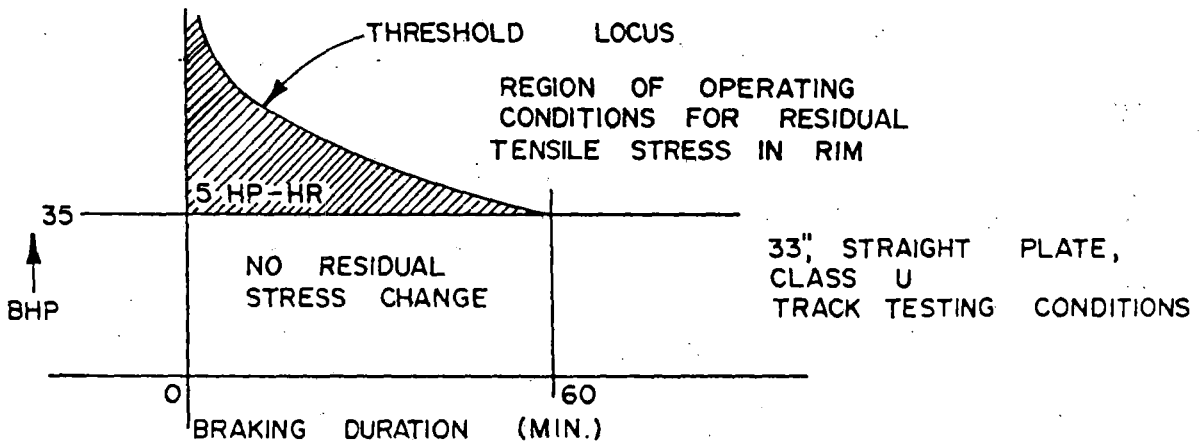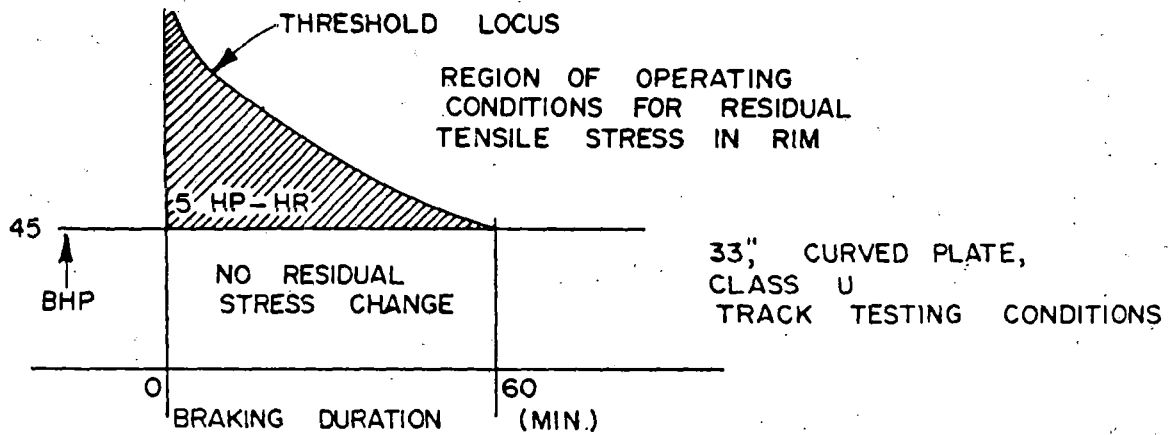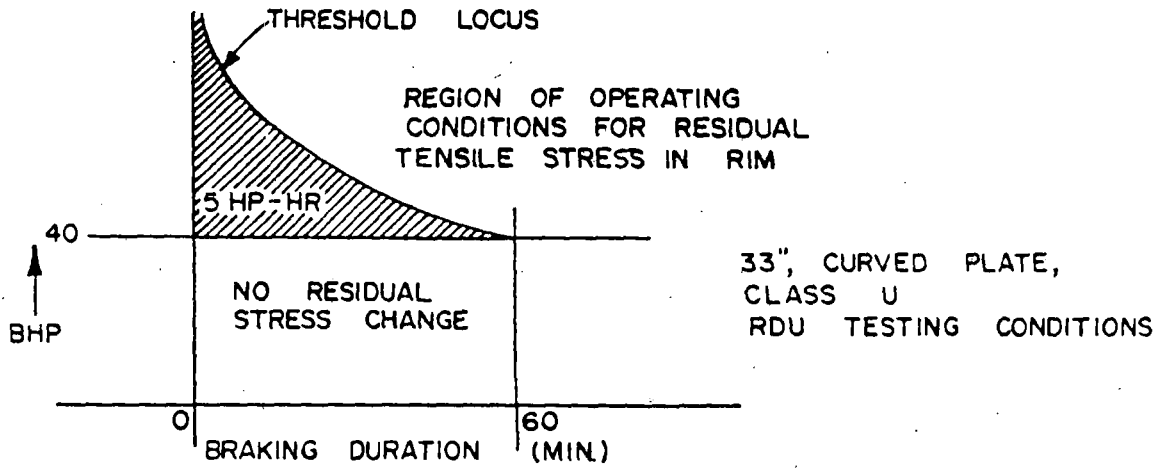STRESS CHANGE IN STRAIGHT PLATE WHEELS

FIGURE 11.52   THRESHOLD LOCI OF BHP -VS- BRAKING DURATION
FOR 33", CLASS U WHEELS UNDER DIFFERENT
TEST CONDITIONS

TABLE 11.8
CALCULATED RIM CIRCUMFERENTIAL STRESSES IN ONE-WEAR WHEELS
AFTER ONE HOUR HEATING

Wheel Size [in.(mm)]	Plate Design	Power Input To Wheel [bhp(kw)]	Maximum Temperature [°F(°C)]	Brake Shoe Position	Circumferential Stress at Indicated Locations			
					Bottom of Back Rim		Maximum on Tread	
					Hot [ksi(MPa)]	Residual [ksi(MPa)]	Hot [ksi(MPa)]	Residual [ksi(MPa)]
36(914)	Curved	48(35.8)	1301(705)	Overhang	-49(-338)	21(145)	-28(-193)	43(296)
			1078(581)	Center	-46(-317)	22(152)	-38(-262)	13(90)
			1006(541)	Override	-44(-303)	20(138)	-37(-255)	33(228)*
36(914)	Straight	48(35.8)	1268(687)	Overhang	-41(-283)	25(172)	-35(-241)	49(338)
			1083(584)	Center	-39(-269)	17(117)	-41(-283)	38(262)
			1043(562)	Override	-37(-255)	4(28)	-36(-248)	40(276)
33(838)	Curved	43(32.1)	1257(681)	Overhang	-46(-317)	20(138)	-29(-200)	44(303)
			1064(573)	Center	-43(-296)	21(145)	-40(-276)	18(124)
			1022(550)	Override	-41(-283)	18(124)	-36(-248)	31(214)*
33(838)	Straight	43(32.1)	1306(708)	Overhang	-42(-290)	30(207)	-37(-255)	49(338)
			1103(595)	Center	-42(-290)	20(138)	-39(-269)	39(269)
			1035(557)	Override	-40(-276)	8(55)	-38(-262)	39(269)
28(711)	Curved	37(27.6)	1314(712)	Overhang	-41(-283)	1(7)	-26(-179)	42(290)
			1112(600)	Center	-33(-228)	2(14)	-30(-207)	8(55)
			1051(566)	Override	-22(-152)	4(28)	-30(-207)	18(124)*
28(711)	Straight	37(27.6)	1285(696)	Overhang	-40(-276)	33(228)	-38(-262)	48(331)
			1090(588)	Center	-41(-283)	22(152)	-39(-269)	45(310)
			1048(564)	Override	-39(-269)	5(34)	-38(-262)	45(310)

*Indicates that the maximum stress occurred on the flange.

Note: With an overhanging brake shoe, the heat is put into the rim from the same node near the front face as in the centered brake shoe to a distance 1-11/16 inches (43 mm) away. With an overriding brake shoe, heat is put into the rim from the tip of the flange to a distance 3-3/8 inches (86 mm) away on a uniform longitudinal basis.

that these high stresses would not contribute to the initiation and propagation of thermal cracks on the tread surface.

The overriding brake shoe leads to high residual stresses in the flange. These high stresses could lead to the development and growth of surface flange cracks, which are important modes of failure in 33 inch diameter Class U wheels.[3]

Note that all three straight-plate designs have about 40 ksi compressive hot circumferential stresses, regardless of the location of heat input. The larger curved-plate wheel designs show lower tread stresses for the overhanging brake shoe case, but the hot stresses in the other two cases are also close to 40 ksi. The 28 inch diameter S-plate design usually shows much lower hot stresses.

There is a significant difference in residual stress patterns between the straight-and curved-plate designs. With the straight-plate design, the highest residual stress on the back rim face results from an overhanging brake shoe. With the curved-plate design, the residual stress at the bottom of the back rim face is almost constant, regardless of brake shoe location.

The largest residual stresses have been predicted for the straight-plate 28 inch diameter wheel design. This wheel type had a very poor service record and has been banned.

11.6   Crack Initiation, Propagation, and Fracture

11.6.1   Cumulative Fatigue Damage Model

The technical literature has been searched for candidate thermomechanical fatigue models that may be appropriate to treat the combination of brake thermal and rail mechanical load cycles that are important in the initiation and growth of a defect to critical size. Attempts to model the wheel failure process have been made and are described below.

Computer Simulation Approach

In the real world, very rarely are stresses measured; the quantity that is measured is strain. Hence a computer simulation of fatigue should be developed with strain as the controlling variable[4].

In his development of the simulation, Martin breaks the stress-strain curve into small elements that are approximated by straight line segments. These segments are based mainly on a constant stress change across each element; the corresponding strains are calculated at the beginning and end of each element. To apply this segmented stress-strain curve to the computer simulation, Martin introduces the concept of availability coefficients. By availability coefficients, he controls how much of each element is used, in sequence, to

simulate the stress behavior of a strain excursion. He also states, without further explanation, that the use of availability coefficients leads to results that are equivalent to rainflow counting, which is the accepted method for obtaining complete cycles from a complex strain history.

The history was first examined by merely breaking the strain range into a series of increments; that is, each "element" obtained had exactly the same amount of strain in it as any other. The computer printout of availability coefficients for each strain reversal could be interpreted to correspond exactly with the rainflow count.

In the next phase, an elemental stress-strain curve was constructed, mainly as suggested by Martin. In other words, most of the elements were constructed with a constant stress range of 2 ksi. As the stress-strain curve bends over at higher stresses, the strain increment becomes larger across the element. This stress-strain behavior has the unfortunate effect of compressing the availability coefficients data, and the computer printout of the availability coefficients for each strain reversal was much harder to follow than the one obtained in the first exercise. It is believed that a strain-based elemental stress-strain curve (rather than one based mainly on stress) will solve the current problem and allow the next step in the development of the computer simulation, which is the introduction of the fatigue behavior.

Difficulties are expected with the introduction of mean stress behavior into the fatigue damage calculation. Another

approach is to use the correction suggested by Morrow, although it is not in closed form. A third approach is to follow that of Landgraf, which is to ignore the mean stress correction entirely. While this may work in the automotive field, the main application here would be to wheels with high tensile residual stress in them, and it would appear that a mean stress correction is necessary.

11.6.1.1 Other Candidate Fatigue Models

Thermomechanical Fatigue Survey and Recommendation

One of the efforts undertaken in support of the assigned task of "developing a cumulative damage low-cycle fatigue model for calculating crack initiation" was to survey the current state of the art. A report of such a survey is included as Appendix 11.1.

This report presents an overview of current life prediction methods for potential application to the analysis of railroad wheel failures originating in the hot tread and rim region of the tread braked wheel. Six groups or classes of theories are reviewed.

1. Simple Time Independent Fatigue Approaches
2. Strain Range Partitioning (SRP)
3. Frequency Modified and Frequency Separation (FM)
4. Energy Based
5. Damage Rate
6. Continuum Damage

Several papers that report recent design applications of some of these methods to diesel and turbine engine components are also summarized. Recommendations for applications in railroad wheel research include: (1) additional cyclic flow behavior testing under thermomechanical fatigue simulation situations; (2) initial trails of the simple time independent elevated temperature fatigue methods (Universal Slope with and without 10% life rule) in wheel life analysis; (3) further critical evaluation and wheel applications of the SRP (Manson, et al.), FM (Coffin) and damage or crack rate (Sehitoglu) methods.

In addition, recent analyses of the propagation of tread thermal cracks reported at the 8th International Wheelset Congress in April 1985 by Meizoso and Sevillano have been reviewed. Their analysis treats the thermal braking cycle only indirectly through its effect on changing the residual stress system that the "elastic" rail contact stresses are superimposed upon.

AAR work sponsored at the University of Illinois by H. Sehitoglu is considering the interaction of thermomechanical strains and surface oxide formation in wheel steel and its effect on short crack development and propagation. This research is being addressed especially for potential application to assess the "damage" contribution of braking cycles to the wheel rim.

11.6.1.2 Evaluation of Back Face Rim Failures

A preliminary attempt has been made to predict the conditions of residual stress and superimposed rail load induced stresses required for crack initiation as well as propagation in one region of the wheel rim not directly subjected to rail contact stresses - the rim back face. This fatigue evaluation considers the range of stresses caused by rail load cycles, the effect of residual stress on crack initiation and propagation, and the possible range of pertinent fatigue properties. A summary of these conditions follows.

For the normal unworn wheel profile, the quasi-static variation in stresses on the back rim caused by rail loading (even that component of load which is most influential - lateral load) is relatively small. From elastic analysis and tests reported by Wetenkamp and Kipp in a 1977 ASME paper, the hoop stress variation at the B1 location for a 20,000 pound lateral load was plotted in Figure 11.53. Note that this stress range is less than 5 ksi.

Detrimental residual stresses such as those induced in the back face rim by very severe braking cycles can reduce the expected wheel life due to crack initiation and/or increase the crack propagation rate. These effects are illustrated in Figure 11.54 for crack initiation based on Manson's mean stress correction, and in Figure 11.55 for crack propagation based on data from Fowler in 1976.

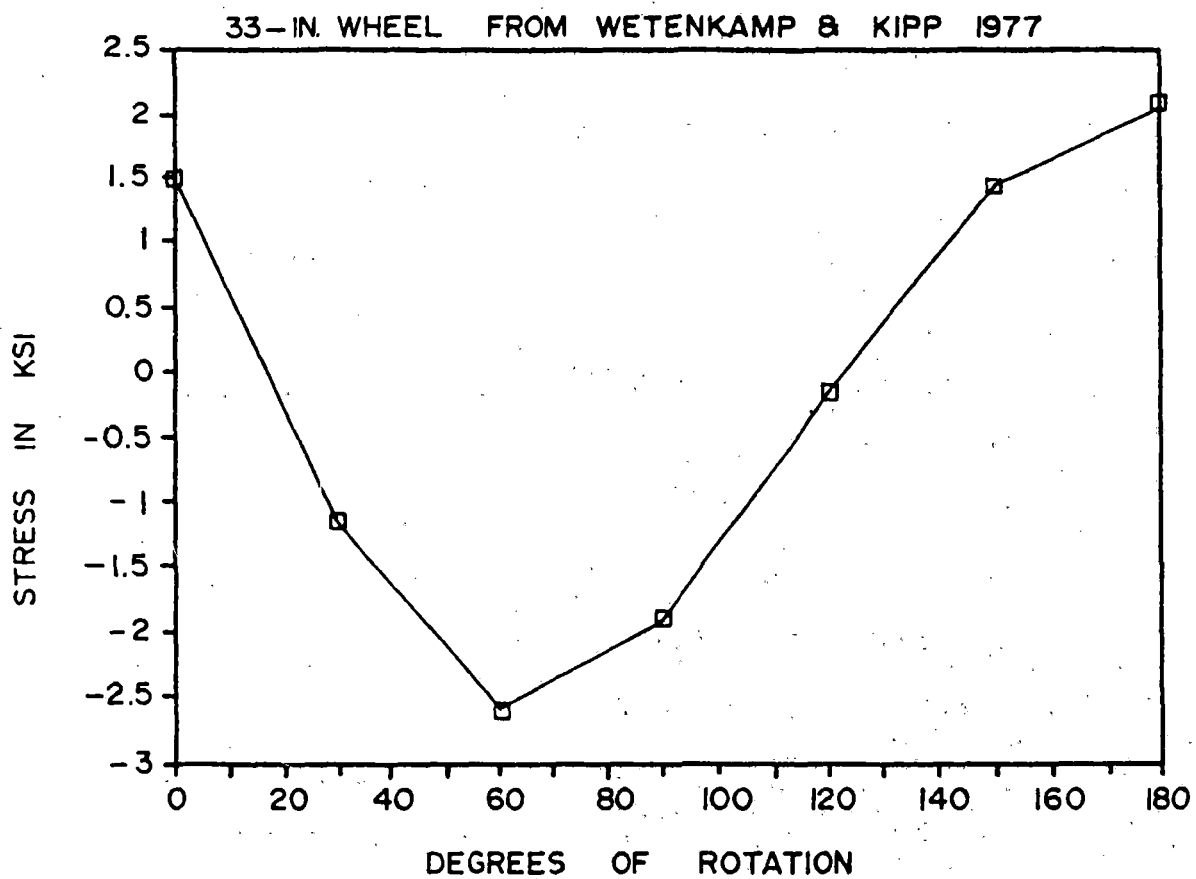The value of hoop residual stress at the B1 location of a

33-IN. WHEEL FROM WETENKAMP & KIPP 1977

FIGURE 11.53   LOW BACK RIM HOOP STRESS FOR 20 KIP LATERAL LOAD
             (WETENKAMP AND KIPP)
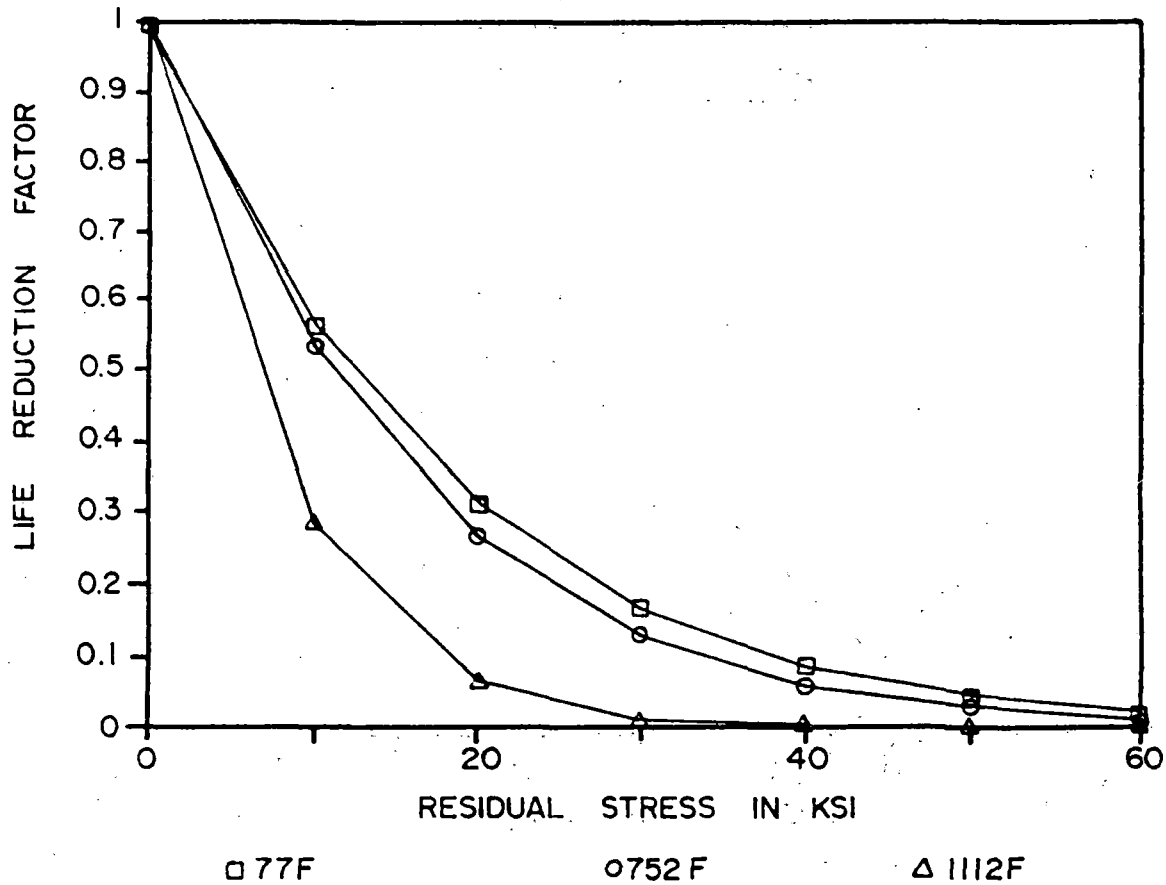
$$L.R.F. = \left[1 - \frac{\sigma_o}{\sigma_f^{'}} \right]^{1/b}$$

b = FATIGUE STRENGTH EXPONENT

σ_o = SUSTAINED MEAN STRESS

$\sigma_f^{'}$ = FATIGUE STRENGTH COEFFICIENT

FROM S.S. MANSON, "HONORING – AND UPDATING – MORROW'S MEAN
STRESS CORRECTION FOR METAL FATIGUE" JOMO' 84

FATIGUE PROPERTIES FROM M.C. FEC, "ELEVATED TEMPERATURE
FATIGUE BEHAVIOR OF CLASS B, C & U WHEEL STEELS"
ASME 1984

FIGURE 11.54 EFFECT OF RESIDUAL (MEAN) STRESS ON CRACK
INITIATION (S.S. MANSON)
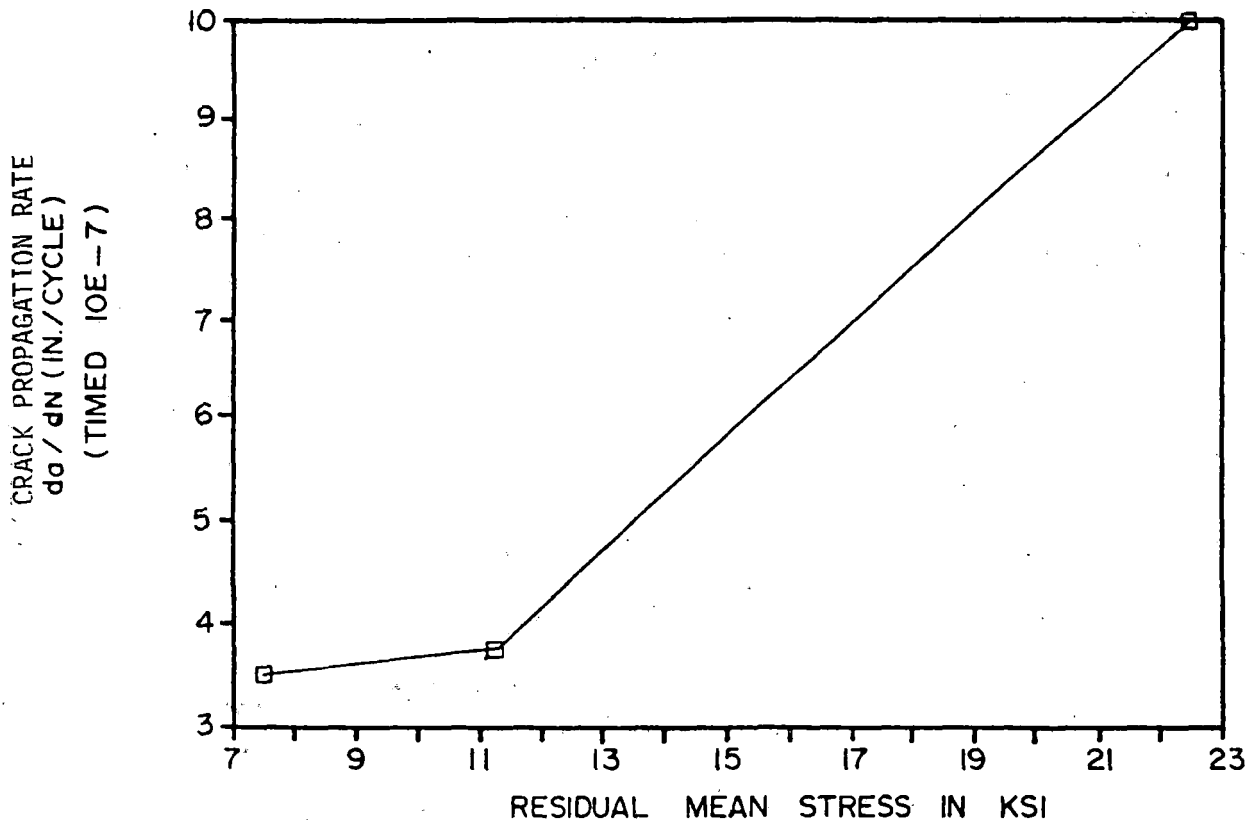
ASSUME   0.2" CRACK
STRESS   RANGE = 15KSI
$\Delta K = \Delta \sigma \sqrt{\pi a}$

FIGURE 11.55   EFFECT OF RESIDUAL STRESS ON CRACK PROPAGATION
(FOWLER)

Class U, CJ33 wheel after a severe 1-hour drag braking cycle at about 44 Bhp may be expected to be in the 22 to 33 ksi range. This level of residual stress is consistent with hole drilling measurements reported in this FRA program as well as analysis described in a later section of this report. From Figure 11.54, it may be seen that a 30 ksi residual or mean stress could be expected to reduce crack initiation life by a factor of 0.17 even for room temperature conditions. Also from Figure 11.55, the crack propagation rate for a 0.2-inch crack subjected to a stress range of 15 ksi might be expected to be increased by a factor of 3 for a residual increase from about 7 ksi to 23 ksi.

The effect of actual fabrication material surface condition (as opposed to laboratory specimen) must be accounted for as Pellini has emphasized ("Guidelines for Establishing Defect Quality Criteria in Fatigue Design", report to AAR, 1979). His "K_f" adjustment (like the notch stress concentration factor) recommended for normal production castings, for example, would be 1.5 for reliable life prediction. Perhaps a value as low as 2.0 (or a fatigue strength reduction factor of 0.5) might be appropriate for some wheels in service.

The combined effect of residual stress and reduced surface quality on crack initiation is illustrated in Figure 11.56 for room temperature Class U steel. The fatigue properties are taken from laboratory tests conducted as part of this program and reported under Task T3. Note that the horizontal axis is given both in terms of reversals (2 x cycles) and miles on 33 inch diameter wheels. Even with these "adjustments" for
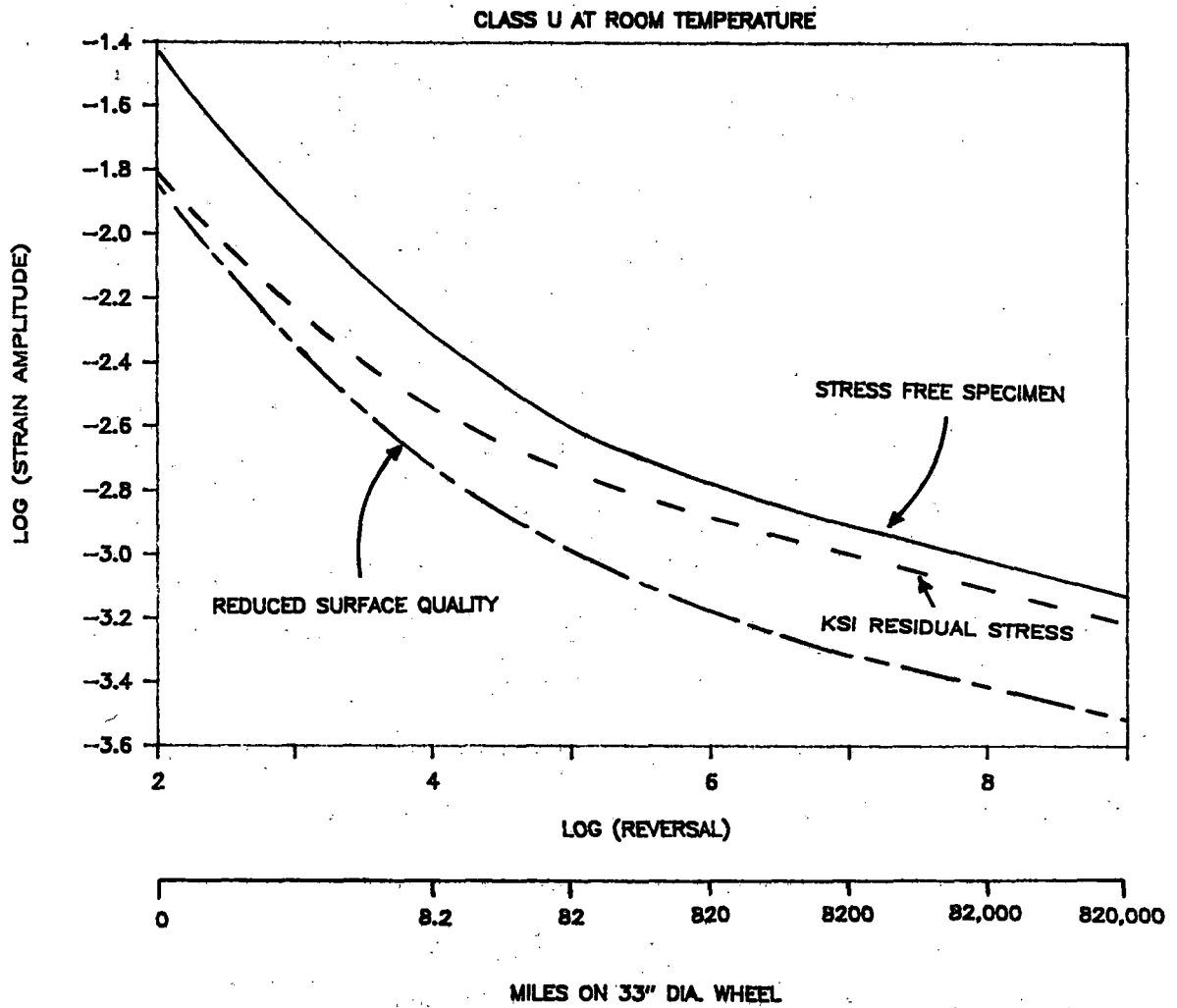
FIGURE 11.56 STRAIN AMPLITUDE/REVERSALS FOR CRACKING

residual stress and surface quality, an applied stress amplitude
as high as 10 ksi would be required to initiate lower back face
cracking in less than a million miles. In view of the
relatively lower rail stress amplitudes in this region of the
wheel predicted from earlier analyses, it appears that other
detrimental loading, geometry, environment or material
conditions must be considered in order to predict crack
initiation here. These observations are generally consistent
with comments made by Wetenkamp in 1977 and by Johnson et al, in
AAR Report #R-560 dated November 1983.

11.6.2   Linear Elastic Fracture Mechanics

One of the objectives of this technical task is to predict
the occurrences of wheel fracture. The interpretation of crack
arrest data and derivation of associated properties is described
in Section 4.0 (Technical Task T3).

A typical fracture analysis approach, which has been
completed is presented below. This analysis uses the residual
stress fields in the rail car wheels and cyclic mechanical
stresses from various field test and theoretical sources. The
entire methodology for the analysis is shown in Figure 11.57.
It may be noted that the fluctuating stress estimate may not be
high enough and not enough load spectra data were available for
this analysis. The results of this analysis, Figure 11.58, lead
to the following conclusions:

   o Residual stresses alone are insufficient to produce a
      life increment less than 200,000 miles.
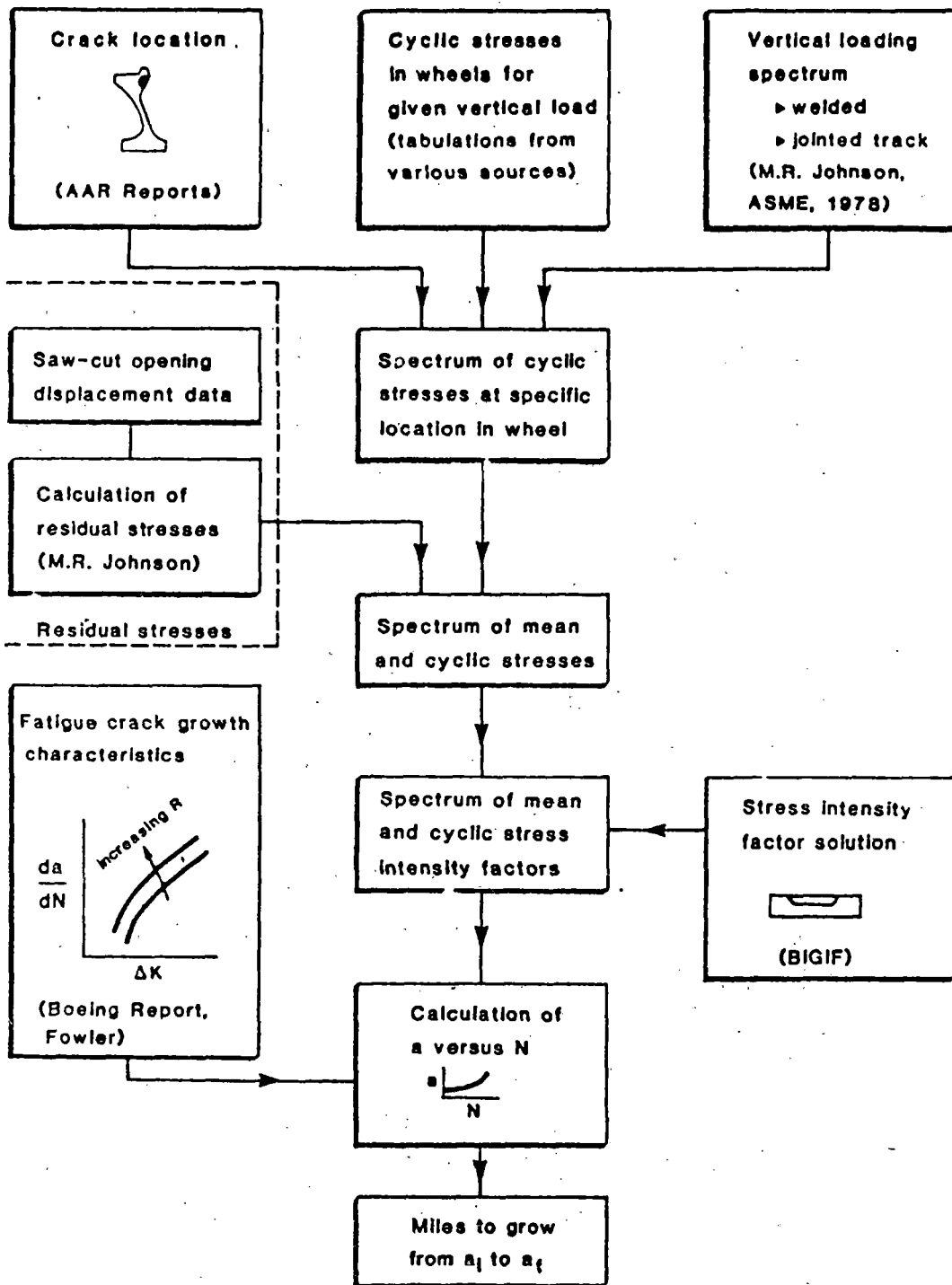
FIGURE 11.57   RESIDUAL STRESS ANALYSIS METHODOLOGY CHART

Location	Wheel Type (Plate)	Residual Stress	Applied Stress Spectrum — Rolling	Braking freq.	σ, ksi	Initial c/a	K_{Ic}, ksi-in$^{1/2}$	CRACK PROP. RATE da/dN	a_{crit}, in	a_{th}, in	Fatigue Life, miles from a_i to a_f (or a_c) 0.25/0.75	0.50/0.75	0.50/a_c	Notes
A	C	I	Std	0	--	3	35	Nom	0.42	~0.25	3.1x10^{10}	0	0	K_{Ic}
A	S	I	Std	0	--	1	35	Nom	0.48	0.42		0.25 0.75	0.50 a_c	c/a
A	C	II	Std	0	--	3	35	Nom	1.22	0.39		0.75		type, res
A	C	I	Std	0	--	3	50	Nom	1.00	~0.25	3.2x10^{10}	5.3x10^8	5.9x10^8	loc
B	C	I	Std	0	--	3	35	Nom	1.26	0.35	0	0	0	fcg
B	C	I	Std	0	--	3	25	Worst	0.92	<0.25		8.0x10^9	8.4x10^9	brakes
B	C	I	Std	1%	25	3	35	Nom	0.92	<0.25		2.0x10^7	2.1x10^7	more brakes
B	C	I	Std	1%	10	3	35	Nom	0.46	<0.25	2.8x10^8	2.0x10^4	2.4x10^4	jointed
B	C	I	Jointed	0	--	3	35	Nom	1.19	~0.25	2.0x10^7	3.2x10^6	3.4x10^6	res.
B	C	I	Jointed	0	--	3	35	Nom	>1.19	>1.19	6.0x10^5	0	0	no res.
B	C	None	Jointed	0	--	3	35	Nom	0.92	0.92	3.3x10^8	2.7x10^6	3.1x10^6	brakes
B	C	III	Jointed	1%	10	3	25	Worst	>2.0	0.84				fcy
B	C	I	Std	0	--	3	35	Nom	0.84	<0.25	1.6x10^8	3.8x10^7	6.0x10^7	high speed
B	C	I	Jointed	0	--	3	35	Worst	0.92	<0.25	2.7x10^6	1.5x10^4	1.8x10^4	fcy
B	C	I	Hi. Sp. Jnt.	0	--	3	35	Nom	1.19	<0.25	2.9x10^7	2.6x10^5	3.3x10^5	no res.
B	C	I	Hi. Sp. Jnt.	0	--	3	25	Worst	1.19	<0.25	2.7x10^5	8.0x10^3	1.0x10^4	fcy
B	C	None	Hi. Sp. Jnt.	0	--	3	25	Worst	0.90	~0.50	—	1.3x10^{10}	1.3x10^{10}	no res.

Location A: Back rim face
B: Front rim face

FIGURE 11.58 SUMMARY OF ANALYSIS RESULTS

o Curved and straight plate wheels are quite similar from a fatigue crack growth standpoint.

o Periodic stress "shifts" due to braking are of lesser influence.

o The crack aspect ratio (length/depth) at the beginning of the incremental life calculation is not influential.

o High cyclic stresses due to high speed on jointed track have some influence, but less than poor fatigue crack growth properties.

11.6.3   Range of Fracture-Critical Crack Sizes

Figure 11.59 describes the wide range of fracture critical cracks (FCC) sizes that resulted in fractures causing derailment.

This information is derived from References (5) and (6). The review of failure analysis reports confirms the relative sizes described in Figure 11.59.

Figures 11.60, 11.61, and 11.62 present the statistical distribution of measured crack sizes, for the failures analyzed by the UP. These data are derived from Reference (6). Reference (5) cites a similar distribution of crack sizes for the case of random selection of fractured wheels.

An important aspect of the frequency distribution of FCC sizes is that the highest fracture frequency is developed for crack sizes on the order of 0.75 inch. This is the surface length, dimension (C). The smallest crack size for failure is
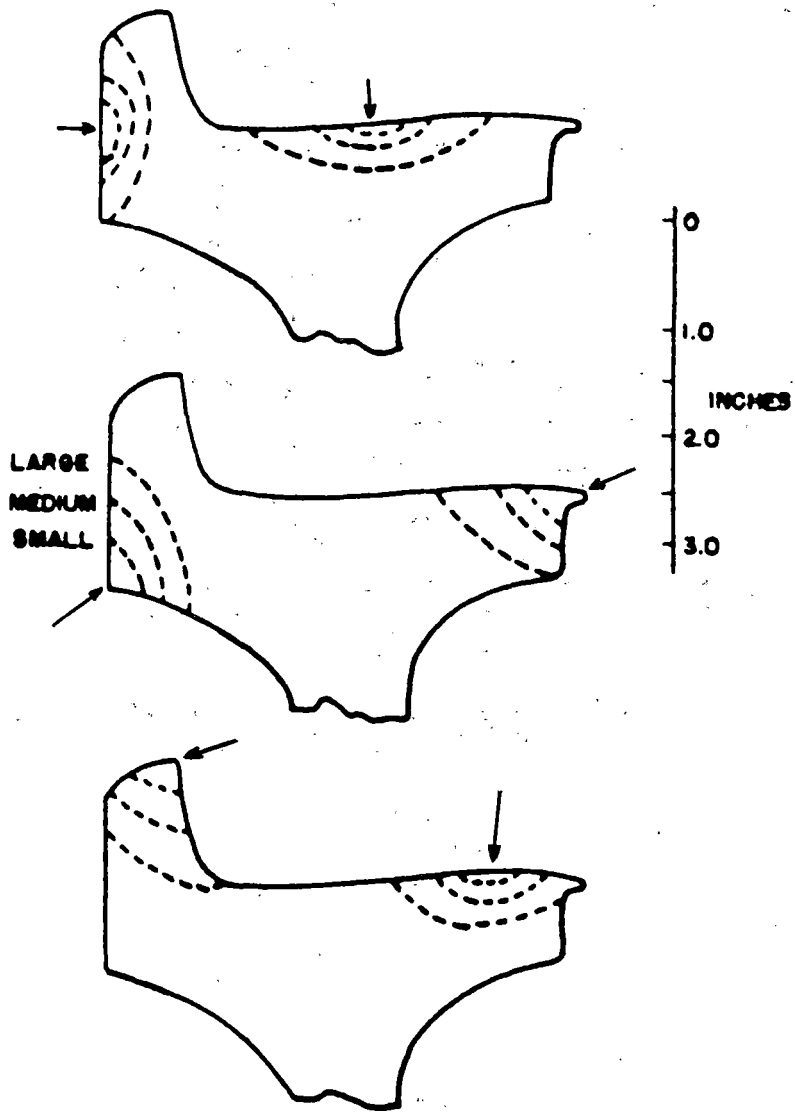
FIGURE 11.59   RANGE OF FRACTURE CRITICAL CRACK SIZES
RESULTING IN DERAILMENTS
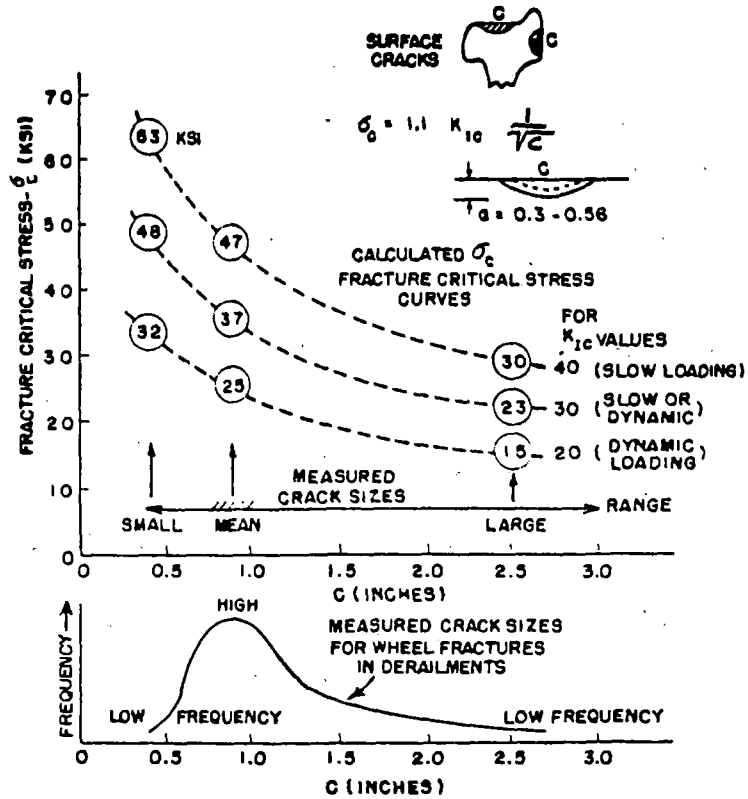(ARROWS INDICATE SITES OF CRACK INITIATION)

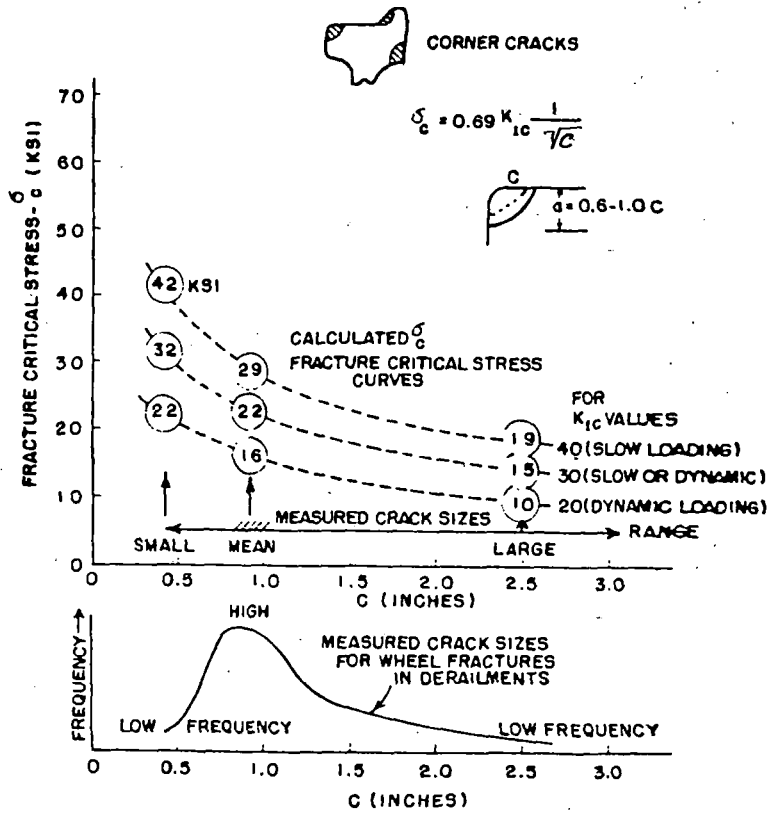FIGURE 11.60   FRACTURE STRESS -VS- CRITICAL CRACK SIZE
FOR SURFACE CRACKS

FIGURE 11.61   FRACTURE STRESS -VS- CRITICAL CRACK SIZE
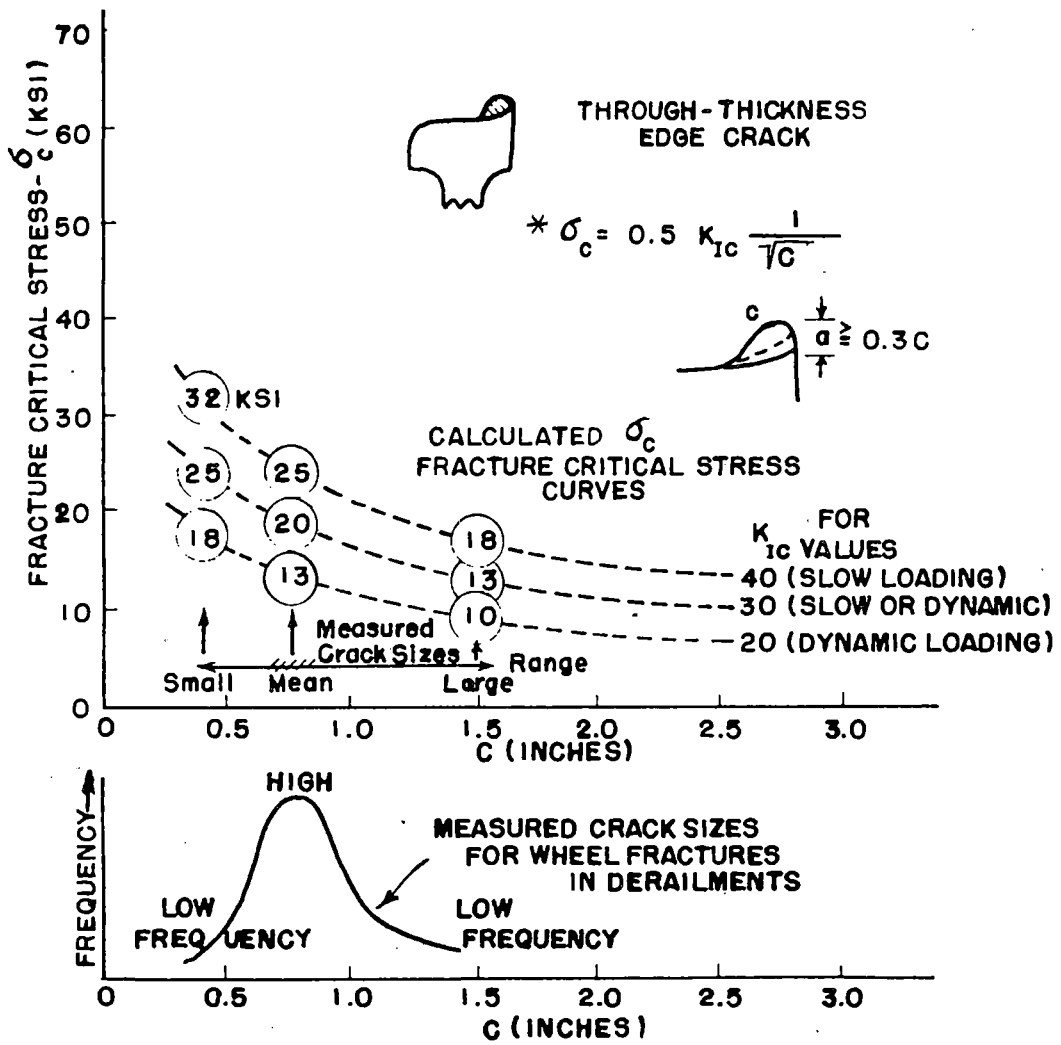FOR CORNER CRACKS

FIGURE 11.62   FRACTURE STRESS -VS- CRITICAL CRACK SIZE
FOR THROUGH-THICKNESS EDGE CRACKS

* C = CRACK LENGTH IN INCHES

on the order of 0.4 inches (C). The largest crack sizes are on the order of 1.5 to 2.5 inches (C). There is a low frequency for development of fractures due to cracks of small and large (C) dimensions.

A plot of the frequency distribution curve for the FCC sizes is presented at the bottom of Figures 11.60, 11.61, and 11.62. The significance of the peak frequency crack sizes is discussed in the following section.

11.7 Calculation of Fracture Critical Stress

Reference K_{IC} (ksi$\sqrt{in}$) fracture properties for cast and wrought B, C, and U wheels is presented in Figure 11.63. The plot is derived from data in Reference (5) and is confirmed by numerous other publications.

Because of similar microstructure and strength levels, the K_{IC} values fall in a narrow range. The lowest values are developed for the case of dynamic (impact) loading rates. These K_{IC} values are representative of highly brittle steels. This very low level of steel fracture properties has been accepted because of the need for high wear resistance.

The uncertainty of the data from the K_{IC} fracture tests ranges from ± 5 to ± 10 ksi$\sqrt{in}$. The smallest value that can be measured with confidence is approximately 20 ksi$\sqrt{in}$.

An envelope as defined in Figure 11.63 provides the best description for the fracture properties of a particular wheel. Characterization of K_{IC} values for each wheel involved
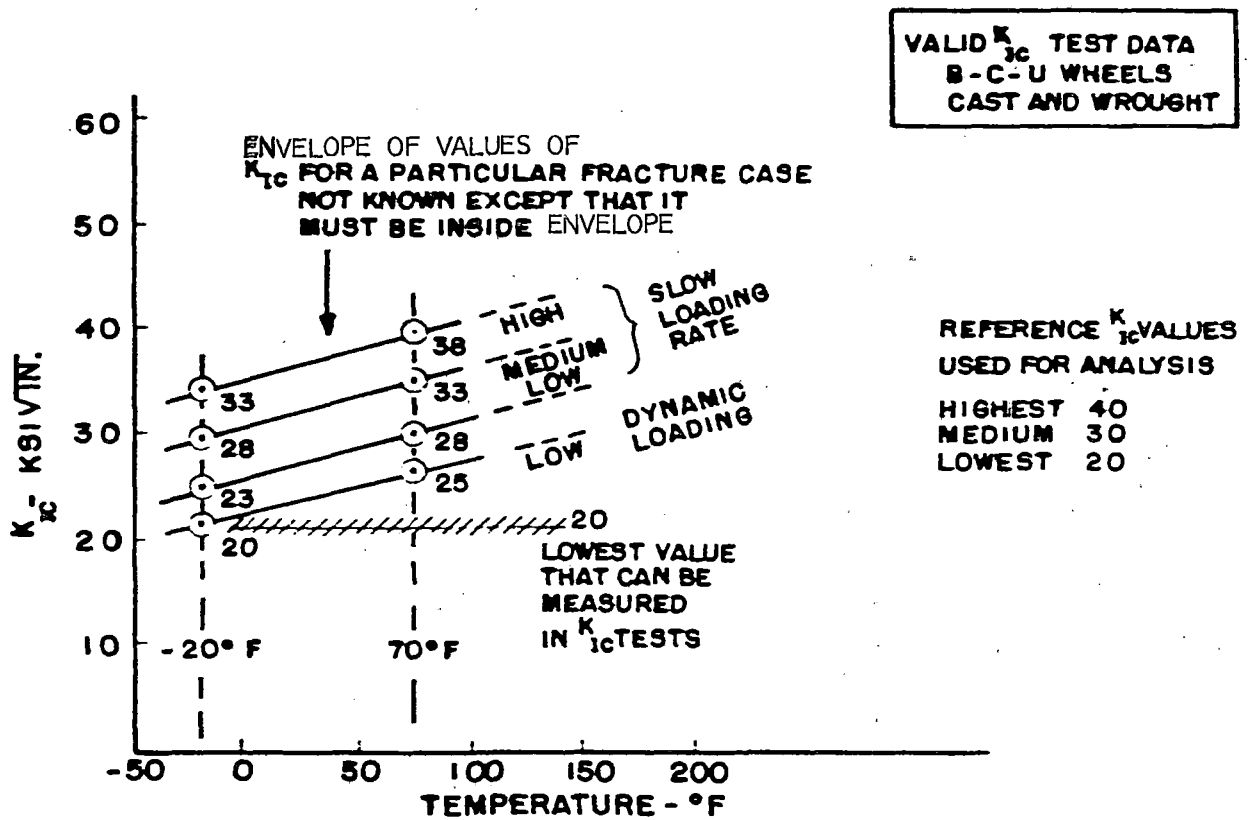
FIGURE 11.63 EXTREMES OF FRACTURE TOUGHNESS VALUE
REPORTED OVER THE TEMPERATURE RANGE OF
$-20^{O}F$ TO $70^{O}F$ $(-29^{O}C$ TO $21^{O}C)$

in a derailment fracture is not practical because it is very expensive and would almost certainly yield K_{IC} values that fall in the envelope.

The K_{IC} values are of primary interest for calculation of the fracture critical stress (FCS) for cases of specific measured crack sizes. For this purpose, the calculations may be made using the Reference K_{IC} values cited in Figure 11.62. The highest value of 40 ksi$\sqrt{in}$ is for the case of slow loading. The medium value of 30 ksi $\sqrt{in}$ is considered to be a representative value.

11.7.1 Calculated Crack Opening Stresses

Figures 11.60, 11.61, and 11.62 present the calculations for FCS for cracks of small, medium, and large sizes. These calculations are made for the Reference K_{IC} values of 20, 30, and 40 ksi $\sqrt{in}$. The calculated stress is the local tensile stress which acts across (90 degrees) the crack. It is best described as a crack-opening stress.

11.7.2 General Conclusions Regarding Failure

The primary conclusions that can be drawn from Figures 11.60, 11.61, and 11.62 and the statistical analyses are explained in Figure 11.63. These observations are:

1. Small cracks do not cause frequent fracture because of the infrequent application of high crack-opening stresses.

2. Therefore, the small cracks grow until their size is sufficiently large to result in fracture <u>for the more frequently applied levels of crack-opening stresses</u>.

3. Only a few cracks grow to larger sizes which can then fail due to lower levels of applied crack-opening stresses.

11.8 <u>Critical Combinations of Factors Causing Fracture Initiation</u>

The prior section indicated that medium size cracks were most frequently responsible for fracture initiation. This observation is supported by the actual measurement of crack sizes for the case of fractures resulting in derailments.

The calculations of fracture critical stresses (FCS) were based on K_{IC} fracture properties involving a narrow range of K_{IC} values. Because of this narrow range, all B, C, and U wheels can be considered to have closely similar fracture properties. Therefore, the calculations of FCS for a specific crack size can be considered to apply to wheels of B, C, and U types. The possible differences due to loading rate are very small and are not statistically of major significance.

It follows that the most frequent cause of fracture initiation is the <u>combination</u> of medium size cracks and medium

level crack-opening stresses. In order to understand the process of failure, several factors must be considered.

One critical factor is the spectrum of tensile stresses that are developed in the rim circumference of the wheels. Cracks grow in size as a result of repeated application of mechanical load and thermal stresses. The growth rate is determined by the stress level and the cyclic frequency.

Another critical factor is the peak stress since fracture occurs at a single application of a stress when the stress is sufficiently high to cause rapid growth of the crack. Therefore, stress peaks in the spectrum of service stresses are a critical factor. The stress peaks represent short pulse events in which normal low levels of repeated applied stresses are exceeded. There are numerous reasons for the development of stress peaks which are superimposed on the spectrum of normal (low) stress cycling. These include wheel impact at joints or switches, truck hunting, and car rocking. Figure 11.64 presents a schematic description of the spectrum of stresses as a function of wheel travel over the rail.

The stress peaks of interest are circumferentially applied tensile stresses which act to open rim or flange cracks. A small part of the wheel circumference is affected by a single stress peak. This is due to the very short time of the stress peaks. This pulse acts only on a small part of the circumference. In failure analysis reports, it is often reported that numerous cracks of the same type and size are present. However, if one crack happens to be at the right
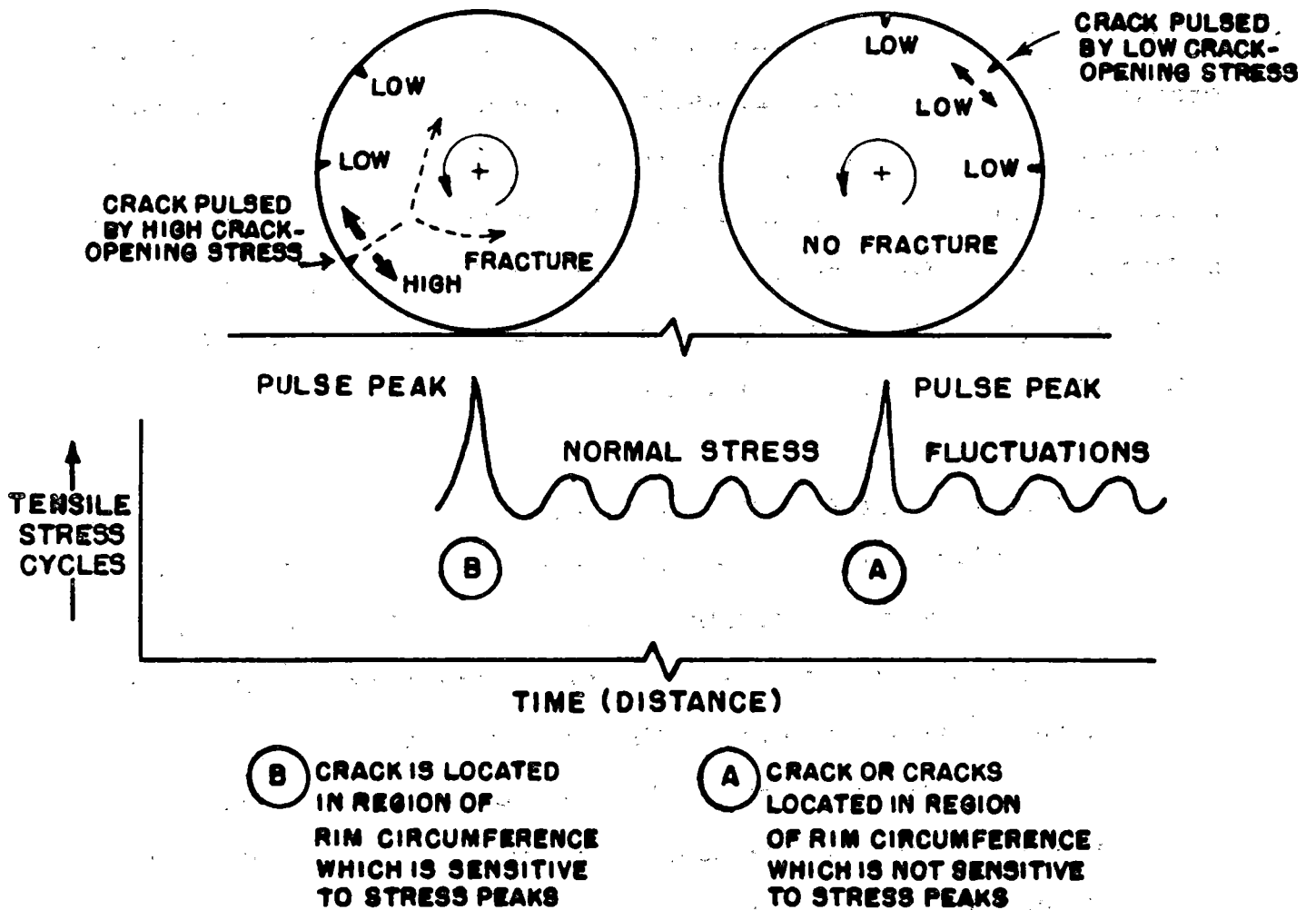
FIGURE 11.64   INFLUENCE ON WHEEL CRACK POSITION
TO LOADING POINT

11-115

place, a pulse can cause it to initiate fracture.

A diagram which tentatively explains the selection is presented schematically in Figure 11.65. According to this diagram, the failure-initiating crack is located in the region of the wheel circumference which is most affected by stress peak pulse. That is, the initiating crack is at the critical place of the wheel when the critical stress peak pulse is applied. This diagram applies to the case of a single crack or multiple cracks. This technical discussion explains the very wide range of crack sizes that result in fracture initiation, and the relatively low fracture rate for wheels that contain cracks of sufficient size for fracture. If the wheels were subjected to uniformly applied (over the circumference) peak stresses, the failure rate would be expected to be higher.

11.9   Observations from Field Experience

1. A straight plate wheel is several times more likely to fail and cause a derailment than a curved plate wheel.

2. During a typical year, approximately one half of the derailments occur during the winter quarter.

3. It is impossible from the service data to conclude if there is any difference in performance between U or B or C wheels due to the lack of data available on population or mileage of heat-treated and nonheat-treated wheels.
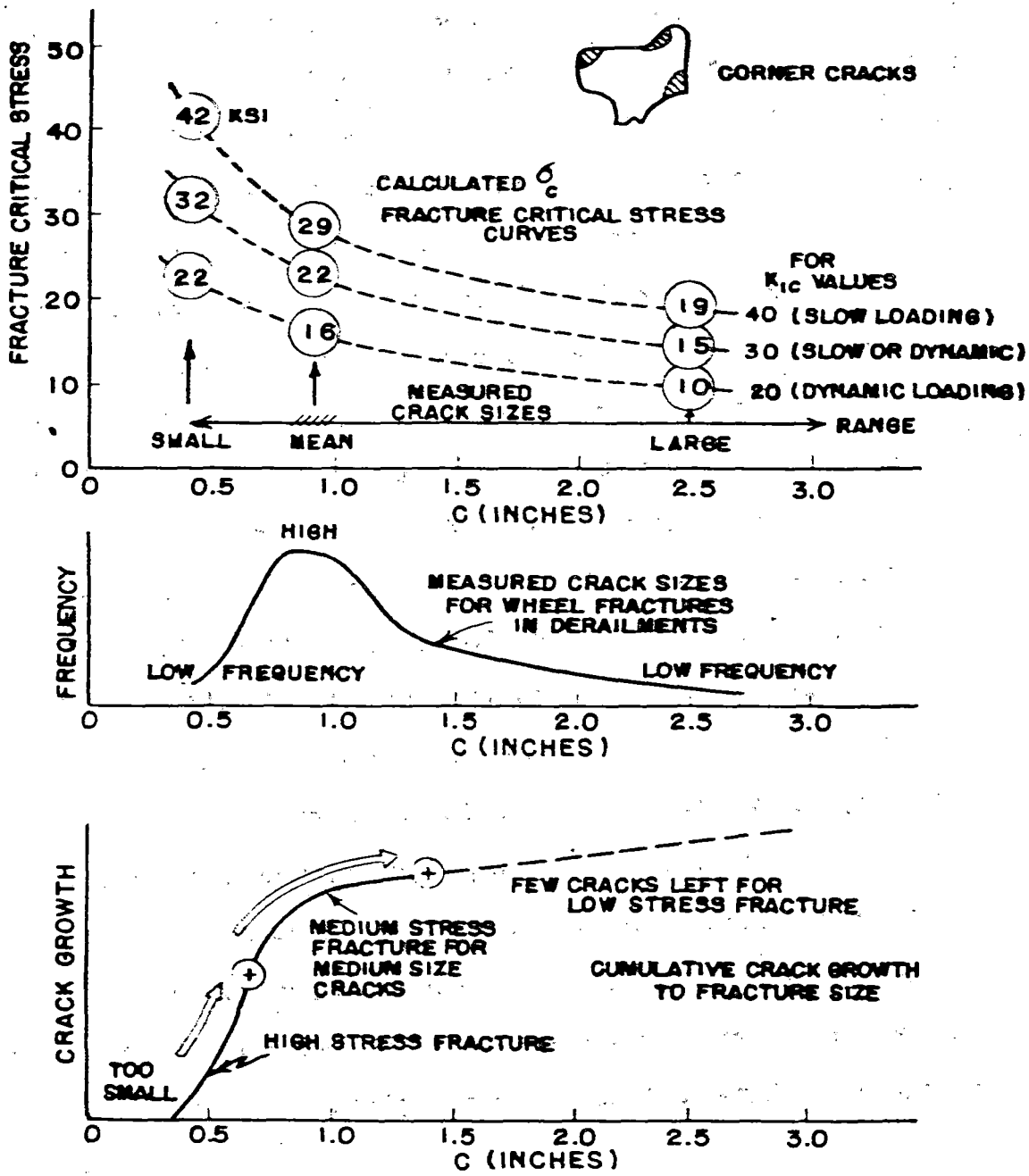
FIGURE 11.65   THE CONTRIBUTION OF CRACK GROWTH TO THE
DISTRIBUTION OF FINAL CRACK SIZE

4. The number of FRA reportable accidents caused by wheel thermal failure is decreasing at a rate of 0.016 accidents per billion ton miles per year (the number of accidents caused by wheel thermal failures was approximately 0.043 per billion ton miles in 1985).

5. Accident statistics indicate that 60 percent of accidents caused by wheel thermal failure involve wheels which are not discolored four inches or more. A survey of 12,000 wheels by one railroad showed that approximately five percent of the wheels were discolored. If this five percent applies to the entire fleet, then any straight plate wheel discolored four inches or more is approximately eight times more likely to fail than any straight plate wheel discolored less than four inches. Service data do not provide sufficient information to determine this ratio by wheel design or class.

6. Examination of over 400 wheels show that thermal cracks that lead to failure are always associated with some type of other mechanical or metallurgical damage.

7. Virtually all curved plate wheel failures originate at the sharp point formed at the intersection of the front flange wear line and the original plane profile.

8. The highest probability for the occurrence of a wheel fracture is found to be when a crack of medium size (3/4-inch) is combined with a medium level combination of residual and service stress (20 to 35 Ksi).

11.10 Analytical Methodology

11.10.1 General Data Correlation and Statistical Analyses

The primary goal of this subtask is to isolate combinations of wheel design and operation that result in critical levels of residual stress. The centralized data base at Pueblo was updated with pertinent data from the wheel saw-cutting, RDU, brake dynamometer (BDU), and track test programs. Residual stress estimates based on hole drilling are available for all of the test wheels. Efforts to correlate indices of braking severity with residual stress changes in the test wheels were made for all the tests completed on BDU, RDU, and track.

11.10.2 Analyses

During braking tests on the RDU, apart from the evaluation of residual stresses by the hole drilling strain gaging method after regular intervals, the thermal and residual strains monitored by high temperature strain gages on a continuous basis during and after testing were reduced for further stress analysis. Fortran programs were written to determine the hoop,

radial, and effective stresses including plastic strains during RDU braking (heating) tests. The brake shoe/wheel interface forces were continuously monitored and the Bhp for each wheel was computed from the acquired data. The temperature levels attained by different locations of the test wheels were monitored so that the actual strains, temperatures, and Bhp's could be interrelated.

The data were analyzed assuming the indices of braking severity to be parameters such as average Bhp dissipated at the brake shoe/wheel interface, and elastic effective stresses computed at various critical locations of the wheel. These indices were correlated with the maximum temperatures attained at different critical locations of the wheel.

Typical correlations between elastic effective stress and maximum temperatures attained at a given location are presented in Figures 11.66 and 11.67. Correlations between elastic effective stress computed at a given critical location and average Bhp at the corresponding wheel/brake shoe interface are presented in Figures 11.68 through 11.70.

11.10.3   Wheel Stress Analysis Programs

The main program selected to perform finite element stress analysis (ANSYS) in support of wheel failure analysis work and other tasks has been qualified and some applications in the programs have been made. A brief summary of the thermal, elastic, and inelastic analyses completed is presented below.
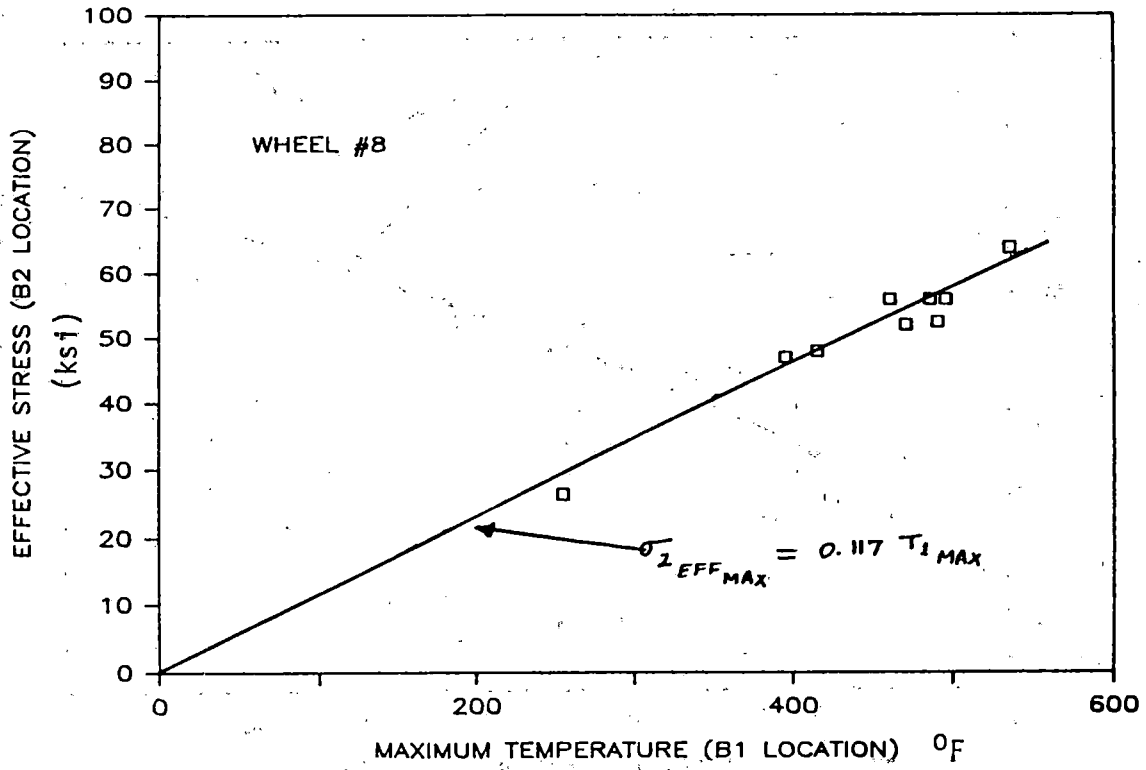
FIGURE 11.66   ELASTIC EFFECTIVE STRESS (B2) -VS- TEMPERATURE (B1),
WHEEL #8
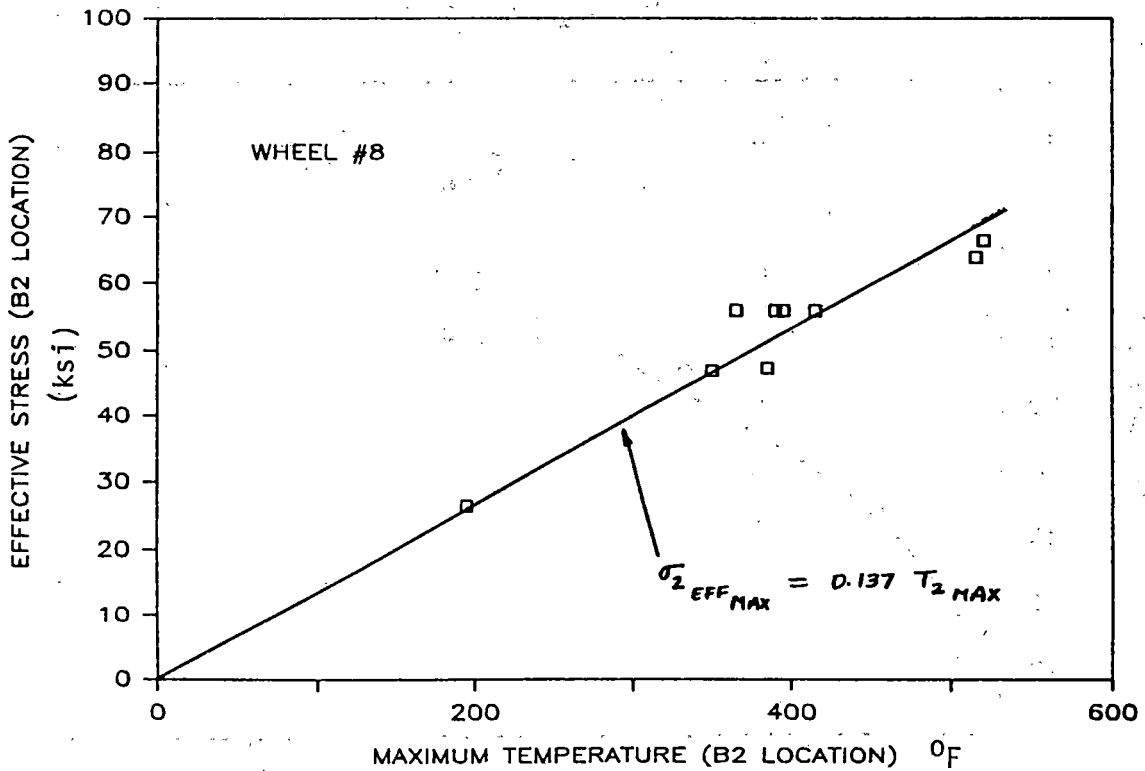
FIGURE 11.67   ELASTIC EFFECTIVE STRESS (B2) -VS- TEMPERATURE (B2),
WHEEL #8

WHEEL #8

$$\sigma_{2_{EFF_{MAX}}} = 10.83 \sqrt{BHP}$$
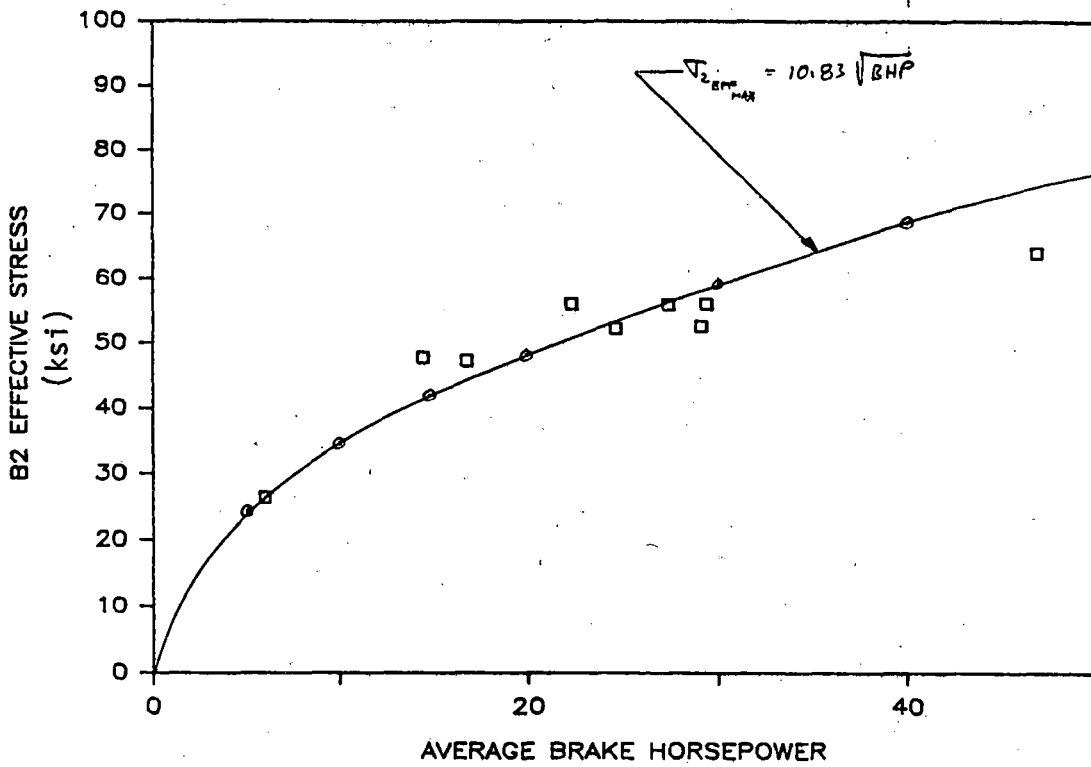
FIGURE 11.68   ELASTIC EFFECTIVE STRESS (B2) -VS- AVERAGE BHP, WHEEL #8

WHEEL #8

$$\sigma_{3_{EFF_{MAX}}} = 12.89 \sqrt{BHP}$$
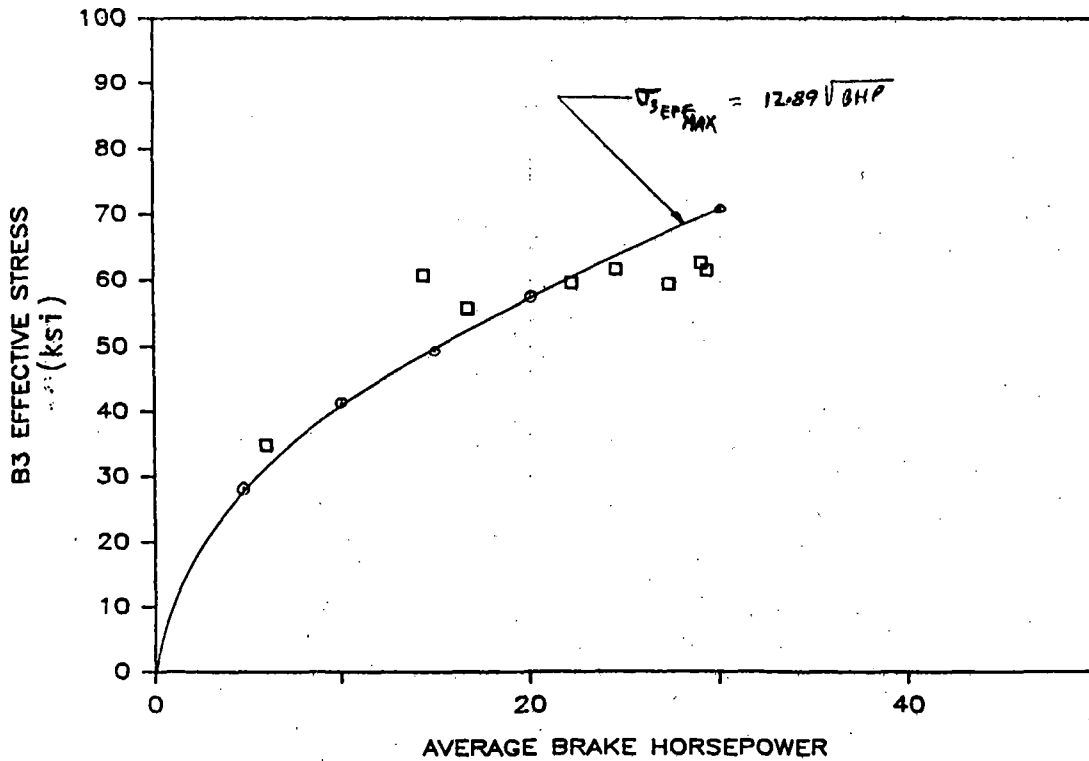
FIGURE 11.69   ELASTIC EFFECTIVE STRESS (B3) -VS- AVERAGE BHP, WHEEL #8

WHEEL #7

$$\sigma_{3_{EFF_{MAX}}} = 11.41 \sqrt{BHP}$$
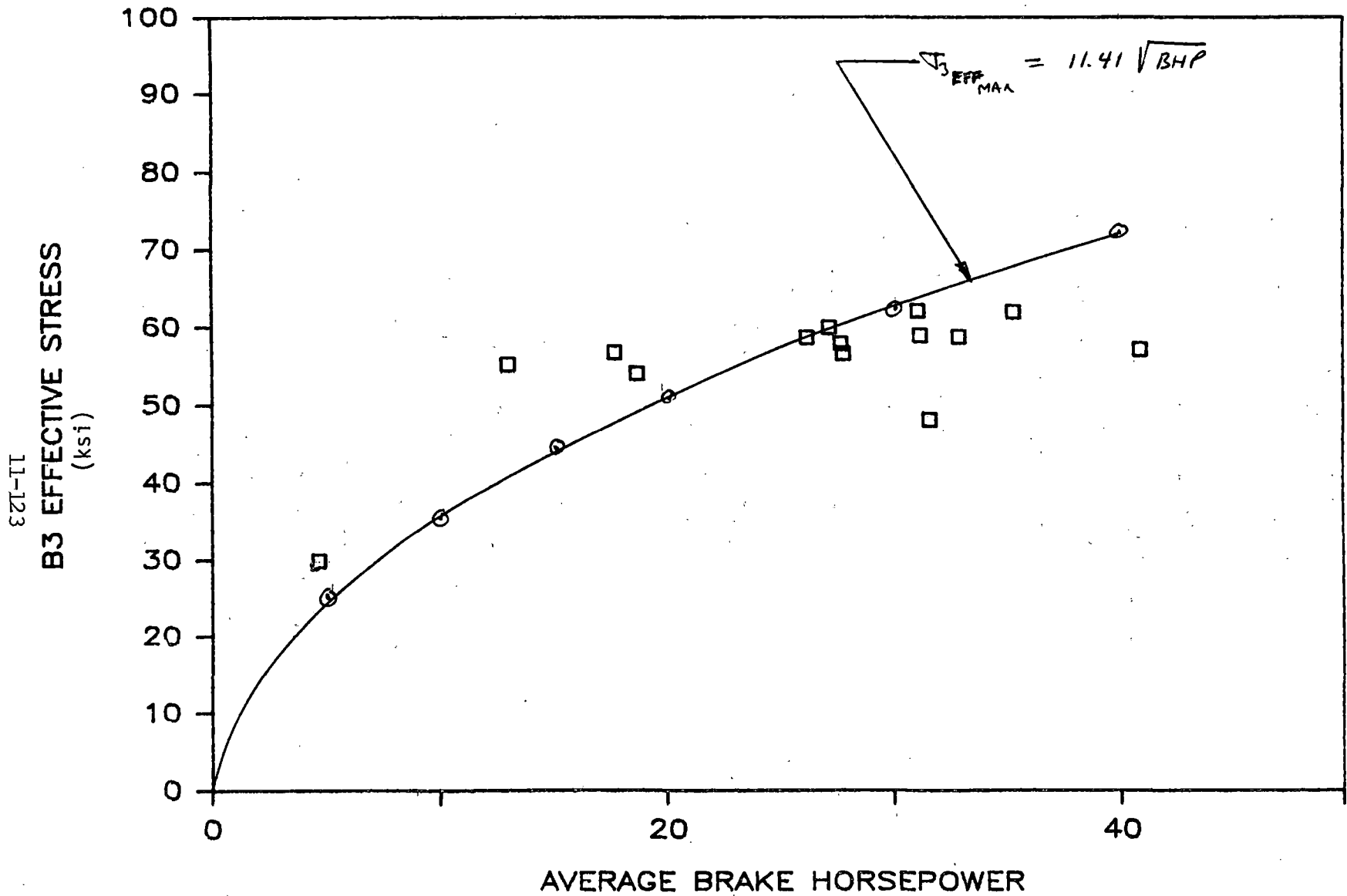
FIGURE 11.70 ELASTIC EFFECTIVE STRESS (B3) -VS- AVERAGE BHP, WHEEL #7

11.10.4   Wheel Temperature Correlation Attempts with ANSYS

The ANSYS computer program is a large-scale, general purpose computer program for the solution of several classes of engineering analyses. Analysis capabilities include static and dynamic; elastic, plastic, creep and swelling; buckling; heat transfer, fluid, and current flow. It is a well established, commercially available computer program that has been leased and used during this program.

Since reliable wheel temperature predictions are an important pre-condition for obtaining good stress results, considerable effort was applied early in the program to a selection and refinement of thermal properties and boundary conditions to give a satisfactory match to prior temperature data from induction heating experiments. These attempts are described under induction heating experiments in this section.

11.10.5   Elastic Analysis

The ANSYS programs have been used routinely at AAR for Thermo-elastic wheel stress analyses in support of AAR Wheel Specification S.660. At present, the elastic option is being used in this research program to estimate the wheel rim stress cycles caused by lateral and vertical rail loading on both new and worn wheel profiles. Finally, ANSYS elastic analyses have been made to estimate the residual stresses revealed by saw-cut opening displacement measurements. This application is

discussed under "Residual Stress Analysis from Saw-Cut Displacement Measurements", in this section.

11.10.6   Inelastic Analyses

The initial effort with ANSYS in this program to account for inelastic behavior of wheel steel was the attempt to predict the total and residual strains observed in the most severely thermally loaded induction heating experiments.   Time or rate independent plastic behavior with the ANSYS kinematic option to account for Bauschinger type unloading was used.   The plastic properties were specified as functions of temperature.

In addition to these ANSYS plasticity analyses, some exploratory or "bench mark" studies were made of the creep or rate sensitive material options in order to support the cyclic stress change material simulation effort.   Simple uniaxial simulations of hypothetical strain and temperature cycles were conducted and compared to the stress cycle predictions of an independent closed form solution for a special case of kinematic hardening with second degree nonlinear creep and temperature dependent properties.   The two solutions were essentially identical, as had been hoped, which encourages further use of the ANSYS material options with more realistic cyclic and rate dependent steel behavior.

11.10.7 Applications

In addition to the overall analytical correlation effort (above) and the inherent task elements relating to cumulative damage modeling and cyclic path dependence of residual stress changes (reported later), specific analyses have been undertaken to support other technical tasks in the program. Progress on these supporting mechanical analysis tasks is summarized below. In some cases, reference is made to these analyses reported as part of another task.

11.11 Detailed Residual Stress

The experimental and analytical portion of detailed residual stress analysis covered under Technical Task T11 is presented in Section 12.0.

11.12 Thermal Cracking

Support for the design of the thermal cracking rig, part of Task 3, has been provided in the form of a transient thermal analysis of a moving heat source (reported under Task 3). This analysis was based on an adaption of Archard's solution (ASME Wear Control Handbook, p. 135) for a temperature rise across a moving hot spot of a given "strength" and speed. It facilitated a preliminary selection of torch thermal ratings and wheel rotating speeds to produce temperatures high enough to produce

transformation to austenite. Austenite is required for transformation to martensite on cooling. Cracking initiates in martensite during further restrained cooling. The details of thermal cracking rig design and test conditions are presented in Section 4.3.

11.13 Wheel/Rail Heat Transfer

The amount of heat transfer at the wheel/rail contact in Technical Task 4 has been estimated based on measurements of the increase of heat content of the "rail" wheel in both the RDU and the brake dynamometer as well as the leading to trailing rail surface temperature measurements reported in Section 5.0.

The first method assumes all the heat transferred through wheel/rail contact raises the internal energy or heat content of the rail-wheel or roller, which is calculated from the temperature rise measured at several radial locations at the end of the braking test. The energy increase in any "ring" region of the rail-wheel is simply the following product:

Ring volume x Steel density x Specific heat of steel x Average temperature increase in ring = I (Btu).

The heat transferred, Q (Btu), during the test period, t (HRS), may be expressed in terms of equivalent horsepower, hp, as:

$$Q = 2544.5 \times hp \times t$$

The heat transfer rate in horsepower may then be obtained by equating the heat transferred and the internal energy increase

during the test period.

$$HP = I \ [Btu] / (2544.5 \times t \ [HRS])$$

This value is a lower bound estimate since convection losses are ignored. Even so, values as high as 8 hp are obtained for nominal 50 Bhp braking tests under full vertical load.

The other method of estimating heat transfer rate is based on the adaption of closed form solutions by Rosenthal (Trans. ASME, Vol. 68, 1946, pp. 849-866). Solutions for the leading and trailing surface temperatures surrounding a moving point and line heat source are described in Appendices 5.2 and 5.3. Applications of this theory are discussed under Technical Task T4 in Section 5.0. Although consistently reliable surface temperature measurements have not yet been achieved, preliminary indications are that temperature differentials of 15°F measured at 16 inches from the contact would be expected theoretically for a heat transfer rate of about 8 hp. Such a temperature differential is within the experimental scatter of the preliminary measurement attempts.

These applications of theoretical heat transfer analysis, including estimated convection heat loss and the effect of contact area, are discussed in detail under Task 4, in Section 5.0.

11.14 Thermal Analysis of Brake Shoes

The detailed brake shoe thermal analysis, in support of the special track and laboratory tests to estimate heat flow into

the brake shoe (Technical Task T7), is presented in Section 6.4.

REFERENCES

1. A. Martin-Meizoso and J. Gil-Sevillano, "Thermal: A Computer Code for Life Prediction of Railway Wheels", Proceeding of the Eight International Wheelset Congress, Madrid, 1985, Paper II.2.

2. A.J. Opinsky, M.W. Joerms, D.H. Stone, and M.R. Johnson, "Effect of Brake Shoe Position on the Development of Residual Stresses in Freight Car Wheels as a Result of Simulated Drag Braking", ASME Paper 85-WA/RT-3, December, 1986.

3. A.J. Opinsky, "An Analysis of Some Railroad Wheel Flange Failures", AAR Report R-571, March, 1984.

4. J. Morrow, J.F. Martin, and N.E. Dowling, "Local Stress Strain Approach to Cumulative Fatigue Damage Analysis", University of Illinois, Report UILU-ENG 74 6001, January, 1974.

5. C.S. Carter, R.G. Caton, and J.L. Guthrie, "Fracture Resistance and Fatigue Crack Growth Characteristics of Railroad Wheels and Axles", Report DOT-TSC-617, April, 1976.

6. A.J. Opinsky, "An Analysis of Some Railroad Wheel Tread Fractures", AAR Report No. R-609, July, 1985.

12.0 DETERMINE RESIDUAL STRESS AND METALLURGICAL CHANGE IN TEST WHEELS (TECHNICAL TASK T11)

The main objective of the Technical Task T11, is to develop detailed residual stress analysis techniques by slicing the test wheels, followed by hole drilling and strain gaging. In consultation with FRA, test wheels were selected from the following assortment:

o   Wheels in as-received condition; analysis will establish baseline stresses.

o   Parabolic plate wheels with known thermal history.

o   Straight plate wheels with known thermal history.

The as-received wheels were sliced, drilled, and strain gaged to map the residual stresses in the test wheel. Required data acquisition and processing procedures were applied to produce analyses of the triaxial residual stresses with the known thermal and mechanical loading histories of the wheels to increase the amount of confidence in the proposed wheel failure mechanisms during the course of research. Since only as-received wheels were analyzed, further correlation was not possible.

12.1 Major Findings/Current Status

Residual Stress Estimation from Saw-Cutting Results

During the execution of the wheel research program, greater experimental emphasis was placed on the wheel saw-cut opening

and strain release measurements than was originally planned in the Statement of Work, in order to take advantage of the method of estimating internal residual stresses by 3D Finite Element Analysis described in Section 11.0. Front face as well as back face saw-cut opening displacements were measured in a total of 31 wheels, for detailed finite element analysis of saw-cut displacement data. Subsequently, greater analytical emphasis was placed on the development of a simple mathematical model to interpret average stress distribution from saw-cut displacement data.

In addition to extended efforts mentioned above which are performed before, during, and after saw-cutting, hole drilling strain-gaging was performed on a number of selected wheels at 3 critical locations in each wheel before saw-cutting. The residual stresses evaluated at these critical locations were correlated with the flange tip displacement (in hoop direction) to saw-cutting at various depths of cut. It was seen that the flange tip displacement at a given depth of cut exhibited a certain relationship with the bi-axial state of stress at the selected critical locations. Linear relationships were established between the bi-axial state of stress at a given location and flange tip displacement (in hoop direction) at selected depths of cut. The stress used to correlate this displacement is an "equivalent" uniaxial stress that would produce the same hoop strain as the measured bi-axial stress components.

This general correlation suggests that a measure of the

residual stress intensity, at least for the lower back rim location, B1, may be estimated from the flange tip saw-cut opening response. A detailed discussion of this analysis is presented in Section 4.6.

The following three extensive efforts were carried out during the overall program:

o   Correlation of residual stress on back rim face (as determined by hole drilling-strain gaging method) and the saw-cut displacement behavior.

o   3D finite element analysis to determine residual stress distribution in 31 rail car wheels from saw-cut displacement data.

o   Closed form analytical model to determine average residual stress distribution in at least 200 service and test wheels.

In view of the above changes in the program, the original effort and emphasis placed on "Detailed Residual Stress Analysis" was reduced and restricted to a limited number of Class U, 33-inch diameter, curved plate wheels.

12.2 Detailed Residual Stress Analysis Efforts

The first wheel analyzed at the Technical Center, Chicago, was a Class U, 33-inch, parabolic plate design, as received from Griffin Wheel Company.

Two methods were proposed and used as the detailed residual stress analysis techniques to be used in the sectioning of

selected wheels.

12.2.1   First Method for Detailed Residual Stress Analysis

The first method involved separating the rim from the plate, removing a quarter section from the rim, slicing a quarter section of the rim into eleven quarter rings, and recording strains and displacements at each stage. After all the cuts were made, drillable strain gages were used on each of the rim sections to detect the presence of any unreleased stresses.

An axisymmetric finite element model of the wheel was constructed, taking care to reflect the manner in which the wheel was cut.   Since the data were obtained in the form of strains, it was decided to simulate mechanical strains with thermal strains.   This method was applied to the data generated from the sectioning of a new, Class U, curved plate wheel. The circumferential stresses obtained (Figure 12.1) show compression over most of the tread and on the front and back face of the rim, and tension inside and on the bottom of the rim plate fillets.

Results and Conclusions (First Method)

Strains generated by the model agreed reasonably well with the input values. Some discrepancies were found due to both the way in which the plate was modeled and also an unaccounted-for rotation of the rim when the rim plate cut was made. The
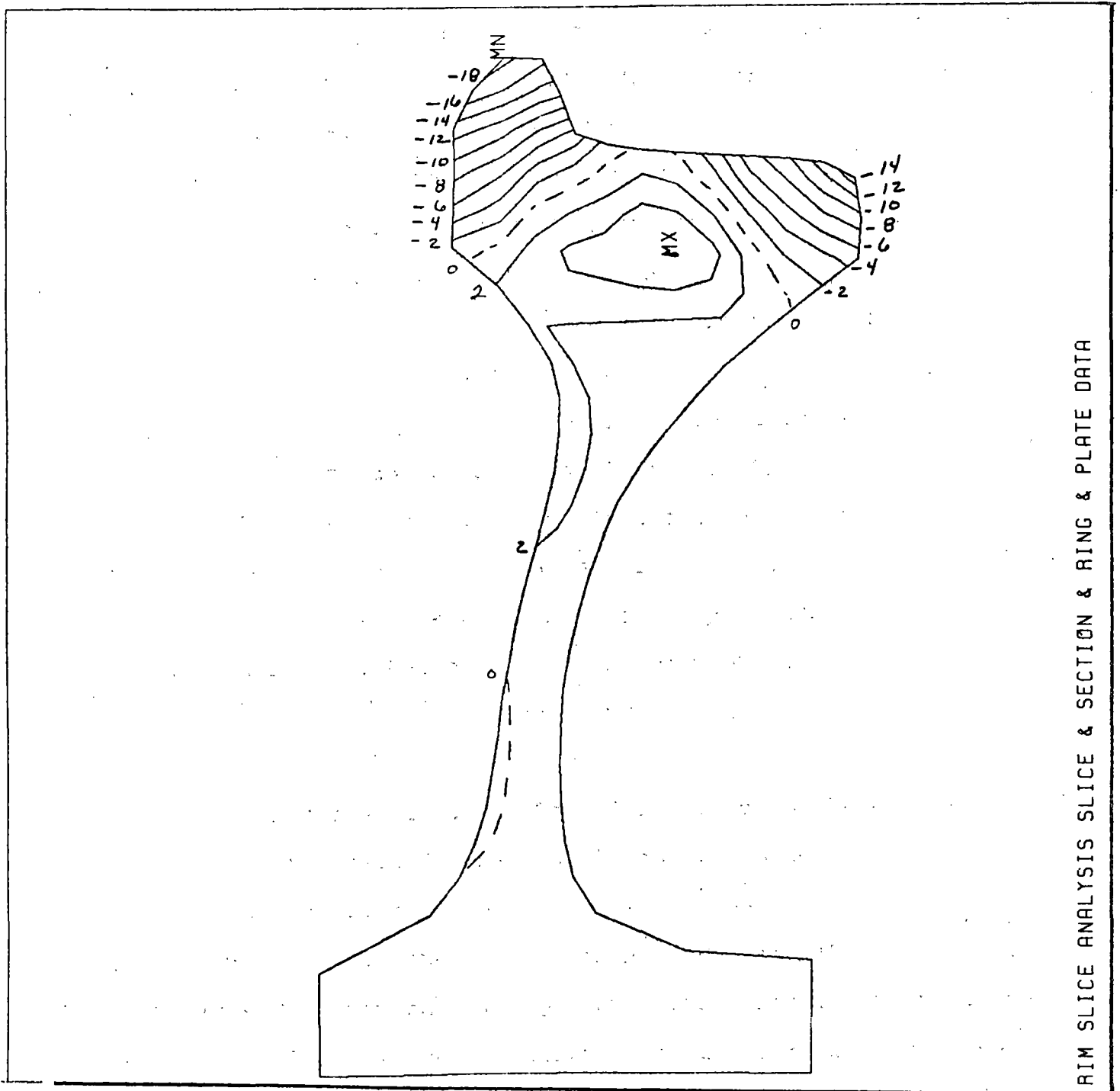
FIGURE 12.1   CIRCUMFERENTIAL RESIDUAL STRESS DISTRIBUTION IN NEW,
33 INCH DIAMETER, CLASS U, WHEEL BY FIRST METHOD

circumferential stresses obtained show compression over most of the tread and on the front and back faces of the rim, and tension inside and on the bottom of the rim plate fillets. Since this was a new Class U wheel, only the relatively small stresses (due to manufacturing) were found. The maximum tensile stress was 6 ksi and the maximum compressive stress was 18.5 ksi at the top of the flange. Both of these occurred in the circumferential direction.

The following conclusions are drawn from the above method of detailed residual stress analysis:

o   The manufacturer of this wheel seems to have introduced compressive residual stresses in the rim during manu- facturing. This matches with the pattern of stress contours found in our analysis at least qualitatively.

o   A major weak point from the standpoint of missing data is the rim plate interface.

12.2.2 Second Method for Detailed Residual Stress Analysis

At TTC, Pueblo, the detailed residual stress analysis of the second wheel (a new Class C, 33-inch, parabolic plate type, as received condition) was undertaken, based on the first method. After the initial strain-gaging of the wheel, the rim of the wheel was separated in a vertical boring mill and strain-gaging on the inside of the separated rim was completed.

At this experimental stage of the detailed residual stress analysis, an additional technique (second method) for detailed

residual stress analysis was presented at a FRA review meeting in September, 1986.

This technique is based on slicing the rim section (after it is parted from the plate) into five rings, preserving the axisymmetric until each ring is radially cut. It was decided that the alternate (multiple ring) method will be followed at TTC to analyze a new Class U wheel, and the results will be compared with the first method which was followed for a similar (new) Class U wheel. It was recommended that if the alternate method was successful, this technique would be used for the detailed residual stress analysis of a thermally abused Class U wheel (wheel #8, from RDU testing).

It was finally decided that the detailed residual analysis under Technical Task 11 would be confined to only Class U, 33-inch diameter curved plate wheels, as follows:

1) New Class U wheel (as-received condition) analyzed using the first method.

2) New Class U wheel (as received condition) analyzed using the alternative technique.

The alternative technique is described in detail, in the following section.

This method is a logical extension of the Sumitomo plate-cut method, where residual hoop stress in the rim is released in just two steps; first by cutting the plate out, and then saw-cutting the rim.

This method is improved by introducing a few slicing operations on the rim before it is radially cut. In this way,

12-7

the resulting residual hoop stress gradient across the rim
section is obtained.

Experimental Procedure

> o   The wheel plate is cut out and separated from the rim
>   to release part of the residual hoop and radial stress
>   in the rim (Figure 12.2).
>
> o   The rim is sliced to make five rings. This procedure
>   results in the release of additional hoop and radial
>   stress (Figure 12.3).
>
> o   All the rings are finally cut radially to release the
>   remaining hoop stress (Figure 12.4).

Analytical Procedure

Axial symmetry is preserved until the last radial cut.
After each cutting/slicing operation, stresses are released on
the cut surface. The stresses relieved in the body are in
equilibrium with the stresses released on the cut surface, and
are determined using finite element analysis. A fine mesh using
1361 nodes was designed for the finite element analysis of the
rim as shown in Figure 12.5. Dotted lines in the figure show
the locations for slicing operation.

The same mesh was used for finite element analysis of
individual slices (Figure 12.3). Two dimensional plane stress
finite element analysis was performed to determine stresses
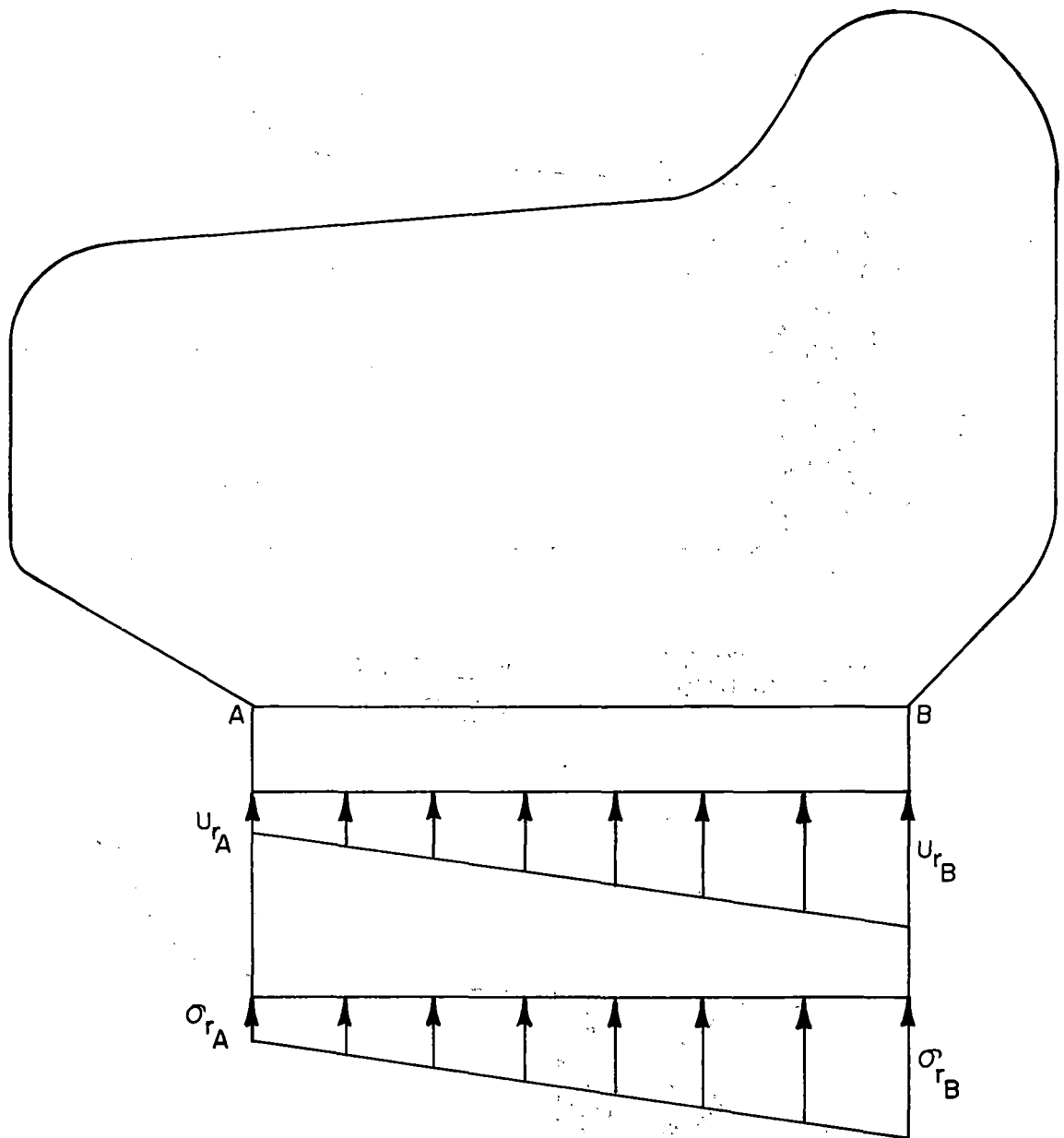
$$U_r = R \cdot \epsilon_\Theta$$

$$\sigma_r = \frac{E}{1-\nu^2} (\epsilon_r + \nu \epsilon_\Theta)$$

U_r = RADIAL DISPLACEMENT   R = RADIUS AT CUT

ϵ_Θ = CIRCUMFERENTIAL ϵ_r = RADIAL STRAIN
       STRAIN

σ_r = RADIAL STRESS

FIGURE 12.2   2-D AXISYMMETRIC ANALYSIS OF THE RIM

SHEAR STRESS
DISTRIBUTION

FIRST SLICE
TOP PORTION

SHEAR STRESS
DISTRIBUTION
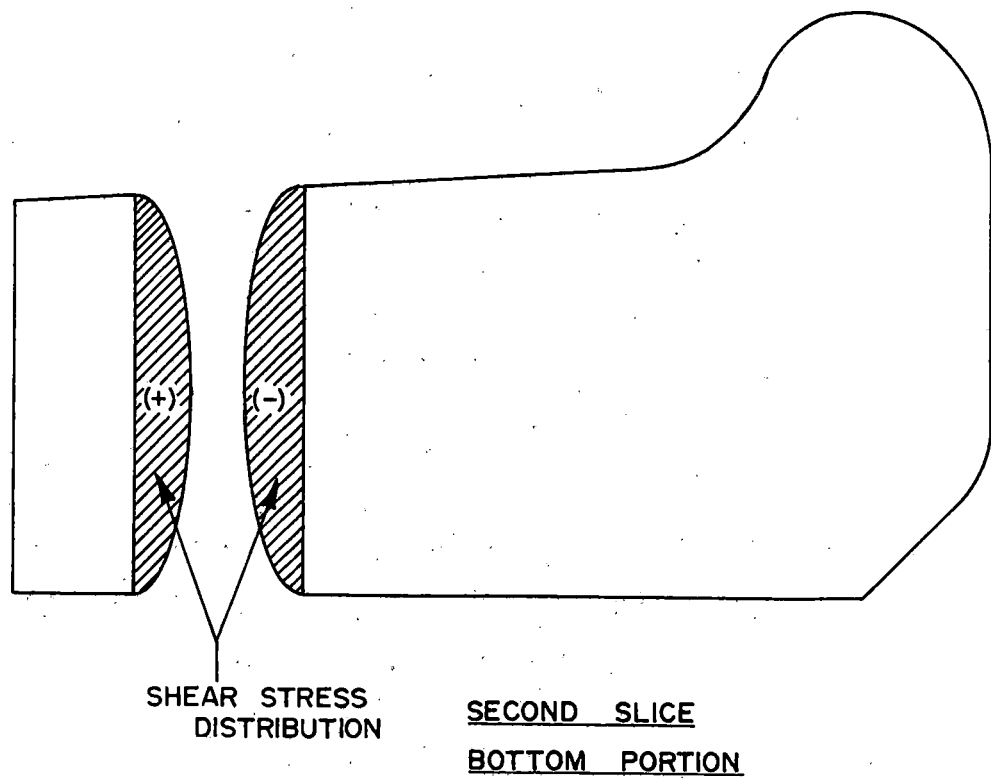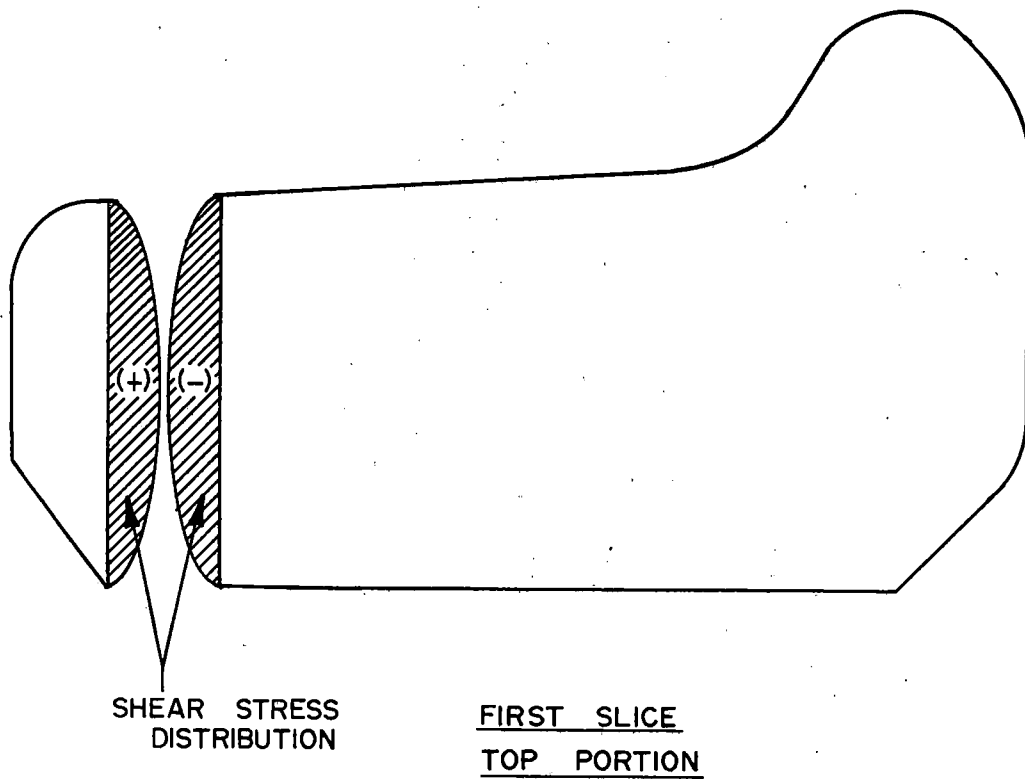
SECOND SLICE
BOTTOM PORTION

FIGURE 12.3   2-D AXISYMMETRIC ANALYSIS OF THE SLICES AND THE
REMAINDER OF THE RIM
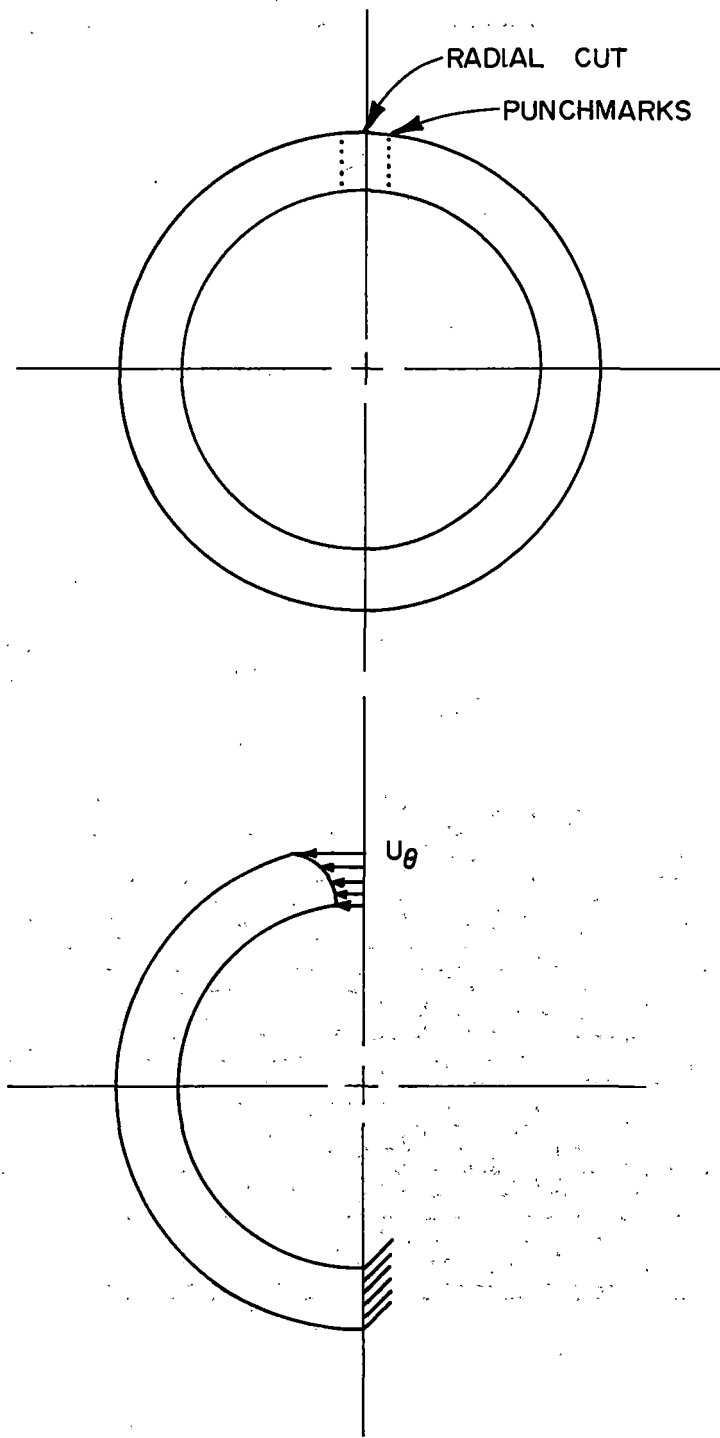
FIGURE 12.4   2-D FINITE ELEMENT ANALYSIS OF INDIVIDUAL
RINGS AFTER RADIAL CUT

SLICE 5

SLICE 1   SLICE 2   SLICE 3   SLICE 4
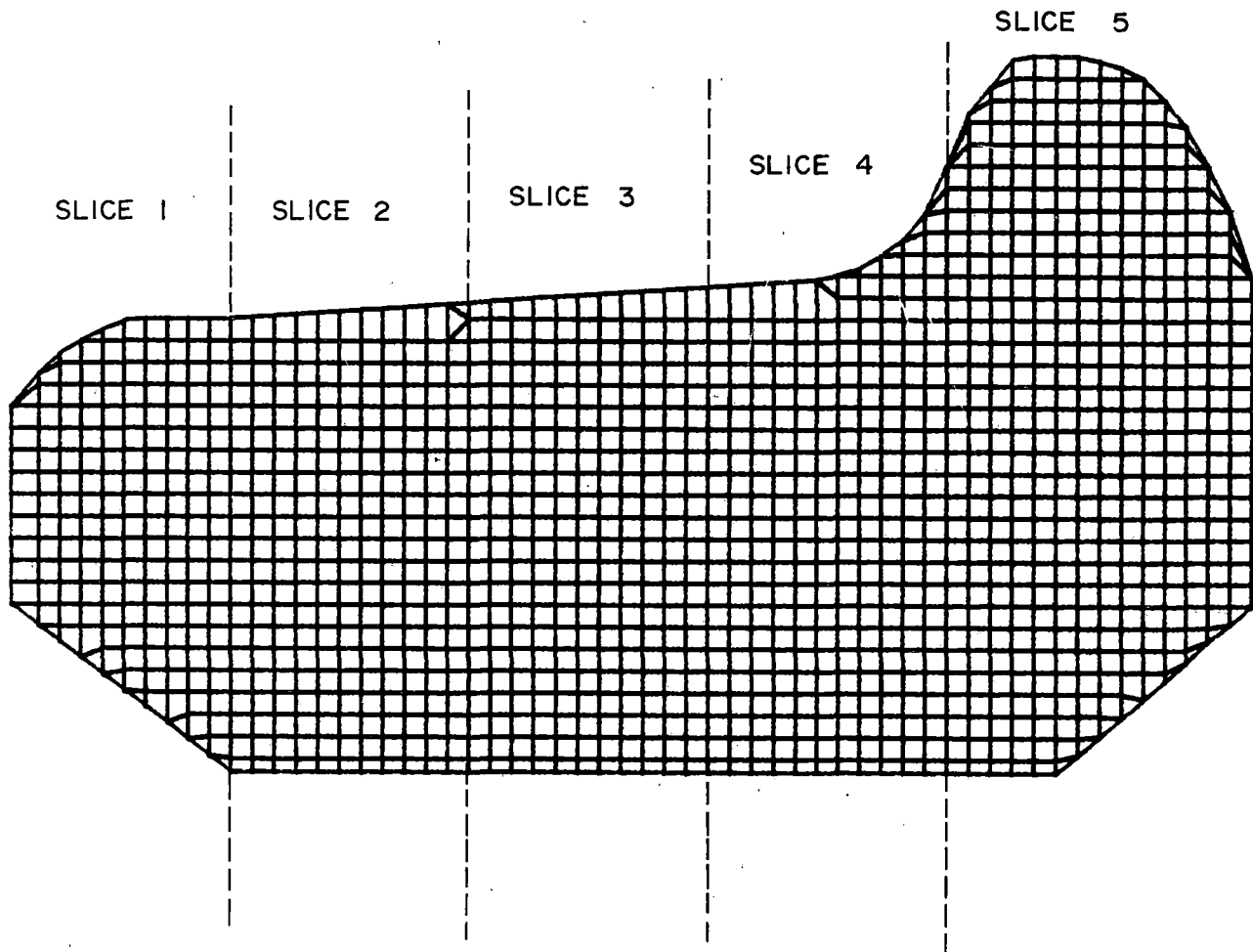
FIGURE 12.5   GENERATED MESH FOR FINITE ELEMENT ANALYSIS

released due to radial saw-cutting of the rings (Figure 12.4). The stresses released through all the operations are combined to arrive at the original residual stress distribution in the rim.

Results of Second Method

The results of the analysis showed a 20 ksi maximum compressive stress on the back face of the rim and 15 ksi maximum compressive stress on the front face of the rim. The corresponding residual hoop stress contours are shown in Figure 12.6.

It should be noted that there were some problems in the measurements during the slicing operation. Therefore, the shear stresses released during slicing of the rim were assumed to be negligible. However, the measurement procedure will be modified for the generation of data required for the finite element analysis of the slices (Figure 12.3). It is our opinion that the present assumption of shear stresses being negligible has a minimal effect on the final stress distribution shown in Figure 12.6.

Recommendations

o   The plate cut-out should be carried out further away from the rim so as to reduce the distance between the two strain gages on either side of the plate. This will minimize the errors due to interpolation.
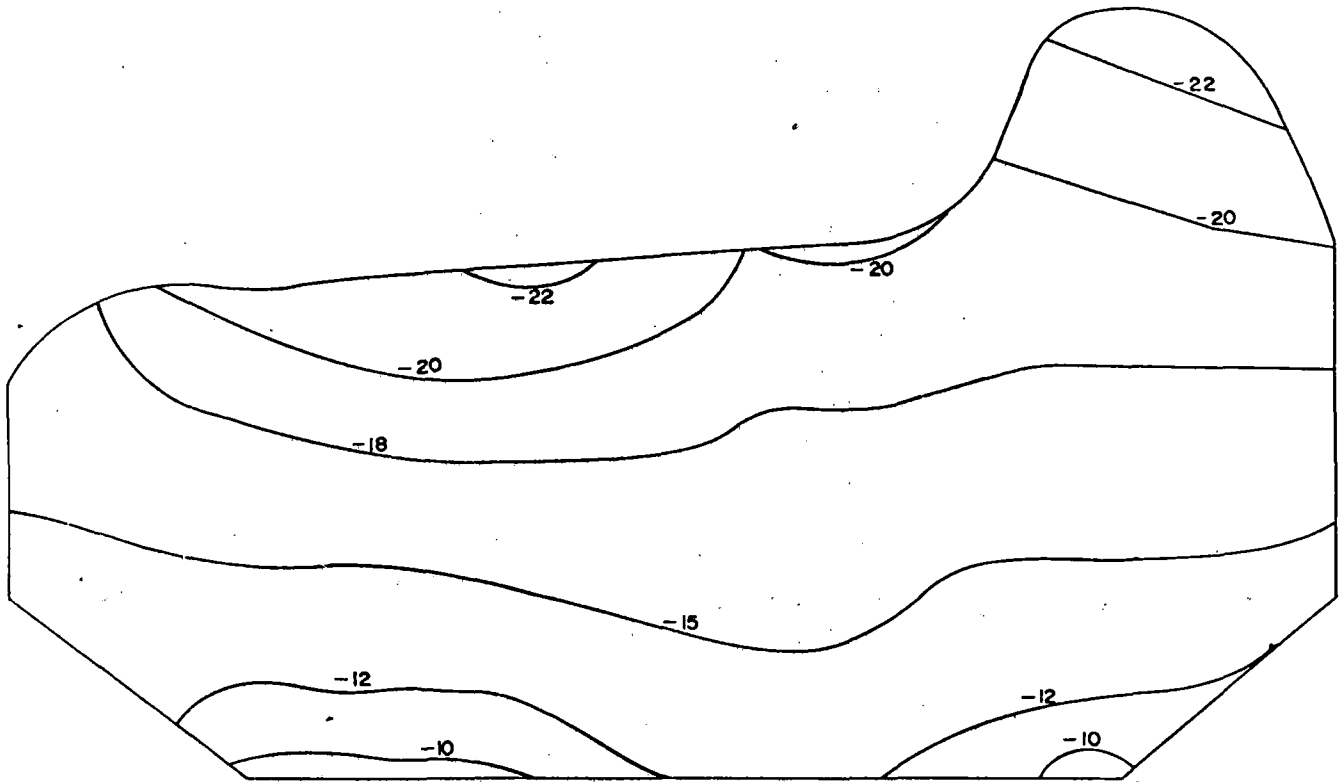
FIGURE 12.6   DISTRIBUTION OF CIRCUMFERENTIAL RESIDUAL STRESS
IN THE RIM OF A CLASS U, CJ-33 (NEW) WHEEL

o   The slicing operation should be slightly modified as shown in Figure 12.7.   Four slices are recommended instead of five.

o   The remainder of the plate should be circumferentially cut to determine residual radial stress distribution.

o   To validate the procedure, at least three more wheels should be analyzed beyond the scope of effort covered under the Wheel Failure Mechanisms Program.

o   Detailed residual stress analysis should be completed on wheel #8 from the RDU test.

General Recommendations

The exercise of the whole section emphasized the determination of stress distribution in the wheel. At this stage, it will be meaningful to initiate studies in the following areas.

o   Modeling of a crack in a stressed wheel.

o   Crack propagation criteria and fracture toughness.

1,2,3 ——► SUGGESTED SEQUENCE
OF SLICING OPERATIONS
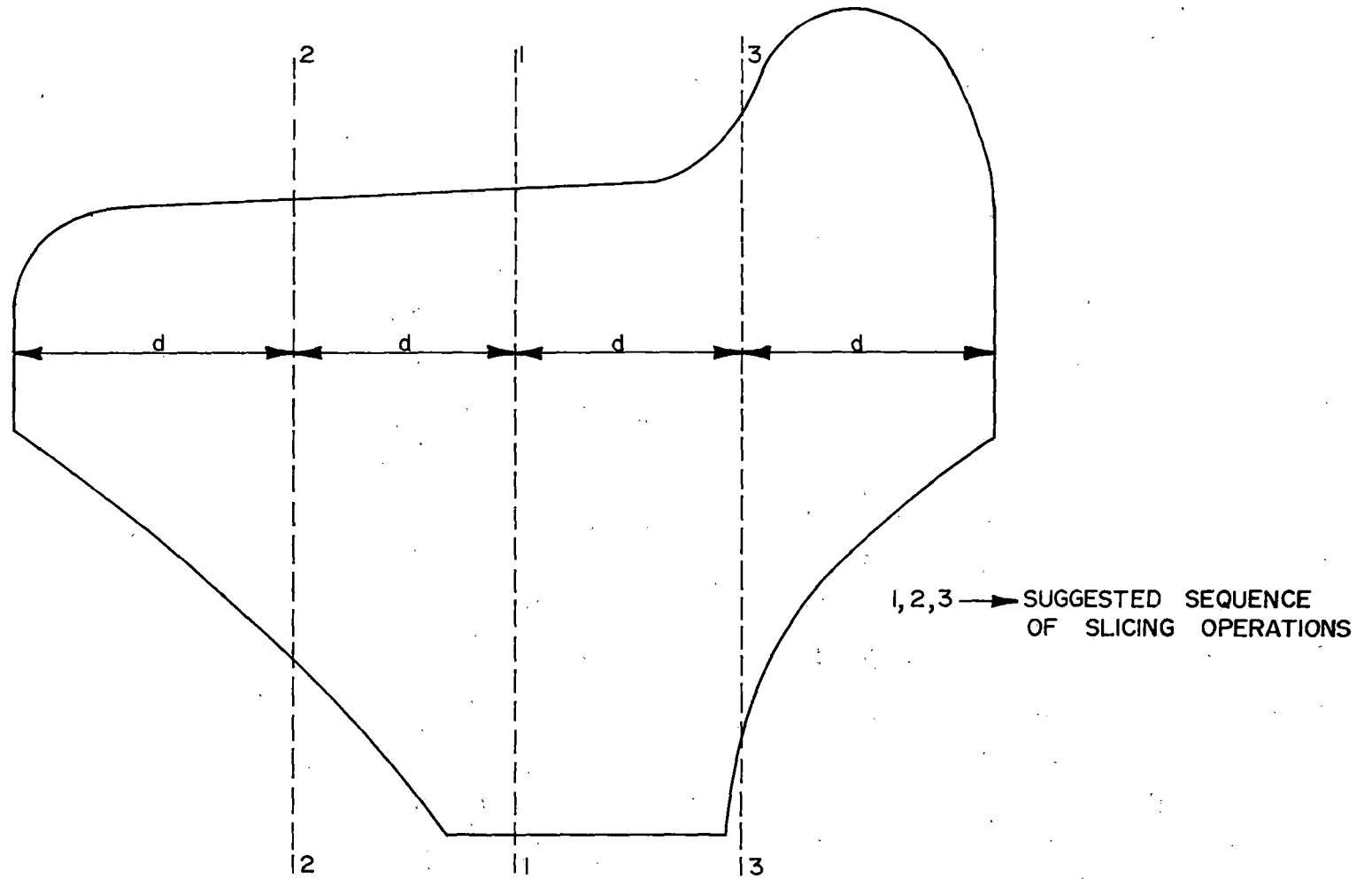
FIGURE 12.7   SUGGESTED SLICING PROCEDURE FOR FUTURE ANALYSIS

13.0 FURNISH SUITABLE BRAKE DYNAMOMETER (TECHNICAL TASK T12)
      MODIFY TTC ROLL DYNAMICS UNIT (TECHNICAL TASK T13)

13.1 Task Statement of Work

Under Technical Task T12 the AAR was required to furnish a
dynamometer at Chicago Technical Center capable of exerting
brake shoe loads and wheel-rail mechanical loads, and able to
sustain a wheel failure without damage. A brake dynamometer
facility with the above features was installed at the AAR
Chicago Technical Center and was made available for this
program, in support of Technical Tasks T4, T6, and T8.

Under Technical Task T13, AAR was required to modify the
Roll Dynamics Unit at the TTC, in support of Technical Task T4
(wheel/rail heat transfer and operating conditions leading to
development of residual stress in wheels).

13.2 Work Description (Technical Task T12)

An Adamson-United dynamometer was purchased from United
States Steel Corporation and installed at the AAR Technical
Center in Chicago. Operations began in October 1984. This
dynamometer, shown in Figure 13.1, is capable of testing rail-
road wheels measuring 28 to 42 inches in diameter at speeds up
to 1500 rpm with a 400 hp d.c. motor. Inertia loads of up to 68
million ft-lbs at top speed are available in increments through
the use of removable fly wheels. The brake system is capable of
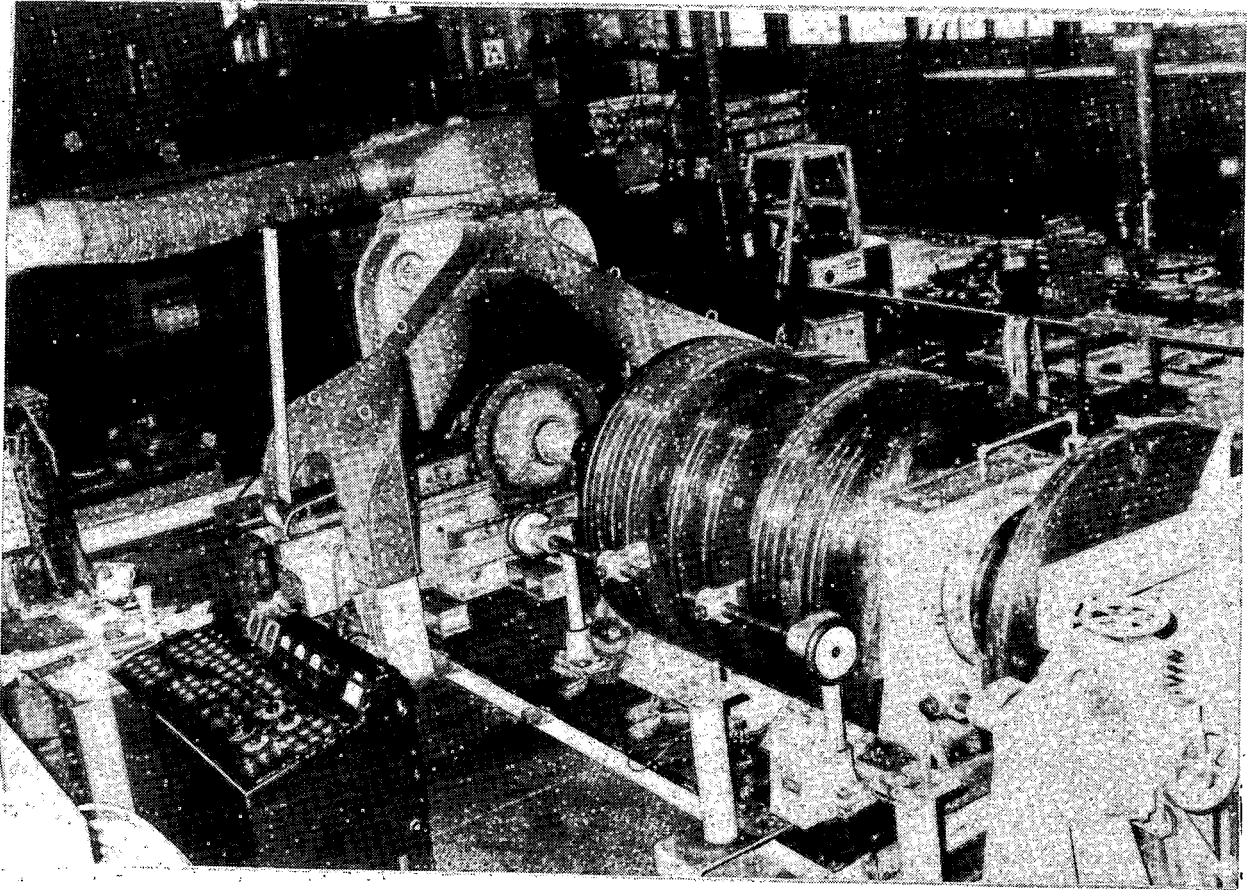
FIGURE 13.1 DYNAMOMETER AT AAR CHICAGO

exerting up to 45,000 pounds on each brake shoe in either a single or clasp arrangement. In addition, vertical loads of up to 70,000 pounds and lateral loads of up to 15,000 pounds can be applied to the tread of the wheel by reaction with the 110-inch diameter track wheel.

Three major test series were completed under Technical Tasks T4, T6, and T8 on the brake dynamometer. As many as fifty wheels were tested, and each wheel was subjected to a series of drag braking cycles in support of Tasks T4 and T6. Several thousand stop braking cycles were conducted on wheels which were tested for crack initiation and propagation in support of Task T8.

13.3 Work Description (Technical Task T13)

The Roll Dynamics Unit at the TTC was successfully modified to accommodate a fully instrumented test truck. A 3-piece truck with conventional brake rigging of a 70-ton capacity open hopper car was used as a test truck on RDU, in support of Technical Task T4. The test truck was supported on one pair of the Roller Module Units (RMU) of the Roll Dynamics Unit and the wheel loads were simulated by hydraulic vertical actuators through load fixtures (Figure 13.2). The complete brake rigging of the truck was retained along with the slack adjustor. The longitudinal restraint system for the truck was specially designed and placed in position with proper reaction support.
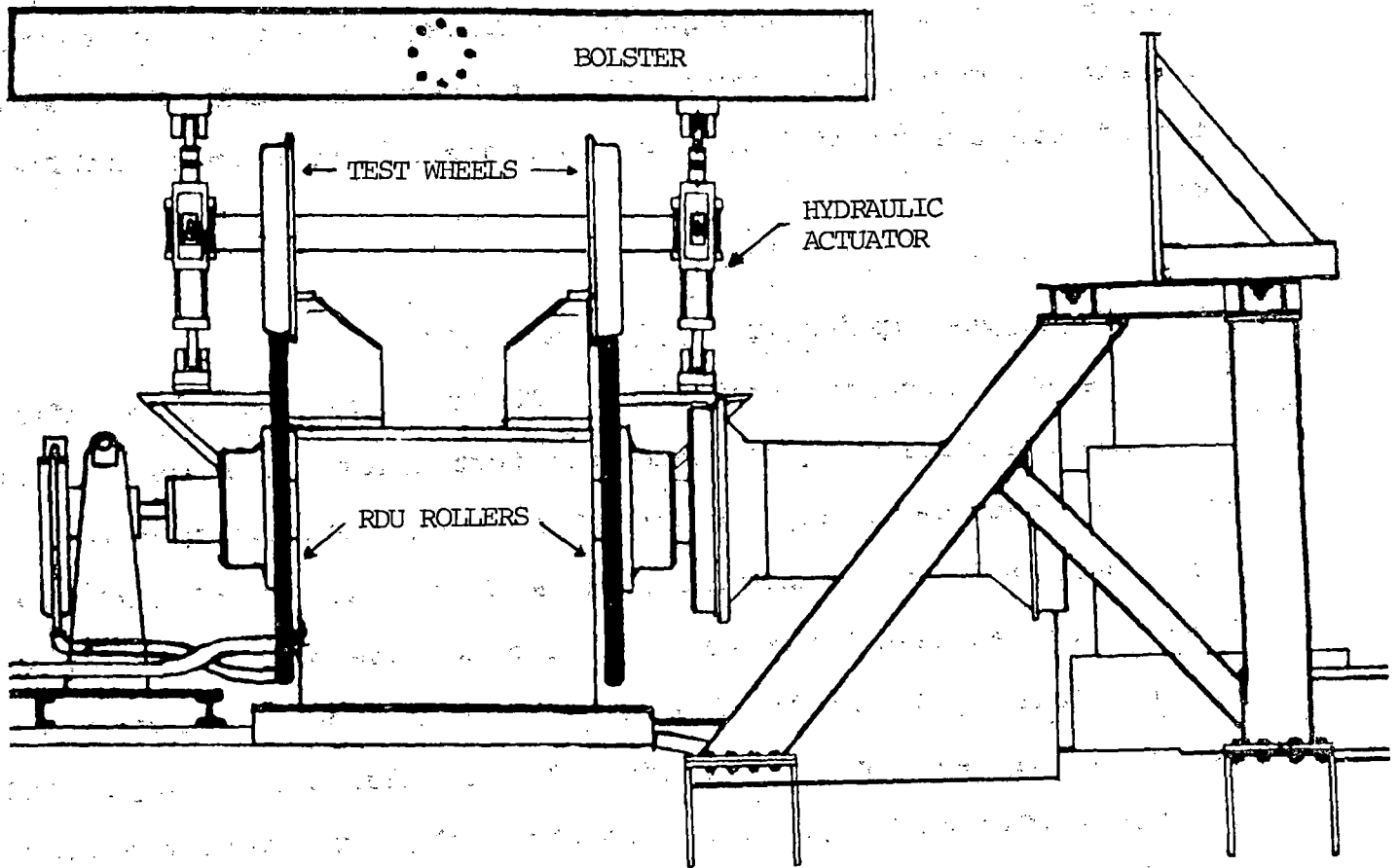
FIGURE 13.2   HOLD-DOWN DEVICE FOR RDU BRAKING TESTS

Each vertical actuator provided a force of 54,000 pounds and the hydraulic power unit and the related control hardware were designed and procured for operating the actuators.

For the simulation of a 70-ton loaded car, reconfiguration of the Roll Module Units (RMU) was performed so that each RMU provided approximately 40,000 pounds of rolling inertia. Each driving train consisted of one Lateral Actuator Thrust Assembly (LATSA), one gear box, one #2 flywheel, and one 600 hp motor, as shown in Figure 13.3.

All the tests in support of Technical Task T4 were performed successfully on RDU, under controlled test conditions. A total of eight Class U, 33-inch diameter (instrumented) wheels were subjected to a major series of drag and stop braking cycles. The wheel temperatures and strains were monitored through slip rings and the brake shoe force were also continuously measured. The operating conditions on RDU for residual stress change in the test wheel rims were subsequently employed during the extensive track testing that followed.
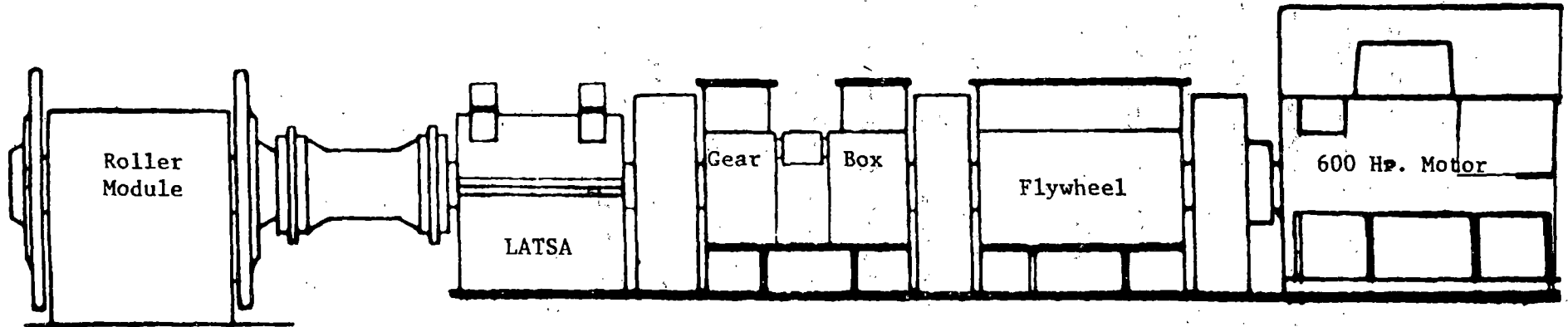
FIGURE 13.3   RMU DRIVE TRAIN RECONFIGURATION FOR RDU BRAKING TESTS

14.0 EVALUATE NDE TECHNIQUES - TECHNICAL TASK T14

The main objective of this technical task was to review and evaluate nondestructive testing techniques for isolating cracked or critically stressed wheels. Initially, an investigation of promising methodologies was to be made through discussions and marketing literature, followed by a critical review and selection of one of the crack detection or residual stress measurement prototypes for evaluation. Limited testing and evaluation of this one device would then be concluded in support of appropriate program tasks at TTC.

Review of State-of-the-Art NDE Techniques

The present state-of-the-art techniques for nondestructive inspection are unable to reliably determine either the presence of cracks or the level of residual stresses in wheels. A brief description of various NDE techniques for determining the level of residual stress and/or the presence of thermal cracks in wheels, is presented below:

14.1 Residual Stress Detection Methods

A. "X-ray Diffraction". The principle of the X-ray diffraction (XRD) technique lies in the fact that the angle at which the X-ray beam is diffracted from the atomic planes of a crystal is indicative of the spacing

14-1

of those planes. When a material is placed under stress, the plane spacing increases (tension) or decreases (compression) and the distance between the atomic planes in the metal changes. From the wave length of X-ray radiation and the angle between the incident and diffracted X-ray beam, the interplanar spacing of the atomic planes reflecting the beam can be measured. Stresses are determined by measuring the strain in the atomic lattice and by relating the strains to stresses through the elastic theory. X-ray diffraction has the following limitation. (1) It is only able to measure surface stresses (~0.001 inch) and is restricted to a small surface area upon which the beam is focused. X-rays may not be able to penetrate surface rust or mill-scale which may require surface preparation; (2) the XRD process is affected by texture and cold work, and, therefore, accurate readings cannot be made on wheel treads that have been cold worked; (3) the technique requires time to analyze sufficient data for a stress determination, typically a few minutes.

B. "Barkhausen Methods". The phenomenon that is the basis of this technique is the abrupt, discontinuous movement of microscopic magnetic domain boundaries that often occurs in ferromagnetic materials under the influence of an external magnetic field.

If a piece of ferromagnetic steel is magnetized, it will elongate in the direction of an applied magnetic field, and conversely, if the same piece is stretched by an applied load, it will be magnetized in the direction of the load. The same occurs with compression, except that the resulting magnetization now occurs at 90 degrees to the direction of compressive load.

To conveniently employ the magnetoelastic interaction for stress investigation, another physical phenomenon is needed. This is the Barkhausen effect, the series of abrupt changes of jumps in the magnetization of a steel when the magnetizing field is gradually altered. Combining these two phenomena leads to a qualitative stress indication so that an increasing tensile stress is accompanied by a growing "Barkhausen noise" level generated by jumps, and an increasing compressive stress by a diminishing noise level. More accurate quantitative data can be obtained through the use of calibration procedures with known loads.

The excitation field is developed by a variable field electromagnet in contact with the specimen. An induction coil between the magnet poles senses changes in specimen magnetization and translates this into an output voltage that is displayed on an oscilloscope. Cycling the external field polarity results in the output amplitude achieving a maxima that is indicative of the material stress state. To develop quantitative stress values from such information, it is necessary to construct a calibration curve of stress

versus Barkhausen noise intensity for the material of interest. Figure 14.1 shows a curve of this type for three different steels.

The Southwest Research Institute study in 1974 established that the Barkhausen phenomenon generated in railroad wheels is sufficiently stress sensitive to be used as a stress indicator. However, there were significant variations and some inconsistencies in the data from wheel to wheel and at similar locations on the same wheel.

An important factor contributing to data variability in the Barkhausen technique is the small volume of material from which the stress indication is obtained. The near surface nature of the Barkhausen effect, when combined with a coil pickup covering an area of only 0.01 square inches, causes the technique to be more sensitive to short range stress gradients and shallow surface conditions than a conventional stress relaxation measurement using strain gages. Despite such characteristics, reasonable qualitative agreement was established for the Barkhausen method.

As a step toward utilizing the Barkhausen noise technique to classify wheels according to the severity of overheating, the SWRI study tentatively identified the area on the back rim surface nearest the tread as that most likely to yield consistent linear results.

An evaluation of 80 wheels by SWRI for an AAR member road found some 16 percent to have high residual stresses using an improved SWRI detector. These data were compared

Steel	Magnetizing	Yield Stress ksi
1	20	36
2	30	58
3	99	103
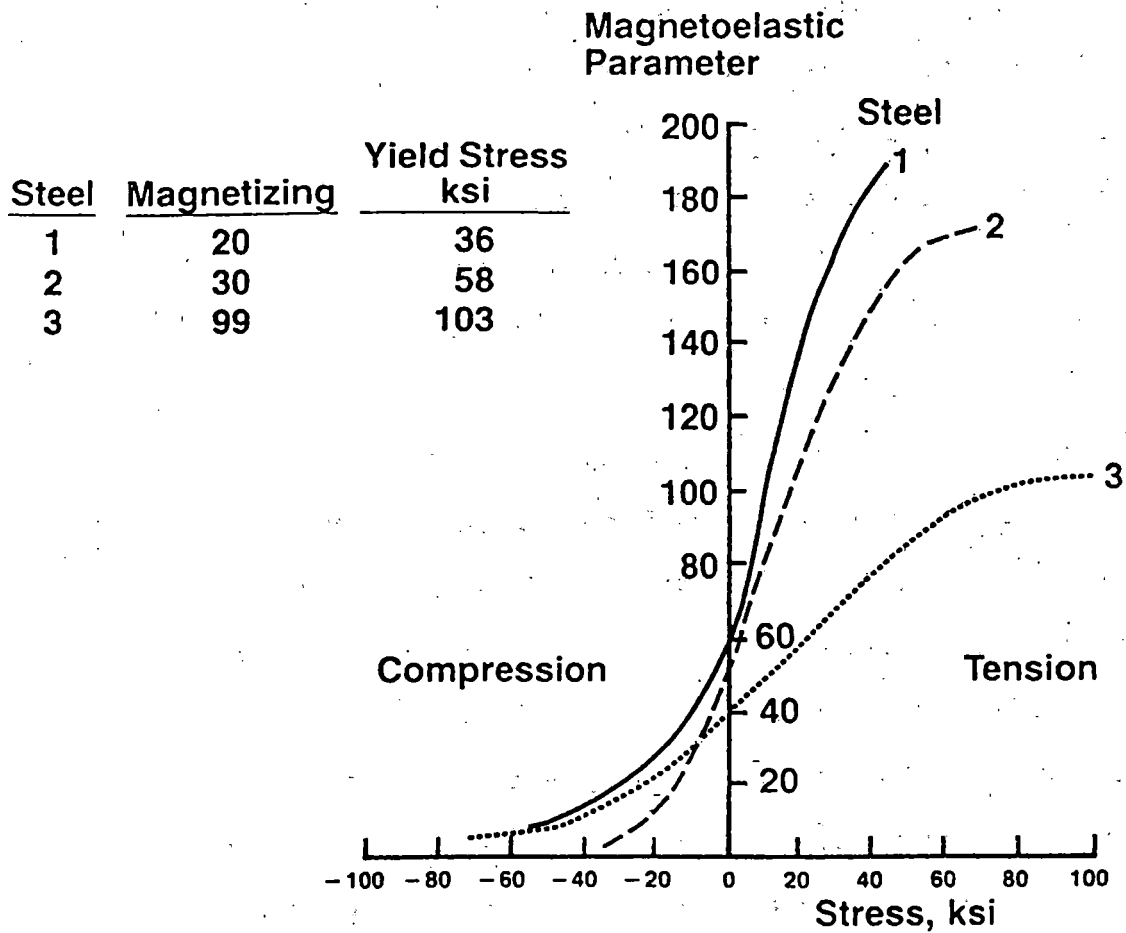
FIGURE 14.1   CALIBRATION OF CURVES FOR THREE DIFFERENT STEELS WITH
INCREASING YIELD STRENGTH FROM 36 KSI TO 103 KSI

to results by an independent saw-cutting program. An evaluation of this technique is given in Table 14.5.

C. "Ultrasonic Bi-Refringence". The principle behind this technique is that the state of stress in a metal influences the propagation velocity of ultrasound. Therefore, the precise measurement of transit times through a known thickness of stressed material can give an indication of the average stress level. The key to obtaining reliable results is the accurate assessment and mitigation of the material variables. Chemistry, preferred orientation, and microstructure affect the sound velocity and must be mitigated through adequate calibration.

This technique has been applied to railroad wheels. The basic procedure was to measure the transit time differential of simultaneously generated 2 MHz pulses through an unstressed reference block and the stressed specimen. This was accomplished using a dual trace oscilloscope to display the two signals and by expanding the time base until individual pulse cycles could be seen. Since a difference in transit time appears as a phase shift in the two signals, the delay - time multiplier on the oscilloscope could be used to determine the differential by making the pulses coincident.

The actual determination of stress in steel is complicated by its anisotropic nature with respect to sound propagation. Under compression, shear waves polarized

parallel to the principal stress axis will travel faster than waves polarized perpendicular to it. The difference between the transit time differentials of the two wave orientations is, thus, a better measure of the average stress than either orientation alone. As applied to the evaluation of wheel rims, the parallel and perpendicular orientations correspond to the circumferential and radial directions, respectively.

The first step in utilizing this technique is the establishment of an acoustic stress constant for wheel material that relates ultrasonic velocity changes to applied stress. This is accomplished by incrementally loading a block of rim steel to simulate the circumferential compressive stresses found in wheels and measuring the transit time differential of pulses traveling in this block and an identical reference block. At each load level, measurements are taken with wave polarization both parallel and perpendicular to the principal stress axis. The difference in transit time differentials of these two polarizations is used, in conjunction with the path length and the value of each load level change, to establish an acoustic stress constant for a typical wheel material.

Once the acoustic stress constant is determined, the average stress across a wheel rim can be calculated by measuring the difference in the radial and circumferential transit time differentials and by knowing the sound path length. In a similar manner, stress changes can be detected

by making measurements before and after the event of interest. It has been demonstrated that accurate measurement of ultrasonic velocity in stressed wheels can be used to evaluate that stress condition. However, the material variability found in wheels of different classes and manufacture would require the use of some independent technique to establish material characteristics prior to any stress measurements. The technique also required an accurate value for the ultrasonic path length, which may necessitate the actual measurement of the rim width of each wheel tested.

D. "Magnetomechanical Acoustic Emission". The Magneto-mechanical Acoustic Emission (MMAE) method is a mechanical counterpart to the magnetic Barkhausen effect. When the level of applied magnetic field is varied, the shift in magnetic domain structures produces ultrasonic waves, which are detected as Acoustic Emission (AE) signals. The MMAE phenomenon's potential as a new nondestructive method for stress measurement was earlier tested with measurements of rail and wheel steels to assess the feasibility of developing a useful instrument for field use. However, tests on this technique on wheels have been inconclusive because it was difficult to distinguish tensile from compressive stresses.

E. "Magnetic/Ultrasonic Technique". Residual stress character-
ization by a magnetic/ultrasonic technique which is
currently being developed at Langley Research Center, holds
promise for a practical nondestructive method adaptable for
rail car wheels. However, this technique is applicable
under laboratory conditions and needs to be adapted for
railroad wheel inspection.

In this method, the state of internal stress in steel
is measured by the material magnetic domain interaction with
both the stress field and the ultrasonic wave propagation.
All the tests to date indicate that this technique is
capable of separating tensile from compressive stress in
steel.

The unique feature of this technique is the measurement
of small changes in ultrasonic wave velocity by the
application of external D.C. magnetic field in the material
under various stress conditions. The fractional change in
the natural velocity ($\Delta V/V$) of a wave propagating along the
external field direction is affected by the uniaxial stress
applied in the same axis. The simultaneous measurements of
magnetic induction confirmed that the stress effect on the
natural velocity curve is dominant in the domain wall motion
region. The slope of $\Delta V/V$ is negative under compression and
positive under tension for steel specimens with different
carbon contents. Results of measurements with residual
stress show exactly the same tendency. Recent measurements
on permanently bent specimens with different radii of

14-9

curvature confirmed the possibility of quantitative stress measurements.

14.2 Crack Detection Methods

Wheel inspection for cracks begins in the manufacturer's shop with procedures defined in Association of American Railroads Specifications M107 and M208 for wrought and cast wheels, respectively. Both outline the same requirements for ultrasonic inspection of rims for inclusions and voids and wet magnetic particle inspection of plate surfaces for discontinuities. Adherence to these specifications effectively sets a minimum quality limit for all new wheels entering service.

The techniques and frequency of in-service inspection are not specified in the Association of American Railroads rules, but are determined by the experience of each performing railroad. All railroads rely principally on visual inspection, with a modest use of magnetic particle or penetrant methods by some. The frequency of inspection is flexible at best, depending heavily on the operating schedule of the vehicle and the repair needs of other components. This lack of explicit inspection intervals, which is inherent in the mobile nature of railroading, places an increased burden on the inspection that does take place to find defects in their earliest stages.

Experience has shown that the vast majority of defective wheels are detected visually before an accident can occur. Despite this basic effectiveness, visual inspection is

characterized by several factors that tend to limit its sensitivity and reliability. Primary among these is its inherent subjectivity. Any system that relies solely on people for critical decisions is subject to the inconsistencies generated by differences in individual motivation, skills, knowledge, and health. Reliable wheel inspection depends heavily on such variables as inspector job satisfaction and visual acuity. The physical condition of the inspection wheel can also influence the ability of visual examination to detect small defects. The presence of oil and dirt on plate surfaces will hide all but the largest plate cracks. Similarly, hot and cold working of the tread can obscure thermal cracks with flowed metal.

A. "Ultrasonics". The science of ultrasonics is being applied to the problem of wheel evaluation in many forms. The search unit of one system fits into a special section of rail that is designed to guide the outer tread of passing wheels over a fluid filled transducer boot. Inside the boot are two oppositely directed transducers set in a gimbaled support that allows them to maintain a constant entry angle to the wheel tread. On contact with a wheel, couplant is sprayed on the boot and an ultrasound pulse is directed circumferentially around the tread as a surface wave by one of the transducers. Initial and multiple order reflections are subsequently received by this transducer from any crack that has developed on the rim faces, tread, or flange. It

is claimed that reliable detection of cracks 0.5 inch long and 0.050 inch deep can be achieved.

After full attenuation of the initial signal has occurred, in about five milliseconds, a second pulse is directed around the wheel in the opposite direction by the second transducer. This dual pulse-echo technique enhances the chances of detecting cracks that are inclined to the surface since they are anisotropic in their ability to reflect sound. The use of dual transducers also allows the analysis of the through-transmitted signal for additional information on the wheels' condition. The attenuation rate of this signal is indicative of the general wheel surface condition and is believed related to the near surface stress level. The time interval between multiple receptions of the through transmitted pulse is used to classify wheels by diameters, and details of the pulse shape can reveal a high flange condition.

A major problem with this system has been its inability to distinguish between benign surface shelling cracks and thermal cracks. It has been suggested that a system employing swept ultrasonic frequencies or dual frequencies may be able to make a distinction between minute shells and true thermal cracks. The swept frequency ultrasonics holds promise for a viable crack detection system and is described separately in this section.

B. "Acoustic Signature Analysis". One of the earliest methods of nondestructively evaluating railroad wheels was to have car inspectors strike them with a hammer and listen to the resulting sound. In this way it was possible to detect many defective wheels because they ring different from good wheels. A more sophisticated version of this technique, known as acoustic signature analysis, is a possible basis for an automatic, in motion, wheel inspection system.

In the acoustic signature method, a wheel is excited by either natural or artificial means into vibrating, and the radiant sound is analyzed for its characteristic spectral content or signature. The introduction of discontinuities, such as cracks, into the wheel will affect the modes of vibration and, consequently, the signature. Early results have shown that impact excitation is the most suitable means of generating sound of sufficient intensity and spectral content in the frequency range (1-5 KH) found to be most sensitive to wheel cracks. In addition, this form of excitation allows the use of damping rate measurements as a supplemental indicator of wheel condition. It has also been established that the best detection system is one using a trackside microphone, near the impactor, to pick up acoustic radiation.

Recent field trails of an acoustic signature system in a joint SP-AAR program have established doubts that this type of system will be able to reliably detect critical size (3/4 inch) thermal cracks.

c.   "Sweep Frequency Ultrasonics (Thermal Crack Detection)".
The reliable, nondestructive detection of railroad wheel
cracks remains an elusive task.   Ultrasonic technology has
been applied by several investigators, and a commercial unit
was produced.   However, difficulties in the separation of
benign surface checking and actual thermal cracks has
prevented a single frequency system from finding wide
application.

The use of sweep frequency ultrasonics in a difference
mode may provide the key to practical, reliable, and
accurate crack detection in rail car wheels.   The frequency
output/input allows for very powerful articulation of signal
properties in conjunction with computer storage of output
that will allow, for example, signal A (wheel/transducer
position 1) to be subtracted from signal B (wheel/transducer
position 2).   This subtraction or difference approach will
readily show the signal difference between A and B.   This
difference can be physically related to a crack that has in
fact changed location through rotation of the wheel with
respect to the fixed input/output transducer positions.

14.3 Screening Criteria

The screening criteria for selecting NDE techniques to
detect cracked or critically stressed wheels are interpreted to
be minimum performance requirements for the three categories of
detection systems that are proposed for use in screening the

14-14

most promising candidate prototypes for subsequent testing and evaluation.

Possible Locations for NDE System Use

The screening criteria to be used in selecting the most promising candidate NDE systems depend on the intended use or area (location) of application of the system. While it is most desirable to have a reliable system for railroad wayside deployment, there are still safety benefits associated with a system capable of use on wheels at repair tracks or even in wheel shops. Therefore, criteria appropriate to all three use scenarios are discussed.

Performance Categories

In each of the three NDE measurement system categories (stress and cracks) there are several performance regions or areas of concern. These are:

1. Accuracy of measurement or detection uncertainty range ± measurement units).

2. Reliability of detection of critical conditions (probability).

3. False alarm rate.

4. Maintainability.

5. Environmental compatibility.

Performance Levels

In addition, within each performance region several levels of performance will be identified. These levels are:

1. Good (possesses necessary capabilities).

2. Sufficient (possesses minimum capabilities).

3. Not Sufficient (marginally useful).

Screening Criteria for Stress and Cracks

The screening criteria, in terms of the above categories, are presented in tabular form in: Table 14.1, for wayside use, for repair track use, and for wheel shop use.

Screening Criteria Evaluation

The following five NDE techniques have been evaluated using the screening criteria developed in Table 14.1.

1. Magnetic Ultrasonic Technique (Residual Stress Detection - NASA Langley)

2. Ultrasonic Bi-Refringence Technique (Residual Stress Detection - NBS, Boulder)

3. Sweep Frequency Ultrasonic Technique (Thermal Crack Detection - JPL)

4. Barkhausen (Residual Stress Measurement)

5. X-ray Diffraction (Residual Stress Measurement)

TABLE 14.1

SCREENING CRITERIA
FOR
RAILROAD WAYSIDE NDE SYSTEMS,
REPAIR TRACKS NDE SYSTEMS,
& WHEEL SHOP NDE SYSTEMS

Category	Performance Level	NDE System Stress	Cracks
Accuracy	Good Sufficient Not Sufficient		
Reliability	Good Sufficient Not Sufficient		
False Alarm Rate	Minimal High Excessive		
Maintainability	Good Sufficient Not Sufficient		
Survivability	Good Sufficient Not Sufficient		
Cost	Excessive Reasonable		

The applicability of the above systems was evaluated with reference to railroad wheels, and the following NDE techniques have been selected for further development and usage under appropriate conditions.

Selected Techniques (not funded by AAR or FRA)

1. "Thermal Crack Detection" - Sweep Frequency Ultrasonic Technique - JPL. The screening criteria evaluation for this technique is presented in Table 14.2.

2. "Residual Stress Detection" - The screening criteria evaluation for Magnetic Ultrasonic Technique, Ultrasonic Bi-Refringence Technique, Barkhausen Method, and X-ray Diffraction Method are presented in Tables 14.3, 14.4, 14.5, and 14.6, respectively.

Two Specific residual stress measurement techniques were pursued by AAR under the Wheel Failure Mechanisms Program. The efforts to accomplish the applicability of these two techniques to railroad wheels are explained in the following section.

14.4 Magnetic/Ultrasonic Technique for Residual Stress
      Measurement

Magnetic/ultrasonic technique for residual stress measurement at NASA, Langley, is the most promising method due to its bulk stress measurement capability combined with the absence of elaborate calibration requirements. A close contact

TABLE 14.2

SCREENING CRITERIA EVALUATION

SCREENING CRITERIA FOR REPAIR TRACK NDE SYSTEMS

TYPE OF SYSTEM: SWEEP FREQUENCY ULTRASONIC (THERMAL CRACK
DETECTION BEING DEVELOPED BY JPL)

| Performance | | NDE System | |
Category	Level	Stress	Cracks
Accuracy	Good Sufficient Not Sufficient	N/A	Good
Reliability	Good Sufficient	N/A	Sufficient
False Alarm Rate	Minimal High Excessive	N/A	Minimal
Maintainability	Good Sufficient Not Sufficient	N/A	Good
Survivability	Good Sufficient Not Sufficient		Sufficient
Cost	Excessive Reasonable	N/A	Reasonable

TABLE 14.3
SCREENING CRITERIA EVALUATION

SCREENING CRITERIA FOR REPAIR TRACK NDE SYSTEMS
WITH POSSIBILITY OF ROLL-BY INSPECTION

TYPE OF SYSTEM: MAGNETIC/ULTRASONIC TECHNIQUE (BEING DEVELOPED AT NASA LANGLEY
RESEARCH CENTER)

| Performance | | NDE System | |
Category	Level	Stress	Cracks
Accuracy	Good Sufficient Not Sufficient	Good	N/A
Reliability	Good Sufficient Not Sufficient	Good (Time=30 sec)	N/A
False Alarm Rate	Minimal High Excessive	Minimal	N/A
Maintainability	Good Sufficient Not Sufficient	Sufficient	N/A
Survivability	Good Sufficient Not Sufficient	Sufficient	N/A
Cost	Excessive Reasonable	Reasonable	N/A

TABLE 14.4

SCREENING CRITERIA EVALUATION

SCREENING CRITERIA FOR WHEEL SHOP NDE SYSTEMS

TYPE OF SYSTEM: ULTRASONIC BI-REFRINGENCE TECHNIQUE (FOR RESIDUAL STRESS MEASUREMENT BEING DEVELOPED BY NBS, BOULDER)

Performance Category	Level	NDE System Stress	Cracks
Accuracy	Good Sufficient Not Sufficient	Good	N/A
Reliability	Good Sufficient Not Sufficient	Sufficient	N/A
False Alarm Rate	Minimal High Excessive	Minimal	N/A
Maintainability	Good Sufficient Not Sufficient	Good	N/A
Survivability	Good Sufficient Not Sufficient	Sufficient	N/A
Cost	Excessive Reasonable	Reasonable	N/A

TABLE 14.5
SCREENING CRITERIA EVALUATION

SCREENING CRITERIA FOR REPAIR TRACK NDE SYSTEMS

TYPE OF SYSTEM: BARKHAUSEN (RESIDUAL STRESS MEASUREMENT)

Performance Category	Level	NDE System Stress	Cracks
Accuracy	Good Sufficient Not Sufficient	Sufficient	N/A
Reliability	Good Sufficient Not Sufficient	(being tested by saw-cutting comparison)	N/A
False Alarm Rate	Minimal High Excessive	Not applicable	N/A
Maintainability	Good Sufficient Not Sufficient	Not known (being evaluated by BN & UP)	N/A
Survivability	Good Sufficient Not Sufficient	Not Sufficient (not good enough for field application)	N/A
Cost	Excessive Reasonable	Unacceptably high. Requires prescreening of wheels, which will miss a large population of wheels with high stresses	N/A

TABLE 14.6
SCREENING CRITERIA EVALUATION

SCREENING CRITERIA FOR REPAIR TRACK NDE SYSTEMS

TYPE OF SYSTEM: X-RAY DIFFRACTION (SURFACE RESIDUAL STRESS MEASUREMENT)

Performance Category	Level	NDE System Stress	Cracks
Accuracy	Good Sufficient Not Sufficient	Good (excellent for surface)	N/A
Reliability	Good Sufficient Not Sufficient	Acceptable	N/A
False Alarm Rate	Minimal High Excessive	Minimal	N/A
Maintainability	Good Sufficient Not Sufficient	Unacceptable	N/A
Survivability	Good Sufficient Not Sufficient	Unacceptable	N/A
Cost	Excessive Reasonable	Acceptable equipment, Unacceptable labor	N/A

is maintained between NASA at Langley AFB and the AAR in the development of a stress measurement prototype. An in-house representative of the AAR was maintained at NASA for a period of 1 year to assist in the improvement of the technique as well as in the construction of a measurement device applicable to railroad wheels.

This joint effort involving AAR, FRA, and NASA has resulted in the assembly of a test system which employs the magneto-acoustic technique to nondestructively determine the residual stress state in railroad wheels.

After successful completion of this lab-oriented phase of the project, two large electromagnet assemblies were built and tested to be both maneuverable and powerful enough to supply a strong magnetic field in wheel rims, and the entire technique was successfully performed using two different computer systems. This latter point is important in that the equipment can conceivably be freed to perform an extension of the lab tests desired, while allowing for simultaneous modifications and manipulations on the upgrade computer system.

The NDE effort covered under the Wheel Failure Mechanisms Program was limited to development of a prototype device that has been made available through FRA in collaboration with NASA Langley. It is capable of making stress measurements in the rim of a full scale railroad wheel.

Proposed Initial Test Matrix to 'Prove' the Capabilities of the Test System

The first task will be to define the optimum test procedure whereby meaningful data can be obtained from wheel samples which would offer a correlation to destructive measurements.

The variables which will be manipulated in the initial tests will include ultrasonic transducer selection, wave mode and propagation direction, magnetic field orientation, and specifics of the magnetization/demagnetization processes.

Appropriate test samples will be wheels which have been subjected to experimentation on the RDU facility at AAR-Pueblo. Complete documentation will include rim area measurements, destructive cutting, and microstructural examination.

It is anticipated that this initial test period will include a demonstration of the test procedure to FRA representatives and interested railroad officials.

Extended Research Efforts - Magnetic Ultrasonic Technique

Following the initial efforts to "prove" the capabilities of the test system, that is, to achieve a documented correlation with destructive testing as a means of determining the stress state in wheels, extensive data collection would then be appropriate. Numerous wheels would be evaluated at AAR-Pueblo to determine, essentially, the range of scatter possible during the examination of large numbers of sample wheels; the

confidence limits of the technique would be defined.

Ultrasonic Bi-Refringence Technique for Residual Stress Measurement

Significant progress has been made in the usage of the electro-magnetic acoustic transducer (EMAT) in the Bi-Refringence technique at the National Bureau of Standards in Boulder, Colorado. The device is applied to the back rim face of a railroad wheel and orthogonally polarized shear horizontal waves are propagated through the thickness of the wheel rim. The arrival times are measured (in pulse-echo) with a precision of 10^{-5} seconds. The difference in arrival times (Bi-Refringence) is related to the difference in principal stresses. TTC cooperated with NBS, Boulder, by supplying full-size wheels and cut samples of wheels. After successful implementation of this technique using EMAT's on the rims of full-size railroad wheels, this method was used to analyze six wheels which were tested on the RDU under Technical Task T4. The preliminary results of the residual stress measurements in the rim were very encouraging.

The NDE effort covered under the Wheel Failure Mechanisms Program is limited to the above level, where an ultrasonic Bi-Refringence system using EMAT's is available at NBS, Boulder, capable of making stress measurements in the rim of a full scale railroad wheel under laboratory conditions.

Future Work Required in Support of the Bi-Refringence Method
Being Tested at NBS, Boulder (beyond the scope of work covered
under Wheel Research Program):

A. To supply 40 slices of wheels (eight from new wheels,
    four per wheel) and the rest of the slices from the
    saw-cut wheels which exhibit closing behavior.

B. To perform hole drilling and strain-gaging at the TTC
    (before eventual saw-cutting) to compare Bi-Refringence
    results.

C. To assist NBS conduct Bi-Refringence analysis on 12
    test wheels before they are saw-cut.

D. To perform closed form analysis using saw-cut
    displacement data to evaluate average residual stress
    distribution in the wheel rim for comparisons with
    Bi-Refringence data.

15.0 M-2 CAR AXLE/BEARING FAILURE TESTS ON RDU (TECHNICAL TASK
      T15)

15.1 Work Statement

AAR was required to conduct an independent study of full
scale testing at the RDU of the TTC to determine rates of
fretting wear and thermal runaway on hollow axle/bearing/wheel
assemblies of commuter rail cars (M-2 Fleet).

15.2 Work Performed

An M-2 fleet truck with hollow axles was instrumented for
temperature observations as well as torque and dynamic
measurements. Tests were conducted on the RDU with four runs of
11,000 and 1,000 miles, during which thermal histories of
bearings that have service-worn grooves between the axle and
roller bearing assembly were examined. Also, static
measurements were made of bearing cup and seal wear ring
movement and any wear which might have occurred between the
bearing cones and the axle. The dynamic performance of a "bent"
axle was compared with a straight hollow axle.

All the required tests were completed and the data obtained
were transmitted to the Transportation Systems Center,
Cambridge, Massachusetts for analysis.

**Wheel Failure Mechanisms of Railroad Cars,
Final Report: Volume 2-Technical Task
Summaries**, 1987
Assocation of American Railroads, BR Rajkumar,
DH Stone